Approche multi-niveaux des modifications précritiques dans l'épilepsie

Louis Cousyn

Thèse de doctorat de Sorbonne Université

École doctorale Cerveau, Cognition, Comportement

Approche multi-niveaux des modifications précritiques dans l'épilepsie

Présentée par **Louis COUSYN**

Pour l'obtention du grade de

DOCTEUR DE SORBONNE UNIVERSITE

Spécialité Neurosciences

Soutenue publiquement le 24 mai 2023, devant un jury composé de :

Pr. Martine GAVARET, Université Paris-Cité	Présidente
Dr. Vera DINKELACKER, Université de Strasbourg	Rapporteuse
Pr. Jean GOTMAN, McGill University	Rapporteur
Pr. William SZURHAJ, Université Picardie Jules Verne	Examinateur
Pr. Vincent NAVARRO, Sorbonne Université	Directeur de thèse
Dr. Mario CHAVEZ, CNRS	Co-encadrant de thèse

Summary

Epilepsy is defined as the repetition of seizures, with varied symptomatology, whose spontaneous and unpredictable nature accounts for the chronic disability in patients. About one-third of patients are resistant to antiseizure medications, i.e. uncontrolled epileptic seizures despite at least two adequate molecules. The study of the mechanisms underlying the transition between an interictal state (literally "between two seizures") and the seizure – also known as ictogenesis – has long suggested the existence of preictal modifications. The preictal state, which refers to the period preceding the seizure, is the cornerstone of seizure prediction methods. Identifying sensitive and specific preictal biomarkers would be an opportunity for therapeutic strategies to stop the "road to the seizure".

My thesis work aimed to characterize preictal states using: i) subjective clinical symptoms; ii) standardized measures of cardiac activity and intracerebral functional connectivity; iii) recordings of *in vivo* neuronal activities and *in vitro* epileptiform activities in patients with epilepsy.

I divided my approach into several levels:

1) The evaluation of prodromal symptoms using daily four-point self-assessment questionnaires in patients: several machine-learning algorithms, based on support vector machine classifiers, have shown good performance prediction of the preictal state. A clinical study using the mobile application Epiday, which was developed based on my thesis work, will prospectively analyze this approach in real-life conditions.

2) The analysis of heart rate variability – as a reflection of sympathetic/parasympathetic balance – during a daily standardized resting-state protocol, which exhibited a good distinction between inter and preictal states by using a classifier. The pseudoprospective analysis showed correct overall probabilistic predictions of the seizure risk but with a moderate sensitivity that requires some adjustments before considering any clinical application.

3) The study of functional connectivity using intracerebral EEG recordings, also during daily resting-state protocols: the classification algorithm based on phase synchrony showed the best performances in distinguishing between inter and preictal states in the theta band. These results were significantly superior to those of the classifier based on interictal epileptiform discharges. The daily probabilistic forecasts of the seizure risk were also promising. Transposing the connectivity data into a hyperbolic space showed similar results.

4) *In vivo* recordings of neuronal activity using intracerebral microelectrodes: I was able to identify a large number of neurons and monitor their activity several hours before the seizure. I intend to continue my thesis work by looking for preictal modifications of the individual and interindividual behavior of these neurons.

5) *In vitro* recordings from postoperative human epileptic brain tissue allowed me to record interictal-like and preictal discharges, which I was able to correlate with data acquired *in vivo*.

My thesis work provided new data suggesting the existence of preictal dynamic modifications, from machine-learning algorithms and the implementation of a daily standardized resting-state protocol. My work paves the way for the analysis of changes in neuronal activities from intracerebral EEG recordings.

Remerciements

Je tiens tout d'abord à adresser mes remerciements à Vincent Navarro, mon directeur de thèse. Vincent, je te remercie pour ton soutien infaillible, ton écoute, ta bienveillance et ta capacité à solutionner tout problème. Merci de m'avoir accordé ta confiance, depuis ma thèse de médecine et durant ces années de thèse de sciences. Je tiens à te faire part de l'admiration, tant sur le plan professionnel qu'humain, que je te porte. Je mesure chaque jour la chance de travailler sous ton aile.

Je tiens également à remercier Mario Chavez, mon co-encadrant de thèse. Mario, ces années de thèse m'ont donné la chance de te rencontrer et de travailler à tes côtés. Ton aide et tes conseils dans l'aboutissement des différents projets, ainsi que ta bonne humeur et ton énergie, ont été cruciaux. Merci de m'avoir fait découvrir l'univers des algorithmes d'apprentissage automatique. Je me souviendrai toujours de nos ateliers dessins de haut vol (le monde de l'art tremble).

J'adresse mes profonds remerciements au Pr. Jean Gotman et au Dr. Vera Dinkelacker pour avoir accepté de juger mon travail de thèse en tant que rapporteurs. Merci du temps que vous consacrerez à la lecture et à l'évaluation de mon travail.

Je tiens à exprimer toute ma gratitude au Pr. Martine Gavaret et au Pr. William Szurhaj pour avoir accepté d'être examinateurs de mes travaux de recherche.

Merci Katia, pour ton aide précieuse, technique comme scientifique, de l'acquisition à l'analyse des données, et également pour ta gentillesse.

Merci à mes co-thésards : Rémy, pour ton aide précieuse sur les routines de connectivité ; Paul, ton aide avec le *spike sorting* a été inestimable ; Aurélie, merci pour tous tes conseils avisés ; Martin, j'espère que nos travaux communs ne s'arrêteront pas là.

Merci à Valerio, Vi-Huong, Claude et Virginie, vos relectures avisées des enregistrements EEG m'ont beaucoup aidé dans mes analyses. Merci également à Stephen pour son aide sur les analyses d'activités neuronales.

Merci à Laurent et Isabelle A., votre soutien en salle m'a permis de me libérer du temps pour mes activités de recherche.

Merci à mes meilleurs internes – ils se reconnaitront – Cendrine, Victor, Vincent G., Alban, François, Vincent L., Margaux et Thomas : grâce à votre autonomie et votre soutien, j'ai pu terminer ma thèse avec un peu plus de sérénité.

Merci également à toute l'équipe paramédicale d'Alajouanine – secrétaires, infirmier·e·s et aide-soignant·e·s – vous êtes trop nombreux·ses pour que je vous nomme mais j'ai une pensée pour chacun·e d'entre vous. Travailler à vos côtés est chaque jour un plaisir, et ce malgré les difficultés actuelles.

À titre plus personnel,

Aux personnes que j'ai connues et à celles que je connaitrai,
À celles que j'ai aimées,
À celles qui n'ont fait que passer et à celles qui sont restées,
À celles disparues, mais dont la mémoire demeure.
Si la vie n'est qu'un passage, puisse-t-il être en la compagnie des meilleurs,
La vôtre*.

Aux anciens souvenirs épris de mélancolie,
Et aux prochains, que l'on souhaite passionnés et embrasés.

Au désordre, au mouvement, au chaos de l'existence qui nous font vaciller,
Mais nous maintiennent animés.

*Cette définition inclut de manière non exhaustive et par ordre d'apparition :
Maman, Papa, Bonne-Maman et Bon-Papa, Barbara, Charles et Jeanne, JP et Flo ;
Agathe, Eugénie, Gaspard, Sophie, Juliette, Salomé, Mimousch, Ghislain ;
Ophélie, Camille, Aicha, Marion, Adèle, Daniele.

Introduce a little anarchy, upset the established order, and everything becomes chaos.

The Joker

(The Dark Knight, Christopher Nolan)

Sommaire

Table des figures

Liste des tableaux

Liste des abréviations, sigles et acronymes

API : application programming interface

AUC : area under the receiver operating characteristic curve

CPU : central processing unit

ECG : électrocardiogramme

ECoG : électrocorticogramme

EDA : activité électrodermale

EEG : électroencéphalogramme

HRV : heart rate variability

IED : interictal epileptiform discharge

iEEG : électro-encéphalogramme intracérébral

IRM : imagerie par résonnance magnétique

IRMf : imagerie par résonnance magnétique fonctionnelle

IZ : irritative zone

LFP : local field potential

MD : mahalanobis distance

MEA : multi-electrode array

MUA : multi-unit activity

NNDD : nearest neighbor data description

PLV : phase-locking value

RS : resting state

SEEG : stéréo-électroencéphalogramme

SPECT : single photon emission computed tomography

SOZ : seizure onset zone

STAY-Y1 : state-trait anxiety inventory form Y1

SUA : single-unit activity

SVDD : support vector data description

SVM : support vector machine

SVM-OC : one-class support vector machine

SVM-TC : two-class support vector machine

Introduction

PARTIE 1. INTRODUCTION GENERALE

I. L'épilepsie : une entité plurielle

1) Données épidémiologiques

Environ 65 millions de personnes à travers le monde, soit 1% de la population mondiale, sont atteintes d'épilepsie (Devinsky et al. 2018). Il s'agit de la 3ème pathologie neurologique la plus fréquente (Vos et al. 2016). Les causes, diverses, peuvent être (Scheffer et al. 2017) :

i) *structurelles* – avec individualisation d'une lésion cérébrale à l'origine de l'épilepsie : sclérose hippocampique, traumatismes crâniens, malformations de développement cortical, infarctus ou hématome cérébral, tumeurs cérébrales, etc. ;

ii) *génétiques*, qu'il s'agisse d'anomalies chromosomiques ou de mutations génétiques, d'épilepsie monogénique ou polygénique, de mutations héréditaires ou *de novo*, germinales ou somatiques ;

iii) *infectieuses* : la neurocysticercose est notamment l'une des causes d'épilepsie les plus fréquentes dans le monde (Carpio et al. 2021);

iv) *autoimmunes* : les crises d'épilepsie ont été décrites dans plus de deux tiers des patients présentant une encéphalite autoimmune, tous types confondus (Graus et al. 2016; Yeshokumar et al. 2021) ;

v) *métaboliques*, regroupant un spectre très large de pathologies ;

vi) et enfin, *inconnues*.

De nombreuses molécules antiépileptiques sont proposées en pratique courante pour contrôler la survenue de crises d'épilepsie. Cependant, environ un tiers des patients ont une épilepsie pharmacorésistante, c'est à dire que les crises persistent malgré l'administration d'au moins deux molécules adéquates. Chez certains de ces patients, une prise en charge chirurgicale peut être proposée, afin de réséquer le foyer épileptogène. Une telle intervention dépendra du type d'épilepsie, de la localisation du foyer, et également de facteurs propres au patient. Un bilan préchirurgical est ainsi recommandé et comporte systématiquement des enregistrement EEG à l'aide d'électrodes de surface voire intracérébrales, afin d'enregistrer les crises d'épilepsie et ainsi localiser leur point de départ.

2) Une pathologie à expression paroxystique

L'épilepsie est un état pathologique chronique susceptible de générer des crises épileptiques, de manière spontanée – en dehors de tout facteur confondant qui pourrait être à l'origine de crises « symptomatiques aiguës » – et répétée – par définition, au moins deux crises à au moins 24 heures d'intervalle. Si ce principe générique permet d'orienter vers un diagnostic d'épilepsie, il n'en reflète cependant pas la pluralité.

Il existe en effet plusieurs types d'épilepsie, eux-mêmes composés de plusieurs types de crises épileptiques. La nouvelle classification des épilepsies de la Ligue Internationale Contre l'Épilepsie (*International League Against Epilepsy*, ILAE) de 2017 propose un diagnostic à plusieurs niveaux (Fisher et al. 2017; Scheffer et al. 2017) :

a) Il convient tout d'abord d'identifier le *type de crises épileptiques* (Figure 1) :

- Crises à début focal : avec/sans rupture de contact ou « déconnexion », avec symptomatologie à composante motrice (automatismes, clonies, posture tonique, etc.) ou non (symptômes sensoriels, cognitifs, végétatifs, etc.), avec ou sans bilatéralisation tonico-clonique secondaire ;
- Crises à début généralisé d'emblée : avec symptomatologie motrice (crise tonico-clonique généralisée, myoclonies, etc.) ou non (crise d'absence) ;
- Crises dont le début, focal ou généralisé, n'est pas identifiable.

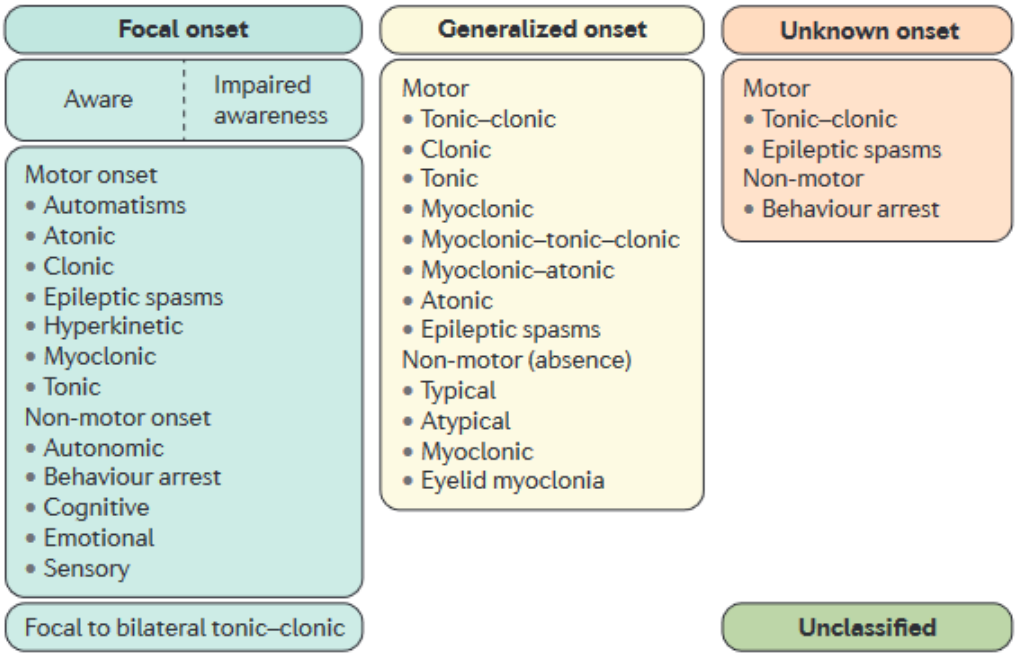

Figure 1. Classification étendue des types de crise d'épilepsie (ILAE 2017)
(Figure issue de Devinsky et al., 2018)

b) Ensuite, le *type d'épilepsie* peut être évoqué (Figure 2) :

- Une épilepsie généralisée, qui se manifeste par des crises généralisées d'emblée ;
- Une épilepsie focale, qui s'exprime par des crises à début focal, avec ou sans rupture de contact, avec ou sans composante motrice, et avec ou sans bilatéralisation tonico-clonique secondaire ;
- Certaines épilepsies peuvent être mixtes, focales et généralisées (e.g. le syndrome de Lennox-Gastaut) ;
- Et certaines indéterminées.

c) Enfin, un *syndrome épileptique* peut parfois être diagnostiqué, à la lumière des informations cliniques, des anomalies EEG et de l'imagerie cérébrale.

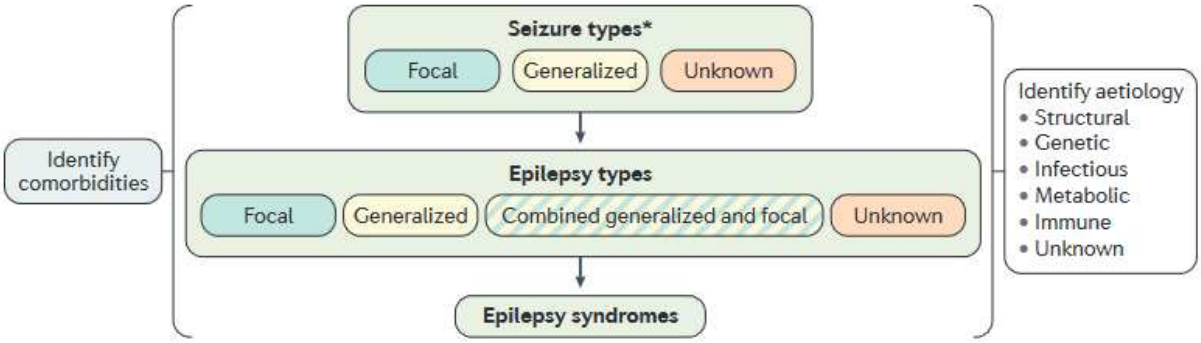

Figure 2. Classification des épilepsies (ILAE 2017)
(Figure issue de Devinsky et al., 2018)

3) Mécanismes physiopathologiques

L'*épileptogenèse* représente les mécanismes sous-tendant le long processus – plusieurs années chez l'humain – de développement au sein d'un tissu cérébral de modifications capables par la suite de générer des crises d'épilepsie (Figure 3). Ces mécanismes sont d'ordre cellulaire (neurogénèse aberrante, gliose réactionnelle, dysfonction de la barrière hémato-encéphalique, etc.), moléculaire, mais également transcriptomique et épigénétique (Devinsky et al. 2018). L'ensemble de ces modifications va amener à un dysfonctionnement de certains canaux ioniques et récepteurs neuronaux, engendrant une hyperexcitabilité cellulaire chronique à l'origine de l'épilepsie.

L'*ictogenèse* désigne les mécanismes impliqués dans l'émergence de crises d'épilepsie – schématiquement définies comme une décharge hypersynchrone de neurones hyperexcitables – par un

tissu cérébral épileptogène. À la différence de l'épileptogenèse, il s'agit d'un processus court sur une échelle de plusieurs secondes à minutes (Figure 3).

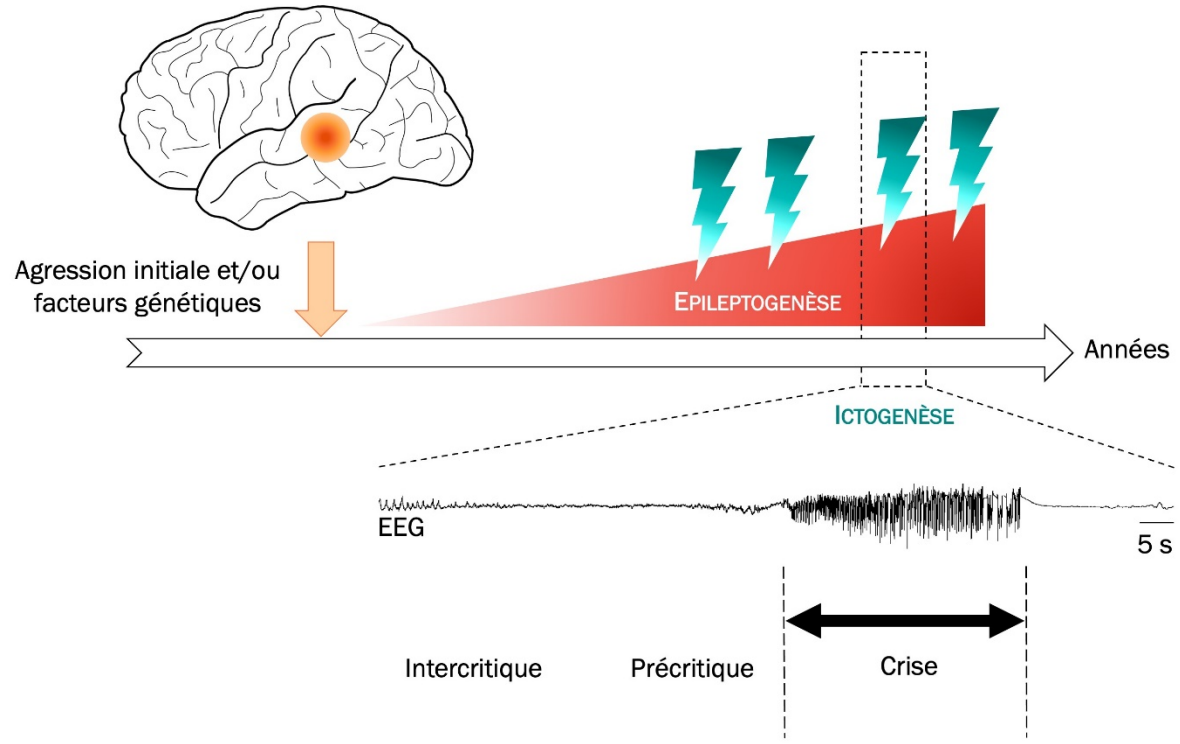

Figure 3. Epileptogenèse et ictogenèse

4) Réseau épileptogène

Plusieurs zones fonctionnelles sont impliquées dans l'épilepsie et composent le réseau épileptogène (Zijlmans et al. 2019) :

- La zone lésionnelle, au sens morphologique ;
- La zone irritative, correspondant à la localisation d'anomalies épileptiques intercritiques visualisées en EEG ;
- Et la zone épileptogène (ou *seizure onset zone*), région d'où émergent les crises et pouvant être délimitée par des explorations EEG et/ou par la tomographie par émission monophotonique (SPECT) (Figure 4).

L'individualisation de ces zones sera particulièrement importante en cas de chirurgie de l'épilepsie – notamment dans le cadre d'épilepsie focale pharmacorésistante – afin de délimiter le foyer à réséquer.

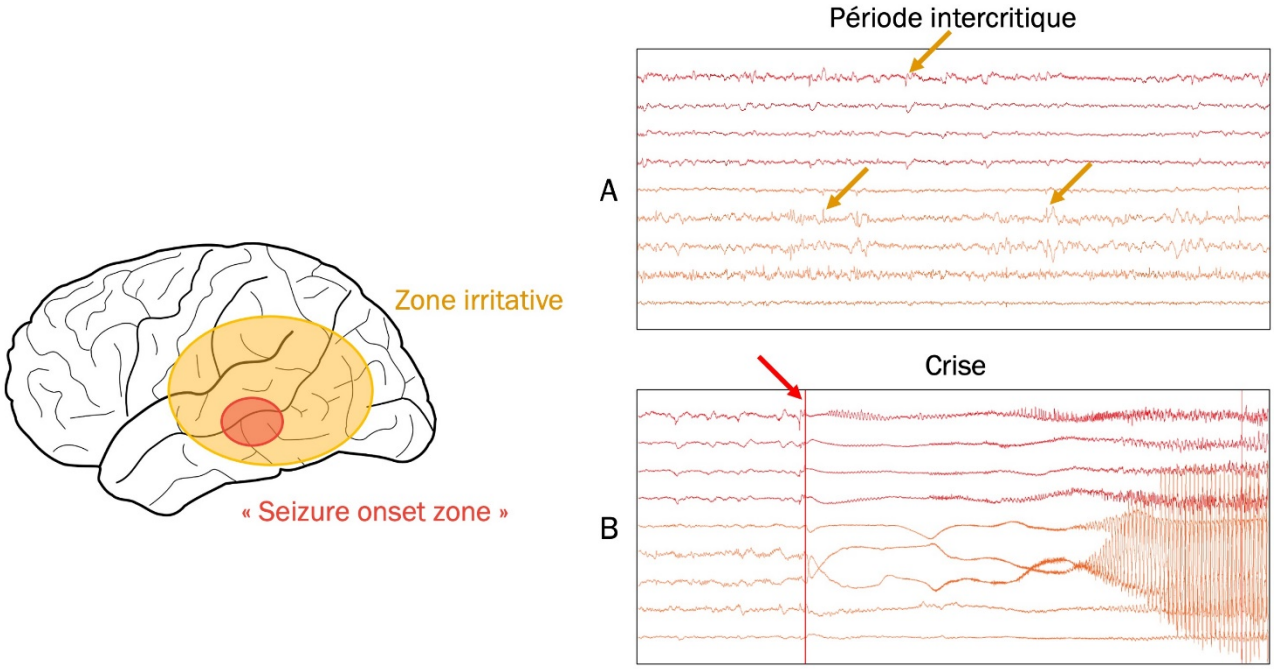

Figure 4. Zones fonctionnelles du réseau épileptogène
A. La zone irritative correspond à la région présentant des anomalies épileptiques intercritiques sur les enregistrements EEG (flèches orange) ; B. La *seizure onset* zone ou zone épileptogène, correspond à la région d'où part la crise en EEG (flèche rouge). La décharge électrique débute sur les électrodes rouges puis se propagent aux électrodes orange.

II. Une exploration électroencéphalographique à plusieurs niveaux

L'électroencéphalographie (EEG) est un examen essentiel dans la prise en charge de l'épilepsie. Elle permet d'enregistrer l'activité électrique du cerveau, et notamment des anomalies intercritiques épileptiques (pointes, pointes-ondes, etc.), signature du potentiel épileptogène chez un patient, et parfois des crises d'épilepsie. Son intérêt est multiple, diagnostique – orientation vers un type d'épilepsie en fonction des anomalies observées – mais également thérapeutique – notamment dans le cadre de la prise en charge des états de mal épileptique – et pronostique. Les électrodes EEG peuvent être placées à différents niveaux.

1) EEG de surface

Les électrodes sont directement placées sur le scalp du patient (Figure 5). Il s'agit de la technique utilisée en pratique courante, en milieu hospitalier ou en cabinet. Les enregistrements peuvent être courts – entre 20 et 30 minutes en moyenne – notamment lors des enregistrements ambulatoires à la recherche d'anomalies épileptiques intercritiques (Figure 6).

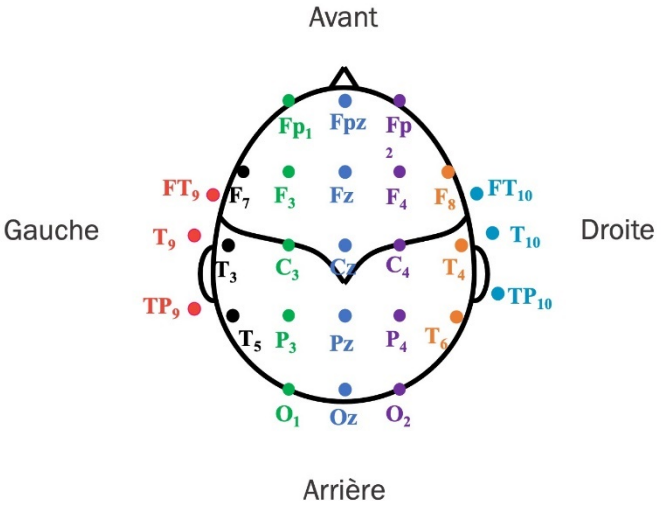

Figure 5. Positionnement des électrodes selon le système 10-20

Figure 6. Anomalies épileptiques intercritiques bitemporales enregistrées en EEG de surface
Pointes-ondes temporales bilatérales asynchrones dans le cadre d'une encéphalite autoimmune à anticorps anti-GAD ; montage référentiel, filtre passe haut : 0,53 Hz, filtre passe bas : 70 Hz, base de temps : 30 sec, gain : 80µV/cm

Des crises d'épilepsie peuvent également être enregistrées, notamment lors d'enregistrements EEG-vidéo continus (24h/24 et 7j/7) de longue durée (10-15 jours en moyenne) au cours du bilan préchirurgical d'une épilepsie focale pharmacorésistante (Figure 7).

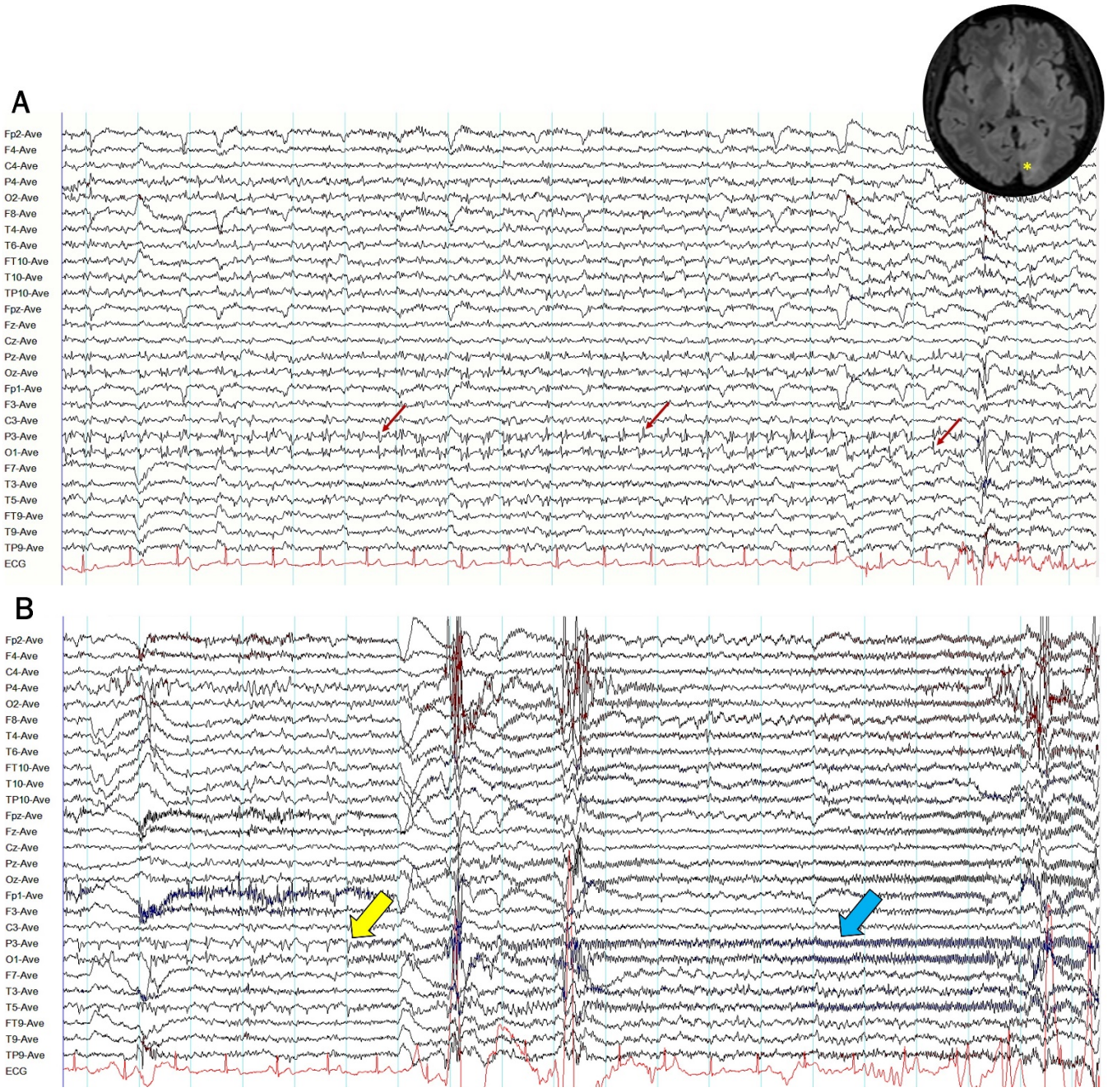

Figure 7. Crise d'épilepsie occipitale enregistrée en EEG de surface

A. Foyer d'anomalies épileptiques intercritiques occipito-pariétales gauches (flèches rouges) périodiques avec aspect « ECG-like » en lien avec une dysplasie corticale (étoile jaune, IRM cérébrale). B. Décharge critique de même localisation constituée initialement de rythmes rapides de faible amplitude (flèche jaune) avec augmentation de la fréquence de décharge et de l'amplitude des anomalies (flèche bleue) et propagation vers d'autres électrodes. Montage référentiel, filtre passe haut : 0,53 Hz, filtre passe bas : 70 Hz, base de temps : 30 sec, gain : 80µV/cm

2) EEG intracérébral

L'implantation d'électrodes intracérébrales en stéréo-électroencéphalographie (SEEG) peut être proposée en deuxième intention dans le cadre du bilan préchirurgical (Parvizi et Kastner 2018). Les électrodes profondes sont placées par voie neurochirurgicale selon une localisation prédéterminée et guidée par les explorations EEG et radiologiques antérieures afin de cibler la zone épileptogène. Les patients sont ensuite enregistrés en SEEG-vidéo continue durant une période moyenne de 21 jours (Figure 8). Chaque électrode profonde dispose de plusieurs contacts, espacés de plusieurs millimètres à centimètres, permettant l'enregistrement des signaux EEG.

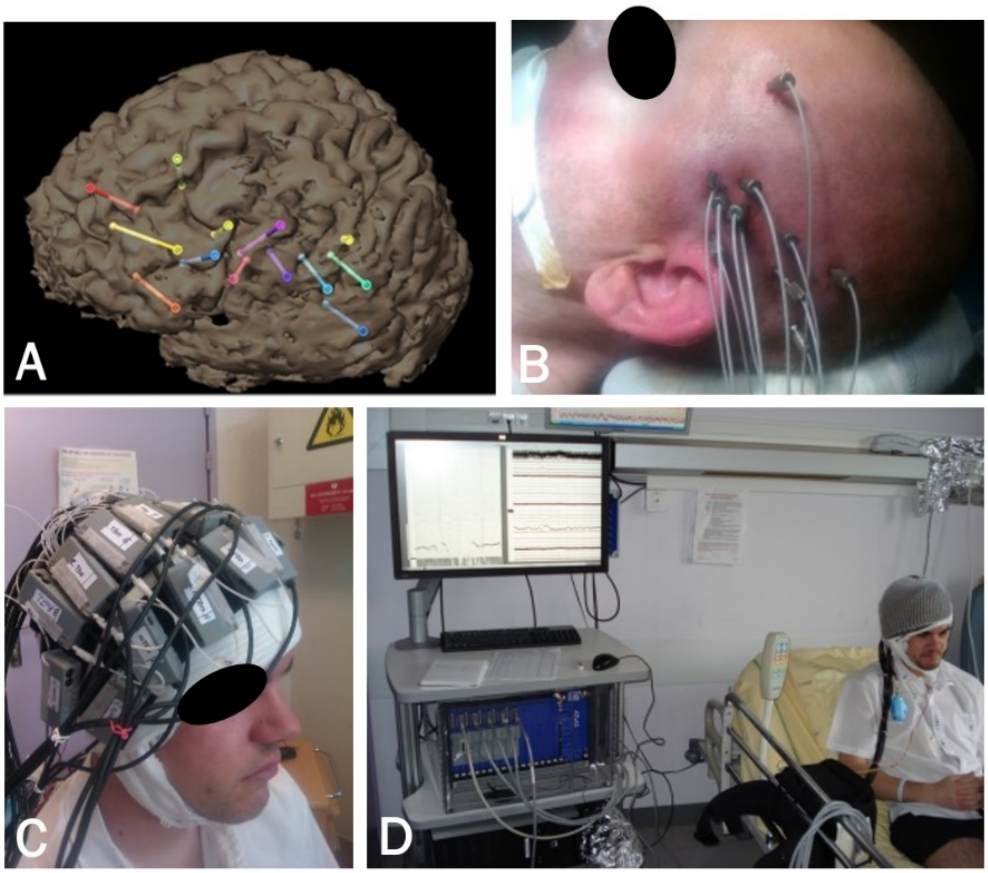

Figure 8. Enregistrement vidéo-EEG intracérébral continu
A. Schéma des localisations/trajectoires des électrodes profondes à implanter ; B. Vue de profil en post-implantation immédiate ; C et D. Enregistrement continu des signaux SEEG dans l'unité d'épileptologie de l'Hôpital Pitié-Salpêtrière (Paris, France).

Des microélectrodes de recherche peuvent être ajoutées aux électrodes profondes classiques (ou « macroélectrodes ») afin d'augmenter la résolution spatiale et enregistrer des potentiels de champ locaux (*local field potentials*, LFP) et des potentiels d'action de neurones (*multi-unit activity*, MUA, et *single-unit activity,* SUA). Plusieurs modèles de microélectrodes ont été développés, comme les macro-microélectrodes Behnke-Fried de Ad-Tech, celles de DIXI, ou les *Utah array* (Fried et al. 1997; Schevon et al. 2008; Despouy et al. 2019).

Notre équipe utilise actuellement les macro-microélectrodes Ad-Tech (Figure 9) : les macroélectrodes ont 4-12 contacts de 1 mm de diamètre, alors que les microélectrodes ont un diamètre de 40 µm, une longueur de 2 à 4 mm et sont constituées chacune de 8 microfils (Lehongre et al. 2022). On obtient ainsi des enregistrements simultanés à plusieurs niveaux de l'activité EEG (Figure 10).

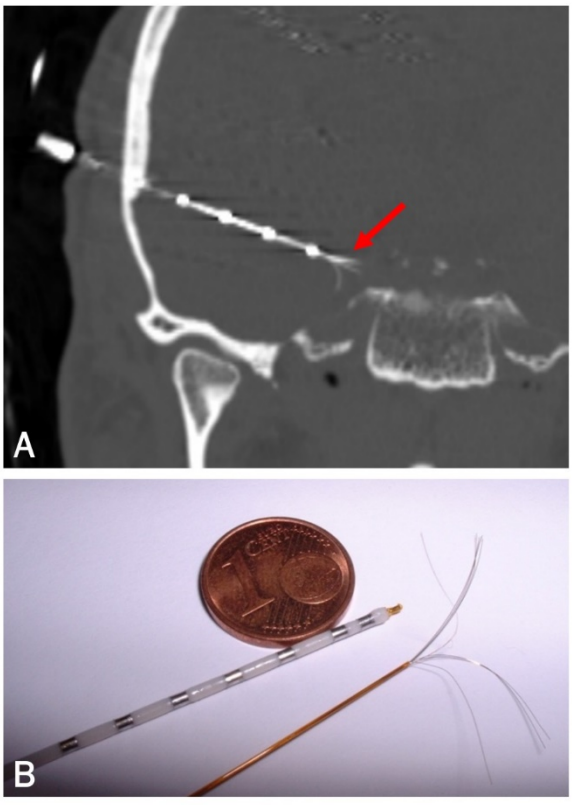

Figure 9. Macro-microélectrodes intracérébrales (Ad-Tech, Wisconsin)
A. Électrode profonde et émergence à son extrémité d'un faisceau de microélectrodes (flèche rouge) visible sur un scanner cérébral en fenêtre osseuse ; B. Électrode profonde à gauche avec visualisation des différents macrocontacts et faisceau de microélectrodes à droite.

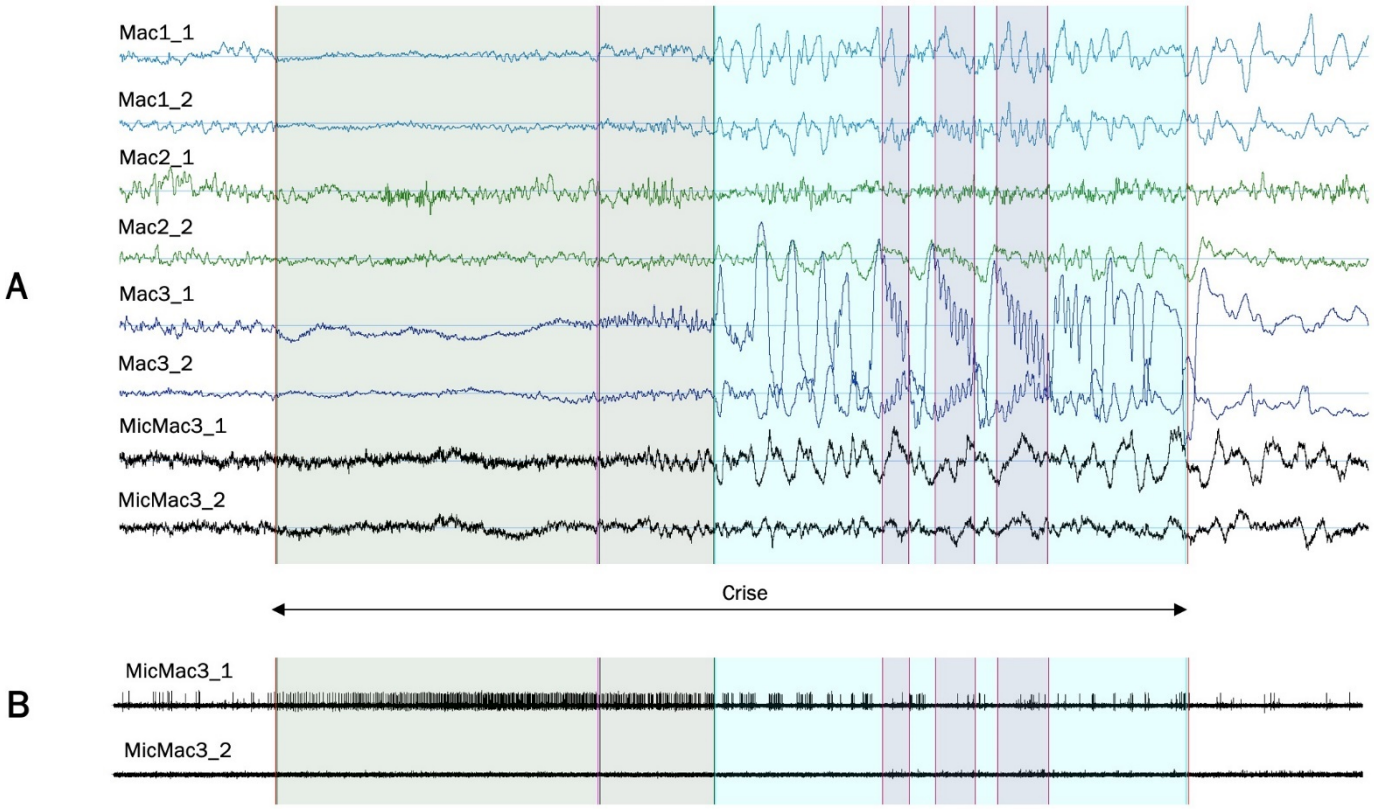

Figure 10. Enregistrement EEG issu de macro-microélectrodes intracérébrales

A. Enregistrement de 3 macroélectrodes (Mac1, Mac2 et Mac3) localisées dans le foyer épileptique – avec chacune 2 macrocontacts (_1 et _2) – et d'une microélectrode (MicMac3, insérée dans la macroélectrode Mac3) avec 2 microfils (_1 et _2). Montage bipolaire, filtre passe haut : 0,1 Hz, filtre passe bas : 200 Hz, base de temps : 30 sec, gain : 150µV/cm ;

B. Visualisation des activités unitaires de neurones après filtrage sur la microélectrode MicMac3_1. Montage bipolaire, filtre passe haut : 300 Hz, filtre passe bas : 3000 Hz, base de temps : 30 sec, gain : 150µV/cm

III. Qu'est-ce que la période précritique ?

1) Un fantasme construit ?

La survenue d'une crise d'épilepsie est un phénomène paroxystique et imprévisible – « un coup de tonnerre dans un ciel serein » – rendant compte du handicap et du retentissement social chez les patients. L'idée d'un état spécifique précédant la crise est donc particulièrement séduisante : elle permettrait une intervention afin de stopper la « route vers la crise », qui pourrait être d'ordre médicamenteuse (prise d'une molécule d'action rapide type benzodiazépines) ou cognitive (techniques de biofeedback, etc.), ou au moins une mise en sécurité du patient pour éviter notamment les chutes traumatiques. L'ensemble des modifications cliniques, radiologiques et EEG en faveur de l'existence d'un état précritique rapportées dans la littérature sera abordé dans le chapitre suivant. Les problématiques que l'on peut déjà soulever est la spécificité de telles modifications et leur capacité à détecter dans un laps de temps raisonnable un état précritique en condition de vie réelle (Figure 11). La période précritique est ainsi la clef de voûte des modèles de prédiction des crises.

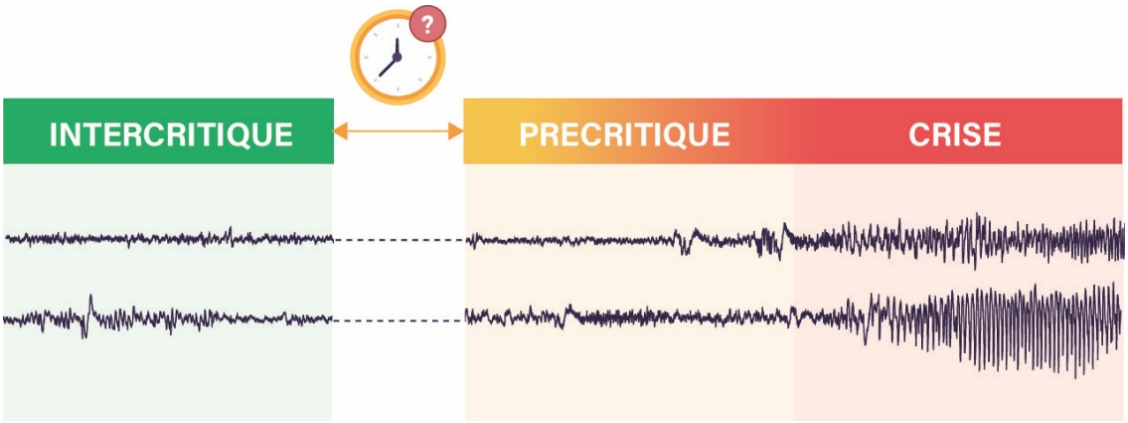

Figure 11. La période précritique
La mise en évidence de modifications précritiques doit être dans un laps de temps suffisant pour permettre une intervention.

2) Le produit insaisissable de dynamiques chaotiques ?

Mettre en évidence des modifications précritiques est toujours un enjeu de taille et la nature des mécanismes sous-tendant l'émergence des crises d'épilepsie ne facilite pas cette tâche. L'épilepsie peut être en effet appréhendée comme un système dynamique, non-linéaire, avec des comportements chaotiques que constituent les changements brutaux d'un état intercritique vers la crise – soit une bifurcation, la transition d'un état vers un autre (Iasemidis et al. 1990; Litt et Echauz 2002; Lehnertz et Litt

2005). Les systèmes chaotiques, imprévisibles du fait d'une sensibilité extrême aux conditions initiales, ne permettent pas une approche déterministe. De plus, peuvent se surajouter des facteurs précipitants stochastiques à même de faire basculer le système vers la crise (Baud et al. 2020). Ainsi, tout comme en météorologie, une approche probabiliste semble particulièrement adaptée à l'identification d'une période précritique en générant une probabilité du risque de crise.

3) Le versant déterministe d'un état procritique ?

L'approche probabiliste amène un nouveau concept, celui d'un état procritique, c'est-à-dire à risque de crise mais sans qu'elle ne survienne nécessairement – ou déterministiquement. Des mécanismes homéostatiques pourraient intervenir pour ne pas basculer vers une période précritique, et enfin la crise (Freestone et al. 2017). La période précritique pourrait alors être considérée comme un état évoluant déterministiquement vers la crise, alors que l'état procritique serait à risque de crise de manière probabiliste (Richardson et Jefferys 2011).

PARTIE 2. ÉTAT DE L'ART DE LA PERIODE PRECRITIQUE

Le concept d'un modèle limité à deux états dans l'épilepsie – c'est-à-dire intercritique/critique – a été remis en question au cours des dernières décennies. L'ictogenèse pourrait inclure un état de transition caractérisé par des modifications de l'excitabilité corticale qui ouvriraient la voie à la survenue d'une crise d'épilepsie. Cet état dit précritique constitue le substrat scientifique des modèles de prédiction des crises. S'il pouvait survenir dans un délai suffisamment long avant le début de la crise afin de détecter un changement d'état cérébral, une intervention susceptible d'arrêter la crise (médicaments, techniques de biofeedback, techniques de stimulation, etc.) ou, au moins, des mesures de mise en sécurité, pourraient être proposées.

Alors qu'une approche déterministe a longtemps été appliquée aux modèles de prédiction – pour prédire la survenue de la prochaine crise – une nouvelle stratégie s'est plus récemment développée. Les stratégies actuelles se veulent plus réalistes et adaptées aux systèmes dynamiques non linéaires. En effet, les approches probabilistes issues des sciences météorologiques sont de plus en plus appliquées aux modèles de prédiction des crises. L'objectif des prévisions de crises est d'estimer la probabilité d'une prochaine crise à tout moment, tandis que les algorithmes de prédiction classiques visent à prédire avec exactitude la survenue d'une prochaine crise. On peut ainsi identifier un état « pro » -critique, c'est-à-dire un état à haut risque de crise d'épilepsie.

I. Une variété d'approches de la période précritique

1) Approches cliniques

- Symptômes prodromaux, auto-prédiction et facteurs précipitants

En 1954, Henri Gastaut rapportait déjà des sensations « prémonitoires » de crises d'épilepsie (Gastaut 1954). Ces symptômes subjectifs, également appelés « prodromes » ou « symptômes prodromaux », peuvent précéder la crise de plusieurs heures – jusqu'à 24 heures – et consistent en des manifestations cognitives (difficultés de concentration, compréhension, à la lecture, etc.), émotionnelles (irritabilité, mauvaise humeur, anxiété, etc.), sensorielles (sensibilité au bruit ou à la lumière, etc.) ou physiques (maux de tête, fatigue, nausées, etc.) (Rajna et al. 1997; Schulze-Bonhage et al. 2006; Scaramelli et al. 2009; Schulze-Bonhage et Haut 2011; Haut et al. 2012; Besag et Vasey 2018). Les symptômes

prodromaux doivent être distingués des symptômes précoces lors des crises focales sans rupture de contact, anciennement appelées « auras », car le mécanisme sous-jacent n'est pas épileptique. En outre, contrairement aux auras, ils sont généralement considérés comme des symptômes négatifs (Figure 12) et ne permettent pas de localiser la zone épileptogène (Petitmengin et al. 2006; Besag et Vasey 2018). La prévalence des symptômes prodromiques varie largement en fonction des cohortes, de 6,2 à 87,1 % des patients (Hughes et al. 1993; Rajna et al. 1997; Lee et No 2005; Schulze-Bonhage et al. 2006; Pinikahana et Dono 2009; Scaramelli et al. 2009).

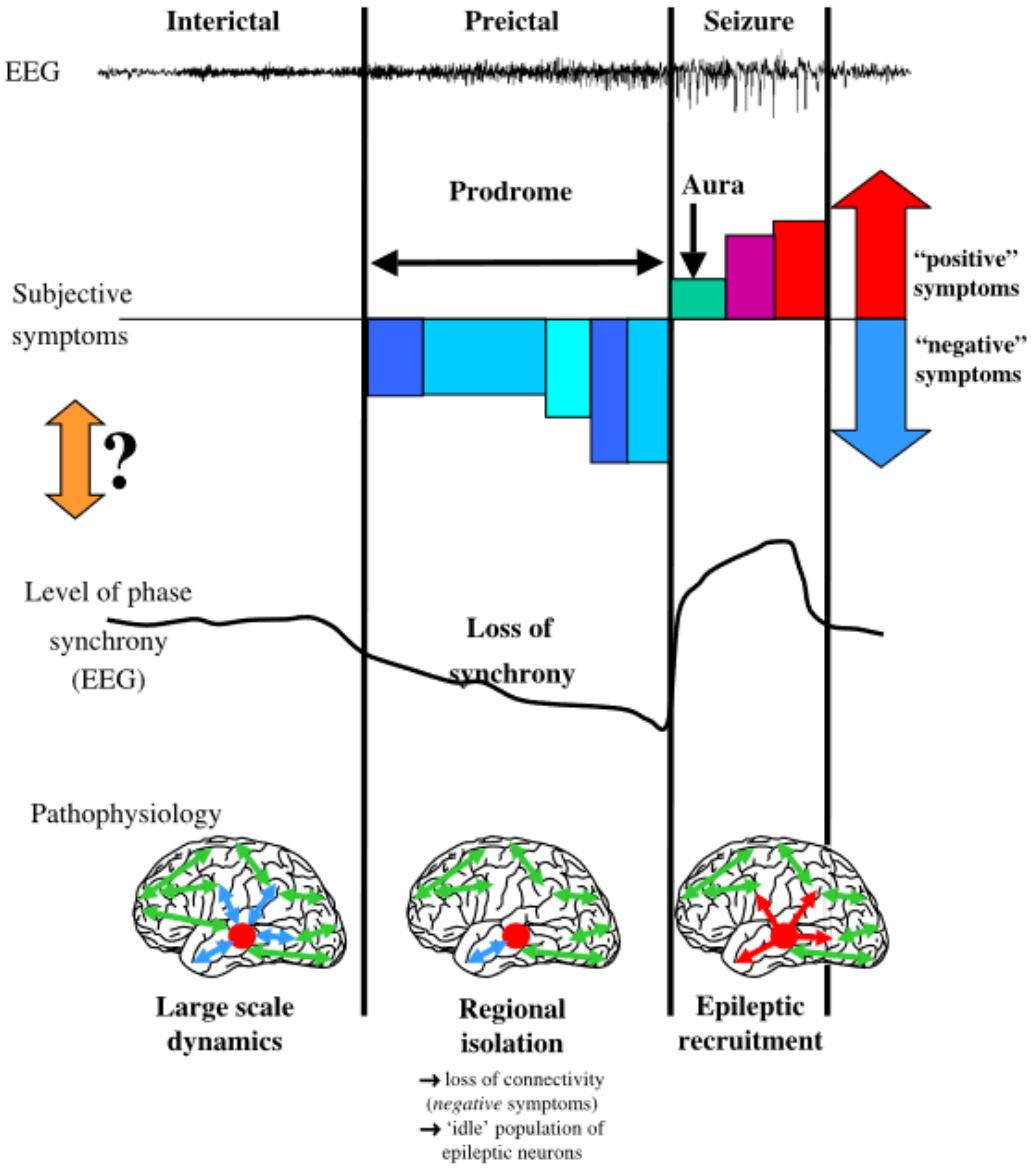

Figure 12. Symptômes prodromaux "négatifs" durant la période précritique
(Figure issue de Petitmengin et al., 2006)

Tableau 1. Études prospectives sur les symptômes prodromaux

OR : odds ratio ; PDA : personal digital assistant ; Se : sensibilité ; Sp : spécificité ; VEEG : vidéo-EEG ; VPN : valeur prédictive négative ; VPP : valeur prédictive positive

Référence	**Conception de l'étude**	**Nombre de patients**	**Symptômes prodromaux**	**Méthode statistique**	**Principaux résultats**
1)	Questionnaire quotidien, VEEG	83	Auto-prédiction des crises dans les 24 prochaines heures (oui/non/ne sait pas)	Modèle à effets mixtes généralisés	Augmentation significative de la probabilité par rapport aux prévisions négatives
2)	Journal, à domicile	71	Auto-prédiction des crises dans les 24 prochaines heures à l'aide d'une échelle de Likert en quatre points	OR et test du Chi-2	Une prédiction positive était associée à un risque deux fois plus élevé de crise (OR 2,25) ; Sp 0,87 ; Se 0,21
3)	Journal, à domicile	71	▪ Identique à (2) ▪ Heures de sommeil ▪ Échelle de 0 à 10 pour l'anxiété et le stress	OR et modèle logit multinomial	- Une augmentation d'une unité du stress et de l'anxiété était associée à un risque accru de crise le jour suivant - L'augmentation du nombre d'heures de sommeil était associée à une réduction du risque de crises - L'auto-prédiction (OR 3,7) et le nombre d'heures de sommeil pendant la nuit précédant la crise sont restés significatifs dans le modèle de régression logistique multinomial
4)	Journal électronique, à domicile	19	▪ Échelle visuelle analogique de 0 à 100 : heureux, triste, détendu, nerveux, vif, ennuyé ▪ Échelle de stress de 0 à 10 ▪ 18 caractéristiques prémonitoires (oui/non) ▪ Heures de sommeil	OR et modèle de régression logistique multivarié	- Plusieurs éléments de l'humeur et 10 caractéristiques prémonitoires étaient associés à un risque accru de crise - Dans les modèles multivariés, une amélioration de 10 points de l'humeur totale diminuait le risque de crise de 25 %, tandis que chaque caractéristique prémonitoire supplémentaire augmentait le risque de crise de 25%

5)	Journal électronique, à domicile	19	▪ Auto-prédiction des crises dans les 24 prochaines heures à l'aide d'une échelle de Likert en 5 points ▪ Échelle visuelle analogique de 0 à 100 : heureux, triste, détendu, nerveux, vif, ennuyé ▪ Échelle de stress de 0 à 10 ▪ 18 caractéristiques prémonitoires (oui/non) ▪ Heures de sommeil	OR et modèle de régression logistique multivarié	- L'OR pour les prédictions dans les 6 heures atteignait 9,31 pour la "quasi certain" - Pour les 9 meilleurs prédicteurs, la sensibilité médiane de l'auto-prédiction était de 0,5 et la spécificité médiane de 0,95 - Dans les modèles multivariés, l'auto-prédiction, le changement d'humeur favorable et le nombre de symptômes prémonitoires étaient significatifs
6)	PDA, à domicile	9	Entrées des symptômes prodromaux actuels (non spécifiés dans l'article)	Se, Sp	Pas de résultat significatif
7)	Questionnaires électroniques, à domicile	64	▪ Auto-prédiction des crises à l'aide d'une échelle de Likert en 5 points ▪ Échelle visuelle analogique de 0 à 100 pour 4 valences d'humeur ▪ Symptômes prémonitoires : 11 éléments (oui/non) ▪ Heures de sommeil	Se, Sp, VPP, VPN	- L'auto-prédiction était associée à la survenue de crises à 6, 12 et 24 heures - Pour la fenêtre de prédiction de 12 heures, la spécificité médiane pour la prédiction des crises était de 0,94 et la sensibilité médiane de 0,10

1) DuBois JM, Boylan LS, Shiyko M, Barr WB, Devinsky O. Seizure prediction and recall. Epilepsy Behav. 2010 May;18(1–2):106–9.
2) Haut SR, Hall CB, LeValley AJ, Lipton RB. Can patients with epilepsy predict their seizures? Neurology. 2007 Jan 23;68(4):262–6.
3) Haut SR, Hall CB, Masur J, Lipton RB. Seizure occurrence: Precipitants and prediction. Neurology. 2007 Nov 13;69(20):1905–10.
4) Haut SR, Hall CB, Borkowski T, Tennen H, Lipton RB. Clinical features of the pre-ictal state: Mood changes and premonitory symptoms. Epilepsy Behav. 2012 Apr;23(4):415–21.
5) Haut SR, Hall CB, Borkowski T, Tennen H, Lipton RB. Modeling seizure self-prediction: An e-diary study. Epilepsia. 2013 Nov;54(11):1960–7.
6) Maiwald T, Blumberg J, Timmer J, Schulze-Bonhage A. Are prodromes preictal events? A prospective PDA-based study. Epilepsy Behav. 2011 Jun;21(2):184–8.
7) Privitera M, Haut SR, Lipton RB, McGinley JS, Cornes S. Seizure self-prediction in a randomized controlled trial of stress management. Neurology. 2019 Nov 26;93(22):e2021–31.

Plusieurs études ont également examiné la valeur de l'auto-prédiction des crises par les patients, c'est-à-dire l'estimation du risque de crise rapportée par les patients eux-mêmes. Le pourcentage de patients ayant une capacité supérieure au hasard de prédire eux-mêmes les crises varie de 21,1 à 47,4 % (Haut et al. 2007a, 2013; Privitera et al. 2019). Les facteurs précipitants (manque de sommeil, stress émotionnel, menstruation, alcool, etc.) sont un autre déterminant important de la survenue des crises, signalés chez 53 à 89,8 % des patients (Nakken et al. 2005; Pinikahana et Dono 2009), pouvant contribuer à l'auto-prédiction des crises.

Plusieurs études ont évalué de manière prospective la capacité des symptômes prodromaux à prédire les crises (Tableau 1). L'auto-prédiction était l'une des variables les plus discriminantes avec une spécificité médiane de 0,87-0,95, mais la sensibilité restait faible, de l'ordre de 0,1-0,5 (Haut et al. 2007a, 2013; DuBois et al. 2010; Privitera et al. 2019). Le manque de sommeil, le stress et certains symptômes prodromaux pourraient être associés à un risque accru de crise d'épilepsie (Haut et al. 2007b, 2012, 2013). Une étude n'a cependant pas donné de résultats significatifs (Maiwald et al. 2011). Une des hypothèses pouvant expliquer ces résultats mitigés serait que les analyses linéaires habituelles ne permettraient pas de saisir la complexité de ces données, ainsi que la catégorisation binaire (oui/non) de certaines variables. L'utilisation d'algorithmes de prédiction non linéaires sur des données échelonnées pourrait ainsi être intéressante.

- Analyses de l'ECG

L'impact direct ou indirect de l'épilepsie sur le système nerveux autonome a été suggéré depuis plus de 20 ans, notamment par l'analyse de la variabilité de la fréquence cardiaque (VFC). En effet, la VFC reflète l'équilibre sympathique/parasympathique (Figure 13) et représente un moyen accessible d'analyser la prépondérance de l'un ou l'autre système par le biais d'une analyse temporelle, fréquentielle et non linéaire (Shaffer et Ginsberg 2017). Une diminution intercritique de la VFC, suggérant une composante parasympathique plus faible, a été mise en évidence chez les patients atteints d'épilepsie par rapport à des témoins sains appariés (Lotufo et al. 2012). Les changements de VFC ont également été signalés comme un moyen prometteur d'identifier les états précritiques (Meisel et Bailey 2019; Leal et al. 2021). La quantité d'informations précritiques issue des enregistrements ECG pourrait même être plus importante que celle des EEG de surface (Meisel et Bailey 2019). Une augmentation du rapport entre les basses fréquences (0,04-0,15Hz) et les hautes fréquences (0,15-0,4Hz), qui reflète une activité sympathique prédominante, a été décrite jusqu'à une heure avant l'apparition de la crise (Kolsal et al. 2014). Plusieurs études ont ainsi développé des algorithmes de prédiction basés sur le VFC. Certains auteurs ont rapporté une sensibilité de

89-91% et un taux de faux positifs de 0,4-0,7 fois par heure (Fujiwara et al. 2016; Billeci et al. 2018) tandis que d'autres ont indiqué une précision de 77,1 % (Giannakakis et al. 2019).

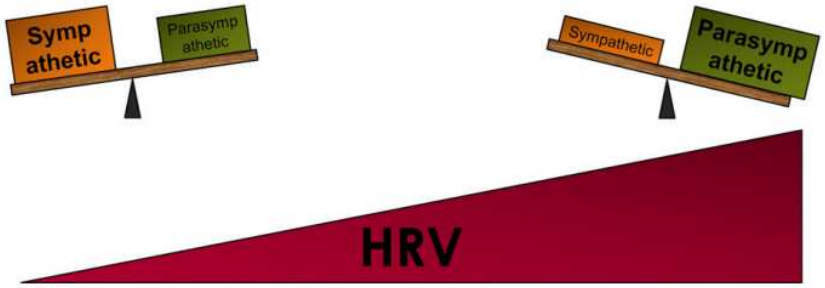

Figure 13. La variabilité de la fréquence cardiaque reflète l'état d'équilibre du système nerveux autonome
(Figure issue de Myers et al., 2018)

- Les cycles dans l'épilepsie

L'excitabilité corticale varie en fonction de l'état de vigilance (cycles veille/sommeil), des fluctuations hormonales (ACTH, cortisol, hormones sexuelles) et d'autres processus physiologiques périodiques (régulation de la glycémie, etc.) (Badawy et al. 2012; Ly et al. 2016). Les anomalies épileptiques intercritiques augmentent généralement pendant les stades N2 et N3 du sommeil et diminuent de manière significative pendant le sommeil paradoxal. En outre, les effets circadiens sur les crises peuvent parfois être estimés en fonction du syndrome épileptique : les patients souffrant d'épilepsie focale frontale sont plus susceptibles d'avoir des crises durant le sommeil, tandis que les patients atteints d'épilepsie myoclonique juvénile ont tendance à avoir plus fréquemment des crises au petit matin.

Les journaux de crises ont été utilisés pour développer des algorithmes de prévision basés sur les cycles de crises – c'est-à-dire les périodicités circadiennes (heures), multidiennes (jours/semaines) ou même circannuelles (mois). Les performances de prévision ont montré dans une étude pseudo-prospective une aire sous la courbe (AUC) de 0,69 à 0,94 et une précision moyenne de 69% (Karoly et al. 2020). La principale limite des approches basées sur les journaux est le risque de sous-déclaration des crises d'épilepsie par les patients, pouvant aller jusqu'à 50 % (Elger et Hoppe 2018). De plus, aucune prévision prospective en condition de vie réelle n'a été évaluée à ce jour.

Le profil circadien des crises peut également être implémenté dans un modèle multimodal afin d'améliorer les performances de prédiction. Un modèle combinant des informations circadiennes et EEG

a donné de meilleures performances qu'un modèle uniquement basé sur l'EEG, avec des résultats de sensibilité plus élevés (Cook et al. 2013; Karoly et al. 2017).

- Les crises d'épilepsie peuvent-elles prédire les crises d'épilepsie ?

L'analyse rétrospective d'enregistrements ultra prolongés (plusieurs années) a révélé, à partir des distributions statistiques des intervalles entre les crises, une occurrence non aléatoire des crises (Cook et al. 2014). Au lieu de prédire la probabilité d'une crise à venir, les approches de prévision du nombre de crises, souvent négligées dans la littérature sur la prédiction des crises, visent à prédire le nombre de crises sur une période future (Goldenholz et al. 2018, 2020; Goldenholz et Westover 2023). En utilisant des données sur de longues périodes, provenant de journaux de crises rapportés par les patients ou d'enregistrements intracrâniens, différentes études ont développé des algorithmes statistiques pour prédire le nombre de crises à venir (Goldenholz et al. 2018, 2020; Wang et al. 2022; Goldenholz et Westover 2023). Ces méthodes permettent également d'incorporer des facteurs extérieurs tels que des variables cliniques, la qualité du sommeil, ou même des informations météorologiques pour fournir une prévision plus robuste aux variations naturelles de la fréquence des crises (Chiang et al. 2018; Payne et al. 2021).

- Des dispositifs portables pour des prévisions ambulatoires ?

Mettre au point un dispositif non invasif adapté à la collecte prospective et prolongée de données et à l'analyse en temps réel constitue un défi pour les décennies à venir. Plusieurs journaux de crises sur smartphone sont disponibles pour l'auto-déclaration des crises et la collecte des symptômes prodromaux. Les capteurs portables tels que les montres, bracelets et bagues intelligents, ou même des patchs autocollants, peuvent recueillir des informations sur la qualité et la quantité du sommeil, la fréquence cardiaque (et la VFC), l'activité électrodermale, l'accélérométrie, etc. Une étude longitudinale a recueilli les caractéristiques du sommeil à partir d'une montre connectée (Fitbit, Fitbit Inc., USA) pendant 17 mois en moyenne et a montré que les variations d'heures de début et de fin de sommeil exposaient à un risque plus élevé de crise le jour suivant que les variations de la durée totale du sommeil (Stirling et al. 2022). L'enregistrement longitudinal de la fréquence cardiaque par montre connectée (Fitbit) a de plus révélé des cycles pluriquotidiens qui se synchronisaient avec l'apparition des crises d'épilepsie (Karoly et al. 2021b).

Les performances de prévision à partir de différentes mesures cliniques combinées (sommeil, fréquence cardiaque et nombre de pas) recueillies par montre connectée (Fitbit) dans un petit échantillon de patients (N=11) ont atteint un AUC moyen de 0,74 pour les probabilités horaires et de 0,66 pour les probabilités journalières (Stirling et al. 2021a). Deux autres études ont utilisé le bracelet E4 (Empatica,

Empatica Inc., USA) pour l'enregistrement prolongé de l'accélérométrie, de la pléthysmographie, de l'activité électrodermale et de la température (Meisel et al. 2020; Nasseri et al. 2021). Les auteurs ont respectivement rapporté un AUC moyen de 0,8 sur 6 patients et une prévision meilleure que le hasard chez 30 des 69 patients (44%).

2) Approches d'imagerie cérébrale

La mesure continue du débit sanguin cérébral de surface (DSC) par des capteurs sous-duraux a mis en évidence une augmentation du débit dans la zone épileptogène 20 minutes avant le début de la crise électrocorticographique, tandis que le DSC dans le cortex non épileptogène diminuait 2 minutes avant le début de la crise. (Weinand et al. 1997). D'autres études ont également constaté une augmentation précritique du DSC régional (rDSC) par tomographie d'émission monophotonique (SPECT) et de la disponibilité de l'oxygène cérébral par spectroscopie proche infrarouge (NIRS), respectivement 11-12 min et 1,5-13 h avant l'apparition de la crise EEG (Baumgartner et al. 1998; Adelson et al. 1999).

Les changements précritiques en IRM fonctionnelle (IRMf) ont été étudiés ultérieurement, en particulier en utilisant le signal dépendant du niveau d'oxygène sanguin (BOLD) comme marqueur du rDSC. Une augmentation du signal BOLD en IRMf a été observée quelques dizaines de secondes à plusieurs minutes avant l'apparition de la crise clinique ou électrique EEG – jusqu'à 20 minutes – et parfois une diminution associée dans une région annexe (Federico et al. 2005; Chaudhary et al. 2012; Vinette et al. 2016).

Il est important de souligner qu'aucun EEG intracérébral n'a été réalisé au cours de ces acquisitions. Il est tout à fait possible qu'une crise ait pu débuter dans une région cérébrale profonde – qui ne serait pas enregistrée par des électrodes placées en surface sur le cuir chevelu ou en ECoG – et les changements observés au cours de la période dite précritique ne seraient le reflet que d'une activité critique occulte. Des données provenant d'un EEG intracérébral et d'une IRMf concomitants sont disponibles pour un seul patient et aucun changement BOLD significatif n'a été observé pendant la période précritique (Chaudhary et al. 2016). La période précritique enregistrée était cependant trop courte – uniquement 30 secondes avant l'apparition de la crise.

Bien qu'intéressantes pour des considérations physiopathologiques, en particulier l'équilibre excitation/inhibition précritique, les approches en IRMf ne sont pas adaptées à une application en pratique clinique dans le domaine de la prédiction des crises d'épilepsie.

3) Approches EEG

- Analyses standards de l'EEG

Anomalies EEG intercritiques

L'EEG intercritique présente une activité physiologique de fond ponctuée par des événements transitoires composées notamment d'anomalies épileptiques intercritiques (pointes, pointes-ondes, etc.), d'anomalies lentes et d'oscillations à haute fréquence (HFO), qui surviennent plus fréquemment que les crises d'épilepsie. Bien que ces événements ne soient associés à aucune manifestation clinique, ils pourraient refléter l'excitabilité corticale (Chvojka et al. 2021; Lai et al. 2023). Des changements dans leur dynamique spatio-temporelle pourraient indiquer une condition particulière qui précède l'apparition des crises d'épilepsie. En effet, il a été démontré que les HFO (100-500 Hz) sont impliqués dans l'initiation des crises et dans les périodes précritiques immédiates (1-5 min avant la crise) (Jefferys et al. 2012; Pearce et al. 2013; Scott et al. 2020, 2021). Certaines études ont toutefois soulevé des doutes quant à leur spécificité à identifier des périodes présentant un risque accru de crises d'épilepsie (Jacobs et al. 2009; Lai et al. 2023). Les premières études ont considéré que l'organisation spatio-temporelle des décharges d'anomalies épileptiques intercritiques jouerait un rôle dans la genèse des décharges critiques (Ralston 1958; Stevens et al. 1972; Lange et al. 1983; Li et al. 2013). Néanmoins, d'autres études portant sur des ensembles de données plus conséquents n'ont pas trouvé de changements systématiques dans les décharges d'anomalies épileptiques intercritiques avant les crises (Gotman et Marciani 1985; Gotman et Koffler 1989; Katz et al. 1991; Chvojka et al. 2021). De même, des oscillations très lentes ont été observées avant l'apparition des crises, mais les données restent insuffisantes pour confirmer une modulation lente de l'excitabilité ou tout autre rôle dans l'ictogenèse (Ren et al. 2011; Constantino et Rodin 2012; Rodin et al. 2014).

Cycles des anomalies épileptiques intercritiques

Les études antérieures sur les figures EEG intercritiques se sont principalement concentrées sur les changements temporels pendant les périodes proches des crises. Néanmoins, des découvertes récentes ont suggéré que la dynamique des anomalies épileptiques intercritiques pouvait être organisée sur des échelles de temps circadiennes, multidiennes et circannuelles. En effet, les algorithmes de prévision des crises ayant pris en compte ces cycles sous-jacents sur des enregistrements EEG ultra prolongés (années) provenant de

dispositifs implantables chroniques ont mis en évidence une probabilité cyclique du risque de crise (Cook et al. 2013; Leguia et al. 2021; Proix et al. 2021).

Figures physiologiques

Le sommeil et l'épilepsie ont une forte influence mutuelle, notamment l'apparition d'anomalies épileptiques intercritiques et de crises à des stades de sommeil particuliers (Derry et Duncan 2013). Il est intéressant de noter que des changements dynamiques dans les fuseaux de sommeil – une réduction significative – ont été mis en évidence avant l'apparition des crises, ce qui pourrait être lié à une perturbation des réseaux cortico-thalamiques avant la décharge critique (Tezer et al. 2014; Rémi et al. 2018).

- Analyse du signal EEG

Les systèmes actuels de prédiction des crises basés sur les données EEG consistent en une acquisition continue suivie i) d'un prétraitement des signaux pour éliminer les artefacts, ii) de l'extraction et de la sélection de caractéristiques les plus informatives, iii) d'une classification pour distinguer les états intercritiques et précritiques, iv) d'un post-traitement pour réduire les faux positifs et, enfin, v) d'une évaluation des performances.

Prétraitement de l'EEG

L'étape de prétraitement vise à supprimer ou à atténuer les artefacts environnementaux ou physiologiques (contractions musculaires, mastication, déglutition, mouvements oculaires, clignements des yeux, etc.) en utilisant de multiples techniques pour augmenter le rapport signal/bruit, telles que les filtres passe-bande, coupe-bande, ou la décomposition en ondelettes (Islam et al. 2020). Même s'il s'agit d'une étape nécessaire pour nettoyer les signaux EEG, les procédures de prétraitement (lissage, normalisation et prétraitement des valeurs aberrantes) peuvent également avoir un impact sur les performances des algorithmes de prédiction (Rasekhi et al. 2013).

Une autre question importante, souvent négligée dans la littérature sur la prédiction des crises, est l'effet de la conduction volumique et l'impact des montages bipolaires ou référentiels sur les mesures (Nunez et al. 1997; Zaveri et al. 2000; Park et al. 2011). Le référencement des signaux EEG originaux à des références artificielles ou l'utilisation de filtres spatiaux (par exemple, le Laplacien) ont été proposés

pour réduire ces biais potentiels (Srinivasan et al. 1998). Des méthodes statistiques spécifiques peuvent également être appliquées pour extraire les caractéristiques de l'EEG et réduire l'impact de la conduction volumique, comme la cohérence imaginaire ou l'indice de retard de phase (*phase-lag index*).

Extraction des caractéristiques

L'extraction des caractéristiques est l'étape au cours de laquelle les informations les plus discriminantes sont extraites des signaux EEG. Fondamentalement, les caractéristiques sont basées sur des mesures univariées de chaque canal, ou multivariées lorsque les informations sont extraites d'une combinaison de plusieurs canaux. Alors que les mesures linéaires sont calculées directement à partir des segments EEG (dans le domaine temporel ou fréquentiel), plusieurs mesures non linéaires, principalement dérivées de la théorie des systèmes dynamiques, ont été proposées pour caractériser les propriétés statistiques plus complexes (Abarbanel et al. 1993; Kantz et Schreiber 2003).

Caractéristiques univariées linéaires

Les caractéristiques linéaires comprennent généralement des moments statistiques dans le domaine temporel (moyenne, variance, coefficient d'asymétrie, coefficient d'aplatissement, caractéristiques de la fonction d'autocorrélation, etc.) ou fréquentiel (centroïde spectral, coefficient d'asymétrie spectrale, puissance absolue ou relative dans les bandes de fréquence standard de l'EEG, etc). Dans plusieurs études de prédiction des crises, les signaux EEG sont modélisés comme la sortie d'un processus autorégressif (AR), d'un processus à moyenne mobile (MA), ou autorégressif à moyenne mobile (ARMA), de sorte que les paramètres du modèle résultant (l'ordre du filtre, les coefficients, l'erreur de prédiction, etc.) servent de caractéristiques pour l'identification de l'état précritique (Mormann et al. 2007). De même, les paramètres obtenus en filtrant les signaux EEG en ondelettes ou d'autres décompositions linéaires temps-fréquence (ondelettes continues, discrètes ou paquets d'ondelettes) ont été utilisés comme caractéristiques dans la prédiction des crises d'épilepsie (Bou Assi et al. 2017; Cherian et Kanaga 2022; Maimaiti et al. 2022). Le principal avantage de ces caractéristiques linéaires est leur simplicité algorithmique et leur facilité d'utilisation notamment dans une configuration en temps réel, ce qui pourrait être intéressant pour une surveillance continue.

Caractéristiques univariées non linéaires

Les signaux cérébraux, à différentes échelles temporelles et spatiales, peuvent être considérés comme la sortie d'oscillateurs non linéaires stochastiques (Lopes da Silva et al. 2003a). La plupart des caractéristiques non linéaires utilisées dans la prédiction des crises sont dérivées de la théorie des systèmes dynamiques, dans laquelle l'EEG est considéré comme une variable observée d'un système dynamique complexe. Certains outils mathématiques permettent de reconstruire, à partir d'une seule observation scalaire, les états sous-jacents du système à chaque instant (Abarbanel et al. 1993; Kantz et Schreiber 2003). La séquence d'états consécutifs dans le temps définit une trajectoire dans l'espace des phases. Dans les premières études sur la prédiction des crises, différents paramètres caractérisant cette trajectoire reconstruite ont été utilisés comme caractéristiques EEG. Les paramètres de la trajectoire tels que la dimension de corrélation (et ses multiples dérivées), les entropies liées à la corrélation, les mesures de flux local, la prédictibilité marginale et les exposants de Lyapunov constituent différentes mesures non linéaires de sa complexité et de sa stabilité (Abarbanel et al. 1993; Kantz et Schreiber 2003). La régularité des trajectoires reconstruites a également été caractérisée par l'analyse et la quantification de leur récurrence, qui fournit différents paramètres liés à la complexité et à la non-linéarité des données observées (Acharya et al. 2011). Pour quantifier la déviation statistique à un moment donné de la trajectoire EEG observée par rapport à la trajectoire reconstruite pendant une période intercritique de référence, certains auteurs ont proposé une mesure non linéaire de dissimilarité (Le Van Quyen et al. 1999, 2000, 2001b). Contrairement aux approches linéaires, certains de ces outils non linéaires permettent de mieux caractériser les fluctuations irrégulières et complexes observées dans les signaux EEG. Néanmoins, la plupart des méthodes dérivées de la théorie du chaos nécessitent une grande quantité d'échantillons pour fournir des estimateurs robustes et sans biais, et sont extrêmement sensibles aux artefacts et aux tendances non stationnaires.

L'entropie d'un système représente le taux de perte d'information sur sa dynamique. Elle reflète le niveau d'incertitude concernant tout état futur et est donc liée à la prédictibilité. Les mesures des trajectoires reconstruites dans l'espace des phases (entropie de Kolmogorov, entropie approximative et l'entropie d'échantillon), mais aussi de la distribution des amplitudes sur des séries temporelles sont couramment utilisées comme estimateurs de leur comportement irrégulier. En effet, différentes familles d'entropies peuvent être utilisées pour caractériser le degré de désordre (ou de régularité) des séries temporelles EEG univariées (Tang et al. 2015). Ces mesures comprennent l'entropie classique de Shannon et ses généralisations, l'entropie de Renyi et l'entropie de Tsalli. Les caractéristiques de prédiction des crises ont également utilisé des entropies multi-échelles pour caractériser la complexité des signaux EEG à des résolutions temporelles de plus en plus grossières (Humeau-Heurtier 2015). De même, les entropies par

ondelettes (spectrales) sont souvent utilisées comme estimateurs de la régularité/du désordre des signaux EEG dans différentes bandes de fréquence.

La fluctuation des oscillations cérébrales contrôle les décharges neuronales en modulant l'excitabilité des neurones. Cette interaction ou modulation des rythmes a été caractérisée par différentes mesures de couplage inter-fréquence qui estiment essentiellement les relations statistiques entre l'amplitude, la phase et la fréquence de deux oscillations provenant de bandes de fréquences différentes (généralement des activités rapides couplées à des oscillations plus lentes) dans un ou deux signaux EEG (Hyafil et al. 2015). Ces caractéristiques, qui comprennent le couplage phase-phase, le couplage phase-fréquence, le couplage phase-amplitude et le couplage amplitude-amplitude, se sont avérées avoir un bon pouvoir discriminant entre les signaux issus des périodes intercritiques, précritiques et critiques (Alvarado-Rojas et al. 2015). D'autres mesures telles que les spectres d'ordre supérieur, ou polyspectres, ont également été utilisées pour identifier les périodes précritiques en quantifiant le couplage de phase entre différents rythmes (Bou Assi et al. 2018). Malgré leur capacité à caractériser des interactions de rythmes complexes, certaines de ces méthodes souffrent de biais statistiques importants qui dépendent des propriétés spectrales du signal étudié, et rendent difficile une comparaison directe des segments EEG avec des dynamiques différentes (Aru et al. 2015; Scherer et al. 2023).

D'autres caractéristiques non linéaires actuellement utilisées dans la prédiction des crises sont basées sur la dynamique symbolique. Les séries temporelles EEG sont transformées en une séquence de symboles en partitionnant la gamme d'amplitudes du signal et en attribuant un symbole à chaque intervalle, ou en faisant correspondre leur valeur à un symbole discret (ou motif ordinal) qui code la manière dont les échantillons consécutifs sont liés les uns aux autres en termes de position et de valeur. La représentation des motifs ordinaux est une méthode non paramétrique qui s'est avérée être une représentation plus précise pour étudier la complexité des séries EEG. L'entropie de permutation, calculée à partir du nombre de motifs ordinaux, et ses différentes extensions et variantes (pondérée, multi-échelle, sensible à l'amplitude, etc.) ont montré un grand potentiel dans les algorithmes de prédiction des crises (Yang et al. 2018; Ra et al. 2021)]. Par rapport à d'autres méthodes non linéaires, la représentation des motifs ordinaux présente l'avantage d'être entièrement pilotée par les données, d'être sensible à plusieurs non-linéarités et d'être robuste aux segments courts et bruités (Ouyang et al. 2013; Ferlazzo et al. 2014).

Malgré l'abondance de la littérature, il n'y a pas à l'heure actuelle d'avantage clair et définitif à utiliser les caractéristiques non linéaires par rapport aux caractéristiques linéaires. L'un des principaux inconvénients des caractéristiques non linéaires de l'EEG est leur haut niveau d'abstraction, qui ne permet pas de comprendre clairement ou même intuitivement les mécanismes à l'origine des crises d'épilepsie.

Caractéristiques multivariées ou connectivité

Le réseau épileptogène comprend des interactions fonctionnelles avec des régions cérébrales parfois distantes et qui pourraient jouer un rôle dans la génération et la propagation des crises (Kramer et Cash 2012). La connectivité EEG a été utilisée comme un traceur potentiel de la transition intercritique/critique (van Mierlo et al. 2014). Au cours des dernières décennies, de nombreuses méthodes ont été proposées pour mesurer la connectivité cérébrale (c'est-à-dire mesurer la similarité statistique entre deux ou plusieurs signaux EEG) sur la base de différents principes allant du traitement des signaux à la modélisation paramétrique et à la théorie de l'information (Lehnertz et al. 2009). Dans le cas des mesures bivariées, les méthodes se répartissent en deux grandes catégories : celles mesurant l'interaction mutuelle et symétrique, et celles mesurant la transmission asymétrique de l'information et généralement associées à des mesures de causalité. À l'intérieur de ces deux catégories, d'autres classifications peuvent être faites en fonction de leur capacité à mesurer des relations linéaires ou non linéaires, à prendre en compte des effets bivariés ou multivariés, et à s'appliquer dans le domaine temporel ou fréquentiel. Les méthodes de connectivité multivariées tentent souvent d'atténuer les effets d'une connectivité parasite entre deux signaux due à la présence d'autres signaux interagissant avec eux (comme l'effet de conduction volumique). Ces méthodes sont basées sur le calcul de probabilités conditionnelles conjointes comme la corrélation partielle, ou sur l'estimation de nombreux paramètres (modèles autorégressifs multivariés) à partir de l'ensemble des signaux.

Parmi les *caractéristiques multivariées linéaires* couramment utilisées dans la prédiction des crises, on peut citer la fonction de corrélation linéaire ou la cohérence spectrale (estimée par des modèles paramétriques ou par la transformée de Fourier) et ses extensions telles que la cohérence imaginaire (développée pour atténuer les effets de conduction volumique) (Ewald et al. 2012; Stam et van Straaten 2012).

La plupart des *mesures multivariées non linéaires* étudiées dans la prédiction des crises sont également dérivées de la théorie des systèmes dynamiques. Comme les entropies conjointes, l'information mutuelle et les régressions non linéaires, les mesures d'interdépendance non linéaires quantifient généralement la similarité entre les trajectoires reconstruites de deux canaux EEG dans un état de phase. En utilisant les caractéristiques de connectivité, des études antérieures ont caractérisé la transition intercritique/critique par des valeurs de couplage, significativement différentes de celles observées pendant la période intercritique (Le Van Quyen et al. 2001a). La synchronie de phase est le processus par lequel deux signaux ou plus tendent à osciller avec une différence de phase constante, indépendamment de leurs amplitudes. Cette mesure de connectivité s'est avérée utile pour quantifier les changements temporels dans les interactions fonctionnelles entre des signaux multicanaux avant la crise (Schindler et al. 2008; Rings et

al. 2019). Différentes versions de la synchronie de phase (partie imaginaire, indice de retard de phase et indice de retard de phase pondéré) ont été appliquées pour identifier et caractériser l'état précritique.

II. Hypothèses physiopathologiques de la période précritique

1) Approches dynamiques

La transition d'un état intercritique à une crise peut être représentée par trois changements dynamiques différents (Figure 14) (Lopes da Silva et al. 2003a).

- Une déformation progressive

La situation idéale serait une transition graduelle dans le temps, avec un recrutement progressif de neurones du réseau épileptogène qui déséquilibrerait un état stable (intercritique) et aboutirait finalement à une crise. Cette conception pourrait permettre d'identifier les modifications précritiques avant l'apparition de la crise.

- Une bifurcation abrupte

En revanche, une transition soudaine et imprévisible vers la crise peut également être envisagée. Une telle conception – sans état précritique – exclurait toute stratégie de prédiction des crises.

- Une conception mixte

Enfin, un modèle double, dans lequel la dynamique physiologique – telle que les changements d'état de vigilance – ouvrirait la voie à une transition abrupte vers la crise, est également possible.

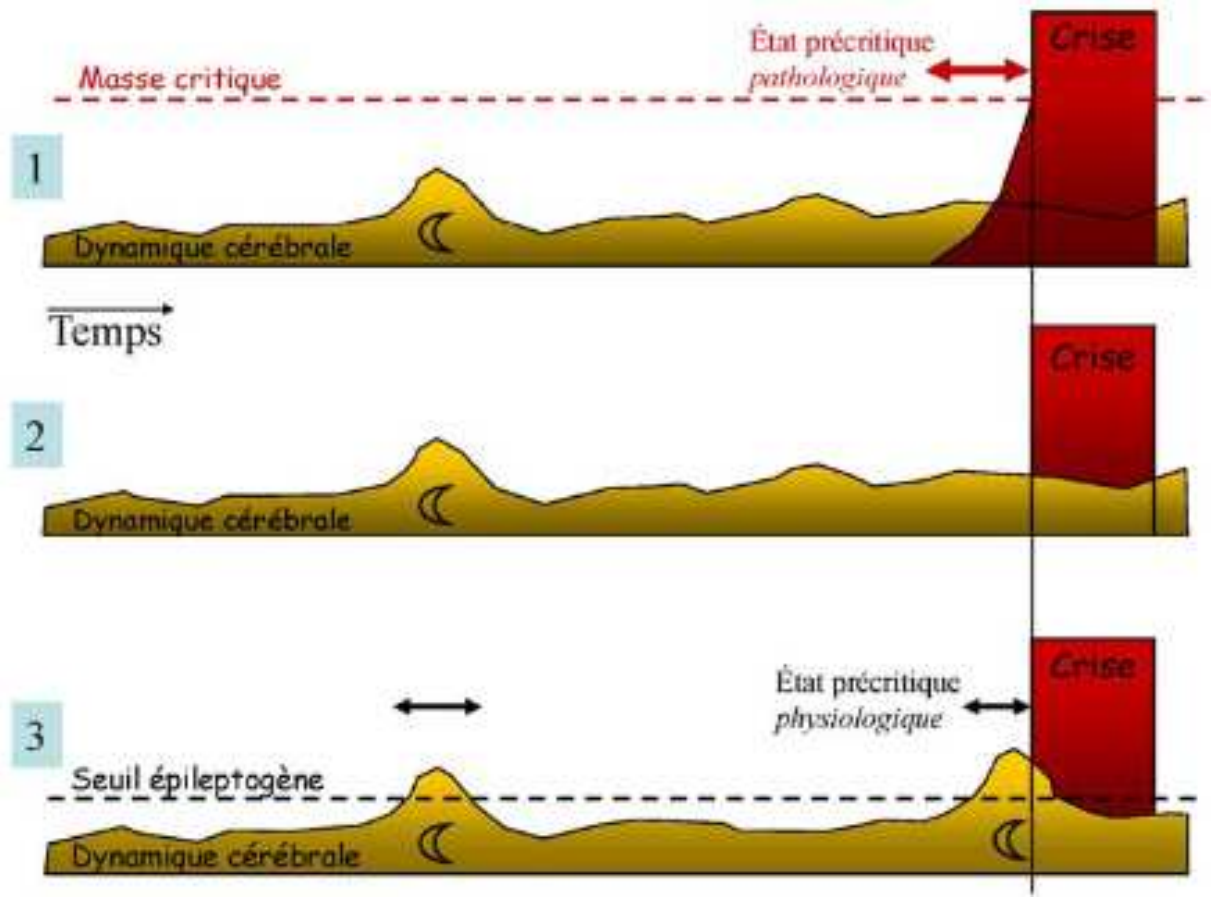

Figure 14. Dynamiques cérébrales précritiques théoriques
1. Déformation progressive ; 2. Bifurcation abrupte ; 3. Conception mixte
(Figure issue de Navarro et al., 2011)

Si l'état précritique est une conception déterministe de l'épilepsie – une augmentation de l'excitabilité corticale amenant invariablement à la survenue d'une crise – l'état procritique est issu d'une conception probabiliste (Figure 15). Il constituerait une période particulièrement à risque de développer une crise qui pourrait finalement aboutir (Baud et al. 2020). Le risque de crise pourrait ainsi fluctuer au cours du temps en suivant les dynamiques d'un système complexe et dépasser un seuil « critique », avec ou sans précipitation par un facteur stochastique.

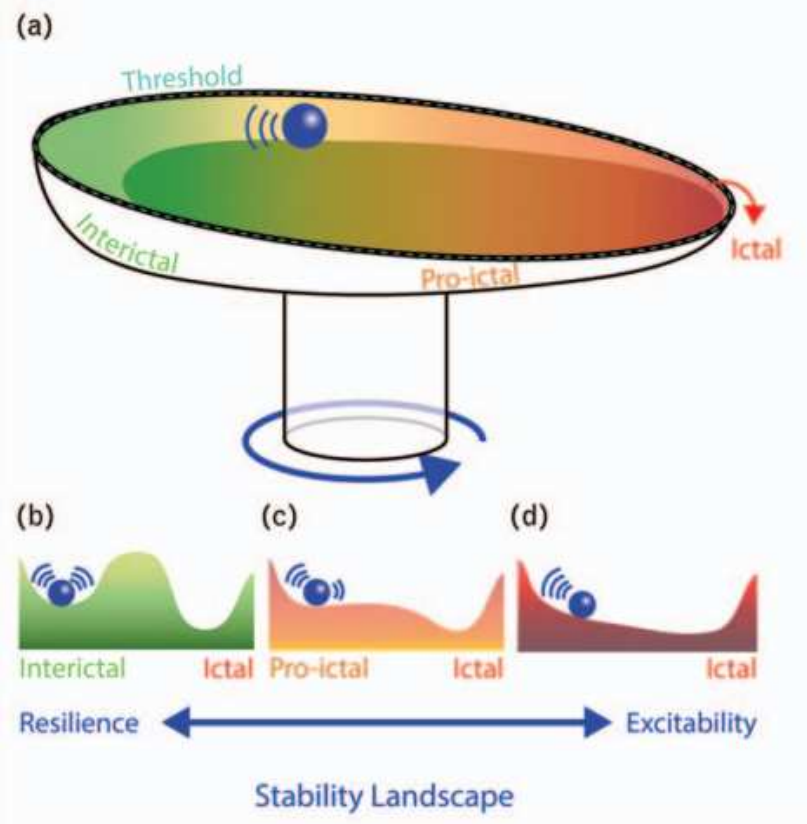

Figure 15. Représentation des dynamiques pro et précritiques
Admettons que les trajectoires de la balle représentent un cycle limite et la chute en dehors du plat la survenue d'une crise d'épilepsie (a). Trois états sont alors possibles : un état où le risque de chute en dehors du plat est faible (b, état intercritique), modéré à élevé (c, état procritique) ou alors inévitable (d). Le risque de crise fluctuerait au cours du temps et un facteur stochastique précipitant pourrait précipiter l'apparition d'une crise.
(Figure issue de Baud et al., 2020).

2) Approches computationnelles

Les modèles computationnels neuronaux ont contribué à élucider certains mécanismes sous-jacents observés dans différents états physiologiques ou pathologiques. Les premiers travaux sur la prédiction des crises ont considéré le cerveau comme un système dynamique pouvant présenter une présenter une période de transition vers la crise (Lopes da Silva et al. 2003a, 2003b). Ces transitions peuvent être modélisées au niveau de neurones individuels, de réseaux de neurones et au niveau de grandes populations de neurones (ou assemblées neuronales). Contrairement aux bifurcations d'activités neuronales modélisées par des modèles cellulaires détaillés (Traub et al. 1989), certaines études ont révélé le rôle clé de la connectivité entre les populations de cellules excitatrices et inhibitrices dans l'apparition des crises d'épilepsie (Kramer

et al. 2007; Takeshita et al. 2007). Plutôt que de décrire la dynamique des neurones individuels (ou couplés en réseaux), les modèles mésoscopiques utilisent une approximation de champ moyen pour décrire l'évolution d'une variable macroscopique de la dynamique intercritique à la dynamique critique (Wendling et al. 2005). Différents modèles neuronaux mésoscopiques ont ainsi été développés pour simuler l'état précritique (van Putten et Zandt 2014; Houssaini et al. 2020; Saggio et al. 2020).

Certaines méthodes de prédiction des crises se sont basées sur des modèles EEG computationnels, dont les paramètres sont estimés à partir des données EEG chez des patients présentant une épilepsie pharmacorésistante (Schindler et al. 2002). Malgré la complexité de l'ajustement d'un modèle EEG, les changements spatio-temporels des paramètres estimés ont révélé des signatures précritiques spécifiques au patient qui pourraient être utilisées pour la prédiction des crises (Aarabi et He 2014). Bien que ces approches aient fourni des informations utiles sur la période de transition précritique, les méthodes d'estimation des paramètres assument certaines conditions sur le substrat neuronal qui ne peuvent pas être facilement vérifiées (par exemple, le rapport excitation/inhibition, le type de couplage entre les populations neuronales, etc). Une intégration théorique des données expérimentales à plusieurs échelles (à la fois électrophysiologique et anatomique) serait nécessaire pour développer des modèles de grandes populations corticales telles que celles enregistrées simultanément par les signaux EEG.

Des techniques d'apprentissage profond ont été récemment proposées pour générer des répliques des segments EEG. Initialement développés pour surmonter le problème du déséquilibre des données dans les études de prédiction, certains auteurs proposent d'utiliser des réseaux antagonistes génératifs (*Generative Adversial Network*) pour synthétiser des échantillons d'EEG (Rasheed et al. 2021a). Cette technique d'augmentation des données pourrait être un modèle génératif alternatif pour améliorer l'ajustement des paramètres dans la modélisation neuronale classique.

3) Données issues des études *in vitro* sur tissus humains et des modèles animaux

Les mécanismes cellulaires et moléculaires de l'ictogenèse peuvent être approchés *in vitro*, notamment à partir de tissus épileptiques humains post-opératoires. Des anomalies épileptiques intercritiques peuvent être enregistrées spontanément dans le subiculum d'une sclérose hippocampique (Cohen et al. 2002). Des crises peuvent également être induites en augmentant l'excitabilité des neurones – en augmentant la concentration du milieu en potassium et en diminuant le magnésium. De telles modifications du milieu extracellulaire ont entraîné l'apparition de décharges critiques, précédées d'un changement de forme des anomalies épileptiques – appelées décharges précritiques (Huberfeld et al.

2011). L'utilisation de différents bloqueurs pharmacologiques a permis de démontrer que les anomalies intercritiques étaient médiées par la transmission GABAergique, alors que les décharges précritiques étaient, en plus, médiées par la transmission glutamatergique.

Les processus d'ictogenèse peuvent, en partie, être liés à la lésion histopathologique sous-jacente. En fonction de la connexion des neurones pathologiques avec le tissu cérébral environnant, les crises de certaines lésions pourraient être associées à une transition précritique, alors que d'autres lésions ne le seraient pas. Les dysplasies corticales focales (DCF) sont des lésions caractérisées par des neurones dysplasiques spécifiques, avec une signature EEG typique : des anomalies épileptiques intercritiques périodiques, qui s'interrompent au début d'une crise. Des décharges précritiques ont été enregistrées *in vitro* à partir de certains tissus avec DCF (Blauwblomme et al. 2019). Une altération de l'expression des co-transporteurs du chlore et un dysfonctionnement de la signalisation GABA ont été associés aux anomalies épileptiques intercritiques, comme dans la sclérose hippocampique. Les mécanismes de transition entre les anomalies intercritiques et les décharges précritiques n'ont cependant pas été mis en évidence.

Les processus d'ictogenèse peuvent également être liés aux microstructures anatomiques du cortex. La physiopathologie de la transition précritique a été principalement étudiée *in vitro* à partir de structures hippocampiques humaines, un archicortex qui présente des réseaux et des sous-types neuronaux spécifiques. Dans le néocortex, les microcircuits sont différents, souvent organisés en colonnes, et il existe un certain nombre d'interneurones différents. Les études *in vitro* sur le néocortex épileptique humain sont rares et les crises ne peuvent pas être facilement enregistrées, à moins qu'elles ne soient provoquées par des bloqueurs du $GABA_A$ (Kandrács et al. 2019), ce qui limite considérablement la généralisation des résultats.

Les limites des études *in vitro* sur les tissus humains pour étudier la transition précritique sont liées à la difficulté d'enregistrer des crises spontanées, ce qui peut être dû à la déconnexion "anatomique" du tissu de toutes les différentes afférences, et à la déconnexion "fonctionnelle" du tissu des influences physiologiques, telles que les états d'éveil, de sommeil et de stress.

La transition entre la période intercritique et la crise peut également être étudiée dans des modèles animaux d'épilepsie. Néanmoins, la généralisation de leurs résultats reste limitée, car les mécanismes pathologiques identifiés sont étroitement liés au facteur déclenchant utilisé dans le modèle. Dans un modèle d'excitabilité élevée au potassium, les mécanismes moléculaires à l'origine des anomalies épileptiques intercritiques et des crises se sont révélés indépendants, car le blocage de la plupart des neurotransmetteurs a inhibé les anomalies épileptiques intercritiques, mais pas les crises (Jensen et Yaari 1988). Dans un modèle de perfusion à forte teneur en potassium et faible teneur en magnésium, le blocage des récepteurs $GABA_A$ a raccourci la période précritique, aboli les anomalies épileptiques intercritiques et

atténué la lente dépolarisation précritique – sans effet sur la durée de la crise – alors que les crises ont été bloquées par le blocage des récepteurs du glutamate. (Zhang et al. 2012). Dans un modèle *in vitro* lié à la 4-aminopyridine, les anomalies épileptiques intercritiques provenant de la région CA3 se propageaient au cortex entorhinal et semblaient limiter l'apparition des crises (Barbarosie et Avoli 1997), ce qui suggère que les anomalies épileptiques intercritiques pourraient refléter un mécanisme compensateur visant à bloquer l'apparition de la crise. Dans un modèle après injection de pilocarpine *in vivo*, utilisant des tétrodes, il a été démontré que des interneurones putatifs étaient progressivement recrutés – augmentation de la synchronie, augmentation de la fréquence de décharge – avant l'apparition des crises, alors que les cellules pyramidales putatives étaient recrutées plus tardivement (Grasse et al. 2013).

L'ensemble des résultats obtenus à partir de tissus épileptiques humains et de modèles animaux d'épilepsie suggère fortement l'existence de changements précritiques, précédant les crises avec un délai de plusieurs secondes ou minutes. La nature de ces changements précritiques semble très variable, soulignant la diversité moléculaire et cellulaire possible des "routes vers la crise", mais aussi la subtilité de la cascade d'événements précédant les crises, qui ne peut être réduite à un simple défaut dans l'équilibre excitation/inhibition.

PARTIE 3. PREDICTION DES CRISES ET ALGORITHMES D'APPRENTISSAGE AUTOMATIQUE

I. Les modèles d'apprentissage automatique

1) Construction et évaluation du modèle

Les techniques d'apprentissage automatique construisent un modèle de prédiction pour identifier les états précritiques en fonction de différentes métriques. Les modèles supervisés apprennent une fonction qui associe une entrée (symptômes prodromaux, caractéristiques ECG ou EEG, etc.) à une sortie, en utilisant des données préalablement labélisées (intercritiques ou précritiques). Les modèles non supervisés apprennent un modèle de reconnaissance à partir d'un ensemble de données non étiquetés.

L'élaboration d'un modèle de prédiction des crises comporte généralement les étapes suivantes :

i) l'apprentissage : les paramètres du modèle sont estimés à partir d'un sous-ensemble des données ;

ii) la validation : les modèles formés sont évalués dans un autre sous-ensemble des données et les hyperparamètres ajustés ;

iii) la phase de test : le modèle final est testé sur un jeu de données distinct afin d'évaluer les performances de prédiction.

Les paramètres du modèle sont généralement optimisés par une procédure de validation croisée (Figure 15). Cette procédure de rééchantillonnage utilise différentes sous-parties des données pour former et tester un modèle sur différentes itérations. La validation croisée a pour but de tester la capacité du modèle à prédire de nouvelles données qui n'ont pas été utilisées pour l'estimer. Il s'agit d'un procédure sûre contre le surajustement (*overfitting*) ou contre le biais de sélection, en particulier sur des ensembles de données limités, car elle suppose que les données sont indépendantes et identiquement distribuées, de même que la procédure de formation/test (King et al. 2021). Néanmoins, dans les études de prédiction des crises, le fractionnement aléatoire des données durant la validation croisée doit être appliqué avec précaution, car les segments adjacents dans le temps sont fortement dépendants, ce qui entraîne des performances optimistes surévaluées (Cherian et Kanaga 2022; West et al. 2023).

Parmi les modèles d'apprentissage automatique les plus populaires utilisés pour la prédiction des crises, on peut citer (Bou Assi et al. 2017; Abbasi et Goldenholz 2019) :

a) l'analyse discriminante linéaire qui établit une combinaison linéaire de caractéristiques qui caractérise ou sépare les états intercritiques et précritiques ;

b) les machines à vecteurs de support (SVM) (Figure 15) qui transposent les données dans un espace à haute dimension où un hyperplan peut séparer les deux classes (intercritiques et précritiques) avec une marge maximale (la distance entre l'hyperplan et les données plus proches) ;

c) la régression logistique qui effectue une classification binaire linéaire représentant l'occurrence ou la non-occurrence d'une classe ;

d) l'algorithme des K plus proches voisins (Figure 15), qui intègre les étiquettes des K voisins les plus proches d'un échantillon pour décider de sa classification finale ;

e) le classifieur bayésien naïf qui apprend le modèle en combinant les probabilités préalables et la vraisemblance des classes.

2) La détection d'anomalies

Le manque d'observations précritiques est une contrainte majeure pour les algorithmes de prédiction des crises, qui nécessitent suffisamment de données des deux classes (intercritiques et précritiques) pour apprendre correctement un modèle. Les méthodes de détection des valeurs aberrantes ou « anomalies », qui ne nécessitent que des données provenant de périodes intercritiques pour former des modèles statistiques, peuvent être utilisées pour identifier les échantillons qui diffèrent de la classe de référence (Wulsin et al. 2011).

3) Modèles d'apprentissage profond

La capacité des algorithmes d'apprentissage profond à extraire automatiquement des caractéristiques représentatives des signaux EEG, sans (ou avec un minimum) de prétraitement et d'intervention manuelle dans les données, ouvre de nouvelles perspectives dans la prédiction des crises d'épilepsie (Rasheed et al. 2021b; Cherian et Kanaga 2022; Shoeibi et al. 2022). Ces modèles apprennent automatiquement grâce aux représentations de plusieurs couches de données transformées. Ces couches sont généralement des neurones artificiels qui appliquent des transformations linéaires aux données d'entrée. Pour que le modèle d'apprentissage profond apprenne des patterns complexes, des couches intermédiaires non linéaires spécifiques (fonctions d'activation) sont ajoutées. Les réseaux sont formés en mettant à jour et en ajustant les poids (et les biais) des neurones à l'aide de techniques d'optimisation. Les

modèles d'apprentissage profond utilisés dans la prédiction des crises comprennent de nombreuses variantes, mais ils peuvent être classés en deux groupes (Wainberg et al. 2018) :

i) les modèles supervisés qui comprennent les réseaux de neurones classiques (Figure 15) ou perceptron, les réseaux neuronaux convolutifs et les réseaux neuronaux récurrents ;

ii) les modèles d'apprentissage non supervisés qui peuvent apprendre à partir de données non étiquetées, parmi lesquels les plus populaires sont les cartes auto-organisatrices, la machine de Boltzmann et les auto-encodeurs. Contrairement aux techniques traditionnelles d'apprentissage automatique qui utilisent des vecteurs de caractéristiques obtenus par des algorithmes traditionnels de traitement du signal, les caractéristiques extraites par ces nouvelles méthodes semblent être plus discriminantes et plus robustes. Néanmoins, l'apprentissage de ces modèles nécessite de nombreux paramètres et donc une grande quantité de données. Malgré leur fort pouvoir discriminant, à l'heure actuelle il n'existe pas de référence pour comparer les multiples architectures, la fonction de perte (pour comparer la sortie observée et prédite), ou les fonctions d'activation et d'optimisation sur les performances des algorithmes.

II. Évaluation des performances d'un modèle

Les performances des modèles de prédiction de crise peuvent être évaluées par différentes métriques (Santos et al. 2018) :

- La précision ou valeur prédictive positive : le rapport du nombre de prédictions correctes d'un état précritique (vrais positifs) sur celui du nombre total de prédictions d'un état précritique, incluant donc les vrais et faux positifs (prédictions incorrectes d'un état précritique) ;
- Le rappel ou sensibilité : le rapport du nombre de vrais positifs sur celui du nombre total d'état précritique à prédire, incluant donc les vrais positifs et les faux négatifs (prédictions incorrectes d'un état intercritique) ;
- Le F1-score, qui combine la précision et le rappel ;
- La spécificité : le rapport entre le nombre de prédictions correctes d'un état intercritique (vrais négatifs) sur celui du nombre total d'état intercritique à prédire, incluant les vrais négatifs et les faux positifs (prédictions incorrectes d'un état précritique) ;
- L'exactitude ou *accuracy*, qui représente la proportion de prédictions correctes (d'un état inter ou précritique) sur l'ensemble des données ;

- Le taux de fausses alarmes, qui correspond à la probabilité d'avoir une prédiction incorrecte d'un état précritique ;
- La courbe ROC (*Receiver Operating Curve*), qui quantifie le rapport entre les prédictions correctes d'un état précritique (vrais positifs) et les prédictions incorrectes d'un état précritique (faux positifs) ;
- L'aire sous la courbe ROC ou AUC (*Area Under the Curve*) qui désigne la surface en dessous de la courbe ROC (Tableau 2).

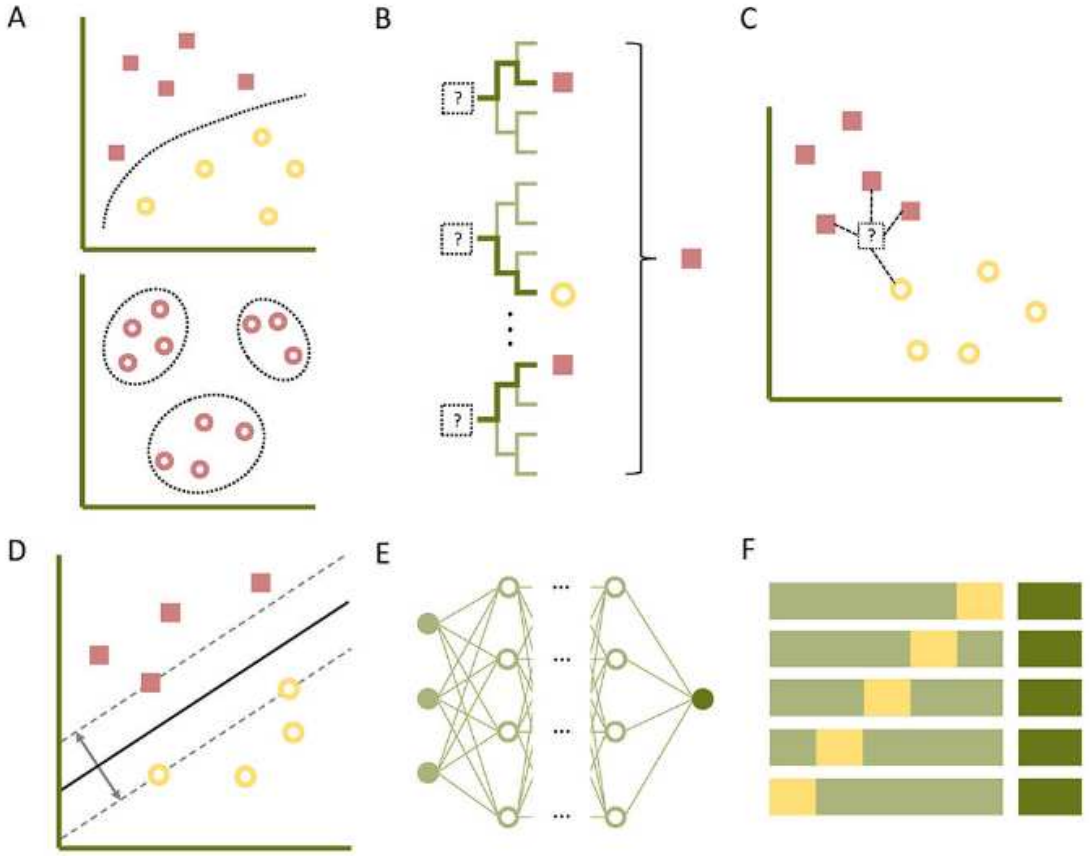

Figure 16. Différents modèles d'apprentissage automatique

A. Un modèle supervisé (en haut) apprend sur des données préalablement labélisées, alors que le modèle non supervisé (en bas) traite des données brutes non traitées pour identifier des groupes. B. L'algorithme *Random Forest* génère des arbres de décision. C. L'algorithme des K plus proches voisins où chaque nouvelle donnée est classée en fonction de la classe des K plus proches voisins (ici K=4). D. Le séparateur à vaste marge crée un hyperplan dans un espace de dimension supérieure pour maximiser la séparation des données avant d'arriver à une couche de sortie. E. Dans les réseaux de neurones artificiels, les données sont traitées par des différentes couches. F. Validation croisée : chaque itération comprend des données d'apprentissage (vert clair), des données de validation (jaune) et des données de test (vert foncé).

(Figure issue de Abbasi et al., 2019)

AUC	0,5	Nulles
	0,6-0,7	Pauvres
	0,7-0,8	Acceptables
	0,8-0,9	Bonnes
	> 0,9	Excellentes

Tableau 2. Valeurs de l'aire sous la courbe (AUC) et performances de classification

III. Les prévisions probabilistes du risque de crise

L'approche probabiliste des stratégies de prédiction des crises nécessite des métriques dédiées pour apprécier l'exactitude des prévisions probabilistes d'un modèle. Ces outils nous viennent notamment des sciences météorologiques qui utilisent depuis longtemps le score de Brier (Brier 1950; Murphy 1973). Le score de Brier peut être appréhendé comme une distance entre la prévision d'un évènement (la crise) et son observation : plus la probabilité prévisionnelle (de 0 à 1) sera proche de l'évènement observé (occurrence ou non), plus le score sera faible. Il est en effet différent de prédire (à tort ou à raison) un risque de crise de 5% ou de 90%. Ainsi, un score de Brier de 0 signifie une prédiction parfaite, alors que 1 est associé aux pires prédictions. Plusieurs études dans le domaine de la prédiction des crises ont implémenté ce score dans leur évaluation de performances (Karoly et al. 2017; Goldenholz et al. 2020; Leguia et al. 2022).

Le score de performance de Brier (ou BSS) est issu d'une comparaison entre les prévisions probabilistes d'un modèle (le risque de crise) et les prévisions d'un système de référence. Dans notre domaine d'application, le système de référence peut correspondre à la fréquence des évènements observés (les crises) sur une période données ce qui constitue une probabilité d'occurrence *a posteriori* (Leguia et al. 2022). Le score de performance de Brier varie de 1 (meilleures performances par le modèle de prédiction), en passant par 0 (performances identiques), à des valeurs négatives (le modèle prédit moins bien que le système de référence).

PARTIE 4. REVUE 1 : CLINICAL INSIGHTS INTO THE PREICTAL STATE: FROM PATHOPHYSIOLOGICAL THEORIES TO FUTURE APPROACHES FOR SEIZURE PREDICTION

Authors

Louis Cousyn[1,2,3], MD, Mario Chavez[2], PhD, Vincent Navarro[1,2,3], MD, PhD

[1] AP-HP, Epilepsy Unit, Neurology Department, Pitié-Salpêtrière Hospital, Paris, France

[2] Paris Brain Institute, ICM (INSERM-U1127, CNRS-UMR7225), Paris, France

[3] Sorbonne University, Paris, France

Correspondence to Prof. Vincent Navarro: Hôpital Pitié-Salpêtrière, 47-83 boulevard de l'Hôpital, 75651 Paris Cedex 13, France; email: vincent.navarro@aphp.fr; phone: +331 42 16 19 40

ORCID numbers:

Louis Cousyn: 0000-0003-1407-5575

Mario Chavez: 0000-0003-0390-4833

Vincent Navarro: 0000-0003-0077-8114

Abstract

The concept of a two-state model in epilepsy – i.e., interictal/ictal – has been widely questioned over the last decades. Ictogenesis may include a transitional state characterized by changes in cortical excitability that could pave the way to the seizure occurrence. This 'pre'-ictal state constitutes the scientific substratum for seizure prediction models. In this work, we first reviewed the multilevel preictal changes. Preictal clinical changes have been reported, including subjective prodromal symptoms, ECG analysis and particularly the heart rate variability – as estimator of the sympathetic/parasympathetic balance – and other measures from wearable multimodal sensors (sleep quantity and quality, electrodermal activity, etc.). Cycles in seizures with circadian, multidien or circannual periodicities have been highlighted through ultra-long-term recordings. Although preictal radiological changes, notably on functional MRI, were described, these approaches seem not suitable for a clinical application. Studies on EEG have sometimes reported preictal spatiotemporal modifications of interictal epileptiform discharges. Signal EEG analysis remains the gold standard for seizure prediction methods: here, we reviewed the necessary processes to implement an EEG-based model, as well as the different features (linear or nonlinear, univariate or multivariate) that have been proposed over decades in the field of seizure prediction. We also reviewed the pathophysiological hypotheses underlying the preictal state, from theoretical conceptions – progressive or abrupt bifurcation – to computational and *in vitro* findings – such as the supposed preictal glutamatergic mediation. Finally, we discussed the clinical and methodological challenges for next-gen seizure prediction models, and the scientific perspectives to better understand the preictal transition and search a preictal signature.

Keywords: Seizure prediction; seizure forecasts; forecasting; ictogenesis; preictal

1. Introduction

The concept of a two-state model in epilepsy – i.e., interictal/ictal – has been widely questioned over the last decades. Ictogenesis may include a transitional state characterized by changes in cortical excitability that could pave the way to the seizure occurrence. This 'pre'-ictal state constitutes the scientific substratum for seizure prediction models. If such a state may occur long enough before the seizure onset to detect a change in brain state, an intervention that may prevent the seizure (medications, biofeedback techniques, stimulation) or, at least, safety measures for the patient, could be proposed.

While a deterministic approach has long been applied in prediction models – to predict the occurrence of the next seizure as a binary event (seizure or not) – a brand new strategy was more recently adopted. Current strategies are intended to be more realistic and suitable for nonlinear dynamic systems. Indeed, probabilistic approaches coming from the meteorological sciences are being increasingly applied to seizure prediction models. The goal of seizure forecasts is to estimate the probability of upcoming seizure at any time, while classical prediction algorithms aim at predicting exactly the next seizure occurrence. Therefore, we can identify a 'pro'-ictal state, i.e., a high-risk state of seizure.

In this work, we aimed at i) reviewing the multilevel preictal changes from subjective symptoms to prediction algorithms from a clinical point of view, ii) discussing the possible pathophysiological underlying mechanisms and iii) addressing the future challenges.

We searched for the terms 'seizure prediction', 'seizure anticipation', 'seizure forecasting', 'preictal period', 'preictal state', 'preictal phase', and 'preictal changes' in titles or abstracts from articles in PubMed, from inception to February 8, 2023. Additional sources of potential interest were also screened. We only reviewed articles in English and generated the final reference list in accordance with their originality, robustness, and relevance to our topic.

2. A variety of approaches of the preictal state

2.1 Clinical approaches

a. Prodromal symptoms, self-prediction, and precipitants

In 1954, Henri Gastaut already reported 'premonitory' sensations of upcoming seizures (1). These subjective symptoms, also called 'prodromes' or 'prodromal symptoms', may precede the seizure onset by several hours – up to 24 hours – and consist of cognitive (trouble concentrating/understanding/reading etc.), emotional (irritability, bad mood, anxiety, etc.), sensorial (light/noise sensitivity, etc.) or physical (headache, fatigue, nausea, etc.) manifestations (2–7). Prodromal symptoms must be distinguished from early subjective symptoms during focal aware seizures, formerly named 'auras', as the underlying mechanism is considered as non-ictal. Besides, unlike auras, they are usually referred to as negative symptoms, and do not provide localization value of the epileptogenic zone (2,8). The prevalence of prodromal symptoms ranges widely from 6.2 to 87.1% of patients (4–6,9–11).

Several studies have also investigated the value of patients' self-prediction of seizure, i.e., the level of likelihood of upcoming seizure(s) reported by the patients themselves. The percentage of patients with an ability above chance to self-predict seizures varied from 21.1 to 47.4 % (12–14). Precipitant factors (sleep deprivation, emotional stress, menstruation, alcohol, etc.) are another strong determinant of seizure occurrence, reported in 53-89.8% of patients (10,15), which may contribute to the self-assessment of seizure likelihood.

It is therefore not surprising that studies prospectively evaluated their ability to predict seizures. Self-prediction was one of the most discriminant variables with median specificity of 0.87-0.95, but sensitivity remained low around 0.1-0.5 (12–14,16). Although sleep deprivation, stress, and some prodromal symptoms could be associated with an increased risk of seizure (3,13,17), some studies did not find significant results (18). One hypothesis is that standard linear analyses might not allow capturing the complexity of these data, as well as the binary (yes/no) categorization of some variables. Using non-linear prediction algorithms on scaled data was suggested as a possible solution, but a prospective real-time analysis must be completed (19).

b. ECG analysis

The direct or indirect impact of epilepsy on the autonomic nervous system has been suggested for more than 20 years, in particular through the analysis of heart rate variability (HRV). Indeed, HRV reflects the sympathetic/parasympathetic balance and represents an accessible way to highlight a modulation of this balance by means of time-, frequency-domain and nonlinear analysis (20). Interictal decreased HRV, suggesting a lower parasympathetic component, was highlighted in patients with epilepsy in comparison with matched healthy controls (21). Changes in HRV were also reported as a promising way to identify preictal states (22,23). The amount of preictal information contained in ECG recordings could even be more consistent than in scalp EEG (22). An increased ratio of low HRV fluctuations (0.04-0.15Hz) over its high frequencies (0.15-0.4Hz), which reflects a predominant sympathetic activity, was described up to one hour before the seizure onset (24). Therefore, several studies implemented HRV-based prediction algorithms. Some authors reported a sensitivity of 89-91% and a false positive rate of 0.4-0.7 times per hour (25,26), while others stated an accuracy of 77.1% (27).

c. Cycles in epilepsy

It is now well understood that cortical excitability varies according to the vigilance state (sleep/wake cycles), hormonal fluctuations (ACTH, cortisol, sexual hormones), and other periodic physiological processes (e.g., blood sugar regulation) (28). Epileptiform interictal discharges (IEDs), for instance, usually increase during non-rapid eye movement (non-REM) sleep stages N2 and N3; and significantly decrease during REM sleep. In addition, the circadian likelihood of seizure can sometimes be estimated according to the epileptic syndrome: patients with frontal lobe epilepsies are more likely to have seizures during non-REM sleep, while patients with juvenile myoclonic epilepsy tend to have more frequently seizures in the early morning.

Seizure diaries have also been used to develop forecasting algorithms based on the seizure cycles – i.e. circadian (hours), multidien (days/weeks) or even circannual (months) periodicities. Forecasting performances in a pseudo-prospective study displayed an AUC from 0.69 to 0.94 and an average accuracy of 69% (29). The main limit of the diary-based approaches is the possible underreporting of self-declared seizures – up to 50% – which may underestimate their rate (30). Besides, no prospective forecasting in real-life conditions has been evaluated yet.

The seizure circadian profile can also be implemented in a multimodal model to enhance the prediction performances. For example, a combined model with circadian and EEG information performed better than a purely EEG-based model with higher sensitivity results (31,32).

d. Can seizure predict seizure?

Retrospective analysis of very long-term (years) recordings has revealed, from the statistical distributions of inter-seizure intervals, a non-random occurrence of seizures (33). Instead of predicting a likelihood of incoming seizure, seizure counts forecasting (an approach often neglected in the seizure prediction literature) aim at predicting the number of seizures on a future period (34–36). Using very long-term (years) data from patient-reported seizures diaries or from very long intracranial recordings, different studies have developed forecasting algorithms to predict seizure counts, or to estimate changes in underlying seizure risks (34–37). Interestingly, these methods allow the incorporation of external factors such as clinical variables, sleep quality, or even weather information to provide a forecast that can be robust to the natural variations of the seizures' frequency (38,39).

e. Wearable devices for ambulatory forecasting?

The challenge for the future will be to develop a suitable and acceptable device for long-term and prospective collection of data and real-time analysis. Several smartphone seizure diaries are available for self-declaration of seizures and collection of prodromal symptoms. Wearable sensors such as smartwatches, smart bands, smart rings, or even stick-on patches can collect physiological information about sleep quality and quantity, heart rate (and HRV), electrodermal activity, accelerometry, etc. A longitudinal study collected sleep features from a smartwatch (Fitbit, Fitbit Inc., USA) for about 17 months and highlighted that variations in sleep onset and offset times were at higher risk of seizure the following day than changes in sleep duration (40). Analysis of longitudinal heart rate smartwatch-based recordings (Fitbit) found multiday cycles that were phase-locked with seizures' occurrence (41).

Forecast performances from different combined clinical metrics (sleep, heart rate, and step count from Fitbit) in a small sample of patients (N=11) reached a mean AUC of 0.74 for hourly probabilities and 0.66 for daily ones (42). Two other studies used the E4 wristband (Empatica, Empatica Inc., USA) for long-term recording of accelerometry, blood volume pulse,

electrodermal activity, and temperature (43,44). Authors reported a mean AUC of 0.8 over 6 patients and better-than-chance forecasting in 30 of 69 patients (44%), respectively.

2.2 Imaging approaches

Continuous measurement of surface cerebral blood flow (CBF) by subdural sensors revealed a CBF increase in the epileptogenic zone 20 minutes prior to the electrocorticographic (ECoG) seizure onset, while CBF in nonepileptogenic cortex decreased 2 minutes before (45). Other studies also found a preictal increase in regional CBF (rCBF) on single photon emission computed tomography (SPECT) and in cerebral oxygen availability on near-infrared spectroscopy (NIRS), respectively 11-12 min and 1.5-13 h prior to the EEG seizure onset (46,47).

Preictal changes on functional MRI (fMRI) were investigated later, in particular using the blood-oxygen-level dependent (BOLD) signal as a marker of rCBF. Although an increased BOLD fMRI signal was observed tens of seconds to several minutes before the clinical or EEG seizure onset – up to 20 minutes –,an associated decrease signal has been also reported (48–50).

It is important to underline that no intracranial EEG was performed during these CBF or fMRI acquisitions. A seizure starting from deep brain areas that would not be recorded by scalp or cortical electrodes remains possible, and changes during the so-called preictal period could be in relation to an occult ictal activity. In a study with concomitant intracerebral EEG and fMRI data in a single patient, no preictal significant BOLD changes were observed (51). The preictal period was, however, too short – 30 seconds – prior to the seizure onset.

Although interesting for pathophysiological considerations, in particular the preictal excitation/inhibition balance, fMRI-based seizure prediction approaches are not suitable for a clinical application.

2.3 EEG analysis

a. Standard EEG analysis

Interictal EEG patterns often displays a physiological background activity punctuated by transient pathophysiological events, including high-frequency oscillations (HFOs), interictal epileptiform discharges (IEDs), and slow wave activities (SWAs), which occur more frequently than seizures. Although such events are not associated with any clinical manifestation, they might reflect the cortical excitability and synchronizability (52,53). Changes in their spatiotemporal dynamic could set a condition that preludes the onset of seizures. Indeed, HFOs (100-500 Hz) have been shown to be involved in seizure initiation, in the immediate periods prior to ictal discharges (1-5 min) (54–57). Some studies, however, raised doubts about the suitability of the HFOs to identify preictal periods with increased likelihood of seizures (53,58). Early studies considered that the spatiotemporal organization of IEDs played a role in the genesis of ictal discharges and were specifically related (59–62). Nevertheless, additional studies with larger datasets found no systematic changes in IEDs prior to seizures (52,63–65). Similarly, very slow oscillations and baseline shifts have been observed prior to seizure onset but limited available evidence is insufficient to suggest a slow modulation of excitability, or any other role in ictogenesis (66–68).

Cycles of IEDs

Previous studies on interictal EEG patterns mainly focused on temporal changes during periods close to seizures. Nevertheless, recent findings suggested that the dynamics of IEDs could be organized over circadian, multidien and circannual timescales. Indeed, seizure forecasting algorithms that considered these underlying cycles of IEDs over very ultra-long-term EEG recordings (years) from chronic implantable devices such as NeuroVista or RNS system (NeuroPace) have revealed cyclical epochs of increased likelihood of seizures (32,69,70).

Physiological EEG patterns prior to seizures

We know sleep and epilepsy have strong mutual influence, notably the occurrence of IEDs and seizures in particular sleep stages (71). Interestingly, dynamical changes in sleep spindles –

namely, a significant reduction – were found before seizure onset, which could be related to a disruption of the cortico-thalamic networks prior to the ictal discharge (72,73)

b. Signal analysis of EEG

Current EEG-based seizure prediction systems generally consist of continuous acquisition of intracerebral or scalp EEG, followed by i) a preprocessing of signals for artifacts removal, ii) extraction and selection of more informative features, iii) classification for discriminating between interictal and preictal states, iv) a postprocessing for reducing false positives and, finally a step of v) performances evaluation.

Preprocessing of the EEG

The preprocessing step aims at removing or attenuating environmental or physiological EEG artifacts (muscle contractions, chewing or swallowing, eye movements or blinks, etc.) using multiple techniques to increase the signal to noise ratio, such as band-pass, notch and adaptive filters, wavelets or data-driven decompositions (74). Although preprocessing procedures (smoothing, normalization, and outliers preprocessing) are necessary step for cleaning EEG segments, they may also impact the performances of seizure prediction algorithms (75).

Another important issue, which is often overlooked in the seizure prediction literature, is the volume conduction effect and the impact of bipolar or referential montages on the extracted measures (76–78). Referencing the original EEG data to artificial references or using spatial filters (e.g., the Laplacian) has been proposed to reduce these potential biases (79). Specific statistical methods (e.g., imaginary coherence, phase-lag index) can be also applied to simultaneously extract EEG features (connectivity parameters) and reduce the impact of volume conduction.

In seizure prediction algorithms, EEG recordings are generally segmented into small windows where meaningful features are extracted from. The typical duration of such segments ranges from 5 to 60 s sliding windows, with or without overlap (80–83). Whereas some studies suggested longer segments (>120 s) may provide a better characterization of brain signals (84), there is no evidence of an optimal duration for EEG segments in seizure prediction. Therefore, choice of the window length must reflect a tradeoff between stationarity assumptions and the ability to capture informative features, which strongly depends on the feature of interest. For

instance, features estimated from slow oscillations require longer data segments than standard first-order EEG statistical moments (mean, variance, etc.).

Features extraction

Features extraction is the step where the most discriminant – and probably non-redundant – information, is extracted from EEG signals. Features are based on univariate measures from every single channel, or multivariate when the information is extracted from a combination of multiple channels. While linear measures characterize basic statistical properties of EEG segments (in time or spectral domain), several non-linear measures, mainly derived from the theory of dynamical systems, have been proposed to characterize high-order properties of univariate or multi-channel signals (85,86).

Linear univariate features. Linear features commonly include statistical moments in time (mean, variance, skewness, kurtosis, characteristics of the autocorrelation function, etc.) or spectral (spectral centroid, spectral skewness, absolute or relative power in the standard EEG frequency bands, etc.) domain. In several seizure prediction studies, EEG signals are modeled as the output of a linear autoregressive (AR), moving average (MA) or an ARMA filter, such that the model parameters (order of the filter, the coefficients, prediction error, etc.) serve as features for pre-ictal identification (87). Similarly, parameters obtained from filtering EEG signals with wavelet or other linear time-frequency decompositions (continuous, discrete wavelet, or wavelet packets filter-banks) have been used as features in seizure prediction (80,82,83). Other nonlinear data-driven decompositions (e.g., the Empirical Mode Decomposition and its different extensions, or the Singular Spectrum Analysis) are often used to decompose EEG signals into a finite number of oscillations, or modes, from which features can be extracted (82,83). Early studies in seizure prediction have been assessed the predictive performances of such parameters in both time and frequency domain. The main advantage of linear features is related to their algorithmic simplicity and easy implementation in a quasi-real-time set-up, which could be of interest for a continuous real-time monitoring.

Nonlinear univariate features. The evidence suggests that neural signals, at different time and spatial scales, can be considered as the output of stochastic nonlinear oscillators (88). Moving average measures of both linear energy (variance) as well as nonlinear energy (a parameter proportional to both signal amplitude and frequency) were among the first nonlinear – but still computationally efficient and simple to calculate – features extracted from EEG to discriminate the preictal state (89). Most of the nonlinear features used in seizure prediction are derived from the dynamical system theory, in which EEG is considered as an observed variable of a dynamical system. Some mathematical tools allow to reconstruct, from a single scalar observation, the underlying states of the system in every time (85,86). Within this framework, the sequence of consecutive states over the time defines a curve in the phase space, which is called state space trajectory. In some pioneering studies, different parameters characterizing such reconstructed trajectory were used as EEG features to detect a significant change prior to seizures. Trajectory's parameters such as correlation dimension (and its multiple derivatives), correlation-related entropies, local flow measures, marginal predictability, and Lyapunov exponents are some of the nonlinear measures of EEG complexity and stability (85,86). The regularity of the reconstructed trajectories was also characterized through the Recurrence Quantification Analysis, which provided different parameters related to the complexity and nonlinearity of the observed EEG data (90). To quantify the statistical deviation at a given time of the observed EEG trajectory from the reconstructed one during a reference interictal period, some authors proposed a state space dissimilarity measure (91–93). In contrast with linear approaches, some of these nonlinear tools yield a better characterization of the irregular and complex fluctuations observed in epileptic EEG signals. Nevertheless, most of methods derived from the chaos theory require a large amount of data to provide robust and unbiased estimators, and they are extremely sensitive to artefacts and nonstationary trends. Further, clear preictal trends on such nonlinear features were found to strongly depend on the electrodes position, type of seizures, etc. (94,95).

The entropy of a system is defined as the rate of information loss about its dynamics. It reflects the level of uncertainty about any future state, and therefore relates to predictability. Measures from reconstructed trajectories in the phase space (Kolmogorov entropy, approximative entropy and its modification, the sample entropy), but also from the amplitudes' distribution of time series were commonly used as estimators of their irregular behavior in seizure prediction literature. Indeed, different families of entropies can be used to characterize the degree of disorder (or regularity) from univariate EEG time series (96). Such measures include the

classical Shannon entropy and its generalizations, the Renyi's and Tsalli's entropy. Seizure prediction methods have also employed multiscale entropies to characterize the complexity of EEG signals at increasingly coarser time resolutions (97). Similarly, wavelet (spectral) entropies are often used as estimators of regularity/disorder of EEG signals at different scales or frequency bands.

Fluctuations of brain oscillations control the timing of neuronal firing by modulating neural excitability. In last years, this interaction or rhythms modulation has been characterized by different measures of cross-frequency coupling (CFC) that basically estimate statistical relationships between the amplitude, phase, and frequency of two oscillations from different frequency bands (generally fast activities coupled to slower oscillations) in one or two EEG signals (98). Such features, that include phase-phase coupling (PPC), phase-frequency coupling (PFC), phase-amplitude coupling (PAC), and amplitude-amplitude coupling (AAC), have been shown to display a good discriminant power between signals from interictal, preictal and ictal periods (99). Other measures such as Higher Order Spectra, also known as polyspectra or spectral representations of third and higher order correlations or moments, have also been used to identify preictal periods by quantifying the phase coupling between different rhythms (100). Despite their capacity to characterize complex rhythms interactions, some of these methods suffer from strong statistical biases that depend on the spectral properties of the studied signal, which renders difficult a straightforward comparison of EEG segments with different spectral dynamics (101,102).

Other nonlinear features currently used in seizure prediction are based on the theory of symbolic dynamics. Here, EEG time series are transformed into a sequence of symbols by partitioning the range of signal amplitudes and assigning a symbol to each interval binning, or by mapping their values to a discrete symbol (ordinal pattern) that encodes how consecutive samples relate to one another in terms of position and value. Ordinal patterns representation is a nonparametric method that been shown to be a more accurate representation to study the complexity of EEG series. The permutation entropy, computed from the number of ordinal patterns distribution, and its different extensions and variants (weighted, multiscale, amplitude-aware, etc.) have been shown a great potential in seizure prediction algorithms (103,104)]. Compared with other nonlinear methods, ordinal patterns representation has the advantage of being fully data-driven, sensitive to several nonlinearities, and robust to short and noisy segments (105,106).

Despite the abundant literature, there is not a clear and definite advantage on the use of nonlinear features over linear ones. A major drawback of nonlinear EEG features is their high level of abstraction, without a clear or intuitive clinical or physiological insight about the mechanisms leading to seizures.

Multivariate (connectivity) features. Large evidence supports the hypothesis of an epileptic network with functional interactions over large brain regions, beyond the epileptogenic network, that can play a role in the generation and early propagation of seizures (107). In past studies, EEG connectivity has been used as a potential tracker of the interictal to ictal transition (108). In the last decades, many methods have been proposed to measure brain connectivity (i.e., measuring the statistical similarity between two or more EEG signals) based on different principles ranging from signal processing to parametric modelling and information theory (109). In the case of bivariate measures, methods fall into two broad categories: those measuring symmetric mutual interaction and those measuring asymmetric information propagation (generally associated to concepts such as causality). Within these two categories, further classifications can be made according to their ability to measure linear or nonlinear relationships, to consider bivariate or multivariate effects, and to apply in the time or frequency domain. Multivariate EEG connectivity methods try often to avoid the emergence of spurious connectivity between two signals that is due to the presence of other signals interacting with them (e.g., produced by the volume conduction effect). These methods are generally based on the computation of joint conditional probabilities (e.g., partial correlation) or on the estimation of many parameters (e.g., multivariate AR models) from the entire set of signals.

Among the linear multivariate features commonly used in seizure prediction, one can mention the linear correlation function or the spectral coherence (estimated by parametric models or by the nonparametric Fourier transform) and its recent extensions such as the imaginary coherence, developed to mitigate the volume conduction effect (110,111).

Most of the nonlinear multivariate measures studied in seizure prediction are also derived from the dynamical systems theory. Like joint entropies, mutual information and nonlinear regressions, nonlinear interdependence measures can quantify the similarity between reconstructed trajectories of two EEG channels in a phase state. Using nonlinear connectivity features, past studies have characterized the interictal to ictal transition by coupling values, significantly different from those observed during the interictal period (112). Phase

synchronization is the process by which two or more signals tend to oscillate with a repeating sequence of relative phase angles, independently of their amplitudes. This connectivity measure has been shown to be a useful measure to quantify temporal changes in functional interactions between multichannel neural signals prior to seizures (113,114). Different versions of the original phase synchrony value (imaginary part of phase-locking value, phase-lag index and weighted phase-lag index) have been applied to identify and characterize the preictal state.

c. Preictal state detection

In early works, the oncoming preictal transition was commonly detected by thresholding the temporal profile of the estimated EEG feature (linear, nonlinear, etc.). Preictal transition was often detected by comparing the probability distributions of a current EEG segment's features and a reference epoch or over successive intervals. Examples of these change point detection methods include the already mentioned dynamical similarity (a non-parametric measure of change dynamics relative to a constant reference EEG epoch, generally far from seizures) (91,93), the cumulative sum or CUSUM algorithm (based on a cumulative sum of deviations from a reference or baseline EEG epoch over the temporal profile of a given feature) (115), and hidden Markov models that can identify epochs of increased preictal transition probability (116). All these methods work well in low dimensional spaces, or for the identification of a single change point. Nevertheless, they are unable to correctly detect multiple change points, or change transitions in high dimensional datasets (117,118).

Machine learning models

In the last decade, significant advances have been made regarding automated seizure prediction algorithms. In contrast with traditional inferential statistics, machine learning (ML) techniques build a prediction model to identify the preictal states, driven by the data structure of the EEG features. Supervised models learn a function that maps an input (EEG features) to an output, by using labeled data (interictal and preictal epochs), whereas unsupervised models learn a pattern recognition from unlabeled datasets. The construction of a seizure prediction model typically involves the steps of i) training (the model parameters are estimated from a subset of learning dataset), ii) validation (trained models are evaluated in a validation dataset and hyperparameters

are tuned), and iii) testing (the final model is tested in a separate dataset to assess the prediction performances). Model's parameters are generally optimized by a cross-validation procedure. This resampling procedure (cross-validation) uses different portions of the data to test and train a model on independent iterations or folds. As the training/testing, the aim of cross-validation is to test the model's ability to predict new data that was not used in estimating it. It is worthy of notice that cross-validation, as the train/test procedure, is a safe procedure against overfitting or selection bias, especially on limited datasets, as it assumes data are independent and identically distributed (119). Nevertheless, in seizure prediction studies, simple random splitting in cross-validation must be carefully applied, as the feature vectors of adjacent segments on time are highly dependent, which results in unrealistic optimistic performances (82,120).

Among the most popular ML models employed in seizure prediction we can mention (80): i) the Linear Discriminant Analysis, which finds a linear combination of features that characterizes or separates the preictal and interictal epochs; ii) Support Vector Machines that map input data into a n-dimensional feature space where an hyperplane separating the two classes with maximum marginal distance can be identified; iii) Logistic Regression that performs a linear binary classification representing the occurrence or non-occurrence of a class; iv) K-nearest neighbors classifier, which integrates the labels from the K nearest neighbors of a sample for deciding its final classification; v) Bayes classifier that learns the model by combining the prior probabilities and classes' likelihood.

Deep learning models

In recent years, the ability of deep learning (DL) algorithms to automatically extract representative features from EEG signals, without (or with minimal) pre-processing and manual intervention in the data, is opening new opportunities in seizure prediction (81,82,121). Most of the DL models automatically learn through representations from multiple layers of transformed data. Such layers are artificial neurons that apply linear transformations to the input data. To make the DL model learn complex patterns, specific nonlinear layers (activation functions) are added in between. Networks are trained by updating and adjusting neurons' weights (and biases) using different optimization techniques. DL models used in seizure prediction include many variants, but they can be classified in two groups: i) supervised models that include the traditional Neural Networks or perceptron, Convolutional Neural Networks

(CNNs), and Recurrent Neural Networks (RNNs); and ii) unsupervised learning models that can learn from unlabeled data, among which the most popular are the Self-Organizing Maps, Boltzmann Machines and AutoEncoders. In contrast with the traditional ML techniques that require EEG parameters obtained by traditional signal processing algorithms, the characteristics automatically extracted by these new DL methods seem to be more discriminant and robust. Nevertheless, such models require many parameters to be learned and therefore a large amount of data. Despite their high discriminating power, there is not a benchmark to compare the multiple architectures, loss (to compare the observed and predicted output), activation and optimization functions on the performances of seizure prediction algorithms.

3. Pathophysiological hypotheses for the preictal state

3.1 Theoretical preictal dynamics

The transition from an interictal state to the seizure can be represented by 3 different dynamical changes already formulated – but still relevant – by Lopes Da Silva et al. (88).

A progressive deformation. The ideal situation would be a gradual transition over time, with a progressive recruitment of neurons from the epileptogenic network that will unbalance a steady (interictal) state and ultimately result in seizure. This conception could allow the identification of preictal modifications prior to the seizure onset.

An abrupt bifurcation. In contrast to a smooth change prior to seizures, a sudden and unpredictable transition toward seizure can be also envisaged. Such a conception – without any preictal state – would exclude any seizure prediction strategy.

A mixed conception. Finally, a dual model, in which physiological dynamics – such as changes in vigilance state – would pave the way for an abrupt transition towards seizure, is also possible.

3.2 Computational approaches

Neural computational models have helped to elucidate some underlying mechanisms of EEG observed in different physiological or pathological states. Early works on seizure prediction considered the brain as a dynamical system that may exhibit a critical transition prior to a seizure (88,122). Such transitions can be modeled at the level of single neurons, networks of neurons, and large populations of neurons. In contrast with bifurcations of neural activities simulated by detailed cellular models (123), some studies have revealed a key role of connectivity between excitatory and inhibitory cell populations on the building up of seizures (124,125). Rather than describing the dynamics of individual (or coupled) neurons, mesoscopic models use a mean field approximation of a macroscopic variable to describe the evolution from interictal to ictal dynamics (126). Different mesoscopic neural models have thus been developed to simulate transitions to the preictal state (127–129).

Some seizure prediction methods are based on more realistic computational EEG models, whose parameters are directly estimated from the ongoing EEG data (130). Despite the complexity of EEG model fitting procedures, the spatio-temporal changes in the estimated parameters revealed patient-specific preictal signatures that could be used for seizure prediction (131). Although such model-based approaches have provided useful insights into the preictal transition, the parameters estimation methods assume some conditions about the neural substrate that cannot be easily verified (e.g., excitatory/inhibitory ratio, type of coupling between neural populations, etc.). A theoretical integration of experimental data from multiple scales (both electrophysiological and anatomical) is therefore necessary to develop parsimonious models of large cortical populations, or neural assemblies, as those recorded by multivariate EEG signals.

Recently, a deep learning technique has been proposed to generate replicas of the observed EEG segments. Originally proposed to overcome the problem of data imbalance in seizure prediction studies, some authors propose the use of Generative Adversarial Networks to synthetize realistic EEG samples (132). This data augmentation technique could be an alternative generative model to improve the parameter fitting in classical neural modeling.

3.3 *In vitro* study from human epileptic tissues and animal models

The cellular and molecular mechanisms of the ictogenesis can be approached in vitro, notably from human post-operative epileptic tissues. Interictal epileptiform discharges (IEDs) have been spontaneously recorded in the subiculum of hippocampal sclerosis (133). In addition, seizures can be induced by increasing the excitability of neurons, rising the potassium concentration and lowering the magnesium. Such modifications of the extracellular medium resulted in the repetitive occurrence of ictal discharges, preceded by a change in the shape of the IEDs – termed preictal discharges (134). The use of different pharmacological blockers allowed to demonstrate that IEDs were mediated by GABAergic transmission, whereas the preictal discharges were, in addition, mediated by glutamatergic transmission.

Ictogenesis processes may, in part, be related to the underlying neuropathological lesion. Depending on the connection of the pathological neurons with the surrounding brain tissue, the seizures of some lesions may be associated with a preictal transition, whereas other lesions may not. The focal cortical dysplasia (FCD) are lesions characterized by specific dysplastic neurons, with a typical EEG signature: periodic IEDs, that interrupt at the beginning of a seizure. Interestingly, preictal discharges were recorded from some FCD tissues, in vitro (135). Altered chloride cotransporters expression and dysfunction of GABA signaling were associated with IEDs, as there were in hippocampal sclerosis. Nevertheless, the mechanisms of the transition from IEDs to the preictal discharges have not been elicited yet.

Ictogenesis processes may also be related to the anatomical microstructures of the cortex. Pathophysiology of the preictal transition was mostly studied in vitro from human hippocampal structures, an archicortex that presents specific networks and neuronal subtypes. In the neocortex, the microcircuitries are different, often organized in columns, and there are several types of interneurons. In vitro studies from the human epileptic neocortex are rare, and seizures cannot be easily recorded, unless they were provoked by $GABA_A$ blockers (136), which strongly limits the generability of the findings.

The limits of the in vitro studies on human tissues to study the preictal transition are related to the difficulty to record spontaneous seizures, which can be due to an “anatomical” disconnection of the tissue from all different afferences, and a “functional” disconnection of the tissue from the physiological influences, such as wake and sleep states and stress.

The transition from interictal to the seizure can also be studied in animal models of epilepsy. Nevertheless, the generability of their findings is limited, because the identified pathological mechanisms are closely related to the triggering factor used in the model. In a model of high potassium-increased excitability, for instance, the molecular mechanisms at the origin of IEDs and seizures were shown to be independent, because the blockage of most neurotransmitters inhibited IEDs, but not the seizures (137). Similarly, in a model of high potassium and low magnesium perfusion, blockade of GABAA receptors shortened the preictal phase, abolished the IEDs, and attenuated the slow preictal depolarization, with no effect on the ictal duration, whereas seizures were blocked by glutamate receptor blockade (138). In a 4-aminopyridine-related in vitro model, IEDs originating in the CA3 region propagate to the entorhinal cortex and were shown to limit the occurrence of ictal discharges (139), suggesting that the IEDs may play in some instances a protective role, avoiding that idle neurons within the epileptogenic zone may recruit themselves and initiate a seizure.

In an *in vivo* pilocarpine model, using tetrodes, putative interneurons were shown to be progressively recruited (increased synchrony, increased firing rate) before the onset of the seizures, whereas putative pyramidal cells were recruited later (140)

Finally, all these findings obtained from human epileptic tissues and animal model of epilepsies strongly suggest the existence of some preictal changes, preceding the seizures with a delay of several seconds or minutes. The nature of these preictal changes seems highly variable, pointing out the possible molecular and cellular diversity of the “routes to the seizure”, but also emphasizing the subtility of the cascade of events before the seizures, that cannot be reduced to a simple default in the balance between excitation and inhibition.

4. Challenges for next-generation prediction models

4.1 Clinical issues

Invasive versus noninvasive techniques

Intracranial EEG is often considered as the gold standard method for seizure prediction model, as it provides a direct access to the spatio-temporal dynamics of the epileptogenic network. In addition to the anatomical proximity, intracranial EEG signals are also less sensitive to external artifacts (e.g., muscle interferences), less influenced by reference electrode issues and volume conduction effects and offer a frequency range larger than scalp EEG. Noninvasive mobile home-based EEG or minimally invasive subscalp EEG are, however, an interesting alternative to develop ambulatory prediction model (141,142).

Chronic implantable devices (as those proposed by NeuroPace or NeuroVista) have been a revolution in terms of recording duration – years, which allowed identifying cycling variations – and remain very promising for future therapeutic strategies. Indeed, those systems integrate a closed-loop brain stimulation that can be triggered by the detection of ictal discharges. Although the RNS system (NeuroPace) can monitor EEG over ultra-long-term period, data cannot be stored (143). We could imagine the identification of patient-specific preictal patterns, through the retrospective analysis of continuous EEG data, which may result in an alert/trigger before the occurrence of ictal discharges.

Fusion of multimodal information

Recordings of long-term extracerebral information such as sleep quantity and quality, heart rate, blood volume pulse, accelerometry, temperature, electrodermal activity, etc. using wearable sensors, are a noninvasive alternative strategy. Although further studies are required to assess their relevance in seizure prediction, combining information from multimodal signals, in association for instance with prodromal symptoms evaluation, could improve their performances.

Impact of forecasts on patients

The impact of daily seizure forecasts delivered to the patient is a critical question. Unlike deterministic predictions – where the output would be binary and thus easily understandable – the probability of seizure is, by definition, uncertain. While a probabilistic approach seems much more appropriate considering the complex dynamics in epilepsy, the interpretation of results raises questions. Indeed, as the risk varies from 0% to 100%, how can intermediate results be interpreted? What is the probability threshold that could indicate a consequent risk and therefore suggest some kind of intervention? One solution might be a mixed approach: a probabilistic prediction to evaluate the risk of seizure, and a deterministic decision for therapeutic action (fast-acting antiepileptic drugs, neurostimulation, etc.).

4.2 Methodological standards

Imbalanced dataset

One of the main statistical issues in seizure prediction algorithms is the imbalance between the number of preictal and interictal data. Most of statistical prediction models tend to be more accurate over the class with the greater number of training samples. Different resampling methods are available (subsampling the interictal samples, or oversampling preictal samples) to alleviate this bias by rebalancing samples of the two classes (144). Some cost-sensitive learning methods may also handle this imbalance issue by assigning higher weights to the minority class samples to modify their preference for the majority class (78,145).

Data leakage in cross-validation

It is a common mistake in seizure prediction to apply the standard cross-validation to the entire time series of features, as they might present temporal correlations over consecutive segments (EEG or any other physiological signal). A random splitting of train and validation datasets generally produces a data leakage, which results in a false high prediction accuracy (82,120). An out-of-time condition in the cross-validation procedure should prevents this data leakage and provides a better and unbiased estimate of the prediction model's performance. Although validation in distant EEG segments seem to be a robust and unbiased approach, the effect of

cycles recently described in epilepsy should be considered (146). Unfortunately, very-long-term EEG recordings required to assess the statistical influence of such confounds on seizure prediction algorithms are, to date, non-available to the scientific community.

In-sample versus out-of-sample optimization

Currently, most of machine learning algorithms use, in a retrospective approach, the entire available dataset to learn and test the prediction models. This in-sample optimization typically results in overestimation of performances, which are generally not reproduced when tested on new data (from new patients or new recordings) for which the learned parameters of the model may no longer be optimal. For any seizure prediction algorithm, the assessment of forecasting performances on a prospective (out-of-sample) or quasi-prospective setup is necessary to evaluate its clinical efficiency (147).

How to interpret false positives?

The detection of false positives should be interpreted according to the underlying methodological strategy: a deterministic (seizure or not) false positive and the probabilistic risk of seizure do not have the same clinical impact (148). Let's consider a proictal state, i.e., a condition which is particularly at risk of upcoming seizures but whose onset could be stopped by the activation of homeostatic mechanisms. Significant differences from an interictal baseline could be noticed without the inexorable occurrence of a seizure. Such a design would have a major influence on the significance of false positives, which could be the transcription of a proictal state that would not necessarily evolve into a preictal state.

Two radically different prediction algorithms based on intracerebral EEG found a strong coherence considering correct but also false predictions (149). This concordance of false-positive results was in favor of real state modifications, but deterministic analyses prevented any proictal consideration.

What would be an ideal prediction model?

Next-gen prediction models could include some key features to optimize the quality of their performances (Figure 1):

- Noninvasive (wearable) or minimally invasive devices, to improve the tolerance, and thus, the patient adherence to long-term recordings;
- Multimodal and multitimescale analysis, to capture signals with different dynamics and also evaluate the cycling physiological phenomena that may influence the occurrence of seizures;
- Patient-specific algorithm, as evidence shows that patient-independent models perform worse than patient-specific models due to high individual variation across patients;
- Probabilistic predictions, to reflect the concept of a proictal state in which seizure may – but not necessary – occur;
- Validation in prospective and real-life conditions, as in-hospital recordings and analysis may provide overoptimistic performances unreachable in real-life context.

In addition, recent progress in circuit design and low power consumption technologies provide a promising perspective for the development of fully embedded seizure prediction systems with more accurate and reliable capacities of feature extraction and machine learning algorithms.

4.3 Scientific perspectives

One strategy to better understand the dynamics of the neuronal activities preceding the seizure consists of following the single-unit activities from *in vivo* microelectrodes. Different types of microelectrodes (AdTech (150), Utah array (151) and DIXI (152)), coupled to spike-sorting methods, have shown their ability to record individual neurons in patients with epilepsy. Such approaches have allowed, for instance, to identify that all neurons recorded in the seizure onset zone were not synchronously recruited at the onset of the seizure, but showed a heterogeneous firing – i.e., some neurons showed an increased firing rate, whereas others exhibited a decrement or no change at all (153,154).

Measures based on the shape and the duration of action potentials allow to distinguish putative interneurons from putative pyramidal cells. Putative interneurons were thus shown to be associated with specific EEG pattern, at the onset of the seizure (155). Efforts must be done to

perform long-term analysis of single neurons activities to research for specific neuronal behaviors preceding the seizures. Such approaches are challenging, because (i) it requires continuous recordings for days and weeks, of large amount of high-quality data; but database are now available (156), (ii) it requires to distinguish between physiological changes – related for example to sleep stages – and pathological changes – behaviors that would be recorded only during seizures and preictal periods, (iii) it requires new methods of data analysis, to identify subtle changes. Such approaches could not be easily applied in a large population of patients, nor for very long periods, but they may uncover neuronal behaviors, related to the preictal period.

Interestingly, deep learning algorithms could distinguish with a good accuracy preictal from interictal multi-unit activities recorded by implanted intracortical multielectrodes in a small group of patients (157).

5. Conclusion

In summary, clinical, radiological and electrophysiological evidence suggest a progressive preictal transition towards the seizure onset, which might be under glutamatergic mediation according to *in vitro* studies. Next-generation seizure prediction models could be based on multimodal and multitimescale analysis from non (or minimally) invasive and wearable devices; and forecast a risk of seizure using a patient-specific algorithm. *In vivo* single-unit activity from microelectrodes could monitor long-term neuronal individual and interindividual behaviors to search a preictal signature.

References

1. Gastaut H. The Epilepsies; Electro-clinical Correlations. Thomas; 1954. 168 p.

2. Besag FMC, Vasey MJ. Prodrome in epilepsy. Epilepsy & Behavior. 2018;83:219-33.

3. Haut SR, Hall CB, Borkowski T, Tennen H, Lipton RB. Clinical features of the pre-ictal state: Mood changes and premonitory symptoms. Epilepsy & Behavior. 2012;23(4):415-21.

4. Rajna P, Clemens B, Csibri E, Dobos E, Geregely A, Gottschal M, et al. Hungarian multicentre epidemiologic study of the warning and initial symptoms (prodrome, aura) of epileptic seizures. Seizure. 1997;6(5):361-8.

5. Scaramelli A, Braga P, Avellanal A, Bogacz A, Camejo C, Rega I, et al. Prodromal symptoms in epileptic patients: Clinical characterization of the pre-ictal phase. Seizure. 2009;18(4):246-50.

6. Schulze-Bonhage A, Kurth C, Carius A, Steinhoff BJ, Mayer T. Seizure anticipation by patients with focal and generalized epilepsy: A multicentre assessment of premonitory symptoms. Epilepsy Research. 2006;70(1):83-8.

7. Schulze-Bonhage A, Haut S. Premonitory features and seizure self-prediction: artifact or real? Epilepsy Res. 2011;97(3):231-5.

8. Petitmengin C, Baulac M, Navarro V. Seizure anticipation: Are neurophenomenological approaches able to detect preictal symptoms? Epilepsy & Behavior. 2006;9(2):298-306.

9. Lee SA, No YJ. Perceived self-control of seizures in patients with uncontrolled partial epilepsy. Seizure. 2005;14(2):100-5.

10. Pinikahana J, Dono J. The lived experience of initial symptoms of and factors triggering epileptic seizures. Epilepsy & Behavior. 2009;15(4):513-20.

11. Hughes J, Devinsky O, Feldmann E, Bromfield E. Premonitory symptoms in epilepsy. Seizure. 1993;2(3):201-3.

12. Privitera M, Haut SR, Lipton RB, McGinley JS, Cornes S. Seizure self-prediction in a randomized controlled trial of stress management. Neurology. 2019;93(22):e2021-31.

13. Haut SR, Hall CB, Borkowski T, Tennen H, Lipton RB. Modeling seizure self-prediction: An e-diary study. Epilepsia. 2013;54(11):1960-7.

14. Haut SR, Hall CB, LeValley AJ, Lipton RB. Can patients with epilepsy predict their seizures? Neurology. 2007;68(4):262-6.

15. Nakken KO, Solaas MH, Kjeldsen MJ, Friis ML, Pellock JM, Corey LA. Which seizure-precipitating factors do patients with epilepsy most frequently report? Epilepsy & Behavior. 2005;6(1):85-9.

16. DuBois JM, Boylan LS, Shiyko M, Barr WB, Devinsky O. Seizure prediction and recall. Epilepsy & Behavior. 2010;18(1-2):106-9.

17. Haut SR, Hall CB, Masur J, Lipton RB. Seizure occurrence: Precipitants and prediction. Neurology. 2007;69(20):1905-10.

18. Maiwald T, Blumberg J, Timmer J, Schulze-Bonhage A. Are prodromes preictal events? A prospective PDA-based study. Epilepsy & Behavior. 2011;21(2):184-8.

19. Cousyn L, Navarro V, Chavez M. Preictal state detection using prodromal symptoms: A machine learning approach. Epilepsia. 2021;62(2):e42-7.

20. Shaffer F, Ginsberg JP. An Overview of Heart Rate Variability Metrics and Norms. Front Public Health. 2017;5:258.

21. Lotufo PA, Valiengo L, Benseñor IM, Brunoni AR. A systematic review and meta-analysis of heart rate variability in epilepsy and antiepileptic drugs. Epilepsia. 2012;53(2):272-82.

22. Meisel C, Bailey KA. Identifying signal-dependent information about the preictal state: A comparison across ECoG, EEG and EKG using deep learning. EBioMedicine. 2019;45:422-31.

23. Leal A, Pinto MF, Lopes F, Bianchi AM, Henriques J, Ruano MG, et al. Heart rate variability analysis for the identification of the preictal interval in patients with drug-resistant epilepsy. Sci Rep. 2021;11:5987.

24. Kolsal E, Serdaroğlu A, Çilsal E, Kula S, Soysal AŞ, Kurt ANÇ, et al. Can heart rate variability in children with epilepsy be used to predict seizures? Seizure - European Journal of Epilepsy. 2014;23(5):357-62.

25. Billeci L, Marino D, Insana L, Vatti G, Varanini M. Patient-specific seizure prediction based on heart rate variability and recurrence quantification analysis. PLoS One. 2018;13(9):e0204339.

26. Fujiwara K, Miyajima M, Yamakawa T, Abe E, Suzuki Y, Sawada Y, et al. Epileptic Seizure Prediction Based on Multivariate Statistical Process Control of Heart Rate Variability Features. IEEE Transactions on Biomedical Engineering. 2016;63(6):1321-32.

27. Giannakakis G, Tsiknakis M, Vorgia P. Focal epileptic seizures anticipation based on patterns of heart rate variability parameters. Computer Methods and Programs in Biomedicine. 2019;178:123-33.

28. Badawy RAB, Freestone DR, Lai A, Cook MJ. Epilepsy: Ever-changing states of cortical excitability. Neuroscience. 2012;222:89-99.

29. Karoly PJ, Cook MJ, Maturana M, Nurse ES, Payne D, Brinkmann BH, et al. Forecasting cycles of seizure likelihood. Epilepsia. 2020;61(4):776-86.

30. Elger CE, Hoppe C. Diagnostic challenges in epilepsy: seizure under-reporting and seizure detection. The Lancet Neurology. 2018;17(3):279-88.

31. Karoly PJ, Ung H, Grayden DB, Kuhlmann L, Leyde K, Cook MJ, et al. The circadian profile of epilepsy improves seizure forecasting. Brain. 2017;140(8):2169-82.

32. Cook MJ, O'Brien TJ, Berkovic SF, Murphy M, Morokoff A, Fabinyi G, et al. Prediction of seizure likelihood with a long-term, implanted seizure advisory system in patients with drug-resistant epilepsy: a first-in-man study. The Lancet Neurology. 2013; 12(6):563-71.

33. Cook MJ, Varsavsky A, Himes D, Leyde K, Berkovic SF, O'Brien T, et al. The Dynamics of the Epileptic Brain Reveal Long-Memory Processes. Front Neurol. 2014; 5:217.

34. Goldenholz DM, Goldenholz SR, Moss R, French J, Lowenstein D, Kuzniecky R, et al. Is seizure frequency variance a predictable quantity? Annals of Clinical and Translational Neurology. 2018;5(2):201-7.

35. Goldenholz DM, Goldenholz SR, Romero J, Moss R, Sun H, Westover B. Development and Validation of Forecasting Next Reported Seizure Using e-Diaries. Annals of Neurology. 2020;88(3):588-95.

36. Goldenholz DM, Westover MB. Flexible realistic simulation of seizure occurrence recapitulating statistical properties of seizure diaries. Epilepsia. 2023;64(2):396-405.

37. Wang ET, Chiang S, Cleboski S, Rao VR, Vannucci M, Haneef Z. Seizure count forecasting to aid diagnostic testing in epilepsy. Epilepsia. 2022;63(12):3156-67.

38. Chiang S, Vannucci M, Goldenholz DM, Moss R, Stern JM. Epilepsy as a dynamic disease: A Bayesian model for differentiating seizure risk from natural variability. Epilepsia Open. 2018;3(2):236-46.

39. Payne DE, Dell KL, Karoly PJ, Kremen V, Gerla V, Kuhlmann L, et al. Identifying seizure risk factors: A comparison of sleep, weather, and temporal features using a Bayesian forecast. Epilepsia. 2021;62(2):371-82.

40. Stirling RE, Hidajat CM, Grayden DB, D'Souza WJ, Naim-Feil J, Dell KL, et al. Sleep and seizure risk in epilepsy: bed and wake times are more important than sleep duration. Brain. 2022;awac476.

41. Karoly PJ, Stirling RE, Freestone DR, Nurse ES, Maturana MI, Halliday AJ, et al. Multiday cycles of heart rate are associated with seizure likelihood: An observational cohort study. EBioMedicine. 2021;72:103619.

42. Stirling RE, Grayden DB, D'Souza W, Cook MJ, Nurse E, Freestone DR, et al. Forecasting Seizure Likelihood With Wearable Technology. Frontiers in Neurology. 2021;12.

43. Meisel C, El Atrache R, Jackson M, Schubach S, Ufongene C, Loddenkemper T. Machine learning from wristband sensor data for wearable, noninvasive seizure forecasting. Epilepsia. 2020;61(12):2653-66.

44. Nasseri M, Pal Attia T, Joseph B, Gregg NM, Nurse ES, Viana PF, et al. Ambulatory seizure forecasting with a wrist-worn device using long-short term memory deep learning. Sci Rep. 2021;11:21935.

45. Weinand ME, Carter LP, El-Saadany WF, Sioutos PJ, Labiner DM, Oommen KJ. Cerebral blood flow and temporal lobe epileptogenicity. Journal of Neurosurgery. 1997;86(2):226-32.

46. Baumgartner C, Serles W, Leutmezer F, Pataraia E, Aull S, Czech T, et al. Preictal SPECT in Temporal Lobe Epilepsy: Regional Cerebral Blood Flow Is Increased Prior to Electroencephalography-Seizure Onset. Journal of Nuclear Medicine. 1998;39(6):978-82.

47. Adelson PD, Nemoto E, Scheuer M, Painter M, Morgan J, Yonas H. Noninvasive Continuous Monitoring of Cerebral Oxygenation Periictally Using Near-Infrared Spectroscopy: A Preliminary Report. Epilepsia. 1999;40(11):1484-9.

48. Federico P, Abbott DF, Briellmann RS, Harvey AS, Jackson GD. Functional MRI of the pre-ictal state. Brain. 2005;128(8):1811-7.

49. Vinette SA, Premji S, Beers CA, Gaxiola-Valdez I, Pittman DJ, Slone EG, et al. Pre-ictal BOLD alterations: Two cases of patients with focal epilepsy. Epilepsy Research. 2016;127:207-20.

50. Chaudhary UJ, Carmichael DW, Rodionov R, Thornton RC, Bartlett P, Vulliemoz S, et al. Mapping preictal and ictal haemodynamic networks using video-electroencephalography and functional imaging. Brain. 2012;135(Pt 12):3645-63.

51. Chaudhary UJ, Centeno M, Thornton RC, Rodionov R, Vulliemoz S, McEvoy AW, et al. Mapping human preictal and ictal haemodynamic networks using simultaneous intracranial EEG-fMRI. NeuroImage: Clinical. 2016;11:486-93.

52. Chvojka J, Kudlacek J, Chang WC, Novak O, Tomaska F, Otahal J, et al. The role of interictal discharges in ictogenesis — A dynamical perspective. Epilepsy & Behavior. 2021;121:106591.

53. Lai N, Li Z, Xu C, Wang Y, Chen Z. Diverse nature of interictal oscillations: EEG-based biomarkers in epilepsy. Neurobiology of Disease. 2023;177:105999.

54. Jefferys JGR, Menendez de la Prida L, Wendling F, Bragin A, Avoli M, Timofeev I, et al. Mechanisms of physiological and epileptic HFO generation. Progress in Neurobiology. 2012;98(3):250-64.

55. Pearce A, Wulsin D, Blanco JA, Krieger A, Litt B, Stacey WC. Temporal changes of neocortical high-frequency oscillations in epilepsy. J Neurophysiol. 2013;110(5):1167-79.

56. Scott JM, Ren S, Gliske SV, Stacey WC. Preictal variability of high-frequency oscillation rates in refractory epilepsy. Epilepsia. 2020;61(11):2521-33.

57. Scott JM, Gliske SV, Kuhlmann L, Stacey WC. Viability of Preictal High-Frequency Oscillation Rates as a Biomarker for Seizure Prediction. Frontiers in Human Neuroscience. 2021;14.

58. Jacobs J, Zelmann R, Jirsch J, Chander R, Dubeau CÉCF, Gotman J. High frequency oscillations (80–500 Hz) in the preictal period in patients with focal seizures. Epilepsia. 2009;50(7):1780-92.

59. Ralston BL. The mechanism of transition of interictal spiking foci into ictal seizure discharges. Electroencephalography and Clinical Neurophysiology. 1958;10(2):217-32.

60. Stevens JR, Lonsbury BL, Goel SL. Seizure occurrence and interspike interval. Telemetered electroencephalogram studies. Arch Neurol. 1972;26(5):409-19.

61. Lange HH, Lieb JP, Engel J, Crandall PH. Temporo-spatial patterns of pre-ictal spike activity in human temporal lobe epilepsy. Electroencephalography and Clinical Neurophysiology. 1983;56(6):543-55.

62. Li S, Zhou W, Yuan Q, Liu Y. Seizure Prediction Using Spike Rate of Intracranial EEG. IEEE Transactions on Neural Systems and Rehabilitation Engineering. nov 2013;21(6):880-6.

63. Gotman J, Marciani MG. Electroencephalographic spiking activity, drug levels, and seizure occurence in epileptic patients. Annals of Neurology. 1985;17(6):597-603.

64. Gotman J, Koffler DJ. Interictal spiking increases after seizures but does not after decrease in medication. Electroencephalography and Clinical Neurophysiology. 1989;72(1):7-15.

65. Katz A, Marks DA, McCarthy G, Spencer SS. Does interictal spiking change prior to seizures? Electroencephalography and Clinical Neurophysiology. 1991;79(2):153-6.

66. Ren L, Terada K, Baba K, Usui N, Umeoka S, Usui K, et al. Ictal very low frequency oscillation in human epilepsy patients. Annals of Neurology. 2011;69(1):201-6.

67. Constantino T, Rodin E. Peri-Ictal and Interictal, Intracranial Infraslow Activity. Journal of Clinical Neurophysiology. 2012;29(4):298.

68. Rodin E, Constantino T, Bigelow J. Interictal infraslow activity in patients with epilepsy. Clinical Neurophysiology. 2014;125(5):919-29.

69. Proix T, Truccolo W, Leguia MG, Tcheng TK, King-Stephens D, Rao VR, et al. Forecasting seizure risk in adults with focal epilepsy: a development and validation study. The Lancet Neurology. 2021;20(2):127-35.

70. Leguia MG, Andrzejak RG, Rummel C, Fan JM, Mirro EA, Tcheng TK, et al. Seizure Cycles in Focal Epilepsy. JAMA Neurology. 2021;78(4):454-63.

71. Derry CP, Duncan S. Sleep and epilepsy. Epilepsy & Behavior. 2013;26(3):394-404.

72. Tezer FI, Rémi J, Erbil N, Noachtar S, Saygi S. A reduction of sleep spindles heralds seizures in focal epilepsy. Clinical Neurophysiology. 2014;125(11):2207-11.

73. Rémi J, Bubeck C, Hartl E, Tezer FI, Noachtar S. Sleep spindle reduction precedes seizures by several epochs. Clinical Neurophysiology. 2018;129(8):1624-5.

74. Islam MS, El-Hajj AM, Alawieh H, Dawy Z, Abbas N, El-Imad J. EEG mobility artifact removal for ambulatory epileptic seizure prediction applications. Biomedical Signal Processing and Control. 2020;55:101638.

75. Rasekhi J, Mollaei MRK, Bandarabadi M, Teixeira CA, Dourado A. Preprocessing effects of 22 linear univariate features on the performance of seizure prediction methods. Journal of Neuroscience Methods. 2013;217(1):9-16.

76. Nunez PL, Srinivasan R, Westdorp AF, Wijesinghe RS, Tucker DM, Silberstein RB, et al. EEG coherency. I: Statistics, reference electrode, volume conduction, Laplacians, cortical imaging, and interpretation at multiple scales. Electroencephalogr Clin Neurophysiol. 1997;103(5):499-515.

77. Zaveri HP, Duckrow RB, Spencer SS. The effect of a scalp reference signal on coherence measurements of intracranial electroencephalograms. Clinical Neurophysiology. 2000;111(7):1293-9.

78. Park Y, Luo L, Parhi KK, Netoff T. Seizure prediction with spectral power of EEG using cost-sensitive support vector machines. Epilepsia. 2011;52(10):1761-70.

79. Srinivasan R, Nunez PL, Silberstein RB. Spatial filtering and neocortical dynamics: estimates of EEG coherence. IEEE Transactions on Biomedical Engineering. 1998;45(7):814-26.

80. Bou Assi E, Nguyen DK, Rihana S, Sawan M. Towards accurate prediction of epileptic seizures: A review. Biomedical Signal Processing and Control. 2017;34:144-57.

81. Rasheed K, Qayyum A, Qadir J, Sivathamboo S, Kwan P, Kuhlmann L, et al. Machine Learning for Predicting Epileptic Seizures Using EEG Signals: A Review. IEEE Reviews in Biomedical Engineering. 2021;14:139-55.

82. Cherian R, Kanaga EG. Theoretical and methodological analysis of EEG based seizure detection and prediction: An exhaustive review. Journal of Neuroscience Methods. 2022;369:109483.

83. Maimaiti B, Meng H, Lv Y, Qiu J, Zhu Z, Xie Y, et al. An Overview of EEG-based Machine Learning Methods in Seizure Prediction and Opportunities for Neurologists in this Field. Neuroscience. 2022;481:197-218.

84. Wiesman AI, da Silva Castanheira J, Baillet S. Stability of spectral estimates in resting-state magnetoencephalography: Recommendations for minimal data duration with neuroanatomical specificity. NeuroImage. 2022;247:118823.

85. Abarbanel HDI, Brown R, Sidorowich JJ, Tsimring LSh. The analysis of observed chaotic data in physical systems. Rev Mod Phys. 1993;65(4):1331-92.

86. Kantz H, Schreiber T. Nonlinear Time Series Analysis. 2e éd. Cambridge: Cambridge University Press; 2003.

87. Mormann F, Andrzejak RG, Elger CE, Lehnertz K. Seizure prediction: the long and winding road. Brain. 2007;130(2):314-33.

88. Lopes da Silva F, Blanes W, Kalitzin SN, Parra J, Suffczynski P, Velis DN. Dynamical diseases of brain systems: different routes to epileptic seizures. IEEE Trans Biomed Eng. 2003;50(5):540-8.

89. D'Alessandro M, Esteller R, Vachtsevanos G, Hinson A, Echauz J, Litt B. Epileptic seizure prediction using hybrid feature selection over multiple intracranial EEG electrode contacts: a report of four patients. IEEE Trans Biomed Eng. 2003;50(5):603-15.

90. Acharya UR, Sree SV, Chattopadhyay S, Yu W, Ang PCA. Application of recurrence quantification analysis for the automated identification of epileptic eeg signals. Int J Neur Syst. 2011;21(03):199-211.

91. Le Van Quyen M, Adam C, Martinerie J, Baulac M, Clémenceau S, Varela F. Spatio-temporal characterizations of non-linear changes in intracranial activities prior to human temporal lobe seizures. European Journal of Neuroscience. 2000;12(6):2124-34.

92. Le Van Quyen M, Martinerie J, Navarro V, Boon P, D'Havé M, Adam C, et al. Anticipation of epileptic seizures from standard EEG recordings. Lancet. 2001;357(9251):183-8.

93. Le Van Quyen M, Martinerie J, Baulac M, Varela F. Anticipating epileptic seizures in real time by a non-linear analysis of similarity between EEG recordings. NeuroReport. 1999;10(10):2149.

94. Lai YC, Harrison MAF, Frei MG, Osorio I. Inability of Lyapunov Exponents to Predict Epileptic Seizures. Phys Rev Lett. 2003;91(6):068102.

95. Harrison MAF, Osorio I, Frei MG, Asuri S, Lai YC. Correlation dimension and integral do not predict epileptic seizures. Chaos. 2005;15(3):033106.

96. Tang L, Lv H, Yang F, Yu L. Complexity testing techniques for time series data: A comprehensive literature review. Chaos, Solitons & Fractals. 2015;81:117-35.

97. Humeau-Heurtier A. The Multiscale Entropy Algorithm and Its Variants: A Review. Entropy. 2015;17(5):3110-23.

98. Hyafil A, Giraud AL, Fontolan L, Gutkin B. Neural Cross-Frequency Coupling: Connecting Architectures, Mechanisms, and Functions. Trends in Neurosciences. 2015;38(11):725-40.

99. Alvarado-Rojas C, Valderrama M, Fouad-Ahmed A, Feldwisch-Drentrup H, Ihle M, Teixeira CA, et al. Slow modulations of high-frequency activity (40–140 Hz) discriminate preictal changes in human focal epilepsy. Sci Rep. 2015;4(1):4545.

100. Bou Assi E, Gagliano L, Rihana S, Nguyen DK, Sawan M. Bispectrum Features and Multilayer Perceptron Classifier to Enhance Seizure Prediction. Sci Rep. 2018;8(1):15491.

101. Aru J, Aru J, Priesemann V, Wibral M, Lana L, Pipa G, et al. Untangling cross-frequency coupling in neuroscience. Current Opinion in Neurobiology. 2015;31:51-61.

102. Scherer M, Wang T, Guggenberger R, Milosevic L, Gharabaghi A. Direct modulation index: A measure of phase amplitude coupling for neurophysiology data. Human Brain Mapping. 2023;44(5):1862-7.

103. Yang Y, Zhou M, Niu Y, Li C, Cao R, Wang B, et al. Epileptic Seizure Prediction Based on Permutation Entropy. Frontiers in Computational Neuroscience. 2018;12.

104. Ra JS, Li T, Li Y. A Novel Permutation Entropy-Based EEG Channel Selection for Improving Epileptic Seizure Prediction. Sensors. 2021;21(23):7972.

105. Ouyang G, Li J, Liu X, Li X. Dynamic characteristics of absence EEG recordings with multiscale permutation entropy analysis. Epilepsy Research. 2013;104(3):246-52.

106. Ferlazzo E, Mammone N, Cianci V, Gasparini S, Gambardella A, Labate A, et al. Permutation entropy of scalp EEG: A tool to investigate epilepsies: Suggestions from absence epilepsies. Clinical Neurophysiology. 2014;125(1):13-20.

107. Kramer MA, Cash SS. Epilepsy as a Disorder of Cortical Network Organization. Neuroscientist. 2012;18(4):360-72.

108. van Mierlo P, Papadopoulou M, Carrette E, Boon P, Vandenberghe S, Vonck K, et al. Functional brain connectivity from EEG in epilepsy: Seizure prediction and epileptogenic focus localization. Progress in Neurobiology. 2014;121:19-35.

109. Lehnertz K, Bialonski S, Horstmann MT, Krug D, Rothkegel A, Staniek M, et al. Synchronization phenomena in human epileptic brain networks. Journal of Neuroscience Methods. 2009;183(1):42-8.

110. Ewald A, Marzetti L, Zappasodi F, Meinecke FC, Nolte G. Estimating true brain connectivity from EEG/MEG data invariant to linear and static transformations in sensor space. NeuroImage. 2012;60(1):476-88.

111. Stam CJ, van Straaten ECW. The organization of physiological brain networks. Clinical Neurophysiology. 2012;123(6):1067-87.

112. Le Van Quyen M, Martinerie J, Navarro V, Baulac And M, Varela FJ. Characterizing neurodynamic changes before seizures. J Clin Neurophysiol. 2001;18(3):191-208.

113. Schindler KA, Bialonski S, Horstmann MT, Elger CE, Lehnertz K. Evolving functional network properties and synchronizability during human epileptic seizures. Chaos. 2008;18(3):033119.

114. Rings T, von Wrede R, Lehnertz K. Precursors of seizures due to specific spatial-temporal modifications of evolving large-scale epileptic brain networks. Sci Rep. 2019;9(1):10623.

115. Aksenova TI, Volkovych VV, Villa AEP. Detection of spectral instability in EEG recordings during the preictal period. J Neural Eng. 2007;4(3):173.

116. Wong S, Gardner AB, Krieger AM, Litt B. A Stochastic Framework for Evaluating Seizure Prediction Algorithms Using Hidden Markov Models. Journal of Neurophysiology. 2007;97(3):2525-32.

117. Rukhsar S, Khan YU, Farooq O, Sarfraz M, Khan AT. Patient-Specific Epileptic Seizure Prediction in Long-Term Scalp EEG Signal Using Multivariate Statistical Process Control. IRBM. 2019;40(6):320-31.

118. Grundy T, Killick R, Mihaylov G. High-dimensional changepoint detection via a geometrically inspired mapping. Stat Comput. 2020;30(4):1155-66.

119. King RD, Orhobor OI, Taylor CC. Cross-validation is safe to use. Nature Machine Intelligence. 2021;3(4):276-276.

120. West J, Bozorgi ZD, Herron J, Chizeck HJ, Chambers JD, Li L. Machine learning seizure prediction: one problematic but accepted practice. J Neural Eng. 2023;20(1):016008.

121. Shoeibi A, Moridian P, Khodatars M, Ghassemi N, Jafari M, Alizadehsani R, et al. An overview of deep learning techniques for epileptic seizures detection and prediction based on neuroimaging modalities: Methods, challenges, and future works. Computers in Biology and Medicine. 2022;149:106053.

122. Lopes da Silva F, Blanes W, Kalitzin SN, Parra J, Suffczynski P, Velis DN. Epilepsies as Dynamical Diseases of Brain Systems: Basic Models of the Transition Between Normal and Epileptic Activity. Epilepsia. 2003;44(s12):72-83.

123. Traub RD, Miles R, Wong RK. Model of the origin of rhythmic population oscillations in the hippocampal slice. Science. 1989;243(4896):1319-25.

124. Kramer MA, Szeri AJ, Sleigh JW, Kirsch HE. Mechanisms of seizure propagation in a cortical model. J Comput Neurosci. 2007;22(1):63-80.

125. Takeshita D, Sato YD, Bahar S. Transitions between multistable states as a model of epileptic seizure dynamics. Phys Rev E. 2007;75(5):051925.

126. Wendling F, Hernandez A, Bellanger JJ, Chauvel P, Bartolomei F. Interictal to ictal transition in human temporal lobe epilepsy: insights from a computational model of intracerebral EEG. J Clin Neurophysiol. 2005;22(5):343-56.

127. van Putten MJAM, Zandt BJ. Neural mass modeling for predicting seizures. Clinical Neurophysiology. 2014;125(5):867-8.

128. Saggio ML, Crisp D, Scott JM, Karoly P, Kuhlmann L, Nakatani M, et al. A taxonomy of seizure dynamotypes. eLife. 2020;9:e55632.

129. Houssaini KE, Bernard C, Jirsa VK. The Epileptor Model: A Systematic Mathematical Analysis Linked to the Dynamics of Seizures, Refractory Status Epilepticus, and Depolarization Block. eNeuro. 2020;7(2).

130. Schindler K, Wiest R, Kollar M, Donati F. EEG analysis with simulated neuronal cell models helps to detect pre-seizure changes. Clinical Neurophysiology. 2002;113(4):604-14.

131. Aarabi A, He B. Seizure prediction in hippocampal and neocortical epilepsy using a model-based approach. Clinical Neurophysiology. 2014;125(5):930-40.

132. Rasheed K, Qadir J, O'Brien TJ, Kuhlmann L, Razi A. A Generative Model to Synthesize EEG Data for Epileptic Seizure Prediction. IEEE Transactions on Neural Systems and Rehabilitation Engineering. 2021;29:2322-32.

133. Cohen I, Navarro V, Clemenceau S, Baulac M, Miles R. On the Origin of Interictal Activity in Human Temporal Lobe Epilepsy in Vitro. Science. 2002;298(5597):1418-21.

134. Huberfeld G, Menendez de la Prida L, Pallud J, Cohen I, Le Van Quyen M, Adam C, et al. Glutamatergic pre-ictal discharges emerge at the transition to seizure in human epilepsy. Nat Neurosci. 2011;14(5):627-34.

135. Blauwblomme T, Dossi E, Pellegrino C, Goubert E, Iglesias BG, Sainte-Rose C, et al. Gamma-aminobutyric acidergic transmission underlies interictal epileptogenicity in pediatric focal cortical dysplasia. Ann Neurol. 2019;85(2):204-17.

136. Kandrács Á, Hofer KT, Tóth K, Tóth EZ, Entz L, Bagó AG, et al. Presence of synchrony-generating hubs in the human epileptic neocortex. J Physiol. 2019;597(23):5639-70.

137. Jensen MS, Yaari Y. The relationship between interictal and ictal paroxysms in an in vitro model of focal hippocampal epilepsy. Annals of Neurology. 1988;24(5):591-8.

138. Zhang ZJ, Koifman J, Shin DS, Ye H, Florez CM, Zhang L, et al. Transition to Seizure: Ictal Discharge Is Preceded by Exhausted Presynaptic GABA Release in the Hippocampal CA3 Region. J Neurosci. 2012;32(7):2499-512.

139. Barbarosie M, Avoli M. CA3-Driven Hippocampal-Entorhinal Loop Controls Rather than Sustains In Vitro Limbic Seizures. J Neurosci. 1997;17(23):9308-14.

140. Grasse DW, Karunakaran S, Moxon KA. Neuronal synchrony and the transition to spontaneous seizures. Experimental Neurology. 2013;248:72-84.

141. Biondi A, Santoro V, Viana PF, Laiou P, Pal DK, Bruno E, et al. Noninvasive mobile EEG as a tool for seizure monitoring and management: A systematic review. Epilepsia. 2022;63(5):1041-63.

142. Stirling RE, Maturana MI, Karoly PJ, Nurse ES, McCutcheon K, Grayden DB, et al. Seizure Forecasting Using a Novel Sub-Scalp Ultra-Long Term EEG Monitoring System. Frontiers in Neurology. 2021;12: 713794.

143. Nagaraj V, Lee ST, Krook-Magnuson E, Soltesz I, Benquet P, Irazoqui PP, et al. Future of seizure prediction and intervention: closing the loop. J Clin Neurophysiol. 2015;32(3):194-206.

144. Varotto G, Susi G, Tassi L, Gozzo F, Franceschetti S, Panzica F. Comparison of Resampling Techniques for Imbalanced Datasets in Machine Learning: Application to Epileptogenic Zone Localization From Interictal Intracranial EEG Recordings in Patients With Focal Epilepsy. Frontiers in Neuroinformatics. 2021;15.

145. Zhou ZH, Liu XY. Training cost-sensitive neural networks with methods addressing the class imbalance problem. IEEE Transactions on Knowledge and Data Engineering. 2006;18(1):63-77.

146. Karoly PJ, Rao VR, Gregg NM, Worrell GA, Bernard C, Cook MJ, et al. Cycles in epilepsy. Nat Rev Neurol. 2021;17(5):267-84.

147. Beniczky S, Karoly P, Nurse E, Ryvlin P, Cook M. Machine learning and wearable devices of the future. Epilepsia. 2021;62(S2):S116-24.

148. Freestone DR, Karoly PJ, Cook MJ. A forward-looking review of seizure prediction. Current Opinion in Neurology. 2017;30(2):167-73.

149. Müller J, Yang H, Eberlein M, Leonhardt G, Uckermann O, Kuhlmann L, et al. Coherent false seizure prediction in epilepsy, coincidence or providence? Clinical Neurophysiology. 2022;133:157-64.

150. Fried I, MacDonald KA, Wilson CL. Single neuron activity in human hippocampus and amygdala during recognition of faces and objects. Neuron. 1997;18(5):753-65.

151. Schevon CA, Ng SK, Cappell J, Goodman RR, McKhann G, Waziri A, et al. Microphysiology of Epileptiform Activity in Human Neocortex: Journal of Clinical Neurophysiology. 2008;25(6):321-30.

152. Despouy E, Curot J, Denuelle M, Deudon M, Sol JC, Lotterie JA, et al. Neuronal spiking activity highlights a gradient of epileptogenicity in human tuberous sclerosis lesions. Clinical Neurophysiology. 2019;130(4):537-47.

153. Truccolo W, Donoghue JA, Hochberg LR, Eskandar EN, Madsen JR, Anderson WS, et al. Single-neuron dynamics in human focal epilepsy. Nat Neurosci. 2011;14(5):635-41.

154. Lambrecq V, Lehongre K, Adam C, Frazzini V, Mathon B, Clemenceau S, et al. Single-unit activities during the transition to seizures in deep mesial structures: Seizures and Single-Unit Activities. Annals of Neurology. 2017;82(6):1022-8.

155. Elahian B, Lado NE, Mankin E, Vangala S, Misra A, Moxon K, et al. Low-voltage fast seizures in humans begin with increased interneuron firing: LVF Onset Seizures. Ann Neurol. 2018;84(4):588-600.

156. Lehongre K, Lambrecq V, Whitmarsh S, Frazzini V, Cousyn L, Soleil D, et al. Long-term deep intracerebral microelectrode recordings in patients with drug-resistant epilepsy: Proposed guidelines based on 10-year experience. NeuroImage. 2022;254:119116.

157. Proix T, Aghagolzadeh M, Madsen JR, Cosgrove R, Eskandar E, Hochberg LR, et al. Intracortical neural activity distal to seizure-onset-areas predicts human focal seizures. PLOS ONE. 2019;14(7):e0211847.

Figure 1. Overview of different approaches to identify preictal changes

Figure 1 legend: Clinical features (prodromal symptoms, seizure diaries, and cycles) and extracerebral signals (eg, ECG, electrodermal activity) can be collected using wearable devices (eg, smartphone, smartwatch). Invasive or mini-invasive techniques can record EEG signals over long-term periods. Physiological cycling variations should be also considered to evaluate the different periodicities that may compose long-term biological signal recordings (top graph). A risk of upcoming seizure may be estimated according to the signal variations during the preictal state: A-B. Specific preictal increase (perfect scenarios) ; C-D: unspecific preictal increase with false positives that can be interpretated as a proictal state or a not specific metric at all (uncertain scenarios) ; E. Physiological variations of a metric (eg, sleep) that may increase the seizure risk but without specificity (physiological scenario).

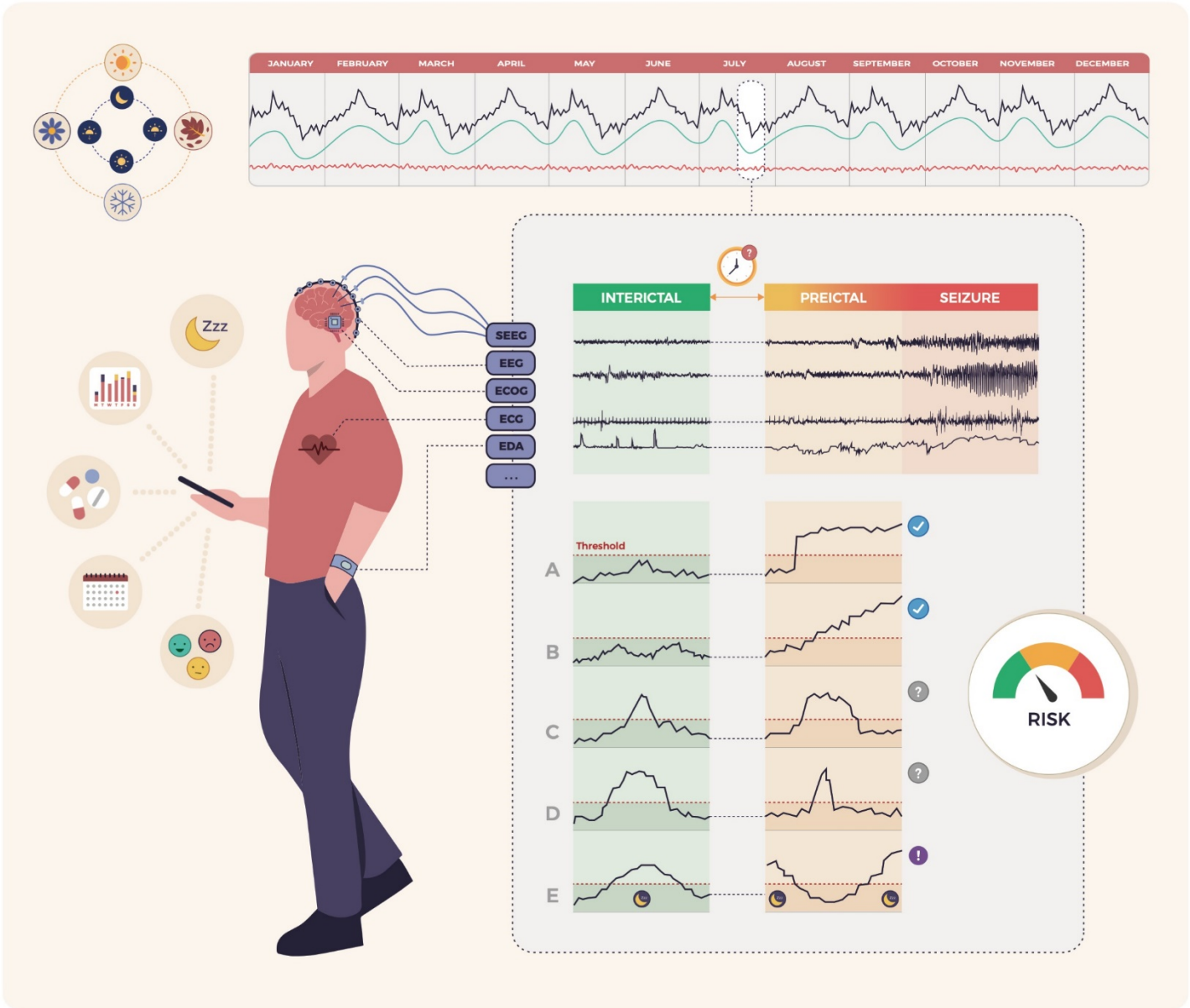

Objectifs

Durant mon travail thèse, je me suis intéressé aux changements d'état pouvant précéder la survenue d'une crise d'épilepsie. Ces modifications précritiques ont été étudiées chez des patients présentant une épilepsie pharmaco-résistantes, à plusieurs échelles :

1) L'étude des modifications cliniques (Articles 1 et 2)

Mon premier niveau d'approche a porté sur l'étude de manifestations cliniques subjectives dans le cadre d'une évaluation quotidienne standardisée. L'identification d'un état précritique a ensuite été réalisée à l'aide de différents modèles d'apprentissage automatique, que l'on pourrait ensuite implémenter dans une application mobile à destination des patients en condition de vie réelle.

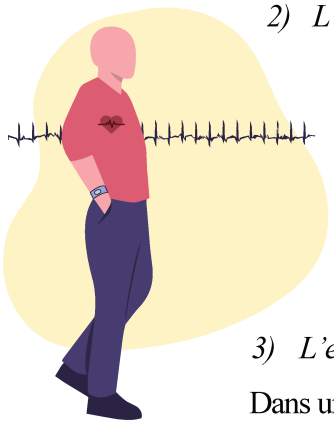

2) L'étude des modifications électrocardiographiques (Article 3)

Mon deuxième niveau d'étude s'est intéressé aux modifications du système nerveux autonome au travers de la variabilité de la fréquence cardiaque. Différentes métriques linéaires et non-linéaires ont été extraites afin d'alimenter des modèles d'apprentissage automatique et estimer le risque de crise quotidien.

3) L'étude des modifications de connectivité intracérébrale (Articles 4 et 5)

Dans un troisième niveau, j'ai évalué les changements quotidiens de connectivité fonctionnelle en EEG intracérébral afin d'émettre des prévisions probabilistes quant au risque de crise.

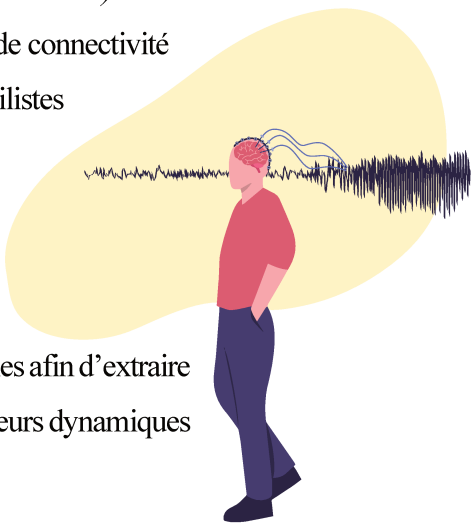

4) L'étude des changements de comportement d'activités unitaires de neurones in vivo

J'ai ensuite analysé des signaux issus de microélectrodes intracérébrales afin d'extraire les activités unitaires de neurones uniques, et j'ai amorcé une évaluation de leurs dynamiques individuels et interindividuels au cours du temps.

5) L'étude des dynamiques de transition précritiques in vitro sur tranches de cortex cérébral

J'ai initié une étude portant sur du tissu cérébral épileptique en per-opératoire afin d'enregistrer *in vitro* des tranches de cortex et tenter de provoquer des crises en modifiant le milieu extracellulaire.

Résultats

PARTIE 1. ÉTUDE DES SYMPTOMES PRODROMAUX DURANT LA PERIODE PRECRITIQUE

I. Classification des états inter et précritiques à l'aide d'une évaluation standardisée quotidienne des symptômes prodromaux

1) Introduction

Plusieurs études ont suggéré l'existence d'une période de transition entre un état intercritique et la survenue de la crise (Kuhlmann et al. 2018b). Cette période « précritique » pouvant précéder la crise constitue la pierre angulaire de tous les modèles de prédiction des crises. Identifier des biomarqueurs précritiques spécifiques demeure néanmoins un défi de taille.

Alors que les informations issues des signaux EEG ont longtemps été plébiscitées, l'analyse des symptômes cliniques a plus récemment émergé. Ainsi, ont été investigués les symptômes cliniques précritiques, autrement nommés « prodromes » ou « symptômes prodromaux », pouvant précéder la crise jusqu'à plusieurs heures. Certaines études ont également mis en évidence l'intérêt d'intégrer l'auto-prédiction – l'appréciation subjective du patient sur le risque de crise à venir – sans les modèles d'anticipation (Haut et al. 2007a, 2013; Privitera et al. 2019).

Dans cette étude, nous avons étudié les performances d'un algorithme de classification binaire, à l'aide de l'évaluation quotidienne et scorée de plusieurs symptômes prodromaux, afin d'identifier un état précritique.

2) Méthodologie

Nous avons créé un *auto-questionnaire* comprenant 24 symptômes cliniques, scorés à l'aide d'une échelle de Likert à 4 points (Tableau 3) :

i. un score d'auto-prédiction de crise ;
ii. 22 symptômes prodromaux, parmi ceux les plus rapportés dans la littérature :
iii. et une échelle d'anxiété (State-Trait Anxiety Inventory forme Y-1, Tableau 4) (Spielberger et al. 1983).

Nous avons fait passer quotidiennement les questionnaires aux 29 patients hospitalisés de mars 2019 à juin 2020 dans l'unité d'épilepsie de l'Hôpital de la Pitié-Salpêtrière (Paris, France) dans le cadre d'un enregistrement vidéo-EEG de scalp continu. Chaque questionnaire était ensuite classé en :

a) *précritique*, si une crise électro-clinique survenait dans les 24h suivantes ;
b) *intercritique*, en l'absence de crise.

Nous avons entraîné un *algorithme de classification* de type machine à vecteurs de support (SVM) sur 70% des données afin qu'il apprenne à distinguer entre les états pré et intercritiques (Chang et Lin 2011). Une phase de test portait ensuite sur les 30% de données restantes afin d'évaluer les performances de notre modèle. Une méthode de *sélection automatique* des variables les plus discriminantes a également été réalisée.

3) Résultats

La combinaison de l'ensemble des symptômes prodromaux, dans la population des 24 patients étudiés, a donné de bonnes performances de prédiction : AUC=0,72, 95% IC [0,61-0,81]. Ces résultats étaient significativement améliorés après sélection automatique des symptômes les plus discriminants : AUC=0,80, 95% IC [0,69-0,88]. Nous avons comparé notre classifieur SVM à un classifieur linéaire « classique » de type Fisher, dont les prédictions ont systématiquement échoué (AUC < 0,6).

Notre approche a permis de distinguer deux états – inter et précritique – à l'aide d'un algorithme pouvant appréhender des distributions complexes de données, qu'elles soient linaires ou non, ce qui n'a pas été le cas avec une approche purement linéaire. De plus, alors que les précédentes études ne relevaient que la présence/absence des symptômes (variables binaires), notre stratégie de cotation en 4 points a permis d'optimiser le niveau de distribution des informations.

Cette partie de mon travail a fait l'objet d'un ***dépôt de brevet*** européen (No. 20306548.7) le 11 décembre 2020 et international (No. PCT/EP2021/085146) le 10 décembre 2021 : « A computer-implemented model for predicting occurrence of a seizure and training method thereof ».

	Pas du tout	**Un peu**	**Modérément**	**Beaucoup**
1. Je me sens **calme**				
2. Je me sens **en sécurité**				
3. Je suis **tendu(e)**				
4. Je me sens **surmené(e)**				
5. Je me sens **à l'aise**				
6. Je suis **contrarié(e)**				
7. L'idée de **malheurs éventuels me tracasse** en ce moment				
8. Je me sens **satisfait(e)**				
9. Je me sens **effrayé(e)**				
10. Je suis **confortable**				
11. Je me sens **confiant(e), sûr(e) de moi**				
12. Je me sens **nerveux(se)**				
13. Je suis **agité(e)**				
14. Je me sens **indécis(e)**				
15. Je suis **détendu(e)**				
16. Je me sens **content(e)**				
17. Je suis **inquiet(ète)**				
18. Je me sens **confus(e)**				
19. Je sens que j'ai les **nerfs solides**				
20. Je me sens **bien**				

Tableau 3 : Échelle d'Anxiété – État de Spielberger (STAI forme Y1)

	Pas du tout	**Un peu**	**Modérément**	**Beaucoup**
1. Je sens que je suis **à risque de faire une crise** d'épilepsie aujourd'hui				
Cognitif				
2. J'ai des **difficultés à me concentrer**				
3. j'ai des **difficultés à comprendre**				
4. J'ai des **difficultés à parler**				
5. J'ai des **difficultés à lire**				
6. J'ai des **difficultés à écrire**				
Sensoriel				
7. Ma vue est **floue, trouble**				
8. Je suis **gêné(e) par la lumière**				
9. Je suis **gêné(e) par le bruit**				
10. J'ai des **acouphènes**, un bourdonnement dans les oreilles				
11. Mon **audition** est **modifiée** (hypersensible ou affaiblie)				
Émotionnel				
12. Je suis de **mauvaise humeur**				
13. Je suis **à fleur de peau, irritable**				
Physique				
14. Je me sens **maladroit(e)**				
15. J'ai des **tremblements**				
16. J'ai une **envie pressante** d'aller aux toilettes				
17. J'ai la **tête qui tourne**, j'ai des vertiges				
18. J'ai des **nausées**				
19. J'ai **mal à la tête**				
20. Je suis **assoiffé(e)**				
21. J'ai très **faim**				
22. Je me sens **bizarre, drôle**				
23. Je me sens **fatigué(e), faible, ou sans énergie**				

Tableau 4 : Échelle des prodromes épileptiques

4) Article 1 : Preictal state detection using prodromal symptoms: a machine learning approach

Received: 12 September 2020 | Revised: 13 December 2020 | Accepted: 13 December 2020

DOI: 10.1111/epi.16804

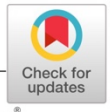

Epilepsia®

BRIEF COMMUNICATION

Preictal state detection using prodromal symptoms: A machine learning approach

Louis Cousyn[1,2,3,4] | **Vincent Navarro**[1,2,3,4] | **Mario Chavez**[2]

[1]Department of Neurology, Epilepsy Unit, Pitié-Salpêtrière Hospital, Public Hospital Network of Paris, Paris, France

[2]Paris Brain Institute, ICM (INSERM-U1127, CNRS-UMR7225), Paris, France

[3]Center of Reference for Rare Epilepsies, Pitié-Salpêtrière Hospital, Paris, France

[4]Sorbonne University, Paris, France

Correspondence
Louis Cousyn, Hôpital Pitié-Salpêtrière, 47-83 boulevard de l'Hôpital, 75651 Paris Cedex 13, France.
Email: louis.cousyn@gmail.com

Abstract

A reliable identification of a high-risk state for upcoming seizures may allow for preemptive treatment and improve the quality of patients' lives. We evaluated the ability of prodromal symptoms to predict preictal states using a machine learning (ML) approach. Twenty-four patients with drug-resistant epilepsy were admitted for continuous video-electroencephalographic monitoring and filled out a daily four-point questionnaire on prodromal symptoms. Data were then classified into (1) a preictal group for questionnaires completed in a 24-h period prior to at least one seizure (n_1 = 58) and (2) an interictal group for questionnaires completed in a 24-h period without seizures (n_2 = 190). Our prediction model was based on a support vector machine classifier and compared to a Fisher's linear classifier. The combination of all the prodromal symptoms yielded a good prediction performance (area under the curve [AUC] = .72, 95% confidence interval [CI] = .61–.81). This performance was significantly enhanced by selecting a subset of the most relevant symptoms (AUC = .80, 95% CI = .69–.88). In comparison, the linear classifier systematically failed (AUCs < .6). Our findings indicate that the ML analysis of prodromal symptoms is a promising approach to identifying preictal states prior to seizures. This could pave the way for development of clinical strategies in seizure prevention and even a noninvasive alarm system.

KEYWORDS

epilepsy, machine learning, preictal state, prodromal symptoms, prodromes, seizure prediction

1 | INTRODUCTION

Epileptic seizures have long been considered to result from an abrupt and unpredictable transition in brain activity. However, recent studies on the underlying mechanisms of transition from an interictal state to seizure (i.e., ictogenesis) suggest some preictal changes.[1] A reliable identification of a high-risk state of seizure may therefore allow for preventive treatment and would improve patients' quality of life. Although electroencephalographic (EEG) signals have been mainly investigated to characterize preictal states,[1] analysis of clinical symptoms is increasingly reported.[2]

Seizures can be preceded by subjective symptoms that are interpreted by the patients as precursors of an upcoming seizure. They can refer to focal aware seizures, formerly called "auras," or to prodromal symptoms, which are not considered to be part of the ictal event. Prodromal symptoms may appear up to 24 h preceding the seizure onset and, as we previously reported,[3] do not share the classical cortical focus-related semiology.

Prodromal symptoms are poorly understood but may reflect changes related to the preictal period. Although not yet specific enough for clinical use, they could refine the pathophysiology of ictogenesis and seizure prediction strategies. Furthermore, some prospective studies (see Table S1) have investigated their ability in seizure prediction and have highlighted premonitory features, although with rather low sensitivities.[4–9]

Although prediction performances of machine learning (ML) algorithms are well known in different clinical fields, they have never been applied to the analysis of prodromal symptoms.[10] In our study, we applied ML methods to evaluate the ability of prodromal symptom scales to identify a preictal state.

2 | MATERIALS AND METHODS

2.1 | Assessment of prodromal symptoms

We collected the 22 most frequently reported prodromal symptoms in the literature[2,3,6,7,11–15] and created a self-rated questionnaire, which also included a self-prediction of seizure. Each item was scored using a four-point Likert scale ranging from "not at all" to "very much so."

2.2 | Measuring anxiety level

We also used the validated State-Trait Anxiety Inventory (STAI) form Y-1 (state anxiety) for daily evaluation of anxiety level. It includes 20 questions with a four-point Likert scale, and scores range from 20 (low) to 80 (high anxiety).

2.3 | Study design and participants

Twenty-nine consecutive patients with drug-resistant epilepsy admitted in the Epilepsy Unit of Pitié-Salpêtrière Hospital (Paris, France) for continuous video-EEG monitoring were included from March 2019 to June 2020. They were required to fill out these questionnaires every morning during their stay. Continuous video-EEG recordings were analyzed to identify seizures during the hospital stay. We excluded patients with a final diagnosis of psychogenic nonepileptic seizures ($n = 1$) or with mistakes in filling out the questionnaires ($n = 4$). The study was also discontinued in one patient because of intercurrent event (severe head injury during a seizure). This study was conducted according to French legislation and was authorized by the national committee for the protection of privacy and personal data (Commission nationale de l'informatique et des libertés, No. 2211991). Patients were informed about the use of their anonymized data in this study.

Every daily questionnaire was then classified into one of the two following groups (Figure 1): (1) preictal group when patients experienced at least one electroclinical seizure in the next 24 h after filling out the questionnaire ($n_1 = 58$) and (2) interictal group for days without any seizure ($n_2 = 190$). To avoid confusion with symptoms from focal aware seizures, questionnaires had to be filled out at least 10 minutes before seizure onset.

2.4 | Univariate between-group comparisons

We applied nonparametric permutation tests ($\alpha = .05$, two-tailed, 10 000 permutations, false discovery rate corrected for multiple comparisons) to compare each prodromal symptom between the interictal and preictal groups.

2.5 | Prediction models

To study predictive values of prodromal symptoms, we evaluated their power to discriminate between interictal and preictal groups. There were two stages in building the prediction model (Figure 1): (1) a training phase, in which a binary classifier (interictal or preictal group) used on 70% of the labeled days to learn the model; and then (2) a testing phase, in which the remaining labeled days were used to evaluate its prediction performance. A cross-validation procedure was used with 10 000 folds.

Classification was performed using self-reported scales of prodromal symptoms and a support vector machine (SVM) classifier.[16] SVM classifiers were chosen because of their robustness for modeling complex data, without any prior assumption about the underlying distribution. In addition, they can use a transformation (kernel) function to project the data into a higher dimensional space; input data that cannot be distinguished in the original space may become separable after transformation into the new high-dimensional feature space (Figure 1). As it is more versatile and powerful than linear or polynomial kernel functions, here we used SVM models with a Gaussian kernel.[17] The kernel width parameter γ was set to be the median pairwise distance among training points.[16]

Classification performance using class-imbalanced data may be biased in favor of the majority class.[18] To prevent this type of bias, we applied SMOTE (synthetic minority oversampling technique), which oversamples points of the minority class based on the similarities between the existing data.[18] To avoid biased models and overoptimistic predictions, the oversampling was applied within each fold of cross-validation.[19] We also controlled the classifiers' performance by using permutation tests.[20]

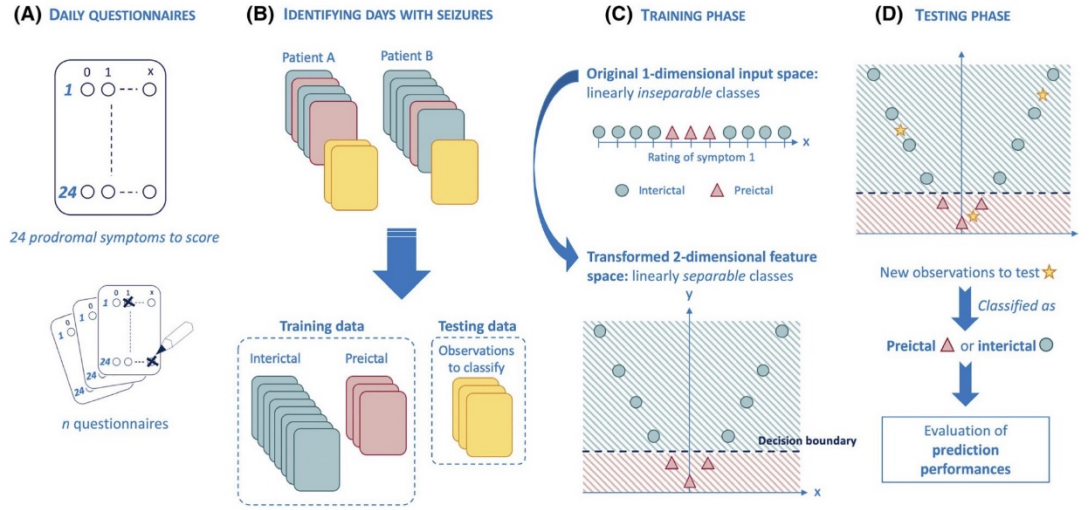

FIGURE 1 General scheme of the prediction method. (A) Daily questionnaires including 24 prodromal symptoms are filled out during *n* days. Each symptom is scored from 0 to *x* (in our study, $x = 3$). (B) Questionnaires are collected daily and grouped into interictal or preictal classes. Some of the data will be used to train the algorithm; the remaining data (indicated in yellow) will be used during the testing phase. (C) Nonlinear transformation of nonseparable data in the original input space; data are mapped into a higher dimensional feature space (from one- to two-dimensional space in this example) where data become separable. The model can be trained and a decision boundary can be fit to separate the two different classes (i.e., interictal and preictal groups). (D) New data (represented here by the yellow star symbols) will be classified into one or another class in accordance to the decision boundary set during the training phase. Prediction performances are finally computed only on testing data

For all prediction parameters considered in this study, the randomization of group labels yielded very low *p*-values < .001 (not shown in Table 1). For completeness, we also compared the results from the SVM classifier with those obtained from a standard linear model (a Fisher's classifier).

Unlike other items, STAI Y-1 scores are discrete variables that range from 20 to 80. To have comparable scales for each item in the prediction models, we converted them into ordinal variables using the same four-point scale as prodromal symptoms: 0 (20–35), 1 (36–50), 2 (51–65), and 3 (66–80).

Classification performance was measured by different attributes (all metrics were computed by applying a cross-validation, excluding the learning period in the classification):

1. *Area under the curve* (AUC) of the receiver operating characteristic curve ranges from .5 (random classification) to 1 (perfect classification).
2. *Sensitivity* evaluates the proportion of true positives that are correctly predicted. It suggests how good the test is at predicting preictal states.
3. *Specificity* evaluates the proportion of true negatives that are correctly predicted. It suggests how good the test is at identifying interictal states.
4. *Accuracy* is the proportion of true results, either true positive or true negative, in our data. It measures the degree of veracity for each prediction. As it may be biased toward the majority class, we also considered the *precision*, also called positive predictive value, which is the fraction of relevant instances among the detected instances.[19]

2.6 | Selection of the most relevant prodromal symptoms

The SVM classifier was first evaluated with the whole set of prodromal symptoms ($N = 24$). Then, "irrelevant" symptoms were removed one by one by a pruning procedure: (1) AUC values were estimated by cross-validation, after removal of each symptom; (2) the symptom without which the model has the highest AUC was removed from the subset of symptoms; and (3) the procedure was repeated with the remaining symptoms. We could identify a set of 11 symptoms that improved the classification performances after their removal (Table 1). If the removal procedure continued, the classification performances decreased considerably.

3 | RESULTS

3.1 | Study patients

Questionnaires of 24 patients were analyzed. Their mean age was 35.0 years (minimum = 22, maximum = 54), and 13

TABLE 1 Predictive values of prodromal symptoms

Univariate analyses							
Prodromal symptoms		***T*-values**	***P*-values**	**Prodromal symptoms**		***T*-values**	***P*-values**
1	Self-prediction of seizure	3.56[a]	0.0008[a]	13	Irritability	0.78	NS
2	Trouble concentrating	0.89	NS	14	Anxiety (STAI-Y1)	1.02	NS
3	Trouble understanding	0.69	NS	15	Clumsiness	0.38	NS
4	Trouble speaking	0.35	NS	16	Tremor	0.64	NS
5	Trouble reading	0.64	NS	17	Urge to urinate	0.97	NS
6	Trouble writing	1.32	NS	18	Spinning head	0.18	NS
7	Blurred vision	0.74	NS	19	Nausea	0.24	NS
8	Light sensitivity	1.29	NS	20	Headache	0.21	NS
9	Noise sensitivity	2.37[a]	0.03[a]	21	Thirst	0.52	NS
10	Tinnitus	1.51	NS	22	Hunger	0.23	NS
11	Hearing impairment	1.97	0.07	23	Funny feeling	1.01	NS
12	Bad mood	0.24	NS	24	Fatigue	1.31	NS

Prediction models	**Fisher's linear classifier**					**SVM classifier**				
	AUC	**Specificity**	**Sensitivity**	**Accuracy**	**Precision**	**AUC**	**Specificity**	**Sensitivity**	**Accuracy**	**Precision**
All symptoms	0.55 [0.40-0.69]	0.67 [0.42-0.86]	0.51 [0.32-0.72]	0.59 [0.48-0.69]	0.60 [0.47-0.76]	**0.72 [0.61-0.81]**	**0.68 [0.54-0.81]**	**0.72 [0.58-0.86]**	**0.70 [0.61-0.78]**	**0.70 [0.61-0.79]**
Most relevant symptoms[b]	0.59 [0.44-0.73]	0.70 [0.49-0.86]	0.54 [0.35-0.74]	0.62 [0.51-0.74]	0.64 [0.51-0.79]	**0.80 [0.69-0.88]**	**0.75 [0.63-0.86]**	**0.77 [0.63-0.89]**	**0.76 [0.68-0.84]**	**0.76 [0.68-0.85]**

Each cell contains the average value across all the folds of permutation and cross-validation tests [95% confidence interval is indicated].

Abbreviations: AUC, area under the curve; NS, not significant.

[a]Statistically significant.

[b]The most relevant symptoms exclude symptoms 5, 6, 8, 10, 12, 14, 15, 19 and 21-23.

patients were women (54.2%). The mean duration of video-EEG monitoring was 10.3 days (minimum = 2 days, maximum = 21 days). Patients had mainly temporal focal epilepsy (n = 14, 58.3%) and a mean number of seizures of 3.8 during the stay (minimum = 0, maximum = 9). Only one patient had generalized epilepsy.

3.2 | A "classical" statistical approach

A linear statistical comparison of groups revealed that the self-prediction of seizure was strongly associated with the preictal group ($p < .001$). Sensory symptoms such as hypersensitivity to noise and hearing impairment also tended to be more frequently reported during the preictal period (respectively, $p = .03$ and $p = .07$; Table 1).

Nevertheless, prediction models based on the Fisher's linear classifier failed in most cases (AUCs < .60) when each symptom was individually analyzed. Predictions also failed when using a combination of the 24 symptoms (AUC = .55, 95% confidence interval [CI] = .40–.69) and no improvements were obtained by the feature removal procedure (AUC = .59, 95% CI = .44–.73).

3.3 | SVM classifier's contributions

SVM-based predictions using individual symptoms failed in most cases (AUCs < .60). However, the combination of all the symptoms provided a good prediction performance (AUC = .72, 95% CI = .61–.81), which was considerably improved using the most relevant symptoms (AUC = .80, 95% CI = .69–.88; Table 1). Refined analyses suggested that the time to seizure (< or ≥6 h after filling the questionnaire) and the daily number of seizures (one or more) have no effect on the prediction of preictal states. The impact of seizure clusters (i.e., ≥3 seizures within a 24-h period[21]) could not be assessed, as only 7 days from six patients were concerned.

Among the 58 days with seizures identified on video-EEG, 45 (77.6%) were reported by patients. To assess prediction performances based on these seizures, the algorithm was trained to detect preictal states using only the reported seizures. Then, we tested its performances to distinguish between interictal and preictal phases, including reported and unreported seizures. Although prediction performances decreased, they remained good using the most relevant symptoms (AUC = .74, 95% CI = .64–.82).

4 | DISCUSSION

Our study highlights the ability of SVM classifiers to identify a preictal state from prodromal symptoms. This new strategy allows capturing complex distribution of data, whether linear or not, which is usually not the case with traditional statistical models. We obtained good prediction performances considering combinations of all the symptoms and of the most relevant ones. In contrast, the prediction model based on linear analyses failed in most cases (AUCs < .6) and thus cannot be considered for clinical use. This confirms the low performances—especially the sensitivity—of standard analyses, as previously reported.[4,7–9,15] In addition, unlike previous studies that used binary variables (yes/no), we applied four-point scales to assess prodromal symptoms, which allowed a more complex distribution of data to be taken into account.

The contrast between the good predictions from symptom combinations and the failure of individual analysis is not surprising. We did not expect to obtain robust predictions based on a single symptom, given difficulties reported in the previous studies. The preictal state seems to be a much more complex condition that may only be captured by combinations of various symptoms.

Only one patient had a generalized epilepsy. We included patients with drug-resistant epilepsy, regardless of the type of epilepsy. However, drug-resistance is more frequent in focal epilepsies and most patients underwent continuous video-EEG as part of the presurgical evaluation.

Our study has several limits. First, it is important to note that, so far, there is no evidence of a direct causality between prodromal symptoms and seizures. Besides, some studies considered prodromal symptoms as not specific enough for common practice and questioned their validity in seizure prediction.[3,8,15] Nevertheless, our results support the hypothesis that prodromal symptoms are associated with preictal states.[4–7,9] A study of the relationship between prodromal symptoms and interictal epileptiform discharges would also be interesting, in particular to better understand the underlying pathophysiological mechanisms. Second, we could not assess patient-specific predictions because of the limited number of seizures per patient. As the SVM classifier required sufficient preictal data to ensure accurate predictions, an individual patient-specific approach was not achievable. A long-term patient follow-up would enable us to collect data over a longer time period and evaluate patient-specific predictions. Third, antiepileptic drug dosage was often reduced (in 19 of 24 patients) to favor seizures. The self-prediction of seizure could have been influenced by these changes, as generally known to the patients. In addition, although only very progressive reduction was applied, the possibility of withdrawal—and not prodromal—symptoms cannot be entirely ruled out. Therefore, future studies could monitor patients without changes in medications, which would replicate the natural course of their epilepsy. Finally, as focal to bilateral and generalized onset tonic-clonic seizures were infrequent compared to focal seizures (10.3% vs. 89.7%), the predictability of these seizure types could not be compared. In addition, awareness during seizures was not always assessed, especially during nocturnal seizures.

Our work provides a useful method that can be highly operable in clinical environments. Furthermore, an effective translation of our approach to a suitable device for long-term monitoring of patients could warn them of the high risk of seizure, allowing them to take precautionary measures.

In summary, our findings suggest that the daily collection of rated prodromal symptoms analyzed through ML algorithms is a promising approach to identifying preictal states prior to seizures. A mobile device would allow for long-term monitoring of patients and evaluation of individual seizure prediction.

ACKNOWLEDGMENTS

This study was supported by the program Investissements d'avenir (ANR-10-IAIHU-06) and grants from the Fondation de l'APHP pour la Recherche–Marie-Laure PLV Merchandising. L.C. was supported by an INSERM Poste d'Accueil and grants from the Journées de Neurologie de Langue Française.

CONFLICT OF INTEREST

V.N. reports fees from boards with UCB Pharma, Eisai, LivaNova, and GW Pharma. Neither of the other authors has any conflict of interest to disclose.

ORCID

Louis Cousyn https://orcid.org/0000-0003-1407-5575
Vincent Navarro https://orcid.org/0000-0003-0077-8114

REFERENCES

1. Kuhlmann L, Lehnertz K, Richardson MP, Schelter B, Zaveri HP. Seizure prediction—ready for a new era. Nat Rev Neurol. 2018;14(10):618–30.
2. Besag FMC, Vasey MJ. Prodrome in epilepsy. Epilepsy Behav. 2018;83:219–33.
3. Petitmengin C, Baulac M, Navarro V. Seizure anticipation: are neurophenomenological approaches able to detect preictal symptoms? Epilepsy Behav. 2006;9(2):298–306.
4. DuBois JM, Boylan LS, Shiyko M, Barr WB, Devinsky O. Seizure prediction and recall. Epilepsy Behav. 2010;18(1–2):106–9.
5. Haut SR, Hall CB, Masur J, Lipton RB. Seizure occurrence: precipitants and prediction. Neurology. 2007;69(20):1905–10.
6. Haut SR, Hall CB, Borkowski T, Tennen H, Lipton RB. Clinical features of the pre-ictal state: mood changes and premonitory symptoms. Epilepsy Behav. 2012;23(4):415–21.
7. Haut SR, Hall CB, Borkowski T, Tennen H, Lipton RB. Modeling seizure self-prediction: an e-diary study. Epilepsia. 2013;54(11):1960–7.

8. Maiwald T, Blumberg J, Timmer J, Schulze-Bonhage A. Are prodromes preictal events? A prospective PDA-based study. Epilepsy Behav. 2011;21(2):184–8.
9. Privitera M, Haut SR, Lipton RB, McGinley JS, Cornes S. Seizure self-prediction in a randomized controlled trial of stress management. Neurology. 2019;93(22):e2021–31.
10. Obermeyer Z, Emanuel EJ. Predicting the future—big data, machine learning, and clinical medicine. N Engl J Med. 2016;375(13):1216–9.
11. Pinikahana J, Dono J. The lived experience of initial symptoms of and factors triggering epileptic seizures. Epilepsy Behav. 2009;15(4):513–20.
12. Scaramelli A, Braga P, Avellanal A, Bogacz A, Camejo C, Rega I, et al. Prodromal symptoms in epileptic patients: clinical characterization of the pre-ictal phase. Seizure. 2009;18(4):246–50.
13. Schulze-Bonhage A, Kurth C, Carius A, Steinhoff BJ, Mayer T. Seizure anticipation by patients with focal and generalized epilepsy: a multicentre assessment of premonitory symptoms. Epilepsy Res. 2006;70(1):83–8.
14. Pinikahana J, Dono J. Initial symptoms, precipitant factors, and techniques to control epileptic seizures: the carer's perspective. Epilepsy Behav. 2009;16(3):442–6.
15. Schulze-Bonhage A, Haut S. Premonitory features and seizure self-prediction: artifact or real? Epilepsy Res. 2011;97(3):231–5.
16. Chang C-C, Lin C-J. LIBSVM: a library for support vector machines. ACM Trans Intell Syst Technol. 2011;2(3):1–27.
17. Schölkopf B, Smola AJ. Learning with kernels: support vector machines, regularization, optimization, and beyond. Cambridge, MA: MIT Press; 2002.
18. Fernández A, García S, Galar M, Prati RC, Krawczyk B, Herrera F. Learning from imbalanced data sets. New York, NY: Springer International Publishing; 2018.
19. Santos MS, Soares JP, Abreu PH, Araujo H, Santos J. Cross-validation for imbalanced datasets: avoiding overoptimistic and overfitting approaches. IEEE Comput Intell Mag. 2018;13(4):59–76.
20. Ojala M, Garriga GC. Permutation tests for studying classifier performance. J Mach Learn Res. 2010;11:1833–63.
21. Haut SR, Shinnar S, Moshé SL. Seizure clustering: risks and outcomes. Epilepsia. 2005;46(1):146–9.

SUPPORTING INFORMATION

Additional supporting information may be found online in the Supporting Information section.

How to cite this article: Cousyn L, Navarro V, Chavez M. Preictal state detection using prodromal symptoms: A machine learning approach. *Epilepsia*. 2021;00:1–6. https://doi.org/10.1111/epi.16804

II. Identification des périodes précritiques à l'aide de méthodes de détection d'anomalies appliquées aux symptômes prodromaux

1) Introduction

La période précritique peut être appréhendée comme un état divergeant d'un état basal physiologique, intercritique. Cette conception ouvre la possibilité à de nouvelles méthodes de classification que sont les algorithmes de « détection d'anomalies ».

Cette approche est particulièrement intéressante dans le domaine de la prédiction des crises. Le nombre de crises d'épilepsie étant parfois limité, les observations précritiques peuvent devenir nettement minoritaires par rapport aux données intercritiques. Or, les algorithmes de classification binaires nécessitent un apprentissage – avec une quantité de données suffisantes – sur les deux classes (inter et précritique). Les méthodes de détection d'anomalies ne requièrent cependant les données que d'une seule classe – dans notre cas, les observations intercritiques – afin d'entraîner l'algorithme (Tax et Duin 1999; Schölkopf et al. 2001; Khan et Madden 2014).

Dans cette étude, nous avons : i) considéré les périodes précritiques comme des « anomalies » et ii) évalué plusieurs méthodes de détection d'anomalies afin d'identifier les périodes précritiques.

2) Méthodologie

Nous avons utilisé la base de données décrites dans l'article 1 (Cousyn et al. 2021).

Les *algorithmes de détection d'anomalies* ont été entrainés sur 80% des observations intercritiques et testés sur les 20% restants des données intercritiques et l'ensemble de celles précritiques. Nous avons évalué les performances de prédiction de 4 méthodes différentes :

a) Distance de Mahalanobis ;
b) Nearest Neigbor Data Description (NNDD) ;
c) Support Vector Data Description (SVDD) ;
d) SVM à une classe.

3) Résultats

Tous les modèles ont montré des performances de prédiction pauvres (AUC $\leq$ 0,6) lorsque que l'ensemble des 24 symptômes était utilisé. Nous avons cependant constaté une amélioration significative après sélection automatique des variables les plus discriminantes. Les meilleures performances de prédiction ont été obtenues avec le modèle SVM à une classe (Figure 17), atteignant un AUC de 0,71,

95% IC [0,63-0,79] (Figure 18). Néanmoins, les performances des autres algorithmes restaient similaires, et les vitesses de calcul parfois plus rapides : le NNDD avait un temps CPU 3 à 5 fois plus court et un AUC de 0,68, 95% IC [0,61-0,76].

Cette approche a permis de montrer que les symptômes prodromaux divergents sont associés aux périodes précritiques. Les méthodes de détection d'anomalies sont une alternative intéressante lorsque le nombre de crises est limité, ne permettant pas d'entraîner efficacement un classifieur binaire.

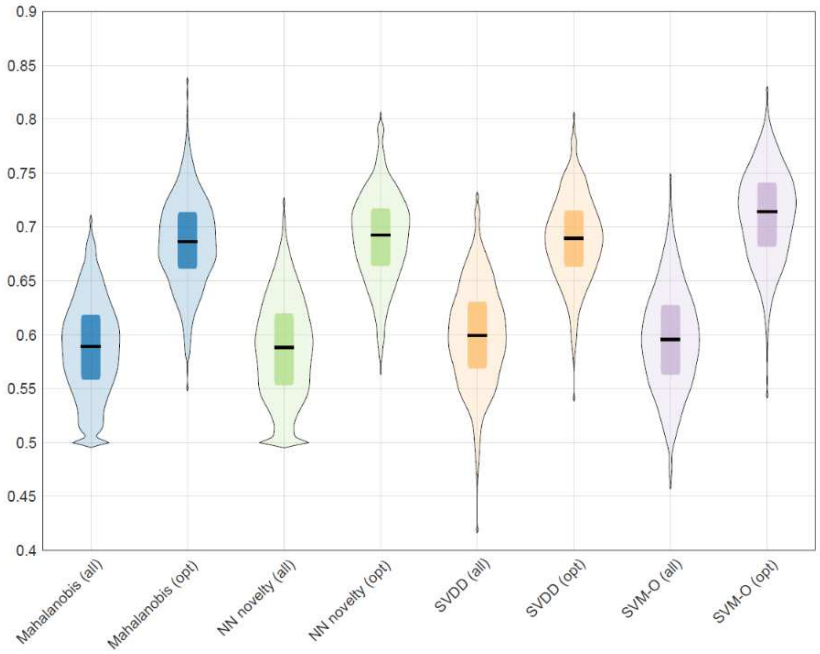

Figure 17 : Comparaison des AUC entre les différentes méthodes de détection d'anomalies
all : ensemble des 24 symptômes ; opt : sélection automatique des variables les plus discriminantes

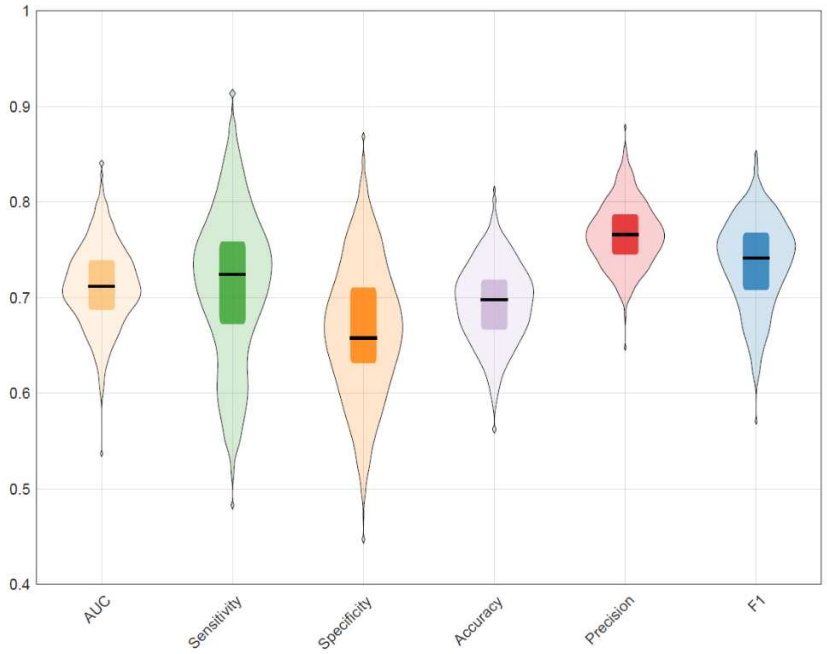

Figure 18 : Performances du modèle SVM à une classe

Article 2 : Outliers in clinical symptoms as preictal biomarkers

Epilepsy Research 177 (2021) 106774

Contents lists available at ScienceDirect

Epilepsy Research

journal homepage: www.elsevier.com/locate/epilepsyres

Short communication

Outliers in clinical symptoms as preictal biomarkers

Louis Cousyn [a,b,*], Vincent Navarro [a,b], Mario Chavez [c]

[a] Paris Brain Institute, Inserm, CNRS, Sorbonne Université, Paris, France
[b] AP-HP, Department of Neurology, Epilepsy Unit, Pitié-Salpêtrière Hospital, Paris, France
[c] CNRS UMR-7225, Pitié-Salpêtrière Hospital, Paris, France

ARTICLE INFO

Keywords:
Epilepsy
Seizure prediction
Prodromal symptoms
Prodromes
Anomaly detection
Machine learning algorithms

ABSTRACT

Previous findings have suggested that a preictal state might precede the epileptic seizure onset, which is the basis for seizure prediction attempts. Preictal states can be apprehended as outliers that differ from an interictal baseline and display clinical changes. We collected daily clinical scores from patients with epilepsy who underwent continuous video-EEG and assessed the ability of several outlier detection methods to identify preictal states. Results from 24 patients suggested that outlying clinical features were suggestive of preictal states and can be identified by statistical methods: AUC = 0.71, 95 % CI = [0.63 – 0.79]; PPV = 0.77, 95 % CI = [0.70 – 0.84]; FPR = 0.31, 95 % CI = [0.21 – 0.44]); and F1 score = 0.74, 95 % CI = [0.64 – 0.81]. Such algorithms could be straightforwardly implemented in a mobile device (e.g., tablet or smartphone), which would allow a longer data collection that could improve prediction performances. Additional clinical – and even multimodal – parameters could identify more subtle physiological modifications.

1. Introduction

Previous findings have suggested that a preictal state might precede the epileptic seizure onset, which is the basis for seizure prediction attempts (Kuhlmann et al., 2018). Identification of specific preictal features remains one of the most challenging aspects in the field of epilepsy. Although most efforts to predict seizures relied on electroencephalographic (EEG) data, an increasing number of studies have focused on the concept of seizure self-prediction (Haut et al., 2007; DuBois et al., 2010; Schulze-Bonhage and Haut, 2011; Mackay et al., 2017; Haut et al., 2013; Privitera et al., 2019). Besides, some clinical symptoms have also been reported as possibly related to preictal states and may precede the seizure by several hours (Schulze-Bonhage et al., 2006). These preictal symptoms, also called premonitory or prodromal symptoms, consist of mood changes, cognitive disturbances, physical symptoms such as headache, tiredness, light/noise sensitivity, etc. (Scaramelli et al., 2009; Haut et al., 2012; Besag and Vasey, 2018).

In a previous study, we highlighted the ability of machine learning models to identify high-risk states for upcoming seizures from clinical features (Cousyn et al., 2021). However, patients often experience a relatively few numbers of days with seizures in comparison with those without seizures. This lack of preictal observations is a major constraint for prediction algorithms, which require sufficient data from both classes (i.e., interictal and preictal) to be properly trained.

Here, we apprehend preictal states as outliers that clinically differ from an interictal baseline and assess the ability of several outlier detection methods – which only require interictal data to train the statistical models – to identify them.

2. Materials and methods

2.1. Clinical evaluation score

We previously reported a daily self-assessment questionnaire with a four-point Likert scale (Cousyn et al., 2021), including 24 clinical features: i) a self-prediction score of seizure, ii) 22 prodromal symptoms, and iii) an anxiety level through the State-Trait Anxiety Inventory form Y-1.

2.2. Patients

Questionnaires were administered every morning to 24 inpatients who underwent continuous video-EEG during the preoperative evaluation of drug-resistant epilepsy (Cousyn et al., 2021). This study was authorized by the French CNIL committee (No. 2211991) and patients were informed about the use of their anonymized data.

* Corresponding author at: Hôpital Pitié-Salpêtrière, 47-83 boulevard de l'Hôpital, 75651, Cedex 13, Paris, France.
E-mail address: louis.cousyn@icm-institute.org (L. Cousyn).

https://doi.org/10.1016/j.eplepsyres.2021.106774
Received 10 July 2021; Received in revised form 26 August 2021; Accepted 20 September 2021
Available online 22 September 2021

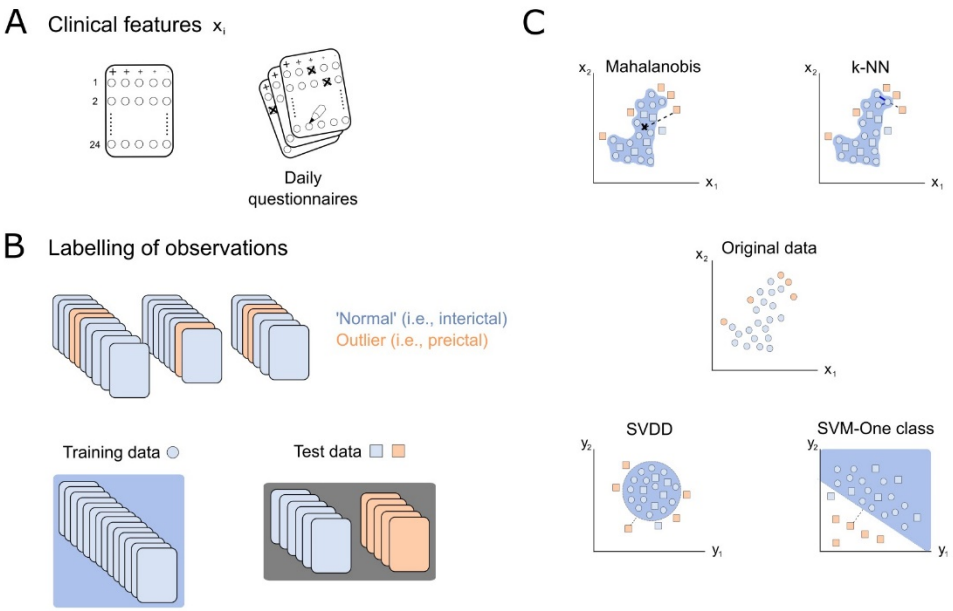

Fig. 1. Overview of the detection of outlying clinical features.
a) Clinical scores are self-reported by patients in daily questionnaires. b) Observations are labelled as those reported the days without seizures (interictal or 'normal' class) and during days with seizures (preictal class). c) For all methods, only interictal observations are used to define the boundary of this normal class. Any point located or mapped outside these boundaries is detected as a preictal outlier.
Abbreviations: k-NN, k-nearest neighbors; SVDD, support vector data description; SVM, support vector machine.

Based on the analysis of video-EEG recordings, questionnaires were divided into: (i) "preictal" observations in case of a seizure occurring in the next 24 h (n = 58), or (ii) "interictal" observations for days without any seizure (n = 190).

2.3. Outlier/anomaly detection methods

We used data from the interictal ("normal") class to train the statistical models so that data from the preictal ("outlying") class were mapped in a different and distant region of the space representation. We applied different outlier (or anomaly) detection methods (Fig. 1 and Supplementary Material):

1 Mahalanobis Distance (MD): an outlier detector that relies on the mean and covariance matrix of the interictal class (Khan and Madden, 2014). The MD-based anomaly score is basically the statistical distance between a test point and the distribution of normal (interictal) data;
2 Nearest Neighbor Data Description (NNDD): a non-parametric method that assumes the local structure of preictal prodromal symptoms (in the original space of representation) is different from that of interictal data (Khan and Madden, 2014). The anomaly score of a point is evaluated by computing the distance to its nearest neighbors in the normal class, normalized by the distances in this local neighborhood;
3 Support vector data description (SVDD): a very robust for modeling non-trivial data, without any prior assumption about the underlying distribution (Tax and Duin, 1999). SVDD uses a transformation (kernel) function to map the interictal data into a high-dimensional feature space where a boundary (a hypersphere covering the points) can be defined. The anomaly score is defined as the distance between a mapped data point and this hypersphere;
4 Support vector machine-one class (SVM-OC): a detector that defines a boundary achieving the maximum separation between the interictal points and the origin (Schölkopf et al., 2001). SVM-OC also applies a kernel transformation such that the decision boundary can enclose the majority of the projected data. For any test point, the anomaly score is defined as the distance to the boundary.

For each outlier detector, a two-step analysis was performed: i) all the 24 clinical features were first used to train/test the statistical model, and then ii) we selected the best features through a pruning procedure to optimize the model (Cousyn et al., 2021) and re-evaluated its performances.

2.4. Prediction performances

We evaluated outlier detectors' performances by developing a cross-validation strategy: for each fold, we first trained detectors on 80 % of interictal observations from all patients (n = 152). The prediction model was then evaluated using the remaining 20 % interictal observations (n = 38) and all the preictal observations (n = 58). This procedure was repeated 1000 times.

Statistical parameters calculated for each fold of cross-validation were: i) the area under the curve (AUC), which summarizes the overall ability of a classifier to discriminate between the two classes and ranges from 0.5 (random) to 1 (perfect classification); ii) the sensitivity, which reflects its ability to identify preictal observations; iii) the specificity, which reflects its ability to identify interictal observations; iv) the positive predictive value (PPV) or precision, which reflects the proportion of correct preictal detections; v) the false positive rate (FPR) that corresponds to the probability of false alarms; and vi) the F1 score that quantifies the trade-off between the PPV and sensitivity.

Table 1
Predictive values of outlying clinical features (median values and 95 % [confidence intervals]).

Clinical features			
1. Self-prediction of seizure	7. Blurred vision	13. Irritability	19. Nausea
2. Trouble concentrating	8. Light sensitivity	14 Anxiety (STAI-Y1)	20. Headache
3. Trouble understanding	9. Noise sensitivity	15. Clumsiness	21. Thirst
4. Trouble speaking	10. Tinnitus	16. Tremor	22. Hunger
5. Trouble reading	11. Hearing impairment	17. Urge to urinate	23. Funny feeling
6. Trouble writing	12. Bad mood	18. Spinning head	24. Fatigue

Prediction models	Mahalanobis distance						NNDD					
	AUC	Specificity	Sensitivity	PPV	FPR	F1	AUC	Specificity	Sensitivity	PPV	FPR	F1
All features	.58 [.5–.67]	.58 [.44–.73]	.62 [.50–.72]	.69 [.62–.77]	.42 [.26–.57]	.66 [.56–.72]	.58 [.50–.67]	.58 [.39–.76]	.6 [.41–.81]	.68 [.62–.76]	.42 [.26–.57]	.64 [.51–.75]
Most relevant features	.68 [.60–.76]	.65 [.54–.70]	.69 [.58–.75]	.76 [.70–.83]	.34 [.21–.45]	.73 [.64–.77]	.68 [.61–.76]	.65 [.52–.81]	.70 [.55–.75]	.75 [.69–.83]	.31 [.18–.47]	.71 [.62–.77]
Prediction models	**SVDD**						**SVM-OC**					
	AUC	Specificity	Sensitivity	PPV	FPR	F1	AUC	Specificity	Sensitivity	PPV	FPR	F1
All features	.6 [.51–.68]	.55 [.39–.76]	.69 [.43–.82]	.68 [.63–.75]	.44 [.25–.60]	.68 [.52–.76]	.60 [.50–.67]	.55 [.39–.71]	.65 [.46–.79]	.69 [.63–.76]	.44 [.26–.58]	.67 [.54–74]
Most relevant features	.69 [.60–76]	.65 [.52–.79]	.70 [.58–.79]	.76 .68	.31 .44	.73 [.65–.78]	**.71 [.63–.79]**	**.72 [.55–.84]**	**.65 [.52–.79]**	**.76 [.70–.83]**	**.34 [.25–.47]**	**.74 [.64–.81]**

Abbreviations: AUC, area under the curve; NNDD, Nearest Neighbor Data Description; SVDD, Support vector data description; SVM-OC, Support vector machine-one class; PPV, positive predictive value; FPR, false positive rate. The most relevant features for the SVM-OC model are: 1, 3, 7, 9, 13, 16 and 24.

3. Results

Our cohort was gender-balanced (13 [54.2 %] females) with a mean age of 35 years (range 22–54 years). Mean seizure frequency was 3.8 seizures (range 0–9) per patient during the hospitalization (mean 10.3 days, range 2–21). Temporal lobe epilepsy was predominant (58.3 % of patients).

All models yielded poor prediction performances when all the 24 clinical features were used (AUCs $\leq$ 0.6; Table 1). Performances were, however, clearly improved by selecting the best variables; in particular, the SVM-OC detector reached good prediction levels (AUC = 0.71, 95 % CI = [0.63 – 0.79]; PPV = 0.77, 95 % CI = [0.70 – 0.84]; FPR = 0.31, 95 % CI = [0.21 – 0.44]); and F1 score = 0.74, 95 % CI = [0.64 – 0.81]).

Considering only preictal observations close to seizures (less than 6 h) or associated with more than one seizure per day did not yield better performances.

4. Discussion

In this study, we found preictal states could be associated with clinical changes that differ from a baseline, i.e. the interictal state. Outlying clinical features were suggestive of a preictal state, which could be identified by outlier detection methods. Although machine learning models trained on both preictal and interictal data provided very good predictions (Cousyn et al., 2021), this approach is highly suitable when preictal observations are less frequent than interictal ones, which is quite a common situation. Our findings suggest that SVM-OC could be the most efficient detector compared to the other algorithms. Nevertheless, other detectors displayed quite similar performances and NNDD also provided faster computations (CPU times were 3–5 times shorter than those in SVM-OC).

It is important to note that our different outlier detectors reached only moderate sensitivities (i.e., preictal state detection) – around 70 %. First, robust identification of outlying clinical states should rely on a large amount of data (Kuhlmann et al., 2018) – which was not achievable in this study. A daily home-based collection of clinical features over a longer period could help increase prediction performances. Second, the selection of the best features was performed through a post-hoc pruning procedure. A prospective study with a larger dataset for parameter optimization would be of interest to reduce the bias of the models. Finally, additional physiological parameters could refine the characterization of preictal-related changes. Autonomic modifications such as heart rate or electrodermal activity could be easily recorded – even at home – using a dedicated wearable device (Kuhlmann et al., 2018; Vieluf et al., 2019). Besides, seizure-precipitating factors (sleep deprivation, menstrual cycles) and circadian rhythms should also be taken into account (Karoly et al., 2017; Baud et al., 2018; Privitera et al., 2019).

A suitable mobile device (e.g., tablet or smartphone) could allow for a long-term and prospective collection of data with real-time analysis. Besides, statistical algorithms could operate on a remote server or directly on the device and be continuously updated with new observations. Another advantage of these prediction algorithms is their easy implementation on any device with an appropriate operating system – including iOS or Android. In addition, one-class classification algorithms require a shorter training – as only interictal observations supply the training database – and can therefore be operational without waiting for a sufficient number of seizures. This could yield a time window for a broad range of therapeutic possibilities, from preventive measures, such as avoiding potentially risky activities, to designing behavioral and/or neurostimulation paradigms that could stop the seizure.

In summary, preictal states may be apprehended as an outlying condition that differs from an interictal baseline and displays clinical changes. Outlier detection methods can highlight these state changes using rated clinical features. Increasing the duration of data collection and the model complexity with additional clinical – and even multimodal – parameters could identify more subtle physiological modifications, which should improve prediction performances.

Declaration of Competing Interest

V. N. reports fees from Boards with UCB Pharma, EISAI, GW Pharma. The remaining authors have no conflicts of interest.

Acknowledgments

This study was supported by the program Investissements d'avenir (ANR-10-IAIHU-06) and grants from the Fondation de l'APHP pour la Recherche (Marie-Laure PLV Merchandising). L.C. was supported by an INSERM "Poste d'Accueil" and grants from the "Journées de Neurologie

de Langue Française".

Appendix A. Supplementary data

Supplementary material related to this article can be found, in the online version, at doi:https://doi.org/10.1016/j.eplepsyres.2021.106774.

References

Baud, M.O., Kleen, J.K., Mirro, E.A., Andrechak, J.C., King-Stephens, D., Chang, E.F., Rao, V.R., 2018. Multi-day rhythms modulate seizure risk in epilepsy. Nat. Commun. 9, 88. https://doi.org/10.1038/s41467-017-02577-y.

Besag, F.M.C., Vasey, M.J., 2018. Prodrome in epilepsy. Epilepsy Behav. 83, 219–233. https://doi.org/10.1016/j.yebeh.2018.03.019.

Cousyn, L., Navarro, V., Chavez, M., 2021. Preictal state detection using prodromal symptoms: a machine learning approach. Epilepsia 62, e42–e47. https://doi.org/10.1111/epi.16804.

DuBois, J.M., Boylan, L.S., Shiyko, M., Barr, W.B., Devinsky, O., 2010. Seizure prediction and recall. Epilepsy Behav. 18, 106–109. https://doi.org/10.1016/j.yebeh.2010.03.011.

Haut, S.R., Hall, C.B., LeValley, A.J., Lipton, R.B., 2007. Can patients with epilepsy predict their seizures? Neurology 68, 262–266. https://doi.org/10.1212/01.wnl.0000252352.26421.13.

Haut, S.R., Hall, C.B., Borkowski, T., Tennen, H., Lipton, R.B., 2012. Clinical features of the pre-ictal state: mood changes and premonitory symptoms. Epilepsy Behav. 23, 415–421. https://doi.org/10.1016/j.yebeh.2012.02.007.

Haut, S.R., Hall, C.B., Borkowski, T., Tennen, H., Lipton, R.B., 2013. Modeling seizure self-prediction: an e-diary study. Epilepsia 54, 1960–1967. https://doi.org/10.1111/epi.12355.

Karoly, P.J., Ung, H., Grayden, D.B., Kuhlmann, L., Leyde, K., Cook, M.J., Freestone, D. R., 2017. The circadian profile of epilepsy improves seizure forecasting. Brain 140, 2169–2182. https://doi.org/10.1093/brain/awx173.

Khan, S.S., Madden, M.G., 2014. One-class classification: taxonomy of study and review of techniques. Knowl. Eng. Rev. 29, 345–374. https://doi.org/10.1017/S026988891300043X.

Kuhlmann, L., Lehnertz, K., Richardson, M.P., Schelter, B., Zaveri, H.P., 2018. Seizure prediction — ready for a new era. Nat. Rev. Neurol. 14, 618–630. https://doi.org/10.1038/s41582-018-0055-2.

Mackay, M., Mahlaba, H., Gavillet, E., Whittaker, R.G., 2017. Seizure self-prediction: myth or missed opportunity? Seizure 51, 180–185. https://doi.org/10.1016/j.seizure.2017.08.011.

Privitera, M., Haut, S.R., Lipton, R.B., McGinley, J.S., Cornes, S., 2019. Seizure self-prediction in a randomized controlled trial of stress management. Neurology 93, e2021–e2031. https://doi.org/10.1212/WNL.0000000000008539.

Scaramelli, A., Braga, P., Avellanal, A., Bogacz, A., Camejo, C., Rega, I., Messano, T., Arciere, B., 2009. Prodromal symptoms in epileptic patients: clinical characterization of the pre-ictal phase. Seizure 18, 246–250. https://doi.org/10.1016/j.seizure.2008.10.007.

Schölkopf, B., Platt, J.C., Shawe-Taylor, J., Smola, A.J., Williamson, R.C., 2001. Estimating the support of a high-dimensional distribution. Neural Comput. 13, 1443–1471. https://doi.org/10.1162/089976601750264965.

Schulze-Bonhage, A., Haut, S., 2011. Premonitory features and seizure self-prediction: artifact or real? Epilepsy Res. 97, 231–235. https://doi.org/10.1016/j.eplepsyres.2011.09.026.

Schulze-Bonhage, A., Kurth, C., Carius, A., Steinhoff, B.J., Mayer, T., 2006. Seizure anticipation by patients with focal and generalized epilepsy: a multicentre assessment of premonitory symptoms. Epilepsy Res. 70, 83–88. https://doi.org/10.1016/j.eplepsyres.2006.02.001.

Tax, D.M.J., Duin, R.P.W., 1999. Support vector domain description. Pattern Recognit. Lett. 20, 1191–1199. https://doi.org/10.1016/S0167-8655(99)00087-2.

Vieluf, S., El Atrache, R., Hammond, S., Touserkani, F.M., Loddenkemper, T., Reinsberger, C., 2019. Peripheral multimodal monitoring of ANS changes related to epilepsy. Epilepsy Behav. 96, 69–79. https://doi.org/10.1016/j.yebeh.2019.02.018.

Supplementary Material for the manuscript: Outliers in clinical symptoms as preictal biomarkers

L. Cousyn[a], V. Navarro[a,b], M. Chavez[c]

[a] *Sorbonne Université, INSERM-U1127. Institut du Cerveau. F-75013 Paris, France*
[b] *Epilepsy Unit, Clinical Neurophysiology Department, AP-HP, Hôpital de la Pitié-Salpêtrière, F-75013, Paris, France.*
[c] *CNRS UMR-7225, Hôpital de la Pitié-Salpêtrière. F-75013 Paris, France.*

Abstract

Here we provide further details about the different anomaly detection methods and prediction assessment metrics used in our manuscript "Outliers in clinical symptoms as preictal biomarkers". We also provide Data and Code Availability Statements

1. Anomaly Detection Methods

1.1. Mahalanobis Distance (MD)

This is a popular unsupervised learning approach to detect outliers [Khan and Madden, 2014]. MD anomaly detection algorithm models the target class as a simple Gaussian distribution. The MD-based anomaly score δ is basically the distance between a test point $\mathbf{x}_i$ and the distribution of normal data in the original the input space given by:

$$\delta_i = (\mathbf{x}_i - \boldsymbol{\mu})^\intercal \Sigma^{-1} (\mathbf{x}_i - \boldsymbol{\mu})$$

where $\boldsymbol{\mu}$ and Σ denote the mean and covariance matrix of the normal class, respectively. At each fold of the cross-validation procedure, $\boldsymbol{\mu}$ and Σ are estimated from the training dataset.

1.2. Nearest Neighbour Data Description (NNDD)

This methods assumes that the local structure of preictal symptoms (in the original space of representation) is different to that of interictal data. In the NNDD method [de Ridder et al., 1998, Khan and Madden, 2014], a test object $\mathbf{x}_i$ is accepted as a member of target class provided that its local density is greater than or equal to the local density of its nearest neighbour in the learning interictal set $NN(\mathbf{x}_i, k)$. The anomaly score computed is simply the ratio between two distances: the distance between the test object $\mathbf{x}_i$ and its k^{th} nearest neighbours in the learning set; and the distance between these nearest points and their k^{th} nearest neighbours. Formally:

$$\delta(\mathbf{x}_i, k) = \frac{d(\mathbf{x}_i, NN(\mathbf{x}_i, k))}{d(NN(\mathbf{x}_i, k), NN(NN(\mathbf{x}_i, k), k))}$$

where $d(x, y)$ denotes the Euclidean distances between objects x and y. Although different numbers of nearest neighbours can be considered (increasing k will decrease the local sensitivity of the method, but it will make it less sensitive to noise), we set $k = 5$ after a cross-validation procedure.

1.3. Support Vector Data Description (SVDD).

This method is a very popular machine learning technique used as outlier or novelty detector for a variety of applications [Tax and Duin, 1999]. In SVDD, the support vector model is trained on data that has only one class, which represents the *normal* or *target* class. This model learns a decision boundary around the target class by fitting a non-linearly transformed hypersphere with minimal volume, such that it encloses almost all points with the minimum radius $R \gg 0$. The method minimises the following error:

$$\mathcal{E}(R, \mathbf{a}, \boldsymbol{\xi}) = R^2 + C \sum_i \boldsymbol{\xi_i}$$

subject to the constraints

$$\|\mathbf{y_i} - \mathbf{a}\|^2 \leqslant R^2 + \boldsymbol{\xi_i}, \quad \boldsymbol{\xi_i} \geqslant 0, \quad \forall i = 1, \ldots, n$$

where R is the radius of the hypersphere, $\mathbf{a}$ is the center of the hypersphere, $\boldsymbol{\xi_i}$ are slack variables allowing training observations $\mathbf{a}$ to fall outside the SVDD boundary, and C is a penalty parameter that governs the trade-off between the size of the sphere and the number of outliers (if $C \geqslant \frac{1}{2}$ all points are ensured to be enclosed). Here, we have set $C = 0.9$. The formulation of SVDD leads to a quadratic programming problem that can be solved by different optimization methods. More details on the algorithmic aspects of SVDD can be found in [Tax and Duin, 1999]. The Support Vector Data Description (SVDD) toolbox used here, and described in § *Data and code availability*, implicitly uses the Matlab function `quadprog` as a solver for the resulting objective functions.

Like traditional Support Vector Machines (SVM), a SVDD firstly uses a nonlinear transformation function defined by a kernel function to project the original data $\mathbf{x_i}$ into a higher dimensional space $\mathbf{x_i} \mapsto \phi(\mathbf{x_i})$. To guarantee the existence of a decision boundary we have used here a Gaussian kernel:

$$k(\mathbf{x_i}, \mathbf{x_j}) = \exp^{\|\mathbf{x_i} - \mathbf{x_j}\|^2 / \sigma}. \tag{1}$$

where $\mathbf{x_i}$ and $\mathbf{x_j}$ denote two feature vectors and the parameter σ is set to be the median pairwise distances among training points [Fukumizu et al., 2009].

The anomaly score δ of a test point $\mathbf{x}_i$ is defined as the distance between the corresponding mapped point $\mathbf{y}_i$ and the target boundary (the hypersphere). At each fold of the cross-validation procedure, the hypersphere radius R is estimated from the learning dataset. The SVDD rejects a given test point as preictal if it falls outside the hypersphere defined over the interictal observations.

1.4. Support vector machine-one class (SVM-OC)

SVM-OC is an anomaly detector also based on SVM models that attempts to learn a decision boundary that achieves the maximum separation between the points of the normal class and the origin [Schölkopf et al., 2001]. SVM-OC separates the training data from the origin by the mean of a separating hyperplane at a distance ρ. To do this, the method minimises the following error:

$$\mathcal{E}(\mathbf{w}, \rho, \boldsymbol{\xi}) = \frac{1}{2}\|w\|^2 + \frac{1}{\nu n}\sum_i \boldsymbol{\xi_i} - \rho$$

subject to the constraints

$$\langle \mathbf{w}, \phi(\mathbf{x_i}) \rangle \geqslant \rho - \boldsymbol{\xi}, \quad \boldsymbol{\xi_i} \geqslant 0, \quad \forall i = 1, \ldots, n$$

where $\mathbf{w}$ is is the normal vector of the hyperplane, $\boldsymbol{\xi_i}$ are also slack variables that are used to model the separation errors, and $\nu \in (0, 1]$ is a parameter that controls the effect of outliers i.e. the hardness or softness of the boundary around the data. This parameter ν can be compared with the parameter C used in the SVDD.

The fitting of SVM-OC models needs to solve a convex programming problem with linear constraints. This so-called quadratic programming problem was solved here by the sequential minimal optimization algorithm [Platt, 1998], implemented in the Matlab function `svmtrain` of the open-source machine learning library LIBSVM (described in § *Data and code availability*).

SVM-OC also uses a Gaussian kernel function to project the data into a higher dimensional space. At each fold of the cross-validation procedure, the anomaly score δ of a test data $\mathbf{x}_i$ is defined as the distance between a mapped point $\mathbf{y}_i$ and the hyperplane defined over the training interictal observations. The SMV-OC rejects a given test point as preictal if this distance is less than ρ.

2. Performance metrics of prediction

Detection performance was measured by different attributes. The following metrics were computed by applying a cross validation, excluding the learning period in the classification:

1. The area under the curve (AUC) of the receiver operating characteristic (ROC). ROC curves represent a sensitivity/specificity pair corresponding to a particular decision threshold. The area under the ROC curves (AUC) summarises the overall ability of a classifier to discriminate between the two classes and ranges from 0.5 (random classification) to 1 (perfect classification)
2. Sensitivity evaluates the proportion of true positives that are correctly predicted. It shows how good the test is at identifying preictal symptoms. It is defined as the ratio $^{\mathrm{TP}}/_{(\mathrm{TP+FN})}$.

3. Specificity is the proportion of the true negatives correctly predicted. The ratio $^{TN}/_{(TN+FP)}$ quantifies how good the test is at identifying normal condition (interictal symptoms).
4. Positive Predictive Value (PPV), or precision, reflects the proportion of correct preictal detections. It was calculated as $^{TP}/_{(TP+FP)}$.
5. False Positive Rate (FPR) corresponds to the probability of false alarms. It is defined as $^{FP}/_{(FP+TN)}$.
6. F1 score is a measure of accuracy that represents the trade-off between the precision and sensitivity, defined as the ratio $^{TP}/_{(TP+0.5(FN+FP))}$

In metrics 2-6, TP and TN denote the correctly classified preictal and interictal symptoms, respectively. FP and FN stand by incorrectly classified interictal and preictal observations, respectively.

3. Data and code availability.

Data: Datasets analysed during the current study are not publicly available due to the patient consents and restrictions of the ethics protocol to protect the privacy of patient involved in the study.

Codes: The Support vector machine-one class (SVM-OC) algorithm is implemented in the open source toolbox LIBSVM, which is freely available at `https://www.csie.ntu.edu.tw/~cjlin/libsvm/`.

The Support Vector Data Description (SVDD) toolbox is freely available at `https://github.com/iqiukp/Support-Vector-Data-Description-SVDD`.

Matlab codes used for ROC-based performance analyses is also available online at `https://www.mathworks.com/matlabcentral/fileexchange/52442-roc-curve`.

Data description Matlab toolbox with the MD, NNDD and SVDD algorithms is available at (copy the address without spaces) `https://www.tudelft.nl/ewi/over-de-faculteit/afdelingen/intelligent-systems/pattern-recognition-bioinformatics/pattern-recognition-bioinformatics/data-and-software/dd-tools`.

All other codes used in this study are available from the corresponding author upon reasonable request.

References

de Ridder D., et al., 1998. An experimental comparison of one-class classification methods, in: *Proceedings of the Fourth Annual Conference of the Advanced School for Computing and Imaging, ASCI'98, Delft, The Netherlands*, pp. 213–218.

Fukumizu K., et al., 2009. Kernel choice and classifiability for RKHS embeddings of probability distributions, in: *Advances in Neural Information Processing Systems*, 22, 1750-1758.

Khan S. S. and Madden M.G., 2014. One-class classification: taxonomy of study and review of techniques. *Knowl. Eng. Rev.* 29, 345–374.

Platt J., 1998. Fast training of support vector machines using sequential minimal optimization, in: *Advances in Kernel Methods –Support Vector Learning*, edited by B. Schölkopf, C. Burges, A. Smola. MIT-Press, Cambridge, Massachusetts.

Schölkopf B., et. al., 2001. Estimating the support of a high-dimensional distribution. *Neural computation* 13, 1443–1471.

Tax D. M. J. and Duin R. P. W., 1999. Support vector domain description. *Pattern Recognit. Lett.* 20, 1191–1199.

III. Évaluation prospective en condition de vie réelle : application mobile Epiday et étude clinique future

1) Introduction

Les résultats de nos deux premières études, renforcés par le dépôt européen et international d'un brevet, nous ont incités à proposer une évaluation des symptômes prodromaux en condition de vie réelle. En effet, l'identification de jours à risque de crise semble envisageable à l'aide d'auto-questionnaires analysés par des algorithmes d'apprentissage automatique, mais les données de nos deux études ont été acquises chez des patients hospitalisés et enregistrés en vidéo-EEG continu.

Nous avons ainsi sollicité l'équipe de développement du département informatique de l'Institut du Cerveau (Clément Rousseau, Séverine Candelier, Mathilde Lannes et Arnaud Couchet), afin de créer une application mobile « Epiday », à destination des patients atteints d'épilepsie. Ce projet a été soutenu par le Département Médico-Universitaire (DMU) Neurosciences de l'Assistance Publique – Hôpitaux de Paris (AP-HP) – Sorbonne Université, et de l'Inserm Transfert (programme CoPoc).

Notre objectif est de mettre en place un outil accessible à un grand nombre de patients permettant d'évaluer quotidiennement, en ambulatoire, les symptômes prodromaux et d'identifier des jours à risque de crise.

2) Architecture du système Epiday

- Interface mobile disponible sur iOS et Android (Figure 19)

L'application Epiday est un véritable « passeport » de l'épilepsie pour les patients, permettant :

- De définir leur épilepsie et leurs différents types de crises (« petites », « moyennes » et « grosses » crises) ;
- De référencer leurs traitements antiépileptiques et leurs posologies ;
- De signaler les crises, en précisant leur type (préalablement référencé) et les éventuels facteurs favorisants ;
- De consulter l'historique des crises ;
- Et enfin, de collecter quotidiennement plusieurs prodromes et facteurs favorisants (sommeil, stress, etc.) à l'aide d'échelles visuelles.

Figure 19 : Interface mobile Epiday

L'application mobile permet au patient de référencer son type d'épilepsie, ses types de crises et ses traitements antiépileptiques, ainsi de tenir un agenda des crises. Les symptômes prodromaux sont évalués par des échelles visuelles.

- Serveurs

Les données remplies par le patient sur l'interface mobile sont ensuite hébergées sur des serveurs. La communication entre l'interface mobile et les serveurs se fait via une API (Application Programming Interface). Les serveurs, agréés pour l'hébergement de données de santé, assurent les fonctions de :

- Stockage des informations sur une base de données ;
- Calcul via les modèles d'apprentissage automatique (entraînement puis prédiction).

- Interface web administrateur

Elle permet aux investigateurs de l'étude d'accéder aux données, de consulter et modifier les informations enregistrées par les patients sur l'interface mobile, et de visualiser les résultats.

Pour un patient donné, on peut ainsi visualiser (Figure 20) :

- L'administration des traitements antiépileptiques et les modifications de posologie au cours du temps ;
- La répartition nycthémérale et mensuelle des crises ;
- Le pourcentage de participation aux échelles visuelles.

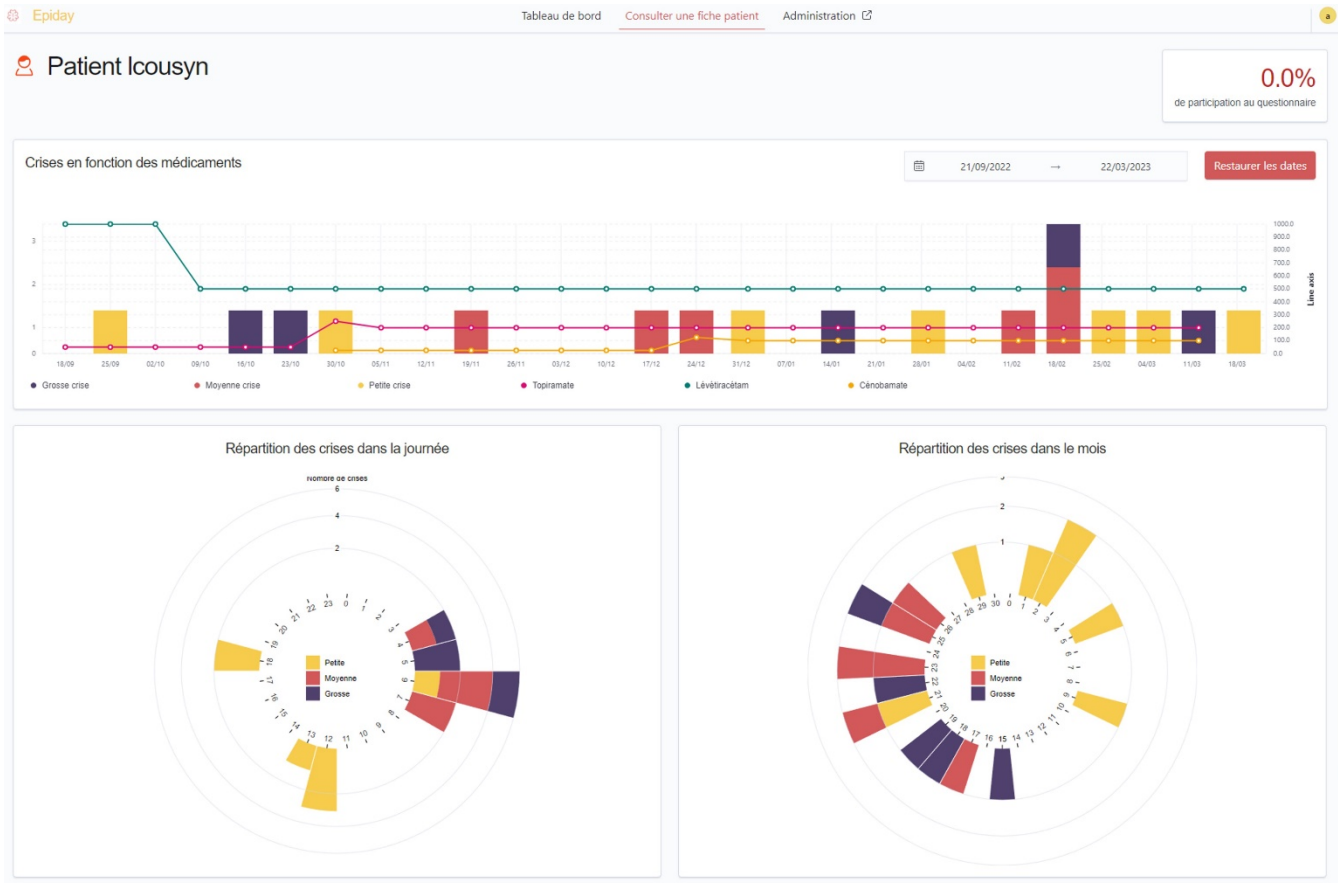

Figure 20 : Visualisation des données patient sur l'interface web d'Epiday
Suivi au cours du temps des crises d'épilepsie et des modifications de traitements antiépileptiques (en haut) ; visualisation de la répartition nycthémérale (en bas à gauche) et mensuelle (en bas à droite) des crises.

Les performances du modèle de prédiction pourront également être représentées, de manière globale sur l'ensemble des patients et individuellement (Figure 21).

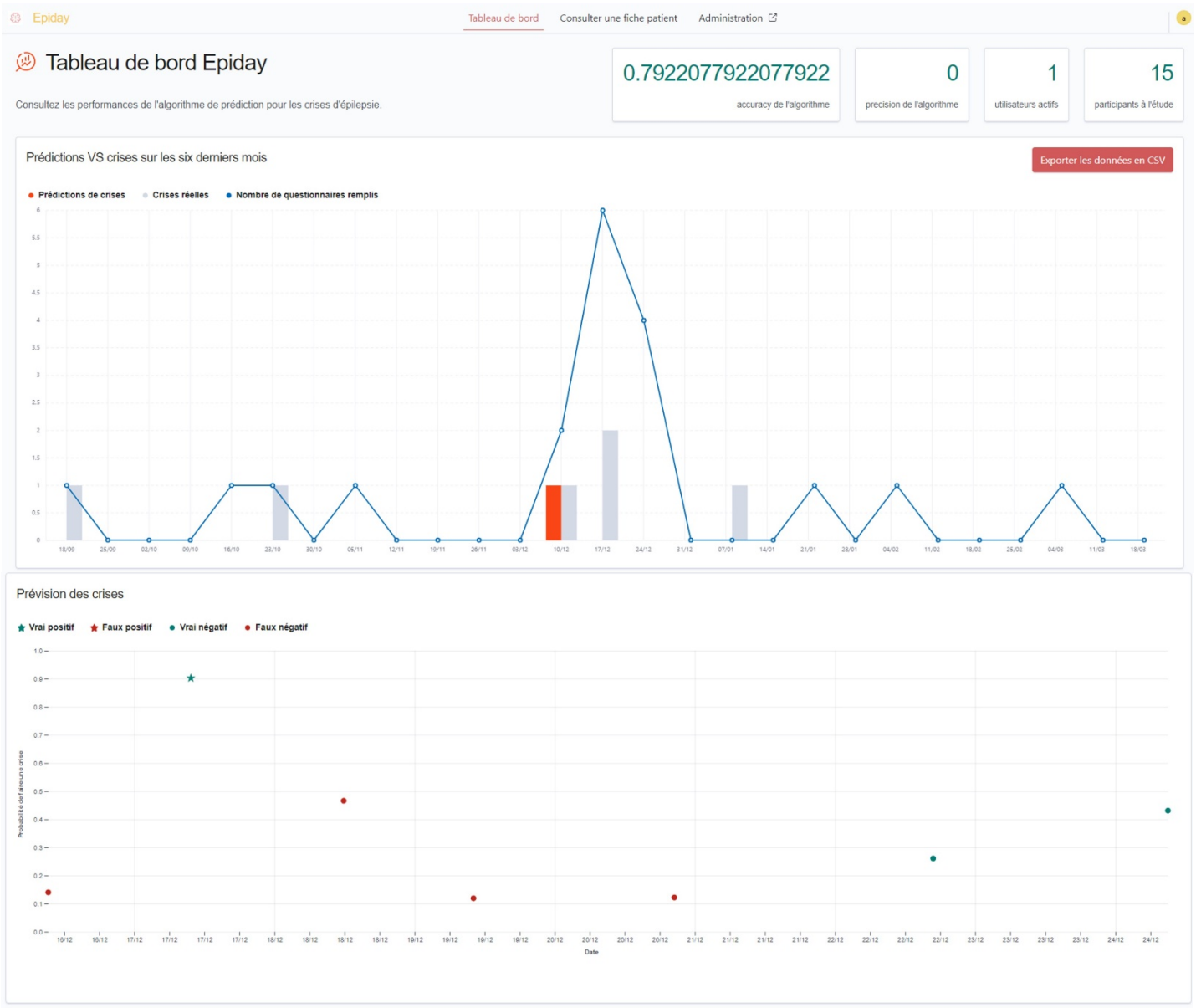

Figure 21 : Visualisation des performances de prédiction
L'interface web permet de représenter sur une échelle de temps le nombre de crises réelles et celui de crises prédites (en haut). Pour chaque prédiction, on peut aussi les représenter en vert (vrai positif ou négatif) ou en rouge (faux positif ou négatif ; en bas).

3) Mise en place d'une étude clinique

L'application mobile, le serveur informatique et l'interface administrateur étant opérationnels, nous souhaitons désormais tester les performances d'Epiday, et ce dans la cadre d'une étude clinique prospective (Loi Jardé 3), en cours de mise en place sous promotion AP-HP.

Les objectifs de cette étude sont :

- Évaluer les performances de prédiction quotidienne du risque de crise de l'application Epiday chez des patients atteints d'une épilepsie pharmaco-résistante ;
- Et, secondairement :
    i. Analyser les cycles (circadiens et multidiens) de crises sur de longues périodes
    ii. Analyser l'adhésion et le niveau de satisfaction de ce nouvel outil chez les patients

Nous ciblons un nombre de 50 patients à inclure, avec les critères suivants :

- Critères d'inclusion :
    - Patients âgés de 18 à 65 ans
    - Épilepsie diagnostiquée depuis au moins 18 mois
    - Imagerie excluant une étiologie d'épilepsie d'aggravation progressive
    - EEG en faveur du diagnostic d'épilepsie au cours des 10 dernières années précédant la sélection
    - Au moins 1 crise par mois
- Critères d'exclusion
    - Antécédents de crises non épileptiques d'origine psychogène
    - Crises non motrices et sans composante observable isolées.

Le suivi prospectif nécessitera l'utilisation quotidienne de l'application mobile sur une période d'au moins 3 mois. La durée de recrutement des patients sera de 2 ans.

Une page d'information sera à disposition des patients sur l'interface mobile (Figure 22). Cette page, en complément des explications données par l'investigateur, a pour but de leur réexpliquer les grands principes de l'étude, la nécessité de remplir quotidiennement les échelles visuelles et de tenir à jour l'agenda des crises. Nous espérons ainsi sensibiliser les patients au besoin de collecter suffisamment de données afin d'entraîner les algorithmes d'apprentissage automatique et générer des prédictions optimales.

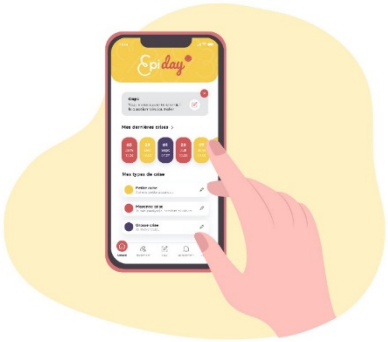

Un suivi quotidien de votre épilepsie

Chaque jour, remplissez des échelles visuelles décrivant au mieux votre état actuel.
Mettez scrupuleusement à jour votre agenda des crises.

Un flux de données sécurisé de A à Z

Les données, anonymes, sont envoyées de votre téléphone vers un serveur sécurisé où seront réalisés les calculs de prédiction. Le médecin peut consulter vos données sur une interface dédiée.

Identification personnalisée des jours à risque de crise

Notre objectif est d'identifier, à l'aide des échelles visuelles quotidiennes, un état qui serait plus à risque de crise d'épilepsie.

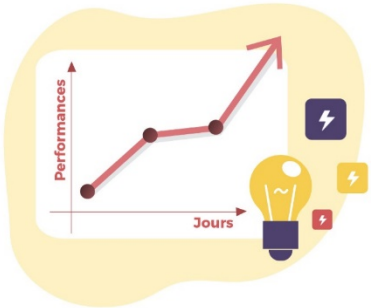

De la régularité pour améliorer les prédictions

Les prédictions se basent sur les données que vous aurez enregistrées. Plus le remplissage des échelles visuelles et de l'agenda des crises sera régulier, au mieux nous pourrons élaborer une prédiction.

Accéder facilement à vos résultats

Vous aurez accès à votre profil personnalisé d'épilepsie : fréquence et types de crises par semaine/mois, périodes « à risque », facteurs favorisant vos crises, etc.

Figure 22 : Page d'information à destination des patients sur l'interface mobile

PARTIE 2. ÉTUDE DE LA VARIABILITE DE LA FREQUENCE CARDIAQUE DURANT LA PERIODE PRECRITIQUE

I. Introduction

La variabilité de la fréquence cardiaque (VFC) ou *heart rate variability* (HRV) reflète l'équilibre entre les deux composantes – sympathique et parasympathique – du système nerveux autonome. Elle correspond aux variations temporelles (en millisecondes) entre deux battements cardiaques, et plus précisément entre deux ondes R consécutives – ou intervalle RR. Alors qu'une prépondérance de la composante sympathique a été décrite durant les crises d'épilepsie, la stimulation du nerf vague (parasympathique) est une stratégie thérapeutique antiépileptique (Myers et al. 2018).

L'identification d'états précritiques, ainsi que des modèles de prédiction des crises, sur la base de la VFC ont montré de bons résultats (Kolsal et al. 2014; Fujiwara et al. 2016; Billeci et al. 2018; Giannakakis et al. 2019).

Dans cette étude, nous avons fait l'hypothèse qu'un déséquilibre du système nerveux autonome, qui peut être estimé par la VFC, pourrait refléter un état « pro »-critique. Nous avons donc évalué les capacités de la VFC durant un protocole de repos quotidien à identifier un état à risque de crise.

II. Méthodologie

Nous avons mis en place un *protocole de repos* standardisé chez les patients hospitalisés pour enregistrement continu EEG intracérébral, dans le cadre du bilan préchirurgical d'une épilepsie focale pharmacorésistante. Le protocole se déroulait comme suit :

- Contrôle préalable de la qualité des signaux ;
- Extinction des sources de stimulation extérieures (téléphone, télévision, radio, etc.) ;
- Débranchement des appareils sur secteur pouvant créer des artefacts (ordinateur, téléphone, lit électrique, etc.) ;
- Le patient avait pour consignes de :
    - Rester calme et immobile autant que possible ;
    - Rester éveillé, les yeux ouverts ;

  - Regarder en direction d'un écran gris et d'éviter les mouvements oculaires brusques et amples ;
  - Éviter tout mouvement ou pensée de nature répétitive (taper du doigt, compter, etc.).
- Enregistrement quotidien entre 10 et 12h du matin ;
- Durée de 10 minutes.

Nous avons réalisé des enregistrements ECG quotidiens de 10 minutes chez 22 patients hospitalisés dans le cadre d'une exploration EEG intracérébrale. Nous avons extrait *31 caractéristiques de la VFC* – issues du domaine temporel et fréquentiel, et d'analyses non-linéaires – sur des fenêtres glissantes de 2 minutes. Chaque fenêtre glissante était ensuite classée en i) précritique, si une crise électro-clinique survenait dans les 24h suivantes, ou ii) intercritique, en l'absence de crise.

Nous avons tout d'abord utilisé un algorithme de classification de type SVM afin d'évaluer les performances de distinction entre les enregistrements inter et précritiques. Une validation croisée « leave-one-day out » a été réalisée : pour chaque itération, un enregistrement de chaque classe était – au hasard – attribué à la phase de test afin qu'il n'y ait pas de fuite d'information entre les jeux de données d'apprentissage et de test. Nous avons ensuite évalué chronologiquement ou de manière « pseudoprospective », les prévisions probabilistes quotidiennes du risque de crise.

III. Résultats

Parmi les 22 patients inclus, seules les données de 15 ont pu être analysées. Pour les 7 exclus, les données étaient insuffisantes, de mauvaise qualité, ou des troubles du rythme ou de la conduction cardiaque étaient rapportés.

Notre première approche de classification standard a montré de mauvaises performances (AUC médian 0,5 [0,41;0,64]) mais qui étaient considérablement améliorées après sélection automatique des variables les plus informatives : AUC 0,75 [0,68;0,99]. Les prévisions probabilistes quotidiennes ont obtenu un score de Brier médian de 0,3 [0,18;0,48]. Sur les 25 jours précritiques, 15 (60%) ont été correctement prédits. Le taux de faux positifs était de 9/37 (24.3%).

Notre approche a montré des performances de classification meilleures que le hasard après sélection automatique des variables. Les prévisions quotidiennes étaient globalement correctes mais le taux important de faux négatifs (40%) – et par conséquent une sensibilité moyenne – nécessite des ajustements avant de considérer toute application clinique. Una approche multimodale serait intéressante.

Cette étude sera bientôt soumise à publication dans une revue scientifique à comité de lecture.

IV. Article 3 : Can heart rate variability identify a high-risk state of upcoming seizure?

Authors

Louis Cousyn[a,b,*], MD, Fedele Dono[c], MD, Vincent Navarro[a,b], MD, PhD, Mario Chavez[d], PhD

[a] Paris Brain Institute (Inserm, CNRS, Sorbonne Université), Paris, France

[b] AP-HP, Department of Neurology, Epilepsy Unit, Pitié-Salpêtrière Hospital, Paris, France

[c] Department of Neuroscience, Imaging and Clinical Sciences, University of Studies G. d'Annunzio Chieti and Pescara Chieti, Italy

[d] CNRS UMR-7225, Pitié-Salpêtrière Hospital, Paris, France

[*] Correspondence to Dr. Louis Cousyn, Hôpital Pitié-Salpêtrière, 47-83 boulevard de l'Hôpital, 75651 Paris Cedex 13, France.

Email: louismarc.cousyn@aphp.fr

Phone: +331 42 16 18 01

ORCID numbers:

Louis Cousyn: 0000-0003-1407-5575

Fedele Dono: 0000-0003-3575-2942

Vincent Navarro: 0000-0003-0077-8114

Mario Chavez: 0000-0003-0390-4833

Abstract

Heart rate variability (HRV) is an accessible and convenient means to assess the sympathetic/parasympathetic balance. Autonomic dysfunctions may reflect a pro-ictal state and occur before the seizure onset. Previous studies have reported HRV-based models to identify preictal states in continuous monitoring. Here, we evaluated the ability of HRV metrics extracted from daily resting-state periods to individualize states at risk of seizure using prediction algorithms. Daily standardized 10-min vigilance-controlled ECG periods were recorded in patients with drug-resistant focal epilepsy who underwent intracerebral EEG. Results from 15 patients suggest that HRV features can identify preictal states with a median AUC of 0.75 [0.68;0.99]. Pseudoprospective daily forecasts yielded a median Brier score of 0.3 [0.18;0.48]. About 60% of preictal days were correctly forecasted, while false positive predictions were noticed in 24% of interictal days. Daily resting HRV seems to capture information about autonomic variations that may reflect a pro-ictal state. The method could be embedded in an ambulatory clinical seizure prediction device, but additional modalities (prodromes, EEG-based features, etc.) should be associated to improve its performances.

Keywords: heart rate variability; autonomic nervous system; epilepsy; seizure forecast; seizure prediction

Highlights

- HRV features from resting state can discriminate between interictal/preictal states
- Daily pseudoprospective forecasts of preictal states yielded fair overall results
- Sensitivity of seizure prediction should be increased
- Multimodal features could improve our model performances
- This approach could be embedded in an ambulatory clinical device

Introduction

Ictal but also interictal autonomic nervous system dysfunctions have been reported, particularly in patients with drug-resistant and temporal lobe epilepsy (Lotufo et al., 2012; Sivathamboo and Perucca, 2021). Heart rate variability (HRV) is an accessible and convenient means to assess sympathetic/parasympathetic dynamics. It refers to time variations between consecutive heartbeats, i.e., the RR interval. While a shift toward sympathetic activity has been described during seizures, stimulation of the vagus nerve, the main component of the parasympathetic nervous system can be used as an antiseizure therapy (Myers et al., 2018).

Some studies have highlighted preictal heart rate changes, especially an increase several seconds or a few minutes before the seizure onset (Bruno et al., 2018). Indeed, modifications in HRV have helped identify preictal states (Leal et al., 2021; Meisel and Bailey, 2019), and some HRV-based seizure prediction models yielded a sensitivity of 89-91% on continuous monitoring (Billeci et al., 2018; Fujiwara et al., 2016; Giannakakis et al., 2019; Kolsal et al., 2014; Myers et al., 2018).

In a recent study, we highlighted that resting-state intracranial EEG connectivity, obtained during short vigilance-controlled periods, can forecast the daily risk of upcoming seizures (Cousyn et al., 2022). We assume that autonomic dysfunctions – which could be assessed by HRV – may also reflect a pro-ictal state and occur before the seizure onset. Here, we evaluated the ability of HRV features extracted from daily resting-state recordings to individualize states at risk of seizure using prediction algorithms.

Materials and Methods

- Patients

Patients with drug-resistant focal epilepsy underwent daily resting-state recordings during their stay for presurgical intracerebral EEG (Ad-Tech® depth electrodes), from January 15, 2019, to July 15, 2022, in the Epilepsy Unit of the Pitié-Salpêtrière University Hospital (Paris, France). All patients gave written informed consent (project C11-16 and C19-55, conducted by INSERM), and an institutional review board (CPP Paris VI and Sud Méditerranée 1) approved the study.

- Recordings

A daily 10-min resting-state protocol was performed between 10 and 12 am. Patients were asked to keep seated, calm, and awake, without repetitive movements or thoughts. External sources of stimulation were systematically turned off (phone, TV, etc.). Patients were simultaneously recorded by iEEG, which is the gold standard to identify electrical seizures. iEEG and electrocardiogram (ECG) signals were recorded after visual quality control.

- HRV measures

RR intervals were first extracted from ECG data. Then, we applied linear and nonlinear HRV measures on 2-min overlapping windows (100-second overlaps) during each 10-min resting-state period. To clean and detect the R peaks of each segment, the Pan-Tompkins QRS detection algorithm was used (Pan and Tompkins, 1985). Thirty-one HRV features including time-domain, frequency-domain, and nonlinear features were computed (Table 1). Only the RR intervals between adjacent, normal and dominant beats were used to compute the HRV features. Segments with less than 100 heartbeats were discarded.

- Classification algorithms

For each patient, we trained SVM classifiers to distinguish between 'interictal' (i.e., no seizure in the next 24 hours) and 'preictal' recordings (i.e., at least one electro-clinical seizure in the next 24 hours) (Figure 1). To avoid any bias, we removed adjacent epochs from training and test sets. To do this, we applied a leave-one-day-out cross-validation: for each fold, one random daily period was removed from the learning dataset and assigned to the testing dataset; each fold randomly used 80% of the 2-min epochs to train and the remaining 20% to test the model; this procedure was repeated 1,000 times. We performed a two-class SVM classifier if at least two days were available from both classes (interictal/preictal), and a one-class SVM classifier if a single daily period was available for any class.

In the SVM models, a Gaussian kernel was applied with the width parameter γ set to the median pairwise distances among training points. We prevented class imbalance-related bias by oversampling data from the minority class using the Synthetic-Minority-Over-sampling-TEchnique (SMOTE) (Liu et al., 2014).

- Daily forecasts

We performed a pseudoprospective approach to evaluate the accuracy of daily forecasts. The model was trained to distinguish between both classes based on the first chronological daily periods that included at least one recording from each class. A Platt scaling was then applied to transform the output of classification models into a probability distribution over classes. For each new daily recording, we obtained a probability of belonging to the preictal state, i.e., the seizure likelihood, by averaging the predicted probability over all tested segments. The accuracy of these probabilistic predictions was estimated by the Brier score – from 0 (perfect forecast) to 1 (worst prediction) (Stirling et al., 2021).

- Features selection

The most discriminant HRV features were automatically selected in each patient through a pruning procedure: i) for each fold, every feature was removed one at a time and the AUC value was calculated; ii) the feature without which the model had the highest AUC was removed; iii) the process was repeated for the remaining features. For daily forecasts, this procedure was applied to the data from the first training days only.

Results

- Study patients

Twenty-two patients underwent the daily resting-state protocol. We excluded patients with insufficient data (< 1 daily recording in one of both classes, N=5), bad ECG signal quality (N=1), and arrhythmia (N=1). Daily recordings from 15 patients were analyzed (Table 2). The median age was 30 years [25;36.5] and 11 patients (73%) were women. Temporal lobe epilepsy was largely predominant (N=14/15). The median duration of recordings was 11 days [8.5;12]. No patient had heart disease and only one took an antiarrhythmic drug (#14, propranolol for essential tremor).

- Standard classification approach

SVM-based classification using all the HRV features yielded poor performances with a median AUC of 0.5 [0.41;0.64]. However, classification performances increase to 0.75 [0.68;0.99] after the automated selection of the most discriminant features (Table 3). Two-thirds of patients yielded an AUC >

0.7. No clear correlations between classification performances and seizure lateralization or epileptogenic focus localization were found.

- Daily forecasting approach

Pseudoprospective daily forecasts required training data from both classes to estimate the seizure likelihood for each testing day, which was possible in 14 of the 15 patients. The median Brier score was 0.3 [0.18;0.48] (Figure 2). Of the 25 preictal days, 15 (60%) were correctly forecasted (probability ≥ 50%), while false positive predictions were noticed in 9/37 (24.3%) interictal days.

Discussion

Our study suggests daily resting HRV measurements could be an interesting tool to evaluate the sympathetic/parasympathetic imbalance that may reflect the risk of upcoming seizure(s). Classification performances were clearly above chance after the selection of the most discriminant features. However, although pseudoprospective daily forecasts yielded fair overall results, the rate of false negative results (40%) – and consequently the sensitivity – requires some adjustments before considering any clinical application.

Our previously reported iEEG connectivity-based model displayed better performances (Cousyn et al., 2022). Indeed, brain connectivity discriminated between interictal/preictal states with a median AUC > 0.7 in 80% of the patients, and a median Brier score of 0.12 for daily forecasts. In addition, more than 90% of preictal days were correctly forecasted with a similar false positive rate (27%). These results suggest that preictal changes in the autonomic nervous system might occur closer to seizure onset than brain connectivity modifications. A fusion analysis of both strategies (EEG and ECG) could be an interesting approach to improve daily forecasts.

Nevertheless, noninvasive HRV measurements are much more convenient for a clinical application, particularly in an ambulatory setup. Several options could enhance the forecasting performances: i) very-long-term recordings from wearable devices to increase the learning dataset (Karoly et al., 2021); ii) additional autonomic features from electrodermal activity or baroreflex sensitivity to better characterize the sympathetic/parasympathetic variations (Sivathamboo and Perucca, 2021); iii) a multimodal approach including also prodromal symptoms and EEG (Meisel et al., 2020; Nasseri et al., 2021; Stirling et al., 2021).

Our study has several limits. First, although we conducted a strict daily standardized vigilance-controlled protocol that ensured the data quality, the limited number of daily recordings could have an impact on the algorithm performance. Although a duration of 2 minutes is minimally required to obtain some HRV features from ECG segments (Task Force of the European Society of Cardiology the North American Society of Pacing Electrophysiology, 1996), longer resting-state recordings would be an interesting strategy to increase performances. Second, we sometimes applied antiseizure medications (ASM) tapering during the stay, which may represent an artificial condition distant from real-life context. However, from a previous study (Cousyn et al., 2022), we did not find any correlation between seizure occurrence and ASM tapering. In addition, evidence suggests that ASM withdrawal does not change significantly HRV features (Stefani et al., 2013). HRV features were obtained at rest, which could explain that no trivial interactions with seizure lateralization, or with epileptogenic focus localization were found.

In summary, daily resting HRV seems to capture information about autonomic variations that may reflect a pro-ictal state, i.e., a high-risk state of upcoming seizure(s). Additional variables (e.g., prodromes, spontaneous baroreflex sensitivity, electrodermal activity, and EEG) could improve prediction performances – in particular the sensitivity – in order to consider a clinical application. An ambulatory long-term multimodal recording with a wearable device could also be a promising approach for seizure forecasting.

Acknowledgments

This study was supported by the program "Investissements d'Avenir" ANR-10-IAIHU-06, and grants from the "Fondation de l'APHP pour la Recherche – Project PRIAM (Kniazeff Fund)". Louis Cousyn was supported by a "Poste d'Accueil" INSERM and grants from the "Journées de Neurologie de Langue Française".

Disclosure of Conflicts of Interest

V.N. reports fees from Boards with UCB Pharma, EISAI, GW Pharma. The remaining authors have no conflicts of interest.

References

Billeci, L., Marino, D., Insana, L., Vatti, G., Varanini, M., 2018. Patient-specific seizure prediction based on heart rate variability and recurrence quantification analysis. PLoS One 13, e0204339. https://doi.org/10.1371/journal.pone.0204339

Bruno, E., Biondi, A., Richardson, M.P., 2018. Pre-ictal heart rate changes: A systematic review and meta-analysis. Seizure - European Journal of Epilepsy 55, 48–56. https://doi.org/10.1016/j.seizure.2018.01.003

Cousyn, L., Messaoud, R.B., Lehongre, K., Frazzini, V., Lambrecq, V., Adam, C., Mathon, B., Navarro, V., Chavez, M., 2022. Daily resting-state intracranial EEG connectivity for seizure risk forecasts. Epilepsia. https://doi.org/10.1111/epi.17480

Fujiwara, K., Miyajima, M., Yamakawa, T., Abe, E., Suzuki, Y., Sawada, Y., Kano, M., Maehara, T., Ohta, K., Sasai-Sakuma, T., Sasano, T., Matsuura, M., Matsushima, E., 2016. Epileptic Seizure Prediction Based on Multivariate Statistical Process Control of Heart Rate Variability Features. IEEE Transactions on Biomedical Engineering 63, 1321–1332. https://doi.org/10.1109/TBME.2015.2512276

Giannakakis, G., Tsiknakis, M., Vorgia, P., 2019. Focal epileptic seizures anticipation based on patterns of heart rate variability parameters. Computer Methods and Programs in Biomedicine 178, 123–133. https://doi.org/10.1016/j.cmpb.2019.05.032

Karoly, P.J., Stirling, R.E., Freestone, D.R., Nurse, E.S., Maturana, M.I., Halliday, A.J., Neal, A., Gregg, N.M., Brinkmann, B.H., Richardson, M.P., La Gerche, A., Grayden, D.B., D'Souza, W., Cook, M.J., 2021. Multiday cycles of heart rate are associated with seizure likelihood: An observational cohort study. EBioMedicine 72, 103619. https://doi.org/10.1016/j.ebiom.2021.103619

Kolsal, E., Serdaroğlu, A., Çilsal, E., Kula, S., Soysal, A.Ş., Kurt, A.N.Ç., Arhan, E., 2014. Can heart rate variability in children with epilepsy be used to predict seizures? Seizure - European Journal of Epilepsy 23, 357–362. https://doi.org/10.1016/j.seizure.2014.01.025

Leal, A., Pinto, M.F., Lopes, F., Bianchi, A.M., Henriques, J., Ruano, M.G., de Carvalho, P., Dourado, A., Teixeira, C.A., 2021. Heart rate variability analysis for the identification of the preictal interval in patients with drug-resistant epilepsy. Sci Rep 11, 5987. https://doi.org/10.1038/s41598-021-85350-y

Liu, N., Koh, Z.X., Chua, E.C.-P., Tan, L.M.-L., Lin, Z., Mirza, B., Ong, M.E.H., 2014. Risk Scoring for Prediction of Acute Cardiac Complications from Imbalanced Clinical Data. IEEE Journal of Biomedical and Health Informatics 18, 1894–1902. https://doi.org/10.1109/JBHI.2014.2303481

Lotufo, P.A., Valiengo, L., Benseñor, I.M., Brunoni, A.R., 2012. A systematic review and meta-analysis of heart rate variability in epilepsy and antiepileptic drugs. Epilepsia 53, 272–282. https://doi.org/10.1111/j.1528-1167.2011.03361.x

Meisel, C., Bailey, K.A., 2019. Identifying signal-dependent information about the preictal state: A comparison across ECoG, EEG and EKG using deep learning. EBioMedicine 45, 422–431. https://doi.org/10.1016/j.ebiom.2019.07.001

Meisel, C., El Atrache, R., Jackson, M., Schubach, S., Ufongene, C., Loddenkemper, T., 2020. Machine learning from wristband sensor data for wearable, noninvasive seizure forecasting. Epilepsia 61, 2653–2666. https://doi.org/10.1111/epi.16719

Myers, K.A., Sivathamboo, S., Perucca, P., 2018. Heart rate variability measurement in epilepsy: How can we move from research to clinical practice? Epilepsia 59, 2169–2178. https://doi.org/10.1111/epi.14587

Nasseri, M., Pal Attia, T., Joseph, B., Gregg, N.M., Nurse, E.S., Viana, P.F., Worrell, G., Dümpelmann, M., Richardson, M.P., Freestone, D.R., Brinkmann, B.H., 2021. Ambulatory seizure forecasting with a wrist-worn device using long-short term memory deep learning. Sci Rep 11, 21935. https://doi.org/10.1038/s41598-021-01449-2

Pan, J., Tompkins, W.J., 1985. A Real-Time QRS Detection Algorithm. IEEE Transactions on Biomedical Engineering BME-32, 230–236. https://doi.org/10.1109/TBME.1985.325532

Sivathamboo, S., Perucca, P., 2021. Interictal autonomic dysfunction. Current Opinion in Neurology 34, 197–205. https://doi.org/10.1097/WCO.0000000000000906

Stefani, M., Arima, H., Mohamed, A., 2013. Withdrawal of anti-epileptic medications during video EEG monitoring does not alter ECG parameters or HRV. Epilepsy Research 106, 222–229. https://doi.org/10.1016/j.eplepsyres.2013.04.003

Stirling, R.E., Grayden, D.B., D'Souza, W., Cook, M.J., Nurse, E., Freestone, D.R., Payne, D.E., Brinkmann, B.H., Pal Attia, T., Viana, P.F., Richardson, M.P., Karoly, P.J., 2021. Forecasting Seizure Likelihood With Wearable Technology. Front Neurol 12, 704060. https://doi.org/10.3389/fneur.2021.704060

Task Force of the European Society of Cardiology the North American Society of Pacing Electrophysiology, 1996. Heart Rate Variability: Standards of Measurement, Physiological Interpretation, and Clinical Use. Circulation 93, 1043–1065. https://doi.org/10.1161/01.CIR.93.5.1043

Table 1. HRV features

Table 1 legend: Detailed description of measures can be found in [Shaffer, F., & Ginsberg, J. P. (2017). An overview of heart rate variability metrics and norms. Frontiers in Public Health, 258] ;[Jeppesen, J., Beniczky, S., Johansen, P., Sidenius, P., & Fuglsang-Frederiksen, A. (2015). Detection of epileptic seizures with a modified heart rate variability algorithm based on Lorenz plot. Seizure, 24, 1-7]; [Piskorski, J., & Guzik, P. (2007). Geometry of the Poincaré plot of RR intervals and its asymmetry in healthy adults. Physiological measurement, 28(3), 287] and [Graff, G., Graff, B., Kaczkowska, A., Makowiec, D., Amigó, J. M., Piskorski, J., Narkiewicz K. & Guzik, P. (2013). Ordinal pattern statistics for the assessment of heart rate variability. The European Physical Journal Special Topics, 222, 525-534.]

HRV features		Definition
Time-domain metrics		
	NumBeats	Number of heartbeats
	hrvMean (ms)	Average RR interval
	SDNN (ms)	Standard deviation of RR intervals
	RMSSD (ms)	Root mean square of successive RR interval differences
	SDANN (ms)	Standard error of average RR intervals
	CVNN	Coefficient of variation of RR intervals
	Heart Rate (bpm)	Heartbeats per minute
	SDNNd (ms)	Contribution of decelerations (increase in RR intervals) to total variability
	SDNNa (ms)	Contribution of accelerations (increase in RR intervals) to total variability
Frequency-domain measures (obtained by the Lomb periodogram)		
	VLF power (ms^2)	Absolute power of the very-low frequency range (0.003-0.04 Hz)
	LF power (ms^2)	Absolute power of the low-frequency range (0.04-0.15 Hz)
	HF power (ms^2)	Absolute power of the high frequency range (0.15-0.4 Hz)
	LFP/HFP	Ratio of LF/HF power
	Normalized LF (nu)	Relative power of the low-frequency range in normal units [LFP/(total power – VLFP)x100]
	Normalized HFP (nu)	Relative power of the high-frequency range in normal units [HFP/(total power – VLFP)x100]
	TP (ms^2)	Total power (0 – 0.5 Hz)
Nonlinear measures from the Poincaré plot of RR intervals, RR(i) vs RR(i-1)		
	SD1/SD2	Ratio of SD1/SD2, i.e., the ratio of short-term to long-term variations (SD1 is the standard deviations of points along the line RR(i) = RR(i-1), and SD2 denotes the standard deviation across the identity line)
	Asd1sd2	Area of ellipse described by SDA and SD2
	CSI	Cardiac sympathetic index: ratio of the longitudinal variability of RR intervals in the Poincaré plot (SD2) by its transverse variability (SD1)
	CVI	Cardiac vagal (parasympathetic) index: logarithm of the product of longitudinal (4∗SD2) and transverse variability (4∗SD1) of RR intervals in the Poincaré plot
	Modified CSI	Modified cardiac sympathetic index (Jeppesen et al., 2015): ratio of the square of the longitudinal variability by its transverse variability

	PI	Porta's index: the number of points (in the Poincaré plot) below the identity line (RR(i) = RR(i-1)), divided by the total number of points except those that are located on the line.
	SD1d (ms^2)	Short-term variance (along the identity line) of contributions of decelerations (prolongation of successive RR intervals)
	SD1a (ms^2)	Short-term variance (along the identity line) of contributions of accelerations (shortening of successive RR intervals)
	SD2d (ms^2)	Long-term variance (across the identity line) of contributions of decelerations (prolongation of successive RR intervals)
	SD2a (ms^2)	Long-term variance of contributions of accelerations (shortening of successive RR intervals)
	C1d (%)	The contribution of SD1d to the total variance along the identity line
	C1a (%)	The contribution of SD1a to the total variance along the identity line
	C2d (%)	The contribution of SD2d to the total variance across the identity line
	C2a (%)	The contribution of SD2a to the total variance across the identity line
Nonlinear measure from RR time series		
	Pen	Permutation entropy of RR intervals: an index of complexity

Table 2. Characteristics of patients

Table 2 legend: RS: resting-state recordings; F: female; M: male; MT: mesial temporal; TPO: temporal-parietal-occipital; FIAS: focal impaired awareness seizures; FAS: focal aware seizures; FBTCS: focal to bilateral tonic-clonic seizures; LTG: lamotrigine; ESL: eslicarbazepine acetate; DZP: diazepam; LCS: lacosamide; ZNS: zonisamide; CLB: clobazam; OXC: oxcarbazepine; PER: perampanel; CBZ: carbamazepine; TPM: topiramate; LVT: levetiracetam; VPA: valproic acid; BVT: brivaracetam; RS: resting states; ET: essential tremor.

Patient		**#1**	**#2**	**#3**	**#4**	**#5**	**#6**	**#7**	**#8**	**#9**	**#10**	**#11**	**#12**	**#13**	**#14**	**#15**
Gender		F	F	F	F	F	M	M	M	F	M	F	F	F	F	F
Age (years)		47	30	18	25	27	39	31	25	38	25	35	31	27	42	24
Location of epileptic focus		Left posterior temporal	Multifocal (right MT and TPO junction)	Right superior frontal gyrus	Left MT	Left posterior temporal	Left temporo-polar	Left MT	Right MT and temporo-polar	Right MT and temporo-polar	Left temporo-polar	Right temporo-polar	Left MT	Bilateral MT	Left MT and temporo-polar	Left temporo-polar
Seizures		FIAS	FIAS	FIAS	FBTCS	FAS, FIAS	FAS, FIAS	FIAS, FBTCS	FAS, FIAS	FIAS	FBTCS	FAS	FIAS, FBTCS	FAS, FIAS	FIAS	FIAS, FBTCS
Antiepileptic drugs		LTG, ESL, DZP	LTG, LCS, ZNS, CLB	LTG, OXC, CLB	ESL, PER, TPM	LTG, OXC	LCS, CBZ	CBZ, PER, ZNS	LVT, LTG	LTG, VPA, CBZ, CLB	CBZ, BRV	CBZ, LTG, CLB	BVT, LTG	ZNS, CBZ	OXC, LCS, ZNS	LTG, TPM
Number of RS	Preictal	2	9	3	2	2	11	1	3	2	2	3	3	2	1	1
	Interictal	5	1	8	10	4	3	15	9	9	9	2	10	10	10	4
Mean delay between preictal RS and seizure onset, hours, min.-max.		6.5, 6-7	9.1, 1.8-21	4.2, 6-15	15.4, 14.5-16.3	0.8, 0.5-1	8.8, 0.3-17	20	17.7, 13-21.5	12.5, 4-21	11.6, 9-14.3	4.1, 1-6.3	8.8, 3.5-18	15.5, 8.3-22.7	15.3	9

Table 3. Preictal-interictal classification after automated selection of HRV features

Table 3 legend: Median AUC values (±deviation)

TC: two-class; OC: one-class; SVM: support vector machine

	Classification performances				
Patient	AUC	Se	Sp	Acc	F1-score
#1 TC-SVM	0.99±0.01	1±0	1±0	0.98±0.03	0.97±0.03
#2 OC-SVM	0.67±0.15	0.61±0.15	0.7±0.2	0.66±0.12	0.65±0.11
#3 TC-SVM	0.74±0.14	0.74±0.15	0.75±0.15	0.73±0.1	0.73±0.12
#4 TC-SVM	0.83±0.17	0.8±0.2	0.85±0.15	0.8±0.15	0.79±0.19
#5 TC-SVM	0.75±0.25	0.8±0.2	0.9±0.1	0.83±0.18	0.8±0.17
#6 TC-SVM	0.98±0.02	1±0	1±0	0.95±0.05	0.95±0.05
#7 OC-SVM	0.59±0.15	0.75±0.1	0.6±0.15	0.68±0.1	0.68±0.07
#8 TC-SVM	0.99±0.01	1±0	0.95±0.05	0.95±0.05	0.95±0.05
#9 TC-SVM	0.51±0.2	0.65±0.2	0.6±0.2	0.6±0.2	0.65±0.11
#10 TC-SVM	0.7±0.3	0.85±0.15	0.8±0.2	0.75±0.18	0.73±0.15
#11 TC-SVM	1±0	1±0	1±0	1±0	1±0
#12 TC-SVM	0.62±0.38	1±0	0.65±0.35	0.68±0.2	0.67±0.15
#13 TC-SVM	0.82±0.19	1±0	0.95±0.05	0.84±0.16	0.84±0.16
#14 OC-SVM	0.69±0.2	0.7±0.15	0.85±0.1	0.73±0.1	0.7±0.16
#15 OC-SVM	1±0	1±0	1±0	1±0	1±0

Figure 1. HRV-based prediction of preictal states

Figure 1 legend: A) For each patient, consecutive daily recordings are considered as days without seizure or 'interictal' class, and days with seizure(s) or 'preictal' class. For each daily 10 min ECG recordings, RR time series are estimated from 2 minute-ECG segments, from which 31 HRV features are extracted. B) Feature selection and prediction models (yellow box) are estimated by a cross-validation procedure. In daily forecasts, the training phase was performed using all the previous days. C) The remaining segments are tested with the learned model (blue box). The probability of belonging to the preictal class, i.e. the estimated seizure likelihood, is thus obtained from the prediction model.

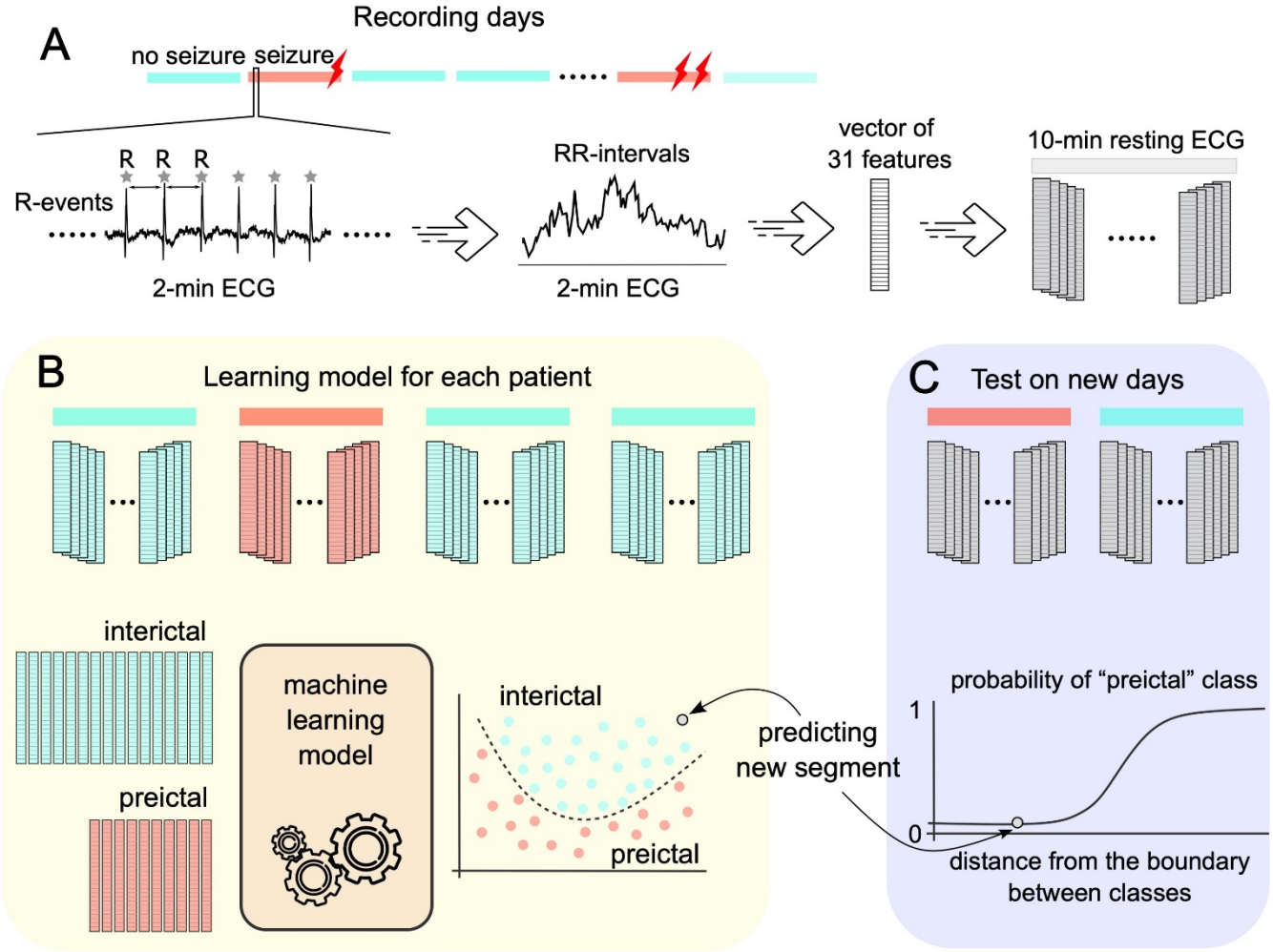

Figure 2. Pseudoprospective daily forecasts

Figure 2 legend: For each patient, consecutive daily recordings were represented by diamonds: white diamonds for days without seizure or 'interictal' class, and black ones for those with seizure(s) or 'preictal' class. For each day to forecast, the training phase was performed using all the previous days. The pruning procedure was performed on the first training dataset (black dashed boxes). Then, we obtained a probability of belonging to the preictal class (below each diamond, in %), i.e., the estimated seizure likelihood. True forecasts are in green, while false ones are in red.

BS: Brier score

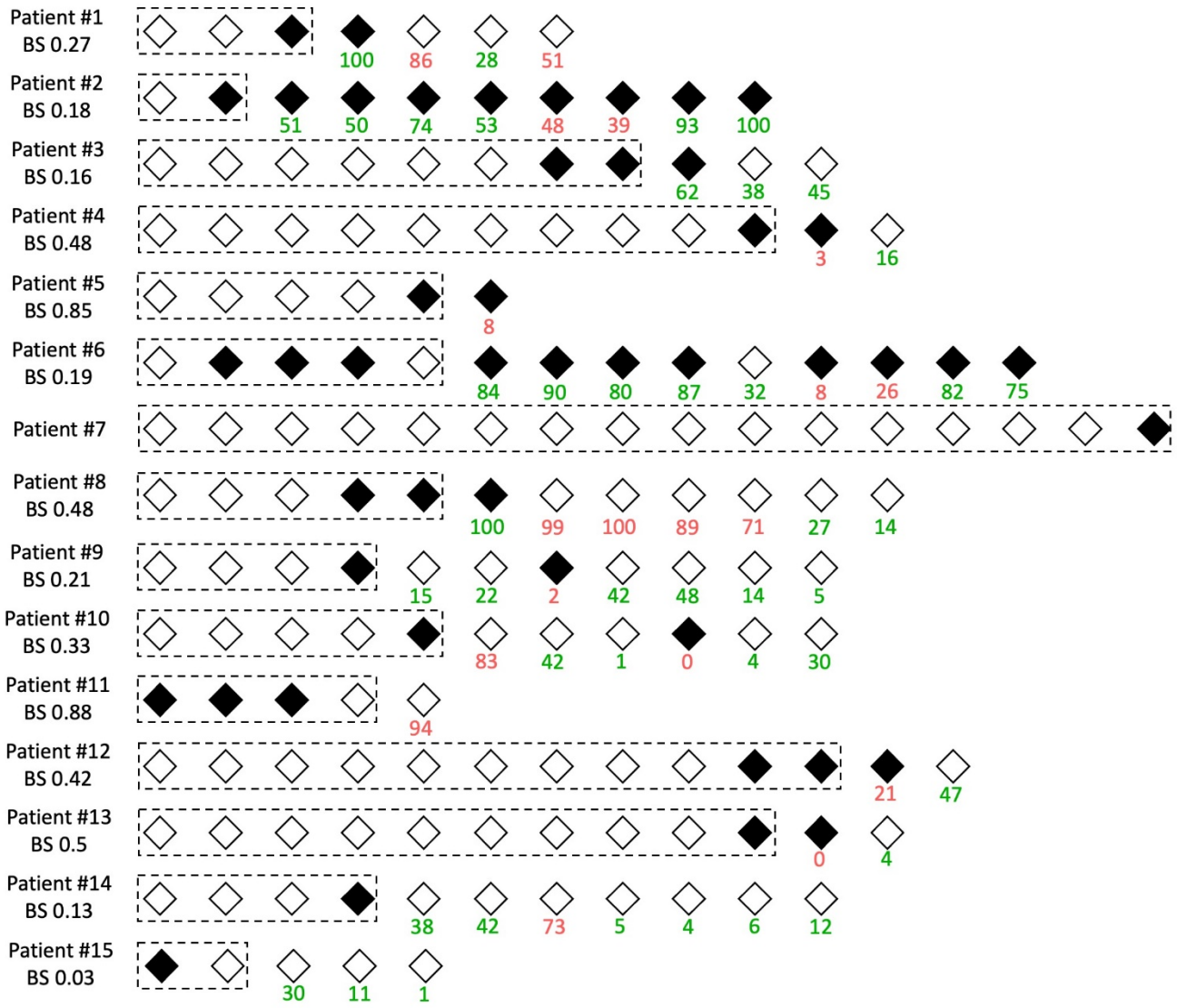

PARTIE 3. ÉTUDE DES MODIFICATIONS PRECRITIQUES DE LA CONNECTIVITE FONCTIONNELLE INTRACEREBRALE

I. Identification des jours à risque de crise à l'aide de la connectivité fonctionnelle intracérébrale

1) Introduction

De par son excellente résolution spatio-temporelle, l'EEG intracérébral est un outil de choix pour l'étude des dynamiques cérébrales précritiques. Plusieurs études ont utilisé des mesures de connectivité EEG intracérébrale pour étudier l'état précritique (Le Van Quyen et al. 2005; van Mierlo et al. 2014; Kuhlmann et al. 2018a). Cependant, l'identification de changements de connectivité précritiques au cours du temps doit nécessairement être interprétée à la lumière des changements induits par les différents états de vigilance. Cette approche nécessite de connaître l'état de vigilance en temps réel ou de disposer de plusieurs périodes de référence pour chaque état. Une mesure quotidienne du risque de crise dans un état de vigilance contrôlé serait plus pratique.

Dans cette étude, nous avons i) évalué les performances de mesures de connectivité EEG intracérébrale durant un protocole de repos standardisé pour identifier un état précritique, puis ii) réalisé des prévisions probabilistes du risque de crise.

2) Méthodologie

Nous avons réalisé des enregistrements quotidiens de 10 minutes au cours d'un protocole de repos standardisé (cf. pages 107-108) auprès de patients hospitalisés pour une exploration vidéo-EEG intracérébrale continue (avec des électrodes profondes Ad-Tech), dans le cadre de la prise en charge de leur épilepsie focale pharmaco-résistante, entre janvier 2019 et juillet 2021.

Chaque enregistrement a ensuite été classé en « précritique » – en cas de crise électro-cliniques survenant dans les 24 heures – ou « intercritique » – en l'absence de crise (Figure 23A).

Pour chaque patient, nous avons i) relu les IRM cérébrales post-implantation afin de ne garder que les macro-contacts situés dans la substance grise, et ii) relu les tracés EEG afin de localiser chaque macro-contact sélectionné : zone de début de crise (*seizure onset zone*), zone irritative ou zone saine putative.

Nous avons estimé la connectivité fonctionnelle à l'aide de mesures de synchronie de phase (*phase-locking value*, PLV) sur des fenêtres glissantes non chevauchantes de 20 secondes dans les différentes bandes de fréquence (du delta au gamma).

Dans un premier temps, nous avons évalué les performances de distinction entre la connectivité intracérébrale de repos des états inter et précritiques à l'aide d'un classifieur SVM et en appliquant une validation croisée de type *leave-one-day-out* afin d'éviter toute fuite d'information (Figure 23B). Nous avons comparé notre modèle à d'autres classifieurs alimentés par :

a) les posologies des médicaments antiépileptiques au cours du temps ;

b) le nombre et l'étendue des anomalies épileptiques intercritiques EEG identifiées par détection automatique ;

c) l'état inter/précritique du jour antérieur (prédiction d'un jour précritique en cas d'enregistrement d'une crise le jour précèdent, et intercritique autrement).

Dans un deuxième temps, nous avons estimé de manière pseudoprospective des probabilités quotidiennes du risque de crise d'épilepsie.

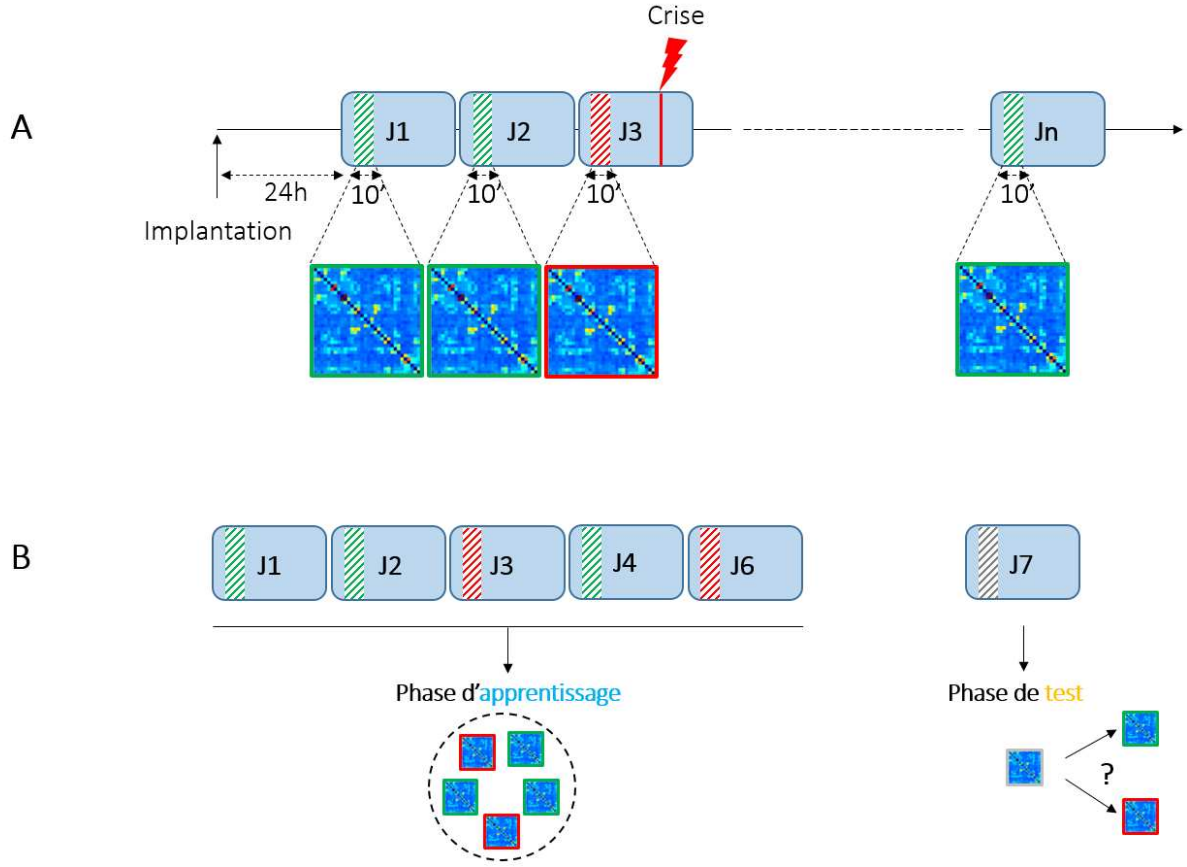

Figure 23. Matrices de connectivité et apprentissage automatique

A. Mesures de connectivité fonctionnelle sur des enregistrements quotidiens de période de repos de 10min, classées en « précritiques » ou « intercritiques ».

B. Un enregistrement quotidien est aléatoirement retiré du jeu de données d'apprentissage (qui sera réalisé uniquement sur les autres jours) pour être assigné uniquement aux données de la phase de test.

3) Résultats

Parmi les 12 patients enregistrés, 10 avaient suffisamment de données dans chacune des deux classes. La première approche a mis en évidence de bonnes performances de discrimination de la connectivité intracérébrale notamment dans la bande de fréquence thêta : 80% des patients avaient un AUC ≥ 0,7, avec un AUC moyen de 0,79 (minimum 0,5, maximum 1). Les modèles basés sur les posologies de médicaments antiépileptiques, les anomalies épileptiques intercritiques EEG ou les informations antérieures n'ont pas permis de distinguer les deux états.

L'approche pseudoprospective a montré de bonnes prévisions probabilistes : 92% des enregistrements précritiques étaient correctement prédits et le taux de faux positifs atteignait 27%. Le score de Brier moyen était de 0,13 (minimum 0, maximum 0,35).

Notre approche a montré de bonnes performances d'identification d'un état précritique et des prévisions quotidiennes précises, à l'aide d'une mesure unique quotidienne. Une évaluation des performances du modèle à l'aide de techniques non invasives (EEG de surface) ou de dispositifs implantables pour enregistrements d'ultra longue durée est cependant nécessaire pour envisager une application en pratique clinique.

4) Article 4 : Daily resting-state intracranial EEG connectivity for seizure risk forecasts

Received: 10 May 2022 | Revised: 1 December 2022 | Accepted: 6 December 2022

DOI: 10.1111/epi.17480

Epilepsia®

BRIEF COMMUNICATION

Daily resting-state intracranial EEG connectivity for seizure risk forecasts

Louis Cousyn[1,2,3,4] | **Rémy Ben Messaoud**[2,5] | **Katia Lehongre**[2] | **Valerio Frazzini**[1,2,3,4] | **Virginie Lambrecq**[1,2,3,4] | **Claude Adam**[1,3] | **Bertrand Mathon**[2,4,6] | **Vincent Navarro**[1,2,3,4] | **Mario Chavez**[2]

[1]Department of Neurology, Epilepsy Unit, Public Hospital Network of Paris, Pitié-Salpêtrière Hospital, Paris, France

[2]Paris Brain Institute, ICM (INSERM-U1127, CNRS-UMR7225), Paris, France

[3]Center of Reference for Rare Epilepsies, Pitié-Salpêtrière Hospital, Paris, France

[4]Sorbonne University, Paris, France

[5]INRIA, ARAMIS Project-Team, Paris, France

[6]Department of Neurosurgery, Public Hospital Network of Paris, Pitié-Salpêtrière Hospital, Paris, France

Correspondence
Louis Cousyn, Department of Neurology, Epilepsy Unit, Public Hospital Network of Paris, Hôpital Pitié-Salpêtrière, 47-83 boulevard de l'Hôpital, 75651 Paris Cedex 13, France.
Email: louismarc.cousyn@aphp.fr

Abstract

Forecasting seizure risk aims to detect proictal states in which seizures would be more likely to occur. Classical seizure prediction models are trained over long-term electroencephalographic (EEG) recordings to detect specific preictal changes for each seizure, independently of those induced by shifts in states of vigilance. A daily single measure—during a vigilance-controlled period—to estimate the risk of upcoming seizure(s) would be more convenient. Here, we evaluated whether intracranial EEG connectivity (phase-locking value), estimated from daily vigilance-controlled resting-state recordings, could allow distinguishing interictal (no seizure) from preictal (seizure within the next 24 h) states. We also assessed its relevance for daily forecasts of seizure risk using machine learning models. Connectivity in the theta band was found to provide the best prediction performances (area under the curve ≥ .7 in 80% of patients), with accurate daily and prospective probabilistic forecasts (mean Brier score and Brier skill score of .13 and .72, respectively). More efficient ambulatory clinical application could be considered using mobile EEG or chronic implanted devices.

KEYWORDS

machine learning, phase synchrony, probabilistic forecasting, SEEG, seizure prediction

1 | INTRODUCTION

Temporal and spatial resolutions of intracranial electroencephalography (iEEG) make it one of the best tools to capture epileptic brain dynamics. In previous studies,[1–3] iEEG connectivity has been used as a potential tracker of the interictal to ictal transition (i.e., preictal state). Classical seizure prediction models are trained over long-term EEG recordings to detect specific preictal changes for each seizure, independently of those induced by shifts in states of vigilance. Nevertheless, this approach requires either a real-time identification of vigilance state, or a combination of different reference interictal states.[4–6] A daily single measure—during a vigilance-controlled period—to estimate the risk of upcoming seizure(s) would be more convenient.

Machine learning models have significantly contributed to improve forecasting performances based on EEG

Vincent Navarro and Mario Chavez contributed equally to this work.

features.[7] Whereas classical seizure prediction models assume that input features (e.g., iEEG connectivity values) will necessarily result in binary outputs (upcoming seizure or not), probabilistic forecasting includes a degree of uncertainty and computes the probability of occurrence of an event.[6] This calibration of the prediction model seems more appropriate to identify a hypothetical *pro*-ictal state in which seizures would be more likely—but not certain—to occur.[8,9]

Herein, we aimed (1) to determine whether patient-specific iEEG connectivity during daily vigilance-controlled resting-state periods was different between days with and without seizure and (2) to prospectively assess its relevance for daily forecasts of seizure risk using calibrated prediction models.

2 | MATERIALS AND METHODS

2.1 | Study design and participants

We recorded resting-state periods in patients with drug-resistant focal epilepsy who underwent iEEG (Ad-Tech depth electrodes) for presurgical evaluation from January 15, 2019 to July 20, 2021, in the Epilepsy Unit of the Pitié-Salpêtrière University Hospital (Paris, France).

The study was conducted according to the recommendations outlined in the Helsinki Declaration and approved by an institutional review board (C11-16 and C19-55 National Institute of Health and Medical Research sponsor).

2.2 | Resting-state protocol

Daily 10-min resting-state periods were recorded usually between 10 a.m. and 12 p.m. and at least 24 h after the electrode implantation to avoid residual effects of general anesthesia. Each recording was conducted under human supervision (L.C.): patients were specifically asked to remain awake, seated, with eyes open, and as calm and still as possible, without repetitive thoughts or movements (counting, finger tapping). They had to stare at a gray computer screen to avoid eye movements. We also limited external stimuli by turning off radio, television, phone, et cetera. Quality control of EEG data was performed during recording and retrospectively.

Each 10-min resting-state period was labeled as "interictal" if no seizure occurred in the next 24 h ($N_1 = 69$), or "preictal" if at least one electroclinical seizure occurred in the next 24 h ($N_2 = 38$). To exclude postictal and ictal periods, we only considered resting-state periods recorded (1) at least 1 h after the last focal seizure and 6 h after the last generalized one, and provided that vigilance had returned to normal; (2) without any ictal or postictal activity; and (3) at least 30 min before the next seizure.

2.3 | iEEG connectivity assessment

Patterns of iEEG connectivity were studied here by means of phase-locking values (PLVs) estimated between pairs of signals.[1,10] To reduce any spurious synchrony produced by the volume conduction, we considered a bipolar montage between pairs of adjacent contacts located in the gray matter of the seizure onset zone (SOZ) and/or the irritative zone (IZ), or from putative "healthy" brain areas without epileptiform activity. We computed connectivity matrices by PLV for 20-s nonoverlapping epochs (30 for each daily recording) between all possible pairs of contacts and in the typical frequency bands (delta, 1–4 Hz; theta, 4–8 Hz; alpha, 8–13 Hz; beta, 13–30 Hz; low gamma, 30–49 Hz; and high gamma, 51–90 Hz).

2.4 | Preictal state discrimination

We first evaluated the ability to discriminate between interictal and preictal epochs using a nonlinear support vector machine (SVM) classifier. As PLVs might be highly correlated between epochs from the same daily recording, which could result in overestimated performances, we considered a leave-one-day-out cross-validation: for each fold, one daily recording from each class (interictal and preictal) was randomly assigned to the testing dataset, whereas the remaining daily periods were used to train the algorithm. In addition, each fold included 70% of the training and testing epochs that were randomly selected, to obtain 10 000 folds with different combinations of data. Two-class SVM was applied in patients ($n = 8$) with at least two resting-state recordings from each class. In patients with only one recording in a given class ($n = 2$), one-class SVM models, which only require data from a single class to train the model, were performed.

For all our SVM models, we used a Gaussian kernel with the width parameter γ set to the median pairwise distances among training points. To prevent any bias related to class-imbalanced training datasets, we applied SMOTE (Synthetic Minority Oversampling Technique), which oversamples points of the minority class based on the similarities between available data, within each cross-validation. We also controlled the classifiers' performance by using permutation tests in which class labels were randomly reassigned. Classification performances of each epoch were assessed by the area under the receiver operating characteristic curve (AUC), which takes values

between .5 for a random classification and 1 for a perfect classification; the F1 score, which is the weighted average of the recall and precision; and the accuracy.

We compared our connectivity-based model to two other models: (1) an SVM classifier based on the number and spread of interictal epileptiform discharges (IEDs) that were automatically detected[11] and (2) a simple classifier that based its predictions on the previous day's state (i.e., preictal if seizure[s] occurred on the previous day, and interictal otherwise).

2.5 | Effect of antiepileptic drug tapering

A medication index was estimated every day, by rescaling the current overall dose (including all antiepileptic drugs [AEDs]) by the overall dose on the first day of recording. In this way, profiles of AED tapering between patients could be compared using a simple index. We then used an SVM classifier to evaluate the ability of daily AEDs doses to discriminate between interictal and preictal periods.

2.6 | Prospective prediction of upcoming seizure(s) for each patient

Daily patient-specific seizure forecasting was prospectively performed. For each day to predict, we trained SVM models on all the iEEG segments from the previous days (at least one from each class) and then computed its probability of belonging to the preictal class, reflecting the risk of upcoming seizures. Daily predictions were obtained by averaging the forecast probabilities from all the iEEG segments. We used Platt scaling to transform the SVM classifier's outputs into a probability distribution over classes by fitting a logistic regression model to the classifier's score.[12] The selection of the most discriminant PLVs from pairs of contacts could be performed (based on data from previous days only) to improve prediction performances using a pruning procedure.[13] During the first training session, the classifier was first evaluated with the whole set of connectivity coefficients. Then, "irrelevant" variables were removed one by one by a pruning procedure: (1) AUC values were estimated after removal of each connection, (2) the connection without which the model had the highest AUC was removed from the subset of connectivity values, and (3) the procedure was repeated with the remaining connections. Finally, we kept the set of connections that yielded the highest performances.

To provide a full evaluation of forecasting models, we computed the Brier score (i.e., the mean squared error over every forecast; from 0 [perfect prediction] to 1 [worst prediction]) and the Brier skill score (BSS), which measures the improvement over a default prediction (given the relatively limited number of recording sessions, default predictions of each patient were estimated as the proportion of interictal/preictal sessions), from 0 (no improvement) to 1 (perfect), with negative values indicating worse performances than default predictions.[6]

3 | RESULTS

3.1 | Study patients

Among the 12 patients who were recorded daily, 10 had at least one resting-state recording from each class (see main characteristics in Table S1). The mean age was 30.7 years (minimum = 18, maximum = 47), and six patients were women. Patients mainly had electrodes in the temporal and the frontal lobes (respectively, $n = 9$ and $n = 4$). Mean number of daily recordings per patient was 10.7 (minimum = 4, maximum = 17), including 3.8 preictal recordings (minimum = 1, maximum = 11).

3.2 | Discrimination between interictal and preictal states

On average, we identified three (minimum = 1, maximum = 6) frequency bands for which connectivity analyses reached AUC ≥ .7 (Table 1). Theta band was found to be the most discriminant band, in particular when considering only contacts from SOZ and IZ: 80% of patients had AUCs of ≥.7 (mean AUC = .79 [minimum = .5, maximum = 1], mean F1 score = .78 [minimum = .62, maximum = 1], and mean accuracy = .77 [minimum = .52, maximum = 1]).

We found that AED tapering had a poor discriminating ability (AUC = .54) to detect preictal periods. Anteriority and IED-based models also displayed weak performances (respectively, mean AUC = .62 and .4; see Table S2).

3.3 | Relevance of daily seizure risk forecasts

Patient-specific predictions were performed in the most discriminant conditions, that is, theta connectivity from SOZ and IZ contacts. Feature selection procedure significantly improved performances in four patients (Figure 1). Of the 24 preictal resting-state recordings, 22 (91.7%) were correctly predicted with a probability of >50%. False positive predictions were observed in six of 22 (27.3%) interictal periods and exclusively occurred after two or more consecutive preictal periods. Mean Brier score and BSS

TABLE 1 Discrimination between interictal and preictal resting states: AUC values

Patient	Frequency band											
	Delta		Theta		Alpha		Beta		Low gamma		High gamma	
#1 TC-SVM	.68 (±.26)	.68 (±.20)	.77 (±.21)	.69 (±.22)	–	–	.84 (±.16)	.81 (±.19)	.76 (±.25)	.74 (±.22)	–	–
#2 OC-SVM	.99 (±.01)	.99 (±.01)	.98 (±.02)	.98 (±.03)	.88 (±.06)	.89 (±.05)	1 (±0)	.89 (±.05)	.98 (±.02)	.97 (±.02)	.93 (±.03)	.91 (±.04)
#3 TC-SVM	.75 (±.17)	.79 (±.17)	.80 (±.15)	.83 (±.15)	.87 (±.12)	.89 (±.11)	.94 (±.06)	.95 (±.05)	.87 (±.13)	.98 (±.03)	–	–
#4 TC-SVM	.90 (±.1)	.97 (±.03)	.83 (±.16)	.93 (±.07)	–	–	–	.66 (±.25)	–	–	–	–
#5 TC-SVM	–	–	.71 (±.22)	.67 (±.14)	–	.74 (±.18)	–	–	–	–	–	–
#6 TC-SVM	1 (±0)	1 (±0)	1 (±0)	1 (±0)	1 (±0)	1 (±0)	1 (±0)	1 (±0)	1 (±0)	1 (±0)	1 (±0)	1 (±0)
#7 TC-SVM	–	–	.77 (±.23)	.80 (±.20)	–	.77 (±.23)	–	.63 (±.35)	–	.71 (±.29)	.67 (±.34)	–
#8 OC-SVM	.65 (±.08)	.61 (±.08)	.62 (±.07)	.70 (±.06)	.75 (±.05)	.82 (±.06)	.70 (±.07)	.74 (±.08)	.83 (±.11)	.62 (±.12)	.84 (±.11)	.66 (±.11)
#9 TC-SVM	–	–	–	–	.65 (±.32)	.69 (±.29)	.66 (±.33)	.67 (±.33)	.93 (±.07)	.93 (±.07)	.98 (±.02)	.98 (±.03)
#10 TC-SVM	–	.66 (±.24)	.92 (±.08)	.97 (±.02)	.65 (±.3)	.78 (±.22)	–	.68 (±.32)	–	–	–	–

Note: For each frequency band, median AUCs (±deviation) obtained from connectivity measures between contacts located in the SOZ or the IZ are shown in the left column, whereas those obtained from measures between all contacts (SOZ, IZ, and putative "healthy" zones) are shown in the right column. We applied two-class SVM models, except for Patients #2 and #8, for whom one-class SVM algorithms were used. "–" indicates an AUC < .6.

Abbreviations: AUC, area under the receiver operating characteristic curve; IZ, irritative zone; OC, one-class; SOZ, seizure onset zone; SVM, support vector machine; TC, two-class.

[Correction added on 13 January 2023, after first online publication: The placement of the headings in Table 1 have been corrected.]

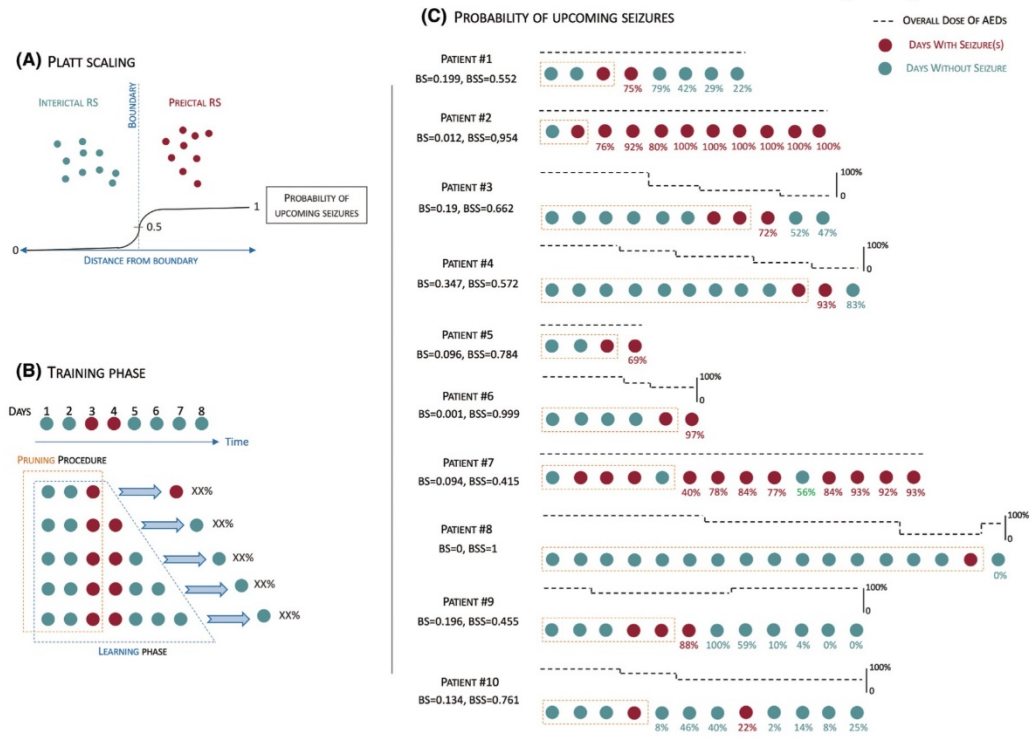

FIGURE 1 Daily forecasting of seizure risk. (A) Platt scaling transforms support vector machine (SVM) classifier outputs (interictal or preictal) into a probability distribution over classes by fitting a logistic regression model to the classifier score. (B) Training phase. For a given day, two-class SVM models were trained on recordings from previous days, including at least one day from each class. A pruning procedure could be performed during the first training session to select the most discriminant phase-locking values and improve the model performance. (C) Testing phase. For each new day, we estimate the probability of belonging to the preictal class, reflecting the risk of upcoming seizure(s), expressed as a percentage below each dot. Green and purple dots represent respectively days without and with seizure(s). To improve prediction performances, a pruning procedure was performed during the first training (orange dashed boxes). The daily medication index—expressed as a percentage of the overall dose of antiepileptic drugs (AEDs)—is represented for each patient by a black dotted line. Patients #1, #2, #5, and #7 had no medication tapering. BS, Brier score; BSS, Brier skill score; RS, resting state.

were .13 (minimum = 0, maximum = .35) and .72 (minimum = .42, maximum = 1), respectively, which suggested a good prediction model.

4 | DISCUSSION

In this study, we found that iEEG connectivity obtained from vigilance-controlled resting-state recordings can discriminate between days with or without seizure, thus providing a promising tool for accurately forecasting the daily risk of upcoming seizure(s). Most of the useful connectivity information seems to be contained in the SOZ and IZ, and theta was the most discriminant frequency band. Several studies in focal epilepsy have already noticed specific network alterations occurring predominantly in the theta frequency band.[14,15] One patient (#6) had perfect performances, which must be related to the especially short delay between resting-state periods and seizures (<1 h on average).

We used vigilance-controlled resting-state recordings to reduce variations in the vigilance condition of the patients, which could induce physiological fluctuations in functional connectivity and thus affect the preictal state predictions.[5] In addition, as iEEG signals might reflect nonlinear interactions, we estimated nonlinear PLVs, and Gaussian SVMs allowed us to deal with complex distributions of data.[16] Our connectivity-based model performed

better than a predictor based on the number and spread of IEDs. A more complex model including other specific EEG markers of epilepsy, such as high-frequency oscillations, would be interesting to develop.

In contrast to classical seizure prediction methods that track changes in EEG dynamics by analyzing long-term recordings, our results suggest that short and daily single resting-state recording could reflect a proictal state, at least at the daily level. Our approach could be evaluated in a suitable device, allowing daily vigilance-controlled resting-state recordings using a wireless ambulatory scalp EEG or ultra-long-term EEG from implanted devices (subscalp or intracranial system), which would be a promising tool to assess the daily risk of upcoming seizure(s).[17,18] A much larger dataset would also allow computing AUCs from predictions of days instead of epochs (composing each daily recording), which could be more clinically relevant. It is important to note that long-term recordings could be affected by connectivity variations, which were not noticeable on our time scale (1–2 weeks per patient), such as postimplantation inflammation-related changes or multidien/circannual cycles of epileptic brain activity.[19,20]

Our study has some limitations. First, the main goal of the hospitalization was to record seizures for presurgical evaluation. Therefore, tapering AEDs may not reflect "real-life" conditions. We did not find obvious correlations between occurrence of seizures and medication adjustment profiles (Figure 1C). Second, we observed a false positive rate of 27.3%. However, this may illustrate the concept of proictal state, that is, a high-risk state of seizure that could be controlled by homeostatic mechanisms.[21] In our study, these false positives were only detected after several consecutive preictal periods, which may represent days with a higher susceptibility of seizures. In two patients (#3 and #7), forecasting probabilities were only slightly above 50% and far below values obtained in preictal states. Finally, given the heterogeneity of electrode location among the patients, we cannot generalize a single unique prediction model. Much larger cohorts of patients are therefore needed to map out the limits of proictal state forecasting.

In summary, our findings suggest that iEEG connectivity, obtained from vigilance-controlled resting-state recordings, can provide a daily and reliable signature of upcoming seizure(s).

AUTHOR CONTRIBUTIONS

Louis Cousyn, Vincent Navarro, and Mario Chavez contributed to the conception and design of the study. All authors contributed to the acquisition and analysis of data. Louis Cousyn, Vincent Navarro, and Mario Chavez contributed to drafting the manuscript and figure.

ACKNOWLEDGMENTS

This study was supported by the program Investissements d'avenir (ANR-10-IAIHU-06), and grants from the Fondation de l'APHP pour la Recherche–Project PRIAM (Kniazeff Fund). L.C. was supported by a Poste d'Accueil (INSERM) and grants from the Journées de Neurologie de Langue Française.

CONFLICT OF INTEREST

V.N. reports fees from boards with UCB Pharma, Eisai, LivaNova, and GW Pharma. The remaining authors have no conflicts of interest.

PATIENT CONSENT

Patients gave written informed consent (project C11-16 and C19-55, conducted by INSERM and approved by the local ethic committees, CPP Paris VI and Sud Méditerranée 1).

ORCID

Louis Cousyn https://orcid.org/0000-0003-1407-5575
Valerio Frazzini https://orcid.org/0000-0003-1187-3352
Bertrand Mathon https://orcid.org/0000-0002-9182-5846
Vincent Navarro https://orcid.org/0000-0003-0077-8114
Mario Chavez https://orcid.org/0000-0003-0390-4833

REFERENCES

1. Le Van QM, Soss J, Navarro V, Navarro V, Robertson R, Chavez M, et al. Preictal state identification by synchronization changes in long-term intracranial EEG recordings. Clin Neurophysiol. 2005;116(3):559–68.
2. van Mierlo P, Papadopoulou M, Carrette E, Boon P, Vandenberghe S, Vonck K, et al. Functional brain connectivity from EEG in epilepsy: seizure prediction and epileptogenic focus localization. Prog Neurobiol. 2014;121:19–35.
3. Kuhlmann L, Karoly P, Freestone DR, Brinkmann BH, Temko A, Barachant A, et al. Epilepsyecosystem.org: crowd-sourcing reproducible seizure prediction with long-term human intracranial EEG. Brain. 2018;141(9):2619–30.
4. Navarro V, Martinerie J, Le Van Quyen M, Baulac M, Dubeau F, Gotman J. Seizure anticipation: do mathematical measures correlate with video-EEG evaluation? Epilepsia. 2005;46(3):385–96.
5. Schelter B, Winterhalder M, Maiwald T, Brandt A, Schad A, Timmer J, et al. Do false predictions of seizures depend on the state of vigilance? A report from two seizure-prediction methods and proposed remedies. Epilepsia. 2006;47(12):2058–70.
6. Karoly PJ, Ung H, Grayden DB, Kuhlmann L, Leyde K, Cook MJ, et al. The circadian profile of epilepsy improves seizure forecasting. Brain. 2017;140(8):2169–82.
7. Abbasi B, Goldenholz DM. Machine learning applications in epilepsy. Epilepsia. 2019;60(10):2037–47.
8. Kuhlmann L, Lehnertz K, Richardson MP, Schelter B, Zaveri HP. Seizure prediction — ready for a new era. Nat Rev Neurol. 2018;14(10):618–30.

9. Baud MO, Proix T, Rao VR, Schindler K. Chance and risk in epilepsy. Curr Opin Neurol. 2020;33(2):163–72.
10. Chavez M, Le Van QM, Navarro V, Baulac M, Martinerie J. Spatio-temporal dynamics prior to neocortical seizures: amplitude versus phase couplings. IEEE Transac Biomed Eng. 2003;50(5):571–83.
11. Janca R, Jezdik P, Cmejla R, Tomasek M, Worrell GA, Stead M, et al. Detection of interictal epileptiform discharges using signal envelope distribution modelling: application to epileptic and non-epileptic intracranial recordings. Brain Topogr. 2015;28(1):172–83.
12. Platt J. Probabilistic outputs for support vector machines and comparisons to regularized likelihood methods. Adv Large Margin Classif. 2000;10:10.
13. Cousyn L, Navarro V, Chavez M. Preictal state detection using prodromal symptoms: a machine learning approach. Epilepsia. 2021;62(2):e42–7.
14. Milikovsky DZ, Weissberg I, Kamintsky L, Lippmann K, Schefenbauer O, Frigerio F, et al. Electrocorticographic dynamics as a novel biomarker in five models of Epileptogenesis. J Neurosci. 2017;37(17):4450–61.
15. van Diessen E, Zweiphenning WJEM, Jansen FE, Stam CJ, Braun KPJ, Otte WM. Brain network Organization in Focal Epilepsy: a systematic review and meta-analysis. PLoS ONE. 2014;9(12):e114606.
16. Aydore S, Pantazis D, Leahy RM. A note on the phase locking value and its properties. Neuroimage. 2013;74:231–44.
17. Cook MJ, O'Brien TJ, Berkovic SF, Murphy M, Morokoff A, Fabinyi G, et al. Prediction of seizure likelihood with a long-term, implanted seizure advisory system in patients with drug-resistant epilepsy: a first-in-man study. Lancet Neurol. 2013;12(6):563–71.
18. Duun-Henriksen J, Baud M, Richardson MP, Cook M, Kouvas G, Heasman JM, et al. A new era in electroencephalographic monitoring? Subscalp devices for ultra–long-term recordings. Epilepsia. 2020;61(9):1805–17.
19. Ung H, Baldassano SN, Bink H, Krieger AM, Williams S, Vitale F, et al. Intracranial EEG fluctuates over months after implanting electrodes in human brain. J Neural Eng. 2017;14(5):056011.
20. Karoly PJ, Rao VR, Gregg NM, Worrell GA, Bernard C, Cook MJ, et al. Cycles in epilepsy. Nat Rev Neurol. 2021;17(5):267–84.
21. Freestone DR, Karoly PJ, Cook MJ. A forward-looking review of seizure prediction. Curr Opin Neurol. 2017;30(2):167–73.

SUPPORTING INFORMATION

Additional supporting information can be found online in the Supporting Information section at the end of this article.

How to cite this article: Cousyn L, Messaoud RB, Lehongre K, Frazzini V, Lambrecq V, Adam C, et al. Daily resting-state intracranial EEG connectivity for seizure risk forecasts. Epilepsia. 2023;64:e23–e29. https://doi.org/10.1111/epi.17480

Supplementary Table 1. Patients' main characteristics

Supplementary table 1 legend: F: female; M: male; MT: mesial temporal; TPO: temporo-parieto-occipital; FIAS: focal impaired awareness seizures; FAS: focal aware seizures; FBTCS: focal to bilateral tonic-clonic seizures; LTG: lamotrigine; ESL: eslicarbazepine acetate; DZP: diazepam; LCS: lacosamide; ZNS: zonisamide; CLB: clobazam; OXC: oxcarbazepine; PER: perampanel; CBZ: carbamazepine; TPM: topiramate; LVT: levetiracetam; VPA: valproic acid; SOZ: seizure onset zone; EIZ: exclusively irritative zone; RS: resting states.

The brain networks were visualized with the BrainNet Viewer (http://www.nitrc.org/projects/bnv/).

		#1	#2	#3	#4	#5	#6	#7	#8	#9	#10
Gender		F	F	F	F	M	F	M	M	M	F
Age, years		47	30	18	25	27	27	39	31	25	38
Location of epileptic focus		Left posterior temporal	Multifocal (right MT and TPO junction)	Right superior frontal gyrus	Left MT	Left precentral	Left posterior temporal	Left temporo-polar	Left MT	Right MT and temporo-polar	Right MT and temporo-polar
Seizures		FIAS	FIAS	FIAS	FBTCS	FAS, FIAS	FAS, FIAS	FAS, FIAS	FIAS, FBTCS	FAS, FIAS	FIAS
Antiepileptic drugs		LTG, ESL, DZP	LTG, LCS, ZNS, CLB	LTG, OXC, CLB	ESL, PER, TPM	LVT, LCS, PER	LTG, OXC	LCS, CBZ	CBZ, PER, ZNS	LVT, LTG	LTG, VPA, CBZ, CLB
Location of electrodes		Bitemporal	Right temporo-parieto-occipital	Right fronto-temporal	Left temporal and fronto-insular	Left pericentral	Left temporo-parieto-occipital	Left fronto-temporal and right frontal	Bitemporal	Right temporo-parietal	Right temporal
Red contacts: SOZ Orange contacts: EIZ Blue contacts: healthy areas		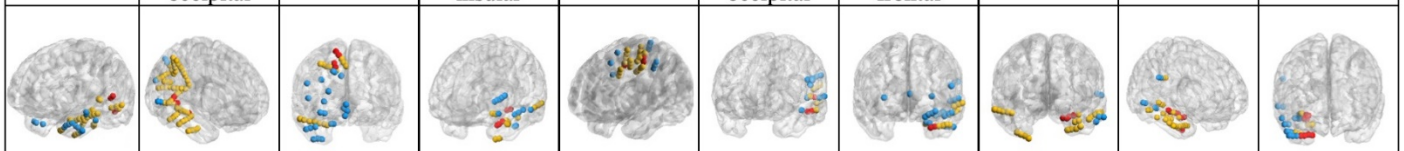									
Number of contacts	SOZ	4	5	4	7	3	4	2	4	10	8
	EIZ	30	58	15	13	22	7	13	23	24	6
	Other areas	14	5	22	12	9	10	25	5	7	17
Number of RS	Preictal	2	10	3	2	2	2	11	1	3	2
	Interictal	6	1	8	10	2	4	3	16	9	10
Mean delay between preictal RS and seizure onset, hours, min.-max.		6.5, 6-7	9.1, 1.8-21	4.2, 6-15	15.4, 14.5-16.3	15.6, 15-16.3	0.8, 0.5-1	8.8, 0.3-17	20	17.7, 13-21.5	12.5, 4-21

Supplementary Table 2. Comparison of classification models

Supplementary table 2 legend: We compared our connectivity-based model to two other models: i) a SVM classifier based on interictal epileptiform discharges (IEDs), that were automatically detected, or 'IED-based model' and ii) a simple classifier that based its predictions on the previous day's state (i.e., "preictal" if seizure(s) occurred on the previous day, and "interictal" otherwise) or 'anteriority-based model'. To assess these prediction models, we estimated AUC, accuracy, and F1-score.

The anteriority-based model yielded an average accuracy value of 0.75, but this value could be overestimated as accuracy does not take into account the class imbalance (i.e., the relative reduced number of preictal days). In this case, the F1-score, which combines the precision and recall, provides a better assessment of model performance. Here, the anteriority-based model yielded a poor F1-score of 0.53, which means that for each correct positive prediction, the model yielded two errors (false negative or false positives). Further, we noticed that, for this dataset, a non-informative (random) model would yield an averaged F1-score of 0.49 (for each patient, this non-informative model's F1-score can be estimated by $2p/[p+1]$, where "p" is the rate of positive events), which is very close to the anteriority-based model's F1-score.

IEDs: interictal epileptiform discharges

	AUC	**Accuracy**	**F1-Score**
Connectivity-based model (theta)	0.79 [min. 0.5 – max. 1]	0.77 [min. 0.52 – max. 1]	0.78 [min.0.62 – max. 1]
IED-based model	0.40 [min. 0.1 – max. 0.72]	0.54 [min. 0.45 – max. 0.69]	0.57 [min. 0.44 – max. 0.7]
Anteriority-based model	0.62 [min. 0.36 – 0.77]	0.75 [min. 0.66 – max. 0.9]	0.53 [min. 0 – max. 0.94]

II. Représentation des réseaux de connectivité intracérébrale dans un espace non euclidien hyperbolique pour la prédiction du risque de crise

1) Introduction

L'analyse des réseaux cérébraux par des mesures issues de la théorie des graphes a montré son intérêt tant pour l'étude de processus cognitifs physiologiques que de mécanismes pathologiques (Reijneveld et al. 2007; Bullmore et Sporns 2009; De Vico Fallani et al. 2014). L'évaluation fonctionnelle et anatomique des réseaux cérébraux, ainsi que leurs dynamiques, est cruciale pour appréhender l'ictogenèse (van Diessen et al. 2013).

Bien que la géométrie euclidienne représente le cadre habituel de notre réalité physique, les géométries non euclidiennes semblent pouvoir capturer davantage les caractéristiques non triviales relatives à la structure hiérarchique ou multi-échelle des données issues de réseaux complexes. Représenter les réseaux de connectivité cérébrale dans un espace non euclidien pourrait ainsi en augmenter le niveau d'informations structurelles et fonctionnelles.

Dans cette étude, nous avons utilisé des géométries non euclidiennes afin de représenter les réseaux de connectivité EEG intracérébrale quotidiens précédemment analysés (Cousyn et al. 2022) et tenté de mettre en évidence des propriétés qui pourraient s'avérer être des biomarqueurs encore plus robustes pour la prédiction des crises.

2) Méthodologie

Nous avons utilisé la base de données présentée dans l'article 4 (pages 129-135).

Des graphes de connectivité ont été créés à partir des matrices de synchronie de phase. Nous avons intégré nos graphes de connectivité dans un espace géométrique hyperbolique et plus précisément dans le modèle du disque de Poincaré. Les méthodes d'intégration ou de plongement de graphes permettent de représenter dans un espace de dimension inférieure des données complexes multidimensionnelles, tout en conservant leur niveau d'informations. Une distribution gaussienne hyperbolique a été définie à partir de l'intégration des graphes de connectivité des périodes intercritiques comme classe de référence. Pour chaque nouveau nœud issu d'un nouveau graphe de connectivité, nous avons estimé son erreur dans le disque hyperbolique en utilisant le modèle gaussien entraîné.

Une approche pseudoprospective a été réalisé afin d'évaluer les prédictions probabilistes quotidiennes du risque de crise

3) Résultats

La précision et le F1-score des prévisions quotidiennes ont progressivement augmenté avec la quantité de données du jeu d'apprentissage. Les résultats médians atteignaient respectivement 1 (min. 0,5, max. 1) et 1 (min. 0,61, max. 1) à partir de 3 enregistrements quotidiens dans chaque classe.

Six patients sur dix n'avaient aucune erreur de prédiction. Le score de Brier moyen était de 0,198 (min. 0,06, max. 0,25).

L'intégration de matrices de connectivité EEG dans un espace hyperbolique pourrait être un outil intéressant afin de représenter la connectivité cérébrale et d'en capturer les informations discriminantes utiles dans les modèles de prédiction des crises.

L'article de cette étude est en cours de préparation afin d'être soumis à publication dans une revue scientifique à comité de lecture.

4) Article 5 : Embedding intracranial EEG connectivity into hyperbolic space as a tool for seizure forecasting

Authors

Martin Guillemaud[a,*], Louis Cousyn[a,b,*], MD, Vincent Navarro[a,b], MD, PhD, Mario Chavez[c], PhD

[*] **Co-first authors**

[a] Paris Brain Institute (Inserm, CNRS, Sorbonne Université), Paris, France

[b] AP-HP, Department of Neurology, Epilepsy Unit, Pitié-Salpêtrière Hospital, Paris, France

[c] CNRS UMR-7225, Pitié-Salpêtrière Hospital, Paris, France

Correspondence to Mario Chavez, Paris Brain Institue, Hôpital Pitié-Salpêtrière, 47-83 boulevard de l'Hôpital, 75651 Paris Cedex 13, France.

Email: mario.chavez@upmc.fr

ORCID numbers:

Louis Cousyn: 0000-0003-1407-5575

Vincent Navarro: 0000-0003-0077-8114

Mario Chavez: 0000-0003-0390-4833

Abstract

In our previous study, we found intracranial EEG connectivity estimated from daily resting-state recordings allowed to identify preictal states. In this study, instead of studying original values of connectivity matrices, we used network embedding methods to capture non-trivial connectivity structures to predict the risk of seizure occurrence. Our approach aimed at exploring non-Euclidean geometries to represent brain networks of epileptic patients, and to work in the most appropriate hidden geometric space representation to unveil properties that could potentially result in robust biomarkers for seizure forecasting.

Our method consists in embedding the connectivity graphs into a hyperbolic geometrical space to find differences between preictal and interictal connectivity networks. We first defined Gaussian distributions in the hyperbolic space for each node using the embedded interictal connectivity networks as a reference class. Using the data of these interictal days, and the associated Gaussian models for each node, we could define a hyperbolic error for each single node that measured the connectivity difference for any new embedded network from the interictal days model.

In a pseudoprospective approach, we used the first n-days from each class to train the model. By means of a Student t-test estimated for each point in the hyperbolic disk, we could compare the embedded connectivity of both classes to define a region of interest (ROI). Once the model was trained, we compared all the embedded networks of the next days we wanted to predict to get hyperbolic error discs. We took the mean error in the ROI and, through a logistic regression function, we calculated the probability of each new day (out of the first n-days) of belonging to the interictal class.

Median accuracy and F1-score of daily probabilistic predictions were respectively 0.75 and 0.74 when only one day from each class was included in the training set. Performances significantly improved with a larger amount of learning data and median accuracy and F1-score reached a value of 1 when three daily recordings were included in both classes. Up to 60% of patients had no error (false positives or negatives) in the predictions.

Embedding intracranial EEG connectivity into a hyperbolic space is a promising tool for seizure forecasting, which may help capture more complex connectivity information than the traditional Euclidean geometry.

Introduction

In the last decades, complex networks have provided an increasingly challenging framework for the study of connected systems (from social sciences to biology and physics), based on the interplay between the wiring architecture and the dynamical properties of the coupled elements [1]. In neurosciences, the representation of brain networks as graphs allows to better describe their non-trivial connectivity properties in a compact and objective way [2,3]. In this mapping of brain data (surface EEG, iEEG, etc.) to networks, nodes usually represent brain regions or recording sites (e.g., EEG electrodes), and edges or links indicate functional connections between them (based on an estimated statistical relationship between the recorded signals).

Regardless of the modality of acquisition, the use of graph analysis in neuroscience has become essential to characterize pathological or physiological brain states in terms of connectivity networks [2-4]. Different graph measures, such as node centrality, communicability and efficiency have been shown to reveal complementary information on brain function in healthy and pathological conditions. However, the latent structure behind these brain network properties is still poorly understood.

Epilepsy is a neurological disorder nowadays conceptualized as a network disease with functionally and/or structurally aberrant connections on virtually all spatial scales [6]. According to this concept, a large-scale epileptic network comprises brain areas that can generate and sustain normal, physiological cortical dynamics during the seizure-free interval, and are mainly involved in the generation, maintenance, spread, and termination of pathophysiological activities such as seizures [6-7]. Network analysis in epilepsy has provided valuable information on seizure onset and propagation, as well as on the functional organization of the brain during the seizure-free interval [7]. During seizures, brain networks have been found to display a more regular structure with less variability [6,7]. Nevertheless, current representations of brain networks fail to provide reliable biomarkers to predict seizure onset [5-7].

Embedding (or vector space) methods find a lower-dimensional space in which high-dimensional complex data can be represented. Modern dimensionality reduction methods learn nonlinear similarities/proximities between points distributed over a hidden manifold in a multidimensional feature space, to preserve, embed (map) and visualize them in a low-dimensional space [8]. Although Euclidean geometry serves as a standard framework for studying our physical reality, increasing evidence suggests that non-Euclidean geometries are the more appropriate framework to capture non-trivial features (e.g., the hierarchical or multiscale structure) often observed in different biological networks, such as the olfactory space, cell development data, single-cell sequencing data, and the brain connectivity [9].

Current networks embedding methods assume a zero-curvature (or flat) space and evaluate the distance between points according to Euclidean metrics. These approaches are, however, limited when dealing with complex hierarchical structures, as the resulting pairwise distances in the embedded spaces are substantially distorted [9]. Recently, spaces with negative curvature (hyperbolic geometries) have attracted a lot of attention as they enable low-distortion embeddings of hierarchical or multi-scale connectivity structures [9-10]. Furthermore, endowed metrics of such spaces allow using some classical machine learning methods such as clustering, prediction, etc. [11].

In complex network analysis, the question of whether it exists a hidden (latent) geometry from which complex connectivity emerges has recently attracted the attention of the community [12-14] and is getting more and more ground. The possibility to find an effective congruency between brain network characteristics and its representation in hyperbolic spaces offers thus the possibility to understand its structure, and address the study of brain organization in a novel and promising framework.

In a previous study [15], we showed that intracranial EEG connectivity estimated from daily resting-state recordings, allowed to identify preictal states. In this study, instead of studying the original values of connectivity matrices, we used network-embedding methods to capture non-trivial connectivity structures to predict the risk of seizure occurrence. Our approach aimed at exploring non-Euclidean geometries to represent functional brain networks of patients with epilepsy, and to work in a more space representation to unveil properties that could potentially result in robust biomarkers for seizure forecasting.

Methods

- Data acquisition

The dataset used in this study was previously presented in [15]. Briefly, daily 10-minute resting-state periods were obtained in 10 patients (mean age 30.7 years) with drug-resistant focal epilepsy who intracranial EEG January 2019, to July 2021. The mean number of daily recordings per patient was 11.

Each daily recorded period was labelled as ‘preictal’ in case of electro-clinical seizure occurred in the next 24 hour, or ‘interictal’ otherwise. The approved by an institutional review board (C11-16 and C19-55 INSERM sponsor).

Connectivity graphs were derived from matrices of synchrony estimated between pairs of signals during 20-second non-overlapping epochs. Phase-locking values (PLV) were obtained in the typical EEG frequency bands (delta 1-4 Hz, theta 4-8 Hz, alpha 8-13 Hz, beta 13-30 Hz, low gamma 30-49 Hz and

high gamma 51-90 Hz). Only contacts in the gray matter were considered and a bipolar montage between adjacent contacts was applied. We classified the location of each contact according to the functional zone: seizure onset zone, irritative zone or 'putative' healthy zone.

- Preictal state forecasts

Our method consisted in embedding connectivity graphs into a hyperbolic geometrical space – more specifically into the Poincaré's disc model – to find differences between preictal and interictal connectivity networks. Connectivity difference for each single node, from the group of networks of interictal days was obtained through the following steps:

i) a filtering step of all the connectivity (PLV) matrices. This step consisted in keeping all the most meaningful connectivity structures by removing the weakest edges until reaching a fixed mean degree of 3 for the whole network [16];

ii) an embedding of all the graphs in the hyperbolic disk by using the coalescent embedding method [10]. Briefly, for a connectivity graph, the weight of the edges was modified using a repulsion attraction rule, giving more weight to edges having a bigger connectivity role for information transmission. The resulting matrix was then projected in a 2-dimensional space with a non-linear dimension reduction method (i.e., Laplacian eigenmaps). Next, the projected nodes underwent an equidistant adjustment in the polar coordinates: the angular coordinates of the nodes were modified by keeping the angular order of the node but standardizing the angle between 2 neighbors' nodes in the circle. Each radius was finally modified according to his rank by ordering the nodes according to their increasing degree (the number of connections in the original graph obtained in step i);

iii) a Gaussian distribution in the hyperbolic space was defined for each node using the embedding of all connectivity matrices of interictal days, considered here as the reference class [14];

iv) for any new embedded connectivity graph, we looked at each node position in the hyperbolic disc and calculated its error using the learned Gaussian model. This error measured the connectivity difference (from each node) from the interictal days model.

In a pseudoprospective approach, we used n-days from each class to train the model (Figure 1). By means of a Student t-test estimated for each point in the hyperbolic disk, we compared the embedded connectivity of both classes to define a region of interest (ROI). Once the model was trained, we compared all the embedded networks of the next days we wanted to predict to get hyperbolic error discs. We took the mean error in the ROI and, through a logistic regression function, we calculated the probability of each

new day (out of the first n-days) of belonging to the interictal class. For each patient, we combined the error values in ROIs obtained from networks at each frequency band, and looked for the combination that provided the best prediction as measured by the AUC values.

Classification performances were firstly assessed by the area under the receiver operating characteristic curve (AUC), which takes values between 0.5 for a random classification to 1 for a perfect classification; and the F1 Score, which is the weighted average of the recall and precision; and the accuracy. To evaluate forecasting performances, we also computed the Brier score, which ranges from 0 (perfect prediction) to 1 (worst prediction) [18].

Results

When only one day (n=1) from each class was included in the training set, the median accuracy of prediction was equal to 0.75 [min. 0.23, max. 1]. Nevertheless, this value raised to 1 [min. 0.5, max. 1] when the model was trained with 3 days from each class, or when considering all the previous days to predict a new day (Figure 2). Similarly, forecasts provided a median F1-score of 0.74 [min. 0.23, max. 1] when using a single day as learning set and a F1-score of 1 [min. 0.61, max. 1] (Figure 2). We compared our method with a simple prediction method that systematically attributed to a new day the category of the previous one (the basic assumption is that when patients have a seizure at a given day, a new seizure is more likely to occur the next day). This simple prediction method provided an accuracy of 0.76. In the most discriminant conditions (with a learning based on at least 3 previous days), the hyperbolic geometry model provided better daily predictions, which clearly suggests that connectivity conveys more discriminant information.

Overall, 6 patients over 10 had no error in the predictions, 2 patients had only one day mispredicted (in both cases, it involved the first interictal day after 2 preictal days) and 2 patients had respectively two and four mispredicted days. Forecasts yielded a mean Brier value was 0.198 (min. 0.06, max. 0.25), which suggested a good prediction model.

Discussion

Our study confirms our previous findings suggesting that intracranial EEG connectivity obtained from vigilance-controlled resting-state recordings can accurately forecast the risk of upcoming seizure. Besides, our results suggest that non-Euclidean geometry might offer a larger dimension of information and increase the discrimination between interictal and preictal states. We highlighted a clear improvement of prediction performances simultaneously with the amount of learning data. We believe long-term or very-long-term recordings could considerably refine our results. In addition, it is interesting to notice that false positives obtained by this method were only detected in two patients, and only occurred immediately after consecutive preictal periods. This might indeed reflect a proictal condition, in which seizures are more likely to happen but homeostatic control mechanisms could stop their emergence.

Specifically, this study reveals that non-Euclidean geometries are an appropriate framework to represent non-trivial connectivity features, providing thus a promising tool for accurately forecasting the daily risk of upcoming seizure(s). It is worthy noticing, however, that alternative non-Euclidean embeddings can be used (eg., spherical, elliptic). Similarly, other hyperbolic spaces such as Lorentz-Klein, d-dimensional Poincaré's ball, or half-space model are alternatives to represent the brain connectivity graphs.

Our study has some limitations. First, the vigilance-controlled resting-state iEEG recordings were obtained from hospitalized patients (candidates for a presurgical evaluation). Although we did not find trivial correlations between occurrence of seizures and the controlled medication tapering, inpatients remain far from real-life conditions. Second, the limited number of patients do not allow a direct generalization of our model. Our results suggest, however, a promising tool in seizure forecasting based on a single daily measure embedding in a non-Euclidean space.

In summary, embedding intracranial EEG connectivity into a hyperbolic space is a promising tool for seizure forecasting, which may help represent complex data and capture discriminant information between interictal and preictal states.

References

[1] S. Boccaletti, V. Latora, Y. Moreno, M. Chavez, and D.-U. Hwang (2006). Complex networks: Structure and dynamics. Physics Reports, 424:175-308.

[2] J. C. Reijneveld, S. C. Ponten, H. W. Berendse, and C. J. Stam (2007). The application of graph theoretical analysis to complex networks in the brain. Clinical Neurophysiology, 118, 2317- 2331.

[3] E. Bullmore and O. Sporns (2009). Complex brain networks: graph theoretical analysis of structural and functional systems. Nature Review Neurosciences, 10 (3), 1-13 .

[4] F. de Vico Fallani, J. Richiardi, M. Chavez, and S. Achard (2014). Graph analysis of functional brain networks: practical issues in translational neuroscience. Philosophical Transactions of the Royal Society B: Biological Sciences, 369(1653) 20130521.

[5] L. Kuhlmann, K. Lehnertz, M.P. Richardson, B. Schelter, and H.P. Zaveri (2018). Seizure prediction—ready for a new era. Nature Reviews Neurology, 14 (10), 618-630.

[6] M.A. Kramer, and S.S Cash (2012). Epilepsy as a disorder of cortical network organization. The Neuroscientist, 18(4), 360-372.

[7] E. van Diessen, S.J. Diederen, K.P. Braun, F.E. Jansen, and C.J. Stam (2013). Functional and structural brain networks in epilepsy: what have we learned? Epilepsia, 54 (11), 1855-1865.

[8] U. Von Luxburg (2007). A tutorial on spectral clustering. Statistics and computing, 17(4), 395-416.

[9] M. Boguñá, I. Bonamassa, M. De Domenico, S. Havlin, D. Krioukov, and M.A. Serrano (2021). Network geometry. Nature Reviews Physics, 3(2), 114-135.

[10] A. Muscoloni, J.M. Thomas, S. Ciucci, G. Bianconi, and C.V. Cannistraci (2017). Machine learning meets complex networks via coalescent embedding in the hyperbolic space. Nature communications, 8(1), 1-19.

[11] T. Hofmann, B. Schölkopf, A.J. Smola (2008). Kernel methods in machine learning. The Annals of Statistics, 36(3), 1171-1220.

[12] A. Allard and M.A. Serrano (2020). Navigable maps of structural brain networks across species. PLoS Computational Biology, 16(2): e1007584.

[13] M. Zheng, A. Allard, P. Hagmann, Y. Alemán-Gómez, M.A. Serrano (2020). Geometric renormalization unravels self-similarity of the multiscale human connectome. Proceedings of the National Academy of Sciences, 117 (33) 20244-20253.

[14] G. Thomas, H. Zaatiti, H. Hajri, N. Baskiotis, and O. Schwander (2019). From Node Embedding To Community Embedding : A Hyperbolic Approach. arXiv [1907.01662], July 2, 2019.

[15] L. Cousyn, R. Ben Messaoud, K. Lehongre, V. Frazzini, V. Lambrecq, C. Adam, B. Mathon, V. Navarro, M. Chavez (2023). Daily resting-state intracranial EEG connectivity for seizure risk forecasts. Epilepsia, 64 (2) e23-e29

[16] F De Vico Fallani, V Latora, and M Chavez (2017). Topological Criterion for Filtering Information in Complex Brain Networks. PLOS Computational Biology, 13 (1) e1005305.

[18] PJ Karoly, H Ung, DB Grayden, et al. (2017). The circadian profile of epilepsy improves seizure forecasting. Brain, 140 (8) 2169-2182.

Figure 1. Prediction method

Figure 1 legend: In this example, days 1 to 5 are used to predict if day 6 is a preictal or interictal day. Interictal days from days 1 to 5 are used to calculate gaussian model distributions for all the nodes. Then all the days from 1 to 5 are used, through the estimation of the error calculated with the learned Gaussian model, to define the region of interest (ROI) of the disc. The values of the training disc in this ROI are used to train a logistic regression model to predict the category of the following day.

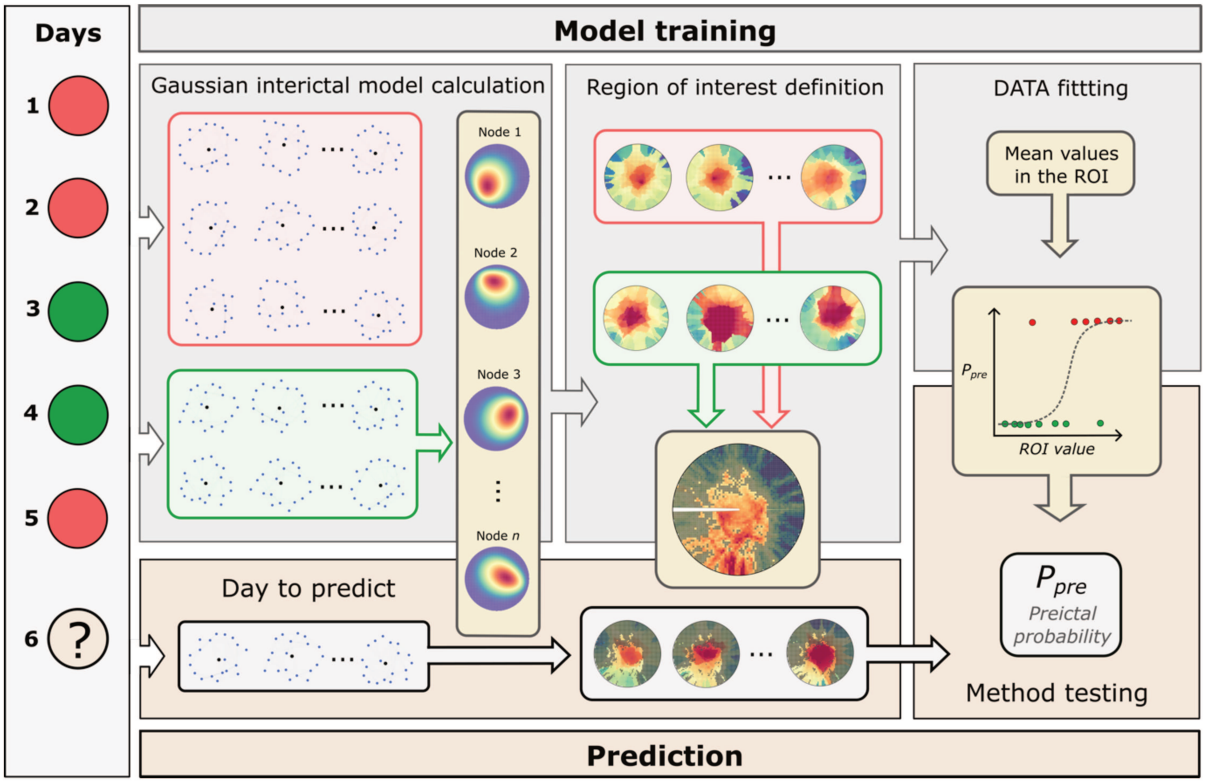

Figure 2. Prediction performances and amount of learning data

Figure 2 legend: Larger amount of learning data significantly improved accuracy and F1-score. Each dot represents the metric performance for one patient. The 'previous day prediction' model refers to the simple approach based on the seizure anteriority.

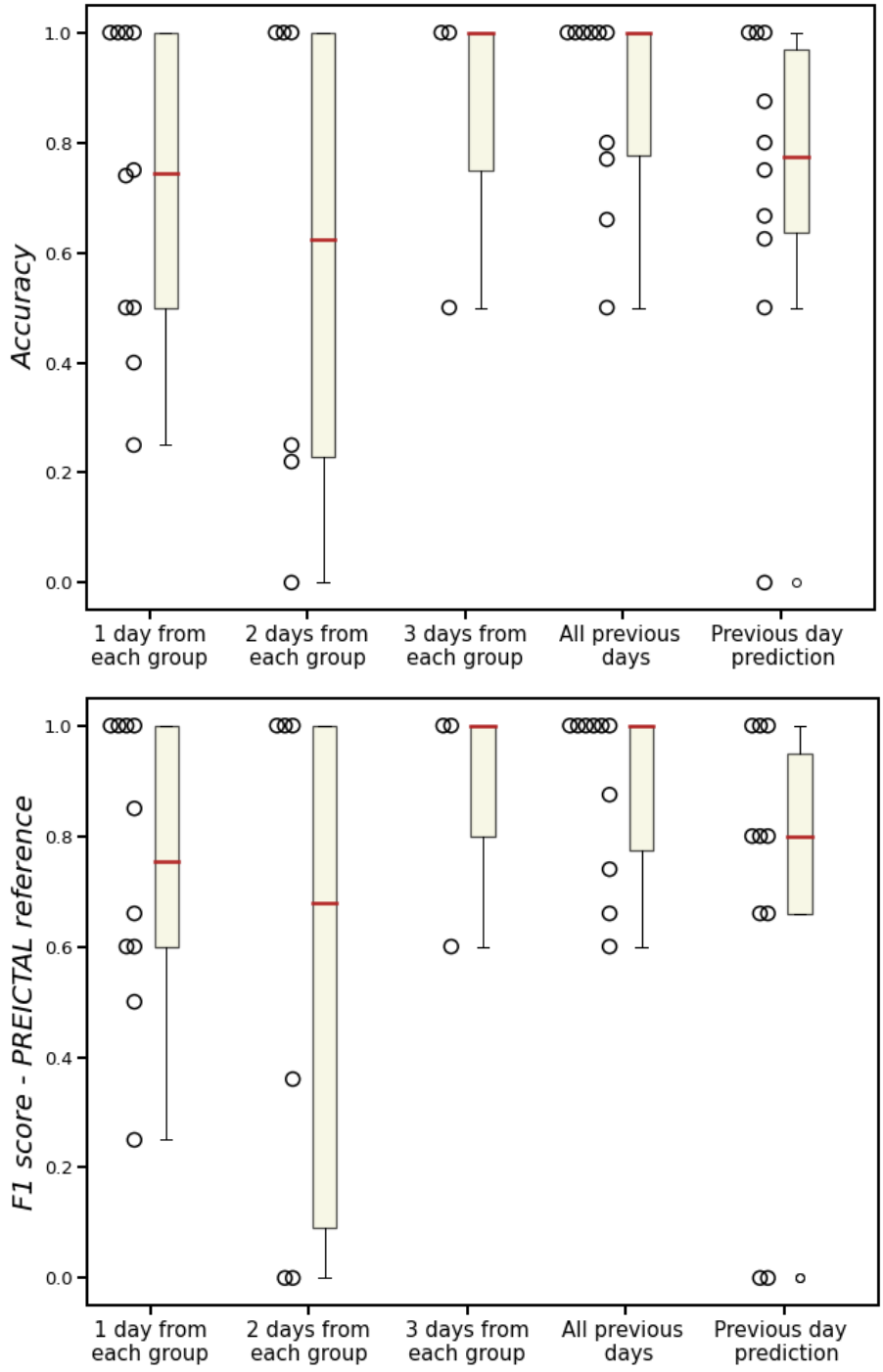

PARTIE 4. ÉTUDE DES ENREGISTREMENTS D'ACTIVITES UNITAIRES DE NEURONES IN VIVO AVANT LES CRISES

I. Introduction

L'utilisation de microélectrodes intracérébrales, intégrées dans les macroélectrodes classiques utilisées en routine dans le cadre des explorations en stéréo-électroencéphalographie, permet d'enregistrer des activités unitaires de neurones. Des comportements hétérogènes ont été individualisées dans des populations de neurones uniques putatifs (*single-unit activity*) lors de l'étude de la phase de transition intercritique/critique : certains neurones augmentaient leur fréquence de décharge, d'autres la diminuaient, alors que certains ne présentaient aucune modification de comportement (Truccolo et al. 2011; Lambrecq et al. 2017).

Nous faisons l'hypothèse que des changements de comportement à l'échelle neuronale – qu'il s'agisse de modifications individuelles ou interindividuelles entre neurones – pourraient survenir durant la période précritique (Figure 24).

L'objectif de cette étude est d'analyser sur des périodes prolongées les comportements neuronaux au cours du temps à la recherche de modifications uni ou multivariées durant la période précritique.

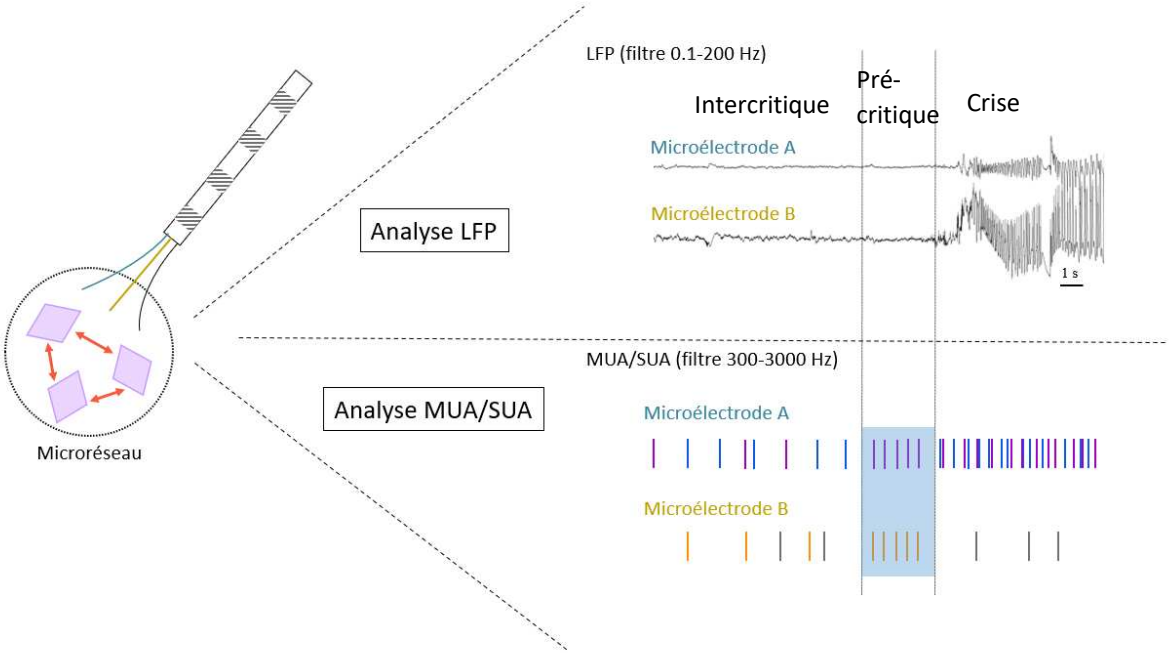

Figure 24. Modifications précritiques hypothétiques de l'activité unitaire de neurones

II. Méthodologie

- Implantations intracérébrales de microélectrodes

L'implantation de macroélectrodes intracérébrales (AdTech®, Wisconsin) a été réalisée dans le cadre des explorations cliniques préchirurgicales d'une épilepsie focale pharmacorésistante chez des patients hospitalisés dans l'unité d'épilepsie de l'Hôpital Pitié-Salpêtrière. Des microélectrodes de recherche ont été insérées à l'extrémité de certaines macroélectrodes. Cette étude a été approuvée par le comité d'éthique local (CPP Paris VI, INSERM C11-16 (2012-2020) ; INSERM C19-55).

- Enregistrements continus de l'EEG intracérébral (EEGi)

Les enregistrements combinés vidéo et EEGi étaient continus, 7j/7 et 24h/24, durant 2 à 3 semaines, dans le but d'enregistrer des crises d'épilepsie électro-cliniques. Nous avons utilisé le système d'acquisition Neuralynx® comportant 160 canaux (ATLAS, Neuralynx®, Inc., Bozeman, MO). La fréquence d'échantillonnage était de 4 kHz pour les macroélectrodes et 32 kHz pour les microélectrodes. Le choix de la référence était un macrocontact situé dans la substance blanche avec le moins possible d'activité pour les macroélectrodes et un des huit microcontacts pour les microélectrodes. Le filtre passe-bande appliqué était de 0,1 Hz-1000 Hz pour les macroélectrodes et 0,1 Hz-4000 Hz pour les microélectrodes. Une description détaillée des techniques d'implantation, du système d'acquisition et de l'amélioration de la qualité des enregistrements par les microélectrodes intracérébrales a été publiée par notre équipe (Annexe 1) (Lehongre et al. 2022).

- Sélection des patients

Parmi les patients enregistrés, nous avons sélectionné ceux présentant :

i) des crises d'épilepsie électro-cliniques enregistrées durant le séjour ;

ii) une microélectrode localisée dans la zone épileptogène ou *seizure onset zone* : une étape de relecture des tracés EEGi a consisté à définir l'emplacement des microélectrodes implantées (*seizure onset zone*, zone irritative, zone saine putative) ;

iii) de l'activité unitaire enregistrée par les microélectrodes : une deuxième étape a ainsi consisté à rechercher la présence d'activités unitaires sur les données brutes durant la période précédant les crises d'épilepsie.

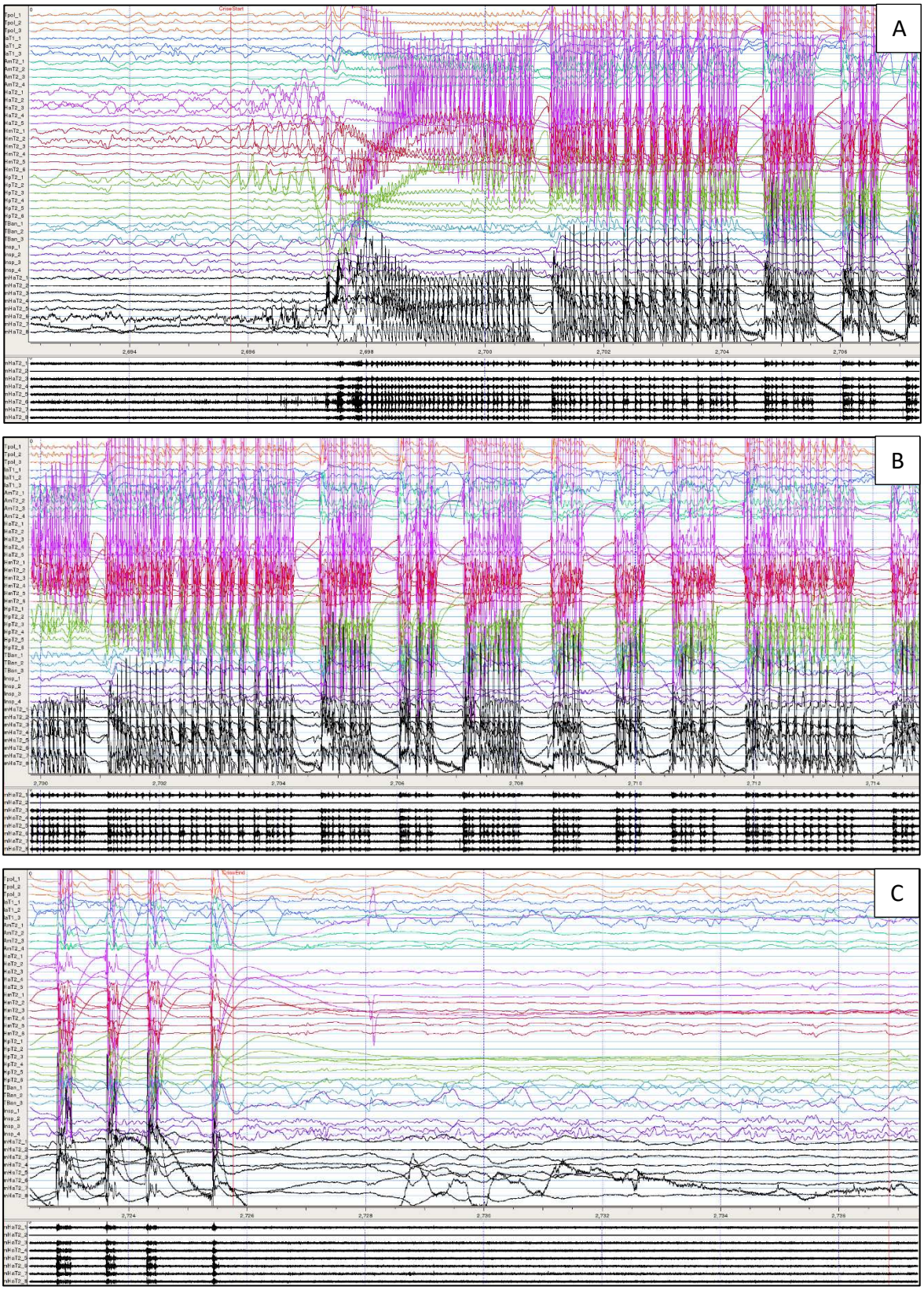

Figure 25. Délimitation de la crise d'épilepsie

Les signaux de couleur représentent les macrocontacts (bande passante 0,1-200Hz, gain 300µV/cm), en noir les microcontacts (bande passante 0,1-200Hz en haut, 300-3000Hz en bas ; gain 150µV/cm). Montages bipolaires, base de temps 15 sec. A) Le début de la crise d'épilepsie est placé au début de l'activité rythmique visualisée sur les macrocontacts hippocampiques (ligne rouge). B) Développement de la crise. C) Placement du marqueur de fin de crise (ligne rouge).

- Sélection des crises d'épilepsie

Une fois les patients sélectionnés, il convenait d'identifier puis sélectionner les crises à étudier. Une relecture des tracés de crise était donc nécessaire pour 1) localiser et marquer le début et la fin électriques de chaque crise (Figure 25), et 2) évaluer la quantité d'activités unitaires enregistrées sur les fichiers précédant la crise, car seules les crises disposant d'activités unitaires durant la période précritique étaient retenues.

- Rejet d'artefacts

Une étape de prétraitement des signaux des microélectrodes était ensuite réalisée sur les fichiers précédant l'apparition des crises sélectionnées des patients inclus. Nous avons choisi de réaliser un rejet d'artefacts manuel (marquage des périodes présentant des artefacts afin de les exclure par la suite des analyses) sur une période de 30min à 4h maximum avant la crise d'épilepsie (Figure 26).

- Tri des potentiels d'action ou *spike sorting*

Une fois les artefacts exclus, nous avons réalisé une détection puis un tri des potentiels d'action ou *spike sorting* en utilisant l'outil Spyking Circus (Yger et al. 2018). Cette méthode permet de détecter les potentiels d'action puis de les trier en activités unitaires putatives de neurones en plusieurs étapes :

i) filtrage : filtre passe-haut > 300 Hz ;

ii) détection des potentiels d'action par seuillage ;

iii) étape de *whitening* sur une période sans potentiel d'action, afin de supprimer les fausses corrélations spatio-temporelles entre les canaux ;

iv) analyse en composantes principales : pour chaque potentiel d'action détecté dans un sous-échantillon, les composantes principales permettant de distinguer au mieux la forme du potentiel sont gardées pour l'étape suivante ;

v) constitution de différents groupes de potentiels d'action ou *clustering* : chaque potentiel d'un sous-ensemble est assigné à un groupe ou *cluster* en fonction du centroïde le plus proche ;

vi) étape d'appariement des potentiels d'action à un groupe ou *cluster* sur l'ensemble des données.

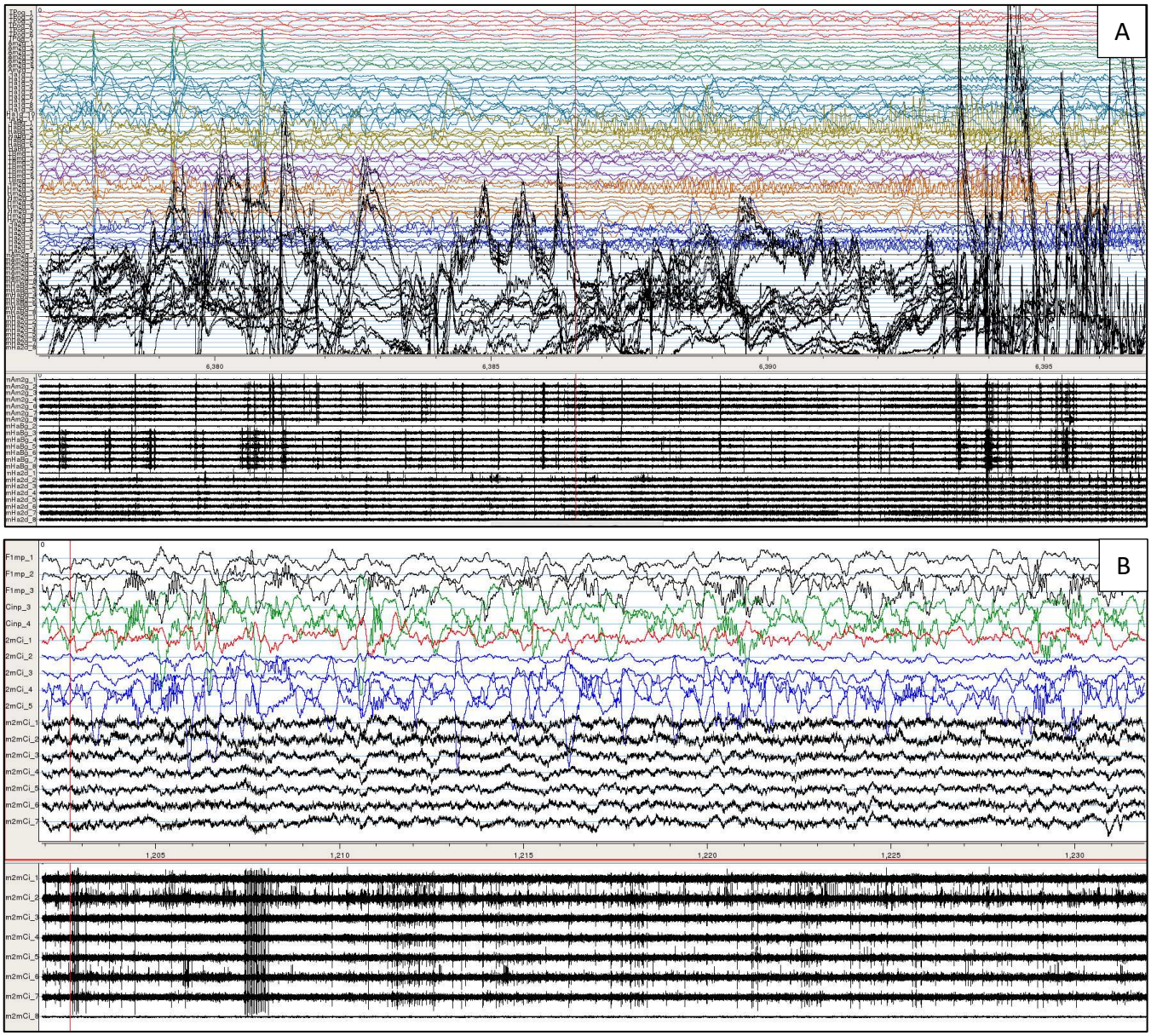

Figure 26. Étape de rejet d'artefacts

Les signaux de couleur représentent les macrocontacts (bande passante 0,1-200Hz, gain 300µV/cm), en noir les microcontacts (bande passante 0,1-200Hz en haut, 300-3000Hz en bas ; gain 150µV/cm). Montages bipolaires, base de temps 20 sec (A) et 30 sec (B). A) Nombreux artefacts amples diffus touchant les microélectrodes (LFP et activités unitaires). Le début de la crise est visible sur les macrocontacts hippocampiques (ligne rouge). B) Autre exemple d'artefacts affectant les microélectrodes, également diffus, mais peu amples et principalement visualisés après filtrage > 300 Hz.

- Visualisation et traitement des données

Nous avons ensuite visualisé nos données en utilisant phy (https://github.com/cortex-lab/phy). Cette interface permet d'afficher les résultats du *spike sorting* : chaque *cluster* d'activités unitaires est représenté, avec la possibilité d'évaluer la fréquence de décharge et la distribution de l'amplitude au cours du temps,

l'intervalle inter-spike (ISI), ainsi qu'un autocorrélogramme ou des corrélogrammes croisés avec les autres *clusters* (Figure 27).

Cette étape permet de contrôler les différents clusters identifiés et de les classer selon qu'il s'agisse d'un cluster d'artefacts, d'un cluster d'activités unitaires (*single-unit activity*, SUA) ou d'un cluster d'activités multi-unitaires (*multi-unit activity*, MUA). On peut également être amené à fusionner deux clusters d'activités unitaires si les différentes métriques orientent vers une activité unitaire de neurone unique putatif (Figure 27).

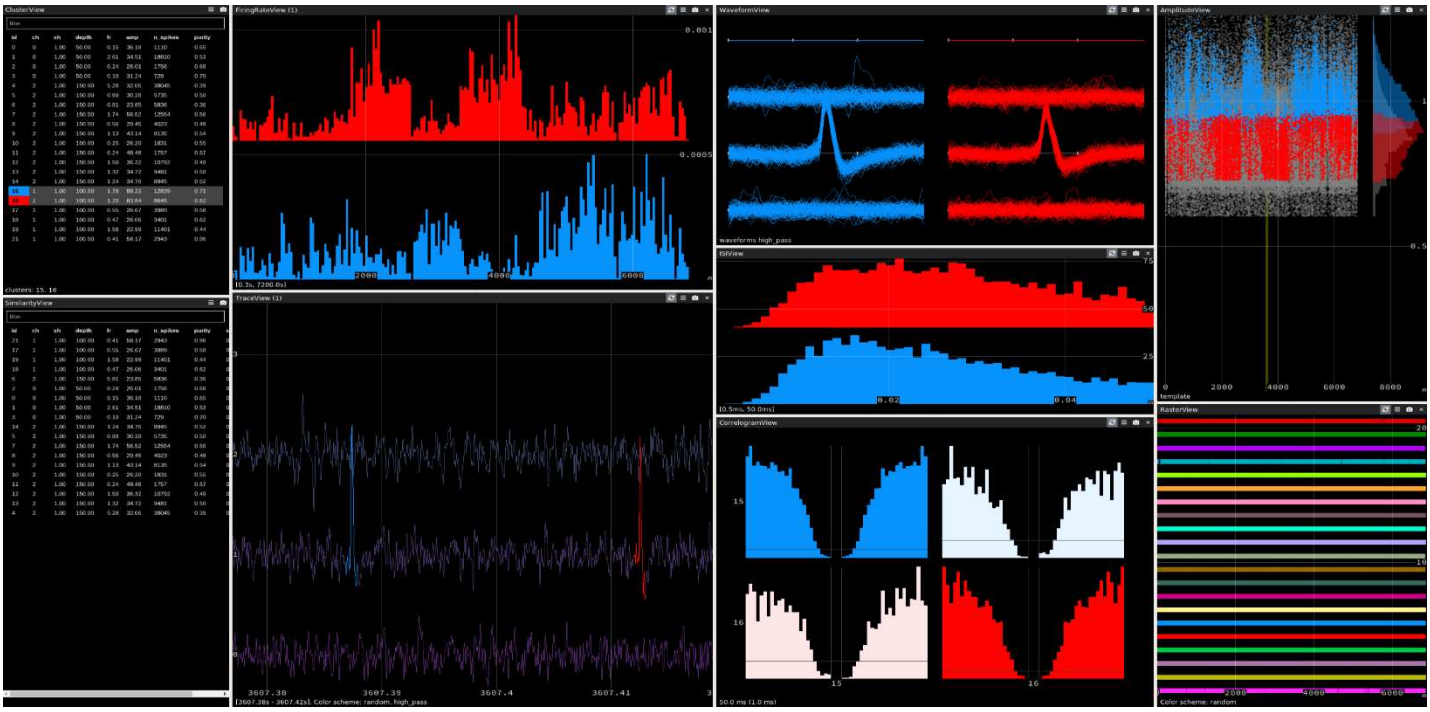

Figure 27. Visualisation des résultats du *spike sorting* sur « phy »
On peut observer les caractéristiques de deux clusters d'activités unitaires, un rouge et un bleu. Les différents paramètres représentés sont la fréquence de décharge au cours du temps (en haut à gauche), la morphologie du potentiel d'action moyen (*waveform*, au milieu et en haut), l'intervalle inter-spike (au centre), les autocorrélogrammes et corrélogrammes croisés (au milieu et en bas) et l'amplitude au cours du temps (en haut à droite). Les caractéristiques très similaires des deux clusters sont en faveur d'un unique neurone et donc d'une fusion des deux clusters.

- Analyses statistiques

Nous avons réalisé des analyses univariés pour chaque cluster : fréquence de décharge (moyenne et écart-type), facteur de Fano, coefficient de variation (CV et CV2) et nombre de *bursts*. Nous avons également étudié les interactions entre neurones par la mesure de synchronie de trains de potentiels d'action. Nous avons utilisé l'interface Spiky et plus précisément la mesure SPIKE-distance (Bozanic et Kreuz 2013; Kreuz et al. 2015). Le SPIKE-distance est une mesure de dissimilarité entre la survenue de plusieurs trains de potentiels d'action (Kreuz et al. 2011, 2013).

III. Résultats préliminaires

Nous avons identifié 23 patients ayant eu au moins une microélectrode sans la *seizure onset zone*. Quatre patients ont été exclus en raison de l'absence de crise enregistrée ou de données inexploitables (artefacts majeurs et/ou absence d'activité unitaire). Sur les 19 patients sélectionnés, les étapes de sélection/marquage des crises, rejet d'artefacts et *spike sorting* ont été réalisées à ce jour chez 8 patients. L'âge moyen était de 33,3 ans (min. 19, max. 55) et 7/8 avaient un foyer épileptique temporal interne. Le nombre moyen de crises par patient ayant pu être analysées durant la période précritique était de 3,4 (min. 1, max. 8).

Nous présentons les données préliminaires de 4 patients, chez qui les étapes de visualisation des données et traitement des différents *clusters* (artefacts, SUA, MUA, fusion) ont pu être appliquées. Un total de 8 périodes précritiques a été analysé, d'une durée moyenne de 2 heures (min. 48.3 minutes, max. 3.7 heures). Nous avons retenu en moyenne 2,5 clusters par période précritique étiquetés *single-unit activity* (min. 0, max. 6), et plus rarement des clusters étiquetés *multi-unit activity* (un cluster retrouvé sur 3 périodes précritiques). Le nombre moyen d'unités par période précritique était de 27628,25 (min. 1516, max. 79937).

Les analyses uni et bivariées n'ont pas montré visuellement de modifications évidentes durant la période précritique (Figures 28 et 29). Des mesures statistiques vont être appliquées afin de déceler des modifications plus subtiles de certains comportements neuronaux (mesures comparatives, comparaison à une période de référence intercritique, etc.).

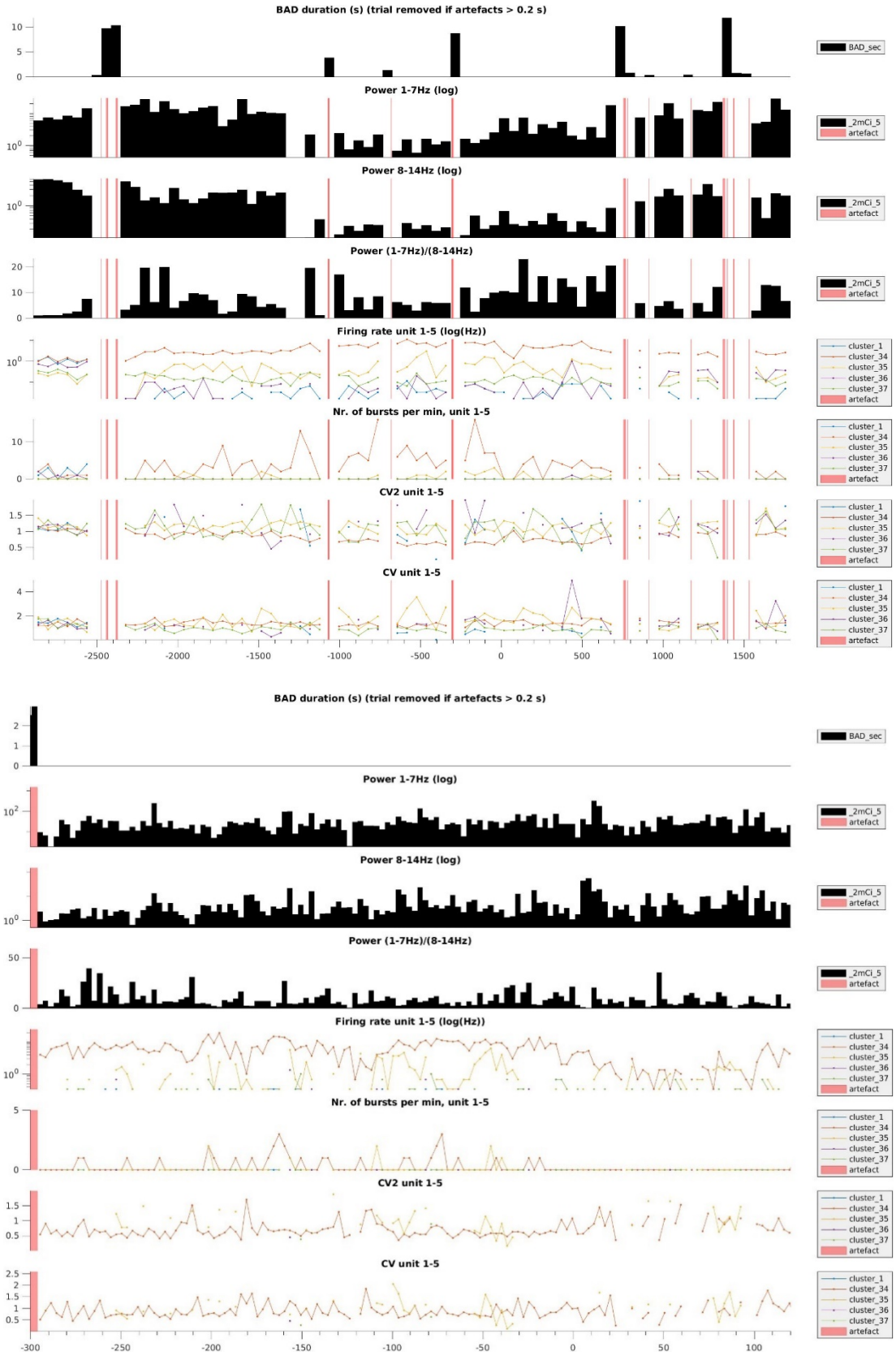

Figure 28. Analyses univariées des activités unitaires au cours du temps

Représentation pour un patient donné des différentes analyses univariées (analyses fréquentielles, fréquence de décharge, nombre de *bursts*, CV et CV2). Le graphe du haut représente la période d'analyse complète et celui du bas un zoom sur les 300 secondes précédant la crise. La crise survient au temps 0.

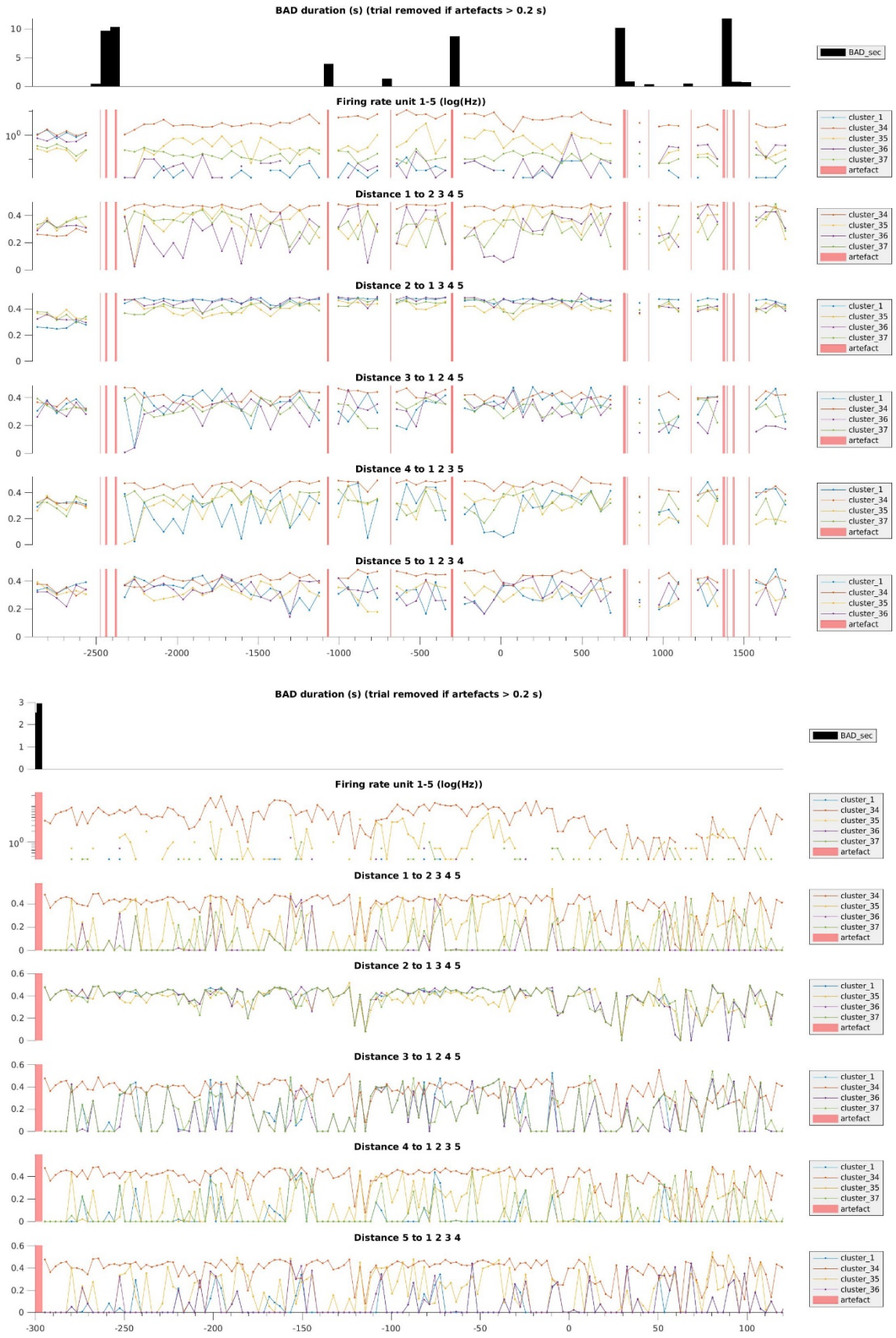

Figure 29. Analyses bivariées des activités unitaires au cours du temps

Représentation pour un patient donné d'une mesure de dissimilarité entre les trains de potentiel d'action de deux neurones putatifs différents. Le graphe du haut représente la période d'analyse complète et celui du bas un zoom sur les 300 secondes précédant la crise. La crise survient au temps 0.

IV. Discussion et perspectives

Nos résultats préliminaires n'apportent pas encore d'arguments pour des modifications précritiques évidentes à l'échelle neuronale. Il ne s'agit cependant que des données issues d'un nombre limité de patients, aussi il est nécessaire de poursuivre les analyses sur l'ensemble de la cohorte de patients sélectionnés. Par ailleurs, les données actuellement analysés présentaient parfois de nombreux artefacts ayant été rejetés durant la phase de prétraitement des signaux.

Je poursuis actuellement les analyses des comportements individuels et interindividuels d'activité unitaire de neurones durant les périodes précritiques. Je compte par la suite effectuer des analyses de type chaîne de Markov, particulièrement adaptées à l'étude des processus dynamiques aléatoires, et qui pourrait s'intéresser aux successions de décharges entre les différents neurones.

PARTIE 5. ÉTUDES IN VITRO SUR TRANCHES DE TISSU CEREBRAL HUMAIN

I. Introduction

Des enregistrements *in vitro* sur tranches de cortex cérébral humain ont pu mettre en évidence des décharges précritiques sous contrôle glutamatergique avec une morphologie particulière précédant la survenue des crises (Huberfeld et al. 2011). Ces études ont été réalisées exclusivement sur des exérèses de sclérose hippocampique. Or, l'hippocampe est un archicortex qui présente des réseaux et des sous-types neuronaux bien particuliers. Dans le néocortex, la microarchitecture est différente, souvent organisée en colonnes, et il y a un nombre d'interneurones différents. Les études *in vitro* du néocortex épileptique humain sont rares, et les crises sont parfois difficiles à enregistrer – à moins d'utiliser des bloqueurs du $GABA_A$ mais ce qui limite considérablement la généralisation des données (Kandrács et al. 2019).

L'étude des modifications précritiques *in vitro* de tissus épileptiques de localisations et d'étiologies différentes pourrait élargir nos connaissances des mécanismes physiopathologiques sous-tendant l'ictogenèse.

L'objectif de cette étude est d'enregistrer *in vitro* des tranches de cortex cérébral épileptique en per-opératoire afin de mettre en évidence des modifications précritiques de comportement des populations neuronales et de les associer à d'éventuelles anomalies histologiques.

Ce travail a été réalisé en collaboration avec Florian Donneger et Jean-Christophe Poncer de l'équipe "Plasticité des réseaux corticaux et épilepsie" de L'institut du Fer à Moulin (INSERM U1270).

II. Méthodologie

- Patients

Nous avons étudié le tissu cérébral épileptique au décours d'une exérèse du foyer épileptogène réalisé dans le cadre de la prise en charge chirurgicale des épilepsies focales pharmacorésistantes. Les patients ont donné leur consentement écrit éclairé.

Cette étude a été approuvée par le comité d'éthique local (étude TIPI, CPP INSERM C16-16).

- Transport et découpe du tissu

Une fois l'exérèse du tissu effectué, il était immédiatement placé dans une solution de transport froide (0-4°C) et oxygénée constituée de : N-méthyl-d-glucamine 93mM, KCl 2,5mM, NaH2PO4 1,2mM, NaHCO3 30mM, HEPES 20mM, D-glucose 20mM, acide ascorbique 5mM, pyruvate de sodium 3mM, MgSO4 10mM et CaCl2 0,5mM. Le pH cible était de 7,4 et l'osmolarité cible de 285-290mOsm.

Le tissu était amené le plus rapidement possible au laboratoire du Fer à Moulin (15-20min). Des tranches de 400µm d'épaisseur étaient découpées par vibratome (HM650V, Microm). Les tranches étaient ensuite placées dans une chambre d'interface pour incubation à 37°C avec du LCR de synthèse oxygéné composé de : D-glucose 10mM, KCl 3,5mM, NaHOC3 26mM, NaH2PO4 1,25mM, NaCl 126mM, CaCl2 1,6mM er MgCl2 1,2mM.

- Enregistrements en MEA

Les tranches étaient ensuite placées une par une dans la chambre d'enregistrement par *multi-electrode array* (MEA) (Figure 30). Nous avons utilisé la station MEA2100 (Multi Channel Systems) équipé de 120 électrodes de 30µm de diamètre et espacées de 100µm, permettant un enregistrement extracellulaire de potentiels de champs locaux. Du LCR de synthèse oxygéné à 37°C était perfusé à un début de 6mL/min.

Une solution pro-convulsivante "haut K+/bas Mg2+" pouvait être perfusée en extracellulaire : D-glucose 10mM, NaHOC3 26mM, NaH2PO4 1,25mM, NaCl 126mM, KCl 6mM, MgCl2 0,25mM, CaCl2 1,6mM.

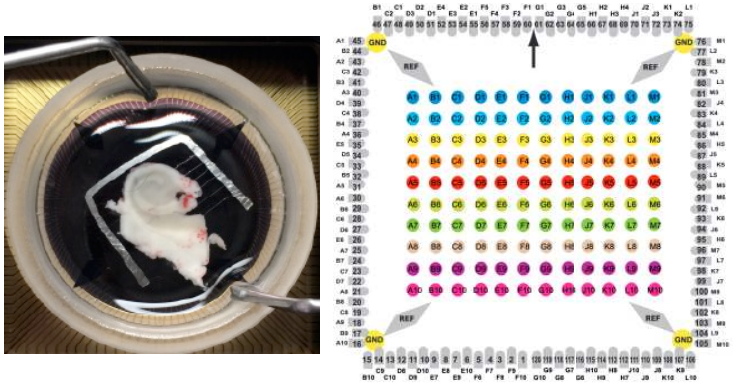

Figure 30. Chambre d'enregistrement MEA
Chambre constituée de 120 électrodes (Multi Channel Systems)

III. Résultats préliminaires

Nous avons pu enregistrer *in vitro* le tissu cérébral réséqué de 6 patients. L'âge moyen des patients était de 23,2 ans (min. 18 ans, max 49 ans). Le foyer de résection était temporal dans 4/6 cas. L'analyse anatomopathologique était négative chez 4/6 patients ; un patient avait une dysplasie corticale focale frontale et une autre patiente une lipofuscinose neuronale focale.

Nous avons enregistré 7 pièces opératoires chez 6 patients. Le nombre moyen de tranches analysées par pièce opératoire était de 7 (min. 3, max. 10). Nous avons mis en évidence des anomalies épileptiques sur 5/7 pièces opératoires, qui n'étaient que très sporadiques et apparues après perfusion de la solution pro-convulsivante sur 2/5 des tissus.

Nous avons réussi à enregistrer des crises sur un des tissus post-opératoires (néocortex temporo-polaire) : sur les 10 tranches analysées, toutes présentaient des activités épileptiques spontanées, et des crises se sont développées sur 9/10 tranches après administration de la solution pro-convulsivante (Figure 31). Chaque décharge était précédée d'une augmentation progressive de l'amplitude des anomalies épileptiques intercritiques (Figure 32).

Nous avons pu enregistrer chez un autre patient des anomalies épileptiques pseudopériodiques (1,2 Hz) très abondantes spontanées (néocortex temporal postérieur), avec une augmentation significative de la fréquence de décharge après ajout de la solution pro-convulsivante (Figure 33). L'administration d'un antagoniste des récepteurs $GABA_A$ (la gabazine) a fait complètement disparaître les anomalies épileptiques localisées et a laissé place à des oscillations diffuses de haute amplitude. L'ensemble a suggéré l'implication d'interneurones gabaergiques dans la genèse des anomalies épileptiques. Ces résultats ont été rapportés dans une revue scientifique en collaboration (Annexe 2) (Frazzini et al. 2022).

IV. Discussion et perspectives

Nous n'avons pu enregistrer des crises que sur un seul des tissus récupérés. L'augmentation progressive d'amplitude des anomalies épileptiques précritiques est concordante avec les modifications de morphologie rapportées au niveau hippocampique durant l'ictogenèse (Huberfeld et al. 2011).

Plusieurs hypothèses peuvent expliquer le peu d'anomalies épileptiques enregistrées. Il peut s'agit de conséquences chirurgicales : le tissu est en effet déconnecté anatomiquement de son réseau épileptique. De plus les tissus enregistrés n'étaient parfois qu'une partie tronquée du foyer épileptique, pour des questions techniques d'exérèse. Ensuite, il était parfois difficile pour les chercheurs d'orienter convenablement la pièce afin de guider la découpe. A la différence de l'hippocampe qui présente des

structures facilement identifiables, nos exérèses néocorticales ne permettaient d'avoir de tels repères. De plus, la distinction de la substance blanche et de la substance grise était parfois compliquée (délitement du tissu, etc.). Enfin, notre technique d'enregistrement était peut-être limitée et une densité plus importante d'électrodes pourrait permettre de mieux couvrir le tissu cérébral et d'augmenter les chances d'enregistrer des activités.

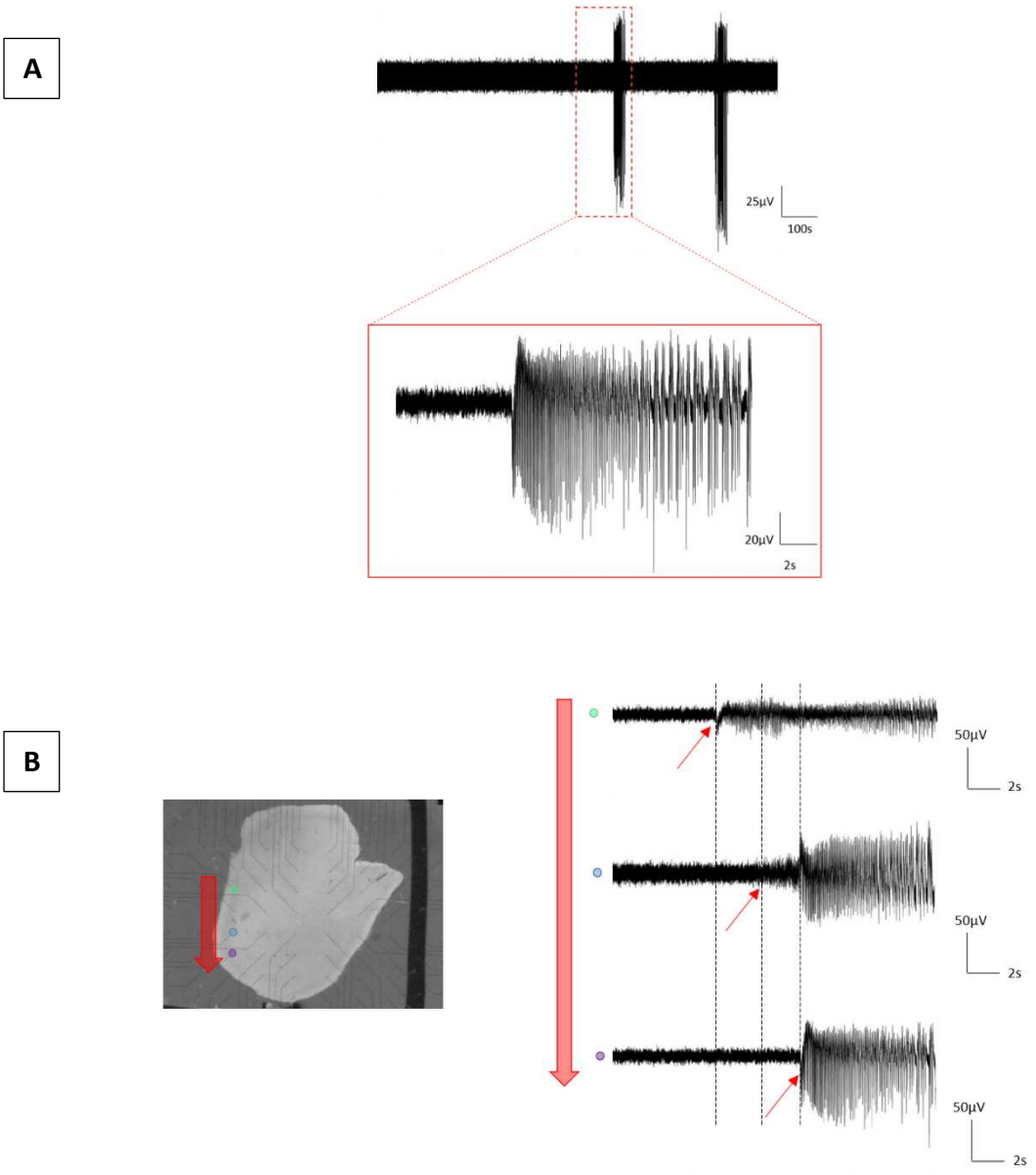

Figure 31. Enregistrement de plusieurs décharges épileptiques en MEA
A. Plusieurs décharges sont enregistrées au cours du temps avec construction temporelle. B. Propagation spatiale des décharges aux différentes électrodes.

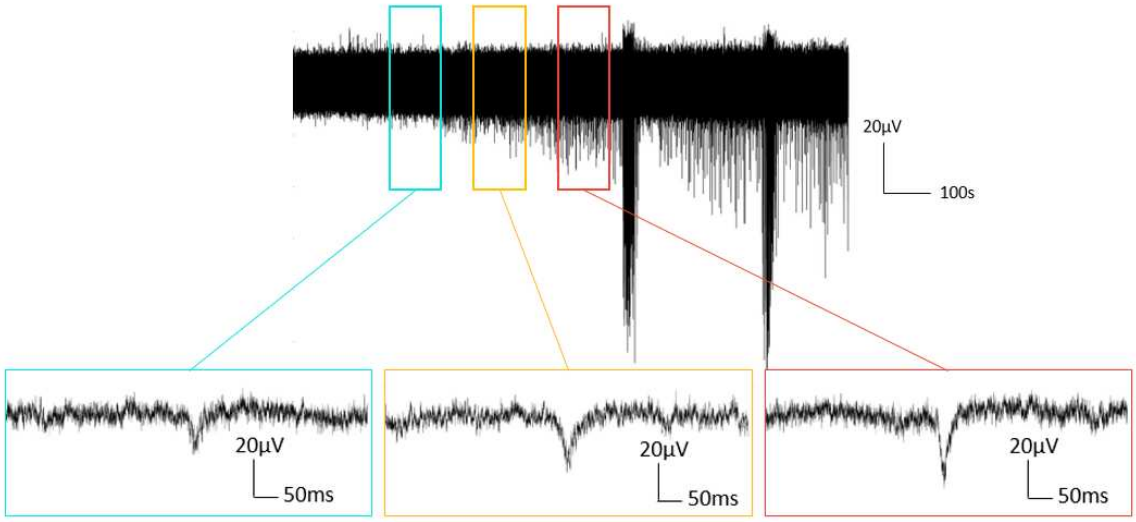

Figure 32. Modification précritique des anomalies épileptiques en MEA
Augmentation progressive de l'amplitude des anomalies épileptiques durant la période précritique.

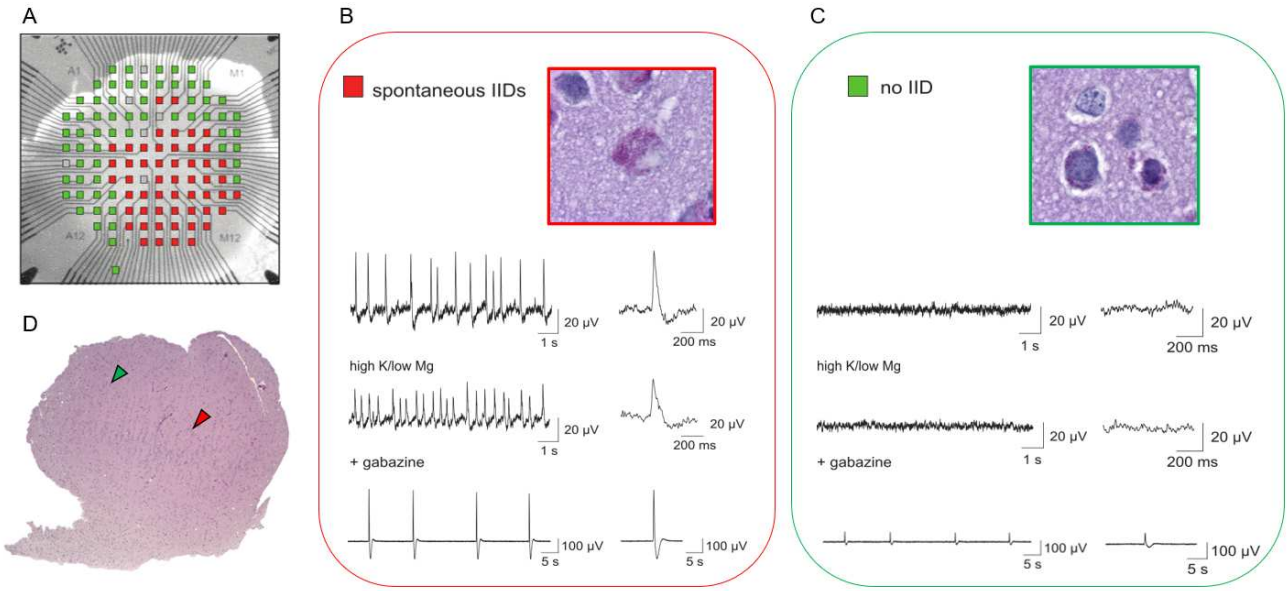

Figure 33. Anomalies intercritiques enregistrées en MEA
Anomalies épileptiques abondantes périodiques avec augmentation de la fréquence de décharge après perfusion d'une solution excitatrice et disparition des anomalies après perfusion de gabazine, un antagoniste des récepteurs $GABA_A$.
(Figure issue de Frazzini et al., 2022)

Discussion générale

Au cours de ce travail, nous avons cherché à identifier des modifications spécifiques d'un état précritique afin d'individualiser des biomarqueurs qui pourraient être appliqués en pratique clinique. L'approche probabiliste de nos modèles de prédiction – adaptée à l'estimation du risque de crise – est en accord avec les données actuelles de la littérature. Les nouvelles stratégies de prédiction des crises s'orientent davantage vers une conception non-déterministe afin de mieux s'adapter aux dynamiques complexes ponctuées d'évènements stochastiques de l'épilepsie.

Nous discuterons d'une part des enjeux cliniques et d'autre part des problématiques méthodologiques soulevés par nos travaux, et enfin nous aborderons les différentes perspectives scientifiques dans l'identification de modifications précritiques.

PARTIE 1. QUELS SONT LES ENJEUX CLINIQUES A RELEVER ?

I. La définition de la période précritique

Par essence, il n'y a pas de définition temporelle ou délimitation claire de la période précritique, puisqu'il s'agirait d'une période de transition d'installation progressive jusqu'à la survenue d'une crise. Si les stratégies initiales visaient à détecter des modifications dans le secondes à minutes précédant la crise, les nouvelles stratégies probabilistes proposent une estimation du risque de crise sur des périodes prolongées pouvant aller jusqu'à 24h avant la crise (Cook et al. 2013; Proix et al. 2021).

Dans nos différentes approches – cliniques, ECG et EEG – nous avons choisi de réaliser une mesure unique quotidienne, au repos, afin d'estimer le risque de crise sur les prochaines 24h. Cette stratégie présente un intérêt pratique évident et repose sur une méthode réaliste dans l'éventualité d'une application pratique. Cependant, une mesure ponctuelle chargée d'estimer une probabilité de crise sur une période beaucoup plus étendue ne peut rendre compte que des dynamiques lentes mais pas de changements d'état rapides. Cette approche, qui est plutôt dédiée à la recherche d'un état procritique, est donc à risque de faux négatifs.

II. Techniques invasives versus non-invasives

Les modèles de prédiction des crises basés sur les données EEG ont principalement été réalisés sur des enregistrements intracrâniens, afin de traiter une information située le plus proche possible du réseau épileptogène – particulièrement en cas de foyer profond (temporal interne, etc.). Le signal recueilli par les EEG intracrâniens est également moins perturbé par des artefacts (musculaires, etc.) et moins sujet aux effets de conduction volumique que celui des EEG de surface. De plus, les EEG de surface enregistrent également avec moins de précision les activités de hautes fréquences et de faibles amplitudes.

Les résultats de notre évaluation de la connectivité cérébrale sont prometteurs et suggèrent des changements au sein du réseau épileptogène et de ses interactions – à petite et plus grande échelle – avec d'autres régions cérébrales qui pourraient refléter une connectivité particulière à risque de crise. Cependant, ces résultats ne sont issus que de la connectivité fonctionnelle intracérébrale, obtenue par le biais d'une intervention neurochirurgicale, nécessitant une hospitalisation continue durant plusieurs jours. Il est donc légitime de se demander si de telles modifications pourraient être individualisées à partir des signaux d'EEG de surface d'une part, et sur des enregistrements réalisés à domicile par le patient d'autre part. Des dispositifs permettant de réaliser des EEG non invasifs à domicile ont été développés ces dernières années (Biondi et al. 2022).

Des dispositifs moins invasifs que les macroélectrodes intracérébrales permettant des enregistrements EEG intracrâniens d'ultra longue durée en ambulatoire sont (ou ont été) également disponibles et en cours d'évaluation dans le domaine de la prédiction des crises (le système RNS de NeuroPace, ou bien le système NeuroVista – finalement non commercialisé) (Cook et al. 2013; Baud et al. 2018; Proix et al. 2021). Ces dispositifs implantables semblent très prometteurs et permettent une stimulation corticale à visée thérapeutique en cas de détection d'une crise d'épilepsie. Il serait intéressant d'évaluer la possibilité de stimulation en cas de détection d'un pattern précritique (Nagaraj et al. 2015; Sisterson et al. 2019).

Une autre question est celle de l'extraction non-invasive de signaux extra-cérébraux, et notamment l'activité ECG, électrodermale, etc. dans les méthodes de prédiction. Si leur enregistrement permet de s'affranchir de tout acte invasif, notamment par l'utilisation des dispositifs portables (montre connectée, smartphone, etc.), on peut s'interroger sur le niveau d'informations dont ils disposent pour identifier un état précritique par rapport aux enregistrements de l'activité cérébrale. Dans notre travail, nous avons en effet mis en évidence des performances nettement moindres des modèles utilisant la variabilité de la fréquence cardiaque au regard de ceux alimentés par les données de connectivité cérébrale. Cependant, les résultats faisaient mieux que le hasard, suggérant que des informations discriminantes pouvaient être

contenues dans les données ECG. Une approche multimodale non-invasive, associant des métriques issues de différentes modalités d'acquisition (cardiaque, sommeil, activité, humeur, etc.) pourrait améliorer les performances de prédiction.

III. Quels impacts de la prédiction pour le patient ?

Dans l'éventualité d'une estimation du risque de crise délivrée quotidiennement au patient, il faut se questionner sur l'effet d'une telle information sur sa vie quotidienne. À la différence d'un modèle déterministe – où la sortie concernant le risque de crise serait binaire : oui ou non – la probabilité du risque de crise est par définition incertaine. Si l'approche probabiliste semble beaucoup plus adaptée, pour des raisons physiopathologiques déjà abordées, la résultant d'un tel modèle amène son lot de questions. Si le principe d'incertitude était méthodologiquement séduisant, il l'est moins lorsque l'on s'interroge sur son application pratique. En effet, si le risque de crise varie de 0% à 100%, comment interpréter des résultats intermédiaires ? En d'autres termes, à partir de quelle probabilité peut-on estimer que le risque de crise est significatif et nécessite une quelconque intervention ?

Le danger est donc une interprétation subjective du risque, qui pourrait amener son lot d'anxiété, de surconsommation de médicaments antiépileptiques « de secours » type benzodiazépines, etc. Une idée serait peut-être une approche mixte : probabiliste pour estimer le risque de crise en fonction des différents paramètres dynamiques, et déterministe pour la sanction thérapeutique – qu'il s'agisse de la prise d'une molécule antiépileptique d'action rapide ou d'une neurostimulation via un dispositif implantable.

De même, l'effet de la prédiction en elle-même – qu'elle soit déterministe ou probabiliste – a nécessairement un effet de renforcement positif ou négatif chez le patient. En cas de démocratisation de la prédiction des crises auprès des patients, un phénomène de prophétie auto-réalisatrice pourrait être observé chez certains d'entre eux. Il serait judicieux, quand les techniques de prédiction seront entre les mains des patients, de recueillir leur expérience et leur avis sur une telle pratique.

PARTIE 2. QUELLES PROBLEMATIQUES METHODOLOGIQUES SONT A PRENDRE EN CONSIDERATION POUR LA PREDICTION DES CRISES ?

Lors de la construction méthodologique de nos différentes études, plusieurs questionnements relatifs à la gestion des jeux de données, aux conditions d'enregistrement ou encore à l'interprétation des résultats se sont imposés à nous, en raison de leur impact possible sur la qualité de nos modèles de prédiction.

I. La gestion des jeux de données

1) Les données déséquilibrées

L'un des principaux problèmes statistiques des algorithmes de prédiction des crises est le déséquilibre entre le nombre de données précritiques et intercritiques disponibles pour la phase d'apprentissage. La plupart des modèles de prédiction statistiques ont en effet tendance à être plus précis pour prédire la classe ayant le plus grand nombre d'échantillons d'entraînement. Pour lutter contre ce déséquilibre en faveur de la classe majoritaire, différentes méthodes de rééchantillonnage sont disponibles. Il peut s'agir d'un sous-échantillonnage de la classe majoritaire (dans notre cas, il s'agira principalement des données intercritiques) ou d'un sur-échantillonnage de la classe minoritaire (le plus souvent, les données précritiques), et ce afin d'atténuer ce biais et de rééquilibrer les données entre les deux classes (Varotto et al. 2021). Certaines méthodes d'apprentissage peuvent traiter ce problème de déséquilibre en attribuant des poids plus élevés aux échantillons de la classe minoritaire afin de modifier leur préférence pour la classe majoritaire (Zhou et Liu 2006; Park et al. 2011).

Nous avons pris en considération ce biais lors de nos différentes approches par une technique de sur-échantillonnage des données de la classe précritique minoritaire basée sur les similarités des données existantes (SMOTE, *synthetic minority oversampling technique*) (Fernández et al. 2018).

2) La fuite de données lors de la validation croisée

La réalisation d'une validation croisée est gage de qualité lors de l'évaluation d'un algorithme de classification (King et al. 2021). Cependant, lorsqu'elle est appliquée sur la totalité des données (EEG ou autre) d'une même série temporelle, elle peut être à l'origine d'un biais courant. En effet, les données d'une

même série temporelle ne sont pas indépendantes, il existe des corrélations temporelles entre les segments consécutifs d'un enregistrement donné. Une division aléatoire des données dans les différents jeux d'apprentissage et de validation est donc source d'une fuite d'information qui sera à l'origine de performances de prédiction faussement élevées (Cherian et Kanaga 2022; West et al. 2023). Il est donc nécessaire d'introduire une condition de temps pour séparer les données d'apprentissage et de validation afin d'obtenir des performances non biaisées. Si la validation sur des segments d'enregistrement distants semble être une approche convenable, l'effet des cycles récemment décrit dans l'épilepsie doit cependant être pris en compte (Karoly et al. 2021a). Malheureusement, les enregistrements de très longue durée nécessaires pour évaluer l'influence statistique de ces facteurs de confusion sur les algorithmes de prédiction ne sont, à ce jour, pas disponibles pour l'ensemble de la communauté scientifique.

Dans nos approches ECG et connectivité, nous avons appliqué une validation particulière appelée *leave-one-day-out* : pour chaque itération, un enregistrement quotidien de chaque classe était attribué au hasard à la phase de test et la phase d'apprentissage était alors réalisée sur le reste des données.

3) Le surapprentissage du modèle

La plupart des algorithmes d'apprentissage automatique utilisent, dans une approche rétrospective, l'ensemble des données disponibles pour apprendre et tester les modèles de prédiction. Cette optimisation à l'intérieur de l'échantillon de données entraîne un surapprentissage et généralement une surestimation des performances du modèle, qui ne sont généralement pas reproduites lorsqu'elles sont testées sur de nouvelles données (provenant de nouveaux patients ou de nouveaux enregistrements) pour lesquelles les paramètres appris du modèle peuvent ne plus être optimaux. Pour tout algorithme de prédiction, l'évaluation des performances de prévision sur une configuration prospective ou quasi-prospective est nécessaire pour évaluer son efficacité clinique (Beniczky et al. 2021).

II. L'état de vigilance lors des enregistrements EEG

Lors de l'étude de la connectivité fonctionnelle cérébrale au cours du temps, nous avons été confrontés au problème de l'état de vigilance du patient. En effet, lors des enregistrements EEG intracérébraux prolongés de plusieurs semaines, le patient alterne constamment entre l'éveil, la somnolence et le sommeil – lui-même constitué de plusieurs states (somment lent léger N1 et N2, sommeil lent profond N3 et sommeil paradoxal). Or, la connectivité cérébrale varie de manière physiologique avec les différents stades de vigilance. Il est donc nécessaire d'interpréter de possibles modifications de la connectivité fonctionnelle à la lumière de l'état de vigilance précis du patient (Schelter et al. 2006), ce qui

n'est possible qu'avec un enregistrement polysomnographique comprenant des capteurs oculaires (afin de mettre en évidence les mouvements oculaires rapides du sommeil paradoxal) et des capteurs musculaires (pour détecter la survenue d'une atonie musculaire propre au sommeil paradoxal), en plus des électrodes EEG de surface permettant de mettre en évidence l'apparition des figures physiologiques liées au sommeil (fractionnement de l'alpha et apparition d'un rythme de fond thêta avec des pointes vertex en N1, complexes K et fuseaux du sommeil en stade N2, activité lente diffuse delta en stade N3).

Un tel montage n'était pas disponible en permanence durant la durée du séjour. Nous avons donc décidé de réaliser des mesures itératives durant un protocole de repos quotidien afin de contrôler l'état de vigilance et de pouvoir comparer la connectivité fonctionnelle entre les périodes intercritiques et précritiques, sans biais lié aux variations physiologiques de la connectivité. Lors de l'étude des modifications de comportement d'activités unitaires de neurones au cours du temps, il conviendra de prendre également en compte ce biais afin de ne pas interpréter comme pathologiques des comportements qui résulteraient de changements physiologiques.

III. L'interprétation des dynamiques précritiques

1) Différents scénarios possibles

Nous avons illustré différents scénarios que l'on pourrait rencontrer lors de l'analyse d'une métrique obtenue à partir des signaux EEG, ECG, ou autre, au cours du temps, à la recherche de modifications qui signeraient un état précritique Figure 34).

Le premier serait le scénario idéal, où une métrique fluctuerait au cours du temps et franchirait un seuil spécifiquement durant la période précritique. Ces modifications pourraient être brutales ou bien progressives au cours du temps.

Le deuxième scénario serait plus problématique en termes d'interprétation. Il s'agit d'une métrique qui franchirait un seuil durant la période précritique, mais également en dehors, amenant à questionner sa spécificité. Dans ce cas précis, étudier les durées de franchissement du seuil est intéressante, afin de les comparer entre les périodes intercritiques et précritiques.

Enfin, un troisième scénario refléterait les variations physiologiques d'une métrique au cours du temps, pouvant être associées à la survenue d'une crise (par exemple, le sommeil). Cependant, les modifications précritiques observées – issues d'un processus physiologique et non pathologique – ne pourraient pas être interprétées comme une signature spécifique de l'état précritique.

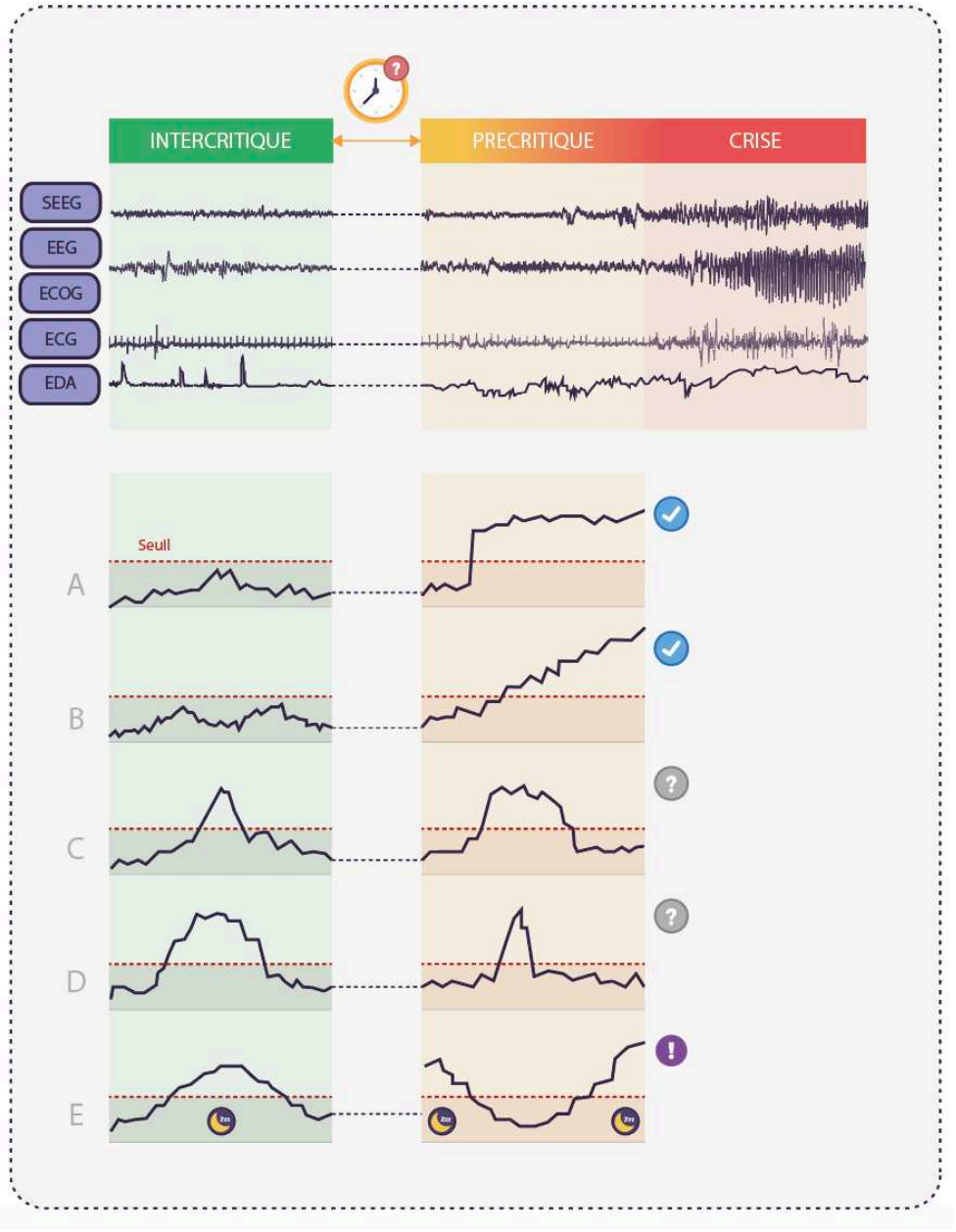

Figure 34. Différents scénarios de dynamiques précritiques
A et B. Scénarios idéaux avec augmentation spécifique d'une métrique (abruptement A, progressivement B) durant la période précritique.
C et D. Scénarios incertains : augmentation d'une métrique durant la période précritique mais également en dehors. Plusieurs possibilités : il peut s'agir de faux positifs reflétant un état procritique mais n'aboutissant pas à une crise, ou alors il s'agit d'une métrique peu spécifique (surtout quand elle dépasse davantage le seul durant la période intercritique, D).
E. Fluctuations physiologiques d'une métrique (par exemple, le sommeil) pouvant augmenter le risque de crise mais sans spécificité.

2) Comment interpréter les faux positifs ?

La détection de faux positifs – des états intercritiques prédits à tort comme précritiques – doit être interprétée à la lumière de méthodologie employée. En effet, il convient de différencier un faux positif déterministe (crise/pas crise) d'un faux positif probabiliste (Freestone et al. 2017). Si l'on considère qu'il existe un état procritique – une condition particulièrement à risque de crise d'épilepsie mais dont la mise en jeu de mécanismes homéostatiques pourrait stopper son apparition – on peut imaginer que des modifications par rapport à un état intercritique de référence puissent être mises en évidence. On observerait ainsi une un changement d'état – suffisamment significatif pour être considéré comme une prédiction positive – sans qu'il n'y ait inexorablement l'apparition d'une crise au décours. Une telle conception aurait une influence majeure sur la signification de faux positifs, qui pourraient être la retranscription d'un état procritique n'évoluant pas un état précritique puis la crise.

Une étude a comparé deux algorithmes de prédiction radicalement différents sur des données d'EEG intracérébral et a mis en évidence une cohérence forte entre les deux méthodes concernant les prédictions (déterministes) de crise correctes mais également erronées (Müller et al. 2022). Cette concordance de résultats faux positifs est en faveur de modifications authentiques mais dont l'analyse déterministe empêche toute considération procritique. Une autre hypothèse est qu'il s'agisse en réalité de phases de sommeil détectées comme un état précritique par les deux algorithmes.

PARTIE 3. QUELLES PERSPECTIVES DANS LE DOMAINE DE LA PREDICTION DES CRISES ?

I. Vers un système de prédiction idéal ?

Les caractéristiques idéales d'un système de prédiction des crises pourraient comprendre, de manière non exhaustive :

- ✓ *Une approche multimodale*

Augmenter les types de sources d'information (EEG, ECG, symptômes prodromaux, etc.) et les combiner pourrait permettre d'évaluer concomitamment plusieurs systèmes, ce qui pourrait notamment être intéressant dans l'hypothèse où ces systèmes suivent des dynamiques temporelles différentes.

- ✓ *Une évaluation à de multiples échelles de temps*

Prendre en compte les différents cycles (circadiens et multidiens notamment) semble nécessaire afin de suivre les dynamiques cycliques de phénomènes physiologiques (sommeil, menstruations, etc.) qui pourraient influer l'apparition des crises.

- ✓ *Un dispositif non invasif*

Si les algorithmes de prédiction des crises ont principalement été étudiés et validés sur des signaux issus d'EEG intracrânien, améliorer la tolérance des dispositifs de recueil de données est primordiale. La réalisation d'EEG mobile à domicile ou l'implantation d'EEG « mini-invasif » sous-cutané pourraient être une alternative (Stirling et al. 2021b; Viana et al. 2021; Biondi et al. 2022), mais leur apport dans le domaine de la prédiction des crises n'a pas été étudié.

- ✓ *Un dispositif portable*

Toujours dans l'optique de favoriser la tolérance (et donc l'adhérence du patient) aux dispositifs d'enregistrement, l'utilisation d'objets portables connectés (montre, téléphone, bague, etc.) semble adéquate. Le recueil d'informations sur le sommeil, la fréquence cardiaque, la température, les cycles de crises, l'état psychologique du patient est possible par ce type de procédé. Des études complémentaires sont cependant nécessaires pour une mise en application clinique.

✓ *Un recueil sur le long terme*

Le recueil de données sur le long terme a pour avantages d'obtenir des informations sur les différents cycles, mais également d'optimiser l'algorithme en augmentant la quantité de données d'apprentissage. Disposer de semaines, voire de mois d'enregistrements, et donc d'un grand nombre de périodes intercritiques et de crises devrait clairement faciliter les méthodes de prédiction.

✓ *Un modèle sur mesure pour chaque patient*

Une approche indépendante du patient peut être proposée notamment en cas de données limitées. Le classifieur est alors conçu à l'aide des données de plusieurs patients. Cependant, les performances seront moindres qu'un modèle spécifique au patient, en raison de la grande variabilité interindividuelle. Pour les approches spécifiques au patient, l'optimisation du modèle est obtenue à partir des données d'un seul sujet, ce qui limite l'adaptabilité du domaine entre les différents patients. Les modèles d'apprentissage profond peuvent également être conçus pour fournir des modèles de prédiction spécifiques au patient (Cherian et Kanaga 2022).

✓ *Une approche probabiliste*

Délivrer une prévision probabiliste semble être la stratégie la plus adéquate aux mécanismes dynamiques complexes sous-tendant l'épilepsie et au concept d'état procritique. Cependant, la décision d'intervention suivant la prévision (prise d'une molécule antiépileptique d'action rapide par exemple) pourrait être déterministe.

✓ *Un procédé ambulatoire*

Tout l'enjeu de la mise en place de dispositifs non ou mini-invasifs, idéalement portables, est leur utilisation par le patient lui-même, à domicile.

✓ *Validé en conditions réelles*

Il est enfin nécessaire que les algorithmes de prédiction des crises étudiés suivent une phase de test, sur de nouvelles données, en condition de vie réelle. En effet, les résultats obtenus en conditions parfaitement contrôlées d'enregistrement et d'analyse, chez des patients hospitalisés, peuvent être surestimés. De plus, une validation prospective est également primordiale. Les analyses pseudoprospectives apportent un certain niveau d'information mais le caractère *stricto sensu* rétrospectif des analyses limite leur généralisation.

II. Microélectrodes intracérébrales et activités neuronales

Nous pensons qu'une des stratégies pour mieux comprendre la dynamique des activités neuronales précédant la crise consistera à suivre les activités d'une seule unité à partir de microélectrodes intracérébrales *in vivo*. Si les précédentes études ont mis en évidence que les neurones enregistrés dans la *seizure onset zone* n'étaient pas recrutés de manière synchrone au début de la crise (Truccolo et al. 2011; Lambrecq et al. 2017), des efforts doivent être faits pour effectuer une analyse à long terme des activités de neurones individuels afin de rechercher des comportements neuronaux spécifiques précédant les crises.

L'étude que j'ai initiée durant ma thèse sur le suivi du comportement des neurones dans les heures précédant les crises devrait fournir des informations très précieuses, sur la diversité de la fréquence de décharge des neurones, leur synchronie, leur propension à décharger en *burst*, avant la survenue des crises. Par la suite, ce type d'étude devra porter sur de plus longues périodes, afin d'appréhender la spécificité d'éventuels changements précritiques.

Mais de telles approches sont difficiles, car :

(i) elles nécessitent des enregistrements continus pendant des jours et des semaines, de grandes quantités de données de haute qualité. Des bases de données sont cependant maintenant disponibles, comme celle établie au sein de mon équipe de recherche (Lehongre et al. 2022) ;

(ii) elles nécessitent de faire la distinction entre les changements physiologiques – liés par exemple aux stades du sommeil – et les changements pathologiques – comportements qui ne seraient enregistrés uniquement pendant les crises et les périodes précritiques ;

(iii) elles nécessitent de nouvelles méthodes d'analyse d'apprentissage automatique, pour identifier des changements subtils de décharges de neurones. De telles approches ne pourraient pas être facilement appliquées à une large population de patients, ni sur de très longues périodes, mais elles pourraient permettre de mettre en évidence des comportements neuronaux liés à la période précritique.

L'étude des activité multi-unitaires par MEA implanté en région néocorticale a permis de distinguer par apprentissage profond les périodes précritiques et intercritiques avec une bonne exactitude dans un petit groupe de patients (Proix et al. 2019).

III. Acquisition, prédiction et intervention en temps réel

Un dispositif idéal pourrait acquérir les données et les traiter afin d'émettre une prévision probabiliste en temps réel à l'aide d'un algorithme directement intégré. Dans les premières études sur la prédiction des crises, les limites de certaines caractéristiques EEG (notamment non-linéaires) étaient liées à leur complexité algorithmique et à la difficulté d'intégrer des algorithmes dans des dispositifs en temps réel. Néanmoins, les progrès récents dans le domaine des processeurs offrent une perspective prometteuse pour le développement de systèmes de prédiction des crises entièrement intégrés.

Le dispositif EEG implantable RNS (NeuroPace) suit en continu les données EEG sur des périodes ultra prolongées de plusieurs années mais ne les enregistre pas (Sun et Morrell 2014). Lorsqu'il détecte une activité électrique pathologique, il peut délivrer une stimulation au sein du foyer épileptique. On pourrait imaginer un système qui suive mais également enregistre l'ensemble des données, afin de mettre en évidence un pattern précritique spécifique chez un patient donné. La stimulation cérébrale pourrait alors se déclencher non pas lorsqu'une crise est détectée, mais en amont, durant la période précritique et ce afin de tenter de stopper la route vers la crise.

Conclusion et perspectives

Plusieurs faisceaux d'arguments dans la littérature convergent vers l'existence d'une transition précritique, entre un état intercritique et la crise. La mise en évidence de modifications spécifiques de cette transition – une signature de l'état précritique – témoigne de ce changement d'état :

- Des modifications cliniques, regroupant : les symptômes prodromaux – manifestations subjectives et « négatives » – mais également l'autoprédiction par le patient lui-même ; l'activité cardiaque et notamment la variabilité de la fréquence cardiaque qui reflète la balance sympathique/parasympathique du système nerveux autonome ;
- Des modifications du débit sanguin cérébral, individualisées en imagerie cérébrale et notamment en IRM fonctionnelle – approche n'étant à l'heure actuelle pas adaptée à une application en pratique clinique ;
- Des modifications de l'activité cérébrale électroencéphalographique : cette approche a l'avantage, par des techniques invasives d'EEG intracérébral, d'offrir une proximité anatomique avec le réseau épileptogène, de disposer d'une excellente résolution spatio-temporelle, et d'être particulièrement adaptée à l'étude des réseaux à dynamiques complexes notamment par des mesures non-linéaires de connectivité.

Les dernières années ont également été marquées par la possibilité, via des enregistrements de très longues durées, d'identifier des cycles de crises sous-tendus par des variations physiologiques, dont la périodicité est de l'ordre du jour (circadien), de plusieurs jours à semaines (multidien) ou bien du mois (circannuel).

La prédiction des crises d'épilepsie, conditionnée par l'identification précoce d'un état précritique, est le graal de nombreux chercheurs et cliniciens depuis plusieurs décennies. La complexité d'étude de tels systèmes – dynamiques, non-linéaires, avec des comportements chaotiques et ponctués d'évènements stochastiques – a souvent remis en question la faisabilité de pouvoir, un jour, prédire avec précision les crises d'épilepsie.

Les nouvelles stratégies de prédiction s'orientent vers une approche empruntée aux sciences météorologiques, les prévisions probabilistes. Le modèle déterministe ne représenterait en effet pas la complexité des systèmes étudiés, avec une réponse – binaire et invariable – jugée trop simpliste par certains. La théorie des probabilités pourrait mieux appréhender ces dynamiques complexes, en apportant un degré d'incertitude qui refléterait les variations du risque de crise au cours du temps. Un état procritique

– où le risque de crise est suffisamment significatif pour se distinguer d'un état de base intercritique – pourrait survenir mais l'évolution, qui mettrait en jeu des processus homéostatiques, ne se ferait pas inexorablement vers un état précritique puis la crise.

L'avènement des nouvelles techniques d'apprentissage automatique – les modèles d'apprentissage profond (Figure 35) – a également rebattu les cartes. Un apprentissage en plusieurs couches de neurones artificiels permettrait aux algorithmes d'apprentissage profond d'obtenir des performances de prédiction supérieures aux algorithmes traditionnels.

Dans notre travail, nous avons appréhendé la période précritique en plusieurs niveaux études :

- *Un niveau clinique*, dans lequel nous avons pu mettre en évidence l'identification d'un état précritique par une combinaison de symptômes cliniques subjectifs et l'utilisation d'algorithmes d'apprentissage automatique. Cette approche a permis de développer une application mobile, afin de valider les performances de nos modèles statistiques de manière prospective et en condition de vie réelle ;
- *Un niveau électrocardiographique*, dans lequel l'étude de caractéristiques linéaires et non-linéaires de la variabilité de la fréquence cardiaque durant un état de repos quotidien a permis de distinguer une période précritique, mais la sensibilité des prévisions probabilistes nécessite d'être améliorée, possiblement par une approche multimodale ;
- *Un niveau électroencéphalographique*, où l'étude de la connectivité fonctionnelle intracérébrale au repos a permis d'identifier avec une bonne précision les états précritiques, et de proposer des prévisions probabilistes prometteuses, au prix évidemment d'une technique d'analyse invasive. Transposer les matrices de connectivité dans un espace non euclidien hyperbolique pourrait permettre d'obtenir un niveau d'informations supérieur ;
- *Un niveau neuronal*, par l'étude des activités unitaires de neurones *in vivo* : nous avons pu identifier et suivre au cours du temps l'activité de neurones durant la période précritique. Nous continuerons ces analyses chez d'autres patientes, puis appliquerons des méthodes statistiques pour évaluer leurs dynamiques individuelles et interindividuelles précritiques ;
- *Un niveau in vitro*, par l'enregistrement des dynamiques précritiques sur tranches fraîches de cortex cérébral.

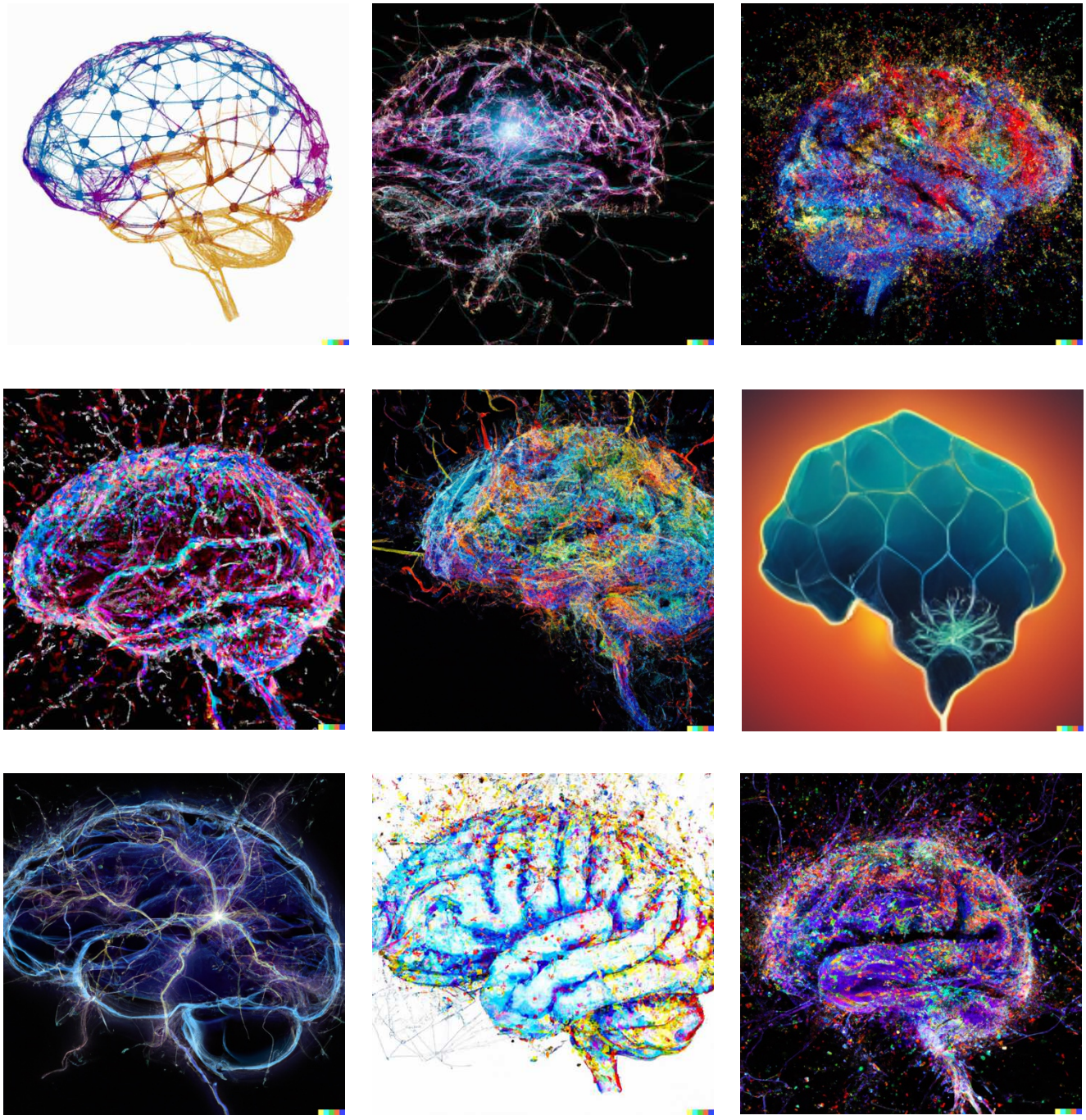

Figure 35. Exemples d'images générées par intelligence artificielle générative
Images créées sur DALL-E (OpenAI)

Je poursuis actuellement mes travaux de recherche sur les enregistrements d'activités unitaires de neurones *in vivo* situés dans la *seizure onset zone*, sur des périodes prolongées de plusieurs heures, afin d'étudier leurs dynamiques précritiques. J'aimerais évaluer les changements de comportement précédant la crise, pour chaque neurone (comportements individuels) et également les comportements d'interaction entre les neurones (comportements interindividuels).

Une étude clinique est également en cours de mise en place afin d'évaluer, de manière prospective et en condition de vie réelle, les performances de prédiction d'une combinaison de variables cliniques (symptômes prodromaux, facteurs favorisants, autoprédiction, cycles de crises) à l'aide de l'application mobile Epiday à destination des patients.

Références

Aarabi A, He B. Seizure prediction in hippocampal and neocortical epilepsy using a model-based approach. Clinical Neurophysiology. 1 mai 2014;125(5):930-40.

Abarbanel HDI, Brown R, Sidorowich JJ, Tsimring LSh. The analysis of observed chaotic data in physical systems. Rev Mod Phys. 1 oct 1993;65(4):1331-92.

Abbasi B, Goldenholz DM. Machine learning applications in epilepsy. Epilepsia. oct 2019;60(10):2037-47.

Acharya UR, Sree SV, Chattopadhyay S, Yu W, Ang PCA. Application of recurrence quantification analysis for the automated identification of epileptic eeg signals. Int J Neur Syst. juin 2011;21(03):199-211.

Adelson PD, Nemoto E, Scheuer M, Painter M, Morgan J, Yonas H. Noninvasive Continuous Monitoring of Cerebral Oxygenation Periictally Using Near-Infrared Spectroscopy: A Preliminary Report. Epilepsia. 1999;40(11):1484-9.

Alvarado-Rojas C, Valderrama M, Fouad-Ahmed A, Feldwisch-Drentrup H, Ihle M, Teixeira CA, et al. Slow modulations of high-frequency activity (40–140 Hz) discriminate preictal changes in human focal epilepsy. Sci Rep. mai 2015;4(1):4545.

Aru J, Aru J, Priesemann V, Wibral M, Lana L, Pipa G, et al. Untangling cross-frequency coupling in neuroscience. Current Opinion in Neurobiology. 1 avr 2015;31:51-61.

Badawy RAB, Freestone DR, Lai A, Cook MJ. Epilepsy: Ever-changing states of cortical excitability. Neuroscience. oct 2012;222:89-99.

Barbarosie M, Avoli M. CA3-Driven Hippocampal-Entorhinal Loop Controls Rather than Sustains In Vitro Limbic Seizures. J Neurosci. 1 déc 1997;17(23):9308-14.

Baud MO, Kleen JK, Mirro EA, Andrechak JC, King-Stephens D, Chang EF, et al. Multi-day rhythms modulate seizure risk in epilepsy. Nat Commun. 8 janv 2018;9(1):88.

Baud MO, Proix T, Rao VR, Schindler K. Chance and risk in epilepsy. Current Opinion in Neurology. avr 2020;33(2):163-72.

Baumgartner C, Serles W, Leutmezer F, Pataraia E, Aull S, Czech T, et al. Preictal SPECT in Temporal Lobe Epilepsy: Regional Cerebral Blood Flow Is Increased Prior to Electroencephalography-Seizure Onset. Journal of Nuclear Medicine. 1 juin 1998;39(6):978-82.

Beniczky S, Karoly P, Nurse E, Ryvlin P, Cook M. Machine learning and wearable devices of the future. Epilepsia. 2021;62(S2):S116-24.

Besag FMC, Vasey MJ. Prodrome in epilepsy. Epilepsy & Behavior. juin 2018;83:219-33.

Billeci L, Marino D, Insana L, Vatti G, Varanini M. Patient-specific seizure prediction based on heart rate variability and recurrence quantification analysis. PLoS One. 25 sept 2018;13(9):e0204339.

Biondi A, Santoro V, Viana PF, Laiou P, Pal DK, Bruno E, et al. Noninvasive mobile EEG as a tool for seizure monitoring and management: A systematic review. Epilepsia. 2022;63(5):1041-63.

Blauwblomme T, Dossi E, Pellegrino C, Goubert E, Iglesias BG, Sainte-Rose C, et al. Gamma-aminobutyric acidergic transmission underlies interictal epileptogenicity in pediatric focal cortical dysplasia. Ann Neurol. févr 2019;85(2):204-17.

Bou Assi E, Gagliano L, Rihana S, Nguyen DK, Sawan M. Bispectrum Features and Multilayer Perceptron Classifier to Enhance Seizure Prediction. Sci Rep. 19 oct 2018;8(1):15491.

Bou Assi E, Nguyen DK, Rihana S, Sawan M. Towards accurate prediction of epileptic seizures: A review. Biomedical Signal Processing and Control. 1 avr 2017;34:144-57.

Bozanic N, Kreuz T. SPIKY: a graphical user interface for monitoring spike train synchrony. BMC Neurosci. juill 2013;14(S1):P225, 1471-2202-14-S1-P225.

Brier GW. Verification of forecasts expressed in terms of probability. Monthly Weather Review. 1 janv 1950;78(1):1-3.

Bullmore E, Sporns O. Complex brain networks: graph theoretical analysis of structural and functional systems. Nat Rev Neurosci. mars 2009;10(3):186-98.

Carpio A, Romo ML, Hauser WA, Kelvin EA. New understanding about the relationship among neurocysticercosis, seizures, and epilepsy. Seizure - European Journal of Epilepsy. 1 août 2021;90:123-9.

Chang CC, Lin CJ. LIBSVM: A library for support vector machines. ACM Trans Intell Syst Technol. 6 mai 2011;2(3):27:1-27:27.

Chaudhary UJ, Carmichael DW, Rodionov R, Thornton RC, Bartlett P, Vulliemoz S, et al. Mapping preictal and ictal haemodynamic networks using video-electroencephalography and functional imaging. Brain. déc 2012;135(Pt 12):3645-63.

Chaudhary UJ, Centeno M, Thornton RC, Rodionov R, Vulliemoz S, McEvoy AW, et al. Mapping human preictal and ictal haemodynamic networks using simultaneous intracranial EEG-fMRI. NeuroImage: Clinical. 1 janv 2016;11:486-93.

Cherian R, Kanaga EG. Theoretical and methodological analysis of EEG based seizure detection and prediction: An exhaustive review. Journal of Neuroscience Methods. 1 mars 2022;369:109483.

Chiang S, Vannucci M, Goldenholz DM, Moss R, Stern JM. Epilepsy as a dynamic disease: A Bayesian model for differentiating seizure risk from natural variability. Epilepsia Open. 2018;3(2):236-46.

Chvojka J, Kudlacek J, Chang WC, Novak O, Tomaska F, Otahal J, et al. The role of interictal discharges in ictogenesis — A dynamical perspective. Epilepsy & Behavior. 1 août 2021;121:106591.

Cohen I, Navarro V, Clemenceau S, Baulac M, Miles R. On the Origin of Interictal Activity in Human Temporal Lobe Epilepsy in Vitro. Science. 15 nov 2002;298(5597):1418-21.

Constantino T, Rodin E. Peri-Ictal and Interictal, Intracranial Infraslow Activity. Journal of Clinical Neurophysiology. août 2012;29(4):298.

Cook MJ, O'Brien TJ, Berkovic SF, Murphy M, Morokoff A, Fabinyi G, et al. Prediction of seizure likelihood with a long-term, implanted seizure advisory system in patients with drug-resistant epilepsy: a first-in-man study. The Lancet Neurology. 1 juin 2013;12(6):563-71.

Cook MJ, Varsavsky A, Himes D, Leyde K, Berkovic SF, O'Brien T, et al. The Dynamics of the Epileptic Brain Reveal Long-Memory Processes. Front Neurol. 24 oct 2014;5:217.

Cousyn L, Ben Messaoud R, Lehongre K, Frazzini V, Lambrecq V, Adam C, et al. Daily resting-state intracranial EEG connectivity for seizure risk forecasts. Epilepsia. 8 déc 2022;

Cousyn L, Navarro V, Chavez M. Preictal state detection using prodromal symptoms: A machine learning approach. Epilepsia. févr 2021;62(2):e42-7.

De Vico Fallani F, Richiardi J, Chavez M, Achard S. Graph analysis of functional brain networks: practical issues in translational neuroscience. Philosophical Transactions of the Royal Society B: Biological Sciences. 5 oct 2014;369(1653):20130521.

Derry CP, Duncan S. Sleep and epilepsy. Epilepsy & Behavior. 1 mars 2013;26(3):394-404.

Despouy E, Curot J, Denuelle M, Deudon M, Jean-Christophe-Sol, Lotterie JA, et al. Neuronal spiking activity highlights a gradient of epileptogenicity in human tuberous sclerosis lesions. Clinical Neurophysiology. janv 2019;

Devinsky O, Vezzani A, O'Brien TJ, Jette N, Scheffer IE, de Curtis M, et al. Epilepsy. Nature Reviews Disease Primers. 3 mai 2018;4:18024.

van Diessen E, Diederen SJH, Braun KPJ, Jansen FE, Stam CJ. Functional and structural brain networks in epilepsy: What have we learned? Epilepsia. nov 2013;54(11):1855-65.

DuBois JM, Boylan LS, Shiyko M, Barr WB, Devinsky O. Seizure prediction and recall. Epilepsy & Behavior. mai 2010;18(1-2):106-9.

Elger CE, Hoppe C. Diagnostic challenges in epilepsy: seizure under-reporting and seizure detection. The Lancet Neurology. mars 2018;17(3):279-88.

Ewald A, Marzetti L, Zappasodi F, Meinecke FC, Nolte G. Estimating true brain connectivity from EEG/MEG data invariant to linear and static transformations in sensor space. NeuroImage. 1 mars 2012;60(1):476-88.

Federico P, Abbott DF, Briellmann RS, Harvey AS, Jackson GD. Functional MRI of the pre-ictal state. Brain. 1 août 2005;128(8):1811-7.

Ferlazzo E, Mammone N, Cianci V, Gasparini S, Gambardella A, Labate A, et al. Permutation entropy of scalp EEG: A tool to investigate epilepsies: Suggestions from absence epilepsies. Clinical Neurophysiology. 1 janv 2014;125(1):13-20.

Fernández A, García S, Galar M, Prati RC, Krawczyk B, Herrera F. Learning from Imbalanced Data Sets. In Cham: Springer International Publishing; 2018.

Fisher RS, Cross JH, D'Souza C, French JA, Haut SR, Higurashi N, et al. Instruction manual for the ILAE 2017 operational classification of seizure types. Epilepsia. 2017;58(4):531-42.

Frazzini V, Mathon B, Donneger F, Cousyn L, Hanin A, Nguyen-Michel VH, et al. Epilepsy related to focal neuronal lipofuscinosis: extra-frontal localization, EEG signatures and GABA involvement. J Neurol. août 2022;269(8):4102-9.

Freestone DR, Karoly PJ, Cook MJ. A forward-looking review of seizure prediction. Current Opinion in Neurology. avr 2017;30(2):167-73.

Fried I, MacDonald KA, Wilson CL. Single neuron activity in human hippocampus and amygdala during recognition of faces and objects. Neuron. mai 1997;18(5):753-65.

Fujiwara K, Miyajima M, Yamakawa T, Abe E, Suzuki Y, Sawada Y, et al. Epileptic Seizure Prediction Based on Multivariate Statistical Process Control of Heart Rate Variability Features. IEEE Transactions on Biomedical Engineering. juin 2016;63(6):1321-32.

Gastaut H. The Epilepsies; Electro-clinical Correlations. Thomas; 1954.

Giannakakis G, Tsiknakis M, Vorgia P. Focal epileptic seizures anticipation based on patterns of heart rate variability parameters. Computer Methods and Programs in Biomedicine. 1 sept 2019;178:123-33.

Goldenholz DM, Goldenholz SR, Moss R, French J, Lowenstein D, Kuzniecky R, et al. Is seizure frequency variance a predictable quantity? Annals of Clinical and Translational Neurology. 2018;5(2):201-7.

Goldenholz DM, Goldenholz SR, Romero J, Moss R, Sun H, Westover B. Development and Validation of Forecasting Next Reported Seizure Using e-Diaries. Annals of Neurology. 2020;88(3):588-95.

Goldenholz DM, Westover MB. Flexible realistic simulation of seizure occurrence recapitulating statistical properties of seizure diaries. Epilepsia. 2023;64(2):396-405.

Gotman J, Koffler DJ. Interictal spiking increases after seizures but does not after decrease in medication. Electroencephalography and Clinical Neurophysiology. 1 janv 1989;72(1):7-15.

Gotman J, Marciani MG. Electroencephalographic spiking activity, drug levels, and seizure occurence in epileptic patients. Annals of Neurology. 1985;17(6):597-603.

Grasse DW, Karunakaran S, Moxon KA. Neuronal synchrony and the transition to spontaneous seizures. Experimental Neurology. 1 oct 2013;248:72-84.

Graus F, Titulaer MJ, Balu R, Benseler S, Bien CG, Cellucci T, et al. A clinical approach to diagnosis of autoimmune encephalitis. Lancet Neurol. avr 2016;15(4):391-404.

Haut SR, Hall CB, Borkowski T, Tennen H, Lipton RB. Clinical features of the pre-ictal state: Mood changes and premonitory symptoms. Epilepsy & Behavior. avr 2012;23(4):415-21.

Haut SR, Hall CB, Borkowski T, Tennen H, Lipton RB. Modeling seizure self-prediction: An e-diary study. Epilepsia. 2013;54(11):1960-7.

Haut SR, Hall CB, LeValley AJ, Lipton RB. Can patients with epilepsy predict their seizures? Neurology. 23 janv 2007a;68(4):262-6.

Haut SR, Hall CB, Masur J, Lipton RB. Seizure occurrence: Precipitants and prediction. Neurology. 13 nov 2007b;69(20):1905-10.

Houssaini KE, Bernard C, Jirsa VK. The Epileptor Model: A Systematic Mathematical Analysis Linked to the Dynamics of Seizures, Refractory Status Epilepticus, and Depolarization Block. eNeuro. 1 mars 2020;7(2).

Huberfeld G, Menendez de la Prida L, Pallud J, Cohen I, Le Van Quyen M, Adam C, et al. Glutamatergic pre-ictal discharges emerge at the transition to seizure in human epilepsy. Nat Neurosci. mai 2011;14(5):627-34.

Hughes J, Devinsky O, Feldmann E, Bromfield E. Premonitory symptoms in epilepsy. Seizure. 1 sept 1993;2(3):201-3.

Humeau-Heurtier A. The Multiscale Entropy Algorithm and Its Variants: A Review. Entropy. mai 2015;17(5):3110-23.

Hyafil A, Giraud AL, Fontolan L, Gutkin B. Neural Cross-Frequency Coupling: Connecting Architectures, Mechanisms, and Functions. Trends in Neurosciences. 1 nov 2015;38(11):725-40.

Iasemidis LD, Chris Sackellares J, Zaveri HP, Williams WJ. Phase space topography and the Lyapunov exponent of electrocorticograms in partial seizures. Brain Topogr. 1 mars 1990;2(3):187-201.

Islam MS, El-Hajj AM, Alawieh H, Dawy Z, Abbas N, El-Imad J. EEG mobility artifact removal for ambulatory epileptic seizure prediction applications. Biomedical Signal Processing and Control. 1 janv 2020;55:101638.

Jacobs J, Zelmann R, Jirsch J, Chander R, Dubeau CÉCF, Gotman J. High frequency oscillations (80–500 Hz) in the preictal period in patients with focal seizures. Epilepsia. 2009;50(7):1780-92.

Jefferys JGR, Menendez de la Prida L, Wendling F, Bragin A, Avoli M, Timofeev I, et al. Mechanisms of physiological and epileptic HFO generation. Progress in Neurobiology. 1 sept 2012;98(3):250-64.

Jensen MS, Yaari Y. The relationship between interictal and ictal paroxysms in an in vitro model of focal hippocampal epilepsy. Annals of Neurology. 1988;24(5):591-8.

Kandrács Á, Hofer KT, Tóth K, Tóth EZ, Entz L, Bagó AG, et al. Presence of synchrony-generating hubs in the human epileptic neocortex. J Physiol. déc 2019;597(23):5639-70.

Kantz H, Schreiber T. Nonlinear Time Series Analysis. 2e éd. Cambridge: Cambridge University Press; 2003.

Karoly PJ, Cook MJ, Maturana M, Nurse ES, Payne D, Brinkmann BH, et al. Forecasting cycles of seizure likelihood. Epilepsia. 2020;61(4):776-86.

Karoly PJ, Rao VR, Gregg NM, Worrell GA, Bernard C, Cook MJ, et al. Cycles in epilepsy. Nat Rev Neurol. mai 2021a;17(5):267-84.

Karoly PJ, Stirling RE, Freestone DR, Nurse ES, Maturana MI, Halliday AJ, et al. Multiday cycles of heart rate are associated with seizure likelihood: An observational cohort study. EBioMedicine. oct 2021b;72:103619.

Karoly PJ, Ung H, Grayden DB, Kuhlmann L, Leyde K, Cook MJ, et al. The circadian profile of epilepsy improves seizure forecasting. Brain. 1 août 2017;140(8):2169-82.

Katz A, Marks DA, McCarthy G, Spencer SS. Does interictal spiking change prior to seizures? Electroencephalography and Clinical Neurophysiology. 1 août 1991;79(2):153-6.

Khan SS, Madden MG. One-class classification: taxonomy of study and review of techniques. The Knowledge Engineering Review. juin 2014;29(3):345-74.

King RD, Orhobor OI, Taylor CC. Cross-validation is safe to use. Nat Mach Intell. avr 2021;3(4):276-276.

Kolsal E, Serdaroğlu A, Çilsal E, Kula S, Soysal AŞ, Kurt ANÇ, et al. Can heart rate variability in children with epilepsy be used to predict seizures? Seizure - European Journal of Epilepsy. 1 mai 2014;23(5):357-62.

Kramer MA, Cash SS. Epilepsy as a Disorder of Cortical Network Organization. Neuroscientist. 1 août 2012;18(4):360-72.

Kramer MA, Szeri AJ, Sleigh JW, Kirsch HE. Mechanisms of seizure propagation in a cortical model. J Comput Neurosci. 1 févr 2007;22(1):63-80.

Kreuz T, Chicharro D, Greschner M, Andrzejak RG. Time-resolved and time-scale adaptive measures of spike train synchrony. Journal of Neuroscience Methods. janv 2011;195(1):92-106.

Kreuz T, Chicharro D, Houghton C, Andrzejak RG, Mormann F. Monitoring spike train synchrony. Journal of Neurophysiology. 1 mars 2013;109(5):1457-72.

Kreuz T, Mulansky M, Bozanic N. SPIKY: a graphical user interface for monitoring spike train synchrony. Journal of Neurophysiology. mai 2015;113(9):3432-45.

Kuhlmann L, Karoly P, Freestone DR, Brinkmann BH, Temko A, Barachant A, et al. Epilepsyecosystem.org: crowd-sourcing reproducible seizure prediction with long-term human intracranial EEG. Brain. sept 2018a;141(9):2619-30.

Kuhlmann L, Lehnertz K, Richardson MP, Schelter B, Zaveri HP. Seizure prediction — ready for a new era. Nature Reviews Neurology. oct 2018b;14(10):618-30.

Lai N, Li Z, Xu C, Wang Y, Chen Z. Diverse nature of interictal oscillations: EEG-based biomarkers in epilepsy. Neurobiology of Disease. 1 févr 2023;177:105999.

Lambrecq V, Lehongre K, Adam C, Frazzini V, Mathon B, Clemenceau S, et al. Single-unit activities during the transition to seizures in deep mesial structures: Seizures and Single-Unit Activities. Annals of Neurology. déc 2017;82(6):1022-8.

Lange HH, Lieb JP, Engel J, Crandall PH. Temporo-spatial patterns of pre-ictal spike activity in human temporal lobe epilepsy. Electroencephalography and Clinical Neurophysiology. 1 déc 1983;56(6):543-55.

Le Van Quyen M, Adam C, Martinerie J, Baulac M, Clémenceau S, Varela F. Spatio-temporal characterizations of non-linear changes in intracranial activities prior to human temporal lobe seizures. European Journal of Neuroscience. 2000;12(6):2124-34.

Le Van Quyen M, Martinerie J, Baulac M, Varela F. Anticipating epileptic seizures in real time by a non-linear analysis of similarity between EEG recordings. NeuroReport. 13 juill 1999;10(10):2149.

Le Van Quyen M, Martinerie J, Navarro V, Baulac And M, Varela FJ. Characterizing neurodynamic changes before seizures. J Clin Neurophysiol. mai 2001a;18(3):191-208.

Le Van Quyen M, Martinerie J, Navarro V, Boon P, D'Havé M, Adam C, et al. Anticipation of epileptic seizures from standard EEG recordings. Lancet. 20 janv 2001b;357(9251):183-8.

Le Van Quyen M, Soss J, Navarro V, Robertson R, Chavez M, Baulac M, et al. Preictal state identification by synchronization changes in long-term intracranial EEG recordings. Clinical Neurophysiology. 1 mars 2005;116(3):559-68.

Leal A, Pinto MF, Lopes F, Bianchi AM, Henriques J, Ruano MG, et al. Heart rate variability analysis for the identification of the preictal interval in patients with drug-resistant epilepsy. Sci Rep. 16 mars 2021;11:5987.

Lee SA, No YJ. Perceived self-control of seizures in patients with uncontrolled partial epilepsy. Seizure. mars 2005;14(2):100-5.

Leguia MG, Andrzejak RG, Rummel C, Fan JM, Mirro EA, Tcheng TK, et al. Seizure Cycles in Focal Epilepsy. JAMA Neurology. 1 avr 2021;78(4):454-63.

Leguia MG, Rao VR, Tcheng TK, Duun-Henriksen J, Kjaer TW, Proix T, et al. Learning to generalize seizure forecasts. Epilepsia. 8 sept 2022;

Lehnertz K, Bialonski S, Horstmann MT, Krug D, Rothkegel A, Staniek M, et al. Synchronization phenomena in human epileptic brain networks. Journal of Neuroscience Methods. 30 sept 2009;183(1):42-8.

Lehnertz K, Litt B. The First International Collaborative Workshop on Seizure Prediction: summary and data description. Clinical Neurophysiology. 1 mars 2005;116(3):493-505.

Lehongre K, Lambrecq V, Whitmarsh S, Frazzini V, Cousyn L, Soleil D, et al. Long-term deep intracerebral microelectrode recordings in patients with drug-resistant epilepsy: proposed guidelines based on 10-year experience. Neuroimage. 19 mars 2022;119116.

Li S, Zhou W, Yuan Q, Liu Y. Seizure Prediction Using Spike Rate of Intracranial EEG. IEEE Transactions on Neural Systems and Rehabilitation Engineering. nov 2013;21(6):880-6.

Litt B, Echauz J. Prediction of epileptic seizures. Lancet Neurol. mai 2002;1(1):22-30.

Lopes da Silva F, Blanes W, Kalitzin SN, Parra J, Suffczynski P, Velis DN. Dynamical diseases of brain systems: different routes to epileptic seizures. IEEE Trans Biomed Eng. mai 2003a;50(5):540-8.

Lopes da Silva F, Blanes W, Kalitzin SN, Parra J, Suffczynski P, Velis DN. Epilepsies as Dynamical Diseases of Brain Systems: Basic Models of the Transition Between Normal and Epileptic Activity. Epilepsia. 2003b;44(s12):72-83.

Lotufo PA, Valiengo L, Benseñor IM, Brunoni AR. A systematic review and meta-analysis of heart rate variability in epilepsy and antiepileptic drugs. Epilepsia. 2012;53(2):272-82.

Ly JQM, Gaggioni G, Chellappa SL, Papachilleos S, Brzozowski A, Borsu C, et al. Circadian regulation of human cortical excitability. Nat Commun. 24 juin 2016;7:11828.

Maimaiti B, Meng H, Lv Y, Qiu J, Zhu Z, Xie Y, et al. An Overview of EEG-based Machine Learning Methods in Seizure Prediction and Opportunities for Neurologists in this Field. Neuroscience. 15 janv 2022;481:197-218.

Maiwald T, Blumberg J, Timmer J, Schulze-Bonhage A. Are prodromes preictal events? A prospective PDA-based study. Epilepsy & Behavior. juin 2011;21(2):184-8.

Meisel C, Bailey KA. Identifying signal-dependent information about the preictal state: A comparison across ECoG, EEG and EKG using deep learning. EBioMedicine. 9 juill 2019;45:422-31.

Meisel C, El Atrache R, Jackson M, Schubach S, Ufongene C, Loddenkemper T. Machine learning from wristband sensor data for wearable, noninvasive seizure forecasting. Epilepsia. 2020;61(12):2653-66.

van Mierlo P, Papadopoulou M, Carrette E, Boon P, Vandenberghe S, Vonck K, et al. Functional brain connectivity from EEG in epilepsy: Seizure prediction and epileptogenic focus localization. Progress in Neurobiology. 1 oct 2014;121:19-35.

Mormann F, Andrzejak RG, Elger CE, Lehnertz K. Seizure prediction: the long and winding road. Brain. 1 févr 2007;130(2):314-33.

Müller J, Yang H, Eberlein M, Leonhardt G, Uckermann O, Kuhlmann L, et al. Coherent false seizure prediction in epilepsy, coincidence or providence? Clinical Neurophysiology. 1 janv 2022;133:157-64.

Murphy AH. A New Vector Partition of the Probability Score. Journal of Applied Meteorology and Climatology. 1 juin 1973;12(4):595-600.

Myers KA, Sivathamboo S, Perucca P. Heart rate variability measurement in epilepsy: How can we move from research to clinical practice? Epilepsia. déc 2018;59(12):2169-78.

Nagaraj V, Lee ST, Krook-Magnuson E, Soltesz I, Benquet P, Irazoqui PP, et al. Future of seizure prediction and intervention: closing the loop. J Clin Neurophysiol. juin 2015;32(3):194-206.

Nakken KO, Solaas MH, Kjeldsen MJ, Friis ML, Pellock JM, Corey LA. Which seizure-precipitating factors do patients with epilepsy most frequently report? Epilepsy & Behavior. 1 févr 2005;6(1):85-9.

Nasseri M, Pal Attia T, Joseph B, Gregg NM, Nurse ES, Viana PF, et al. Ambulatory seizure forecasting with a wrist-worn device using long-short term memory deep learning. Sci Rep. 9 nov 2021;11:21935.

Nunez PL, Srinivasan R, Westdorp AF, Wijesinghe RS, Tucker DM, Silberstein RB, et al. EEG coherency. I: Statistics, reference electrode, volume conduction, Laplacians, cortical imaging, and interpretation at multiple scales. Electroencephalogr Clin Neurophysiol. nov 1997;103(5):499-515.

Ouyang G, Li J, Liu X, Li X. Dynamic characteristics of absence EEG recordings with multiscale permutation entropy analysis. Epilepsy Research. 1 mai 2013;104(3):246-52.

Park Y, Luo L, Parhi KK, Netoff T. Seizure prediction with spectral power of EEG using cost-sensitive support vector machines. Epilepsia. 2011;52(10):1761-70.

Parvizi J, Kastner S. Promises and limitations of human intracranial electroencephalography. Nat Neurosci. avr 2018;21(4):474-83.

Payne DE, Dell KL, Karoly PJ, Kremen V, Gerla V, Kuhlmann L, et al. Identifying seizure risk factors: A comparison of sleep, weather, and temporal features using a Bayesian forecast. Epilepsia. 2021;62(2):371-82.

Pearce A, Wulsin D, Blanco JA, Krieger A, Litt B, Stacey WC. Temporal changes of neocortical high-frequency oscillations in epilepsy. J Neurophysiol. sept 2013;110(5):1167-79.

Petitmengin C, Baulac M, Navarro V. Seizure anticipation: Are neurophenomenological approaches able to detect preictal symptoms? Epilepsy & Behavior. sept 2006;9(2):298-306.

Pinikahana J, Dono J. The lived experience of initial symptoms of and factors triggering epileptic seizures. Epilepsy & Behavior. 1 août 2009;15(4):513-20.

Privitera M, Haut SR, Lipton RB, McGinley JS, Cornes S. Seizure self-prediction in a randomized controlled trial of stress management. Neurology. 26 nov 2019;93(22):e2021-31.

Proix T, Aghagolzadeh M, Madsen JR, Cosgrove R, Eskandar E, Hochberg LR, et al. Intracortical neural activity distal to seizure-onset-areas predicts human focal seizures. PLOS ONE. 22 juill 2019;14(7):e0211847.

Proix T, Truccolo W, Leguia MG, Tcheng TK, King-Stephens D, Rao VR, et al. Forecasting seizure risk in adults with focal epilepsy: a development and validation study. The Lancet Neurology. 1 févr 2021;20(2):127-35.

van Putten MJAM, Zandt BJ. Neural mass modeling for predicting seizures. Clinical Neurophysiology. 1 mai 2014;125(5):867-8.

Ra JS, Li T, Li Y. A Novel Permutation Entropy-Based EEG Channel Selection for Improving Epileptic Seizure Prediction. Sensors. janv 2021;21(23):7972.

Rajna P, Clemens B, Csibri E, Dobos E, Geregely A, Gottschal M, et al. Hungarian multicentre epidemiologic study of the warning and initial symptoms (prodrome, aura) of epileptic seizures. Seizure. oct 1997;6(5):361-8.

Ralston BL. The mechanism of transition of interictal spiking foci into ictal seizure discharges. Electroencephalography and Clinical Neurophysiology. 1 mai 1958;10(2):217-32.

Rasekhi J, Mollaei MRK, Bandarabadi M, Teixeira CA, Dourado A. Preprocessing effects of 22 linear univariate features on the performance of seizure prediction methods. Journal of Neuroscience Methods. 15 juill 2013;217(1):9-16.

Rasheed K, Qadir J, O'Brien TJ, Kuhlmann L, Razi A. A Generative Model to Synthesize EEG Data for Epileptic Seizure Prediction. IEEE Transactions on Neural Systems and Rehabilitation Engineering. 2021a;29:2322-32.

Rasheed K, Qayyum A, Qadir J, Sivathamboo S, Kwan P, Kuhlmann L, et al. Machine Learning for Predicting Epileptic Seizures Using EEG Signals: A Review. IEEE Reviews in Biomedical Engineering. 2021b;14:139-55.

Reijneveld JC, Ponten SC, Berendse HW, Stam CJ. The application of graph theoretical analysis to complex networks in the brain. Clinical Neurophysiology. 2007;118:2317-31.

Rémi J, Bubeck C, Hartl E, Tezer FI, Noachtar S. Sleep spindle reduction precedes seizures by several epochs. Clinical Neurophysiology. 1 août 2018;129(8):1624-5.

Ren L, Terada K, Baba K, Usui N, Umeoka S, Usui K, et al. Ictal very low frequency oscillation in human epilepsy patients. Annals of Neurology. 2011;69(1):201-6.

Richardson MP, Jefferys JGR. Introduction—Epilepsy Research UK Workshop 2010 on "Preictal Phenomena". Epilepsy Research. déc 2011;97(3):229-30.

Rings T, von Wrede R, Lehnertz K. Precursors of seizures due to specific spatial-temporal modifications of evolving large-scale epileptic brain networks. Sci Rep. 23 juill 2019;9(1):10623.

Rodin E, Constantino T, Bigelow J. Interictal infraslow activity in patients with epilepsy. Clinical Neurophysiology. 1 mai 2014;125(5):919-29.

Saggio ML, Crisp D, Scott JM, Karoly P, Kuhlmann L, Nakatani M, et al. A taxonomy of seizure dynamotypes. Skinner FK, Frank MJ, Van Drongelen W, Valiante TA, éditeurs. eLife. 21 juill 2020;9:e55632.

Santos MS, Soares JP, Abreu PH, Araujo H, Santos J. Cross-Validation for Imbalanced Datasets: Avoiding Overoptimistic and Overfitting Approaches. IEEE Comput Intell Mag. nov 2018;13(4):59-76.

Scaramelli A, Braga P, Avellanal A, Bogacz A, Camejo C, Rega I, et al. Prodromal symptoms in epileptic patients: Clinical characterization of the pre-ictal phase. Seizure. mai 2009;18(4):246-50.

Scheffer IE, Berkovic S, Capovilla G, Connolly MB, French J, Guilhoto L, et al. ILAE classification of the epilepsies: Position paper of the ILAE Commission for Classification and Terminology. Epilepsia. 1 avr 2017;58(4):512-21.

Schelter B, Winterhalder M, Maiwald T, Brandt A, Schad A, Timmer J, et al. Do False Predictions of Seizures Depend on the State of Vigilance? A Report from Two Seizure-Prediction Methods and Proposed Remedies. Epilepsia. 2006;47(12):2058-70.

Scherer M, Wang T, Guggenberger R, Milosevic L, Gharabaghi A. Direct modulation index: A measure of phase amplitude coupling for neurophysiology data. Human Brain Mapping. 2023;44(5):1862-7.

Schevon CA, Ng SK, Cappell J, Goodman RR, McKhann G, Waziri A, et al. Microphysiology of Epileptiform Activity in Human Neocortex: Journal of Clinical Neurophysiology. déc 2008;25(6):321-30.

Schindler K, Wiest R, Kollar M, Donati F. EEG analysis with simulated neuronal cell models helps to detect pre-seizure changes. Clinical Neurophysiology. 1 avr 2002;113(4):604-14.

Schindler KA, Bialonski S, Horstmann MT, Elger CE, Lehnertz K. Evolving functional network properties and synchronizability during human epileptic seizures. Chaos. sept 2008;18(3):033119.

Schölkopf B, Platt JC, Shawe-Taylor J, Smola AJ, Williamson RC. Estimating the support of a high-dimensional distribution. Neural Comput. juill 2001;13(7):1443-71.

Schulze-Bonhage A, Haut S. Premonitory features and seizure self-prediction: artifact or real? Epilepsy Res. déc 2011;97(3):231-5.

Schulze-Bonhage A, Kurth C, Carius A, Steinhoff BJ, Mayer T. Seizure anticipation by patients with focal and generalized epilepsy: A multicentre assessment of premonitory symptoms. Epilepsy Research. juill 2006;70(1):83-8.

Scott JM, Gliske SV, Kuhlmann L, Stacey WC. Viability of Preictal High-Frequency Oscillation Rates as a Biomarker for Seizure Prediction. Frontiers in Human Neuroscience. 2021;14.

Scott JM, Ren S, Gliske SV, Stacey WC. Preictal variability of high-frequency oscillation rates in refractory epilepsy. Epilepsia. 2020;61(11):2521-33.

Shaffer F, Ginsberg JP. An Overview of Heart Rate Variability Metrics and Norms. Front Public Health. 28 sept 2017;5:258.

Shoeibi A, Moridian P, Khodatars M, Ghassemi N, Jafari M, Alizadehsani R, et al. An overview of deep learning techniques for epileptic seizures detection and prediction based on neuroimaging modalities: Methods, challenges, and future works. Computers in Biology and Medicine. 1 oct 2022;149:106053.

Sisterson ND, Wozny TA, Kokkinos V, Constantino A, Richardson RM. Closed-Loop Brain Stimulation for Drug-Resistant Epilepsy: Towards an Evidence-Based Approach to Personalized Medicine. Neurotherapeutics. 1 janv 2019;16(1):119-27.

Spielberger C, Gorsuch R, Lushene R, Vagg P, Jacobs G. Manual for the State-Trait Anxiety Inventory (Form Y1 – Y2). Vol. IV, Palo Alto, CA: Consulting Psychologists Press; 1983.

Srinivasan R, Nunez PL, Silberstein RB. Spatial filtering and neocortical dynamics: estimates of EEG coherence. IEEE Transactions on Biomedical Engineering. juill 1998;45(7):814-26.

Stam CJ, van Straaten ECW. The organization of physiological brain networks. Clinical Neurophysiology. 1 juin 2012;123(6):1067-87.

Stevens JR, Lonsbury BL, Goel SL. Seizure occurrence and interspike interval. Telemetered electroencephalogram studies. Arch Neurol. mai 1972;26(5):409-19.

Stirling RE, Grayden DB, D'Souza W, Cook MJ, Nurse E, Freestone DR, et al. Forecasting Seizure Likelihood With Wearable Technology. Frontiers in Neurology. 2021a;12.

Stirling RE, Hidajat CM, Grayden DB, D'Souza WJ, Naim-Feil J, Dell KL, et al. Sleep and seizure risk in epilepsy: bed and wake times are more important than sleep duration. Brain. 13 déc 2022;awac476.

Stirling RE, Maturana MI, Karoly PJ, Nurse ES, McCutcheon K, Grayden DB, et al. Seizure Forecasting Using a Novel Sub-Scalp Ultra-Long Term EEG Monitoring System. Frontiers in Neurology. 2021b;12.

Sun FT, Morrell MJ. The RNS System: responsive cortical stimulation for the treatment of refractory partial epilepsy. Expert Rev Med Devices. nov 2014;11(6):563-72.

Takeshita D, Sato YD, Bahar S. Transitions between multistable states as a model of epileptic seizure dynamics. Phys Rev E. 31 mai 2007;75(5):051925.

Tang L, Lv H, Yang F, Yu L. Complexity testing techniques for time series data: A comprehensive literature review. Chaos, Solitons & Fractals. 1 déc 2015;81:117-35.

Tax DMJ, Duin RPW. Support vector domain description. Pattern Recognition Letters. 1 nov 1999;20(11):1191-9.

Tezer FI, Rémi J, Erbil N, Noachtar S, Saygi S. A reduction of sleep spindles heralds seizures in focal epilepsy. Clinical Neurophysiology. 1 nov 2014;125(11):2207-11.

Traub RD, Miles R, Wong RK. Model of the origin of rhythmic population oscillations in the hippocampal slice. Science. 10 mars 1989;243(4896):1319-25.

Truccolo W, Donoghue JA, Hochberg LR, Eskandar EN, Madsen JR, Anderson WS, et al. Single-neuron dynamics in human focal epilepsy. Nat Neurosci. mai 2011;14(5):635-41.

Varotto G, Susi G, Tassi L, Gozzo F, Franceschetti S, Panzica F. Comparison of Resampling Techniques for Imbalanced Datasets in Machine Learning: Application to Epileptogenic Zone Localization From Interictal Intracranial EEG Recordings in Patients With Focal Epilepsy. Frontiers in Neuroinformatics. 2021;15.

Viana PF, Duun-Henriksen J, Glasstëter M, Dümpelmann M, Nurse ES, Martins IP, et al. 230 days of ultra long-term subcutaneous EEG: seizure cycle analysis and comparison to patient diary. Annals of Clinical and Translational Neurology. 2021;8(1):288-93.

Vinette SA, Premji S, Beers CA, Gaxiola-Valdez I, Pittman DJ, Slone EG, et al. Pre-ictal BOLD alterations: Two cases of patients with focal epilepsy. Epilepsy Research. 1 nov 2016;127:207-20.

Vos T, Allen C, Arora M, Barber RM, Bhutta ZA, Brown A, et al. Global, regional, and national incidence, prevalence, and years lived with disability for 310 diseases and injuries, 1990–2015: a systematic analysis for the Global Burden of Disease Study 2015. The Lancet. oct 2016;388(10053):1545-602.

Wainberg M, Merico D, Delong A, Frey BJ. Deep learning in biomedicine. Nat Biotechnol. oct 2018;36(9):829-38.

Wang ET, Chiang S, Cleboski S, Rao VR, Vannucci M, Haneef Z. Seizure count forecasting to aid diagnostic testing in epilepsy. Epilepsia. 2022;63(12):3156-67.

Weinand ME, Carter LP, El-Saadany WF, Sioutos PJ, Labiner DM, Oommen KJ. Cerebral blood flow and temporal lobe epileptogenicity. Journal of Neurosurgery. 1 févr 1997;86(2):226-32.

Wendling F, Hernandez A, Bellanger JJ, Chauvel P, Bartolomei F. Interictal to ictal transition in human temporal lobe epilepsy: insights from a computational model of intracerebral EEG. J Clin Neurophysiol. oct 2005;22(5):343-56.

West J, Bozorgi ZD, Herron J, Chizeck HJ, Chambers JD, Li L. Machine learning seizure prediction: one problematic but accepted practice. J Neural Eng. janv 2023;20(1):016008.

Wulsin DF, Gupta JR, Mani R, Blanco JA, Litt B. Modeling EEG Waveforms with Semi-Supervised Deep Belief Nets: Fast Classification and Anomaly Measurement. J Neural Eng. juin 2011;8(3):036015.

Yang Y, Zhou M, Niu Y, Li C, Cao R, Wang B, et al. Epileptic Seizure Prediction Based on Permutation Entropy. Frontiers in Computational Neuroscience. 2018;12.

Yeshokumar AK, Coughlin A, Fastman J, Psaila K, Harmon M, Randell T, et al. Seizures in autoimmune encephalitis—A systematic review and quantitative synthesis. Epilepsia. 2021;62(2):397-407.

Yger P, Spampinato GL, Esposito E, Lefebvre B, Deny S, Gardella C, et al. A spike sorting toolbox for up to thousands of electrodes validated with ground truth recordings in vitro and in vivo. Kleinfeld D, éditeur. eLife. 20 mars 2018;7:e34518.

Zaveri HP, Duckrow RB, Spencer SS. The effect of a scalp reference signal on coherence measurements of intracranial electroencephalograms. Clinical Neurophysiology. 1 juill 2000;111(7):1293-9.

Zhang ZJ, Koifman J, Shin DS, Ye H, Florez CM, Zhang L, et al. Transition to Seizure: Ictal Discharge Is Preceded by Exhausted Presynaptic GABA Release in the Hippocampal CA3 Region. J Neurosci. 15 févr 2012;32(7):2499-512.

Zhou ZH, Liu XY. Training cost-sensitive neural networks with methods addressing the class imbalance problem. IEEE Transactions on Knowledge and Data Engineering. janv 2006;18(1):63-77.

Zijlmans M, Zweiphenning W, van Klink N. Changing concepts in presurgical assessment for epilepsy surgery. Nat Rev Neurol. oct 2019;15(10):594-606.

Annexes

NeuroImage 254 (2022) 119116

Contents lists available at ScienceDirect

NeuroImage

journal homepage: www.elsevier.com/locate/neuroimage

Long-term deep intracerebral microelectrode recordings in patients with drug-resistant epilepsy: Proposed guidelines based on 10-year experience

Katia Lehongre[a,1], Virginie Lambrecq[a,b,c,1], Stephen Whitmarsh[a], Valerio Frazzini[a,b,c], Louis Cousyn[a,c], Daniel Soleil[d], Sara Fernandez-Vidal[a], Bertrand Mathon[a,e], Marion Houot[f,g,h], Jean-Didier Lemaréchal[a,i], Stéphane Clemenceau[e,2], Dominique Hasboun[a,j], Claude Adam[c], Vincent Navarro[a,b,c,k,*]

[a] *Sorbonne Université, Paris Brain Institute – Institut du Cerveau, ICM, INSERM, CNRS, APHP, Pitié-Salpêtrière Hospital, Paris France*
[b] *AP-HP, EEG Unit, Neurophysiology Department, Pitié-Salpêtrière Hospital, DMU Neurosciences, Paris, France*
[c] *AP-HP, Epilepsy Unit, Pitié-Salpêtrière Hospital, DMU Neurosciences, Paris, France*
[d] *Bureau d'Etudes CEMS, 801 Route d'Eyguieres, 13 560 Senas, France*
[e] *AP-HP, Neurosurgery Department, Pitié-Salpêtrière Hospital, Paris, France*
[f] *Centre of Excellence of Neurodegenerative Disease (CoEN), AP-HP, Pitié-Salpêtrière Hospital, Paris, France*
[g] *Institute of Memory and Alzheimer's Disease (IM2A), Department of Neurology, AP-HP, Pitié-Salpêtrière Hospital, Paris, France.*
[h] *Clinical Investigation Centre, Institut du Cerveau et de la Moelle épinière (ICM), Pitié-Salpêtrière Hospital Paris, France*
[i] *Institut de Neurosciences des Systèmes, Aix-Marseille Université, Marseille, France*
[j] *AP-HP, Neuroradiologiy Department, Pitié-Salpêtrière Hospital, Paris, France*
[k] *AP-HP, Center of Reference for Rare Epilepsies, Pitié-Salpêtrière Hospital, Paris, France*

ARTICLE INFO

Keywords:
Drug-resistant epilepsy
sEEG
Human
Microelectrode
Multi-unit activity
Technical guidelines

ABSTRACT

Purpose: Human neuronal activity, recorded *in vivo* from microelectrodes, may offer valuable insights into physiological mechanisms underlying human cognition and pathophysiological mechanisms of brain diseases, in particular epilepsy. Continuous and long-term recordings are necessary to monitor non predictable pathological and physiological activities like seizures or sleep. Because of their high impedance, microelectrodes are more sensitive to noise than macroelectrodes. Low noise levels are crucial to detect action potentials from background noise, and to further isolate single neuron activities. Therefore, long-term recordings of multi-unit activity remains a challenge. We shared here our experience with microelectrode recordings and our efforts to reduce noise levels in order to improve signal quality. We also provided detailed technical guidelines for the connection, recording, imaging and signal analysis of microelectrode recordings.

Results: During the last 10 years, we implanted 122 bundles of Behnke-Fried hybrid macro-microelectrodes, in 56 patients with pharmacoresistant focal epilepsy. Microbundles were implanted in the temporal lobe (74%), as well as frontal (15%), parietal (6%) and occipital (5%) lobes. Low noise levels depended on our technical setup. The noise reduction was mainly obtained after electrical insulation of the patient's recording room and the use of a reinforced microelectrode model, reaching median root mean square values of 5.8 μV. Seventy percent of the bundles could record multi-units activities (MUA), on around 3 out of 8 wires per bundle and for an average of 12 days. Seizures were recorded by microelectrodes in 91% of patients, when recorded continuously, and MUA were recorded during seizures for 75 % of the patients after the insulation of the room. Technical guidelines are proposed for (i) electrode tails manipulation and protection during surgical bandage and connection to both clinical and research amplifiers, (ii) electrical insulation of the patient's recording room and shielding, (iii) data acquisition and storage, and (iv) single-units activities analysis.

* Corresponding author at: AP-HP, Epilepsy Unit, Pitié-Salpêtrière Hospital, 47-83 Boulevard de l'Hôpital, Paris 75013, France.
E-mail address: vincent.navarro@aphp.fr (V. Navarro).

[1] These authors contributed equally to this work.

[2] In Memoriam: Dr. Stéphane Clemenceau (1960 - 2021) was a great neurosurgeon, who has spent his entire career in the Department of Neurosurgery at The Pitié-Salpêtrière Hospital (Paris). He founded the epilepsy surgery unit in 1990 and developed advanced techniques for epilepsy surgery, particularly for mesial temporal lobe resections. He was one of the first neurosurgeons to use MRI-guidance instead of angiography for intracranial EEG electrode implantations.

https://doi.org/10.1016/j.neuroimage.2022.119116.
Received 26 August 2021; Received in revised form 23 February 2022; Accepted 15 March 2022
Available online 19 March 2022.

Conclusions: We progressively improved our recording setup and are now able to record (i) microelectrode signals with low noise level up to 3 weeks duration, and (ii) MUA from an increased number of wires . We built a step by step procedure from electrode trajectory planning to recordings. All these delicate steps are essential for continuous long-term recording of units in order to advance in our understanding of both the pathophysiology of ictogenesis and the neuronal coding of cognitive and physiological functions.

1. Introduction

Intracranial electroencephalography (iEEG) investigation prior to epilepsy surgery represents a rare opportunity to access human neuronal assemblies function *in vivo* for extended periods of time. A surgical implantation of intracerebral electrodes can delineate the epileptogenic focus, called the seizure onset zone (SOZ), when non-invasive electroencephalography (EEG) and neuroimaging have been insufficient to localize the epileptogenic focus in drug-resistant patients (Crandall et al., 1963; Engel et al., 2005; Reif et al., 2016; Zijlmans et al., 2019).

Different types of electrodes can be surgically implanted, alone or in combination: subdural strip electrodes, grid electrodes, or depth electrodes for stereoelectroencephalography (sEEG). All of these electrodes contain several *macrocontacts*, spaced several millimeters to centimeters apart. Each macrocontact has a size of a few mm and measures neuronal activity from a large population of neurons (Buzsáki et al., 2012; Parvizi and Kastner, 2018).

Microelectrodes have small contact areas at the tip of isolated wires, with a diameter of around 40 µm. Compared to macrocontacts, *microwires* provide two main advantages: an increased spatial resolution, allowing the recording of local field potentials (LFPs) at submillimeter scale from small neuronal assemblies; and the ability to record action potentials of sampled neurons, i.e.multi-unit activities (MUAs) from which single-unit activities (SUAs) can be isolated after spike sorting (Pedreira et al., 2012; Stacey et al., 2013). The first acute recordings of units in the human mesial temporal lobe were made in 1971, during and between seizures (Verzeano et al., 1971). Macroelectrodes have been modified to allow the insertion of a flexible bundle of microwires (Babb et al., 1973). Subsequently, *microelectrodes* have been inserted for the duration of the iEEG in the epileptogenic focus in humans (Babb and Crandall, 1976; Wyler et al., 1982) and different microelectrode types have been developed. Hybrid depth electrodes have microcontacts interspaced between macrocontacts (Howard et al., 1996). In the Ad-Tech Behnke-Fried macro-microelectrodes model (Fried et al., 1997), microwires are inserted through the macroelectrode shaft, protruding into the cerebral tissue beyond the tip of the depth macroelectrode. In the DIXI hybrid macro-microelectrodes model, the microwires exit the macroelectrode shaft between macrocontacts and have a tetrode rather than a single-wire configuration (Despouy et al., 2019). The Utah array is a two dimensional array of 4 mm × 4 mm that contains 96 microelectrodes and can be implanted at the surface of the cortex (Schevon et al., 2008). Lastly, high density poly(3,4-ethylenedioxythiophene) polystyrene sulfonate (PEDOT:PSS) microelectrodes were recently proposed, for acute recordings in the operative room during surgery (Paulk et al., 2021).

Microelectrodes are implanted in patients with epilepsy for research purposes and the analysis of the LFP, MUA or SUA recorded have provided valuable insights into neuronal codes or underlying physiological processes, as well as cognition (Axelrod et al., 2019; Ekstrom et al., 2003; Fried et al., 1997; Kim et al., 2019; Kreiman et al., 2000; Lakretz et al., 2021; Mormann et al., 2008; Quiroga et al., 2005). Recordings allow testing of cognitive processes such as working and episodic memory, with temporal precision through single-trial studies in brain areas without epileptic activities. For example, important findings were obtained in the mesial temporal lobe, in the amygdala and hippocampus with Behnke-Fried electrodes (Fried et al., 1997), where the isolation of SUA was essential to describe individual neurons' behaviors. Itzak Fried's group described category specific SUA, such as imagery neurons in the human mesial temporal lobe (Kreiman et al., 2000) and place cells in the human hippocampus (Ekstrom et al., 2003). Some mesial temporal lobe SUAs could be selectively activated by distinct pictures of given objects, landmarks or individuals, such as "Jennifer Aniston neuron" (Quiroga et al., 2005). Long-term recordings (up to 3 weeks) during presurgical implantation allow dedicated time periods for cognitive tasks, which can be repeated over several days and weeks. This has obvious value for studying memory encoding and retrieval (Kornblith et al., 2017; Rutishauser et al., 2021; Staresina et al., 2019).

Microelectrode recordings have also been a major tool for investigating the pathophysiology of epilepsy, notably the ictogenesis, i.e. how the brain initiates seizures. Epileptic seizures on EEG are the main electrophysiological marker of epilepsy. Recognizing the most precocious and faster components of the ictal discharge is a key step in identifying the SOZ (Fisher et al., 1992; Talairach and Bancaud, 1966; Wendling et al., 2003). Microelectrodes inserted in the SOZ can capture single-unit activities at the beginning and the development of seizures and help to describe SOZ networks (Lambrecq et al., 2017; Schevon et al., 2012, 2008). In addition, according to the waveform and firing properties of isolated neurons through spike sorting, it is possible to distinguish putative pyramidal cells and interneurons, and to describe their respective involvement in the generation of seizures (Elahian et al., 2018; Truccolo et al., 2011; Weiss et al., 2016). Microelectrodes have also been used to describe single unit behaviors during interictal events like epileptic spikes and have shown heterogeneous firing patterns (Alvarado-Rojas et al., 2013; Despouy et al., 2019; Keller et al., 2010; Ulbert et al., 2004). Microelectrodes can also detect other epileptic markers that are not detected on adjacent macroelectrodes, such as high frequency oscillations (HFOs), specifically in the fast ripple band (250-500 Hz). Initially identified from microelectrode recordings, HFOs were assumed to be generated by small neuronal assemblies of about one mm^3 (Zijlmans et al., 2017). Microelectrodes have also revealed microseizures as discrete rhythmic activities that would not be detected by macroelectrodes, due to the better resolution of microelectrodes for sampling the local field potentials of much smaller neuronal assemblies (Schevon et al., 2008; Staba et al., 2014; Stead et al., 2010).

Detection of units on microelectrodes signal requires a high signal to noise ratio (SNR), that depends on the noise level in the signal but also on the distance of the electrode from the soma of the neuron (Rey et al., 2015; Buzsáki et al., 2012). The higher the noise level is, the more difficult it is to detect action potentials of lower amplitude. The accuracy of the spike sorting algorithm to assign the action potentials detected to different neurons will also be affected by a high noise level because of an alteration of the action potential waveforms (Buccino et al., 2020; Chaure et al., 2018; Wild et al., 2012). As for all electrophysiological recordings, electro-magnetic noise from the surrounding environment, as well as movement artifacts are major noise sources for the signal. Therefore, and because it is not possible to move the microwire of the Behnke-Fried electrode to approach the soma of a neuron, it is crucial to decrease those noise sources, especially because microwires have a very small diameter, that makes them very fragile and sensitive to noise (Misra et al., 2014).

Furthermore, epileptic events, in particular seizures, have unpredictable occurrences and require continuous and long-term electrophysiological monitoring to be recorded. Studying LFPs and unit activity during those events is only possible with stable high quality microelectrode recordings during the whole monitoring period. Long-term microelectrode recordings are also essential for physiological and cognitive stud-

ies at the cellular level. However, continuous and long-term recordings with microelectrodes are technically highly challenging. Thanks to a strong collaboration between several clinical teams of Pitié-Salpêtrière Hospital (Paris, France) and a research center (Paris Brain Institute), located on the hospital's site, we started to record epileptic patients with Behnke-Fried microelectrodes in 2010.

The aim of this paper is to share our experience of the last 10-year with continuous long-term microelectrode recordings and bring recommendations complementary to already published methodological papers. Electrode manipulation during the surgery is a crucial step to avoid noise resulting from wire degradation and has been described in several papers (Misra et al., 2014; Minxha et al., 2018). Detailed quantification of noise level depending on technical setting is important as well to adopt the best methodology, but has not been quantified and described in detail from our knowledge. We have described the technical issues we faced, and the different improvements we made to reduce the noise level on the signal, which is crucial to increase the possibilities to record MUA and SUA. We have first described our current recording methodology in the Method section. The improvement of our data quality over time is reported in the Results section with detailed noise level measures and a quantification of multi-units recordings depending on different material setups. In addition, we have summarized the main technical guidelines, from surgery to recordings, that we found essential to improve the quality of microelectrode recordings.

2. Materials and methods

2.1. Patients

Since 2010, fifty-six patients with refractory focal epilepsy underwent a presurgical intracerebral electrode investigation with additional microelectrodes. The aim of the clinical intracerebral investigation was to determine the SOZ when non-invasive explorations were inconclusive. Non-invasive explorations included medical history, neurological examination, brain imaging (e.g. MRI, PET, SPECT) and long-term scalp video-EEG monitoring. The continuous (24/7) video-EEG monitoring with intracranial electrodes took place in the Epilepsy Unit of the Pitié-Salpêtrière Hospital (Paris, France) and started the day after the implantation. Recordings lasted for 2 to 3 weeks, depending on whether enough informative seizures were recorded. All patients provided informed and written consent for the implantation of microelectrodes, which received approval from local ethic committees (CPP Paris VI, CNRS, 2004, 2006; INSERM C11-16, C19-55).

2.2. Planning of stereotactic electrode placement

Electrode planning was carried out by epileptologists, neurosurgeons and neuroradiologists, days or weeks before implantation. Macroelectrode trajectories and targets were defined only based on clinical objectives. They were very specific to each patient and trajectories were not necessarily orthogonal to the brain surface. The planification of macro-microelectrodes trajectories was not influenced by the decision of adding a microelectrode. Microelectrodes were added to a macroelectrode when there was enough gray matter beyond the last macrocontact for the microwires to expand into. As the original 20 mm length of the microwires was too long, they were cut at a length calculated during trajectory planning.

Until end of 2017, macroelectrode trajectories were planned according to a stereotactic Leksell frame and based on pre-implantation brain MRI, using iplan® stereotaxy, version 3.0, BrainLAB System (Budke et al., 2018; Ringel et al., 2009). Since the end of 2017, the ROSA robot (Zimmerbiomet, Ind., USA) has been used to assist the surgery. However, the ROSA planning software did not allow to map 3D cortical surfaces or to visualize multiple electrode trajectories simultaneously. Therefore, the STIM core facility of the Paris Brain Institute developed a stereotactic sEEG toolbox (EPILOC). One of its modules, STEREO-PLAN (Fernandez-Vidal et al., 2019), allows clinicians to perform sEEG planning. EPILOC includes several image processing pipelines: corregistation of multimodal pre-operative sequences, anatomical segmentations and computation of patient specific models and a dedicated 3D SLICER (Fedorov et al., 2012) graphic interface. The graphic interface allows to visualize all the previous pipeline results, referenced to the ACPC native orientation, and to easily plan and edit trajectories with different depth electrode models. Multiple structural and metabolic imaging modalities (such as PET and SPECT data) can also be merged in the native patient space, to add further information pertinent to the planning of intracerebral trajectories.

2.3. Surgical placement of the electrodes

The stereotactic implantation of intracranial electrodes was performed in the Department of Neurosurgery. Prior to the insertion of microelectrodes into the dedicated hollow macroelectrodes, microwires were cut by the neurosurgeon to the desired length defined during the planning (generally 2-3 mm, Supp. Fig. 1). They were cut using Yasargil microscissors, all at the same length and perpendicularly to the electrode axis, and then gently bend outwards until they had a splayed pattern, like an "umbrella", that will be maintained when they extend in the brain. (Fig. 1). This splayed pattern provides a better chance of recording action potentials (Babb et al., 1973; Misra et al., 2014). All electrodes were fixed on the skull with hollow screws that prevent post-surgical movement of the electrodes (*anchor bolts*: ADTECH LSBK1-BX-06 length 13mm, and LSBK1-AX-06 length 21mm). Once all intracranial electrodes were implanted, the patient's skin was cleaned and sanitized with soap, water and betadine. The head was then prepared for long-term video-EEG recording with careful bandaging (Fig. 2 and Table 1), necessary to avoid any damage to the electrodes and to improve comfort of the patient during hospitalization.

A post-operative CT-scan and MRI were always performed after implantation and merged with the presurgical MRI to verify the electrodes' positions (see 2.6.2). An X-ray was also performed to confirm the spreading of the microelectrodes.

2.4. Connection to the recording system

Patients were connected to the acquisition system during the first day after implantation. First, all supplemental EEG scalp electrodes were placed on the patient's head (where there were no implanted electrodes). A ground electrode was placed under the collarbone, and 2 ECG electrodes were placed on the chest. Secondly, the depth electrode tails were connected to CABRIO connectors (Ad-Tech ®, Wisconsin) for the macroelectrodes and CHET headstages (Neuralynx®, Inc., Bozeman, MO) for the microelectrodes (Fig. 3, Tables 2 and 3). Connecting the tails is a crucial step in the electrode manipulation and requires a lot of care. We therefore established a procedure to increase the patient's comfort, avoid any wrong manipulation and tensile load on the electrode tails that could break the wires, and avoid any tension on connection cables that could lead to disconnection. To maintain sterility, the bandage done in the surgery room was not removed until the patient was discharged. Steps G to J from Fig. 3 were redone every 2 to 3 days in order to repaste the scalp electrodes, but connectors were not moved to avoid manipulating the electrode tails.

2.5. Recording material

2.5.1. Electrodes

The number of macroelectrodes that were implanted in each patient ranged from 4 to 13, including 1-4 hybrid macro-microelectrodes. All electrodes were produced by Ad-Tech Medical Instrument Corporation (Ad-Tech®, Wisconsin). The standard macroelectrodes consisted of 4-12 platinum contacts of 1 mm of diameter, 2.41 mm of length and 5 mm of inter-contact distance with nickel-chromium wiring and polyurethane

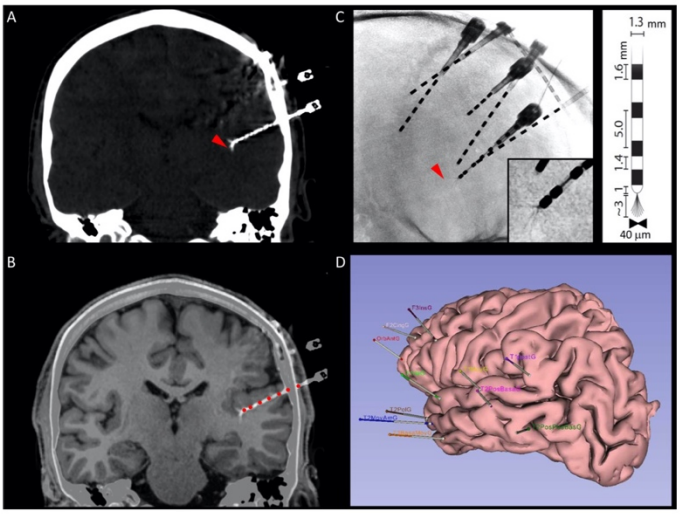

Fig. 1. Multimodal microelectrode identification. A. Cranial CT Scan on a coronal plan showing the trajectory of the macroelectrodes and the localization of microelectrode bundles (red arrow). **B.** Automated superposition of the CT scan with the anatomical T1 MRI, allowing the visualization of microelectrodes' position in the brain parenchyma together with the automated identification of macroelectrode contacts (red circles) along the intracerebral trajectory. **C.** Radiographic image showing the bidimensional location of intracerebral electrodes. The red arrow indicates the location of a microelectrode bundle, seen in the previous pictures. *Inset's*: magnification of microelectrode wires. Note the spreading of the microwires. *Inset's on the right*: Schematic representation of the macro-micro electrode geometry. **D.** 3D Epiloc anatomical reconstruction of subject cortical anatomy, showing the implantation scheme of the intracerebral macroelectrodes.

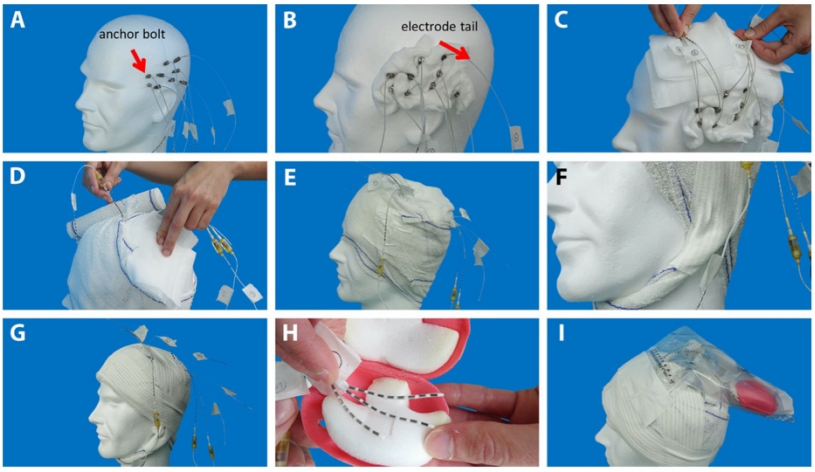

Fig. 2. Main steps for the surgical bandage. A. Surgically implanted macroelectrodes and macro-microelectrodes. The arrow shows an anchor bolt. **B.** Compresses wrapped around the anchor bolts of macro and microelectrodes. The arrow shows an electrode tail. **C.** Bundling of tails in one or two parts above the head. **D.** Fixing together with compresses and bandages while avoiding to cover the electrode tails. **E.** Output of electrode tails through the bandage in 2 different sites. **F.** Making a chin strap. **G.** Coronal and sagittal adhesive strips to hold the bandage in place. **H.** Infusion protection box to protect microelectrodes before connection. **I.** Protection of all connectors and boxes in a plastic bag placed above the head, before connection in the patient's room.

Table 1
Guidelines on electrode tails manipulation and protection during surgical bandage.

	Corresponding pictures from Fig. 2
Wrapping of compresses around the anchor bolts for the patient's comfort (to prevent irritation of the skin around the anchor) and to avoid sharp bending of the electrode tails at the anchor bolt outputs.	A -> B
Grouping of the electrode tails toward the desired output from the bandage. It is important to maximize the output length of the tails from the bandage to avoid any bending or pulling during the connection of the tails to the connectors. If the distance between the electrodes is too long, two outputs from the bandage should be prepared.	C
Covering of the head with bandages without covering the electrode tails and with respect to the prepared output of tails.	D -> G
Protection of microelectrode tails in an infusion box maintained in a plastic bag at the top of the head, to avoid any bad manipulation of tails between the surgery and the connection (i.e. during CT scan / MRI, sleep, etc.).	H + I

tubing. The macro-microelectrodes (Behnke-Fried model) included both a hollow macroelectrode and a microelectrode bundle that spread out from the tip of the macroelectrode. The macroelectrode part of the micro-macroelectrode consisted of 8 (BF08R-SP05X-000, BF08R-SP71X-0C2) or 9 (BF09R-SP05X-0MF, BF09R-SP61X-0BB) platinum contact electrodes of 1.3 mm of diameter and 1.57 mm of length, embedded on the surface of a polyurethane tube with a hollow lumen. The microelectrode, consisted of a bundle of 8 (model 1: WB08R-SP00X-0AA) or 9 (model 2: WB09R-SP00X-0AA; model 3: WB09R-SP00X-014) platinum-iridium microwires of 40 µm diameter and 20 mm length. For all models, the microelectrode bundle was inserted through the hollow macroelectrode, protruding 3-6 mm into the cerebral tissue beyond the tip of the macroelectrode. For model 2 and 3, the 9th wire was un-insulated and was provided for a possible use as reference. The suppression of the insulation on several millimeters confers to this electrode a lower impedance and therefore a capacity to record from a larger neuronal

Fig. 3. Main steps for the electrode connection. A&B. Bandage preparation with holes to add scalp electrodes outside the implanted zone. **C.** Placement of scalp electrodes. **D.** Pasting of velcro bands on the bandage. **E.** Connection and placement of the connectors on the velcro bands. The arrows show the 2 connector types: CABRIO connectors from Ad-Tech and CHETs from Neuralynx. *Note that Neuralynx CHETs are closed with a plastic clip to prevent them from opening. These clips are made of small electrical raceways. Simple tape can be used too, but is less handy and often leaves the CHET sticky when removed.* **F.** Grouping of all the connector cables within a bandage. **G.** Covering of the connectors with compresses. **H.** Covering of the connectors with the "conductive tissue". **I.** Covering and stabilizing with 2 bandages. **J.** Final covering with a net. **K.** Connection to the headboxes. The arrow shows a head box. **L.** Placement of the headboxes in a bag. **M&N.** Fixation of the input and output cables on the bag. The arrows show how the cables are fixed. **O.** The bag is carried by the patient when moving.

Table 2
Guidelines on electrode tails manipulation and protection during connection.

	Corresponding pictures from Fig. 3
Opening of small bandage parts outside the implanted zone, to create access for scalp electrodes	A + B
Placement and pasting of scalp electrodes	C
Preparation of velcro bands that will be used to fix the connectors on the head and prevent any pulling on the electrode tails: •Pasting of velcro bands on the wrap, outside the implanted area but preferentially on the top of the head, where the patient will not lie on while sleeping. •Pasting of small complementary pieces of velcro on all connectors	D
Connection and placement of the connectors on the velcro without pulling and bending of tails and cables. Electrode tails, especially for micros, must be handled very carefully to avoid unnecessary tensile load. The placement will be done: •According to the length of tail available •With all connector cables in the same direction in order to join them on a single side of the patient •With some compresses under tails to avoid bending if necessary	E + F
Wrapping of all connector cables together for the comfort of the patient but also to prevent from pulling on them	F
Covering of tails and connectors with compresses to smooth the compression of the cables with the bandage. Compresses should also be added under the macro-microelectrode tails if needed	G
Covering of the compresses with an electrically conductive silver cloth (Stretch conductive fabric, Less EMF Inc., Latham NY 12110, USA) to shield poorly isolated electrode tails. The tissue is grounded to the patient through an alligator clip attached to the tissue	H
Covering with a bandage and a tubular net bandage to maintain the connectors and the tissue on the patient's head	I + J
Connection of the connector cables to the headboxes and placing of the headboxes in a waist bag that will be carried by the patient if he needs to move. To prevent any disconnection, the connector cables and the output tether cables are attached to the bag. The tether cables are also attached to the amplifier carriage before their connection to the amplifier.	K -> O

Table 3
Glossary.

Name	**Definition**
Electrode tail (Fig. 2B)	Output of the electrode from the brain
CABRIO connector (Fig. 3E)	Ad-Tech electrode connector
CHET (Fig. 3E)	Neuralynx electrode connector
HeadBox (Fig. 3K)	Connection box used to connect electrode connectors and send the signal to the amplifiers
Tether cable	Connection cable from the headboxes to the amplifier

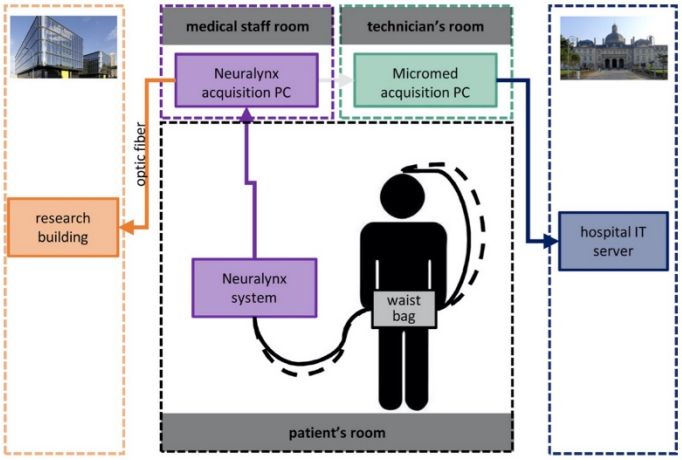

Fig. 4. Current acquisition setup. Signals recorded from macro and microelectrodes are acquired by the research Neuralynx system and sent from the Neuralynx acquisition PC to the clinical Micromed acquisition PC through a direct network connection. The research and clinical acquisition PC send respectively the data to the research and clinical servers to fill the respective databases. The research building is located in the hospital and has a direct network connection to the epilepsy center building via a dedicated optic fiber. Black dashed lines represent cables for macroelectrodes, black plain lines represent cables for microelectrodes.

population, with less sensitivity to action potentials from surrounding neurons (Jurczynski et al., 2021). Model 3 was the same as model 2, but with an epoxy reinforcement on the area of attachment between tails of the microelectrode and macroelectrode (Supp Fig. 1), supposed to reduce the risk of failure at this weak point.

Additional scalp electrodes were also recorded (T9, FT9, Fp1, Fz, Fp2, FT10, T10, O1, Oz, O2, EKG). In the last 23 patients, electrodes essential for polysomnographic recordings (C4 or C3, M1 or M2, E1, E2 and EMG) were added.

2.5.2. Amplifiers

Over the last 10 years, three successive acquisition setups have been used, each one bringing specific improvements (Fig. 4 and Supp. Fig. 2).

Oct. 2010 - Jun. 2012 - Macro and micro recorded on 2 different amplifiers (11 patients): For the first microelectrode recordings, macro and microelectrode signals were acquired on two different amplifiers. All macroelectrode signals were recorded continuously with the clinical amplifier (SD LTM, Micromed® S.p.A., Italy, 128 channels at 1024 Hz), and microelectrode signals were recorded a few hours per day, with the Lynx amplifier (Digital Lynx, Neuralynx®, Inc., Bozeman, MO, 32 channels at 32 kHz, Supp. Fig. 2.A). Macro and micro signals were synchronized offline with the help of an analogical trigger sent to both systems during acquisition.

Nov. 2012 - Oct. 2018 - Macro and micro recorded on same amplifiers (39 patients): In 2012, the Neuralynx system was upgraded to the ATLAS amplifier (Atlas, Neuralynx®, Inc., Bozeman, MO), to record with up to 160 electrodes. Contrary to the previous system, the ATLAS amplifier also allowed the recording from all macro and microelectrodes simultaneously, as well as continuously during the whole clinical investigation of the patient, i.e. up to 3 weeks. Signals from macroelectrodes and microelectrodes were recorded at 4 and 32 kHz, respectively. Because clinicians need access to the data via the clinical database, the signal of the macroelectrodes (and the microelectrodes when the total number of electrodes did not exceed 128) was also recorded by the clinical Micromed systems (1024 Hz). To record the signal in parallel, the signal was split using a specific cable provided by Neuralynx (MDR50), with a Neuralynx connection on one side and touch proof outputs for the Micromed HeadBoxes on the other side (Supp. Fig. 2.B).

Nov. 2018 - current - Macro and micro recorded on a unique amplifier (6 patients): In 2018, the Micromed acquisition software was updated with a network connection between the Neuralynx and Micromed systems, allowing for a real-time data transfer from the Neuralynx acquisition system to the Micromed software and database. Consequently, since 2018 only the ATLAS amplifier has been used to record all electrodes continuously and during the whole clinical investigation (Fig. 4). This new setup avoided a duplication of the electrode connections to two different amplifiers, which was a source of possible connection errors as each electrode was connected twice. Potential noise issues related to the fact that two amplifiers were grounded together, were also avoided. The acquisition sampling rate on Neuralynx was set to 4096 Hz for the macroelectrodes and 32768 Hz for the microelectrodes. Signal from all electrodes was downsampled to 1024 Hz for Micromed.

All Neuralynx recordings were realized with Neuralynx Cheetah acquisition software.

2.5.3. Reference and patient ground

Macroelectrode reference: For recordings with the Micromed system (before Nov. 2018), a scalp reference electrode was used, placed as close as possible to the vertex of the head (Cz). For recordings with the Neuralynx system, the reference can be chosen from any of the recorded electrodes and can be different for macro and microelectrodes. For the macroelectrodes, when available, a contact in the white matter with a flat EEG signal and without epileptic activity, was selected. If such electrode contact was not available, the Cz scalp electrode was used. The latter was avoided when possible, because scalp electrodes are more likely to record muscle artifacts and to get detached from the skin, which introduces noise in all data.

Microelectrode reference: For each microelectrode, a microwire from the same bundle, with no MUA and no artifacts, was used as reference, to avoid injecting these activities in all electrodes. For model 1 and the large majority of model 2 and 3, one of the 8 microwires was selected. Using the un-insulated reference microwire for model 2 and 3 resulted most of the time in a higher noise level in the microelectrode signals, probably because the difference of impedance between the electrodes was too high. It was used only for 3 patients. Using a normal microwire as reference will enhance detection of very local activities but also eliminate all common activities recorded by the microwires, especially the slow components of the LFP that are generated from the averaged activity of a larger neuronal population. The un-insulated reference, on the contrary, will better preserve the slow components of the LFP but can also inject the same LFP activity in all microwires because of the difference of impedance and amplitude of signal captured by the electrodes. The impact on the LFP, whatever the wire used as reference, can vary depending on the distance between the microwires in the brain, which is unpredictable with the Behnke-Fried electrodes (Jurczynski et al., 2021).

Signal quality of microelectrodes was daily checked. If MUAs or artifacts appeared on all wires, which usually meant that the reference was

contaminated by those activities, another microwire of the microelectrode bundle was selected as a reference.

Ground: A scalp electrode on the collarbone was used for the patient's ground. Before November 2018, when 2 different amplifiers were used, the same patient's ground was used for both by using a jumper cable.

2.6. Data management

2.6.1. Storage

Microelectrodes are recorded at high sampling rate (32 kHz in our configuration) which can lead to an important amount of data to manage and store when acquired continuously for several weeks. A single channel recorded at 32 kHz for 2 h weighs almost 0.5 GB. In 2 to 3 weeks, a continuous recording of around 100 macro and microelectrodes, including 8 to 32 microwires accumulates 2 to 3 TB of data.

Because the research center (Paris Brain Institute) and the epilepsy unit are located on the hospital grounds in different buildings with separated network infrastructures, an optic fiber was extended from the epilepsy unit to the servers of the research center, allowing a direct data transfer since Feb. 2013. Every night, the data acquired by the Neuralynx system was transferred to the server at the Paris Brain Institute, allowing for a quick visualization and analysis by researchers. Before storage on the server, all data was pseudo-anonymized if not already done at the acquisition. All recorded data were segmented into files of 2 h maximum to optimize their reading access with the different visualization and analysis softwares. As Cheetah software did not allow segmentation without losing samples between files, recordings were usually launched for 24 h and segmented offline with Matlab software to 2 h without data loss. Data were organized by patients with standardized nomenclature and organization to facilitate access to the desired dataset. Acquisition settings, imagery and clinical information were added to each patient's folder. Access to the data was secured with personal ID and password, and obtained on demand for collaborators. Data acquired by the clinical softwares was stored and managed by the hospital IT infrastructure.

2.6.2. Electrode localisation and visualization

Within the EPILOC toolbox, two modules have been developed to localize implanted electrodes and their contacts spatially and anatomically. They were based on several image processing pipelines, using Brainvisa (Rivière et al., 2011, https://brainvisa.info/web/) and Freesurfer (http://surfer.nmr.mgh.harvard.edu/), that were built to: 1) compute anatomical models from the structural MRI preoperative sequence, 2) normalize this sequence on MNI template, 3) coregister pre- and post-operative sequences in the patient native space with the structural preoperative MRI as reference, using a block matching algorithm, 4) automatically localize depth sEEG electrodes on CT postoperative sequences, by segmentation of electrode artifacts present on the postoperative TDM and their classification using their distance to the theoretical trajectories planned on the stereotactic guidance device (ROSA or Leksell), 5) label all the contacts using the MNI atlases and the patient specific anatomical models. A first module allowed to check and correct, if necessary, potential mismatches of the automatic localization stage. The second module called EPILOC-VIEW created an interface that allowed users to navigate easily on a 3D scene, where all the results of different pipelines were merged. The user had the possibility to navigate among the different implanted electrodes and contacts and focus on each electrode by choosing a classical view or a view along the axis of the electrode, which was important to better identify the traces of the microelectrodes (Fig. 1). The structural image normalization allowed to report all the patient's data in the MNI space and visualize them in both native and MNI spaces. Microelectrodes were detected on the postoperative 3D CT scan. The superimposition with the pre-implantation MRI sequences allowed the identification of the individual anatomical localization. Their localization in the seizure onset zone (SOZ) was extracted from the clinical reports.

2.6.3. Signal visualization

It is often necessary to inspect the raw signal not only to check data quality and artifacts, but also to annotate pathological or physiological activities for further analyses. However, data acquired since 2012 was difficult to read with available software. Macro and microelectrodes signals were acquired at different sampling rates which is typically not supported in software for EEG visualization. Furthermore, before 2012 data were acquired on different amplifiers, and saved in different data files and formats. Data duplication due to conversion to different data formats becomes a storage issue with continuous recordings. In response to these issues, an in-house EEG/MEG software, MUSE (Ducorps et al., 2010) (Supp. Fig. 3), was updated to visualize macro and microelectrode signals directly from different file formats and at different sampling rates. For macro and microelectrode signals that were acquired on different amplifiers, the analog synchronization triggers were used offline to find the delay between the signals and to synchronize two visualization windows. When macro and microelectrode signals were acquired synchronously on the same Neuralynx system, all signals could be visualized at their original sampling rate. The MUSE software also gives the possibility to filter macro and microelectrodes separately at different frequencies and to annotate artifacts and events of interest (i.e. seizures, interictal activities, etc).

2.7. Noise / data quality

2.7.1. Room isolation and noise measurements

Because of their high impedance (Stacey et al., 2013), microelectrodes are more sensitive to artifacts than macroelectrodes. The most pervasive noise comes from the electrical recording environment, especially at 50/60Hz. The signal to noise ratio (SNR) can be insufficient if the electrical environment is too noisy, which in turn will prevent the detection of action potentials. The most effective way to reduce noise in the data is first to prevent or reduce it, e.g., by changing the electrical setup of the recording room. The hospital room used for the intracranial investigation was part of a building built in the 1960s. EMC-ZM (Electromagnetic Compatibility - Zero Method, Soleil et al., 1992, http://danielsoleil.com) measurements were performed and uncovered that the EEG recording room was full of noisy sources from electrical power distribution. Therefore, in 2014 a specific electrical installation, called "Low-Noise", was performed to approach 0 Vp and 0 Ap, i.e. no electrical noise (Fig. 5). This installation involved the followings:

- the creation of an isolated ground plane of reference made of a copper sheet of 0.3 mm thickness covering the floor of the room and itself protected by an antistatic coating;
- the electric power of the building, before arriving to the room, was isolated with a low capacitor coupling transformer whose output was a two-phase 230V rms, with its mid-point connected to the reference plane;
- all subsequent distribution of the current to the room outlets was filtered by low HF-losses capacitors until outlets of the room to obtain the Low-Noise. The two-phase and filtered power supply remove the electric radiation of the main cords;
- all outlet grounds of the room were shortetly referenced to the ground plane. All metallic objects (bed, table, chair, etc…) in the room were connected to the ground plane of reference when possible.

Noise measurements were done with a "Clean Energy Meter" (Hager, HagerGroup, Blieskastel, Germany) before and after the improvements. This measuring tool is a voltmeter that measures peak unreversed voltages after elimination of 50 Hz power supply with a high pass filter. Switched to an Ampere meter, it can be used to check that there is no current, even at 50 Hz, near the conductors connected to the isolated ground plane.

All the works were in accordance with NFC 15-100 and NFC 15-211 and the measurements were in line with IEC 61 000 -6 and -16.

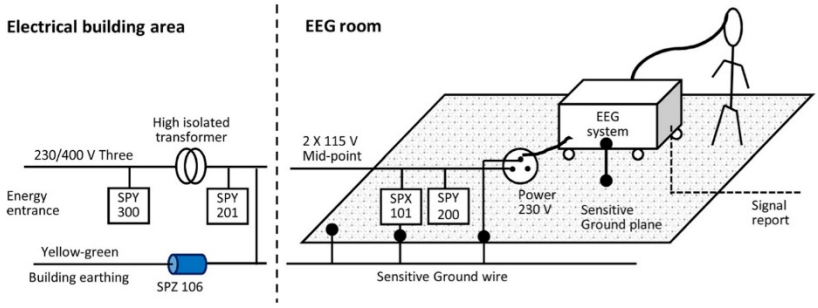

Fig. 5. Synoptic electrical diagram of the electrical installation in the patient's room. SPX 101: Hardening filter 2 phases. SPY 300: Capacitor bloc 3 phases 4.7 µF. SPY 200: Capacitor bloc 2 phases 4.7 µF. SPY 201: Capacitor bloc 2 phases 15 µF. SPZ 106: Magnetical bloc, hole 10 mm - Clean Energy HAGER.

Table 4
Description of main time periods of recording.

Time Period	Date	Recording system for macro-electrodes	Recording system for micro-electrodes	Electrical shielding of the room	Electrode model	Number of patients
1	Oct. 2010 - Jun. 2012	Neuralynx	Micromed	no	1	11
2	Nov. 2012 - Jul. 2014	Neuralynx + Micromed	Neuralynx + Micromed	no	1 or 2	14
3	Nov. 2014 - Oct. 2016	Neuralynx + Micromed	Neuralynx + Micromed	yes	1 or 2	14
4	Feb. 2017 - Oct. 2018	Neuralynx + Micromed	Neuralynx + Micromed	yes	3	11
5	Nov. 2018 - Sept. 2019	Neuralynx	Neuralynx	yes	3	6

2.7.2. Signal quality measures and statistics

In order to estimate the SNR of the microelectrode recordings, the root mean square (RMS) was calculated on 10 minutes of signal filtered between 300 and 3000 Hz, from 15 periods blindly selected without a priori on data quality but equally distributed in time, over the whole recording of each patient. No selection regarding the signal quality was done in order to keep an objective overview of the continuous recording and the possible quality variation in time.

According to the literature and our observations, low levels of noise increase the possibility to detect action potentials in the signal and the accuracy of the spike sorting (Buccino et al., 2020; Chaure et al., 2018; Wild et al., 2012). To test whether a decrease in noise was associated with an increase in action potential recordings, the presence of MUA was visually checked on filtered signals using MUSE software (300-300 Hz) and reported. The following measures were realized for each bundle: the number of wires recording at least once MUA along the 15 periods, referred as overall MUA; the number of wires recording MUA the first day of recording (day 0), after 1 week (day 6) and after 2 weeks (day 13), referred as time-dependent MUA. The first day of recording started the day following the implantation.

According to the improvement steps (new recording system, electrical shielding of the room, reinforced electrode model) of our recording procedure, five major time periods could be identified from 2010 to 2020 and are summarized in Table 4. Variation of RMS values and MUA quantification measured at the different time periods were evaluated using Generalized Linear Mixed Models (GLMMs).

RMS: For the RMS, a GLMM with identity link and normal distribution was used, with RMS values for each of the 15 distributed periods of each patient's wire as the dependent variable, the time period and the number of days after the first recording day as the fixed effects and the patients' ID with the wire's ID nested as the random intercept effects. In order to compare the proportion of extreme RMS values in each time period, they were identified as RMS values > Q3 + 1.5xIQR, with Q3 and IQR calculated on all RMS values, and a pairwise Fisher's exact test was performed between time periods and extreme RMS values identification. As RMS values were right-skewed, they were log10 transformed.

MUA: For the MUA, to test whether the overall MUA differed between time periods or was related to RMS values, two GLMMs with log link and Poisson distribution were performed, with the overall MUA quantification as the dependent variable, the time periods or the median RMS of each bundle as the fixed effects and the patients' ID as the random intercept effects. Lastly to test whether the number of wires recording MUA differed between time periods and days of recording, a GLMM with log link and Poisson distribution was performed, with the time-dependent MUA quantification as the dependent variable, the time periods and the day of recording as the fixed effects and the patients' ID as the random intercept effects. To test whether there was a difference between the time periods according to the day of recording, the interaction between the time periods and the day of recording was added as a fixed effect in the previous model.

For RMS and MUA, type II Wald chi-square tests were used to test main effects and interactions and post hoc pairwise comparisons were carried out when appropriate. Mean difference estimates (MDE) ± standard errors (SE) and mean ratio estimates (MRE) ± SE were reported for post-hoc comparisons of RMS and MUA respectively. For all analysis and figures, RMS values from the microwires used as reference were excluded.

The signal measures were calculated with Matlab (MATLAB. (2019) *version* 9.7.0 *(R2019b)*. Natick, Massachusetts: The MathWorks Inc.) and statistical analyses and figures were achieved using R 4.1.2 (R Foundation for Statistical Computing, Vienna, Austria. URL "https://www.R-project.org".)) and lme4 package (v1.1-27.1, Bates et al., 2014, p. 4) for GLMM fit, emmeans package (v1.7.2, Lenth, 2020) for post-hoc comparisons and model representation, optimx package (v2021.1.12, Nash, 2011) for GLMM convergence, and RVAideMemoire package (v0.9.81, Hervé) for pairwise Fisher's exact test .

2.8. LFP-MUA/SUA pipeline analysis of epileptic events

To illustrate the type of analysis that can be performed on epileptic events, this section presents a procedure developed in our lab to investigate the firing behavior of neurons during interictal epileptic spikes (IEDs), which are brief paroxysmal electrographic discharges that can be observed visually on EEG. Microelectrode wires were first selected, based on whether they showed MUA and IEDs. Artifacts and IEDs were annotated manually on the basis of visual observation of the microelectrodes. All annotations were done with MUSE, a software developed in-house to allow the visualization of both macro and micro electrodes. Spike sorting was then done using Spyking Circus (Yger et al., 2018), according to the procedure outlined in detail in their reference docu-

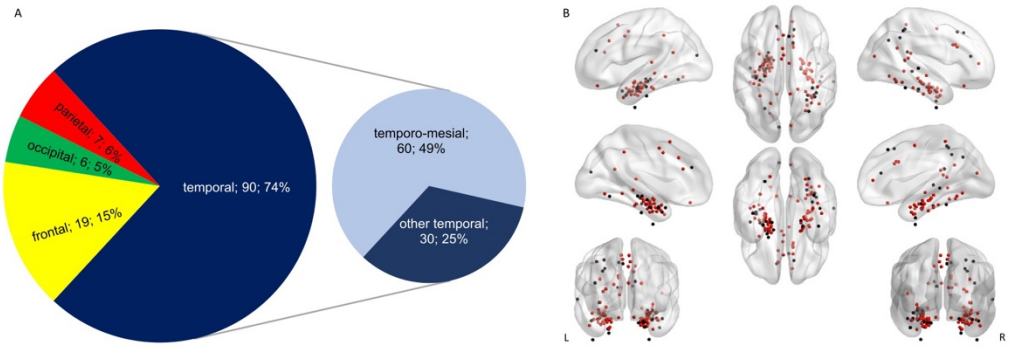

Fig. 6. Microelectrode localization. A. Distribution diagram of the electrode localizations with a detailed focus for the temporal lobe. The temporo-mesial region includes: hippocampal formation, amygdala, parahippocampus. The first number near the brain region's name indicates the number of microelectrodes in the corresponding region, the 2d number indicates the percentage of microelectrodes. **B.** 3D MNI normalized localizations of the microelectrodes. Each dot is a microelectrode bundle. Red dots correspond to microelectrode bundles that recorded MUA and black dots correspond to microelectrode bundles that did not record MUA. The 3D figure was realized using BrainNet viewer (www.nitrc.org). *Note that some dots appear outside of the brain because of the imprecision of the MNI normalization, especially for electrodes at the border of the temporal lobes where the MRI quality is not as good as for the rest of the brain.*

mentation (https://spyking-circus.readthedocs.io/en/latest/) and reference article (Yger et al., 2018) . In short, Spiking Circus uses a combination of density-based clustering and template matching algorithms to automatically cluster the detected action potentials into putative single units. Data is temporally whitened, and action potentials (APs) are automatically detected at 6 (or higher) median absolute deviations (MAD) of high-pass filtered (> 300 Hz) signal. APs that occurred during annotated artifacted periods were ignored, their inclusion would affect the spike sorting accuracy. Clusters that were not stable across the recording were discarded from further analysis. Clusters were further evaluated whether they reflected putative single-unit activity (SUA) or multi-unit activity (MUA) based on their inter-spike-interval (ISI), the percentage of refractory period violation, the consistency of their firing rate and amplitude over time, and their waveform morphology. IEDs were automatically aligned according to their cross-correlation. Average LFPs and spike times were then time-locked to the IEDs and plotted on the same time-axis. The analyses pipeline was implemented using custom MATLAB scripts (https://github.com/stephenwhitmarsh/EpiCode), and used FieldTrip (Oostenveld et al., 2011), a MATLAB (The Mathworks Inc., Natick, Massachusetts) toolbox for MEEG and spike analyses.

3. Results

3.1. Database description

From October 2010 to September 2020, 56 patients (31 women; age: mean = 33 years, range:18-60; duration of epilepsy: mean = 16 years, range:4-40) were implanted with a total of 122 microelectrode bundles (range: 1-4 per patient). Electrodes were mostly localized in the temporal lobe (n=90; 74%), with a predominance in the mesial temporal cortex (n=60), including hippocampal formation (n=31), amygdala (n=14), parahippocampus (n=6). Microelectrodes were also placed within frontal (n=19, 15%), parietal (n=7, 6%) and occipital (n=6, 5%) lobes (Fig. 6A). Most microelectrode bundles were in gray matter or lesioned tissue (n=99; 81%), but some spread in the white matter (n=4; 3%) or in extraparenchymal regions (n=13; 11%). In the temporal lobe, the proportion of microelectrodes in extraparenchymal regions was 6/22 for amygdala, 2/44 for hippocampal formation, and 3/9 for temporo-basal regions.

Signal from microelectrodes was recorded from 55 patients and 119 microbundles; one patient at TimePeriod 1 could not be recorded for technical reasons. For the first 10 patients from TimePeriod 1, microelectrodes were recorded a few hours (1-4 h) per day, for 10 days on average, with a total duration of 14.5 h on average. For the next 45 patients, microelectrodes were recorded continuously for an average of 16.2 days (min = 5 days, max = 27 days). Twenty-seven among the 122 microelectrodes were located in the SOZ (Fig. 6B).

During TimePeriod 1, seizures could be recorded with microelectrodes for 50% of the patients with a total of 33 seizures (5/10 patients, with 1 to 17 seizures/patient). Microelectrodes were in the SOZ for 2 patients. During TimePeriod 2 to 5, seizures could be recorded with microelectrodes for 91% of the patients (41/45 patients, with 2 to > 50 seizures per patient). Microelectrodes were in the SOZ for 16 patients.

3.2. Signal quality measures

3.2.1. Electrical noise in the room

Room measurements before and after the new electrical installation revealed that the noise level in the patient's room decreased from values around 8V High Frequency (HF) peak-to-peak to less than 0.1 V peak-to-peak, corresponding to a 35 dB of reduction .

3.2.2. Data SNR

The LMM investigating RMS differences over recording time periods revealed a significant effect of the time period (Chi^2 = 99.29, p<0.001, Fig. 7, Table 5 for descriptive statistics). Compared to TimePeriod 2, RMS values were significantly lower during TimePeriod 1 (MDE ± SE = -0.50±0.06, p<0.001), when micro and macroelectrodes were recorded separately, and during TimePeriod 3 (MDE±SE = -0.33±0.06, p<0.001), TimePeriod 4 (MDE±SE = -0.47±0.06, p<0.001) and TimePeriod 5 (MDE±SE = -0.46±0.07, p<0.001) after the room has been electrically isolated. There was also a significant difference between TimePeriod 1 and 3, with lower values during TimePeriod 1 (MDE±SE = -0.17±0.06, p=0.037), but no significant difference between the other time periods (p>0.05). The difference between TimePeriod 3 and 4 was not significant but the median RMS value was higher during TimePeriod 3. The number of outliers differed between all time periods (pairwise Fisher's exact test, all p<0.001, Table 5 for descriptive statistics) apart between Time Period 4 and Time Period 5. The period with less outliers was Time Period 1, followed by Time Period 4 and 5, Time Period 3 and Time Period 2.

Moreover the LMM revealed a slight but significant increase of the RMS over days of recordings (estimate±SE = 5.53e-03±6.23e-04, Chi^2 = 78.77, p<0.001, Supp. Fig. 4). Individual data are presented in

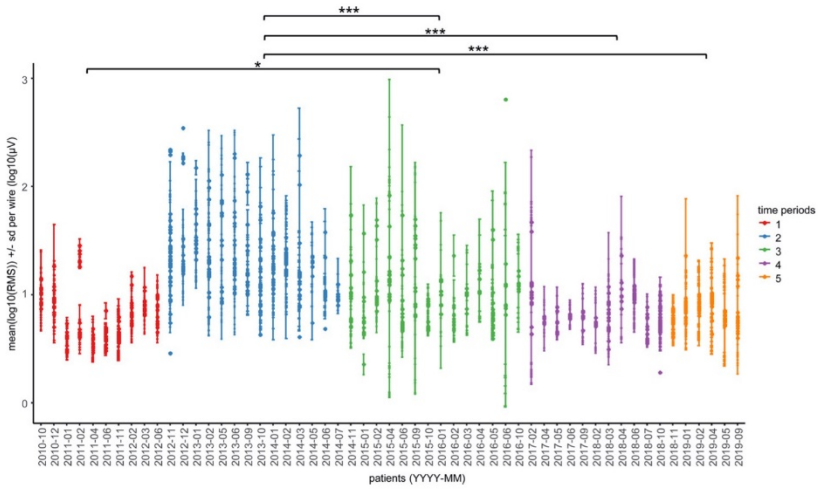

Fig. 7. RMS per wire and day for each patient. Each dot represents the mean of RMS values measured over days for each wire. Note that the y axis is expressed on a log10 scale, values of 1, 2 and 3 corresponding respectively to 10µV, 100µV and 1000µV. Dots are plotted according to the log10(RMS) mean value and the patient ID expressed in year-month (YYYY-MM). Bars represent the standard deviation of the log10(RMS) values of each wire. The color code distinguishes the 5 time periods (red: TimePeriod 1, blue: TimePeriod 2, green: TimePeriod 3, purple: TimePeriod 4, orange: TimePeriod 5). The patient's room was electrically cleaned between TimePeriod 2 and TimePeriod 3. The electrode model was changed to the reinforced model 3 between Time Period 3 and Time Period 4. Significant differences between time periods are indicated with stars (*: 0.05 > p < 0.01; **: 0.01 > p < 0.001; ***: p < 0.001).

Table 5
Descriptive statistics of each time period.

Time Period	RMS (µV)						MUA (nb wires/bundle)			
	N total	Outliers		Median	Q1	Q3	N total	Median	Q1	Q3
		N	%							
1	1527	3	0.20	6.30	4.48	9.15	19	2	0	4
2	3497	412	11.78	16.96	9.80	36.21	34	0.5	0	2
3	2718	101	3.72	6.45	4.73	11.72	26	3	0.25	4.75
4	2336	33	1.41	5.87	4.73	8.10	20	3	1	6
5	1654	34	2.05	5.82	4.53	8.26	15	4	1.5	5.5

Supp. Fig. 5. A GLMM with the interaction between recording day and the patient ID as the fixed effects precised significant positive correlation between RMS and days of recording for 25/55 patients, distributed in all time periods. The correlation was not significant for 19/55 patients and significantly negative for 11/55 patients.

3.2.3. MUA

For 70% of recorded microelectrode bundles (82/119), at least 1 wire from the microelectrode bundle showed MUA, with an average of 3 wires per bundle. The proportion of bundles recording MUA differed between time periods and reached 70.1 %, 50 %, 73.1 %, 85 % and 80 % for TimePeriod 1 to 5 respectively.

As can be observed on Fig. 8A, the relation between the RMS values and the number of wires recording MUA at least once was not linear. The maximum number of wires recording MUA was observed for RMS value around 7.4 µV. Above 7.4 µV the number of wires recording MUA decreased when RMS values increased, while below 7.4 µV the relation was inverted. A first GLMM focusing on RMS values > 7.4µV and testing the relation between the number of wires recording MUA and the RMS values, confirmed a significant negative impact of high RMS values on the number of wires per bundle recording MUA (estimate±SE = -0.07±0.03, Chi^2 = 47, p=0.034). A second GLMM focusing on RMS values < 7.4 and testing the relation between the number of wires recording MUA and the RMS values, confirmed a positive correlation (estimate±S = 0.47±0.08, Chi^2 = 34.27, p<0.001).

The GLMM testing whether overall MUA differed between time periods revealed a significant time period effect (Chi^2 = 16.52, p=0.002, Fig. 8B, Table 5 for descriptive statistics). There were significantly less wires per bundle recording MUA during TimePeriod 2 than during TimePeriod 3 (MRE)±SE = 0.42±0.12, p=0.016), TimePeriod 4 (MRE± SE = 0.34±0.11, p=0.007) and TimePeriod 5 (MRE± SE = 0.33±0.11, p=0.006).

The GLMM testing the time-dependent MUA revealed a significant effect of the time period (Chi2 = 17.96, p=0.001) and of the day of MUA measure (Chi2 = 57.59, p<0.001). Significantly less wires per bundle recorded MUA during TimePeriod 2 compared to TimePeriod 4 (MRE±SE = -1.53±0.40, p=0.001) and 5 (MRE±SE = -1.48±0.44, p=0.007). The number of wires recording MUA significantly differed between all days of recordings (day0 vs. day6: (MRE±SE = 1.62±0.19, p=0.001, day6 vs. day13: (MRE±SE = 1.97±0.33, p=0.002, day0 vs. days13: (MRE±SE = 3.19±0.51, p<0.001, Fig. 8C). The introduction of the interaction between the time periods and the day of MUA measure as fixed effects in the model did not reveal any significant interaction (Fig. 8C).

Interestingly, for 52 bundles, the total number of wires recording MUA at least once during the whole recording period, was higher than the number of wires recording MUA the first day of recording, reflecting the fluctuation from day to day of the presence of MUA on wires (see Supp. Fig. 3).

No MUA were recorded in 37 microbundles. For the majority of cases, this could be attributed to a localization outside gray matter, i.e. extraparenchymal (12 bundles), white matter (3 bundles), or a failure in the extrusion from the macroelectrode (4 bundles were not visible on the CT scan). For 8 bundles, the mean RMS was high (> 10µV). Finally, for 9 bundles there was no clear reason for the lack of MUA, as they were in the gray matter with RMS values < 5 µV.

As one of our objectives was to record as many seizures as possible with MUA, we looked at the number of patients for whom it was possible to record seizures with MUA. For 33 patients, we could record at least 1 seizure (range 1 to 10) with MUA on at least one microelectrode signal. Those 33 patients correspond to 40% of patients during TimePeriod 1,

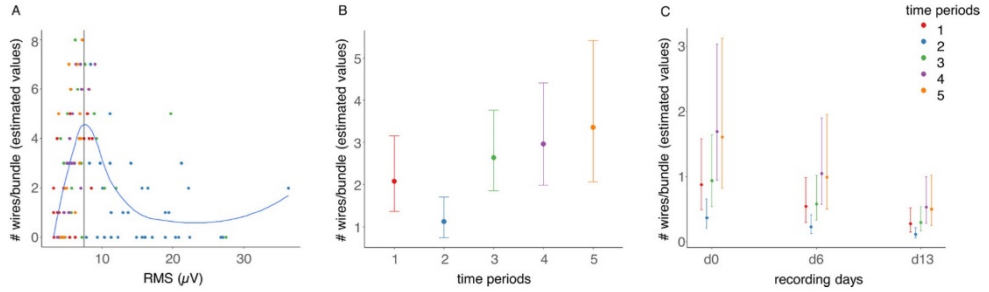

Fig. 8. Number of wires per bundle recording MUA. A. Representation of the number of wires per bundle recording at least once MUA during the whole recording, in relation to the median of RMS values measured on all wires of the bundle. The blue line fits the data with the LOESS method which uses local averaging. The vertical black line is plotted at the peak of the fitting line. **B.** Representation of the estimated marginal means of the number of wires per bundle recording at least once MUA during the whole recording for each time period given by the GLMM. Bars represent low and high 95% confidence intervals. **C.** Representation of the estimated marginal means of the number of wires per bundle recording at least once MUA values for each time period and day of recording (0-6-13) given by the GLMM. Bars represent low and high 95% confidence intervals. For all plots each dot represents a bundle and the color code distinguishes the 5 time periods (red: TimePeriod 1, blue: TimePeriod 2, green: TimePeriod 3, purple: TimePeriod 4, orange: TimePeriod 5). Significant differences between time periods are indicated with stars (*: $0.05 > p < 0.01$; **: $0.01 > p < 0.001$; ***: $p < 0.001$).

but with few seizures per patient, 28% of patients during TimePeriod 2, and 76% of patients during TimePeriod 3 to 5. Among those 33 patients, 12 had the microelectrodes recording MUA localized in the SOZ.

3.3. Example of analysis pipeline for long-term continuous recording of epileptic activity

The continuous and long-term recordings described here allows for manual or automatic annotation of epileptic events during active and passive wake state, as well as during sleep. Fig. 9 gives an example of the analysis pipeline described in the method (Section 2.8). Epileptic spikes were visible on both macro- and microelectrodes (Fig. 9A & B). The high-passed signal of the microelectrode showed action potentials, i.e MUA (Fig. 9C). Spike-sorting analysis isolated two different single neurons, i.e SUA (red and blue), with different morphologies (Fig. 9F) and firing properties (as noted, by the histogram of their inter-spike intervals; Fig. 9G). The firing rates of both neurons correlated with the LFP of the IEDs (Fig. 9D & E).

4. Discussion

During the last 10 years, we collected a database of 119 microelectrode recordings in patients with epilepsy. Most microelectrodes were implanted in mesial temporal regions, consistent with the predominance of temporal epilepsies (Blumcke et al., 2017). Our post-implantation imaging analysis also revealed that most of the microelectrodes were in gray matter as expected, but some were in white matter or meninges. This mistargetings can be related to our implantation strategy: the deepest macrocontact is placed in the mesial cortex and microwires must extend from there toward the inner part of the brain. During the trajectory planning, the estimated length for the microwires always comprises a margin of error of some mm, in case of potential deviation of the macroelectrode trajectory during the implantation. However, more deviation can occur and prevent the microelectrode from reaching the targeted localization. We observed more mistargetings of gray matter in some cerebral regions, such as amygdala, compared to other regions such as hippocampus, probably because the volume of gray matter beyond the tip of the electrode is smaller in amygdala. Nevertheless, the addition of microelectrodes did not increase the risk of hemorrhages and infectious complications (Mathon et al., 2015).

The analysis of the noise level and the presence of MUA on our microelectrode recordings showed a progressive improvement related to several technical changes. The analyses were performed on blindly selected files equally distributed along the whole recording, in order to have the most objective overview of noise levels. The electrical insulation of the patient's room came out as a major effect, and the use of the reinforced micro-bundle had smaller but not negligible consequences. Most RMS values of the filtered microelectrode signal from the last time periods (i.e., our current recording configuration), were relatively low. For Time Period 4 and 5, more than 85% and nearly 70 % of the measures were < 7.4 μV during the 1st and 2d week respectively, while they were below 10 % for Time Period 2. The number of wires per bundle recording MUA significantly increased over time periods—from 2010 to 2020. The quality improvement of the data was efficient from the first days of the recording and allowed to keep a better quality (lower RMS and more wires with MUA) until the end of the recording. The reduction of RMS values in our data increased our possibilities to record MUA and therefore the probability to better isolate SUA through spike sorting (Buccino et al., 2020; Chaure et al., 2018; Wild et al., 2012). This relation between MUA and SUA was indeed observed in several analyses conducted on our data. The more MUA were present in the recordings, the more SUA could be isolated. According to Fig. 8A, it seems that reaching a RMS < 10 μV is important to obtain a SNR high enough to catch action potentials. The fact that we observed less MUA for RMS below 5 μV can probably be explained by a very low electrical and physiological noise, i.e. the lack of MUA on the signal contributes to the RMS reduction of the filtered signal. Interestingly, during our first microelectrodes recordings (TimePeriod 1), when microelectrodes were recorded separately from the macroelectrodes and for only a couple of hours per day, we obtained lower RMS, more MUA than during TimePeriod 2 and less outliers than during all other time periods. This might be explained by the presence of researchers during the whole recording, systematically trying to reduce noise, i.e. by shielding all cables and starting to record only when the noise level was low. The transition to a single amplifier for macro and microelectrodes (TimePeriod 2) was first associated with a decrease of signal quality. However the decrease of RMS values during TimePeriod 2 reveals the impact of the improvements realized at all steps from implantation to recordings. The significant difference in RMS values between TimePeriod 2 and TimePeriod 3 highlights the importance of the electrical insulation of the patient room, whose financial cost was balanced by the major noise reduction. However, modifying the electrical installation is not always possible and it will also not prevent some electrical noise sources. Shielding cables to prevent surrounding electromagnetic interference and avoiding ground loops is essential (see Misra et al., 2014, for details). We could observe 50/60Hz noise reduction in the microelectrodes by covering their poorly shielded tail with a conductive tissue grounded to the patient (Stretch conductive fabric, Less EMF Inc., Latham NY 12110, USA). Furthermore, like

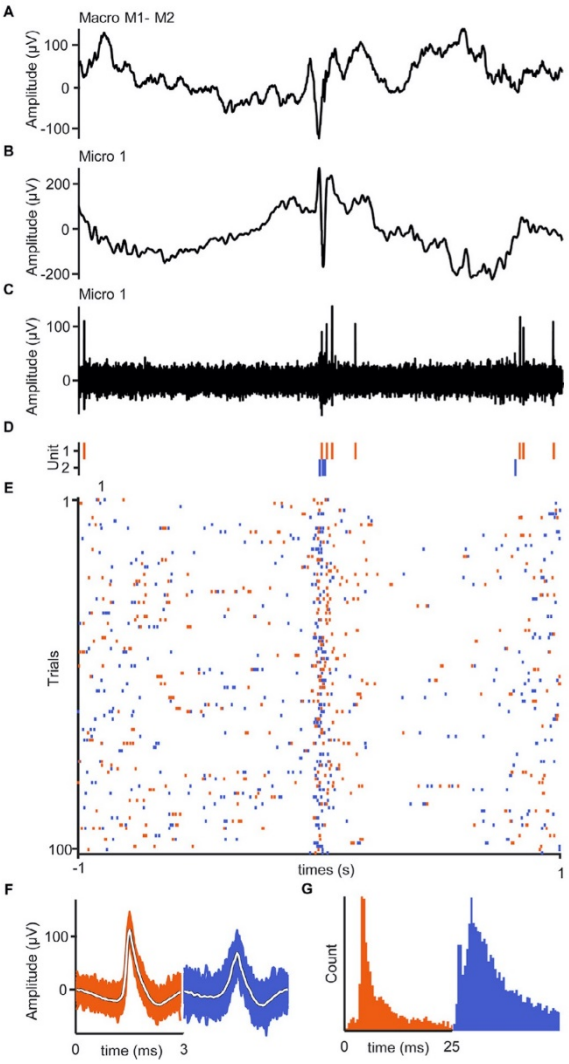

Fig. 9. Example of single units time-locked to the LFP of IEDs. A. IED recorded by a macro contact. The macroelectrode iEEG signal is shown on a bipolar montage (M1-M2). **B.** Same IED as in A recorded by a micro wire (Micro 1) at the tip of the macroelectrode represented in A, the signal is low-pass filtered at 50 Hz. **C.** Same signal as B but high-pass filtered at 500Hz. The filtered signal shows action potentials (multi-units activity). **D.** Spike sorting of Micro 1 signal resulted in a separation of action potentials into two different putative single units (red and blue color code). Red and blue lines represent the occurence in time of action potentials of each unit. **E.** Raster plot of 100 IEDs recorded by Micro 1. Action potential times of each unit (red and blue) were time-locked to the IEDs, showing clear synchronization. **F.** Action potential waveforms of each unit: 1000 random time courses with superimposed average. **G.** Inter-spike-interval histogram of each unit.

for all electrophysiological recordings, any electrical device plugged in an outlet that touches the patient, the bed/chair where the patient is sitting, or the connectors and tether cables, will introduce 50/60Hz noise and should be avoided. Therefore, if the patient needs to use a computer or his phone, they should preferably run on battery. However, even on battery, a laptop can be a source of noise for the microelectrodes when the patient touches the keyboard. One solution, especially for cognitive tasks where responses are mandatory, is to use optical cables to connect to button response boxes. Wireless keyboards or mouses might also work, but should first be tested regarding the responses delays and jitters. The patient's bed, if it is electrically motorized, can also be a source of noise. If it is the case, unplugging or using a manual bed should be considered. We also experienced that keeping a loose scalp electrode connected to the Neuralynx amplifier was another source of slow wave artifacts for all electrodes connected to the same input board of 32 channels. Hanging scalp electrodes have the impedance of the headbox or system input and behave like an antenna in the air that will pick up the noise in the environment.

The reference is also important for reducing noise levels. Even if references can always be changed offline, the use of the best reference during acquisition enhances the chances to have a good signal. For example, if the reference is damaged and sensitive to movements/noise and is likely to saturate, then all signals will saturate and it will not be possible to gain signal by offline re-referencing. A good reference also contributes to on-line estimates of the signal quality, so that the recording setup can be adapted when necessary. Because we often observed, like Misra et al 2014, an increase in noise level with the un-insulated wire, we mostly preferred a normal microwire for model 2 and 3, despite the impact on the LFP. This is not the choice of all centers recording with microelectrodes, probably because of the possibility to re-reference off-line prior spike-sorting if needed. Several re-referencing techniques can be used like using a local reference or the average of all wires. In addition to those classical techniques, Jurczynski and colleagues (Jurczynski et al., 2021) also proposed an adaptive version of the zero-reference method. The impact of the un-insulated wire that differs from one patient to another would need further investigation, as well as the impact on unit recordings and spike sorting.

Any damage of the microwire will increase not only the impedance of the electrode (Misra et al., 2014) and 50/60Hz noise, but also artifacts due to movement. Damage can happen at any time between the surgery and the end of recording, especially when the electrode was manipulated and could explain a decrease in data quality. Therefore, we established a procedure from the surgery to the end of recording (Tables 1 & 2), where at each step, electrodes are manipulated carefully: by the neurosurgeons when they cut the wires and insert them into the macroelectrode, by the nurses when they wrap the head with the bandage, and by the technicians when they connect the tails to the connectors. Interestingly, we observed less extreme RMS values (less outliers), probably related to less damage of wires, after switching to the more resistant model of the Behnke-Fried microelectrode. Noisy channels were in general present from the beginning of the recording, revealing a degradation of the electrode more likely to occur between the surgery and the beginning of the recording than during the recording. The reinforcement of the electrode seems therefore to decrease the risk of breaking and improves the quality of the recordings during the whole acquisition.

We also observed that the RMS values slightly increased over time and that this was associated with less MUA recordings. The increase in RMS might be due to an increase in the microwires' impedance, as observed on another electrode model (Despouy et al., 2020). The loss of MUA could also be due to the inflammatory reaction around the microelectrodes, which insertion in the neural tissue can cause gliosis leading to the loss of sensitivity of the recording (Babb et al., 1973; Polikov et al., 2005). Despite the reduced number of wires recording MUA at the end of the recording, it often happened that MUA appeared on new wires or reappeared after a 'silent' interval. This fluctuation would need further exploration. However we hypothesize that it might be due to a slight movement of the electrode or the brain, as previously described (Babb et al., 1973), allowing the wire to record from other neurons than the previous ones. Alternatively, it might be due to changes in impedance due to movements of the electrode tail.

Improved quality of continuous and long-term recording from microelectrodes, increases the possibility to record seizures with micro-

Table 6
Summary of main guidelines.

Main guidelines
Very careful manipulation of the microelectrodes at all steps (Figs. 2 & 3 /Tables 1 & 2)
Prefer the most robust Ad-Tech microelectrode if you use Ad-Tech electrodes (Section 2.5.1)
If possible, the recording room should be shielded or have a clean electrical installation (Section 2.7.1)
Shield as much as possible (cables, electrode tails; Section 4.)
Avoid ground loops (Section 4.)
No electrical device plugged in an outlet should touch directly or indirectly the patient (Section 4.)
If possible, reduce to a single amplifier. If not, both amplifier should be connected to the same outlet and grounded to the same patient's ground (Section 2.5.2)
The patient should never be connected to the electrical ground for safety reasons
Do not connect scalp electrodes to Neuralynx if they are not pasted to the patient' skin (Section 4.)
Prepare an appropriate IT infrastructure in case of long-term recording of microelectrodes, to collect the high amount of data generated

electrodes, which is a crucial requirement to study ictogenesis and the cellular mechanisms related to seizures emergence. Our data shows that it was indeed necessary to record continuously from macro and microelectrode, in order to capture seizures whose occurrence is unpredictable. A first analysis of 38 seizures from 9 patients, recorded by microelectrodes within the SOZ showed that neuronal spiking activity at seizure initiation was highly heterogeneous and not hypersynchronous (Lambrecq et al., 2017). However, recording from the seizure-onset-zone remains a challenge, which by definition, is unknown at the beginning of the intracranial investigation. In addition, Behnke-Fried micro-macroelectrodes can only record deep structures like the mesial temporal structures, but are not tailored for sampling neocortical structures. On the contrary, cortical multielectrode arrays (Utah arrays) provide coverage of neocortical structures, but provoke cortical damage and can only be used on structures that will be surgically removed. Hybrid electrode models with microwires protruding between macrocontacts, e.g. DIXI tetrodes (MICRODEEP® Micro-Macro Depth Electrode), are a good way to record units in more superficial cortical areas (Despouy et al., 2020, 2019).

The number of wires per bundle that recorded MUA remained quite low, around 3 out of 8 (range 0-8), and did not seem to be only a SNR issue as very low RMS with no MUA could be observed. The absence of MUA might also be related to the distance between the wires and active neurons. One solution would be to adapt the length of the microwires, once implanted in the brain in order to try to get closer to neurons if no MUA is recorded. As far as we know, DIXI tetrodes are the only electrode model proposing such a technology that allows to pull out the wires up to 2 mm. Beside, another interesting feature of DIXI microelectrodes is their *tetrode* configuration rather than single wires, which should allow better separation of single units based on the spatial distribution of action-potential recordings. Most unsupervised spike sorting software can use the tetrode configuration to separate detected action potentials in different units (Buccino et al., 2020).

Keeping 3 weeks of continuous recording, including microelectrodes at high sampling rate, generates a large amount of data to be stored, backuped, analyzed and shared. This is only possible with an efficient IT infrastructure, allowing high storage capacity but also fast and secured data access. As an example, we generate around 2 TB of data per patient. In addition to the storage capacity, there is also the question of data organization, including all the metadata related to the patient and the recordings. Each patient investigation is different in terms of electrode localisation, SOZ, medication and all those metada are necessary to analyze the electrophysiological data, to study epilepsy or cognitive processings. A structured database becomes essential when the number of patients increases. We therefore developed a secure survey and database that can include clinical information, electrode localization and technical settings. Another possibility, which is not mutually exclusive, is to adopt the BIDS dataformat (Holdgraf et al., 2019), that is standardized, adapted for data sharing and gives the possibility to add metadata for each recording. Finally, a good organization combined to a suitable analysis pipeline (see Section 2.8 and Fig. 9), a powerful spike sorting tool tailored for long-term data (Buccino et al., 2020; Chaure et al., 2018; Niediek et al., 2016; Rey et al., 2015; Wild et al., 2012, Yger et al. 2018) and high computational capabilities are essential keys to achieve analyses of large amounts of collected data.

5. Conclusion and perspectives

We showed that it is feasible to record high quality, long-term and continuous microelectrode signals *in vivo* in patients with epilepsy. Our procedure allows the recording of both LFP and single neurons activity during physiological (as wakefulness and sleep) and pathological (as interictal epileptiform discharges and seizures) periods. We shared our experience to improve the quality of these recordings and we proposed several technical guidelines (Tables 1, 2 and 6), that are complementary to other methodological papers on microelectrodes recordings (Minxha et al., 2018; Misra et al., 2014 for Behnke-Fried electrodes; Despouy et al., 2020 for Dixi macro-microelectrodes). We described in detail head wrappings after the surgery that are crucial steps in the electrode manipulation, and quantify noise level depending on acquisition setup and environnement.

Studying ictogenesis in focal epilepsies using intracerebral microelectrodes is faced with a great number of specific challenges: (i) to record in the actual SOZ, (ii) to record unitary activity during seizures, (iii) to follow the same neuron over time during different epileptic events, and (iv) to be faced to great interindividual variability. In the future, the increased availability of microelectrode technology and shared recording-protocols will increase the pool of human microelectrode data among neuroscientists and help overcome these difficulties. Progress will likely come from additional technical advancements, like the development of a mobile microelectrodes which could be moved further in or out when unitary activities are lost, or the development of non-penetrating cortical microelectrode arrays (Khodagholy et al., 2015). Microelectrodes show great potential in the field of epilepsy (Chari et al., 2020). In the coming decades, we expect that they will increasingly contribute to deciphering the cellular mechanisms of seizure generation and to establish new markers of the epileptogenic focus.

CRediT author statement

Conceptualization: Katia Lehongre, Virginie Lambrecq, Vincent Navarro

Methodology: Katia Lehongre, Virginie Lambrecq, Stephen Whitmarsh, Vincent Navarro

Software: Katia Lehongre, Stephen Whitmarsh, Valerio Frazzini, Sara Fernandez-Vidal, Jean-Didier Lemarechal, Dominique Hasboun,

Formal analysis: Katia Lehongre, Virginie Lambrecq, Stephen Whitmarsh, Valerio Frazzini, Marion Houot

Resources: Katia Lehongre, Virginie Lambrecq, Valerio Frazzini, Louis Cousyn, Daniel Soleil, Bertrand Mathon, Stéphane Clemenceau, Dominique Hasboun, Claude Adam, Vincent Navarro

Writing - original draft: Katia Lehongre, Virginie Lambrecq, Stephen Whitmarsh, Valerio Frazzini, Louis Cousyn, Daniel Soleil, Sara Fernandez-Vidal, Bertrand Mathon, Jean-Didier Lemarechal, Stéphane Clemenceau, Dominique Hasboun, Claude Adam, Vincent Navarro

Writing - review & editing: Katia Lehongre, Virginie Lambrecq, Stephen Whitmarsh, Valerio Frazzini, Louis Cousyn, Daniel Soleil, Sara Fernandez-Vidal, Bertrand Mathon, Marion Houot, Jean-Didier Lemarechal, Dominique Hasboun, Claude Adam, Vincent Navarro

Supervision & Funding acquisition: Vincent Navarro

Declaration of Competing Interest

D. Soleil is the manager of the CEMS society. The other authors have no conflict of interest in relation with this work.

Acknowledgments

This work received support from the “Investissements d’avenir” program (ANR-10-IAIHU-06), and from the Fondation Assistance Publique Hôpitaux de Paris (EPIRES – Marie Laure PLV Merchandising). We thank all the nurses and technicians for their involvement in the microelectrode recordings. We thank Charlotte Lebaz, Pauline Marijon, Corinne Lascaut, Ghislaine Therme, Nadège Manelle and Sabine Dedenis for their kind participation in the realization of the pictures for the Figs. 2 and 3.

Supplementary materials

Supplementary material associated with this article can be found, in the online version, at doi:10.1016/j.neuroimage.2022.119116.

References

Alvarado-Rojas, C., Lehongre, K., Bagdasaryan, J., Bragin, A., Staba, R., Engel, J., Navarro, V., Le Van Quyen, M., 2013. Single-unit activities during epileptic discharges in the human hippocampal formation. Front. Comput. Neurosci. 7, 140. doi:10.3389/fncom.2013.00140.

Axelrod, V., Rozier, C., Malkinson, T.S., Lehongre, K., Adam, C., Lambrecq, V., Navarro, V., Naccache, L., 2019. Face-selective neurons in the vicinity of the human fusiform face area. Neurology 92, 197–198. doi:10.1212/WNL.0000000000006806.

Babb, T.L., Carr, E., Crandall, P.H., 1973. Analysis of extracellular firing patterns of deep temporal lobe structures in man. Electroencephalogr. Clin. Neurophysiol. 34, 247–257. doi:10.1016/0013-4694(73)90252-6.

Babb, T.L., Crandall, P.H., 1976. Epileptogenesis of human limbic neurons in psychomotor epileptics. Electroencephalogr. Clin. Neurophysiol. 40, 225–243. doi:10.1016/0013-4694(76)90147-4.

Bates, D., Mächler, M., Bolker, B., Walker, S., 2014. Fitting Linear Mixed-Effects Models using lme4. ArXiv14065823 Stat.

Blumcke, I., Spreafico, R., Haaker, G., Coras, R., Kobow, K., Bien, C.G., Pfäfflin, M., Elger, C., Widman, G., Schramm, J., Becker, A., Braun, K.P., Leijten, F., Baayen, J.C., Aronica, E., Chassoux, F., Hamer, H., Stefan, H., Rössler, K., Thom, M., Walker, M.C., Sisodiya, S.M., Duncan, J.S., McEvoy, A.W., Pieper, T., Holthausen, H., Kudernatsch, M., Meencke, H.J., Kahane, P., Schulze-Bonhage, A., Zentner, J., Heiland, D.H., Urbach, H., Steinhoff, B.J., Bast, T., Tassi, L., Lo Russo, G., Özkara, C., Oz, B., Krsek, P., Vogelgesang, S., Runge, U., Lerche, H., Weber, Y., Honavar, M., Pimentel, J., Arzimanoglou, A., Ulate-Campos, A., Noachtar, S., Hartl, E., Schijns, O., Guerrini, R., Barba, C., Jacques, T.S., Cross, J.H., Feucht, M., Mühlebner, A., Grunwald, T., Trinka, E., Winkler, P.A., Gil-Nagel, A., Toledano Delgado, R., Mayer, T., Lutz, M., Zountsas, B., Garganis, K., Rosenow, F., Hermsen, A., von Oertzen, T.J., Diepgen, T.L., Avanzini, G.EEBB Consortium, 2017. Histopathological findings in brain tissue obtained during epilepsy surgery. N. Engl. J. Med. 377, 1648–1656. doi:10.1056/NEJMoa1703784.

Buccino, A.P., Hurwitz, C.L., Garcia, S., Magland, J., Siegle, J.H., Hurwitz, R., Hennig, M.H., 2020. SpikeInterface, a unified framework for spike sorting. eLife 9, e61834. doi:10.7554/eLife.61834.

Budke, M., Avecillas-Chasin, J.M., Villarejo, F., 2018. Implantation of depth electrodes in children using VarioGuide® frameless navigation system: technical note. Oper. Neurosurg. Hagerstown Md 15, 302–309. doi:10.1093/ons/opx192.

Buzsáki, G., Anastassiou, C.A., Koch, C., 2012. The origin of extracellular fields and currents — EEG, ECoG, LFP and spikes. Nat. Rev. Neurosci. 13, 407–420. doi:10.1038/nrn3241.

Chari, A., Thornton, R.C., Tisdall, M.M., Scott, R.C., 2020. Microelectrode recordings in human epilepsy: a case for clinical translation. Brain Commun. 2, fcaa082. doi:10.1093/braincomms/fcaa082.

Chaure, F.J., Rey, H.G., Quian Quiroga, R., 2018. A novel and fully automatic spike-sorting implementation with variable number of features. J. Neurophysiol. 120, 1859–1871. doi:10.1152/jn.00339.2018.

Crandall, P.H., Walter, R.D., Rand, R.W., 1963. Clinical applications of studies on stereotactically implanted electrodes in temporal-lobe epilepsy. J. Neurosurg. 20, 827–840. doi:10.3171/jns.1963.20.10.0827.

Despouy, E., Curot, J., Denuelle, M., Deudon, M., Jean-Christophe-Sol Lotterie, J.-A., Reddy, L., Nowak, L.G., Pariente, J., Thorpe, S.J., Valton, L., Barbeau, E.J., 2019. Neuronal spiking activity highlights a gradient of epileptogenicity in human tuberous sclerosis lesions. Clin. Neurophysiol. doi:10.1016/j.clinph.2018.12.013.

Despouy, E., Curot, J., Reddy, L., Nowak, L.G., Deudon, M., Sol, J.-C., Lotterie, J.-A., Denuelle, M., Maziz, A., Bergaud, C., Thorpe, S.J., Valton, L., Barbeau, E.J., 2020. Recording local field potential and neuronal activity with tetrodes in epileptic patients. J. Neurosci. Methods 341, 108759. doi:10.1016/j.jneumeth.2020.108759.

Ducorps, A., Lemarechal, J.-D., Schwartz, D., Yahia-Cherif, L., 2010. A user-friendly software suite for MEG, EEG, EcoG /Intracranial-EEG data analysis. Presented at the Biomag - 17th International Conference on Biomagnetism, Dubrovnik, Croatia.

Ekstrom, A.D., Kahana, M.J., Caplan, J.B., Fields, T.A., Isham, E.A., Newman, E.L., Fried, I., 2003. Cellular networks underlying human spatial navigation. Nature 425, 184–188. doi:10.1038/nature01964.

Elahian, B., Lado, N.E., Mankin, E., Vangala, S., Misra, A., Moxon, K., Fried, I., Sharan, A., Yeasin, M., Staba, R., Bragin, A., Avoli, M., Sperling, M.R., Engel, J., Weiss, S.A., 2018. Low-voltage fast seizures in humans begin with increased interneuron firing: excitatory/inhibitory imbalance and LVF onset seizures. Ann. Neurol. doi:10.1002/ana.25325.

Engel, A.K., Moll, C.K.E., Fried, I., Ojemann, G.A., 2005. Invasive recordings from the human brain: clinical insights and beyond. Nat. Rev. Neurosci. 6, 35–47. doi:10.1038/nrn1585.

Fedorov, A., Beichel, R., Kalpathy-Cramer, J., Finet, J., Fillion-Robin, J.-C., Pujol, S., Bauer, C., Jennings, D., Fennessy, F., Sonka, M., Buatti, J., Aylward, S., Miller, J.V., Pieper, S., Kikinis, R., 2012. 3D Slicer as an image computing platform for the quantitative imaging network. Magn. Reson. Imaging 30, 1323–1341. doi:10.1016/j.mri.2012.05.001.

Fernandez-Vidal, S., Frazzini, V., Lambrecq, V., Navarro, V., Dormont, D., Mathon, B., Adam, C., Bardinet, E., Hasboun, D., 2019. Modular Stereotactic Planning Toolbox for SEEG Procedures Presented at the World Society for Stereotactic and Functional Neurosurgery.

Fisher, R.S., Webber, W.R., Lesser, R.P., Arroyo, S., Uematsu, S., 1992. High-frequency EEG activity at the start of seizures. J. Clin. Neurophysiol. Off. Publ. Am. Electroencephalogr. Soc. 9, 441–448. doi:10.1097/00004691-199207010-00012.

Fried, I., MacDonald, K.A., Wilson, C.L., 1997. Single neuron activity in human hippocampus and amygdala during recognition of faces and objects. Neuron 18, 753–765. doi:10.1016/s0896-6273(00)80315-3.

Holdgraf, C., Appelhoff, S., Bickel, S., Bouchard, K., D’Ambrosio, S., David, O., Devinsky, O., Dichter, B., Flinker, A., Foster, B.L., Gorgolewski, K.J., Groen, I., Groppe, D., Gunduz, A., Hamilton, L., Honey, C.J., Jas, M., Knight, R., Lachaux, J.-P., Lau, J.C., Lee-Messer, C., Lundstrom, B.N., Miller, K.J., Ojemann, J.G., Oostenveld, R., Petridou, N., Piantoni, G., Pigorini, A., Pouratian, N., Ramsey, N.F., Stolk, A., Swann, N.C., Tadel, F., Voytek, B., Wandell, B.A., Winawer, J., Whitaker, K., Zehl, L., Hermes, D., 2019. iEEG-BIDS, extending the brain imaging data structure specification to human intracranial electrophysiology. Sci. Data 6, 102. doi:10.1038/s41597-019-0105-7.

Howard, M.A., Volkov, I.O., Granner, M.A., Damasio, H.M., Ollendieck, M.C., Bakken, H.E., 1996. A hybrid clinical-research depth electrode for acute and chronic in vivo microelectrode recording of human brain neurons. Technical note. J. Neurosurg. 84, 129–132. doi:10.3171/jns.1996.84.1.0129.

Jurczynski, P., Cam, S., Rossion, B., Ranta, R., 2021. Separating local and propagated contributors to the Behnke-fried microelectrode recordings. In: Proceedings of the 14th International Joint Conference on Biomedical Engineering Systems and Technologies. Presented at the 14th International Conference on Bio-inspired Systems and Signal Processing. SCITEPRESS - Science and Technology Publications, pp. 343–350 Online Streaming, — Select a Country — doi:10.5220/0010349303430350.

Keller, C.J., Truccolo, W., Gale, J.T., Eskandar, E., Thesen, T., Carlson, C., Devinsky, O., Kuzniecky, R., Doyle, W.K., Madsen, J.R., Schomer, D.L., Mehta, A.D., Brown, E.N., Hochberg, L.R., Ulbert, I., Halgren, E., Cash, S.S., 2010. Heterogeneous neuronal firing patterns during interictal epileptiform discharges in the human cortex. Brain 133, 1668–1681. doi:10.1093/brain/awq112.

Khodagholy, D., Gelinas, J.N., Thesen, T., Doyle, W., Devinsky, O., Malliaras, G.G., Buzsáki, G., 2015. NeuroGrid: recording action potentials from the surface of the brain. Nat. Neurosci. 18, 310–315. doi:10.1038/nn.3905.

Kim, K., Ladenbauer, J., Babo-Rebelo, M., Buot, A., Lehongre, K., Adam, C., Hasboun, D., Lambrecq, V., Navarro, V., Ostojic, S., Tallon-Baudry, C., 2019. Resting-state neural firing rate is linked to cardiac-cycle duration in the human cingulate and parahippocampal cortices. J. Neurosci. Off. J. Soc. Neurosci. 39, 3676–3686. doi:10.1523/JNEUROSCI.2291-18.2019.

Kornblith, S., Quian Quiroga, R., Koch, C., Fried, I., Mormann, F., 2017. Persistent single-neuron activity during working memory in the human medial temporal lobe. Curr. Biol. CB 27, 1026–1032. doi:10.1016/j.cub.2017.02.013.

Kreiman, G., Koch, C., Fried, I., 2000. Imagery neurons in the human brain. Nature 408, 357–361. doi:10.1038/35042575.

Lakretz, Y., Ossmy, O., Friedmann, N., Mukamel, R., Fried, I., 2021. Single-cell activity in human STG during perception of phonemes is organized according to manner of articulation. NeuroImage 226, 117499. doi:10.1016/j.neuroimage.2020.117499.

Lambrecq, V., Lehongre, K., Adam, C., Frazzini, V., Mathon, B., Clemenceau, S., Hasboun, D., Charpier, S., Baulac, M., Navarro, V., Le Van Quyen, M., 2017. Single-unit activities during the transition to seizures in deep mesial structures: seizures and single-unit activities. Ann. Neurol. 82, 1022–1028. doi:10.1002/ana.25111.

Mathon, B., Clemenceau, S., Hasboun, D., Habert, M.-O., Belaid, H., Nguyen-Michel, V.-H., Lambrecq, V., Navarro, V., Dupont, S., Baulac, M., Cornu, P., Adam, C., 2015. Safety profile of intracranial electrode implantation for video-EEG recordings in drug-resistant focal epilepsy. J. Neurol. 262, 2699–2712. doi:10.1007/s00415-015-7901-6.

Minxha, J., Mamelak, A.N., Rutishauser, U., 2018. Surgical and electrophysiological techniques for single-neuron recordings in human epilepsy patients. In: Sillitoe, R.V. (Ed.), Extracellular Recording Approaches, Neuromethods. Springer New York, New York, NY, pp. 267–293. doi:10.1007/978-1-4939-7549-5_14.

Misra, A., Burke, J., Ramayya, A., Jacobs, J., Sperling, M., Moxon, K., Kahana, M., Evans, J., Sharan, A., 2014. Methods for implantation of micro-wire bundles and optimization of single/multiunit recordings from human mesial temporal lobe. J. Neural Eng. 11, 026013. doi:10.1088/1741-2560/11/2/026013.

Mormann, F., Kornblith, S., Quiroga, R.Q., Kraskov, A., Cerf, M., Fried, I., Koch, C., 2008. Latency and selectivity of single neurons indicate hierarchical processing in the human medial temporal lobe. J. Neurosci. Off. J. Soc. Neurosci. 28, 8865–8872. doi:10.1523/JNEUROSCI.1640-08.2008.

Niediek, J., Boström, J., Elger, C.E., Mormann, F., 2016. Reliable analysis of single-unit recordings from the human brain under noisy conditions: tracking neurons over hours. PLoS One 11, e0166598. doi:10.1371/journal.pone.0166598.

Oostenveld, R., Fries, P., Maris, E., Schoffelen, J.-M., 2011. FieldTrip: open source software for advanced analysis of MEG, EEG, and invasive electrophysiological data. Comput. Intell. Neurosci. 2011, 156869. doi:10.1155/2011/156869.

Parvizi, J., Kastner, S., 2018. Promises and limitations of human intracranial electroencephalography. Nat. Neurosci. 21, 474–483. doi:10.1038/s41593-018-0108-2.

Paulk, A.C., Yang, J.C., Cleary, D.R., Soper, D.J., Halgren, M., O'Donnell, A.R., Lee, S.H., Ganji, M., Ro, Y.G., Oh, H., Hossain, L., Lee, J., Tchoe, Y., Rogers, N., Kiliç, K., Ryu, S.B., Lee, S.W., Hermiz, J., Gilja, V., Ulbert, I., Fabó, D., Thesen, T., Doyle, W.K., Devinsky, O., Madsen, J.R., Schomer, D.L., Eskandar, E.N., Lee, J.W., Maus, D., Devor, A., Fried, S.I., Jones, P.S., Nahed, B.V., Ben-Haim, S., Bick, S.K., Richardson, R.M., Raslan, A.M., Siler, D.A., Cahill, D.P., Williams, Z.M., Cosgrove, G.R., Dayeh, S.A., Cash, S.S., 2021. Microscale physiological events on the human cortical surface. Cereb. Cortex 31, 3678–3700. doi:10.1093/cercor/bhab040.

Pedreira, C., Martinez, J., Ison, M.J., Quian Quiroga, R., 2012. How many neurons can we see with current spike sorting algorithms? J. Neurosci. Methods 211, 58–65. doi:10.1016/j.jneumeth.2012.07.010.

Polikov, V.S., Tresco, P.A., Reichert, W.M., 2005. Response of brain tissue to chronically implanted neural electrodes. J. Neurosci. Methods 148, 1–18. doi:10.1016/j.jneumeth.2005.08.015.

Quiroga, R.Q., Reddy, L., Kreiman, G., Koch, C., Fried, I., 2005. Invariant visual representation by single neurons in the human brain. Nature 435, 1102–1107. doi:10.1038/nature03687.

Reif, P.S., Strzelczyk, A., Rosenow, F., 2016. The history of invasive EEG evaluation in epilepsy patients. Seizure 41, 191–195. doi:10.1016/j.seizure.2016.04.006.

Rey, H.G., Pedreira, C., Quian Quiroga, R., 2015. Past, present and future of spike sorting techniques. Brain Res. Bull., Adv. Electrophysiol. Data Anal. 119, 106–117. doi:10.1016/j.brainresbull.2015.04.007.

Ringel, F., Ingerl, D., Ott, S., Meyer, B., 2009. VarioGuide: a new frameless image-guided stereotactic system–accuracy study and clinical assessment. Neurosurgery 64, 365–371. doi:10.1227/01.NEU.0000341532.15867.1C, discussion 371-373.

Rivière, D., Geffroy, D., Denghien, I., Souedet, N., Cointepas, Y., 2011. Anatomist: a Python Framework for Interactive 3D Visualization of Neuroimaging Data Presented at the Python in Neuroscience Workshop.

Rutishauser, U., Reddy, L., Mormann, F., Sarnthein, J., 2021. The architecture of human memory: insights from human single-neuron recordings. J. Neurosci. Off. J. Soc. Neurosci. 41, 883–890. doi:10.1523/JNEUROSCI.1648-20.2020.

Schevon, C.A., Ng, S.K., Cappell, J., Goodman, R.R., McKhann, G., Waziri, A., Branner, A., Sosunov, A., Schroeder, C.E., Emerson, R.G., 2008. Microphysiology of epileptiform activity in human neocortex. J. Clin. Neurophysiol. 25, 321–330. doi:10.1097/WNP.0b013e31818e8010.

Schevon, C.A., Weiss, S.A., McKhann, G., Goodman, R.R., Yuste, R., Emerson, R.G., Trevelyan, A.J., 2012. Evidence of an inhibitory restraint of seizure activity in humans. Nat. Commun. 3, 1060. doi:10.1038/ncomms2056.

Soleil, D., Badier, J.-M., Lemesle, M., 1992. Zero" solution for shielding and electrical protection in a unit for electroencephalographic recording. In: 1992 14th Annual International Conference of the IEEE Engineering in Medicine and Biology Society. Presented at the 1992 14th Annual International Conference of the IEEE Engineering in Medicine and Biology Society, pp. 1134–1135. doi:10.1109/IEMBS.1992.5761389.

Staba, R.J., Stead, M., Worrell, G.A., 2014. Electrophysiological biomarkers of epilepsy. Neurother. J. Am. Soc. Exp. Neurother. 11, 334–346. doi:10.1007/s13311-014-0259-0.

Stacey, W.C., Kellis, S., Greger, B., Butson, C.R., Patel, P.R., Assaf, T., Mihaylova, T., Glynn, S., 2013. Potential for unreliable interpretation of EEG recorded with microelectrodes. Epilepsia 54, 1391–1401. doi:10.1111/epi.12202.

Staresina, B.P., Reber, T.P., Niediek, J., Boström, J., Elger, C.E., Mormann, F., 2019. Recollection in the human hippocampal-entorhinal cell circuitry. Nat. Commun. 10, 1503. doi:10.1038/s41467-019-09558-3.

Stead, M., Bower, M., Brinkmann, B.H., Lee, K., Marsh, W.R., Meyer, F.B., Litt, B., Van Gompel, J., Worrell, G.A., 2010. Microseizures and the spatiotemporal scales of human partial epilepsy. Brain J. Neurol. 133, 2789–2797. doi:10.1093/brain/awq190.

Talairach, J., Bancaud, J., 1966. Lesion, "irritative" zone and epileptogenic focus. Confin. Neurol. 27, 91–94. doi:10.1159/000103937.

Truccolo, W., Donoghue, J.A., Hochberg, L.R., Eskandar, E.N., Madsen, J.R., Anderson, W.S., Brown, E.N., Halgren, E., Cash, S.S., 2011. Single-neuron dynamics in human focal epilepsy. Nat. Neurosci. 14, 635–641. doi:10.1038/nn.2782.

Ulbert, I., Heit, G., Madsen, J., Karmos, G., Halgren, E., 2004. Laminar analysis of human neocortical interictal spike generation and propagation: current source density and multiunit analysis in vivo. Epilepsia 45, 48–56. doi:10.1111/j.0013-9580.2004.04011.x.

Verzeano, M., Crandall, P.H., Dymond, A., 1971. Neuronal activity of the amygdala in patients with psychomotor epilepsy. Neuropsychologia 9, 331–344. doi:10.1016/0028-3932(71)90029-7.

Weiss, S.A., Alvarado-Rojas, C., Bragin, A., Behnke, E., Fields, T., Fried, I., Engel, J., Staba, R., 2016. Ictal onset patterns of local field potentials, high frequency oscillations, and unit activity in human mesial temporal lobe epilepsy. Epilepsia 57, 111–121. doi:10.1111/epi.13251.

Wendling, F., Bartolomei, F., Bellanger, J.J., Bourien, J., Chauvel, P., 2003. Epileptic fast intracerebral EEG activity: evidence for spatial decorrelation at seizure onset. Brain J. Neurol. 126, 1449–1459. doi:10.1093/brain/awg144.

Wild, J., Prekopcsak, Z., Sieger, T., Novak, D., Jech, R., 2012. Performance comparison of extracellular spike sorting algorithms for single-channel recordings. J. Neurosci. Methods 203, 369–376. doi:10.1016/j.jneumeth.2011.10.013.

Wyler, A.R., Ojemann, G.A., Ward, A.A., 1982. Neurons in human epileptic cortex: correlation between unit and EEG activity. Ann. Neurol. 11, 301–308. doi:10.1002/ana.410110311.

Yger, P., Spampinato, G.L., Esposito, E., Lefebvre, B., Deny, S., Gardella, C., Stimberg, M., Jetter, F., Zeck, G., Picaud, S., Duebel, J., Marre, O., 2018. A spike sorting toolbox for up to thousands of electrodes validated with ground truth recordings in vitro and in vivo. eLife 7, e34518. doi:10.7554/eLife.34518.

Zijlmans, M., Worrell, G.A., Dümpelmann, M., Stieglitz, T., Barborica, A., Heers, M., Ikeda, A., Usui, N., Le Van Quyen, M., 2017. How to record high-frequency oscillations in epilepsy: a practical guideline. Epilepsia 58, 1305–1315. doi:10.1111/epi.13814.

Zijlmans, M., Zweiphenning, W., van Klink, N., 2019. Changing concepts in presurgical assessment for epilepsy surgery. Nat. Rev. Neurol. 15, 594–606. doi:10.1038/s41582-019-0224-y.

Journal of Neurology (2022) 269:4102–4109
https://doi.org/10.1007/s00415-022-11024-y

ORIGINAL COMMUNICATION

Epilepsy related to focal neuronal lipofuscinosis: extra-frontal localization, EEG signatures and GABA involvement

Valerio Frazzini[1,2,3] · Bertrand Mathon[2,3,4] · Florian Donneger[2,7,8] · Louis Cousyn[1,2,3] · Aurélie Hanin[2] · V.-H. Nguyen-Michel[1] · Claude Adam[1] · Virginie Lambrecq[1,2,3] · Sophie Dupont[1,3,5] · Jean Christophe Poncer[2,7,8] · Franck Bielle[2,3,6] · Vincent Navarro[1,2,3]

Received: 11 October 2021 / Revised: 7 February 2022 / Accepted: 11 February 2022 / Published online: 7 March 2022

Abstract

Focal neuronal lipofuscinosis (FNL) is an uncommon epileptic disorder related to an excess of lipofuscin accumulation within dysmorphic-appearing neurons (DANs), whose epileptogenic mechanisms are still poorly understood. It shares some clinical and neuroimaging similarities with focal cortical dysplasia of type IIb (FCDIIb), but it represents a different pathological entity. Here, we identified two patients with FNL among a 10-year cohort of 323 patients who underwent neurosurgery for a focal pharmacoresistant epilepsy. We describe the electroclinical, metabolic and neuropathological features of both patients with FNL who benefited from a comprehensive presurgical investigation. While the previous reports showed frontal lobe localization of the lesion, FNL was identified in the temporal lobe, in one of our patients. EEG investigations in both patients showed striking focal and rich interictal activity resembling that described in FCDIIb. Besides focal intraneuronal lipofuscin accumulation, the neuropathological analysis demonstrated that somata of DANs were surrounded by a large amount of GABAergic presynaptic buttons, suggesting the involvement of interneurons in the epileptogenicity of FNL. To further explore the role of GABAergic transmission in the generation of epileptiform activity in FNL, we performed in vitro multi-electrode array recordings on the post-surgery tissue from one patient. Spontaneous interictal-like discharges (IILDs) were identified only in the restricted area displaying the highest density of lipofuscin-containing DANs, suggesting a close correlation between the density of lipofuscin-containing neurons and epileptogenicity. Moreover, IILDs were blocked by the GABAA receptor antagonist gabazine. All together, these findings showed how GABA signaling may contribute to the generation of interictal-like activity in FNL tissue.

Keywords Lipofuscinosis · Focal seizures · SEEG · Dysmorphic appearing neurons · Focal cortical Dysplasia · MEA · GABA

Abbreviations

DANs	Dysmorphic-appearing neurons
FCDIIb	Focal cortical dysplasia of type IIb
FLE	Frontal lobe epilepsy
FNL	Focal neuronal lipofuscinosis
STG	Superior temporal gyrus
MEA	MultiElectrode Array

Franck Bielle and Vincent Navarro contributed equally to this work.

✉ Vincent Navarro
vincent.navarro@aphp.fr

1 Epilepsy Unit, Department of Neurology and EEG Unit, Department of Clinical Neurophysiology, AP-HP, Pitié Salpêtrière Hospital, Reference Center for Rare Epilepsies, 75013 Paris, France

2 Paris Brain Institute, ICM, INSERM, CNRS, 75013 Paris, France

3 Sorbonne Université, 75013 Paris, France

4 Department of Neurosurgery, AP-HP, Pitié Salpêtrière Hospital, 75013 Paris, France

5 Rehabilitation Unit, AP-HP, Pitié-Salpêtrière Hospital, Paris, France

6 Department of Neuropathology, AP-HP, Pitié Salpêtrière Hospital, 75013 Paris, France

7 Inserm UMR-S 1270, 75005 Paris, France

8 Institut du Fer À Moulin, 75005 Paris, France

Journal of Neurology (2022) 269:4102–4109

Introduction

Focal neuronal lipofuscinosis (FNL) corresponds to an excess of lipofuscin accumulation within dysmorphic-appearing neurons (DANs) and was described as the pathological hallmark of a distinct type of pharmaco-resistant frontal lobe epilepsy (FLE) [1, 2]. While FNL shares some clinical and neuroimaging features with focal cortical dysplasia of type IIb (FCDIIb), it represents a different neuropathological entity currently described in seven patients [1, 3]. To date, it is still unclear if FNL displays peculiar ictal or interictal electrophysiological features and little is known about the basis of its epileptogenicity. Here, we describe the electroclinical, metabolic and neuropathological features of two patients with focal pharmaco-resistant epilepsy due to FNL who benefited from a comprehensive presurgical investigation. Post-surgical specimen from one patient was further explored using multi-electrode array recordings in vitro to explore the microscopic organization of the locally generated epileptiform activity. The goal of the study is to offer a multilevel description of this challenging epileptogenic pathology with particular emphasis on the relationship between neurophysiological and neuropathological features.

Methods

We screened all patients who underwent epilepsy surgery between January 2010 and December 2020 in the Pitié-Salpêtrière Hospital and for which neuropathological examinations were available. On a total of 323 patients, we identified 2 patients whose histological examination revealed microscopic abnormalities compatible with FNL. Both patients underwent a complete presurgical evaluation in the Epileptology Unit of the Pitié-Salpêtrière Hospital. It included 3 T brain MRI, 27-electrode long-term video-EEG recordings (MicroMed System, Italy) and interictal 18FDG-PET. Interictal and ictal (SISCOM) Tc-99 m-HMPAO SPECT evaluation were performed in both patients. For patient 1, we conducted an intracerebral SEEG investigation exploring the right temporal, parietal and occipital lobes. Nine intracerebral electrodes (AdTech®) were inserted using the robotic ROSA® device (Medtech). Signals were continuously and synchronously recorded at 4 kHz using a hardware filter at 0.01 Hz (Atlas Recording System; NeuraLynx, Tucson, AZ, USA). Post-implantation electrode locations were based on a pre-implantation 3 T 3D-MRI, post-implantation 1.5 T 3D-MRI and CT scan, integrated using the Epiloc toolbox, an in-house developed plugin for the 3D-Slicer visualization software. The study design and report are in accordance with the STROBE statement [4].

Neuropathology

After surgery, brain specimens were formalin-fixed and paraffin-embedded. Three micrometers-thick tissue sections were studied by hematoxylin–eosin, Periodic Acid Schiff (PAS) and Luxol blue stainings or were processed for immunostainings by a fully automated stainer Ultra (Ventana, Roche) using diaminobenzidine as a chromogen and the following primary antibodies and dilutions: monoclonal mouse anti-non phosphorylated neurofilament SMI32 (Biolegend, 1/1000), mouse monoclonal anti-p62 (Becton Dickinson, 1/500), polyclonal rabbit anti-glutamate decarboxylase 65 & 67 (Sigma, 1/3000).

Human tissue and multi-electrode recordings

A written consent was obtained for the in vitro study, according to a procedure validated by the national ethical committee (TIPI project, INSERM C16-16). Cortical specimens collected in the operating room were immediately transported in ice-cold (0–4 °C), oxygenated solution (O2/CO2 95/5%), containing (in mM): N-methyl-d-glucamine 93, KCl 2.5, NaH2PO4 1.2, NaHCO3 30, HEPES 20, D-glucose 20, ascorbic acid 5, sodium pyruvate 3, MgSO4 10 and CaCl2 0.5 (300–310 mOsm, pH 7.4) and transported within 15 min to the laboratory. Transverse cortical slices (400 µm thick) were prepared in the same solution using a vibratome (HM650V, Microm). They were maintained at 37 °C in an interface chamber containing artificial cerebrospinal fluid (ACSF) composed of (in mM): D-glucose 10, KCl 3.5, NaHOC3 26, NaH2PO4 1.25, NaCl 126, CaCl2 1.6 and MgCl2 1.2 (290 mOsm), equilibrated with 5% CO2 in 95% O2. Multielectrode array recordings were performed using a MEA2100 station (Multi Channel Systems) equipped with a 120-microelectrode array chamber (12×12 layout, 30 µm titanium nitride electrodes spaced 100 µm). Slices were maintained in the recording chamber using a home-made platinum-nylon harp and superfused with pre-warmed (37 °C) oxygenated ACSF at a rate of 6 ml/min. Slices were imaged using a video-microscope table (MEA-VMT1, Multi Channel Systems) to register the location of electrodes with respect to the slice. Extracellular signals were acquired at a sampling rate of 10 kHz and post-hoc filtered with a low pass Bessel filter (order 2; 40 Hz) using Multi Channel Experimenter (MultiChannelSystems). Analyses were performed offline using homemade software (Matlab, The Mathworks).

Results

Clinical presentation

Patient 1, a 24-year-old woman, suffered from focal epilepsy since the age of 12. Seizures consisted of dizziness and spatiotemporal disorientation, followed by loss of awareness and atonia, sometimes associated with falls. Patient 2, a 30-year-old woman, developed focal seizures since the age of 3 months. A mild right hemiplegia appeared during the second year of life. Seizures were controlled by pharmacological treatment until the age of 26, then the patient experienced a progressive increase in seizure frequency. Seizures usually consisted of paresthesia of the right hemi-body, including the face, followed by hypertonic contraction and then clonus of the upper limb. Awareness was preserved.

Structural and metabolic imaging

In patient 1, brain MRI was normal (Fig. 1a, left). Brain ^{18}FDG-PET found a right temporal hypometabolism including the lateral cortex, up to the parieto-temporal junction

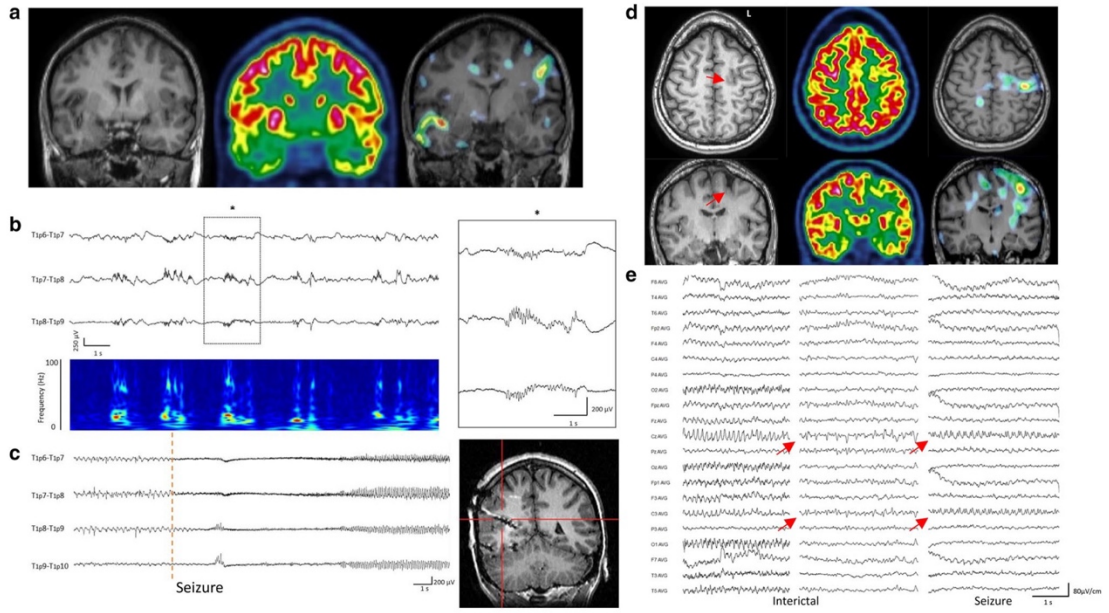

Fig. 1 Imaging, metabolic and electrophysiological features of two epileptic patients with a final diagnosis of FNL. **a**, Brain MRI and metabolic imaging from patient 1. Left panel: anatomical T1WI MRI showing no obvious lesion. Middle Panel: interictal PET showing hypometabolism in the right temporal lobe. Right panel: ictal versus interictal SPECT showing an area of hyperperfusion in the right temporopolar cortex, in particular within the superior temporal gyrus. The radiotracer was injected 27 s after the seizure onset. **b**, Interictal pattern recorded from contacts 6 to 9 of the intracerebral electrode located in the right superior temporal gyrus (see brain location on the right part of panel **c**). Interictal activity consisted of periodic discharges of fast oscillations superimposed on isolated or repetitive slow waves, sometime entangled with isolated epileptic spikes. The insert shows a magnification of the sEEG trace enclosed in the dotted rectangle. T1p: *T1* superior temporal gyrus, *p* posterior. sEEG signals are showed in bipolar montage. Lower panel: Time–Frequency Analysis (TFA) of interictal sEEG signal showed overhead (T1p7–8 channel). TFA showed periodic modulation of frequency power at around 30 Hz together with spots of higher frequency power up to 80 Hz. **c**, Left panel: Representative trace of a seizure from patient 1. Seizures were found to originate from brain tissue around the contacts 6–7-8 of the electrode T1p, and consisted of a low voltage fast activity. Right panel: Anatomical MRI showing the trajectory of the intracerebral electrode exploring the posterior part of the right superior temporal lobe. **d**, Brain MRI and metabolic imaging from patient 2. Left, upper and lower panel: axial and coronal view of brain T1WI MRI. Discrete focal blurring of the cortico-subcortical junction of the bottom of the superior left frontal sulcus (red arrow). Middle, upper and lower panel: axial and coronal view of the ^{18}FDG-PET showing hypometabolism of the left superior frontal sulcus. Right, upper and lower panel: axial and coronal view of the ictal versus interictal SPECT disclosing an area of cortical hyperperfusion centered on the lesion and the left inferior pre-central cortex. **e**, Representative traces of interictal and ictal scalp EEG of patient 2. EEG showed intermittent low amplitude rhythmic spiky activity at 6–7 Hz, on the left fronto-central and anterior midline electrodes (left panel). Interictal activity can also acquire a pseudoperiodic, short interval, appearance (middle panel). During seizures (right panel), the rhythmic ictal abnormalities showed a peculiar "sawtooth" morphology. EEG signals are showed with an average reference montage

and the pericentral region (Fig. 1a, middle panel). Ictal versus interictal SPECT (SISCOM) disclosed a hyperperfused area in the right temporopolar cortex, predominating in the superior temporal gyrus (STG; Fig. 1a right). In patient 2, brain MRI demonstrated a focal blurring at the cortico-subcortical junction of the bottom of the superior left frontal sulcus (Fig. 1d, left panel). This lesion was hypometabolic on ^{18}FDG-PET (Fig. 1d, middle). Ictal versus interictal SPECT disclosed a cortical hyperperfusion involving the lesion, extending to the homolateral inferior pre-central cortex (Fig. 1d, right panel).

EEG investigations

In patient 1, surface EEG disclosed spikes and sharp waves on the right temporal lobe. Based on the electrophysiological and metabolic features, the patient 1 underwent to a first intracranial investigation (stereoelectroencephalography, SEEG) exploring the left lateral and antero-basal temporal cortices, the left temporal pole, the left amygdalohippocampal complex and entorhinal cortex. Left orbitofrontal cortex was also explored. This SEEG investigation did not identify the origin of seizures, pointing to a more posterior location of the seizure onset zone (SOZ). A second SEEG investigation explored the posterior part of the left temporal lobe, the temporo-occipital junction and the left inferior parietal lobule (Supplementary Fig. 1). This latter SEEG investigation identified a highly active focus of interictal epileptiform discharges in the posterior part of the right STG (Fig. 1b). They consisted of quasi-continuous periodic spikes and spikes and waves with superimposed short-lasting bursts of fast activity during wakefulness. The latter increased dramatically during non-REM sleep, and appeared as short-interval (1–2 s), periodic discharges at 80 Hz oscillations (brushes), alternating with transient suppression of background activity (Fig. 1b). Recorded seizures consisted of a low voltage fast activity at seizure onset and originated from the same contacts where the interictal discharges (IIDs) were identified. (Fig. 1c). In patient 2, scalp EEG showed quasi-continuous rhythmic (6–7 Hz), low amplitude spikes/sharp waves interictal epileptiform discharges, on the left fronto-central electrodes (Fig. 1e). Seizures mainly occurred during sleep and consisted of a left frontocentral rhythmic ictal activity with a "sawtooth" morphology (Fig. 1e, right panel).

Surgery outcome

In patient 1, surgical cortectomy removed the posterior part of right STG (Fig. 2a, left right part). In patient 2, surgery removed the bottom of the posterior part of the superior left frontal sulcus (Fig. 2b, right panel). No significative reduction of seizure frequency was achieved after one year since surgery (ILAE Class 5) in both patients. These results are in line with previous observation on FNL surgery [1].

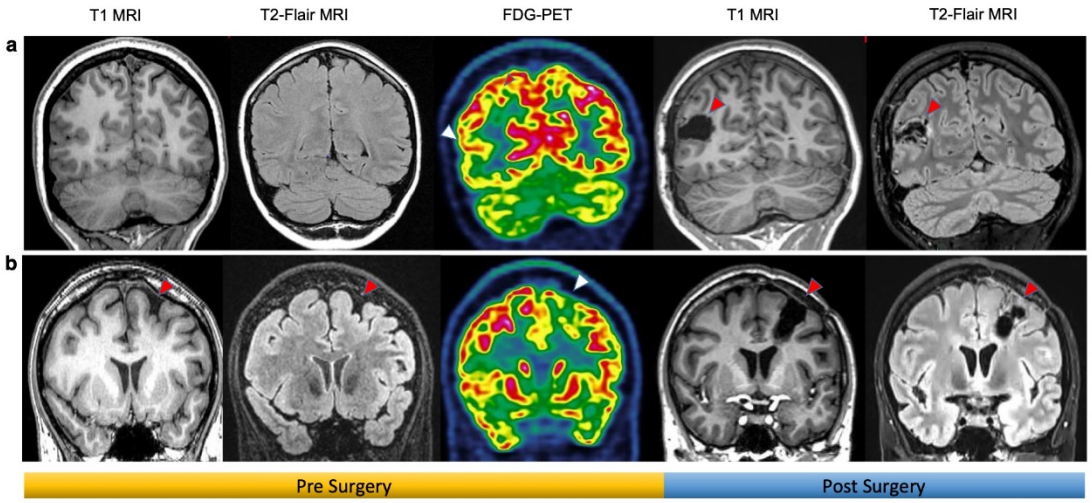

Fig. 2 Pre and Post-surgery neuroimaging showing the postsurgical cavity. **a** (from the left to the right): presurgical T1WI and T2 Flair WI from patient 1, showing no evident macroscopic focal lesion. Interictal ^{18}FDG-PET showing the posterior part of the right temporal hypometabolism. Post-surgery T1WI and T2 Flair MRI showing the post-surgical cavity located in the posterior part of right STG. **b**, Pre-surgical T1WI and T2 Flair WI from patient 2, showing a focal blurring at the cortico-subcortical junction of the bottom of the superior left frontal sulcus. Interictal ^{18}FDG-PET showing a focal hypometabolism associated to the lesion. Post-surgery T1WI and T2 Flair MRI showing the post-surgical cavity located in the bottom of the posterior part of the superior left frontal sulcus

Both patients underwent a second surgical intervention to remove the tissue surrounding the previous postsurgical cavity. These surgeries did not modify seizure frequency in both patients after the following months.

Neuropathological study

In both patients, neuropathological analysis of first postsurgical specimens disclosed enlarged, pyramidal or globoid neurons resembling DANs (Fig. 3a). The cytoplasm of DANs was markedly distended, showing intracellular granular material on hematoxylin–eosin. Granular material was both PAS and Luxol blue positive, suggesting excessive lipofuscin accumulation (Fig. 3b). All DANs were negative for anti-GAD staining, suggesting that they were not interneurons (Fig. 3b). p62—a protein involved in ubiquitin-proteasome system and in autophagy [5, 6]—was weakly expressed in DANs, in contrast to the strong expression found in abnormal cells of FCDIIb (Fig. 3a) [1]. The somata of lipofuscin-containing DANs were surrounded by crown-like, GAD-immunopositive puncta, compatible with peri-somatic GABAergic presynaptic buttons (Fig. 3b and c). Interestingly, no normal pyramidal neuron in the specimen showed a similar morphological feature (Fig. 3b). In both patients, lipofuscin-containing neurons showed a heterogeneous distribution within the resected tissues. Some lipofuscin-containing DANs were organized in clusters while others appeared as isolated cells. The resected tissue was fragmented, which did not allow to control the presence of neuronal lipofuscinosis at margins of the resections. The neuropathological examination of cerebral specimens after second surgery showed rare lipofuscine-containing neurons for patient 1 and no pathological neuron for patient 2.

In vitro electrophysiological recordings from post-surgery human tissue from patient 1

To correlate these morphological features with neuronal activity, we next performed in vitro recordings from the second postsurgical specimens from patient 1 using multielectrode arrays. Spontaneous, periodic (1.2 Hz), interictal-like discharges (IILDs) were identifiable in a restricted area of the slice (red electrodes in Fig. 4a). Upon application of a pro-convulsive extracellular solution (9 mM K+; 0.25 mM

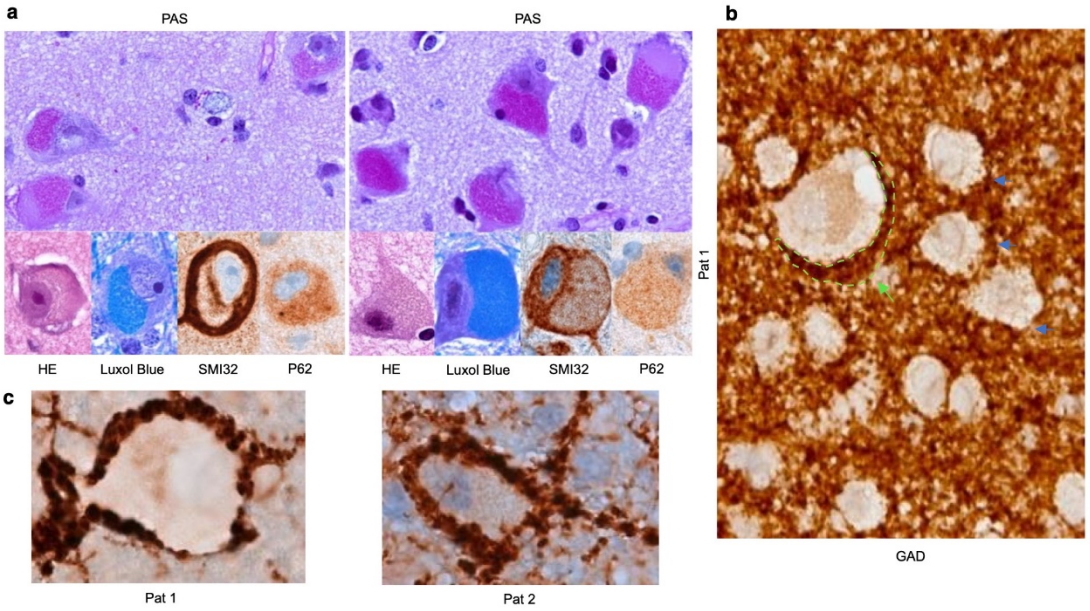

Fig. 3 Neuropathological analysis of the postsurgical specimen from Patient 1 and 2. **a**, Upper pictures: periodic Acid Schiff (PAS) coloration. In both patients dysmorphic-appearing neurons (DANs) showed intracytoplasmic granular accumulation on PAS. Lower pictures: intracytoplasmic granular accumulation was also stained by hematoxylin–eosin and displayed Luxol blue positivity, all suggesting of lipofuscin material. DANs showed strong ring-like labeling with anti-neurofilament SMI32 antibodies. DANs showed a weak positivity for p62. **b**, Anti-GAD staining revealed that DANs neurons are not inhibitory cells. DANs were surrounded by multiple extracellular, perisomatic puncta, compatible with presynaptic GABAergic boutons. This finding was observed only around DANs (dotted green lines with arrow), and not around neurons of normal appearance (blue arrows). **c**, Perisomatic GABA staining of the DANs was found in both patients

Journal of Neurology (2022) 269:4102–4109

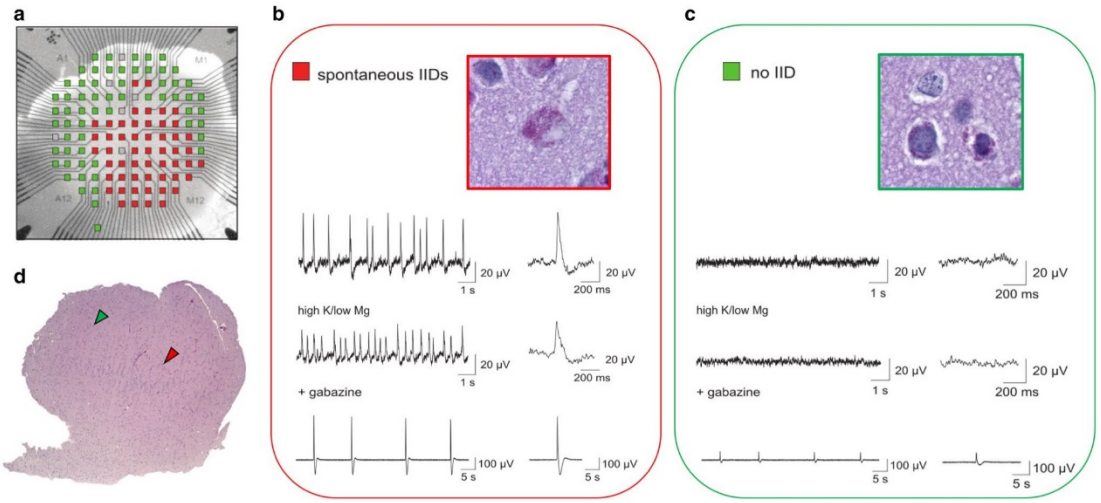

Fig. 4 Gabazine suppresses spontaneous interictal-like discharges (IILDs) recorded in vitro in human FNL tissue. **a**, Example of a cortical slice from a post-operative tissue, recorded on a 120-channel multielectrode array. The schematic representation of the electrode layout is superimposed on the image of the slice. Electrodes recording spontaneous IILDs are shown in red whereas those without IILDs are shown in green. Noisy electrodes are represented in grey and were not used for recording. Note that the epileptogenic zone is restricted to a portion of the slice. **d**, Same slice as in A, stained with PAS for lipofuscin visualization. Arrows indicate the sites from which insets in panels **b**–**c** were obtained. **b**–**c**, Representative local field potential recordings from both spontaneously active (**b**, red) and inactive (**c**, green) areas from the slice shown in panels **a**–**d**. Insets, magnification of the areas indicated with red (**b**) and green (**c**) arrows, respectively, in panel **d**. Note the presence of a dysmorphic neuron containing a strong intracytoplasmatic lipofuscin staining (purple) in the spontaneously active area. Top traces, spontaneous IILDs represented on different timescales, recorded from a red (**b**) but not a green (**c**) electrode. Middle traces, upon perfusion with a pro-convulsive solution (9 mM K+, 0.25 mM Mg2+, 1.6 mM Ca2+), the frequency of IILDs increased while their amplitude was reduced. No activity was induced in areas without spontaneous IILDs. Lower traces, upon addition of gabazine (10 µM), IILDs were suppressed and replaced with large amplitude, rhythmic, LFP oscillations spreading throughout the slice

Mg2+, 1.6 mM Ca2+), the frequency of IILDs increased by 27% whereas their amplitude decreased by 58% (Fig. 4b). However, no ictal-like activity was induced outside the spontaneously active area. Importantly, this area also displayed the highest density of lipofuscin-containing DANs (Fig. 4b, red arrow; Fig. 4c, red contoured square) which were virtually absent from the silent areas (Fig. 3b, green arrow; Fig. 4d, green contoured square). These findings suggest a correlation between the density of lipofuscin-containing neurons and epileptogenicity. Finally, since DANs were surrounded by a high density of putative perisomatic GABAergic synaptic boutons, we tested the role of GABA signaling in the generation of epileptic activity. Thus, application of the specific GABAA receptor antagonist gabazine (10 µM) resulted in the complete suppression of epileptiform activity detected on previously active electrodes and the emergence of slow, high-amplitude LFP oscillations in the whole slice.

Discussion

FNL is a rare and recently described pathology [1, 2]. According to the reports of a total of seven patients, FNL was systematically located in the frontal lobes. Here, we report that FNL can also be identified in the temporal lobe, as shown in one of our two patients. Previous reports did not provide details on EEG findings. Here, we report, in both patients, strikingly focal and rich interictal EEG activities. They consisted of focal rhythmic or periodic interictal epileptiform discharges resembling those described in FCDIIb [7, 8]. However, in line with the previous reports on FNL [1], surgical outcome was not satisfying in our two patients, when compared to that observed with FCD patients [1, 2, 8]. It is not clear whether these differences are due to a greater difficulty in

correctly delineating and resecting the affected tissue or to differences in network organizations around the lesion as compared with FCDIIb. Neuropathological examination of post-operative tissues from both patients showed intraneuronal lipofuscin accumulation within dysmorphic neurons, a hallmark of FNL. In line with a previous report, post-surgical tissues from our patients revealed a cortical and juxtacortical location of FNL 1 [1, 2]. Contrary to FCDIIb, lipofuscin-containing DANs were less clustered, appearing as small group of pathological cells as well as isolated ones. In addition, all DANs were GAD-immunonegative, suggesting they were not GABAergic interneurons (Fig. 3c). In contrast, their soma were surrounded by a crown-like zone of dense GABAergic presynaptic buttons. This suggested GABAergic interneurons may either contribute to the epileptogenicity of FNL or, impose an inhibitory restraint to the propagation of epileptiform activity [12–14], or both. A similar organization was reported in FCDIIb, where interneurons provide increased GABAergic innervation of DANs [9, 10]. In addition, hypertrophic basket formations established by putative parvalbumin interneurons also surround DANs in FCDs [11]. The contribution of GABAergic interneurons to epileptic activity is, however, a highly dynamic and multifaceted process. Thus, whereas GABA-mediated inhibition may prevent the spread of epileptic activity [12–14], GABAA receptor-mediated currents can also paradoxically promote epileptiform activity [15] due to altered neuronal chloride homeostasis resulting in depolarizing and excitatory GABA signaling [20, 21]. Consistent with this scenario, spontaneous seizure generation in vivo was associated with increased GABAergic interneuron activity preceding pyramidal neuron activity [16]. In human FCD tissue recorded in vitro, epileptiform activity was initiated by synchronizing mechanisms relying on GABAA receptors [16–19]. Our in vitro data from FNL resective tissue demonstrate that the epileptogenic zone is confined within a highly restricted area enriched in lipofuscin-rich neurons. In addition, we showed that spontaneous IILDs were blocked by the GABAA receptor antagonist gabazine which, however, induced widespread, large amplitude LFP oscillations beyond the limits of the spontaneously active area. These observations suggest GABA signaling in FNL tissue may both contribute to the generation of interictal-like activity and constrain the spreading of synchronous, epileptiform activity. In conclusion, we suggest that FNL is not exclusive of FLE but can be found in other types of focal epilepsies such as temporal lobe epilepsy. Although FNL and FCDIIb represent two distinct pathologies, they share some neuropathological and electrophysiological features. Histological analyses reveal an abnormal density of GABAergic terminals around the soma of lipofuscin-containing DANs, suggesting a role of GABAergic interneurons in epileptic activities. In vitro electrophysiological recordings from resected tissue further supported this hypothesis.

Supplementary Information The online version contains supplementary material available at https://doi.org/10.1007/s00415-022-11024-y.

Funding This work received support from the "Investissements d'avenir" program ANR-10-IAIHU06, and from the Fondation Assistance Publique Hôpitaux de Paris (EPIRES—Marie Laure PLV Merchandising)

Declarations

Conflicts of interest On behalf of all authors, the corresponding author states that there is no conflict of interest. We confirm that we have read the journal's position on issues involved in ethical publication and affirm that this report is consistent with those guidelines. Valerio Frazzini, Bertrand Mathon, Florian Donneger, Louis Cousyn, Aurélie Hanin, Vi-Huong Nguyen-Michel, Claude Adam, Virginie Lambrecq, Jean Christophe Poncer reports no disclosure. Sophie Dupont reports fees from Boards with UCB Pharma, EISAI, Liva Nova, GW Pharma, Takeda, Novartis. Franck Bielle reports funding of research out of the scope of this article by Abbvie, a next-of-kin employed by Bristol-Myers Squibb, fees of travel and conference out of the scope of this article by Bristol-Myers Squibb, Vincent Navarro reports fees from Boards with UCB Pharma, EISAI, Liva Nova, GW Pharma.

Ethical approval The study was performed in accordance with the ethical standards as laid down in the 1964 Declaration of Helsinki and its later amendments or comparable ethical standards.

References

1. Liu JY, Reeves C, Diehl B et al (2016) Early lipofuscin accumulation in frontal lobe epilepsy. Ann Neurol 80(6):882–895
2. Mhatre R, Jagtap SA, Kurwale N, Santhoshkumar R, Deshmukh Y, Mahadevan A (2020) Frontal lobe epilepsy with focal neuronal lipofuscinosis—case report of a rare entity. Epilepsy Behav Rep. 14:100369
3. Blümcke I, Thom M, Aronica E et al (2011) The clinicopathologic spectrum of focal cortical dysplasias: a consensus classification proposed by an ad hoc task force of the ILAE diagnostic methods commission. Epilepsia 52(1):158–174
4. Cuschieri S (2019) The STROBE guidelines. Saudi J Anaesth 13(1):S31–S34
5. Iyer A, Prabowo A, Anink J et al (2014) Cell injury and premature neurodegeneration in focal malformations of cortical development. Brain Pathol 24:1–17
6. Ichimura Y, Komatsu M (2010) Selective degradation of p62 by autophagy. Semin Immunopathol 32:431–436
7. Epitashvili N, San Antonio-Arce V, Brandt A et al (2018) Scalp electroencephalographic biomarkers I epilepsy patients with focal cortical dysplasia. Ann Neurol 84(4):564–575
8. Tassi L, Garbelli R, Colombo N et al (2012) Electroclinical, MRI and surgical outcomes in 100 epileptic patients with type II FCD. Epileptic Disord 14(3):257–266
9. Garbelli R, Munari C, De Biasi S, Vitellaro-Zuccarello L, Galli C, Bramerio M, Mai R, Battaglia G, Spreafico R (1999) Taylor's cortical dysplasia: a confocal and ultrastructural immune histochemical study. Brain Pathol 9:445–461

10. Tassi L, Colombo N, Garbelli R, Francione S, Lo Russo G, Mai R, Cardinale F, Cossu M, Ferrario A, Galli C, Bramerio M, Citterio A, Spreafico R (2002) Focal cortical dysplasia: neuropathological subtypes, EEG, neuroimaging and surgical outcome. Brain 125:1719–1732
11. Alonso-Nanclares L, Garbelli R, Sola RG, Pastor J, Tassi L, Spreafico R, DeFelipe J (2005) Microanatomy of the dysplastic neocortex from epileptic patients. Brain 128:58–173
12. Schevon CA, Weiss SA, McKhann G, Goodman RR, Yuste R, Emerson RG (2012) Evidence of a inhibitory restraint of seizure activity in humans. Nat Commun 3:1060
13. Trevelyan AJ, Sussillo D, Watson BO, Yuste R (2006) Modular propagation of epileptiform activity: evidence for an inhibitory veto in neocortex. J Neurosci 26(48):12447–12455
14. Trevelyan AJ, Sussillo D, Yuste R (2007) Feedforward inhibition contributes to the control of epileptiform propagation speed. J Neurosci 27:3383–3387
15. Avoli M, de Curtis M (2011) GABAergic synchronization in the limbic system and its role in the generation of epileptiform activity. Prog Neurobiol 95(2):104–132
16. Elahian B, Lado NE, Mankin E, Vangala S, Misra A, Moxon K, Fried I, Sharan A, Yeasin M, Staba R, Bragin A, Avoli M, Sperling M, Engel J, Weiss SA (2018) Low-voltage fast seizures in humans begin with increased interneuron firing. Ann Neurol 84(4):588–600
17. Andre VM, Flores-Hernandez J, Cepeda C, Starling AJ, Nguyen S, Lobo MK, Vinters HV, Levine MS, Mathern GW (2004) NMDA receptor alterations in neurons from pediatric cortical dysplasia tissue. Cereb Cortex 14:634–646
18. Cepeda C, Chen JC, Wub JY, Fisher RS, Vinters HV, Mathern GW, Levine MS (2014) Pacemaker GABA synaptic activity may contribute to network synchronization in pediatric cortical dysplasia. Neurobiol Dis 62:208–217
19. Avoli M, Louvel J, Mattia D, Olivier A, Esposito V, Pumain R, D'Antuono M (2003) Epileptiform synchronization in the human dysplastic cortex. Epileptic Disord 5(Suppl 2):45–50
20. Lévesque M, Ragsdale D, Avoli M (2019) Evolving mechanistic concepts of epileptiform synchronization and their relevance in curing focal epileptic disorders. Curr Neuropharmacol 17(9):830–842
21. Cohen I, Navarro V, Clemenceau S, Baulac M, Miles R (2002) On the origin of interictal activity in human temporal lobe epilepsy in vitro. Science 298:1418–1421

Cellular and Molecular Life Sciences (2022) 79:16
https://doi.org/10.1007/s00018-021-04088-y

REVIEW

The LGI1 protein: molecular structure, physiological functions and disruption-related seizures

Paul Baudin[1] · Louis Cousyn[1,2] · Vincent Navarro[1,2,3]

Received: 31 August 2021 / Revised: 7 December 2021 / Accepted: 9 December 2021

Abstract
Leucine-rich, glioma inactivated 1 (LGI1) is a secreted glycoprotein, mainly expressed in the brain, and involved in central nervous system development and physiology. Mutations of LGI1 have been linked to autosomal dominant lateral temporal lobe epilepsy (ADLTE). Recently auto-antibodies against LGI1 have been described as the basis for an autoimmune encephalitis, associated with specific motor and limbic epileptic seizures. It is the second most common cause of autoimmune encephalitis. This review presents details on the molecular structure, expression and physiological functions of LGI1, and examines how their disruption underlies human pathologies. Knock-down of LGI1 in rodents reveals that this protein is necessary for normal brain development. In mature brains, LGI1 is associated with Kv1 channels and AMPA receptors, via domain-specific interaction with membrane anchoring proteins and contributes to regulation of the expression and function of these channels. Loss of function, due to mutations or autoantibodies, of this key protein in the control of neuronal activity is a common feature in the genesis of epileptic seizures in ADLTE and anti-LGI1 autoimmune encephalitis.

Keywords LGI1 · Kv1 · AMPA receptors · Genetic epilepsy · Autoimmune encephalitis

Introduction

The epilepsies affect more than 1% of the world population and have diverse causes and prognoses. While mutations of genes encoding ion channels are the most frequent cause of inherited epilepsies, other mechanisms may be involved. For instance leucine-rich, glioma inactivated 1 protein (LGI1) is a secreted synaptic protein and mutations of LGI1 are associated with autosomal dominant lateral temporal lobe epilepsy (ADLTE) [1–3]. In addition, auto-antibodies against LGI1 are linked to an autoimmune encephalitis (AE). It is becoming clear that such auto-immune disorders are responsible for many unexplained drug-resistant epilepsies [4–6]. AE with anti-LGI1 antibodies is the second most frequent type of AE, and is characterized by limbic encephalitis associated with pathognomonic tonic–dystonic seizures (TDS) [7–10].

LGI1 is a member of the LGI protein family. This family consists of secreted glycoproteins with a leucine-rich repeat (LRR) domain and an epitempin (EPTP) domain, which influence several aspects of nervous system development and physiology [11]. LGI1 was initially described as a putative tumor suppressor, since it was found at a chromosomal translocation breakpoint in a glioma cell line [12]. LGI1 was also underexpressed in glioblastoma cells [12–14] and reduced tumor cell proliferation and migration [15–17]. However, the link to cancer remains controversial. LGI1 is expressed at low levels in glial cells [18], and tumors are not associated with either ADLTE [19] or with the AE linked to LGI1 auto-antibodies [20].

This review first examines the molecular structure, expression and physiological functions of LGI1. We then discuss how disruption of LGI1 functions, due to either genetic mutations or auto-antibodies, contributes to genetic or autoimmune epileptic syndromes.

Paul Baudin and Louis Cousyn have contributed equally to this work

✉ Vincent Navarro
vincent.navarro@aphp.fr

[1] Sorbonne Université, Paris Brain Institute – Institut du Cerveau, ICM, INSERM, CNRS, AP-HP, Pitié-Salpêtrière Hospital, Paris, France

[2] AP-HP, Epilepsy Unit, Pitié-Salpêtrière Hospital, DMU Neurosciences, Paris, France

[3] AP-HP, Center of Reference for Rare Epilepsies, Pitié-Salpêtrière Hospital, 47-83 Boulevard de l'Hôpital, 75013 Paris, France

Published online: 30 December 2021

Structure, expression of LGI1 and molecular partners

LGI1 structure and domain organization

The human *LGI1* gene, located in the chromosomal region 10q24, is 39.6 kb long and consists of eight exons and seven introns. It encodes a 2.2 kb transcript. The mouse *LGI1* gene shares 91% of its nucleotide sequence with its human orthologue, resulting in 97% amino acid sequence identity [12, 21]. LGI1 is a protein of 557 amino acids with a molecular weight of 64 kDa [12]. It includes an N-terminal leucine-rich repeat (LRR) domain and a C-terminal epitempin repeat (EPTP) domain, also called epilepsy-associated repeat (EAR) domain (Fig. 1). LGI1 has no transmembrane domain, and cleavage of the signal peptide at the N-terminal extremity produces a mature protein of 60 kDa. LGI1 is a secreted glycoprotein [1–3, 22, 23]. Before secretion, LGI1 is N-glycosylated on the N192, N127 and N422 residues in the endoplasmic reticulum [3, 24].

The LRR domain is composed of four leucine-rich patterns, each of 24 amino acids, and has a cysteine cluster on each side. It is coded by exons 1 to 6 [21, 25, 26]. The EPTP domain is coded by the exons 7 and 8. It contains a seven-bladed beta-propeller, with each blade composed of four-stranded antiparallel β-sheets of around 45 amino acids [26–29]. LRR and EPTP domains are both thought to mediate interactions with other proteins [28, 30].

LGI1 expression profile

Various commercial antibodies directed against LGI1 have been shown to cross-react with other members of the LGI protein family [1, 24, 31, 32]. This lack of specificity might seem to preclude analysis of LGI1 protein distribution by immunohistochemistry. However, anti-LGI1 antibodies purified from auto-immune encephalitis patients are known to be specific [33, 34].

In mouse and human tissue, *LGI1* transcripts are expressed at high levels in the brain, at moderate levels in spinal cord, and are not detected in heart, liver, lungs, placenta, or pancreas [12, 25, 35–37]. In mouse brain, *LGI1* expression is higher in neurons, than in glial cells [24, 35, 38]. *LGI1* is expressed by both excitatory and inhibitory neurons. Ohkawa et al. [33] used dual hybridization in situ to show that in mouse hippocampus, *LGI1* mRNA

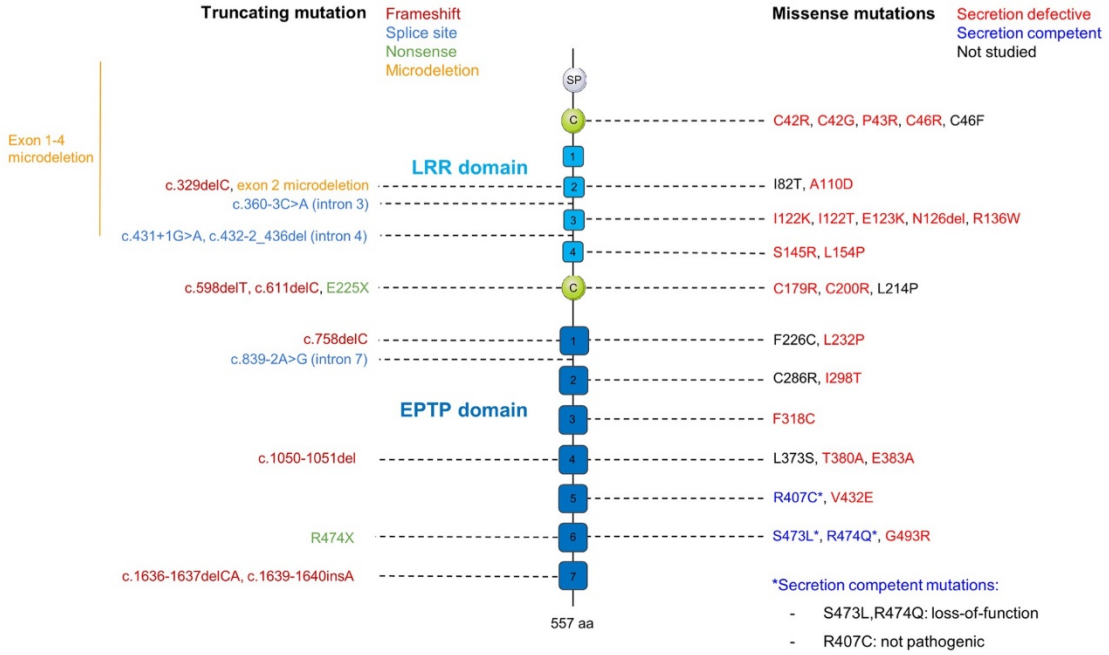

Figure 1 Domain organization of LGI1 and localization of mutations linked to ADLTE. Mutations are distributed along the whole gene sequence, without domain-preference. The list of mutations was compiled from Boillot and Baulac, 2016 [95] and Yamagata and Fukai, 2020 [96]. SP: signal peptide (cleaved in mature protein); C: cysteine cluster

was coexpressed with vGluT1, the vesicular glutamate transporter 1, specific to excitatory neurons, and also with GAD67, glutamate decarboxylase 67kD, an inhibitory cell marker.

In adult mice, *LGI1* mRNA levels are higher in the hippocampus, other limbic structures and neocortex. Hippocampal mRNA signals are most strongly associated with CA3 pyramidal cells and granule cells of the dentate gyrus, with lower expression in the CA1 subfield [1, 39–41]. The application of serum and cerebrospinal fluid (CSF) IgG from anti-LGI1 AE patients to mouse brain sections, revealed strong LGI1 labeling in hippocampal neuropil [7, 33]. In slices from LGI1$^{-/-}$ mice hippocampus, viral re-expression of LGI1 showed expression in both axons and dendrites [42]. A spatially restricted expression suggested LGI1 is secreted in paracrine fashion. LGI1 has been shown to be enriched at synapses [43, 44] and the axon initial segment of hippocampal neurons [45, 46].

LGI1 mRNA is expressed in diverse neocortical areas, with some variability between layers: cortical layers V–VI have higher expression levels than layers I–IV. In adult mice, *LGI1* transcripts are detected in the amygdala, piriform cortex, entorhinal cortex and cerebellum. In the cerebellum, anti-LGI1 antibodies from AE patients induce labeling at basket cell synapses but not on the soma of Purkinje cells. *LGI1* transcripts are absent or expressed at low levels in the olfactory bulb, diencephalon and brainstem [2, 7, 36, 39–41].

A developmental time profile of LGI1 expression has been resolved using Western blot analysis of mouse brain lysates. It shows LGI1 protein first appears during late embryonic development (E15) and increases until adulthood [2, 37, 38, 47–49]. During embryogenesis, LGI1 expression is not restricted to differentiated neurons but is rather diffuse [31, 49]. This diffuse expression seems to be regulated in a spatial and temporal manner [31]. LGI1 is associated with certain immature migrating neurons [31]. This orchestrated time profile sustains the idea that LGI1 plays a significant role in normal brain development (cf. paragraph 3.1).

LGI1 interactors

LGI1 protein network

Protein partners of LGI1 have been identified by affinity purification in knock-in (KI) mice expressing an epitope-tagged LGI1 protein. Partner proteins from the precipitated complex linked to LGI1 were identified by mass spectrometry and Western Blot [50]. The most abundant proteins identified in this way were ADAM22 (A Disintegrin and Metalloproteinase 22) and ADAM23. Less abundant proteins included ADAM11, postsynaptic membrane-associated guanylate kinase proteins (MAGUKs: PSD95, PSD93 and SAP97), Kv1 channels, presynaptic scaffolding proteins (CASK and Lin7), and the 14–3–3 protein, a known partner of ADAM22 [50, 51]. Some of the identified proteins share some functional attributes with LGI1. As we will describe, genetic disruptions of *LGI1* produce animals which exhibit generalized epileptic seizures during early postnatal life [37, 50, 52]. Similar seizures were seen in animals in which *ADAM11* [53], *ADAM22* [54], *ADAM23* [55] and *KCNA1* and *KCNA2*—which code for Kv1 channel subunits [56, 57]—genes are inactivated.

Membrane receptors for LGI1: ADAM11, ADAM22, ADAM23 and Nogo receptor 1

ADAM proteins Members of the ADAM protein family are components of multi-molecular protein complexes which include LGI1 [50]. The extracellular domain of ADAM proteins contains a metalloproteinase-like domain, a disintegrin domain, a cysteine-rich domain and an epidermal growth factor (EGF)-like domain. Three ADAM proteins (ADAM22, ADAM23 and ADAM11) bind to LGI1 and are exclusively expressed in the CNS [58]. They all lack a zinc-binding motif resulting in a catalytically inactive metalloproteinase domain due to the absence of critical amino acids at this site [58–60].

Further insight into the nature of the multi-molecular protein complex was obtained by immunoprecipitation based on tagged ADAM22 rather than LGI1 [44]. Affinity purification showed that partner proteins included LGI family members (LGI1 to LGI4), ADAM proteins (ADAM11, ADAM22 and ADAM23), pre and postsynaptic MAGUKs and scaffold proteins, presynaptic Kv1 channels, and the 14–3–3 protein partner of ADAM22. Close similarities of protein complexes based on tagged LGI1 or ADAM22 suggest they form part of the same pathway.

One isoform of ADAM22 contains an intracellular C-terminal PDZ binding motif specifically interacting with the third PDZ domain of the MAGUK family protein PSD95 [2]. LGI1 and ADAM22 are the two main components of the protein complex associated with PSD95, identified by immunoprecipitation [2]. PSD95 acts as a postsynaptic anchor for proteins at excitatory synapses. It contributes to synaptogenesis and synaptic plasticity among other processes [61]. ADAM11 and ADAM23 lack the PDZ domain binding motif and, therefore, do not directly interact with PSD95, suggesting other partners [55]. Binding to PSD95, suggests ADAM22 and LGI1 are localized at the postsynaptic side of the synaptic cleft. Time-lapse imaging of mCherry tagged ADAM22 and ADAM23 in cell culture, provides further support for a postsynaptic location of ADAM22 and suggests that ADAM23 may be located presynaptically. Axonal transport of ADAM23 was largely anterograde, while ADAM22 was predominantly transported in a retrograde sense [46].

However, this assumed localization may not be completely resolved. ADAM22 is also enriched presynaptically in the axonal compartment at the axon initial segment [46]. Further studies may bring clarification.

ADAM proteins act as chaperone-like proteins for LGI1 as well their role in anchoring LGI1 to the cell membrane. They participate in LGI1 maturation and N-glycosylation processes [46]. Furthermore, ADAM22 and ADAM23 colocalize with LGI1 in axonal transport vesicles [46], suggesting possible interdependent interactions for their transport and subcellular distribution. Membrane expression of LGI1 is strongly decreased in ADAM22$^{-/-}$ and ADAM23$^{-/-}$ mice [62], as is ADAM22 and ADAM23 expression in LGI1$^{-/-}$ animals [50, 62], providing further evidence for interactions between ADAM family proteins and LGI1.

Nogo receptor 1 (NgR1) The Nogo receptor 1, NgR1, is coded by the *RTN4R* gene. It is a 473 amino acid protein, which contains a signal peptide, eight LRR domains, an LRR C-terminal flanking domain cysteine rich, a unique region and a glycosylphosphatidylinositol membrane anchorage site [63]. NgR1 interacts directly with LGI1 [48, 64]. It co-immunoprecipitates with ADAM22 from rat brain lysate suggesting functional interactions exist [48]. However, it is not present in the multi-molecular protein complex recovered by LGI1 purification, nor in those purified by immunoprecipitation based on tagged ADAM22, Kv1, or PSD95 [2, 44, 50, 65]. The absence of NgR1 in these protein complexes is hard to explain. We speculate that NgR1 binding to LGI1 may be weaker than that to the ADAM receptors and associated proteins. This hypothesis could be usefully tested.

One study showed that the NgR1–ADAM22 complex could facilitate binding of LGI1 to ADAM22 [48]. However, LGI1 also bound NgR1 independently in HEK293T cells [48]. In this way LGI1 seems to act as a competitive inhibitor of NgR1, antagonizing the effects of growth inhibition mediated by the ligands Nogo66, myelin-associated glycoprotein (MAG) and oligodendrocyte myelin glycoprotein (OMPG) [48].

Trans-synaptic assemblies of LGI1

Immunoprecipitation studies suggest that LGI1 interacts with both pre and postsynaptic molecules. It is co-immunoprecipitated with presynaptic anti-Kv1.1 antibodies [65], and with postsynaptic anti-PSD95 antibodies [2]. In addition, both pre and postsynaptic proteins are present in the LGI1-purified multi-molecular complex [50]. Moreover, ADAM22 and ADAM23 co-immunoprecipitated from wild-type mice brain lysates but not those derived from LGI1$^{-/-}$ mice [50]. Based on this evidence, the LGI1 protein has been suggested to form a trans-synaptic bridge between the ADAM23 and ADAM22 proteins [50].

Superresolution imaging has recently provided more details on interactions between LGI1 and ADAM22 using an epitope-tagged ADAM22 KI animal [26]. Cryo-electron microscopy demonstrated 1:1, 2:2 and 3:3 ADAM22-LGI1 complexes in solution, in a ratio of approximately 6:3:1. Crystallization of the 2:2 ADAM22–LGI1–LGI1–ADAM22 hetero-tetramer [26] showed that LGI1 binds to the metalloproteinase-like domain of ADAM22 via its EPTP domain. This LGI1–EPTP domain alone is sufficient to mediate ADAM22 binding. This binding is mediated by interactions between the amino acids Trp398, Tyr408 and Tyr409 of ADAM22 and a hydrophobic pocket in the EPTP beta propeller of LGI1. The LGI1–ADAM22 complex dimerizes through binding between LRR domains of pairs of LGI1 molecules, thus forming 2:2 dimer-of-dimer heterotetramers [26] (Fig. 2A).

This dimerization is consistent with a trans-synaptic role for 2:2 ADAM22–LGI1 assemblies. The length of the 2:2 heterotetramer is estimated at 19 nm [26], which is close to the size of the synaptic cleft [66]. Different LGI1–ADAM complexes could be possible, since LGI1 may similarly bind to ADAM22, ADAM23 and ADAM11 [26, 29]. Experimental evidences for the existence of this trans-synaptic complex in vivo, and of the association with different ADAM proteins, remain to be conclusively demonstrated.

In addition to the trans-synaptic complex, LGI1 is also enriched at the axon initial segment, where it colocalizes with ADAM22 and Kv1 channels [45, 46]. Complexes at this site may involve 1:1 or 3:3 ADAM–LGI1 assemblies.

Physiological functions of LGI1

Role of LGI1 during development

LGI1 is required for a normal brain development

LGI1 is expressed during late development in the mouse and expression increases to reach a peak during the first two postnatal weeks (cf. paragraph 2.2). A role for LGI1 in brain development was inferred from structural abnormalities in animals from which LGI1 is genetically deleted. The cortex of early postnatal LGI1−/− mice (P7–P20) shows a diffuse dysplasia together with an abnormal neuronal layer organization [67]. Cortical dysplasia is also induced in mice by conditional inactivation of LGI1 in nestin immunopositive cells, but not in GFAP cells, CAMK2a cells or parvalbumin cells [68]. This data suggests that cortical malformations may result from a loss of LGI1 function in neuronal precursor cells during development. In a different LGI1−/− mouse, cortical malformations were not observed but neuronal loss

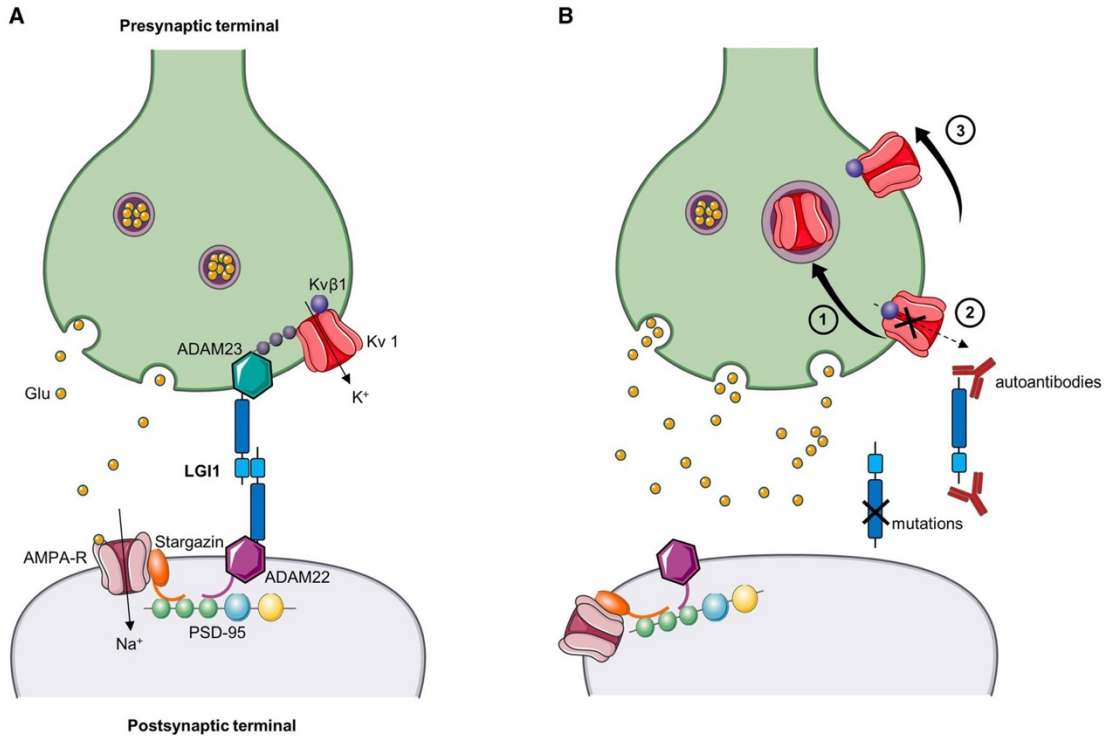

Figure 2 Synaptic organization of LGI1 and disruption by mutations and autoantibodies. **A** Organization of LGI1 in a trans-synaptic complex with protein partners, and indirect functional interactions with presynaptic Kv1 channels and postsynaptic AMPA-Rs. **B** Pathogenic disruptions of LGI1, either by loss-of-function mutation or by autoantibodies. LGI1 alterations were shown to disrupt both Kv1 channels and AMPA-R expression and function. This could result from (1) internalization of Kv1 channels with their protein complex [133], (2) a decrease in Kv1 current, through fast-inactivation mediated by Kvβ1 [65, 86], (3) removal of Kv1 channels and AMPA-R from the synapse, or decreased expression [45, 85, 133, 138]. The loss of Kv1 currents enhances neurotransmitter release and so increases synaptic glutamate levels. Similarly, internalization, loss of channel function or changes in synaptic expression might be involved for AMPA-R channels. These may be the most promising candidate mechanisms that link LGI1 disruption to seizures. We used Servier Medical Art to create the figure

occurred in the CA1 and CA3 areas, and the thickness of the granule cell layer was enhanced with neuronal dispersion [37]. Defects in cerebellar foliation have been detected in P2–P4 LGI1−/− animals together with a reduction in thickness of the external granule cell layer [69].

LGI1 enhances neurite growth and synapse formation and maturation

Several studies suggest that LGI1 controls synapse numbers and activity. In LGI1−/− mice, cortical and hippocampal neurons receive fewer synapses and synaptic signaling is reduced [64, 67]. Conversely, application of LGI1 to cultured hippocampal neurons over 6 days increased synapse numbers [64]. LGI1 stimulates dendritic growth of neurons in culture, and enhances axonal growth by suppressing myelin-induced growth cone collapse [48, 55].

Interactions between LGI1 and the Nogo receptor 1, NgR1, (cf. paragraph 2.3.2) are suggested to mediate these effects on axonal and dendritic growth and also on the formation and maturation of synapses [64]. When occupied by its myelin-derived agonist ligands, NgR1 activates RhoA signaling. This small GTPase acts to limit synapse numbers in development [70], and is crucial for normal neuronal morphogenesis [71]. Hippocampal neurons of NgR1−/− mice receive more synapses than control mice [64]. Work on LGI1−/− mice suggests that LGI1 inhibits RhoA activation via NgR1 [64]. Thus, the NgR1–LGI1 balance would regulate RhoA activity during development, and in this way affect synaptic number and function.

LGI1 may also affect neuronal maturation through its interactions with proteins of the ADAM family. Indeed, LGI1–ADAM22 and LGI1–ADAM23 interactions have been shown to influence neuronal development [55]. Furthermore,

NgR1 and ADAM22 interact directly, although it is not clear whether ADAM proteins and NgR1 participate in independent LGI1-associated pathways, or function as co-receptors for LGI1. Both arrangements may coexist.

Distinct LGI1−/− mouse strains have provided opposite evidence on LGI1 influences on neuronal process growth and synaptogenesis [43, 62]. Electron microscopy provided no evidence that dendritic growth or synaptogenesis were altered in different LGI1−/− mice. The reasons for these inconsistencies are unknown, and further work is needed to understand differences between animals with LGI1 deletions.

LGI1 regulates neuronal myelination

Electron microscopy examination of LGI1−/− mice has suggested LGI1 facilitates myelination in the central and peripheral nervous system [72]. In addition, recent data has shown that LGI1 may control the differentiation of oligodendrocyte precursor cells [38]. In LGI1−/− animals the expression of TSC1 (tuberous sclerosis complex 1) was reduced, which could be responsible for an upregulating activity of the mTORC1 complex in oligodendrocytes. Since mTORC activity is known to affect CNS myelination [73], over-activation in LGI1−/− mice could tend to reduce myelination [38].

Roles of LGI1 in the control of neuronal ion channels

LGI1 regulates presynaptic voltage-dependant K^+ current through Kv1 channels

Kv1 channels are a family of K^+ channels, which are expressed as protein tetramers of 4 alpha subunits, each with 6 transmembrane domains. Eight alpha subunits have been described so far (Kv1.1–Kv1.8). They can assemble into homotetramers or heterotetramers. Different combinations control the biophysics, pharmacology and dynamics of K^+ currents and also sites of membrane insertion and channel mobility [74]. Alpha subunits may be associated with accessory intracellular beta subunits which modify channel properties and currents [75]. Kv1 channels are expressed ubiquitously and exhibit great diversity in expression, topography, and associated subunits [74, 76]. Expression levels are high in axons and terminal boutons as well as somata and dendrites. Kv1 channels are enriched and colocalize with LGI1 in axon initial segments [45, 46].

K^+ currents mediated by Kv1 channels activate at membrane potentials near neuronal firing threshold [77] thus operating to prevent hyperexcitability by limiting and delaying neuronal firing [78, 79]. Kv1 channels control action potential shape, timing and frequency and transmitter release from axonal terminals [79–82]. Kv1.1 subunits tend to promote fast activating, slowly inactivating outward K^+ currents in response to depolarization [74], which are blocked by the specific inhibitor dendrotoxin-K [83, 84].

Interactions between Kv1 and LGI1 suggest that LGI1 affects Kv1 expression and functional properties. Co-immunoprecipitation studies with anti-LGI1 antibodies precipitate Kv1 channels, and reciprocally LGI1 protein was isolated in co-immunoprecipitation work based on anti-Kv1.1 antibodies [50, 65]. However, LGI1 does not bind directly to Kv1, but interactions are mediated indirectly via proteins of the ADAM family and PSD95-like MAGUKs [44]. LGI1 does not interact in the same way with all different Kv1 subunits. In $LGI1^{-/-}$ mice, Kv1.1 and Kv1.2 expression, but not that of Kv1.4 and Kv1.6, was considerably reduced [45, 85].

Functional interactions between LGI1 and Kv1.1 were first described by Schulte et al. in a heterologous expression system [65]. LGI1 potentiated K^+ currents by blocking fast-inactivation of Kv1.1 channels, which is mediated by the beta subunit Kvβ1. Similarly, LGI1, associated with ADAM22, potentiates K^+ currents in HEK293 cells transfected with Kv1.1/Kv1.4 [86]. Furthermore in $LGI1^{-/-}$ mice, axonal expression of Kv1.1 channels in CA3 pyramidal cells is strongly decreased, as well as Kv1.1 currents, which increases neuronal excitability [45]. Dendrotoxin-K, the specific Kv1.1 antagonist, increases neuronal excitability and transmitter release in wild-type neurons, but not in neurons lacking LGI1 [45], confirming that LGI1 acts on Kv1.1 channels.

LGI1 regulates postsynaptic AMPA-R channels

Glutamate-activated ionotropic AMPA receptors (AMPA-R) underlie fast, excitatory synaptic transmission in the mammalian brain. They are heterotetramers formed by diverse assemblies of AMPA-receptor subunits GluR1 to GluR4. When activated by synaptically released glutamate, ion flux through a membrane pore opened in the receptor mediates a postsynaptic excitatory current [87].

While the multi-molecular protein complex derived by immunoprecipitation of tagged LGI1 did not contain AMPA-R, it did contain PSD95 and SAP97 [50], which both interact with AMPA-Rs. PSD95 is a scaffolding protein, which stabilizes AMPA-R at the postsynaptic membrane [61]. It binds, through its two first PDZ domains, to stargazin protein which in turn binds to AMPA-R subunits [88]. SAP97 is another anchoring protein of the MAGUK family. It binds directly through its second PDZ domain, to a PDZ ligand motif on the C-terminus of the GluR1 subunit [89]. An alternatively spliced version of ADAM22 also possesses a C-terminal cytoplasmic PDZ ligand motif which binds to the third PDZ motif of PSD95 [2].

PSD95 overexpression increases the number of AMPA-R expressed at postsynaptic sites and so increases the

amplitude of synaptic events [61, 88]. This effect was abolished in LGI1$^{-/-}$ mice and in KI mice expressing a mutated version of ADAM22 without its PDZ binding site to PSD95 [42, 44]. These data suggest that both LGI1 and ADAM22 are needed for PSD95 membrane anchoring of AMPA-R. Postsynaptic stabilization of AMPA-R is thus indirectly linked to LGI1, via complexes of either ADAM22–PSD95–stargazin or ADAM22–PSD95–SAP97.

LGI1 may also regulate AMPA-R mediated synaptic currents. Application of LGI1 protein to acute slices of rat hippocampus enhanced EPSC amplitudes [2]. Inversely, AMPA-R currents decreased in slices from LGI1$^{-/-}$ mice or from animals expressing mutated ADAM22 [42, 44, 50]. Moreover, AMPA-R currents were restored by LGI1-expressing lentivirus injections in hippocampal slice culture from LGI1$^{-/-}$ mice [42]. Thus LGI1 directly enhances postsynaptic events presumably by recruiting AMPA-Rs to postsynaptic sites. AMPA-R decrease in LGI1$^{-/-}$ mice was not a consequence of seizures in these animals, as the study of Lovero et al. [42] reported AMPA-R alteration in P8 mice, before the emergence of spontaneous seizures (cf. paragraph 4.1.2).

Some of these findings have been disputed in work with other strains of LGI1$^{-/-}$ mice. Other studies reported no differences in AMPA-R expression or in EPSC properties compared to control mice [43, 52]. The reasons for those discrepancies remain unclear. However, a number of different approaches, including LGI1$^{-/-}$ mice, ADAM22 KI mice expressing a non-functional ADAM22, as well as PSD95 overexpression in LGI1$^{-/-}$ and ADAM22-mutated mice, tend to conclude that LGI1 acts on molecules that stabilize AMPA-Rs at post-synaptic sites and so enhances the number of receptors expressed. These findings are congruent with data from protein interaction studies.

Human pathologies related to LGI1 disruption

Genetic disruption of LGI1

Autosomal dominant lateral temporal lobe epilepsy (ADLTE)

In 1995, Ottman et al. reported a familial focal epilepsy with autosomal dominant inheritance linked to chromosome 10q [90]. Predominant auditory features were suggestive of a lateral temporal lobe onset. LGI1 mutations were identified a few years later in several families with autosomal dominant lateral temporal lobe epilepsy [25, 35, 39]. Although heterozygous mutations in reelin, *RELN*, have also been reported in ADLTE families [91], LGI1 mutations remain predominant and are identified in about one-half of cases [35, 39, 92]. A reduced penetrance around 70% is described [25, 35, 39, 92–94].

The first symptoms of ADLTE occur during adolescence or early adulthood. Focal aware seizures—formerly known as 'auras'—with auditory features are the most suggestive manifestations. Ictal auditory symptoms are reported in 62% of patients and seizures are reportedly triggered by sudden sounds, such as a phone ringing for about 20% of them [93]. Initial ictal symptoms include simple sounds, such as buzzing, ringing and humming, or more complex hallucinations, such as voices or music. Positive or negative auditory illusions include altered sound volumes or frequencies. Patients may experience other less common types of focal aware seizures: visual or olfactory hallucinations, dysmnesic features (déjà-vu), or vertigo. 20% of patients describe ictal aphasia [93, 94] as a receptive aphasia, formerly called Wernicke's aphasia. Focal to bilateral tonic–clonic seizures affect about two thirds of patients [93]. Brain MRI scans are frequently normal, while EEG records may reveal temporal epileptiform activity. ADLTE is generally well controlled by antiepileptic drugs. However, drug treatment must be maintained for life, since relapses are frequent when drugs are withdrawn.

LGI1 mutations: a loss-of-function pathophysiology

At least 45 distinct mutations of LGI1 have been identified in ADLTE patients. Lists of mutations were published in 2016 and 2020 [95, 96], and no new mutations of LGI1 have been reported since 2020. Of the 45 mutations, there are 30 missense (67%), 7 frameshift (16%), 4 in splicing donor or acceptor sites (9%), 2 nonsense (4.5%) and 2 microdeletions (4.5%). The mutations are homogeneously distributed throughout the *LGI1* sequence, with no specific domain preference (Fig. 1).

Three lines of LGI1$^{-/-}$ mice have been generated to model pathophysiological effects of a genetic loss of LGI1 function [37, 50, 52]. They exhibit similar behavioral phenotypes. Spontaneous generalized epileptic seizures appeared during the second postnatal week at a frequency of approximately one per hour. Ictal EEG events originated earlier in the hippocampus than in the cortex [37]. Weight gain in these young animals was strongly reduced when seizures emerged and LGI1$^{-/-}$ mice died prematurely during the third postnatal week [37, 50, 52]. No spontaneous epileptic seizures have been observed in LGI1$^{+/-}$ mice. Their survival was normal, as was their fertility [37, 50, 52]. However, at one month, they were more sensitive than LGI1$^{+/+}$ mice to the induction of seizures by the convulsant pentylenetetrazole (PTZ) [50] and by sound stimulation [37]. Thus, LGI1 loss of functions leads to an epileptic phenotype, in a gene-dose dependent manner.

The function of LGI1 mutations associated with ADLTE has been assessed. Frameshift, splice-site, nonsense and deletion mutations seem likely to induce loss of function, since protein sequences are strongly altered. Most missense mutations tested (21/24) show defects in secretion, while 3/24 are secretion competent [96]. The loss of secretion may result from abnormal protein conformations which would lead to premature degradation by quality control machinery. This hypothesis was tested for the E383A mutation, with a transgenic LGI1$^{-/-}$ model made to express the mutated protein [62], and also for the L385R mutation, in a transgenic rat model [97]. Both animal models exhibited generalized seizures and died prematurely between the second and fourth week of life. Both mutated proteins were unstable and prematurely degraded. The chemical corrector, 4-phenylbutyric acid, which acts to stabilize misfolded proteins, improved secretion of the mutated LGI1 and reduced seizure susceptibility in LGI1–E383A mice, suggesting possible conformational alterations in the LGI1–E383A protein [62].

The three secretion-competent LGI1 mutations were also functionally assessed. The S473L mutation impairs LGI1 binding to ADAM22 but not to ADAM23 [26, 62]. The R474Q mutation did not alter LGI1–ADAM22 or LGI1–ADAM23 binding, but did suppress LGI1 dimerization [26]. The third secretion-competent LGI1 mutation, R407C, did not affect LGI1–ADAM binding, or LGI1–LGI1 binding. Lethal epilepsy was not detected in LGI1$^{-/-}$ mice crossed with transgenic mice to overexpress wild-type LGI1 [50]. Expression of LGI1–R407C in LGI1$^{-/-}$ mice rescued the phenotype, as observed with re-expression of wild-type LGI1. Such a rescue did not occur with the S473L and R474Q mutations [26, 62]. These data suggest that the R407C mutation is non-pathogenic. In contrast, for the pathogenic but secretion-competent mutations S473L and R474Q, function is lost but with no major effects on protein conformation. If the R407C mutation is not pathogenic, could its detection in one ADLTE family [98] be a false-positive? Possibly mutation of a different gene, such as reelin [91], might be involved in this family.

In summary, most LGI1 mutations induce a loss of function which is independent of the type of mutation and its localization in the gene, leading to the epileptic disease. Genotype–phenotype correlations are, therefore, absent. No differences were found between truncating and missense mutations, or between the mutations from different sites along the gene. No correlation has been established between different mutations and their respective penetrance [95, 99, 100]. In addition, the behavioral phenotype of LGI1$^{+/-}$ mice overexpressing LGI1–S473L or LGI1–R474Q was similar to that of LGI1$^{+/-}$ mice, suggesting the absence of dominant-negative effects [62].

Autoimmune disruption of LGI1

Autoimmune encephalitis associated with antibodies directed against LGI1

An AE with antibodies targeting the LGI1 protein was reported in 2010 [7, 9]. Before this report, a group of AE syndromes involving central and peripheral nervous systems had been identified and related to antibodies directed against the voltage-gated potassium channel complex, or VGKC [101]. Anti-VGKC antibodies were later shown to target either LGI1 or contactin-associated protein-like2 (CASPR2), which are two protein members of the VGKC complex [7, 9]. The term 'anti-VGKC encephalitis' has now been redefined as two distinct subgroups—anti-LGI1 encephalitis and anti-CASPR2 encephalitis—with distinct symptoms and prognosis.

Anti-LGI1 encephalitis is the second most common subtype of AE-related to anti-neuropil antibodies—after anti-NMDA (N-methyl-d-aspartate) receptor encephalitis. It represents about 25% (range 17.6–34.6%) of all AE subtypes [102–106], and is the most frequently observed subtype in epilepsy units [107].

Demographic characteristics Patients with anti-LGI1 AE have a median age of 65 in the largest cohort ($n = 196$) [20] and from 56 to 60 in other significant cohorts [108–111]—which could explain an association with Alzheimer's disease. Patients are more often males than females in a ratio of 2:1 [8, 10, 20, 108–113]. Data from several cohorts suggests a genetic predisposition exists with a strong association to Human Leukocyte Antigen (HLA) class II alleles. HLA-DRB1*07:01 was found in 88–91% of patients [114–117]. In a large cohort of anti-LGI1 AE patients, non-carriers of this allele were younger (median age: 46), more frequently female, with fewer psychiatric symptoms and less frontal lobe dysfunction [117].

Clinical phenotypes Two brain regions—motor cortex and the mesial temporal lobe—are mainly affected by anti-LGI1 AE and clinical phenotypes differ accordingly (Fig. 3) [10]. When the motor cortex is involved, tonic–dystonic seizures (TDS) are generated. They have also been termed faciobrachial dystonic seizures (FBDS) and are pathognomonic of anti-LGI1 encephalitis. When the mesial temporal lobe is involved, clinical symptoms are indicative of a limbic encephalitis.

Clinical characteristics of TDS are described in Table 1 and supported by a video recording in the Online Resource 1. We tend to prefer the term tonic–dystonic seizure (TDS) to faciobrachial dystonic seizure (FBDS), since face involvement may be variable or absent, although both terms are used. TDS events in video-EEG recordings are

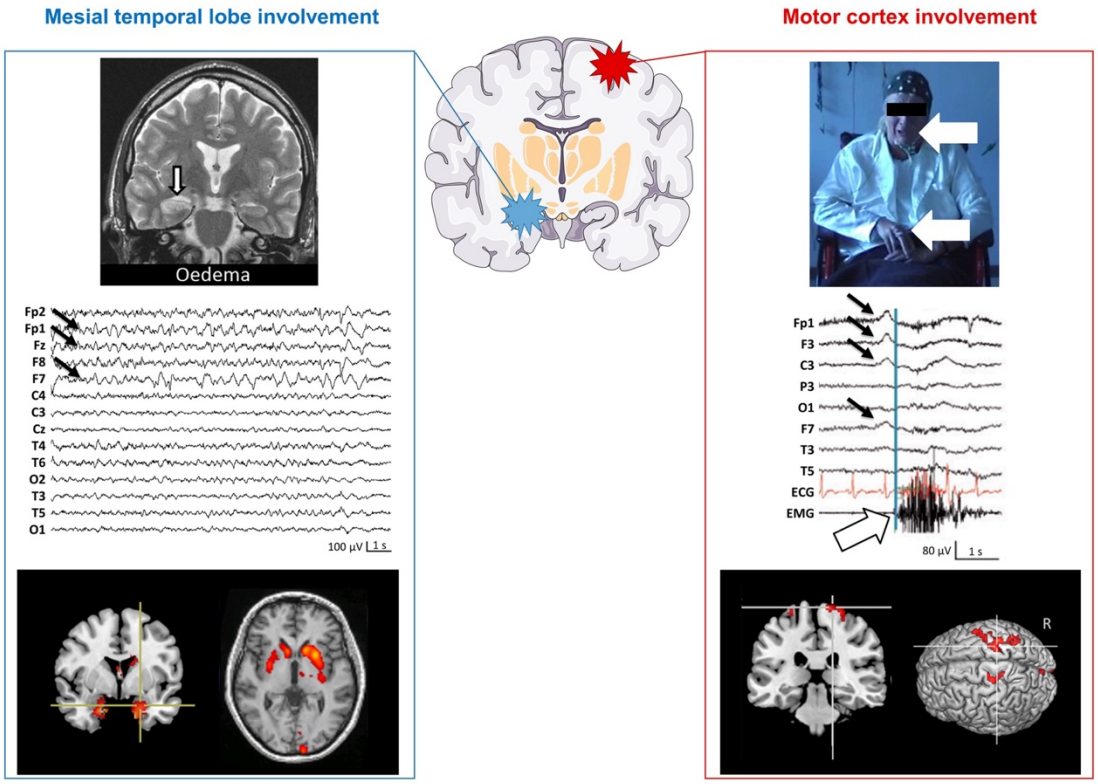

Figure 3 Two main targets of anti-LGI1 encephalitis: mesial temporal lobe and motor cortex. Left, Mesial temporal lobe involvement. Hippocampal hyper-intensity and edema can be found on the brain MRI (top left, coronal T2 image), as well as focal fronto-temporal lobe seizures (middle left; arrows indicate the EEG channels involved in the seizure) on EEG, and hippocampal hypermetabolism on F18–FDG–PET (bottom left; coronal view, superimposed on brain MRI). A striking bilateral striatal hypermetabolism is often detected in anti-LGI1 AE. Right, Motor cortex involvement. Tonic–dystonic seizures (TDS), also called faciobrachial dystonic seizures (FBDS), occur as in the top right (tonic contraction of the right hemiface and arm). Concomitant scalp EEG shows a fronto-central slow wave (middle right, black arrows) before the contralateral muscle contraction (white arrow, right arm EMG). F18–FDG–PET (bottom right) shows a hypermetabolism located on the primary motor cortex. EEG, MRI, and F18–FDG–PET figures are reproduced with permission from Navarro et al. 2016 [10]

preceded by a specific and highly reproducible slow wave [10, 118, 119]. This wave, which can be easily missed, lasts around 500 ms and arises from fronto-central electrodes contralateral to the TDS. EEG analysis using average montage and co-recording of EMG activity of the corresponding muscles can help better identify this slow wave (Fig. 3, right). In EMG records, the tonic component of the TDS is characterized by a 'rhombus'-like shape of duration 1–2 s. Polymyographic records revealed two different EMG profiles associated with TDS [10]. In 2/5 patients, EMG activity was continuous, corresponding to a purely tonic spasm. In 3/5 patients, EMG activity consisted of short rhythmic bursts corresponding to a tonic spasm with superimposed short duration (20–40 ms) myoclonus. The temporal and spatial organization of the jerks was compatible with rapid pyramidal conduction along the corticospinal pathway, as for cortical myoclonus. Taken together, these features support a cortical origin for TDS. Finally, 18F-fluoro-deoxy-glucose (18F-FDG) positron emission tomography (PET) showed a strong increase of metabolism in contralateral primary motor cortex (Fig. 3, right) [10]. These observations suggest TDS originates in the motor cortex. MRI unilateral signal abnormalities and PET strong bilateral hypermetabolism in basal ganglia—in particular the striatum—may be detected in anti-LGI1 AE with TDS [120, 121]. MRI changes (T1 and/or T2 hyperintensities) have also been found in basal ganglia in some patients [120, 121]. While the motor cortex activation may generate the tonic phase of TDS [10], the striatum involvement might cause the dystonic posture [122].

Table 1 Main characteristic of TDS, also called FBDS, in anti-LGI1 AE

Duration	Brief motor events around 1 s
Location	Unilateral hemiface and upper limb (*i.e.*, FBDS), or unilateral upper and lower limbs, and less frequently the trunk
Lateralization	- One side at disease onset - Later, possibly both sides, usually independently - 'A bascule' TDS can also occur and consist in seizures affecting on one side then the other one after a few seconds
Type of movement disorders	- Tonic component, which mimics epileptic spasms - Dystonic component, which can be seen in the fingers and the hand, sometimes associated with brief automatisms
Consequences	- Falls or 'drop attacks' when affecting lower limbs - Vocalization when affecting the head
Consciousness	Rarely associated with a loss of consciousness, but 'classical' seizures from frontal or temporal lobes can emerge after disease progression
Triggers	Sometimes triggered by surprise (ring, etc.), movement or strong (positive or negative) emotions
State of vigilance	Occurring during both awakening and sleep stages
Evolution	Progressive increase in frequency: from 1 TDS per week to 1 TDS every 2–3 min

Limbic encephalitis (Fig. 3, left) is often characterized by mesial temporal lobe seizures and cognitive disorders of subacute onset (typically less than 3 months). Patients with anti-LGI1 AE may initially experience focal mesial temporal lobe seizures (MTLS) with no loss of consciousness, mainly including vegetative symptoms (ascending epigastric feeling, hot and cold feeling, pilo-erection), as well as sudden fear or anxiety, which may be misdiagnosed as psychiatric symptoms. Dysmnesic symptoms (déjà-vu, déjà-vécu) can also occur, but rather in patients suffering from epilepsy in relation to a hippocampal sclerosis as late sequelae, without any active dysimmune encephalitis. The duration of seizures in patients with limbic encephalitis is typically a few seconds, and their frequency may reach 30–40 per day. Focal seizures with impaired awareness and automatisms, and focal to bilateral tonic–clonic seizures and status epilepticus may occur thereafter or as the first manifestation. Cognitive disorders associated with limbic encephalitis center on memory impairment, largely involving episodic verbal and visuospatial memories, due to hippocampal involvement. Confusion and disorientation can also be identified. Mean Mini-Mental State Examination (MMSE) score is 20–23.5 points, indicating a mild cognitive impairment [10, 108, 123, 124]. MRI scan can be normal at the early beginning of the disease, especially when limbic symptoms are discrete. Hippocampal edema can be seen thereafter (Fig. 3, left). At later stage, after the disease is controlled by immunomodulatory drugs, hippocampal edema, defined by an increased volume, disappears. In later stages, signs of hippocampal sclerosis may be seen, including T2/FLAIR hypersignal associated with atrophy and loss of internal structure. 18F-FDG PET highlights hippocampal hypermetabolism in active limbic encephalitis. Frontal and temporal lobe hypometabolism is typical in patients with cognitive impairment.

Hyponatremia is reported in about two thirds of AE patients (39–69%) [7, 9, 10, 20, 108–110, 112]. It is thought to result from a syndrome of inappropriate antidiuretic hormone secretion (SIADH), which may originate from a hypothalamic involvement. Accordingly, a link between hyponatremia and mesial temporal involvement with major cognitive disorders was reported [8, 10]. Peripheral nervous system may also be involved. Peripheral neuropathy and peripheral nerve hyperexcitability have been reported in approximately 5–10% of patients with anti-LGI1 AE [20, 125]. Neuropathic pain usually displays a length-dependent pattern and responds to immunotherapy [125].

Clinical evolution of the disease Anti-LGI1 AE originates either in the motor cortex or the mesial temporal structures. Later, both regions can be affected (Fig. 4). In some patients TDS is initially unilateral and may become bilateral with time. Similarly, the mesial temporal lobe may first be affected unilaterally before the encephalitis may affect bilateral cortical structures and severe cognitive impairment ensues. As knowledge on the syndrome improves, the delay between symptom onset and diagnosis has decreased, from about 12 months a decade ago to 1–3 months at present. The disease usually follows a monophasic time course. Relapses appear to occur in 25–41% of patients, usually in the first year after recovery [126–128]. Sequels of an initial encephalitis usually stem from a delayed diagnosis, associated with a temporal lobe involvement. For instance an early hippocampal edema can evolve into hippocampal sclerosis and induce MTLE. Epileptic seizures persist in about 20% of patients after treatment and recovery from encephalitis. Administration of corticosteroids may protect against this evolution [109, 128]. In older patients, interaction with Alzheimer's disease processes can aggravate cognitive dysfunc-

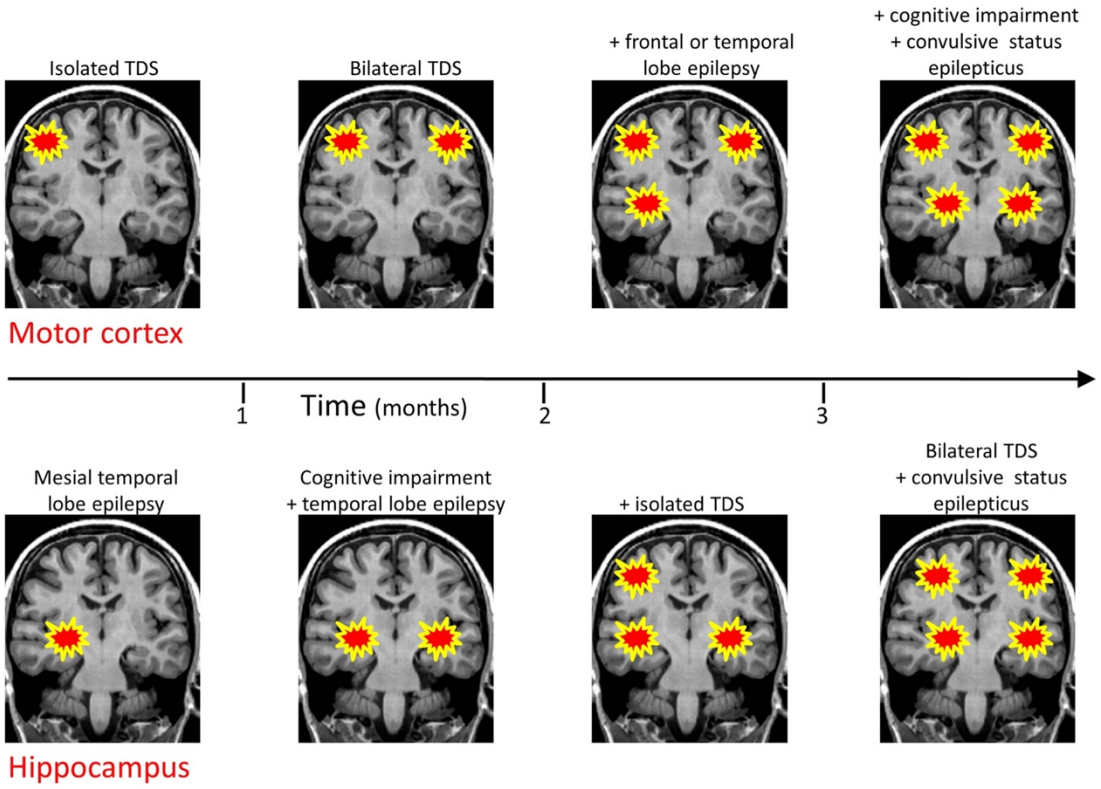

Figure 4 Natural clinical history of anti-LGI1 encephalitis. At disease onset unilateral motor cortex (unilateral TDS, top left) or mesial temporal lobe (isolated mesial temporal lobe seizure, bottom left) may be equally affected structures. The further evolution is characterized by bilateral involvement, leading to either bilateral TDS, or cognitive disorders and MTLS. Finally, both structures, motor cortex and mesial temporal lobe, may be involved. The figure is reproduced with permission from Navarro et al. 2016 [10]

tion. CSF biomarkers should be explored to understand such interactions.

Biological findings Antibodies against LGI1 are mainly IgG4 subtypes [129–131]. They can be identified in both CSF and blood. Antibodies can sometimes be detected only in blood. IgG4 are not pro-inflammatory antibodies, but rather mediate inhibitory protein–protein interactions with their targets [132]. CSF may be normal, and in contrast to anti-NMDAR AE, pleocytosis is rare and moderate. To exert their pathological effects on their antigens, autoantibodies have to access the CNS. Entry of autoantibodies into the CNS can occur via diffusion of IgG, or via the passage of B cells, from the periphery to the CNS, across the blood brain barrier. On study reported B cell IgG synthesis in the CNS of 3 anti-LGI1 AE patients [34]. It is not known if this mechanism could coexist with peripheral IgG diffusion to CNS, which is suggested by the approximately 100 times more concentrated antibodies in the serum compared to the CSF [133]. The role of inflammation in anti-LGI1 AE remains to be clarified. Possibly 'encephalopathy' could be a better description since there may be no direct inflammation, even if hippocampal edema is observed probably resulting from inflammation due to excitotoxic processes [134] (Fig. 3, left).

Treatments TDS and MTLE are poorly controlled by standard antiepileptic drugs [102, 130, 135, 136]. Immunomodulatory and immunosuppressive treatments acting on B lymphocytes and immunoglobulins are more efficient. High doses of corticosteroids with intravenous polyclonal immunoglobulins are often used as a first-line therapy. Alternatively plasma exchange can be used; rituximab has also been used. Other drugs have also been used, such as cyclophosphamide. Only one double-blind placebo-controlled study was reported in anti-LGI1 AE and suggested the efficacy of intravenous polyclonal immunoglobulins in

reducing seizure frequency [137]. However, there is still no class 1 evidence for the use of specific drugs.

Anti-LGI1 antibodies inhibit LGI1

When an antibody has been linked to an autoimmune disease, it is crucial to determine whether it plays an active role in the pathophysiology or whether it is just an effective biomarker. For anti-LGI1 AE, the absence of major inflammatory reactions in the CSF, and IgG4 subtype of most autoantibodies in patients (cf. paragraph 4.2.1) tend to favor a humoral rather than a cellular dysimmune reaction. The reversal of symptoms by immunotherapy also suggests that antibodies mediate AE, and not cytotoxic T lymphocytes which would induce irreversible tissue lesions.

The effects of human anti-LGI1 antibodies have been studied on neurons, in vitro and in vivo. Anti-LGI1 antibodies are polyclonal and recognize epitopes of both the LRR and EPTP domains of LGI1 [33, 34, 133] which have recently been shown to initiate distinct pathophysiological effects [34, 133]. A recent study showed that binding to the EPTP domain impairs interactions between LGI1 and ADAM22 and also ADAM23. This disruption is similar to that induced by the secretion-competent mutation S473L (cf. paragraph 4.1.2). In contrast antibody binding to the LRR domain induces internalization of LGI1 and its membrane receptors.

Antibody injections into mouse hippocampus or cerebral ventricles, reduce expression of Kv1 and AMPA-R channels after 7–14 days [133, 138], reproducing effects observed in LGI1$^{-/-}$ mice (cf. paragraph 4.1.2). AMPA-R expression was also decreased after adding anti-LGI1 antibodies to rat hippocampal neurons in culture medium [33]. Anti-LGI1 antibodies consistently increased neuronal excitability, regardless of the domain targeted, in vitro [34] and in vivo [133, 138]. In vivo infusion of antibodies in mice, reduces synaptic long-term potentiation [133, 138], and induced reversible memory deficits [138].

Surprisingly seizures did not emerge, even if intracerebral anti-LGI1 antibody injection in vivo decreased expression of Kv1 and AMPA-R channels and increased neuronal excitability [133, 138]. AE evolves over weeks or months, so perhaps a 2 week exposure to antibodies, which decreased channel expression by ~ 15%, did not suffice to trigger seizures [138]. For comparison, Kv1.1 expression was reduced by ~ 50% from control in LGI1 KO mice that exhibited frequent generalized seizures [45, 85]. Thus, antibody infusion, critical to demonstrate pathogenicity, may not be the optimal method to explore human epileptic phenotypes.

In summary, LGI1 autoantibodies change neuronal and synaptic function so as to increase neuronal excitability. This loss of LGI1 function in AE is a pathophysiological common point with changes induced by LGI1 mutations in ADLTE patients (Fig. 2B). Seizures represent a common pathological point for AE and ADLTE, even if many clinical symptoms differ sharply.

Conclusion

This review has explored consequences of the loss of function of LGI1, a feature common to ADLTE, a genetic syndrome and AE, an autoimmune disease. Reduced Kv1 currents due to loss of LGI1 function led to an increased neuronal excitability and activity, in both genetic and autoimmune animal models, which seem likely to contribute to epileptic disorders linked to LGI1.

LGI1 also controls AMPA-R expression. Precise details on mechanisms have added support to this previously controversial hypothesis. However, it remains unclear how a reduced efficacy of fast synaptic excitation could favor the emergence of seizures in the genetic syndrome ADLTE or in the immune related AE. The same question remains to be answered for anti-AMPA-R AE patients, who may also exhibit seizures in estimated 28% of patients [139]. One proposed mechanism involves a specific decrease of AMPA-R activity in inhibitory interneurons [33]. However, conditional inactivation of LGI1 in either glutamatergic cells or in parvalbumin-containing interneurons [32] did not support this hypothesis. Conditional inactivation in glutamatergic cells sufficed to trigger seizures, but deletion of LGI1 limited to parvalbumin cells did not induce seizures. Thus seizures in LGI$^{-/-}$ mice may depend on an increased efficacy of excitatory cells rather than a disinhibitory reduction in interneuron efficacy. A reduced AMPA-R expression could also be involved in some non-epileptic symptoms of ADLTE and anti-LGI1 AE patients.

Evidence that LGI1 mutations induce an aberrant brain organization, with abnormal neuronal and synaptic morphologies, suggests that subtle developmental abnormalities may also contribute to seizures resulting from LGI1 mutations in ADLTE. More severe epileptic phenotypes result when LGI1 is deleted during embryogenesis than when deletions are made during adult life [32]. Developmental effects might partly explain different clinical profiles of ADLTE patients and anti-LGI1 AE patients, for whom LGI1 is inhibited in a fully mature brain.

LGI1 has emerged as a major molecular influence on the regulation of brain development, neuronal excitability and synaptic transmission and plasticity. Comprehension of this physiology is crucial to understand normal brain function as well as the pathophysiological syndromes reviewed here. Better understanding of the physiology, pharmacology and biochemistry will open new therapeutic approaches, such as targeting LGI1 molecular partners, or designing anti-epileptic drugs to target the altered cellular and synaptic currents.

Supplementary Information The online version contains supplementary material available at https://doi.org/10.1007/s00018-021-04088-y.

Acknowledgements We thank Richard Miles, for critical reading of the manuscript.

Author contributions Original draft preparation and editing: PB, LC, VN.

Funding Agence nationale de la recherche, 'Investissements d'avenir' program ANR-10–IAIHU-06. Fondation pour la Recherche Médicale, grant FDT202012010523. Fondation Assitance Publique-Hôpitaux de Paris (EPIRES, Marie Laure PLV Merchandising).

Availability of data and materials Not applicable.

Declarations

Conflict of interest V.N. reports personal fees from UCB, Liva Nova, and EISAI, outside the submitted work. The other authors declare that they have no competing interests.

Informed consent The authors affirm that patients provided informed consent for publication of the images in Fig. 3 and in Online Resource 1.

Consent for publication All authors gave their consent for publication.

References

1. Senechal KR, Thaller C, Noebels JL (2005) ADPEAF mutations reduce levels of secreted LGI1, a putative tumor suppressor protein linked to epilepsy. Hum Mol Genet 14:1613–1620. https://doi.org/10.1093/hmg/ddi169
2. Fukata Y, Adesnik H, Iwanaga T et al (2006) Epilepsy-related ligand/receptor complex LGI1 and ADAM22 regulate synaptic transmission. Science 313:1792–1795. https://doi.org/10.1126/science.1129947
3. Sirerol-Piquer MS, Ayerdi-Izquierdo A, Morante-Redolat JM et al (2006) The epilepsy gene LGI1 encodes a secreted glycoprotein that binds to the cell surface. Hum Mol Genet 15:3436–3445. https://doi.org/10.1093/hmg/ddl421
4. Dalmau J, Geis C, Graus F (2017) Autoantibodies to synaptic receptors and neuronal cell surface proteins in autoimmune diseases of the central nervous system. Physiol Rev 97:839–887. https://doi.org/10.1152/physrev.00010.2016
5. Goodfellow JA, Mackay GA (2019) Autoimmune encephalitis. J R Coll Physicians Edinb 49:287–294. https://doi.org/10.4997/JRCPE.2019.407
6. Husari KS, Dubey D (2019) Autoimmune epilepsy. Neurotherapeutics 16:685–702. https://doi.org/10.1007/s13311-019-00750-3
7. Irani SR, Alexander S, Waters P et al (2010) Antibodies to Kv1 potassium channel-complex proteins leucine-rich, glioma inactivated 1 protein and contactin-associated protein-2 in limbic encephalitis, Morvan's syndrome and acquired neuromyotonia. Brain 133:2734–2748. https://doi.org/10.1093/brain/awq213
8. Irani SR, Michell AW, Lang B et al (2011) Faciobrachial dystonic seizures precede Lgi1 antibody limbic encephalitis. Ann Neurol 69:892–900. https://doi.org/10.1002/ana.22307
9. Lai M, Huijbers MG, Lancaster E et al (2010) Investigation of LGI1 as the antigen in limbic encephalitis previously attributed to potassium channels: a case series. Lancet Neurol 9:776–785. https://doi.org/10.1016/S1474-4422(10)70137-X
10. Navarro V, Kas A, Apartis E et al (2016) Motor cortex and hippocampus are the two main cortical targets in LGI1-antibody encephalitis. Brain 139:1079–1093. https://doi.org/10.1093/brain/aww012
11. Pakozdy A, Patzl M, Zimmermann L et al (2015) LGI proteins and epilepsy in human and animals. J Vet Intern Med 29:997–1005. https://doi.org/10.1111/jvim.12610
12. Chernova OB, Somerville RP, Cowell JK (1998) A novel gene, LGI1, from 10q24 is rearranged and downregulated in malignant brain tumors. Oncogene 17:2873–2881. https://doi.org/10.1038/sj.onc.1202481
13. Krex D, Hauses M, Appelt H et al (2002) Physical and functional characterization of the human LGI1 gene and its possible role in glioma development. Acta Neuropathol 103:255–266. https://doi.org/10.1007/s004010100463
14. Besleaga R, Montesinos-Rongen M, Perez-Tur J et al (2003) Expression of the LGI1 gene product in astrocytic gliomas: downregulation with malignant progression. Virchows Arch 443:561–564. https://doi.org/10.1007/s00428-003-0874-3
15. Kunapuli P, Chitta KS, Cowell JK (2003) Suppression of the cell proliferation and invasion phenotypes in glioma cells by the LGI1 gene. Oncogene 22:3985–3991. https://doi.org/10.1038/sj.onc.1206584
16. Kunapuli P, Kasyapa CS, Hawthorn L, Cowell JK (2004) LGI1, a putative tumor metastasis suppressor gene, controls in vitro invasiveness and expression of matrix metalloproteinases in glioma cells through the ERK1/2 pathway. J Biol Chem 279:23151–23157. https://doi.org/10.1074/jbc.M314192200
17. Nadia G, Masola V, Quartesan S et al (2006) Increased expression ofLGI1 gene triggers growth inhibition and apoptosis of neuroblastoma cells. J Cell Physiol 207:711–721. https://doi.org/10.1002/jcp.20627
18. Piepoli T, Jakupoglu C, Gu W et al (2006) Expression studies in gliomas and glial cells do not support a tumor suppressor role for LGI11. Neuro Oncol 8:96–108. https://doi.org/10.1215/15228517-2005-006
19. Gu W, Brodtkorb E, Piepoli T et al (2005) LGI1: a gene involved in epileptogenesis and glioma progression? Neurogenetics 6:59–66. https://doi.org/10.1007/s10048-005-0216-5
20. Gadoth A, Pittock SJ, Dubey D et al (2017) Expanded phenotypes and outcomes among 256 LGI1/CASPR2-IgG-positive patients. Ann Neurol 82:79–92. https://doi.org/10.1002/ana.24979
21. Somerville RPT, Chernova O, Liu S et al (2000) Identification of the promoter, genomic structure, and mouse ortholog of LGI1. Mamm Genome 11:622–627. https://doi.org/10.1007/s003350010128
22. Chabrol E, Gourfinkel-An I, Scheffer IE et al (2007) Absence of mutations in the LGI1 receptor ADAM22 gene in autosomal dominant lateral temporal epilepsy. Epilepsy Res 76:41–48. https://doi.org/10.1016/j.eplepsyres.2007.06.014
23. de Bellescize J, Boutry N, Chabrol E et al (2009) A novel three base-pair LGI1 deletion leading to loss of function in a family with autosomal dominant lateral temporal epilepsy and migraine-like episodes. Epilepsy Res 85:118–122. https://doi.org/10.1016/j.eplepsyres.2009.02.007
24. Head K, Gong S, Joseph S et al (2007) Defining the expression pattern of the LGI1 gene in BAC transgenic mice. Mamm Genome 18:328–337. https://doi.org/10.1007/s00335-007-9024-6
25. Gu W, Wevers A, Schröder H et al (2002) The LGI1 gene involved in lateral temporal lobe epilepsy belongs to a new

subfamily of leucine-rich repeat proteins. FEBS Lett 519:71–76. https://doi.org/10.1016/S0014-5793(02)02713-8
26. Yamagata A, Miyazaki Y, Yokoi N et al (2018) Structural basis of epilepsy-related ligand–receptor complex LGI1–ADAM22. Nat Commun 9:1546. https://doi.org/10.1038/s41467-018-03947-w
27. Scheel H (2002) A common protein interaction domain links two recently identified epilepsy genes. Hum Mol Genet 11:1757–1762. https://doi.org/10.1093/hmg/11.15.1757
28. Staub E, Pérez-Tur J, Siebert R et al (2002) The novel EPTP repeat defines a superfamily of proteins implicated in epileptic disorders. Trends Biochem Sci 27:441–444. https://doi.org/10.1016/S0968-0004(02)02163-1
29. Leonardi E, Andreazza S, Vanin S et al (2011) A computational model of the LGI1 protein suggests a common binding site for ADAM proteins. PLoS ONE 6:e18142. https://doi.org/10.1371/journal.pone.0018142
30. Kobe B, Kajava AV (2001) The leucine-rich repeat as a protein recognition motif. Curr Opin Struct Biol 11:725–732. https://doi.org/10.1016/s0959-440x(01)00266-4
31. Silva J, Wang G, Cowell JK (2011) The temporal and spatial expression pattern of the LGI1 epilepsy predisposition gene during mouse embryonic cranial development. BMC Neurosci 12:43. https://doi.org/10.1186/1471-2202-12-43
32. Boillot M, Huneau C, Marsan E et al (2014) Glutamatergic neuron-targeted loss of LGI1 epilepsy gene results in seizures. Brain 137:2984–2996. https://doi.org/10.1093/brain/awu259
33. Ohkawa T, Fukata Y, Yamasaki M et al (2013) Autoantibodies to epilepsy-related LGI1 in limbic encephalitis neutralize LGI1-ADAM22 interaction and reduce synaptic AMPA receptors. J Neurosci 33:18161–18174. https://doi.org/10.1523/JNEUROSCI.3506-13.2013
34. Kornau H, Kreye J, Stumpf A et al (2020) Human cerebrospinal fluid monoclonal LGI1 autoantibodies increase neuronal excitability. Ann Neurol 87:405–418. https://doi.org/10.1002/ana.25666
35. Morante-Redolat JM (2002) Mutations in the LGI1/Epitempin gene on 10q24 cause autosomal dominant lateral temporal epilepsy. Hum Mol Genet 11:1119–1128. https://doi.org/10.1093/hmg/11.9.1119
36. Furlan S, Roncaroli F, Forner F et al (2006) The LGI1/epitempin gene encodes two protein isoforms differentially expressed in human brain. J Neurochem 98:985–991. https://doi.org/10.1111/j.1471-4159.2006.03939.x
37. Chabrol E, Navarro V, Provenzano G et al (2010) Electroclinical characterization of epileptic seizures in leucine-rich, glioma-inactivated 1-deficient mice. Brain 133:2749–2762. https://doi.org/10.1093/brain/awq171
38. Xie Y-J, Zhou L, Wang Y et al (2018) Leucine-rich glioma inactivated 1 promotes oligodendrocyte differentiation and myelination via TSC-mTOR signaling. Front Mol Neurosci 11:231. https://doi.org/10.3389/fnmol.2018.00231
39. Kalachikov S, Evgrafov O, Ross B et al (2002) Mutations in LGI1 cause autosomal-dominant partial epilepsy with auditory features. Nat Genet 30:335–341. https://doi.org/10.1038/ng832
40. Herranz-Pérez V, Olucha-Bordonau FE, Morante-Redolat JM, Pérez-Tur J (2010) Regional distribution of the leucine-rich glioma inactivated (LGI) gene family transcripts in the adult mouse brain. Brain Res 1307:177–194. https://doi.org/10.1016/j.brainres.2009.10.013
41. Smedfors G, Olson L, Karlsson TE (2018) A Nogo-like signaling perspective from birth to adulthood and in old age: brain expression patterns of ligands, receptors and modulators. Front Mol Neurosci 11:42. https://doi.org/10.3389/fnmol.2018.00042
42. Lovero KL, Fukata Y, Granger AJ et al (2015) The LGI1–ADAM22 protein complex directs synapse maturation through regulation of PSD-95 function. Proc Natl Acad Sci USA 112:E4129–E4137. https://doi.org/10.1073/pnas.1511910112
43. Boillot M, Lee C-Y, Allene C et al (2016) LGI1 acts presynaptically to regulate excitatory synaptic transmission during early postnatal development. Sci Rep 6:21769. https://doi.org/10.1038/srep21769
44. Fukata Y, Chen X, Chiken S et al (2021) LGI1–ADAM22–MAGUK configures transsynaptic nanoalignment for synaptic transmission and epilepsy prevention. Proc Natl Acad Sci USA 118:e2022580118. https://doi.org/10.1073/pnas.2022580118
45. Seagar M, Russier M, Caillard O et al (2017) LGI1 tunes intrinsic excitability by regulating the density of axonal Kv1 channels. Proc Natl Acad Sci USA 114:7719–7724. https://doi.org/10.1073/pnas.1618656114
46. Hivert B, Marien L, Agbam KN, Faivre-Sarrailh C (2019) ADAM22 and ADAM23 modulate the targeting of the Kv1 channel-associated protein LGI1 to the axon initial segment. J Cell Sci. https://doi.org/10.1242/jcs.219774
47. Ribeiro PAO, Sbragia L, Gilioli R et al (2008) Expression profile of Lgi1 gene in mouse brain during development. J Mol Neurosci 35:323–329. https://doi.org/10.1007/s12031-008-9096-0
48. Thomas R, Favell K, Morante-Redolat J et al (2010) LGI1 Is a nogo receptor 1 ligand that antagonizes myelin-based growth inhibition. J Neurosci 30:6607–6612. https://doi.org/10.1523/JNEUROSCI.5147-09.2010
49. Kusuzawa S, Honda T, Fukata Y et al (2012) Leucine-rich glioma inactivated 1 (Lgi1), an epilepsy-related secreted protein, has a nuclear localization signal and localizes to both the cytoplasm and the nucleus of the caudal ganglionic eminence neurons: nuclear translocation of Lgi1. Eur J Neurosci 36:2284–2292. https://doi.org/10.1111/j.1460-9568.2012.08129.x
50. Fukata Y, Lovero KL, Iwanaga T et al (2010) Disruption of LGI1–linked synaptic complex causes abnormal synaptic transmission and epilepsy. Proc Natl Acad Sci USA 107:3799–3804. https://doi.org/10.1073/pnas.0914537107
51. Gödde NJ, D'Abaco GM, Paradiso L, Novak U (2006) Efficient ADAM22 surface expression is mediated by phosphorylation-dependent interaction with 14–3-3 protein family members. J Cell Sci 119:3296–3305. https://doi.org/10.1242/jcs.03065
52. Yu YE, Wen L, Silva J et al (2010) Lgi1 null mutant mice exhibit myoclonic seizures and CA1 neuronal hyperexcitability. Hum Mol Genet 19:1702–1711. https://doi.org/10.1093/hmg/ddq047
53. Kole MJ, Qian J, Waase MP et al (2015) Selective loss of presynaptic potassium channel clusters at the cerebellar basket cell terminal pinceau in adam11 mutants reveals their role in ephaptic control of Purkinje cell firing. J Neurosci 35:11433–11444. https://doi.org/10.1523/JNEUROSCI.1346-15.2015
54. Sagane K, Hayakawa K, Kai J et al (2005) Ataxia and peripheral nerve hypomyelination in ADAM22-deficient mice. BMC Neurosci 6:33. https://doi.org/10.1186/1471-2202-6-33
55. Owuor K, Harel NY, Englot DJ et al (2009) LGI1-associated epilepsy through altered ADAM23-dependent neuronal morphology. Mol Cell Neurosci 42:448–457. https://doi.org/10.1016/j.mcn.2009.09.008
56. Smart SL, Lopantsev V, Zhang CL et al (1998) Deletion of the KV1.1 potassium channel causes epilepsy in mice. Neuron 20:809–819. https://doi.org/10.1016/S0896-6273(00)81018-1
57. Brew HM, Gittelman JX, Silverstein RS et al (2007) Seizures and reduced life span in mice lacking the potassium channel subunit Kv1.2, but hypoexcitability and enlarged Kv1 currents in auditory neurons. J Neurophysiol 98:1501–1525. https://doi.org/10.1152/jn.00640.2006
58. Edwards D, Handsley M, Pennington C (2008) The ADAM metalloproteinases. Mol Aspects Med 29:258–289. https://doi.org/10.1016/j.mam.2008.08.001

59. Sagane K, Yamazaki K, Mizui Y, Tanaka I (1999) Cloning and chromosomal mapping of mouse ADAM11, ADAM22 and ADAM23. Gene 236:79–86. https://doi.org/10.1016/s0378-1119(99)00253-x
60. Liu H, Shim AHR, He X (2009) Structural characterization of the ectodomain of a disintegrin and metalloproteinase-22 (ADAM22), a neural adhesion receptor instead of metalloproteinase. J Biol Chem 284:29077–29086. https://doi.org/10.1074/jbc.M109.014258
61. El-Husseini AE, Schnell E, Chetkovich DM et al (2000) PSD-95 involvement in maturation of excitatory synapses. Science 290:1364–1368
62. Yokoi N, Fukata Y, Kase D et al (2015) Chemical corrector treatment ameliorates increased seizure susceptibility in a mouse model of familial epilepsy. Nat Med 21:19–26. https://doi.org/10.1038/nm.3759
63. Fournier AE, GrandPre T, Strittmatter SM (2001) Identification of a receptor mediating Nogo-66 inhibition of axonal regeneration. Nature 409:341–346. https://doi.org/10.1038/35053072
64. Thomas RA, Gibon J, Chen CXQ et al (2018) The Nogo receptor ligand LGI1 regulates synapse number and synaptic activity in hippocampal and cortical neurons. eNeuro. https://doi.org/10.1523/ENEURO.0185-18.2018
65. Schulte U, Thumfart J-O, Klöcker N et al (2006) The epilepsy-linked Lgi1 protein assembles into presynaptic Kv1 channels and inhibits inactivation by Kvbeta1. Neuron 49:697–706. https://doi.org/10.1016/j.neuron.2006.01.033
66. Savtchenko LP, Rusakov DA (2007) The optimal height of the synaptic cleft. Proc Natl Acad Sci U S A 104:1823–1828. https://doi.org/10.1073/pnas.0606636104
67. Silva J, Sharma S, Cowell JK (2015) Homozygous deletion of the LGI1 gene in mice leads to developmental abnormalities resulting in cortical dysplasia: loss of LGI1 leads to cortical dysplasia. Brain Pathol 25:587–597. https://doi.org/10.1111/bpa.12225
68. Silva J, Qin H, Cowell JK (2019) Selective inactivation of LGI1 in neuronal precursor cells leads to cortical dysplasia in mice. Genesis 57:e23268. https://doi.org/10.1002/dvg.23268
69. Xie Y-J, Zhou L, Jiang N et al (2015) Essential roles of leucine-rich glioma inactivated 1 in the development of embryonic and postnatal cerebellum. Sci Rep 5:7827. https://doi.org/10.1038/srep07827
70. Wills ZP, Mandel-Brehm C, Mardinly AR et al (2012) The Nogo receptor family restricts synapse number in the developing hippocampus. Neuron 73:466–481. https://doi.org/10.1016/j.neuron.2011.11.029
71. Luo L (2000) Rho GTPases in neuronal morphogenesis. Nat Rev Neurosci 1:173–180. https://doi.org/10.1038/35044547
72. Silva J, Sharma S, Hughes B et al (2010) Homozygous inactivation of the LGI1 gene results in hypomyelination in the peripheral and central nervous systems: hypomyelination in LGI1 null mice. J Neurosci Res 88:3328–3336. https://doi.org/10.1002/jnr.22496
73. Lebrun-Julien F, Bachmann L, Norrmén C et al (2014) Balanced mTORC1 activity in oligodendrocytes is required for accurate CNS myelination. J Neurosci 34:8432–8448. https://doi.org/10.1523/JNEUROSCI.1105-14.2014
74. Ovsepian SV, LeBerre M, Steuber V et al (2016) Distinctive role of KV1.1 subunit in the biology and functions of low threshold K+ channels with implications for neurological disease. Pharmacol Ther 159:93–101. https://doi.org/10.1016/j.pharmthera.2016.01.005
75. Dodson PD, Forsythe ID (2004) Presynaptic K+ channels: electrifying regulators of synaptic terminal excitability. Trends Neurosci 27:210–217. https://doi.org/10.1016/j.tins.2004.02.012
76. Trimmer JS (2015) Subcellular localization of K+ channels in mammalian brain neurons: remarkable precision in the midst of extraordinary complexity. Neuron 85:238–256. https://doi.org/10.1016/j.neuron.2014.12.042
77. Guan D, Lee JCF, Tkatch T et al (2006) Expression and biophysical properties of Kv1 channels in supragranular neocortical pyramidal neurones. J Physiol 571:371–389. https://doi.org/10.1113/jphysiol.2005.097006
78. Guan D, Lee JCF, Higgs MH et al (2007) Functional roles of Kv1 channels in neocortical pyramidal neurons. J Neurophysiol 97:1931–1940. https://doi.org/10.1152/jn.00933.2006
79. Cudmore RH, Fronzaroli-Molinieres L, Giraud P, Debanne D (2010) Spike-time precision and network synchrony are controlled by the homeostatic regulation of the D-type potassium current. J Neurosci 30:12885–12895. https://doi.org/10.1523/JNEUROSCI.0740-10.2010
80. Yellen G (2002) The voltage-gated potassium channels and their relatives. Nature 419:35–42. https://doi.org/10.1038/nature00978
81. Ovsepian SV, Steuber V, Le Berre M et al (2013) A defined heteromeric K_V1 channel stabilizes the intrinsic pacemaking and regulates the output of deep cerebellar nuclear neurons to thalamic targets: K_V1 channel governs cerebellar output to thalamus. J Physiol 591:1771–1791. https://doi.org/10.1113/jphysiol.2012.249706
82. Guan D, Pathak D, Foehring RC (2018) Functional roles of Kv1-mediated currents in genetically identified subtypes of pyramidal neurons in layer 5 of mouse somatosensory cortex. J Neurophysiol 120:394–408. https://doi.org/10.1152/jn.00691.2017
83. Wang FC, Bell N, Reid P et al (1999) Identification of residues in dendrotoxin K responsible for its discrimination between neuronal K+ channels containing Kv1.1 and 1.2 alpha subunits. Eur J Biochem 263:222–229. https://doi.org/10.1046/j.1432-1327.1999.00494.x
84. Harvey AL, Robertson B (2004) Dendrotoxins: structure-activity relationships and effects on potassium ion channels. CMC 11:3065–3072. https://doi.org/10.2174/0929867043363820
85. Zhou L, Zhou L, Su L et al (2018) Celecoxib ameliorates seizure susceptibility in autosomal dominant lateral temporal epilepsy. J Neurosci 38:3346–3357. https://doi.org/10.1523/JNEUROSCI.3245-17.2018
86. Lancaster E, Burnor E, Zhang J, Lancaster E (2019) ADAM23 is a negative regulator of Kv1.1/Kv1.4 potassium currents. Neurosci Lett 704:159–163. https://doi.org/10.1016/j.neulet.2019.04.012
87. Henley JM, Nair JD, Seager R et al (2021) Kainate and AMPA receptors in epilepsy: cell biology, signalling pathways and possible crosstalk. Neuropharmacology 195:108569. https://doi.org/10.1016/j.neuropharm.2021.108569
88. Schnell E, Sizemore M, Karimzadegan S et al (2002) Direct interactions between PSD-95 and stargazin control synaptic AMPA receptor number. Proc Natl Acad Sci U S A 99:13902–13907. https://doi.org/10.1073/pnas.172511199
89. von Ossowski L, Tossavainen H, von Ossowski I et al (2006) Peptide binding and NMR analysis of the interaction between SAP97 PDZ2 and GluR-A: potential involvement of a disulfide bond. Biochemistry 45:5567–5575. https://doi.org/10.1021/bi051989
90. Ottman R, Risch N, Hauser WA et al (1995) Localization of a gene for partial epilepsy to chromosome 10q. Nat Genet 10:56–60. https://doi.org/10.1038/ng0595-56
91. Dazzo E, Fanciulli M, Serioli E et al (2015) Heterozygous reelin mutations cause autosomal-dominant lateral temporal epilepsy. Am J Hum Genet 96:992–1000. https://doi.org/10.1016/j.ajhg.2015.04.020
92. Michelucci R, Poza JJ, Sofia V et al (2003) Autosomal dominant lateral temporal epilepsy: clinical spectrum, new epitempin mutations, and genetic heterogeneity in seven European families:

familial lateral temporal epilepsy. Epilepsia 44:1289–1297. https://doi.org/10.1046/j.1528-1157.2003.20003.x
93. Michelucci R, Pasini E, Malacrida S et al (2013) Low penetrance of autosomal dominant lateral temporal epilepsy in Italian families without LGI1 mutations. Epilepsia 54:1288–1297. https://doi.org/10.1111/epi.12194
94. Bisulli F, Naldi I, Baldassari S et al (2014) Autosomal dominant partial epilepsy with auditory features: a new locus on chromosome 19q13.11-q13.31. Epilepsia 55:841–848. https://doi.org/10.1111/epi.12560
95. Boillot M, Baulac S (2016) Genetic models of focal epilepsies. J Neurosci Methods 260:132–143. https://doi.org/10.1016/j.jneumeth.2015.06.003
96. Yamagata A, Fukai S (2020) Insights into the mechanisms of epilepsy from structural biology of LGI1–ADAM22. Cell Mol Life Sci 77:267–274. https://doi.org/10.1007/s00018-019-03269-0
97. Baulac S, Ishida S, Mashimo T et al (2012) A rat model for LGI1-related epilepsies. Hum Mol Genet 21:3546–3557. https://doi.org/10.1093/hmg/dds184
98. Striano P, Busolin G, Santulli L et al (2011) Familial temporal lobe epilepsy with psychic auras associated with a novel LGI1 mutation. Neurology 76:1173–1176. https://doi.org/10.1212/WNL.0b013e318212ab2e
99. Rosanoff MJ, Ottman R (2008) Penetrance of LGI1 mutations in autosomal dominant partial epilepsy with auditory features. Neurology 71:567–571. https://doi.org/10.1212/01.wnl.0000323926.77565.ee
100. Nobile C, Michelucci R, Andreazza S et al (2009) LGI1 mutations in autosomal dominant and sporadic lateral temporal epilepsy. Hum Mutat 30:530–536. https://doi.org/10.1002/humu.20925
101. Vincent A, Buckley C, Schott JM et al (2004) Potassium channel antibody-associated encephalopathy: a potentially immunotherapy-responsive form of limbic encephalitis. Brain 127:701–712. https://doi.org/10.1093/brain/awh077
102. de Bruijn MAAM, van Sonderen A, van Coevorden-Hameete MH et al (2019) Evaluation of seizure treatment in anti-LGI1, anti-NMDAR, and anti-GABA $_{B}$ R encephalitis. Neurology 92:e2185–e2196. https://doi.org/10.1212/WNL.0000000000007475
103. Shen C, Fang G, Yang F et al (2020) Seizures and risk of epilepsy in anti-NMDAR, anti-LGI1, and anti-GABABR encephalitis. Ann Clin Transl Neurol 7:1392–1399. https://doi.org/10.1002/acn3.51137
104. Ilyas-Feldmann M, Prüß H, Holtkamp M (2021) Long-term seizure outcome and antiseizure medication use in autoimmune encephalitis. Seizure 86:138–143. https://doi.org/10.1016/j.seizure.2021.02.010
105. Qiao S, Wu H-K, Liu L-L et al (2021) Characteristics and prognosis of autoimmune encephalitis in the East of China: a multicenter study. Front Neurol 12:642078. https://doi.org/10.3389/fneur.2021.642078
106. Shan W, Yang H, Wang Q (2021) Neuronal surface antibody-medicated autoimmune encephalitis (limbic encephalitis) in China: a multiple-center retrospective study. Front Immunol 12:621599. https://doi.org/10.3389/fimmu.2021.621599
107. Cousyn L, Lambrecq V, Houot M et al (2021) Seizures in autoimmune encephalitis: specific features from a systematic comparative study. Epileptic Disord. https://doi.org/10.1684/epd.2021.1355
108. Qiao S, Wu H, Liu L et al (2021) Clinical features and long-term outcomes of anti-leucine-rich glioma-inactivated 1 encephalitis: a multi-center study. NDT 17:203–212. https://doi.org/10.2147/NDT.S292343
109. Lin N, Liu Q, Chen J et al (2021) Long-term seizure outcomes in patients with anti-leucine-rich glioma-inactivated 1 encephalitis. Epilepsy Behav 122:108159. https://doi.org/10.1016/j.yebeh.2021.108159
110. Li T-R, Zhang Y-D, Wang Q et al (2021) Clinical characteristics and long-term prognosis of anti-LGI1 encephalitis: a single-center cohort study in Beijing. China Front Neurol 12:674368. https://doi.org/10.3389/fneur.2021.674368
111. Zhao Q, Sun L, Zhao D et al (2021) Clinical features of anti-leucine-rich glioma-inactivated 1 encephalitis in northeast China. Clin Neurol Neurosurg 203:106542. https://doi.org/10.1016/j.clineuro.2021.106542
112. van Sonderen A, Schreurs MWJ, de Bruijn MAAM et al (2016) The relevance of VGKC positivity in the absence of LGI1 and Caspr2 antibodies. Neurology 86:1692–1699. https://doi.org/10.1212/WNL.0000000000002637
113. Binks SNM, Veldsman M, Easton A et al (2021) Residual fatigue and cognitive deficits in patients after leucine-rich glioma-inactivated 1 antibody encephalitis. JAMA Neurol 78:617. https://doi.org/10.1001/jamaneurol.2021.0477
114. Kim T-J, Lee S-T, Moon J et al (2017) Anti-LGI1 encephalitis is associated with unique HLA subtypes: HLA subtypes in anti-LGI1 encephalitis. Ann Neurol 81:183–192. https://doi.org/10.1002/ana.24860
115. van Sonderen A, Roelen DL, Stoop JA et al (2017) Anti-LGI1 encephalitis is strongly associated with HLA-DR7 and HLA-DRB4: anti-LGI1 encephalitis. Ann Neurol 81:193–198. https://doi.org/10.1002/ana.24858
116. Binks S, Varley J, Lee W et al (2018) Distinct HLA associations of LGI1 and CASPR2-antibody diseases. Brain 141:2263–2271. https://doi.org/10.1093/brain/awy109
117. Muñiz-Castrillo S, Haesebaert J, Thomas L et al (2021) Clinical and prognostic value of immunogenetic characteristics in anti-LGI1 encephalitis. Neurol Neuroimmunol Neuroinflamm 8:e974. https://doi.org/10.1212/NXI.0000000000000974
118. Wennberg R, Steriade C, Chen R, Andrade D (2018) Frontal infraslow activity marks the motor spasms of anti-LGI1 encephalitis. Clin Neurophysiol 129:59–68. https://doi.org/10.1016/j.clinph.2017.10.014
119. Liu X, Han Y, Yang L et al (2020) The exploration of the spectrum of motor manifestations of anti-LGI1 encephalitis beyond FBDS. Seizure 76:22–27. https://doi.org/10.1016/j.seizure.2019.12.023
120. Flanagan EP, Kotsenas AL, Britton JW et al (2015) Basal ganglia T1 hyperintensity in LGI1-autoantibody faciobrachial dystonic seizures. Neurol Neuroimmunol Neuroinflamm 2:e161. https://doi.org/10.1212/NXI.0000000000000161
121. Liu X, Shan W, Zhao X et al (2020) The clinical value of 18F-FDG-PET in autoimmune encephalitis associated with LGI1 antibody. Front Neurol 11:418. https://doi.org/10.3389/fneur.2020.00418
122. Brüggemann N (2021) Contemporary functional neuroanatomy and pathophysiology of dystonia. J Neural Transm (Vienna) 128:499–508. https://doi.org/10.1007/s00702-021-02299-y
123. Celicanin M, Blaabjerg M, Maersk-Moller C et al (2017) Autoimmune encephalitis associated with voltage-gated potassium channels-complex and leucine-rich glioma-inactivated 1 antibodies - a national cohort study. Eur J Neurol 24:999–1005. https://doi.org/10.1111/ene.13324
124. Hang H, Zhang J, Chen D et al (2020) Clinical characteristics of cognitive impairment and 1-year outcome in patients with anti-LGI1 antibody encephalitis. Front Neurol 11:852. https://doi.org/10.3389/fneur.2020.00852
125. Ramanathan S, Tseng M, Davies AJ et al (2021) LGI1- versus CASPR2-antibody neuropathic pain: clinical and biological comparisons. Ann Neurol. https://doi.org/10.1002/ana.26189
126. van Sonderen A, Thijs RD, Coenders EC et al (2016) Anti-LGI1 encephalitis: clinical syndrome and long-term follow-up.

Neurology 87:1449–1456. https://doi.org/10.1212/WNL.0000000000003173
127. Chen W, Wang M, Gao L et al (2021) Neurofunctional outcomes in patients with anti-leucine-rich glioma inactivated 1 encephalitis. Acta Neurol Scand. https://doi.org/10.1111/ane.13503
128. Smith KM, Dubey D, Liebo GB et al (2021) Clinical course and features of seizures associated with LGI1-antibody encephalitis. Neurology. https://doi.org/10.1212/WNL.0000000000012465
129. Ariño H, Armangué T, Petit-Pedrol M et al (2016) Anti-LGI1–associated cognitive impairment: presentation and long-term outcome. Neurology 87:759–765. https://doi.org/10.1212/WNL.0000000000003009
130. Thompson J, Bi M, Murchison AG et al (2018) The importance of early immunotherapy in patients with faciobrachial dystonic seizures. Brain 141:348–356. https://doi.org/10.1093/brain/awx323
131. Bien CG, Bien CI, Dogan Onugoren M et al (2020) Routine diagnostics for neural antibodies, clinical correlates, treatment and functional outcome. J Neurol 267:2101–2114. https://doi.org/10.1007/s00415-020-09814-3
132. Koneczny I (2018) A new classification system for IgG4 autoantibodies. Front Immunol 9:97. https://doi.org/10.3389/fimmu.2018.00097
133. Ramberger M, Berretta A, Tan JMM et al (2020) Distinctive binding properties of human monoclonal LGI1 autoantibodies determine pathogenic mechanisms. Brain 143:1731–1745. https://doi.org/10.1093/brain/awaa104
134. González-Burgos I, Velázquez-Zamora DA, Beas-Zárate C (2009) Damage and plasticity in adult rat hippocampal trisynaptic circuit neurons after neonatal exposure to glutamate excitotoxicity. Int J Dev Neurosci 27:741–745. https://doi.org/10.1016/j.ijdevneu.2009.08.016
135. Irani SR, Stagg CJ, Schott JM et al (2013) Faciobrachial dystonic seizures: the influence of immunotherapy on seizure control and prevention of cognitive impairment in a broadening phenotype. Brain 136:3151–3162. https://doi.org/10.1093/brain/awt212
136. Feyissa AM, Lamb C, Pittock SJ et al (2018) Antiepileptic drug therapy in autoimmune epilepsy associated with antibodies targeting the leucine-rich glioma-inactivated protein 1. Epilepsia Open 3:348–356. https://doi.org/10.1002/epi4.12226
137. Dubey D, Britton J, McKeon A et al (2020) Randomized placebo-controlled trial of intravenous immunoglobulin in autoimmune LGI1/CASPR2 epilepsy. Ann Neurol 87:313–323. https://doi.org/10.1002/ana.25655
138. Petit-Pedrol M, Sell J, Planagumà J et al (2018) LGI1 antibodies alter Kv1.1 and AMPA receptors changing synaptic excitability, plasticity and memory. Brain. https://doi.org/10.1093/brain/awy253
139. Zhang T-Y, Cai M-T, Zheng Y et al (2021) Anti-alpha-amino-3-hydroxy-5-methyl-4-isoxazolepropionic acid receptor encephalitis: a review. Front Immunol 12:652820. https://doi.org/10.3389/fimmu.2021.652820

Progress in Neurobiology 213 (2022) 102262

Contents lists available at ScienceDirect

Progress in Neurobiology

journal homepage: www.elsevier.com/locate/pneurobio

Kv1.1 channels inhibition in the rat motor cortex recapitulates seizures associated with anti-LGI1 encephalitis

Paul Baudin [a], Stephen Whitmarsh [a], Louis Cousyn [a,b], Delphine Roussel [a], Sarah Lecas [a], Katia Lehongre [a], Stéphane Charpier [a], Séverine Mahon [a,1], Vincent Navarro [a,b,c,*,1]

[a] Sorbonne Université, Paris Brain Institute – Institut du Cerveau, ICM, INSERM, CNRS, APHP, Pitié-Salpêtrière Hospital, Paris, France
[b] AP-HP, Epilepsy Unit, Pitié-Salpêtrière Hospital, DMU Neurosciences, Paris, France
[c] AP-HP, Center of Reference for Rare Epilepsies, Pitié-Salpêtrière Hospital, Paris, France

ARTICLE INFO

Keywords:
LGI1
Kv1.1
Tonic-dystonic seizures
Epilepsy
Autoimmune encephalitis

ABSTRACT

Autoimmune encephalitis associated with antibodies directed against the leucine-rich glioma inactivated 1 (LGI1) protein is responsible for specific tonic-dystonic motor seizures. Although dysfunctions in neuronal excitability have been associated with anti-LGI1 autoantibodies, their relation to seizures remain inconclusive. We developed a new in vivo experimental rat model to determine whether inhibition of Kv1.1 channels by dentrotoxin-K (DTX) in the primary motor cortex (M1) could recapitulate the human seizures and to elucidate their subtending cortical mechanisms. Comparing electro-clinical features of DTX-induced seizures in rats with those recorded from a cohort of anti-LGI1 encephalitis patients revealed striking similarities in their electro-encephalographic (EEG) signature, frequency of recurrence and semiology. By combining multi-site extracellular and intracellular recordings of M1 pyramidal neurons in DTX rats, we demonstrated that the blockade of Kv1.1 channels induced a sequence of changes in neuronal excitability and synaptic activity, leading to massive suprathreshold membrane depolarizations underlying the paroxysmal EEG activity. Our results suggest the central role of Kv1.1 channels disruption in the emergence of anti-LGI1-associated seizures and suggest that this new rodent model could serve future investigations on ictogenesis in autoimmune encephalitis.

1. Introduction

Autoimmune encephalitis is a group of neurological diseases, which can be associated with the production of autoantibodies targeting synaptic proteins, and it is responsible for an increasing number of unexplained pharmacoresistant epilepsies (Crisp et al., 2016; Dalmau et al., 2017; Husari and Dubey, 2019). One of the most frequent autoimmune encephalitis, caused by the production of antibodies directed against the leucine-rich, glioma inactivated 1 (LGI1) protein, is characterized by limbic encephalitis and tonic-dystonic motor seizures (TDS). The evolution of the disease, generally within months, results in a progressive bilateral involvement of limbic and motor brain structures (Navarro et al., 2016) and a gradual increase in seizures frequency, possibly leading to life-threatening status epilepticus. A delay in diagnosis or treatment can thus have deleterious consequences and lead to irreversible lesions, such as hippocampal atrophy (Ghimire et al., 2020; Griffith et al., 2020; X. Liu et al., 2020; R. Liu et al., 2020; Ramanathan et al., 2021). While limbic encephalitis is a common syndrome in different autoimmune encephalitis, TDS are specific to anti-LGI1 autoimmune encephalitis (Irani et al., 2011; Navarro et al., 2016). TDS, also known as faciobrachial dystonic seizures, consist in a brief tonic contraction of the upper limb, which ends in a dystonic posture, sometimes associated with ipsilateral hemi-face and lower limb contraction. We recently demonstrated that TDS originate from the primary motor cortex (M1) (Navarro et al., 2016) and that the muscular contraction is preceded by a focal, contralateral, fronto-central slow wave on the electroencephalogram

Abbreviations: AMPAR, α-amino-3-hydroxy-5-methyl-4-isoxazolepropionic acid receptor; AP, action potential; DTX, dendrotoxin-K; ECoG, electrocorticogram; EEG, electroencephalogram; *F-I*, frequency-current; G_m, membrane conductance; KO, knock-out; LFP, local field potential; M1, primary motor cortex; MUA, multi-unit activity; R_m, membrane resistance; SD, standard deviation; SU, single-unit; TDS, tonic-dystonic seizure; TDW, tonic-dystonic wave; τ_m, membrane time constant; *V-I*, voltage-current; V_m, membrane potential.

* Correspondence to: 47-83 Boulevard de l'Hôpital, Paris 75013, France.
E-mail address: vincent.navarro@aphp.fr (V. Navarro).

[1] These authors contributed equally to this work.

https://doi.org/10.1016/j.pneurobio.2022.102262
Received 8 November 2021; Received in revised form 3 February 2022; Accepted 8 March 2022
Available online 10 March 2022

(EEG) (X. Liu et al., 2020; R. Liu et al., 2020; Navarro et al., 2016; Wennberg et al., 2018). Although immunotherapy reduces the incidence and severity of seizures over time, TDS usually persist for several weeks after starting treatment and cannot be controlled with current anti-epileptic drugs (de Bruijn et al., 2019; Feyissa et al., 2018; Irani et al., 2013; Thompson et al., 2018).

The secreted neuronal protein LGI1 takes part in a trans-synaptic complex, including Kv1.1 voltage-dependent potassium channels and glutamatergic α-amino-3-hydroxy-5-methyl-4-isoxazolepropionic acid receptors (AMPAR) (Fukata et al., 2021; Schulte et al., 2006; Yamagata et al., 2018). LGI1 is also enriched at the axon initial segment, where it co-localizes with Kv1.1 channels as well (Hivert et al., 2019; Seagar et al., 2017). Anti-LGI1 antibodies are known to prevent fixation of LGI1 to its pre- and postsynaptic partners or to induce the internalization of the LGI1-associated protein complex (Ramberger et al., 2020), resulting in decreased expression, and functional alterations, of Kv1.1 channels and AMPAR (Kornau et al., 2020; Ohkawa et al., 2013; Petit-Pedrol et al., 2018; Ramberger et al., 2020). Specifically, the application of anti-LGI1 antibodies to hippocampal cultures has been shown to increase the excitability of CA3 pyramidal neurons through a reduction of their excitation threshold (Kornau et al., 2020). This effect could be mimicked by the application of the selective Kv1.1 channels blocker dendrotoxin-K (DTX) (Grissmer et al., 1994; Wang et al., 1999), suggesting a role of these K^+ channels in the expression of the antibody-induced effects. Similar changes in the excitability of cortical and hippocampal pyramidal neurons have also been observed in slices from LGI1 knock-out (KO) mice and correlated with a reduced expression of Kv1.1 and Kv1.2 channels, as well as a decrease in K^+ currents (Seagar et al., 2017; Zhou et al., 2018).

Although Kv1.1 channels, which finely tune neuronal excitability, may have a role in seizures initiation, the relations between the loss of Kv1.1 and the emergence of TDS remain unclear. Indeed, previous studies using chronic – up to two weeks – infusion of anti-LGI1 antibodies in the hippocampus or cerebral ventricles did not report epileptic activity, despite a decrease in the expression of Kv1.1 channels (Petit-Pedrol et al., 2018; Ramberger et al., 2020). Here, we developed a new in vivo pharmacological rodent model to test the hypothesis that a blockade of Kv1.1 channels is sufficient for the development of the characteristic TDS. This was achieved by comparing the seizures induced in adult rats by infusion of DTX in M1, the main cortical target in humans (Navarro et al., 2016), with TDS recorded in a cohort of patients with anti-LGI1 encephalitis. Remarkably, the rodent model reliably generated motor seizures whose properties, including EEG signature, frequency of occurrence and symptoms, were very similar to the TDS recorded in patients. By performing multi-site extracellular and intracellular recordings in our model, we also demonstrated that the paroxysmal EEG activity during TDS was subtended in M1 deep-layer pyramidal neurons by a massive membrane depolarization and synchronous high-frequency action potentials (APs) discharge. Analysis of synaptic activity and firing dynamics during interictal periods led us to propose the first diachronic scenario for the initiation of TDS, which emerged from a progressive increase in the level of activity in cortical neurons and local synaptic networks.

2. Materials and methods

2.1. Human studies

Anti-LGI1 encephalitis patients, admitted in the Epilepsy Unit of the Pitié-Salpêtrière Hospital (Paris, France) between 2010 and 2019 with at least one episode of TDS recorded on the EEG, were retrospectively included ($n = 12$). EEG was recorded with 21 scalp electrodes positioned according to the 10–20 system. Total duration of EEG recordings ranged from 0.5 to 10 h per patient. EMG from muscles of the upper limb was simultaneously recorded in 9 out of 12 patients, the position of the electrodes being adapted to the location of the most visible contraction. Patient behavior was simultaneously recorded with video. Data from several recording systems (Medatec®, Belgium; Micromed®, Italy; Nicolet®, USA) were reviewed in an average reference montage. EEG and EMG signals were acquired at 256 Hz or 512 Hz, and high-pass filtered at 0.1 Hz. The main clinical and biological data, therapeutics, and outcomes of patients are provided in table S1. Investigations were conducted in accordance with the French legislation and authorized by CNIL committee (No. 2,211,991). All patients were informed about the use of their anonymized data, and provided verbal consent.

2.2. Multi-scale electrophysiological recordings in the rodent model

Animal care and manipulation were carried out in accordance with the European Committee Council Directive (2010/63/EU) and approved by the French Ministry for Research and the local Ethical Committee (APAFIS no. 8302-2017113017466765). Experiments were performed on male Sprague Dawley rats, aged of 2–4 months and weighting 200–450 g ($n = 44$).

2.2.1. Freely-moving animals

Rats ($n = 19$) were anesthetized with 2 – 4% isoflurane (Osalia) and placed in a stereotaxic frame. DTX (200 ng, 0.5 µl; Alomone Labs) was loaded into a 10 µl Hamilton syringe injector and slowly (0.1 $\mu l.min^{-1}$) injected perpendicularly to the brain surface at 1 mm depth into the left M1 (AP, +2 mm; ML, 2.6 mm) (Paxinos and Watson, 1997). The doses of DTX were adjusted in pilot experiments to generate frequent seizures without induction of a status epilepticus (Bagetta et al., 1996). EEG activity was monitored through two stainless-steel screws (0.86 mm diameter) implanted into the right and left M1 and a reference electrode placed over the cerebellum. Intramuscular bipolar stainless-steel EMG electrodes were placed in the front paw extensors. After DTX injection, rats were placed in freely moving conditions and connected to a computer-assisted video-EEG system (Deltamed LTM, Natus®). EEG and EMG signals were acquired at 4096 Hz and high-pass filtered at 0.1 Hz. At the end of experiments, animals were euthanized by an overdose of euthasol (0.6 $ml.kg^{-1}$; TVM) and brains were cut into coronal sections for histological processing. Brain sections were then stained with cresyl violet to localize electrode tips.

2.2.2. Sedated animals

In sedated animals ($n = 7$ control and 20 DTX rats), the monitoring of electrocorticographic activity (ECoG) in M1 was combined with local field potential (LFP) and multi-unit activity (MUA) recordings, or with intracellular recordings of subjacent pyramidal neurons. Rats were initially anesthetized with 2 – 4% isoflurane and underwent tracheotomy for artificial ventilation (room air, 80 $breaths.min^{-1}$, 2.6 $ml.cycle^{-1}$) under neuromuscular blockade (gallamine triethiodide, 40 mg/2 h i.m.; Sigma-Aldrich®). They were placed in a stereotaxic frame and a small craniotomy was made above M1 to allow DTX injection and multiscale recordings. Isoflurane anesthesia was discontinued after the surgical procedures. Analgesia and sedation were then maintained by local infiltration of lidocaine 2% (Centravet) to incision and pressure points and repeated injection of sufentanil (3 $\mu g.kg^{-1}$ every 30 min, i.p.; Piramal). Sedation with sufentanil was chosen as it does not alter the spontaneous activity and excitability of cortical cells (Altwegg-Boussac et al., 2014) and does not interfere with the induction-expression of focal and generalized seizures (Langlois et al., 2010; Depaulis et al., 2016). Heart rate and ECoG activity were continuously monitored to assess the depth of sedation. The stability of physiological parameters, i.e. end-tidal carbon dioxide concentration ($EtCO_2$), oxygen saturation (SpO_2) and core temperature (37 °C), was ensured throughout the experiments (Altwegg-Boussac et al., 2017). DTX injection (40 ng, 0.5 µl) was performed after completion of the surgery, under sufentanil sedation. The first seizure was observed on average 15.9 ± 12.6 min (range: 2–44, $n = 20$ rats) after DTX injection. Control rats were injected with 0.5 µl of phosphate buffer saline (PBS, VWR chemicals).

ECoG activity was recorded with of a low impedance (~60 kΩ) silver electrode placed on the dura above M1, and a reference electrode apposed on a contralateral temporal muscle. ECoG signals were amplified with a differential *AC* amplifier (Model 1700; A-M Systems), filtered between 0.1 Hz and 1 kHz, and digitized at 3 kHz (CED 1401 Micro3; Spike2 software version 7.20, Cambridge Electronic Design) for off-line analysis.

Recordings of LFP and MUA were performed using a 16-channel (250-μm electrode separation distance) silicon-based probe (35 μm site IrOx, ATLAS Neuroengineering®) inserted into the M1, 200 μm anterior to the injection site. LFP signals were amplified and filtered between 0.1 Hz and 6 kHz, using a DigitalLynx (NeuraLynx®) amplifier, and digitized at 32 kHz for post hoc analysis.

Intracellular recordings were performed with glass micropipettes filled with 2 M potassium acetate (50–90 MΩ) in the vicinity of the DTX injection site. Recordings were obtained from cortical neurons ($n = 33$ from 20 rats) located in the M1 layer 5 at depths ranging from 950 to 2200 μm below the cortical surface (Paxinos and Watson, 1997; Wilent and Contreras, 2004). Current-clamp recordings were amplified with an Axoclamp 900 A amplifier (Molecular Devices) operating in bridge mode, bandpass filtered between *DC* and 30 kHz, and digitized at 30 kHz. Recorded cortical neurons were identified on-line as pyramidal cells on the basis of their distinctive intrinsic firing patterns in response to direct stimulations (Steriade, 2004), and off-line by their morphological features (Fig. 3A). Extracellular *DC* potentials were obtained immediately after the loss of intracellular recordings with the same microelectrodes (Fig. 3B). Intracellularly recorded neurons were filled with neurobiotin (1% added to the pipette solution; Vector Laboratories) through repeated injections of depolarizing current pulses (0.5–1 nA; 100–200 ms) applied at 1–2 Hz during the last 10–15 min of the recording sessions (Williams et al., 2016). At the end of experiments, rats were euthanized with euthasol and transcardially perfused with 4% paraformaldehyde in PBS. Brains were removed and cut in coronal sections for histological processing. For LFP experiments, brain sections were stained with cresyl violet to localize injector and silicon probe tracks. The morphology of neurobiotin-filled neurons was revealed as previously described (Williams et al., 2016). All recovered neurons were located in layer 5 of left M1 and possessed the typical morphological features of deep-layer pyramidal neurons (Steriade, 2004; Wilent and Contreras, 2004; Williams et al., 2016).

2.3. Signal analysis

Analysis was performed with a combination of Fieldtrip (release 20,200,919) (Oostenveld et al., 2011) and custom-developed scripts in MATLAB (The Mathworks Inc., version R2019b). Custom analysis scripts can be found at https://github.com/Paul-Baudin/EpiCode/tree/master/projects/dtx. Intracellular signals were analyzed with Spike2 software (Cambridge Electronic Design, version 9.08b).

2.3.1. EEG and EMG signals.

EEG signals were first low-pass filtered at 70 Hz and EMG records were high-pass filtered at 10 Hz. The regularity of tonic-dystonic wave (TDW) occurrence was calculated with the CV2 method (Altwegg-Boussac et al., 2014): here $CV2 = (2|\Delta t_{i+1} - \Delta t_i|) / (\Delta t_{i+1} + \Delta t_i)$, and $\Delta t_i = t_i - t_{i-1}$ is the inter-TDW-interval. TDW half-width was the duration of TDW at half-amplitude. Analysis of rodent data was restricted to the first 10 h following DTX injection. Artefacted trials were discarded for the morphological analysis. The start and end of the tonic-dystonic muscular contraction was defined as the first (and last) event crossing a threshold set at 3 times the standard deviation (SD) of the baseline rectified EMG signal.

2.3.2. LFP and MUA records

For spike detection, the raw wide-band signal was filtered (> 300 Hz) and negative deflections > 6 median absolute deviations of the filtered trace were considered as spikes. A combination of density-based clustering and template matching algorithms were used to automatically cluster the detected spikes (Yger et al., 2018). Clusters were evaluated as to whether they reflected putative single-unit (SU) or multi-unit (MU) activities, based on the ISI distribution, the percentage of refractory period violation (RPV = ISI < 2 ms) and the spike waveform profile. Analysis was restricted to putative SUs located in layer 5. Spike activity of selected units was time-aligned to the peak of each TDW and trials were averaged to construct peri-stimulus time histograms (PSTHs) and spike density plots. Units were classified according to their firing rate change in a time period starting 200 ms before and ending 2 s after the TDW peak. Non-parametric cluster-based permutation tests (Maris and Oostenveld, 2007) were used to determine significant changes relative to the baseline, taken as the − 2 to − 1 s period preceding the TDW peak. SUs showing a significant increase in firing rate during more than 95% of the defined period were classified as 'prolonged increase'. SUs with a significant increased firing rate during less than 80% of the TDW were classified as 'transient increase'. None of the recorded units exhibited an enhanced discharge for more than 80%, and less than 95%, of the TDW period. SUs with no significant increase (or decrease) in firing were classified as 'no change/decrease'. Spike duration was measured between the trough and the following peak of the SU average trace (Barthó et al., 2004) (Fig. 2A). Bursts were defined as sequences of two or more spikes from the same unit with ISI shorter than 10 ms (Watson et al., 2016). To examine time-dependent changes during interictal periods, firing frequency was computed every second and inter-seizure duration was normalized to allow averaging of the different epochs.

2.3.3. Intracellular records

Average membrane potential (V_m) of cortical neurons was calculated as the mean of the distribution of spontaneous subthreshold neuronal activity and the magnitude of V_m fluctuations was quantified as the SD of the distribution (SD V_m). V_m and SD V_m values, mean spontaneous firing rate and firing regularity (estimated with the CV2 method) were extracted from recordings of at least 1 min. Voltage threshold of action potentials (APs) was defined as the V_m at which the dV_m/dt first exceeded 10 $mV.ms^{-1}$ (Mahon and Charpier, 2012).

Voltage–current (*V–I*) relationships were constructed from the mean V_m drops (ΔV_m) evoked by hyperpolarizing current pulses of varying intensity (−0.2 to −1 nA; 100 ms duration; every 0.5 s; $n > 10$ trials per intensity). ΔV_m was measured at the peak of the hyperpolarizing voltage deflection, immediately after the end of the membrane capacitance charge, to avoid interference with a possible hyperpolarization-activated depolarizing sag potential (Pape, 1996). Once the linearity of the *V–I* relations was attested, membrane resistance (R_m) was calculated as the slope of the corresponding linear fit (Fig. 5A, dashed lines) (Williams et al., 2016). To assess dynamical changes of the integrative properties of cortical neurons during TDWs, we applied brief repeated hyperpolarizing (−0.6 nA, 20 ms duration, every 100 ms) current pulses and measured the corresponding mean ΔV_m (Fig. 3C). The membrane time constant (τ_m) was derived from an exponential decay fit applied to the initial phase of the mean hyperpolarization evoked by current pulses of -0.2 or -0.4 nA. Neuronal transfer function, which describes the cell output firing frequency as a function of injected depolarizing current pulses of increasing intensity (*F–I* relationship, 0.1–2 nA, 200 ms pulses at 1 Hz; $n > 10$ trials per intensity), was quantified in DTX and control conditions. Linear regression of *F–I* curves yielded the threshold current for AP generation (I_{th}; *x*-intercept) and the neuronal gain (γ; slope) (Altwegg-Boussac et al., 2017, 2014; Mahon and Charpier, 2012). Latency and temporal precision of the first evoked AP was measured on current pulses inducing a similar firing frequency (20 –40 Hz) in control and DTX neurons (Fig. 5C).

Dynamic changes of V_m, SD V_m and frequency content of subthreshold intracellular activity during the inter-seizure epochs were assessed over successive periods of 30 s and expressed as function of baseline values (defined as the first 30 s of the interictal period). Time

was normalized to permit averaging across neuronal population. Time-frequency maps were constructed using a multitaper decomposition analysis with a sliding time window of 1 s (Oostenveld et al., 2011), after removing of APs which were replaced by a piecewise cubic hermite polynomial interpolation.

2.4. Statistical analysis

Statistical analysis was performed with MATLAB. Differences between groups were assessed using the Wilcoxon signed-rank test, the Mann-Whitney rank-sum test or one-way ANOVA when appropriate. Correlations were evaluated by means of Pearson's rho values and their level of significance. The sequential rejective Benjamini-Hochberg test procedure was used to correct for multiple comparisons (Benjamini and Hochberg, 1995). Results are represented as mean ± SD and $P < 0.05$ was considered a significant effect.

3. Results

3.1. Inhibition of Kv1.1 channels in the rodent motor cortex recapitulates the human TDS

We first sought to determine whether an acute inhibition of Kv1.1 channels in the rodent M1, through focal injection of DTX, was able to reproduce the human TDS and the coincident large-amplitude slow EEG wave. Validation of the pharmacological model was based on a comparative assessment of the consequences of Kv1.1 blockade with the TDS-related electroclinical correlates recorded by simultaneous EEG, EMG and video monitoring in a cohort of 12 anti-LGI1 encephalitis patients (Supplementary Table 1). Patients exhibited the previously described postural changes (Irani et al., 2011; Navarro et al., 2016; Wennberg et al., 2018; X. Liu et al., 2020; R. Liu et al., 2020), consisting of a brief (~1 s) distal tonic contraction of the upper limb, ending in a dystonic posture of the fingers, which was sometimes associated with a contraction of the ipsilateral hemi-face (Fig. 1A, right) (Supplementary Movie 1). The number of TDS per patient was highly variable (30.4 ± 35 seizures, range: 3–114, $n = 12$ patients), and their frequency ranged from 5 to 31 seizures per hour (13.5 ± 7.4 h^{-1}, $n = 12$ patients) (Fig. 1A, right). As previously reported (X. Liu et al., 2020; R. Liu et al., 2020; Navarro et al., 2016; Wennberg et al., 2018), clinical TDS was systematically preceded by a slow EEG wave, which was exclusively detected from the fronto-central electrodes (Fig. 1A, left and Supplementary Fig. 1). Due to its systematic association with the tonic-dystonic contraction, we called this EEG wave a 'tonic-dystonic wave' (TDW). This abnormal EEG waveform, arising from apparently normal background cortical activity, was unilateral and contralateral to the tonic-dystonic contraction. TDWs were temporally correlated with a robust increase in EMG activity recorded from the muscles of the upper limb (Fig. 1A and C, left records). Within each patient, TDWs recurred with some temporal regularity, as indicated by the CV2 values of inter-TDW intervals (0.7 ± 0.3, range: 0.2–1.3, $n = 365$ TDWs from 12 patients) (Fig. 1A, right). Cortical TDWs, the burst of EMG activity and TDS were robustly associated in each patient, suggesting a causal link between the cortical event and the motor symptoms of the seizure.

We attempted to reproduce these clinical and EEG features in freely-moving rodents by blocking the activity of Kv1.1 channels in M1 via a focal injection of DTX in the layer 5, which contains the soma of corticospinal neurons. Monitoring EEG activity from ipsilateral and contralateral M1 and EMG signals from the front paw extensors (Fig. 1B and C) after DTX injection revealed electroclinical symptoms strikingly similar to those recorded in patients. In all tested rats, large-amplitude slow negative EEG waves emerged from a normal background EEG pattern with a frequency ranging from 13.6 to 45.8 per hour (27.9 ± 8.6 h^{-1}, $n = 1832$ waves from 9 DTX rats) (Fig. 1B, right). Similarly as in anti-LGI1 autoimmune encephalitis patients, the slow EEG waves in rodents recurred regularly (Inter-wave intervals CV2 = 0.3 ± 0.07; range: 0.2–0.4, $n = 9$ rats) (Fig. 1B, right) and were systematically accompanied by a burst of EMG activity (Fig. 1B and C, right). Seizures in rodents were highly stereotyped, characterized by a tonic-dystonic contraction of the anterior paw extensors contralateral to the DTX injection site, and an upward-lateral displacement of the head (Fig. 1B, right) (Supplementary Movie 2). Tonic-dystonic episodes were systematically preceded by the slow EEG wave, which can therefore be similarly named TDW by analogy with the human pathology.

Although patients and DTX rats both showed analogous association between TDWs and the increase in EMG activity (Fig. 1C, left), differences were observed as well. The duration at half-amplitude of the human TDW (half-width duration = 512 ± 124 ms, $n = 243$ TDWs from 12 patients) was significantly longer as compared to the TDW in rodents (half-width duration = 320 ± 79 ms, $n = 1\,354$ TDWs from 9 DTX rats; $P = 0.001$) (Fig. 1C and D, top). This was accompanied by an increased duration of the tonic contraction in patients (Patients, 1.2 ± 0.7 s, $n = 9$ versus DTX rats, 0.4 ± 0.1 s, $n = 5$; $P = 0.001$) (Fig. 1 C and D) and an augmented delay between the onset of the TDW and the beginning of the change in EMG activity (Patients, 432 ± 210 ms, $n = 9$ versus DTX rats, 54.0 ± 12.6 ms, $n = 5$; $P = 0.001$) (Fig. 1C).

In DTX rats, TDWs were systematically followed by a transient epoch (0.8–1.5 s) of attenuated EEG activity, preceding a longer period (16.3 ± 8.7 s) of ictal activity (Fig. 1B, left). Ictal activity consisted in negative oscillations at 8–16 Hz, followed by rhythmic (3–8 Hz) spike and polyspike discharges (Fig. 1B and Supplementary Fig. 2). This ictal pattern could be detected, albeit strongly attenuated, in M1 contralateral to the DTX injection site (Fig. 1B), suggesting partial trans-callosal propagation to the homotypic cortex. This sustained ictal activity always caused rhythmic muscular contractions and tonic-clonic seizures in DTX rats (Fig. 1B, left and Supplementary Movie 3).

Supplementary material related to this article can be found online at doi:10.1016/j.pneurobio.2022.102262.

3.2. Profiles of cortical neurons firing during the DTX-induced TDW

We next investigated changes in cortical neurons activity during TDWs. We recorded ECoG activity in M1, together with multi-site extracellular recordings ($n = 5$ rats) (Fig. 2A, left) or intracellular recordings from layer 5 pyramidal neurons ($n = 10$ rats) (Fig. 3A).

LFP and MUA were collected at different depths in M1 from sedated DTX rats and spike sorting was used to extract the activity of putative single units (SUs) located in layer 5 (Fig. 2A and Supplementary Fig. 2A). Shape and half-width of TDWs in sedated animals did not significantly differ from those measured in freely-moving rats (Awake, 320 ± 79 ms, $n = 1354$ TDWs from 9 rats versus Sedated, 291 ± 111 ms, $n = 637$ TDWs from 7 rats; $P = 0.8$) (Fig. 2A middle, inset). The firing rate of the majority of SUs (62/65) was modulated by the occurrence of TDWs. Three distinct firing profiles could be identified. The largest group of neurons (46/65) displayed a strong transient increase in firing rate during the TDWs, from 2.8 ± 4.6 Hz in baseline ($n = 4232$ TDWs from 46 SUs) to 8.1 ± 7.2 Hz ($P < 0.001$) during the TDW period ('transient increase' group) (Fig. 2B, left). A maximal firing frequency of 48.1 ± 42 Hz was reached at the peak of the TDW, indicating a tight synchronization of discharge among this group of neurons (Fig. 2B and C, left). This pronounced enhancement in firing activity, which lasted on average 0.65 ± 0.6 s (from 0.02 to 1.7 s, $n = 46$ SUs), rapidly collapsed after the TDW. The firing activity following TDWs was either similar ($n = 21/46$ SUs) or statistically lowered ($n = 25$ SUs; $P < 0.05$) as compared to baseline (Fig. 2B and C, left).

A second group of neurons ($n = 10/65$) was characterized by a marked and prolonged TDW-related increase in firing, which persisted for at least 2 s after the end the ECoG wave ('prolonged increase' group) (Fig. 2B, middle). The increase in firing started at the onset of the TDW and reached a maximal value of 35.1 ± 18.2 Hz ($n = 10$ SUs) at the peak negativity of the TDW, suggesting again a synchronized discharge among cortical neurons (Figs. 2B and C, middle). The average firing of

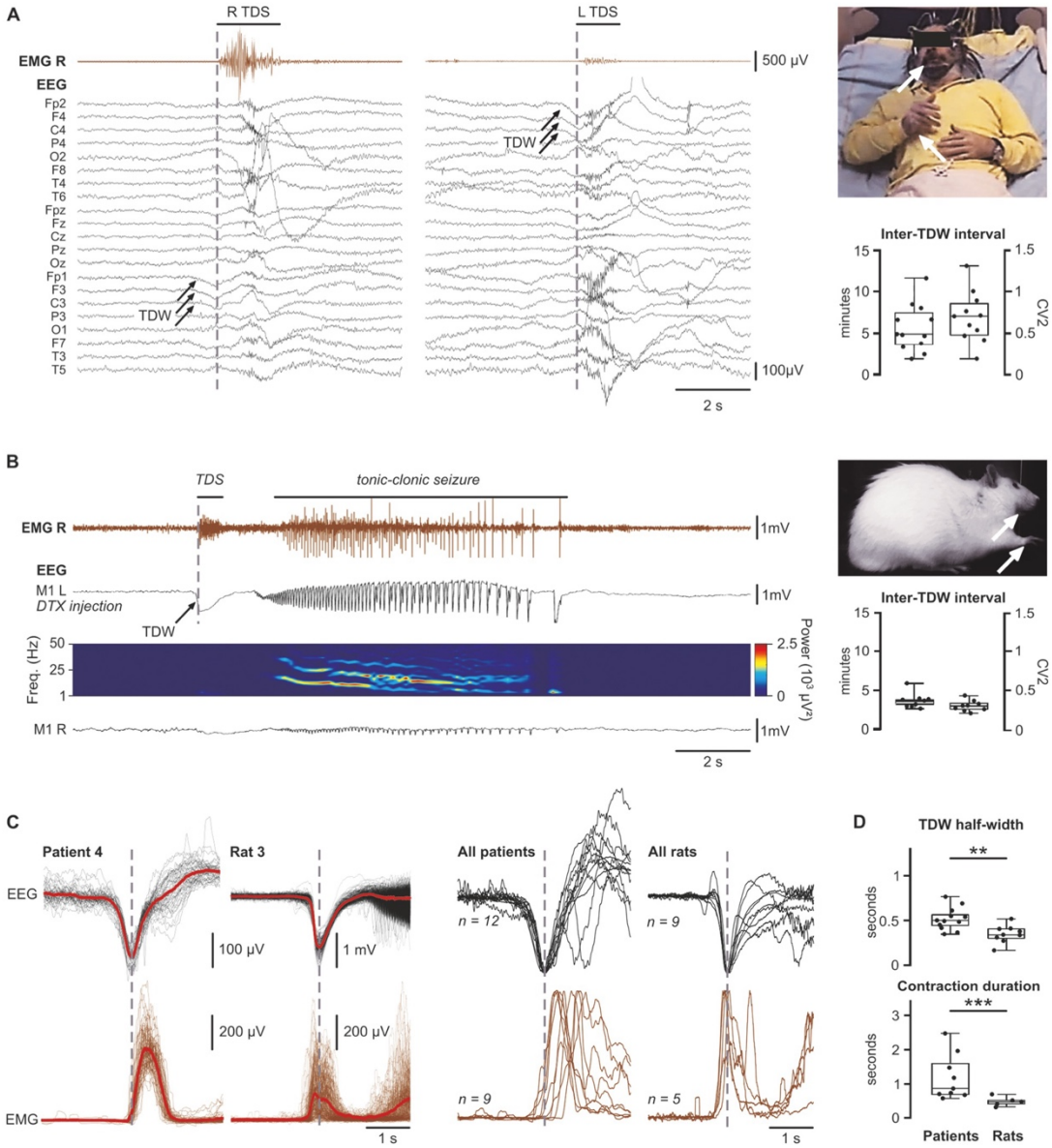

Fig. 1. Electroclinical features of tonic-dystonic seizures in anti-LGI1 encephalitis patients and DTX rats. (A) Typical EEG (black traces) and EMG (right arm; brown traces) records during tonic-dystonic seizures affecting the right (R TDS) or left (L TDS) limbs in anti-LGI1 encephalitis patients. TDS consisted in a tonic contraction of the upper limb and the hemi-face (arrows in the picture at right), followed by a dystonic posture of the fingers. The left- or right-sided tonic-dystonic contraction was consistently preceded by a contralateral large amplitude negative slow wave (tonic-dystonic wave, TDW) on a few adjacent fronto-central EEG electrodes (arrows). Dashed lines mark the beginning of tonic-dystonic contraction. The summary plot (right) illustrates the periodicity and regularity of occurrence (CV2) of TDWs ($n = 12$ patients). (B) EEG records from the left (L) and right (R) primary motor cortices (M1) (black traces) in a freely-moving rat, and corresponding EMG activity of the front paw extensors (EMG R, brown trace), following the injection of DTX in the left M1. The rodent TDW in M1L was correlated in time with the right-sided tonic-dystonic contraction (dashed line), and shortly (0.8–1.5 s) followed by a tonic-clonic seizure associated with paroxysmal oscillations on the EEG. The temporally-aligned time-frequency map illustrates the evolution of the EEG frequency content. The picture at right illustrates a tonic-dystonic contraction of the right upper limb and ipsilateral hemi-face in a DTX rat. Population data of TDW's periodicity and regularity are shown on the bottom right ($n = 9$ rats). (C-D) Comparison of TDW and tonic-dystonic contraction between patients and DTX rats. (C) Left, Superimposition of single TDWs collected from Patient #4 and from Rat #3 (black traces) and corresponding envelope of rectified EMG activities (brown traces). The peak of TDWs was taken as the time reference for alignment of the records. The red traces correspond to averages. Right, Superimposition of the average TDWs computed for all patient ($n = 12$) and DTX rats ($n = 9$), and corresponding envelopes of EMG activity. EEG and EMG traces have been normalized in amplitude and aligned according to the peak of TDWs. (D) Population data comparing the half-duration amplitude (half-width) of TDWs and muscular contraction duration between patients ($n = 12$) and rats ($n = 9$). $^{**}P < 0.01$, $^{***}P < 0.001$ (two-tailed Mann-Whitney rank-sum test).

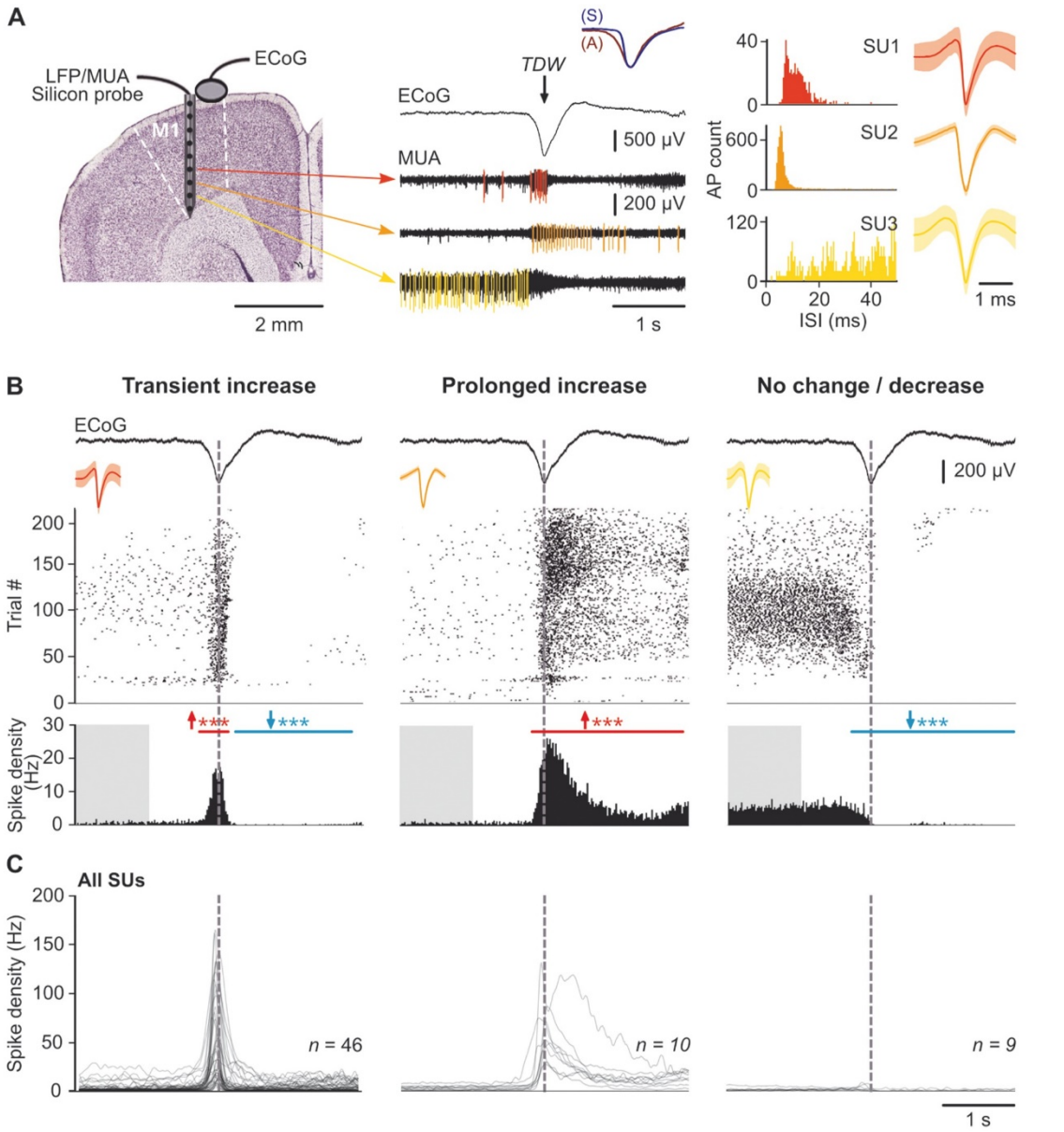

Fig. 2. Extracellular firing profiles of M1 neurons during the TDW. (A) Schematic drawing of recordings arrangement and isolation of SU activities. LFP were recorded in M1 using a 16-channel silicon probe, in conjunction with an ECoG in a sufentanil-sedated DTX rat (left). LFP records from layer 5 were high-pass filtered at 300 Hz to extract MUA (black records) and the firing profile of SUs (colored traces) during the TDW in the ECoG (middle). Note in the inset the great similarity between the TDWs recorded in awake (A) and sedated (S) animals (amplitude is normalized). Three examples of average (± SD) spike waveforms and corresponding inter-spike-intervals (ISI) distributions are shown at right. (B) Raster plots of spike activity (top) and corresponding peri-stimulus time histogram (bin = 10 ms; bottom) from three representative SUs (same cells as in A) sorted according to their firing change in association with the surface TDW: 1) a 'Transient increase' (left), 2) a 'Prolonged increase' (middle) or, 3) a lack of change or even a decrease ('No change/decrease', right). Gray dashed lines mark TDW peaks. Significance was assessed with a cluster-based permutation test comparing firing activity during the TDW with baseline firing (gray shaded area). The horizontal red and blue bars respectively indicate significant positive and negative clusters. ***$P < 0.001$. (C) Superimposed average ($n = 53$–219 TDWs) spike densities computed for all SUs in each group ('transient increase', $n = 46$; 'prolonged increase', $n = 10$; 'no change/decrease', $n = 9$).

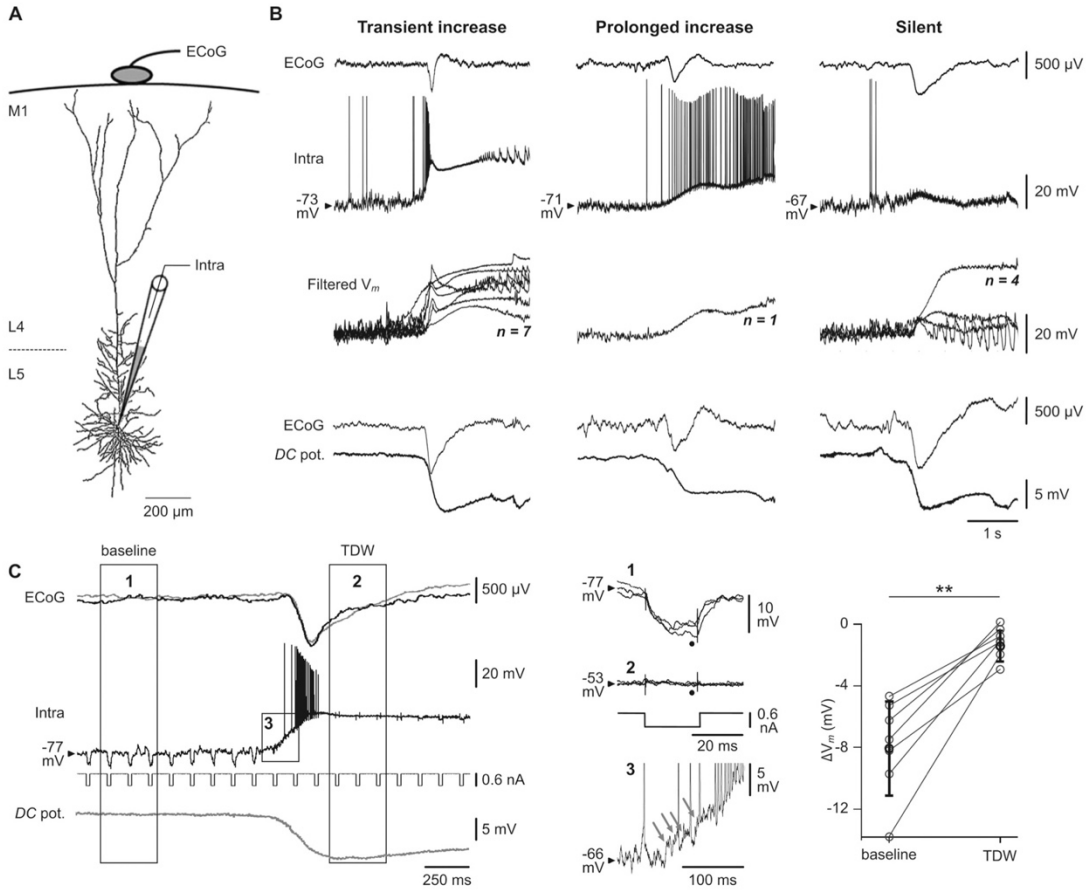

Fig. 3. Intracellular correlates of the TDW in pyramidal M1 neurons. (A) Reconstruction of a layer 5 M1 pyramidal neuron intracellularly recorded (Intra) in conjunction with the ECoG activity from a DTX rat. (B) Top, Short epochs of intracellular activity from three M1 neurons showing a transient increase, a prolonged increase or a decrease in their firing rate in association with the TDW. V_m value are indicated on the left of the traces. Middle, Superimposed (by matching V_m values before TDW) subthreshold cell activity (after removal of APs and low-pass filtering at 70 Hz) from the cortical neurons of the three groups showing TDW-associated membrane depolarizations. Bottom, ECoG TDW and corresponding *DC* potential extracellularly recorded at the end of the intracellular recordings illustrated in the top panel. Time calibration applies for all traces. (C) ECoG activity (top traces) simultaneously recorded with *DC* potential (lower trace) or intracellular activity of a M1 neuron (middle trace) during the repeated injection of current pulses (−0.6 nA, 20 ms, every 100 ms) in baseline and during the TDW. Expansion of three voltage deflections (measured at the time indicated by the black dots) during baseline (1) and TDW (2) periods are shown superimposed on the right. The expanded frame (3) shows that the onset of the TDW-associated depolarization (in absence of current pulses) is sculpted by the temporal summation of depolarizing synaptic potentials (oblique arrows). The summary graph illustrates the decrease in current-induced V_m changes during the TDW as compared to baseline ($n = 7$ neurons). $^{**}P < 0.01$ (two-tailed Wilcoxon signed-rank test).

this group of SUs during the TDW (12.9 ± 8.8 Hz, $n = 1960$ TDWs) remained above baseline until the appearance of the ECoG ictal oscillations ($P < 0.001$), despite a slow decrease after TDW termination (Figs. 2B and C, middle).

A third group of neurons ($n = 9/65$) consisted of SUs whose firing rate was either reduced ($n = 6$) during the TDW or not significantly modified ($n = 3$) ('no change/decrease' group) (Figs. 2B and C, right). These cells were thus not involved in the global increase in neuronal activity accompanying the occurrence of TDWs. The firing frequency of the 'decreased' neurons changed from 1.7 ± 1.8 Hz, ($n = 800$ TDWs from 6 SUs) in baseline to 0.31 ± 0.35 Hz during the ECoG wave ($P < 0.05$), corresponding to a decrease of 78 ± 19% (49–97%) (Figs. 2B and C, right).

SUs from the three groups did not significantly differ in cortical location (transient increase: 1627 ± 474 µm from the cortical surface, $n = 46$; prolonged increase: 1844 ± 257 µm, $n = 10$; no change/decrease: 1440 ± 233 µm, $n = 9$; $P = 0.12$), baseline firing frequency (transient increase: 2.8 ± 4.6 Hz, $n = 46$; prolonged increase: 2.6 ± 2.2 Hz, $n = 10$; no change/decrease: 1.7 ± 1.8 Hz, $n = 9$; $P = 0.54$) and burst propensity (transient increase: 15.9 ± 41.8 min^{-1}, $n = 46$; prolonged increase: 1.4 ± 3.7 min^{-1}, $n = 10$; no change/decrease: 3.4 ± 9.0 min^{-1}, $n = 9$; $P = 0.4$). According to their mean spike duration (transient increase: 0.68 ± 0.25 ms, $n = 46$; prolonged increase: 0.67 ± 0.24 ms, $n = 10$; no change/decrease: 0.86 ± 0.14 ms, $n = 9$; $P = 0.12$), recorded neurons can be assumed to be mainly putative pyramidal cells (Barthó et al., 2004).

3.3. Intracellular correlates of the TDW

To further explore the cellular mechanisms subtending the TDW, we combined ECoG monitoring with intracellular recordings of M1 neurons near the DTX injection site ($n = 12$ neurons from 10 rats) (Fig. 3A). Cells

were located in the M1 layer 5 and displayed the characteristic current-evoked firing profiles of pyramidal neurons, including regular spiking ($n = 9$) and intrinsic bursting ($n = 3$) patterns (Fig. 5B). Laminar location and cellular typology of neurons were further confirmed by subsequent histological reconstruction of neurobiotin-loaded cells ($n = 6$) (Fig. 3A). Before TDW, spontaneous activity of pyramidal neurons was characterized by a small-amplitude and fluctuating background synaptic drive leading to a mean V_m of − 71.9 ± 4 mV (from −77.5 to −64.7 mV, $n = 12$ neurons), causing a firing rate of 1.5 ± 3.7 Hz ($n = 10$ out 12 neurons) (Fig. 3B, top).

Consistent with the three categories of SUs identified with extracellular recordings, the majority of intracellularly recorded neurons ($n = 7$ out of 12) displayed a transient increase in their firing at the occurrence of the TDW (Fig. 3B, left). This was associated with an abrupt positive shift of the membrane voltage, which reached a mean value of − 48.8 ± 7.5 mV (from −60.7 to −38.3 mV, $n = 7$ neurons) at the peak of the TDW (Fig. 3B, left middle). This large membrane depolarization (13.4–34.3 mV), triggered by the temporal summation of depolarizing synaptic events (arrows in Fig. 3C, central), elicited a brief (0.04–0.8 s) period of high-frequency APs discharge (83 ± 50 Hz, $n = 7$ neurons), in time with the corresponding TDW (Fig. 3B left, top and 3C). The membrane depolarization further increased in magnitude after termination of the TDW, resulting in the silencing of cortical neurons likely due to a 'depolarization block' process known to prevent APs triggering (Bikson et al., 2003). Another group of neurons did not fire in relation with the TDW ('silent group', $n = 4$ neurons) (Fig. 3B right, top). Their intracellular behavior was variable, and included large and sustained depolarization shifts ($n = 1$), lasting depolarizations of smaller amplitude ($n = 2$) and subthreshold membrane oscillations ($n = 1$) (Fig. 3B right, middle). Finally, in one neuron, the TDW was associated with a sustained suprathreshold depolarization that persisted for at least 2 s after the end of the ECoG wave ('prolonged increase' group) (Fig. 3B, middle top). The three distinct TDW-related intracellular behaviors were reproducible over successive paroxysms and were not associated with differences in layer location, general cell morphology and intrinsic electrical membrane properties (Supplementary Table 2).

To assess collective changes in the activity of M1 neurons during the TDW, the microelectrode was slowly removed at the end of intracellular recordings to capture the LFP associated with TDWs ($n = 7$ rats). We found that the initial deflection of the ECoG wave coincided with a large negative *DC* shift (−7.8 ± 1.9 mV, $n = 7$) in each group of neurons (Fig. 3B, bottom paired records). This suggested that the TDW-related V_m depolarization observed in most of neurons was caused by a massive transmembrane current, recorded as a large voltage negativity in the extracellular space within the M1 network and captured as the TDW by ECoG electrodes. This hypothesis was confirmed by the measurement of R_m during the TDW and attendant *DC* shift (Fig. 3C, left gray traces). Negative current pulses of short duration were repeatedly applied (−0.6 nA, 20 ms, every 100 ms) through the intracellular pipette before and during the TDW (Fig. 3C, left). The current-induced membrane potential drops were considerably reduced in all tested cells during the TDW-associated cell depolarization (baseline, 8.0 ± 3.1 mV versus TDW, 1.3 ± 1.0 mV, $n = 7$ neurons; $P = 0.016$), leading in three neurons to a quasi-canceling of the membrane resistance (< 5 MΩ) (Fig. 3C, right). This large decrease in R_m likely resulted from an increase in synaptic conductance due to the synchronized discharge of a majority of M1 neurons during the TDW.

3.4. Cortical neurons initiating the TDW are more active and hyperexcitable

To get insights into the cellular and network mechanisms responsible for the emergence of TDW and TDS in our rat model, we compared the ongoing activity, integrative properties and excitability of M1 neurons between control rats, receiving a single vehicle injection in M1 ($n = 11$ neurons from 5 rats), and DTX rats ($n = 22$ neurons from 15 rats). Measurements in DTX rats were made at distance from the seizures (post-seizure delay = 76 ± 45 s, pre-seizure delay = 62 ± 42 s, $n = 22$ neurons).

Control cortical neurons and DTX-treated neurons in between seizures were characterized by fast and irregular synaptic fluctuations (Fig. 4A), leading to unimodal V_m distributions (Fig. 4A, right). Although the average membrane polarization was similar in both groups ($P = 0.6$), the magnitude of V_m fluctuations (SD V_m) was significantly attenuated in DTX neurons ($P = 0.007$) (Fig. 4A and B). The spontaneous firing rate was increased in the DTX group ($P = 0.04$) and the AP discharge became more regular ($P = 0.01$) (Fig. 4A and B). This increase in spontaneous firing was accompanied by a lowering of the voltage AP threshold ($P = 0.005$) (Fig. 4B).

We then compared the membrane resistance (R_m) and the membrane time constant (τ_m), which respectively control the efficiency of synaptic currents to displace V_m and the capacity of a neuron to summate synaptic potentials in time. Voltage-current (*V-I*) relations were linear, indicating a lack of membrane rectification in the hyperpolarizing direction in the two groups (Fig. 5A). However, the slope of the *V-I* relation was steeper in the DTX group, resulting in larger R_m values (∼ + 45%) as compared to control condition ($P = 0.02$) (Fig. 5A). As expected, this was associated with an increase in τ_m in DTX-treated neurons ($P = 0.04$) (Fig. 5A).

The high-frequency firing in the majority of M1 neurons during the TDW could result, at least in part, from an exacerbated intrinsic excitability in DTX condition. We thus compared the frequency-current (*F–I*) relations of cortical pyramidal neurons, i.e. their output firing in response to excitatory inputs of increasing intensity, between control ($n = 8$) and DTX ($n = 9$) neurons. Series of depolarizing current pulses were applied to both groups of neurons to compute the threshold current for AP generation and the slope of the frequency-current (*F-I*) curves (neuronal gain) (Fig. 5B). The current threshold was consistently reduced by ∼48% in DTX pyramidal cells ($P = 0.04$), while the slope of *F-I* curves remained unaffected ($P = 0.9$) (Fig. 5B). This indicates an amplification of M1 neurons responsiveness to weak synaptic inputs and a stability of their neuronal gain after DTX injection. The coordinated firing of most M1 neurons during TDW could result from an increase in the temporal reliability of cells discharging in response to suprathreshold excitation. We thus compared the latency and temporal precision of the first AP induced by suprathreshold depolarizing current steps in DTX and control neurons (Fig. 5C). Accordingly, we observed that the latency of evoked APs and the SD of the first AP latency were indeed substantially reduced in DTX neurons ($P = 0.004$ and $P = 0.02$ respectively) (Fig. 5C).

3.5. Progressive changes in cortical neurons activity during inter-ictal periods

The ictogenic mechanisms underlying the high recurrence of TDS at the paroxysm of anti LGI1-encephalitis remain unknown. To investigate this question, we attempted to determine whether the DTX-induced TDW was preceded by time-dependent changes in neuronal and synaptic activities within M1.

We first searched for possible dynamic modifications in the firing rate of extracellularly recorded DTX M1 neurons between successive TDWs (Fig. 6A). The majority of neurons ($n = 34/65$ SUs; 52%) showed a progressive increase in their discharge frequency, which culminated at the approach of the TDW (Fig. 6A and B). Indeed, their mean firing rate, which was 1.1 ± 2.1 Hz after termination of a seizure reached 2.3 ± 2.9 Hz just before the next TDW (mean increase of ∼103%; average rate of increase of 0.3 ± 0.5 $Hz.min^{-1}$; $P < 0.001$) (Fig. 6B right, red curves). In a second neuronal population ($n = 22$ SUs; 34%), the initial interictal firing frequency (2.5 ± 5.1 Hz, $n = 22$ SUs) was not significantly modified over the interictal periods ($P = 0.15$) (Fig. 6B right, black curves). Finally, 9 SUs exhibited a substantial decrease in their firing rate over the inter-seizure period, from 3.6 ± 3.2 Hz to 1.0

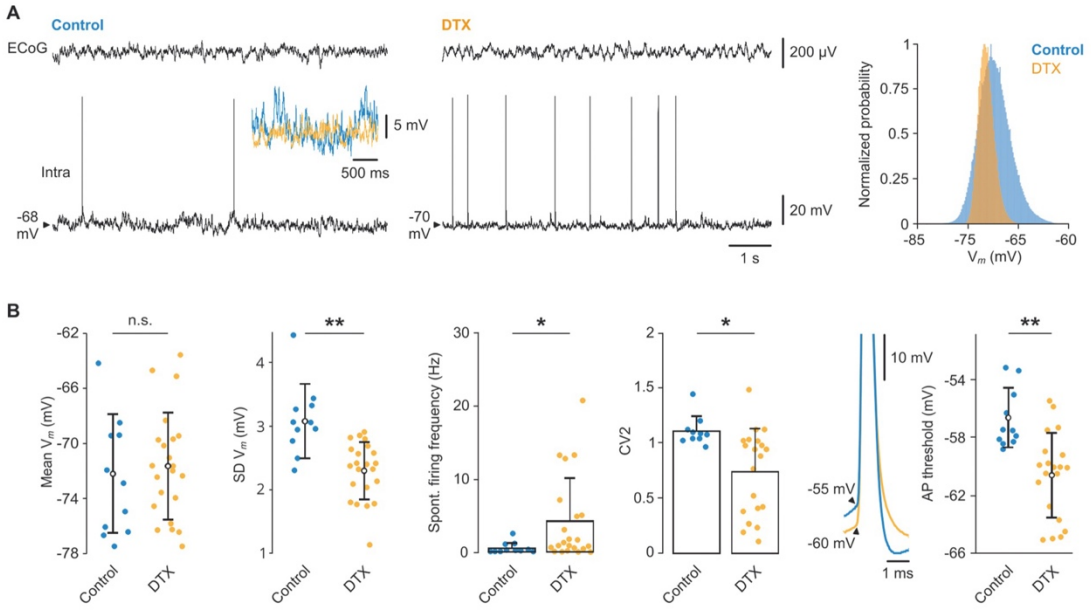

Fig. 4. Spontaneous activity of M1 neurons is increased in DTX rats. (A) Simultaneous recordings of M1 ECoG and intracellular activity from a subjacent pyramidal cell in control (left) and DTX (middle) condition. Inset, *DC* superimposition of spontaneous synaptic activities (2.5 s duration) recorded in the control (blue) and DTX (orange) neuron. Right, distribution of V_m values from the two illustrated neurons. (B) Summary plots comparing mean V_m, SD V_m, spontaneous firing frequency, and CV2 of spike intervals in control (blue circles) and DTX (orange circles) condition. Right, *DC* superimposition of average ($n > 10$) spontaneous APs recorded in a DTX and a control neuron. Spikes are truncated for commodity. Population analysis revealed a significant decrease in the voltage firing threshold in DTX neurons as compared to control ($n = 11$ control and $n = 22$ DTX neurons). *$P < 0.05$, **$P < 0.01$, n.s., not significant (two-tailed Mann-Whitney rank-sum test with Benjamini-Hochberg's post hoc correction).

± 1.0 Hz ($n = 9$ SUs; $P < 0.001$) (Fig. 6B right, blue curves). In contrast, all the neurons recorded in control rats exhibited a stable firing frequency over comparable periods of time ($n = 45$ SUs; Fig. S3 A and B).

The increase in extracellular firing observed in most neurons during inter-ictal epochs could originate from various non-exclusive processes, including a progressive membrane depolarization, an increased amplitude of V_m fluctuations, a change in background synaptic patterns or a lowering of the voltage AP threshold. To test for these different mechanisms, we further analyzed the dynamics of intracellular activities during the inter-TDS period (Fig. 6C and D). In a majority of neurons (~67%), we observed a slow membrane depolarization (from −73.6 ± 4.6 to −71.8 ± 4.1 mV, rate of V_m change = 0.74 ± 0.48 mV.min^{-1}, $n = 8/12$ neurons) accompanied by a significant increase in the amplitude of V_m fluctuations over time ($n = 5/12$ neurons) (Fig. 6D, left and middle, red lines). The four remaining cells exhibited a slight decrease or a lack of change in their V_m and SD V_m values over the course of the interictal period (Fig. 6D, left and middle, blue and black lines). A time-dependent analysis of the frequency content of background synaptic activity also revealed a robust increase in the power of frequencies above 20 Hz, preceding the TDW (Fig. 6C, bottom and D, right). Finally, comparing measurements of voltage AP threshold just after (−59.8 ± 3.1 mV, $n = 10$ neurons) or immediately before (−59.2 ± 2.7 mV, $n = 10$ neurons) seizure occurrence indicated an absence of significant change over the interictal period ($P = 0.11$, Wilcoxon signed-rank test). We did not observe time-dependent changes in neuronal properties of intracellularly recorded neurons from control rats ($n = 11$ neurons) (Fig. S3 C and D).

4. Discussion

4.1. A new model to study anti-LGI1 associated motor seizures

Different strategies have been used by the past to establish a causal link between LGI1 disruption and seizures in anti-LGI1 autoimmune encephalitis. One of the main in vivo approaches, crucial to demonstrate the pathogenicity of autoantibodies, was to develop mouse models of the disease by infusion of total immunoglobulins or purified anti-LGI1 antibodies from patients into the hippocampus or cerebral ventricles for seven to fourteen days. While these experimental procedures were effective in decreasing the expression of Kv1.1 channels and/or AMPAR and in perturbing synaptic transmission within the hippocampus (Petit-Pedrol et al., 2018; Ramberger et al., 2020), they did not permit the emergence of seizures. As anti-LGI1 encephalitis evolves for several weeks or months before reaching a severe phenotype, it is likely that the 10–15% decrease in Kv1.1 channels expression obtained after two weeks of infusion was too small to produce sufficient excitability changes in neurons and networks to trigger epileptic activity (Petit-Pedrol et al., 2018). Interestingly, generalized seizures observed in LGI1 KO mice (Chabrol et al., 2010; Fukata et al., 2010; Yu et al., 2010) are often associated with more than 50% decrease in Kv1.1 channels density as compared to control mice (Seagar et al., 2017; Zhou et al., 2018).

As an alternative strategy, we decided to target the pathophysiological mechanisms downstream to LGI1, through a direct pharmacological inhibition of Kv1.1 channels whose expression and/or function is known to be impaired by the down-regulation of LGI1 (Kornau et al., 2020; Lugarà et al., 2020; Petit-Pedrol et al., 2018; Ramberger et al., 2020; Seagar et al., 2017; Zhou et al., 2018). Our results demonstrate that blocking Kv1.1 channels in the rodent motor cortex faithfully recapitulated the human phenotype of anti-LGI1 encephalitis. First, the

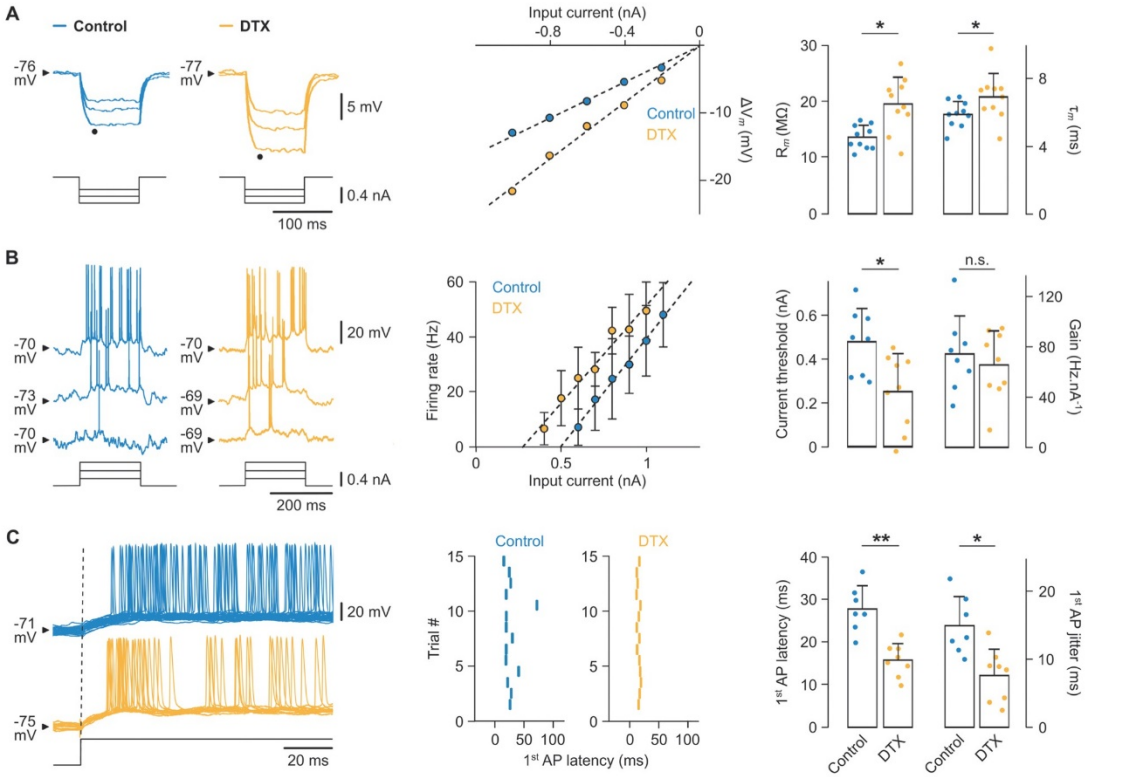

Fig. 5. DTX M1 pyramidal neurons are more excitable. (A) Left, Average ($n = 16$–28 trials) voltage responses of M1 pyramidal neurons (top traces), recorded from a rat intracortically-injected with PBS (Control) or DTX, to negative current pulses of increasing intensity (bottom traces) and corresponding *V-I* plots. The black dots indicate the timing of ΔV_m measurements. Here and in the following panels, the pre-pulse V_m is indicated on the left of the traces. Blue and orange traces correspond to control and DTX condition, respectively. Dashed lines in *V-I* plots correspond to the best linear regression ($r^2 > 0.99$ for both condition). Right, Summary plot comparing mean (± SD) values of R_m and τ_m in both conditions ($n = 10$ neurons). (B) Firing responses of a M1 pyramidal neuron (top traces) to depolarizing currents steps of increasing intensity (bottom traces) in control and DTX condition, and corresponding *F-I* curves. Each symbol corresponds to the mean (± SD) firing rate calculated from 20 to 25 successive trials. Dashed lines correspond to the best linear regression ($r^2 > 0.95$) in the two conditions. Pooled current threshold and gain values from neurons in control ($n = 8$) and DTX condition ($n = 9$) are compared on the right. (C) Left, Fourteen overlaid firing responses (the first 100 ms are illustrated) of a M1 neuron in control and DTX rats. The corresponding raster plots of the first evoked AP are illustrated on the right of the traces. Right, Mean values of first AP latency and jitter in control ($n = 7$) and DTX condition ($n = 8$). $^*P < 0.05$, $^{**}P < 0.01$, n.s., not significant (two-tailed Mann-Whitney rank-sum test with Benjamini-Hochberg's post hoc correction).

tonic-dystonic contraction, characteristic of these motor seizures, was systematically observed in the rodent model (see Supplementary movies 1 and 2 for comparison between species). Second, the high incidence and regularity of seizure occurrence measured in the rodent model were similar to those observed in our cohort of anti-LGI1 encephalitis patients. Finally, in both species, the TDS were always preceded by a stereotyped slow cortical wave of large amplitude in the M1 EEG. However, our acute pharmacological experimental model does not embrace the full spectrum of complex disturbances mediated by the anti-LGI1 antibodies. In particular, a dysfunction in AMPAR, as observed in LGI1 KO mice and in mice treated with human anti-LGI1 antibodies (Fukata et al., 2010; Petit-Pedrol et al., 2018; Yu et al., 2010; Zhou et al., 2009), and its possible consecutive modulation of the excitation/inhibition balance could participate to the initiation of seizure activity. As previously proposed (Ohkawa et al., 2013), a decreased AMPAR function in inhibitory interneurons could reduce the inhibitory impact on excitatory pyramidal cells, causing an overall network hyperactivity. However, this hypothesis is not supported by a study conducted in LGI1 conditional KO mice since a specific inhibition of LGI in pyramidal neurons was sufficient to generate seizures, whereas no spontaneous seizures were observed after a selective deletion of LGI1 in interneurons (Boillot et al., 2014). Future studies combining dysfunctions of both Kv1.1 channels and AMPAR will be needed to appreciate the specific contribution of LGI1's synaptic partners.

4.2. A putative scenario for the generation of the TDW and the TDS

By performing extracellular and intracellular recordings of M1 neurons in the rodent model, we demonstrated that the selective blockade of Kv1.1 channels initiates a cascade of changes in neuronal excitability and network activity that concur to generate recurrent large-amplitude slow EEG waves closely resembling the human TDWs.

Kv1.1 channels conduct a critical K^+ current that activates at membrane potentials close to the AP voltage threshold (Guan et al., 2006) and prevents hyperexcitability by limiting and delaying the neuronal discharge (Cudmore et al., 2010; Guan et al., 2007). Accordingly, we found that the intrinsic excitability of M1 pyramidal neurons poisoned with DTX was consistently increased. This was expressed as a reduction in both current and voltage threshold for AP triggering, resulting in a facilitation of their spontaneous and evoked discharge. Similar effects of DTX on neuronal excitability, attributed to a direct inhibitory action on Kv1.1 channels (Guan et al., 2007; Higgs and Spain, 2011; Li et al., 2012;

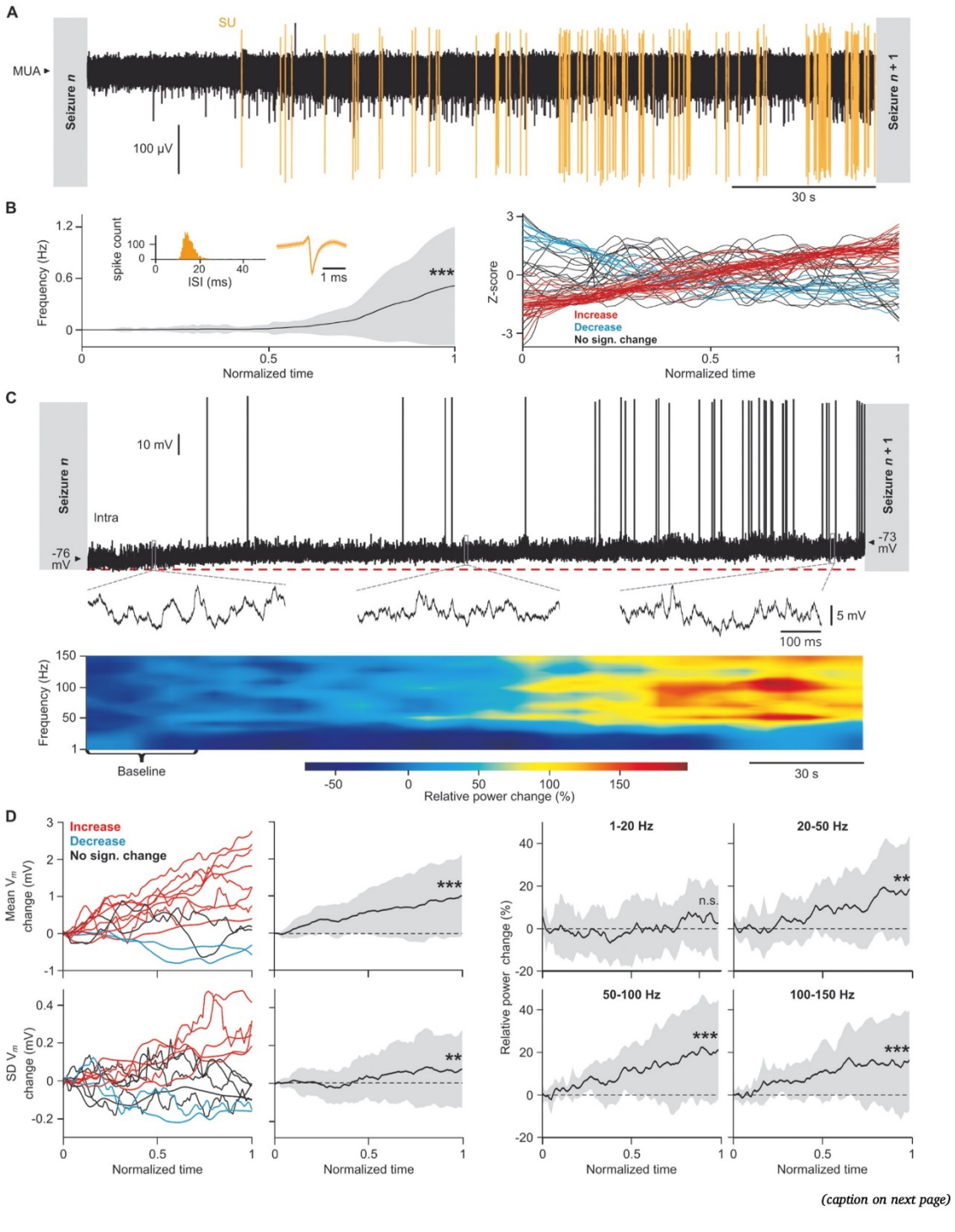

(caption on next page)

Fig. 6. Progressive neuronal changes over the interictal periods. (A) Examples of MU (black trace) and SU (orange trace) activities in between seizures (gray shaded areas). (B) Left, Evolution of the mean (± SD) firing rate of the SU illustrated in (A) along inter-seizure periods ($n = 219$), after normalization of the duration of interictal episodes. ISI distribution and average spike waveform profile are shown in inset. Right, Mean firing rate (normalized with a z-score) for all sorted SUs ($n = 65$, $n = 53$–219 inter-seizure periods per SU). The majority of cells showed a progressive increase in their spike frequency in between seizures (red lines, $n = 34/65$; $P < 0.05$, Pearson correlation), with the remaining neurons either exhibiting a decrease (blue lines, $n = 9$ $P < 0.05$) or an absence of significant change (black lines, $n = 22$, $P > 0.05$) in their firing rate. (C) Top, Intracellular activity of a M1 pyramidal neuron during the inter-seizure period (top traces) and expanded view of short periods of subthreshold synaptic activity (lower traces). A time-frequency map of subthreshold neuronal activity is shown below the records. The frequency power is normalized by the baseline power. (D) Top left, mean V_m computed over a sliding-time window of 30 s (each line corresponds to a single neuron). Pearson's correlation revealed a significant depolarization ($n = 8$), a lack of change ($n = 2$) or a hyperpolarization ($n = 2$) of V_m during inter-seizure periods. The evolution in time of mean V_m (± SD) computed over all neurons is shown at right. Bottom left, Similar measurements and statistics applied to the SD V_m. Right, Interictal evolution of the mean (± SD) relative power change computed for four different frequency bands. Note the increased power for frequencies above 20 Hz. $^{**}P < 0.01$, $^{***}P < 0.001$, n.s., not significant (Pearson's correlation with Benjamini-Hochberg's post hoc correction).

Morgan et al., 2019), have been previously reported in pyramidal neurons (Bekkers and Delaney, 2001; Cudmore et al., 2010; Guan et al., 2007; Higgs and Spain, 2011; Morgan et al., 2019) and in neocortical GABAergic interneurons (Goldberg et al., 2008; Li et al., 2012). Interestingly, we also showed that the hyperexcitability of pyramidal neurons after DTX injection was accompanied by a shorter latency and a lower variability of their current-evoked AP discharge, as well as an increased regularity of their spontaneous firing, as previously observed (Cudmore et al., 2010; Higgs and Spain, 2011; Morgan et al., 2019).

Previous in vitro investigations in hippocampal slices from LGI1 KO mice or mice infused with LGI1 antibodies reported enhanced glutamate release probability and excitatory synaptic transmission (Boillot et al., 2016; Petit-Pedrol et al., 2018; Seagar et al., 2017; Yu et al., 2010), likely caused by a decrease in presynaptic expression of Kv1.1 (Petit--Pedrol et al., 2018; Seagar et al., 2017). Our in vivo data showing a reduction in the amplitude of Vm fluctuations in M1 pyramidal neurons after DTX are difficult to reconcile with such an increased glutamatergic neurotransmission. One possible explanation would be a parallel increase in inhibitory synaptic transmission, due to a DTX-induced increased excitability of fast-spiking interneurons (Goldberg et al., 2008; Li et al., 2012), which would produce a robust shunting effect on pyramidal cells membrane (Tremblay et al., 2016). A reduction in AMPA receptor function (Fukata et al., 2010; Ohkawa et al., 2013), which is proposed to be a homeostatic response to the increase in presynaptic glutamatergic transmission (Seagar et al., 2017), might provide an alternative mechanism.

We also found that the enhanced excitability of DTX-treated pyramidal cells was accompanied by an increase in their input resistance, an unexpected result since Kv1.1 channels are not activated at resting membrane potentials (Bekkers and Delaney, 2001; Guan et al., 2018). Although the precise origin of this change in R_m remains to be established, it is possible that the blockade of Kv1.1 triggers a downregulation of other voltage-gated channels, which would be responsible for the decrease in membrane conductance at rest. Such cross-modulation of ionic conductances has already been described in other forms of encephalopathy and epilepsy (Lezmy et al., 2020; Simkin et al., 2021; Zhang et al., 2021).

The DTX-induced modifications of membrane properties in

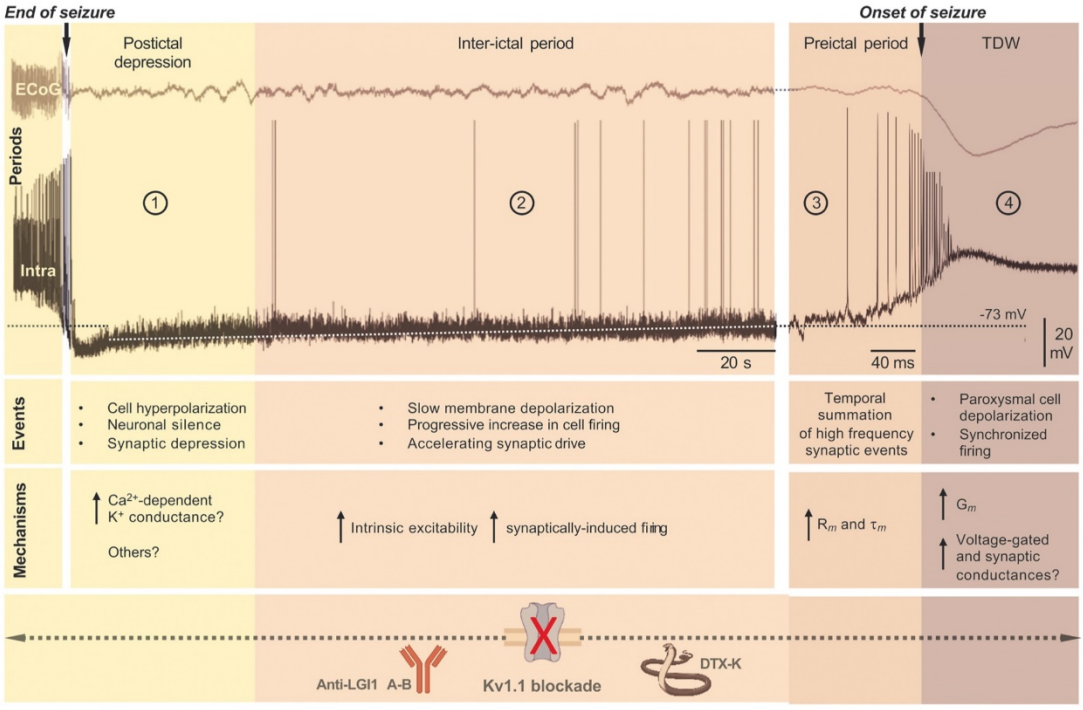

Fig. 7. Diachronic scenario that could explain the cyclic recurrence of seizures after disruption of Kv1.1 channels. See Discussion for explanations on each step of this scenario.

individual neurons observed at the injection site are likely to be responsible for dynamic modifications within the M1 network that will favor paroxysmal synchronized activities. We therefore propose the following diachronic scenario to explain the cyclic recurrence of seizures. We observed in most DTX pyramidal cells an enhanced membrane polarization immediately after seizures, despite a lack of change in the average interictal V_m values compared to control neurons. This relative neuronal hyperpolarization after seizure termination likely results from the activation of Ca^{2+}-dependent K^+ conductance, caused by intense firing and consecutive increase in intracellular Ca^{2+} concentration during the preceding seizure activity (Fig. 7, period 1), as previously proposed for post-ictal depression in other types of neocortical seizures (Timofeev et al., 2004). Neurons then progressively recover a more depolarized membrane potential, instigating a progressive increase in firing rate amplified by the facilitating effect of Kv1.1 channels blockade on intrinsic and synaptically-induced firing (Fig. 7, period 2) (Ovsepian et al., 2016). This increase in firing rate among M1 neurons could result in an amplification of the background synaptic drive through local synaptic interactions that may participate in the progressive membrane depolarization (Altwegg-Boussac et al., 2014) and facilitate the coupling between excitatory postsynaptic potentials and APs (Guan et al., 2007; Ovsepian et al., 2016). It may thus explain the increased frequency of ongoing synaptic events in M1 neurons observed just before seizures, and the triggering – through a temporal summation facilitated by an increased membrane time constant – of a paroxysmal depolarization in a majority of neurons (Fig. 7, periods 3 and 4). The abnormally large positive shift in membrane potential underlying the TDW closely resembles the monolithic epileptic event called "paroxysmal depolarization shift" (Prince, 1968), which is due to the synergistic effects of voltage-gated and synaptic conductances (G_m in Fig. 7) (Hotka and Kubista, 2019). In line with this scenario, we found that the TDW-associated depolarizations were associated with a collapse of membrane resistance values in pyramidal neurons. The synchronization of TDW-related paroxysmal depolarizations within the motor cortex, attested by the large-amplitude negative *DC* shift simultaneously recorded in the extracellular space, likely elicited a robust and coordinated discharge among M1 cortical neurons, including those of the pyramidal tract initiating the tonic muscular contractions.

The decreased firing observed in a minority of M1 neurons during the TDW could result from a collateral inhibition originating from local interneurons, activated by the pyramidal neurons subtending the paroxysmal depolarization. This process, known to control the spatial extent of excitation among M1 neurons (Georgopoulos and Stefanis, 2007), could account for the relatively focused motor response to the TDW. Relying on the strong similarity of TDW and TDS between anti-LGI1 encephalitis patients and the rodent model, we can envisage similar ictogenic processes in humans.

5. Conclusions

In this work, we developed a new in vivo rodent model to determine the role of Kv1.1 channels in the emergence of motor seizures associated with anti-LGI1 encephalitis. We demonstrated in freely-moving animals that a focal inhibition of Kv1.1 channels by DTX-K in M1 circuits promoted the emergence of seizure activity that closely resembled the TDS recorded in our cohort of anti-LGI1 encephalitis patients. Motor seizures in the rodent model were characterized by a tonic-dystonic contraction of the upper limbs that was always preceded by a stereotyped large amplitude slow wave in the M1 EEG. Like in human patients, TDS in rodents had a high incidence and a regular frequency of occurrence. Our single cell recordings in the rodent model indicated that the loss of Kv1.1 channels caused an increased excitability of M1 pyramidal neurons, expressed as an increased membrane resistance, a decreased activation threshold, a reduced latency and improved precision of their evoked firing. Our results also indicate that these cellular changes were responsible for a progressive increase in the level of activity and synchronization within the M1 network during interictal periods, ultimately leading to the triggering in a majority of neurons of a massive suprathreshold membrane depolarization reflected in the EEG by the paroxysmal TDW. This robust and synchronized firing of M1 neurons during the TDW is likely responsible for the initiation of the characteristic tonic contraction associated with these seizures.

Our findings, providing the first description of the pathophysiological mechanisms underlying the recurrence of TDS, could be of valuable interest not only for the understanding of ictogenesis in autoimmune encephalitis but also to the study of brain pathologies associated with deficiency in Kv1 channels (Chow and Leung, 2020; D'Adamo et al., 2020). Our results also opens up the way to new treatments through the discovery of molecules that could rescue Kv1.1 inhibition, by a direct targeting of its regulatory mechanisms (Niespodziany et al., 2019) or through compensatory mechanisms such as potentiation of other K^+ currents.

Funding

This work was supported by the Agence nationale de la recherche, France, 'Investissements d'avenir' program [grant numbers ANR-10-IAIHU-06, ANR-11-INBS-0011-NeurATRIS]; the Fondation pour la Recherche Médicale, France [grant number FDT202012010523, PB]; and the Fondation Assitance Publique-Hôpitaux de Paris, France [EPIRES, Marie Laure PLV Merchandising].

CRediT authorship contribution statement

Conceptualization: PB, SC, SM, VN. Methodology: PB, SW, SC, SM, VN. Investigation: PB, DR, SL. Resources: PB, LC, KL. Formal analysis: PB, SW. Visualization: PB, SW, SC, SM, VN. Funding acquisition: PB, SC, SM, VN. Project administration: SC, SM, VN. Supervision: SC, SM, VN. Writing – original draft: PB, SC, SM, VN. Writing – review & editing: SW, LC, DR, SL, KL.

Competing interests

V.N. reports personal fees from UCB, Liva Nova, and EISAI, outside the submitted work. The other authors declare that they have no competing interests.

Data Availability

The data that support the findings of this study are available from the corresponding author, upon reasonable request.

Appendix A. Supporting information

Supplementary data associated with this article can be found in the online version at doi:10.1016/j.pneurobio.2022.102262.

References

Altwegg-Boussac, T., Chavez, M., Mahon, S., Charpier, S., 2014. Excitability and responsiveness of rat barrel cortex neurons in the presence and absence of spontaneous synaptic activity in vivo. J. Physiol. 592, 3577–3595. https://doi.org/10.1113/jphysiol.2013.270561.

Altwegg-Boussac, T., Schramm, A.E., Ballestero, J., Grosselin, F., Chavez, M., Lecas, S., Baulac, M., Naccache, L., Demeret, S., Navarro, V., Mahon, S., Charpier, S., 2017. Cortical neurons and networks are dormant but fully responsive during isoelectric brain state. Brain J. Neurol. 140, 2381–2398. https://doi.org/10.1093/brain/awx175.

Bagetta, G., Iannone, M., Palma, E., Nistico, G., Dolly, J.O., 1996. N-methyl-d-aspartate and nonn-methyl-d-aspartate receptors mediate seizures and CA1 hippocampal damage induced by dendrotoxin-K in rats. Neuroscience 71, 613–624.

Barthó, P., Hirase, H., Monconduit, L., Zugaro, M., Harris, K.D., Buzsáki, G., 2004. Characterization of neocortical principal cells and interneurons by network interactions and extracellular features. J. Neurophysiol. 92, 600–608. https://doi.org/10.1152/jn.01170.2003.

Bekkers, J.M., Delaney, A.J., 2001. Modulation of excitability by α-dendrotoxin-sensitive potassium channels in neocortical pyramidal neurons. J. Neurosci. 21, 6553–6560. https://doi.org/10.1523/JNEUROSCI.21-17-06553.2001.

Benjamini, Y., Hochberg, Y., 1995. Controlling the false discovery rate: a practical and powerful approach to multiple testing. J. R. Stat. Soc. Ser. B Methodol. 57, 289–300.

Bikson, M., Hahn, P.J., Fox, J.E., Jefferys, J.G.R., 2003. Depolarization block of neurons during maintenance of electrographic seizures. J. Neurophysiol. 90, 2402–2408. https://doi.org/10.1152/jn.00467.2003.

Boillot, M., Huneau, C., Marsan, E., Lehongre, K., Navarro, V., Ishida, S., Dufresnois, B., Ozkaynak, E., Garrigue, J., Miles, R., Martin, B., Leguern, E., Anderson, M.P., Baulac, S., 2014. Glutamatergic neuron-targeted loss of LGI1 epilepsy gene results in seizures. Brain 137, 2984–2996. https://doi.org/10.1093/brain/awu259.

Boillot, M., Lee, C.-Y., Allene, C., Leguern, E., Baulac, S., Rouach, N., 2016. LGI1 acts presynaptically to regulate excitatory synaptic transmission during early postnatal development. Sci. Rep. 6. https://doi.org/10.1038/srep21769.

de Bruijn, M.A.A.M., van Sonderen, A., van Coevorden-Hameete, M.H., Bastiaansen, A.E. M., Schreurs, M.W.J., Rouhl, R.P.W., van Donselaar, C.A., Majoie, M.H.J.M., Neuteboom, R.F., Sillevis Smitt, P.A.E., Thijs, R.D., Titulaer, M.J., 2019. Evaluation of seizure treatment in anti-LGI1, anti-NMDAR, and anti-GABA B R encephalitis. Neurology 92, e2185–e2196. https://doi.org/10.1212/WNL.0000000000007475.

Chabrol, E., Navarro, V., Provenzano, G., Cohen, I., Dinocourt, C., Rivaud-Péchoux, S., Fricker, D., Baulac, M., Miles, R., LeGuern, E., Baulac, S., 2010. Electroclinical characterization of epileptic seizures in leucine-rich, glioma-inactivated 1-deficient mice. Brain 133, 2749–2762. https://doi.org/10.1093/brain/awq171.

Chow, L.W.C., Leung, Y.-M., 2020. The versatile Kv channels in the nervous system: actions beyond action potentials. Cell. Mol. Life Sci. CMLS 77, 2473–2482. https://doi.org/10.1007/s00018-019-03415-8.

Crisp, S.J., Kullmann, D.M., Vincent, A., 2016. Autoimmune synaptopathies. Nat. Rev. Neurosci. 17, 103–117. https://doi.org/10.1038/nrn.2015.27.

Cudmore, R.H., Fronzaroli-Molinieres, L., Giraud, P., Debanne, D., 2010. Spike-time precision and network synchrony are controlled by the homeostatic regulation of the D-type potassium current. J. Neurosci. 30, 12885–12895. https://doi.org/10.1523/JNEUROSCI.0740-10.2010.

D'Adamo, M.C., Liantonio, A., Rolland, J.-F., Pessia, M., Imbrici, P., 2020. Kv1.1 channelopathies: pathophysiological mechanisms and therapeutic approaches. Int. J. Mol. Sci. 21, E2935 https://doi.org/10.3390/ijms21082935.

Dalmau, J., Geis, C., Graus, F., 2017. Autoantibodies to synaptic receptors and neuronal cell surface proteins in autoimmune diseases of the central nervous system. Physiol. Rev. 97, 839–887. https://doi.org/10.1152/physrev.00010.2016.

Depaulis, A., David, O., Charpier, S., 2016. The genetic absence epilepsy rat from Strasbourg as a model to decipher the neuronal and network mechanisms of generalized idiopathic epilepsies. J. Neurosci. Methods 260, 159–174. https://doi.org/10.1016/j.jneumeth.2015.05.022.

Feyissa, A.M., Lamb, C., Pittock, S.J., Gadoth, A., McKeon, A., Klein, C.J., Britton, J.W., 2018. Antiepileptic drug therapy in autoimmune epilepsy associated with antibodies targeting the leucine-rich glioma-inactivated protein 1. Epilepsia Open 3, 348–356. https://doi.org/10.1002/epi4.12226.

Fukata, Y., Lovero, K.L., Iwanaga, T., Watanabe, A., Yokoi, N., Tabuchi, K., Shigemoto, R., Nicoll, R.A., Fukata, M., 2010. Disruption of LGI1-linked synaptic complex causes abnormal synaptic transmission and epilepsy. Proc. Natl. Acad. Sci. 107, 3799–3804. https://doi.org/10.1073/pnas.0914537107.

Fukata, Y., Chen, X., Chiken, S., Hirano, Y., Yamagata, A., Inahashi, H., Sanbo, M., Sano, H., Goto, T., Hirabayashi, M., Kornau, H.-C., Prüss, H., Nambu, A., Fukai, S., Nicoll, R.A., Fukata, M., 2021. LGI1–ADAM22–MAGUK configures transsynaptic nanoalignment for synaptic transmission and epilepsy prevention. Proc. Natl. Acad. Sci. 118, e2022580118 https://doi.org/10.1073/pnas.2022580118.

Georgopoulos, A.P., Stefanis, C.N., 2007. Local shaping of function in the motor cortex: motor contrast, directional tuning. Brain Res. Rev. 55, 383–389. https://doi.org/10.1016/j.brainresrev.2007.05.001.

Ghimire, P., Khanal, U.P., Gajurel, B.P., Karn, R., Rajbhandari, R., Paudel, S., Gautam, N., Ojha, R., 2020. Anti-LGI1, anti-GABABR, and Anti-CASPR2 encephalitides in Asia: a systematic review. Brain Behav. 10. https://doi.org/10.1002/brb3.1793.

Goldberg, E.M., Clark, B.D., Zagha, E., Nahmani, M., Erisir, A., Rudy, B., 2008. K+ channels at the axon initial segment dampen near-threshold excitability of neocortical fast-spiking GABAergic interneurons. Neuron 58, 387–400. https://doi.org/10.1016/j.neuron.2008.03.003.

Griffith, S.P., Malpas, C.B., Alpitsis, R., O'Brien, T.J., Monif, M., 2020. The neuropsychological spectrum of anti-LGI1 antibody mediated autoimmune encephalitis. J. Neuroimmunol. 345, 577271 https://doi.org/10.1016/j.jneuroim.2020.577271.

Grissmer, S., Nguyen, A.N., Aiyar, J., Hanson, D.C., Mather, R.J., Gutman, G.A., Karmilowicz, M.J., Auperin, D.D., Chandy, K.G., 1994. Pharmacological characterization of five cloned voltage-gated K+ channels, types Kv1.1, 1.2, 1.3, 1.5, and 3.1, stably expressed in mammalian cell lines. Mol. Pharm. 45, 1227–1234.

Guan, D., Lee, J.C.F., Tkatch, T., Surmeier, D.J., Armstrong, W.E., Foehring, R.C., 2006. Expression and biophysical properties of Kv1 channels in supragranular neocortical pyramidal neurones. J. Physiol. 571, 371–389. https://doi.org/10.1113/jphysiol.2005.097006.

Guan, D., Lee, J.C.F., Higgs, M.H., Spain, W.J., Foehring, R.C., 2007. Functional roles of Kv1 channels in neocortical pyramidal neurons. J. Neurophysiol. 97, 1931–1940. https://doi.org/10.1152/jn.00933.2006.

Guan, D., Pathak, D., Foehring, R.C., 2018. Functional roles of Kv1-mediated currents in genetically identified subtypes of pyramidal neurons in layer 5 of mouse somatosensory cortex. J. Neurophysiol. 120, 394–408. https://doi.org/10.1152/jn.00691.2017.

Higgs, M.H., Spain, W.J., 2011. Kv1 channels control spike threshold dynamics and spike timing in cortical pyramidal neurones: Kv1 channels control threshold dynamics. J. Physiol. 589, 5125–5142. https://doi.org/10.1113/jphysiol.2011.216721.

Hivert, B., Marien, L., Agbam, K.N., Faivre-Sarrailh, C., 2019. ADAM22 and ADAM23 modulate the targeting of the Kv1 channel-associated protein LGI1 to the axon initial segment. J. Cell Sci. 132. https://doi.org/10.1242/jcs.219774.

Hotka, M., Kubista, H., 2019. The paroxysmal depolarization shift in epilepsy research. Int. J. Biochem. Cell Biol. 107, 77–81. https://doi.org/10.1016/j.biocel.2018.12.006.

Husari, K.S., Dubey, D., 2019. Autoimmune epilepsy. Neurotherapeutics 16, 685–702. https://doi.org/10.1007/s13311-019-00750-3.

Irani, S.R., Michell, A.W., Lang, B., Pettingill, P., Waters, P., Johnson, M.R., Schott, J.M., Armstrong, R.J.E., Zagami, S., Bleasel, A., Somerville, A., Smith, E.R., Vincent, S.M. J., A, 2011. Faciobrachial dystonic seizures precede Lgi1 antibody limbic encephalitis. Ann. Neurol. 69, 892–900. https://doi.org/10.1002/ana.22307.

Irani, S.R., Stagg, C.J., Schott, J.M., Rosenthal, C.R., Schneider, S.A., Pettingill, P., Pettingill, R., Waters, P., Thomas, A., Voets, N.L., Cardoso, M.J., Cash, D.M., Manning, E.N., Lang, B., Smith, S.J.M., Vincent, A., Johnson, M.R., 2013. Faciobrachial dystonic seizures: the influence of immunotherapy on seizure control and prevention of cognitive impairment in a broadening phenotype. Brain 136, 3151–3162. https://doi.org/10.1093/brain/awt212.

Kornau, H., Kreye, J., Stumpf, A., Fukata, Y., Parthier, D., Sammons, R.P., Imbrosci, B., Kurpjuweit, S., Kowski, A.B., Fukata, M., Prüss, H., Schmitz, D., 2020. Human cerebrospinal fluid monoclonal LGI1 autoantibodies increase neuronal excitability. Ann. Neurol. 87, 405–418. https://doi.org/10.1002/ana.25666.

Langlois, M., Polack, P.-O., Bernard, H., David, O., Charpier, S., Depaulis, A., Deransart, C., 2010. Involvement of the thalamic parafascicular nucleus in mesial temporal lobe epilepsy. J. Neurosci. Off. J. Soc. Neurosci. 30, 16523–16535. https://doi.org/10.1523/JNEUROSCI.1109-10.2010.

Lezmy, J., Gelman, H., Katsenelson, M., Styr, B., Tikochinsky, E., Lipinsky, M., Peretz, A., Slutsky, I., Attali, B., 2020. M-current inhibition in hippocampal excitatory neurons triggers intrinsic and synaptic homeostatic responses at different temporal scales. J. Neurosci. Off. J. Soc. Neurosci. 40, 3694–3706. https://doi.org/10.1523/JNEUROSCI.1914-19.2020.

Li, K.-X., Lu, Y.-M., Xu, Z.-H., Zhang, J., Zhu, J.-M., Zhang, J.-M., Cao, S.-X., Chen, X.-J., Chen, Z., Luo, J.-H., Duan, S., Li, X.-M., 2012. Neuregulin 1 regulates excitability of fast-spiking neurons through Kv1.1 and acts in epilepsy. Nat. Neurosci. 15, 267–273. https://doi.org/10.1038/nn.3006.

Liu, R., Zhang, M., Liu, L., Chen, G., Hou, Y., Wang, M., Li, J., 2020. Neuronal surface antibody syndrome: a review of the characteristics of the disease and its association with autoantibodies. Neuroimmunomodulation 27, 1–8. https://doi.org/10.1159/000507448.

Liu, X., Han, Y., Yang, L., Wang, B., Shao, S., Feng, Y., Pang, Z., Du, Y., Lin, Y., 2020. The exploration of the spectrum of motor manifestations of anti-LGI1 encephalitis beyond FBDS. Seizure 76, 22–27. https://doi.org/10.1016/j.seizure.2019.12.023.

Lugarà, E., Kaushik, R., Leite, M., Chabrol, E., Dityatev, A., Lignani, G., Walker, M.C., 2020. LGI1 downregulation increases neuronal circuit excitability. Epilepsia 61, 2836–2846. https://doi.org/10.1111/epi.16736.

Mahon, S., Charpier, S., 2012. Bidirectional plasticity of intrinsic excitability controls sensory inputs efficiency in layer 5 barrel cortex neurons in vivo. J. Neurosci. 32, 11377–11389. https://doi.org/10.1523/JNEUROSCI.0415-12.2012.

Maris, E., Oostenveld, R., 2007. Nonparametric statistical testing of EEG- and MEG-data. J. Neurosci. Methods 164, 177–190. https://doi.org/10.1016/j.jneumeth.2007.03.024.

Morgan, P.J., Bourboulou, R., Filippi, C., Koenig-Gambini, J., Epsztein, J., 2019. Kv1.1 contributes to a rapid homeostatic plasticity of intrinsic excitability in CA1 pyramidal neurons in vivo. ELife 8, e49915. https://doi.org/10.7554/eLife.49915.

Navarro, V., Kas, A., Apartis, E., Chami, L., Rogemond, V., Levy, P., Psimaras, D., Habert, M.-O., Baulac, M., Delattre, J.-Y., Honnorat, J., et al., 2016. Motor cortex and hippocampus are the two main cortical targets in LGI1-antibody encephalitis. Brain 139, 1079–1093. https://doi.org/10.1093/brain/aww012.

Niespodziany, I., Mullier, B., André, V.M., Ghisdal, P., Jnoff, E., Moreno-Delgado, D., Swinnen, D., Sands, Z., Wood, M., Wolff, C., 2019. Discovery of a small molecule modulator of the Kv1.1/Kvβ1 channel complex that reduces neuronal excitability and in vitro epileptiform activity. CNS Neurosci. Ther. 25, 442–451. https://doi.org/10.1111/cns.13060.

Ohkawa, T., Fukata, Y., Yamasaki, M., Miyazaki, T., Yokoi, N., Takashima, H., Watanabe, M., Watanabe, O., Fukata, M., 2013. Autoantibodies to epilepsy-related LGI1 in limbic encephalitis neutralize LGI1-ADAM22 interaction and reduce synaptic AMPA receptors. J. Neurosci. 33, 18161–18174. https://doi.org/10.1523/JNEUROSCI.3506-13.2013.

Oostenveld, R., Fries, P., Maris, E., Schoffelen, J.-M., 2011. FieldTrip: open source software for advanced analysis of MEG, EEG, and invasive electrophysiological data. Comput. Intell. Neurosci. 2011, 1–9. https://doi.org/10.1155/2011/156869.

Ovsepian, S.V., LeBerre, M., Steuber, V., O'Leary, V.B., Leibold, C., Oliver Dolly, J., 2016. Distinctive role of KV1.1 subunit in the biology and functions of low threshold K+ channels with implications for neurological disease. Pharmacol. Ther. 159 (93–101) https://doi.org/10.1016/j.pharmthera.2016.01.005.

Pape, H.C., 1996. Queer current and pacemaker: the hyperpolarization-activated cation current in neurons. Annu. Rev. Physiol. 58, 299–327. https://doi.org/10.1146/annurev.ph.58.030196.001503.

Paxinos, G., Watson, C.R., 1997. The Rat Brain in Stereotaxic Coordinates. Academic Press.

Petit-Pedrol, M., Sell, J., Planagumà, J., Mannara, F., Radosevic, M., Haselmann, H., Ceanga, M., Sabater, L., Spatola, M., Soto, D., Gasull, X., Dalmau, J., Geis, C., 2018.

LGI1 antibodies alter Kv1.1 and AMPA receptors changing synaptic excitability, plasticity and memory. Brain. https://doi.org/10.1093/brain/awy253.
Prince, D.A., 1968. The depolarization shift in "epileptic" neurons. Exp. Neurol. 21, 467–485. https://doi.org/10.1016/0014-4886(68)90066-6.
Ramanathan, S., Al-Diwani, A., Waters, P., Irani, S.R., 2021. The autoantibody-mediated encephalitides: from clinical observations to molecular pathogenesis. J. Neurol. 268, 1689–1707. https://doi.org/10.1007/s00415-019-09590-9.
Ramberger, M., Berretta, A., Tan, J.M.M., Sun, B., Michael, S., Yeo, T., Theorell, J., Bashford-Rogers, R., Paneva, S., O'Dowd, V., Dedi, N., Topia, S., Griffin, R., Ramirez-Franco, J., El Far, O., Baulac, S., Leite, M.I., Sen, A., Jeans, A., McMillan, D., Marshall, D., Anthony, D., Lightwood, D., Waters, P., Irani, S.R., 2020. Distinctive binding properties of human monoclonal LGI1 autoantibodies determine pathogenic mechanisms. Brain 143, 1731–1745. https://doi.org/10.1093/brain/awaa104.
Schulte, U., Thumfart, J.-O., Klöcker, N., Sailer, C.A., Bildl, W., Biniossek, M., Dehn, D., Deller, T., Eble, S., Abbass, K., Wangler, T., Knaus, H.-G., Fakler, B., 2006. The epilepsy-linked Lgi1 protein assembles into presynaptic Kv1 channels and inhibits inactivation by Kvbeta1. Neuron 49, 697–706. https://doi.org/10.1016/j.neuron.2006.01.033.
Seagar, M., Russier, M., Caillard, O., Maulet, Y., Fronzaroli-Molinieres, L., De San Feliciano, M., Boumedine-Guignon, N., Rodriguez, L., Zbili, M., Usseglio, F., Formisano-Tréziny, C., Youssouf, F., Sangiardi, M., Boillot, M., Baulac, S., Benitez, M.J., Garrido, J.-J., Debanne, D., El Far, O., 2017. LGI1 tunes intrinsic excitability by regulating the density of axonal Kv1 channels. Proc. Natl. Acad. Sci. 114, 7719–7724. https://doi.org/10.1073/pnas.1618656114.
Simkin, D., Marshall, K.A., Vanoye, C.G., Desai, R.R., Bustos, B.I., Piyevsky, B.N., Ortega, J.A., Forrest, M., Robertson, G.L., Penzes, P., Laux, L.C., Lubbe, S.J., Millichap, J.J., George, A.L., Kiskinis, E., 2021. Dyshomeostatic modulation of Ca2+-activated K+ channels in a human neuronal model of KCNQ2 encephalopathy. ELife 10, e64434. https://doi.org/10.7554/eLife.64434.
Steriade, M., 2004. Neocortical cell classes are flexible entities. Nat. Rev. Neurosci. 5, 121–134. https://doi.org/10.1038/nrn1325.
Thompson, J., Bi, M., Murchison, A.G., Makuch, M., Bien, C.G., Chu, K., Farooque, P., Gelfand, J.M., Geschwind, M.D., Hirsch, L.J., Somerville, E., Lang, B., Vincent, A., Leite, M.I., Waters, P., Irani, S.R., Faciobrachial Dystonic Seizures Study Group, Dogan-Onugoren, M., Rae-Grant, A., Illes, Z., Szots, M., Malter, M., Widman, G., Surges, R., Archibald, N., Reid, J., Duncan, C., Richardson, A., Lilleker, J., Iorio, R., Blaabjerg, M., Abeler, K., Shin, Y., 2018. The importance of early immunotherapy in patients with faciobrachial dystonic seizures. Brain 141, 348–356. https://doi.org/10.1093/brain/awx323.
Timofeev, I., Grenier, F., Steriade, M., 2004. Contribution of intrinsic neuronal factors in the generation of cortically driven electrographic seizures. J. Neurophysiol. 92, 1133–1143. https://doi.org/10.1152/jn.00523.2003.
Tremblay, R., Lee, S., Rudy, B., 2016. GABAergic interneurons in the neocortex: from cellular properties to circuits. Neuron 91, 260–292. https://doi.org/10.1016/j.neuron.2016.06.033.
Wang, F.C., Bell, N., Reid, P., Smith, L.A., McIntosh, P., Robertson, B., Dolly, J.O., 1999. Identification of residues in dendrotoxin K responsible for its discrimination between neuronal K+ channels containing Kv1.1 and 1.2 alpha subunits. Eur. J. Biochem. 263, 222–229. https://doi.org/10.1046/j.1432-1327.1999.00494.x.
Watson, B.O., Levenstein, D., Greene, J.P., Gelinas, J.N., Buzsáki, G., 2016. Network homeostasis and state dynamics of neocortical sleep. Neuron 90, 839–852. https://doi.org/10.1016/j.neuron.2016.03.036.
Wennberg, R., Steriade, C., Chen, R., Andrade, D., 2018. Frontal infraslow activity marks the motor spasms of anti-LGI1 encephalitis. Clin. Neurophysiol. 129, 59–68. https://doi.org/10.1016/j.clinph.2017.10.014.
Wilent, W.B., Contreras, D., 2004. Synaptic responses to whisker deflections in rat barrel cortex as a function of cortical layer and stimulus intensity. J. Neurosci. Off. J. Soc. Neurosci. 24, 3985–3998. https://doi.org/10.1523/JNEUROSCI.5782-03.2004.
Williams, M.S., Altwegg-Boussac, T., Chavez, M., Lecas, S., Mahon, S., Charpier, S., 2016. Integrative properties and transfer function of cortical neurons initiating absence seizures in a rat genetic model: epileptic seizures and information processing. J. Physiol. 594, 6733–6751. https://doi.org/10.1113/JP272162.
Yamagata, A., Miyazaki, Y., Yokoi, N., Shigematsu, H., Sato, Y., Goto-Ito, S., Maeda, A., Goto, T., Sanbo, M., Hirabayashi, M., Shirouzu, M., Fukata, Y., Fukata, M., Fukai, S., 2018. Structural basis of epilepsy-related ligand–receptor complex LGI1–ADAM22. Nat. Commun. 9. https://doi.org/10.1038/s41467-018-03947-w.
Yger, P., Spampinato, G.L., Esposito, E., Lefebvre, B., Deny, S., Gardella, C., Stimberg, M., Jetter, F., Zeck, G., Picaud, S., 2018. A spike sorting toolbox for up to thousands of electrodes validated with ground truth recordings in vitro and in vivo. ELife 7, e34518.
Yu, Y.E., Wen, L., Silva, J., Li, Z., Head, K., Sossey-Alaoui, K., Pao, A., Mei, L., Cowell, J. K., 2010. Lgi1 null mutant mice exhibit myoclonic seizures and CA1 neuronal hyperexcitability. Hum. Mol. Genet. 19, 1702–1711. https://doi.org/10.1093/hmg/ddq047.
Zhang, T.-Y., Cai, M.-T., Zheng, Y., Lai, Q.-L., Shen, C.-H., Qiao, S., Zhang, Y.-X., 2021. Anti-alpha-amino-3-hydroxy-5-methyl-4-isoxazolepropionic acid receptor encephalitis: a review. Front. Immunol. 12, 652820 https://doi.org/10.3389/fimmu.2021.652820.
Zhou, Y.-D., Lee, S., Jin, Z., Wright, M., Smith, S.E.P., Anderson, M.P., 2009. Arrested maturation of excitatory synapses in autosomal dominant lateral temporal lobe epilepsy. Nat. Med. 15, 1208–1214. https://doi.org/10.1038/nm.2019.
Zhou, Lin, Zhou, Liang, Su, L., Cao, S.-L., Xie, Y.-J., Wang, N., Shao, C.-Y., Wang, Y.-N., Zhou, J.-H., Cowell, J.K., Shen, Y., 2018. Celecoxib ameliorates seizure susceptibility in autosomal dominant lateral temporal epilepsy. J. Neurosci. 38, 3346–3357. https://doi.org/10.1523/JNEUROSCI.3245-17.2018.

Journal of Neurology
https://doi.org/10.1007/s00415-022-11004-2

ORIGINAL COMMUNICATION

Neuron Specific Enolase, S100-beta protein and progranulin as diagnostic biomarkers of status epilepticus

Aurélie Hanin[1,2] · Jérôme Alexandre Denis[3,4] · Valerio Frazzini[1,2] · Louis Cousyn[1,2] · Françoise Imbert-Bismut[5] · Benoit Rucheton[5] · Dominique Bonnefont-Rousselot[5,6] · Clémence Marois[7] · Virginie Lambrecq[1,2,3] · Sophie Demeret[7] · Vincent Navarro[1,2,3,8]

Received: 1 December 2021 / Revised: 29 January 2022 / Accepted: 30 January 2022

Abstract

Status epilepticus (SE) is a life-threatening prolonged epileptic seizure. A rapid diagnosis is fundamental to initiate antiepileptic treatment and to prevent the development of neurological sequels. Several serum and cerebrospinal fluid biomarkers have been proposed to help in the diagnosis of SE. Nevertheless, previous studies were conducted on too small patient cohorts, precluding the utilization of interesting biomarkers for the SE diagnosis. Here, we aimed to assess the ability of Neuron Specific Enolase (NSE), S100-beta protein (S100B) and progranulin to help in the diagnosis of SE in a large cohort of patients (36 control patients, 56 patients with pharmacoresistant epilepsy and 82 SE patients). Blood NSE, S100B and progranulin levels were higher in SE patients when compared with control patients or patients with pharmacoresistant epilepsy. Both NSE and progranulin levels were higher in cerebrospinal fluid from SE patients when compared with control patients. The receiver-operating characteristics curves revealed good accuracy at detecting SE for serum S100B (AUC 0.748) and plasma progranulin (AUC 0.756). The performances were lower for serum NSE (AUC 0.624). Eighty-four percent of patients with serum S100B levels above 0.09 ng/mL presented with a SE, whereas 90% of patients without SE had serum S100B levels lower than 0.09 ng/mL. Serum S100B levels were not significantly different according to SE etiology, SE semiology or SE refractoriness. Our results confirm that NSE, S100B and progranulin levels are increased after SE. We suggest that serum S100B levels might be added to clinical evaluation and electroencephalogram to identify difficult-to-diagnose form of SE.

Keywords Status epilepticus · Diagnosis · Etiology · Neuron Specific Enolase · S100-beta protein · Progranulin

✉ Vincent Navarro
vincent.navarro@aphp.fr

1 Sorbonne Université, Institut du Cerveau - Paris Brain Institute - ICM, Inserm, CNRS, AP-HP, Pitié-Salpêtrière Hospital, Paris, France

2 AP-HP, Epilepsy Unit and Clinical Neurophysiology Department, DMU Neurosciences, Pitié-Salpêtrière Hospital, Paris, France

3 Sorbonne Université, Paris, France

4 AP-HP, Endocrine and Oncological Biochemistry Department, Pitié-Salpêtrière Hospital, Paris, France

5 AP-HP, Metabolic Biochemistry Department, Pitié-Salpêtrière Hospital, Paris, France

6 UTCBS, CNRS, INSERM, Université de Paris, Paris, France

7 AP-HP, Neuro-Intensive Care Unit, Pitié-Salpêtrière Hospital, Paris, France

8 AP-HP, Center of Reference for Rare Epilepsies, Pitié-Salpêtrière Hospital, Paris, France

Abbreviations

CONT	Control patients
CSF	Cerebrospinal fluid
EEG	Electroencephalogram
EPI	Pharmacoresistant epileptic patients
ICU	Intensive Care Unit
NPV	Negative predictive value
NSE	Neuron Specific Enolase
NRSE	Non-refractory status epilepticus
PPV	Positive predictive value
PSRSE	Prolonged super-refractory status epilepticus
ROC	Receiver-operating characteristics
RSE	Refractory status epilepticus
S100B	S100-beta protein
SE	Status epilepticus

Published online: 21 February 2022

Introduction

Status epilepticus (SE) is a life-threatening prolonged epileptic seizure, related to various etiologies and with heterogeneous clinical presentations [1]. Sustained SE may lead to brain injury, and is associated with worse clinical outcomes and higher mortality [2]. The rapid diagnosis of SE is fundamental to urgently initiate antiepileptic treatments [3]. Diagnosis of convulsive SE is mostly based on clinical examination. In contrast, the diagnosis of non-convulsive SE requires an electroencephalogram (EEG) recording [4]. Here, we looked for the impact of SE on three biochemical markers levels and we wondered if these biochemical markers could be used to identify difficult-to-diagnose form of SE.

We considered Neuron Specific Enolase (NSE), S100-beta protein (S100B) and progranulin, which have previously been proposed as SE biomarkers [5]. They reflected, respectively, the neuronal injury (NSE), the astroglial injury (S100B) and the activation of microglia (progranulin) that occur in SE. Increased cerebrospinal fluid (CSF) NSE levels were reported in patients with cryptogenic or remote SE [6]. Increased serum NSE levels were also reported in patients with sustained SE with a peak between 24 and 48 h after the SE onset [7, 8]. Despite good characteristics (good neuronal specificity, stability in the body fluids, a rapid and reliable biochemical assessment), NSE is not currently used as a diagnosis SE biomarker. This can be explained as most previous studies were conducted on too small patient cohorts (between 2 and 31 patients) precluding the utilization of NSE as a validated diagnosis biomarker for SE [9]. S100B was mostly studied in isolated seizures, but increased CSF S100B levels were reported in a rat model of SE [10–12]. S100B was not previously studied in human SE. Nevertheless, its rapid assessment and its ability to distinguish isolated epileptic seizures from psychogenic non-epileptic seizures make S100B a promising biomarker for SE diagnosis [12]. A higher expression of progranulin was observed in activated microglia and macrophages following pilocarpine-induced SE in rats [13]. However, progranulin levels in CSF were not significantly increased compared to patients who underwent a lumbar puncture after a single tonic–clonic seizure [14].

Here, we evaluated the diagnosis value of these three biomarkers in a large cohort of patients. They were measured in blood samples from SE patients, control patients and patients with pharmacoresistant epilepsy as well as in CSF samples from some SE patients and control patients.

First, we assessed the ability of NSE, S100B and progranulin to identify SE patients.

Second, we investigated the impact of SE etiology, SE semiology and the delay of blood or CSF collection after the ongoing SE onset on the biomarker's levels.

Methods

Study design, setting and participants

We prospectively enrolled adult patients admitted in intensive care unit (ICU) and neurology units of the Pitié-Salpêtrière Hospital, from February 2013 to March 2021. The protocol was approved by our local ethic committee (2012, CPP Paris-VI) and sponsored by INSERM (C16-16, 20152482). Patients or relatives were informed and gave their consent. The study design and report are in accordance with the STROBE statement [15].

Eligible SE patients were patients aged at least 18 years, with an ongoing SE, either a generalized convulsive SE, either a focal convulsive or focal non-convulsive SE diagnosed according to the International League Against Epilepsy criteria [1]. The SE end was defined as the absence of seizures after the anesthetic's withdrawal. Physicians from ICU and neurology units excluded: patients with a subtle SE defined by minor and erratic myoclonic movements in patients with severely impaired consciousness; patients with post-anoxic SE; patients whose SE was linked to a pathological condition, such as trauma or subarachnoid aneurysmal hemorrhage, who needed immediate surgery and for whom the biomarkers could be elevated due to the underlying disease [16, 17]. Patients for whose parent, guardian or other reliable person refused permission or patients who refused themselves permission were also excluded. Enrolled patients were divided into four groups according to their SE etiology: acute, progressive, remote and cryptogenic [18]. The type of SE was further categorized into three groups: non-refractory SE (NRSE), refractory SE (RSE) and prolonged super-refractory SE (PSRSE) [19]. The RSE was defined as a failure of at least two appropriately selected and dosed parenteral medications including a benzodiazepine, without any specific SE duration [19]. The PSRSE was defined as a RSE that persists for more than 7 days, with ongoing need for anesthetics [19]. The type of SE was further categorized into three groups according to the SE semiology: generalized convulsive SE, focal convulsive SE and focal non-convulsive SE. None of the patients had a generalized non-convulsive SE.

Eligible patients with pharmacoresistant epilepsy (EPI) were aged at least 18 years and hospitalized for a video-EEG monitoring pre-surgical evaluation ($n=17$) or for a resection of the epileptic focus ($n=39$). Patients who refused permission and patients for whose the date of the last seizure cannot be reported were excluded.

Eligible control patients (CONT) were aged at least 18 years and hospitalized in neurology units for non-acute disorders. A clinical neurological evaluation and a lumbar puncture were performed for all CONT patients. Patients with previous history of epilepsy or patients whose symptoms were linked to an acute pathological condition (trauma, hemorrhage) were excluded as well as patients with an abnormal lumbar puncture (i.e., pleocytosis, increased protein levels, intrathecal synthesis). The diagnoses for these patients were psychogenic disorders or non-inflammatory peripheral neuropathies.

Biochemical assays

Blood and CSF samples were centrifuged at 3500 rpm for 10 min. Hemolytic samples (hemoglobin concentration above 47 mg/dL) were excluded.

The NSE and S100B assays were performed using, respectively, immunofluorimetric assays and electrochemiluminometric sandwich immunoassays (Kryptor®, Brahms and Modular®E170, Roche Diagnostics). The lowest detections were 0.8 ng/mL for NSE and 0.005 ng/mL for S100B. The coefficients of variation (CV) were found to be lower than 5% for all controls used.

Progranulin measurements were performed using the progranulin-human-ELISA kit (Adipogen, Coger SAS, France). All the samples were analyzed in duplicated and progranulin measurements was repeated when CV between duplicated measures were higher than 15%.

Statistical analysis

Analyses were performed with R Software (R.3.5.0).

We first performed Kruskal–Wallis test to evaluate subgroups impact. Then, pairwise comparisons were performed using Student or Mann–Whitney when appropriate. The Benjamini–Hochberg test procedure was used to correct for multiple comparisons. Correlations between blood levels and the time between SE onset and blood sampling were evaluated by calculating respective Spearman's rho values and their level of significance. To assess the ability of biomarkers to diagnose SE, we computed the area under the receiver-operating characteristics (ROC) curve and reported sensitivity and specificity for the best cut-off which was defined accordingly to the Youden's index [20]. Quantitative variables were expressed as mean with standard deviation. All statistical were two-sided with a type I error rate of 5%.

Data availability

All anonymized data are available on request.

Results

The study cohort is represented in Fig. 1A. Main demographic data are shown in Table 1. Blood samples were collected for 36 CONT patients, 56 EPI patients and 82 SE patients. CSF samples were collected for 38 CONT patients and 34 SE patients.

Blood samples and CSF samples were collected, respectively, on average 7 (± 12) and 11 (± 17) days after the SE onset. All the blood and the CSF samples were collected in patients with an ongoing SE. Twenty-nine EPI patients (52%) showed a seizure in the last 48 h before the blood collection.

NSE, S100B and progranulin as diagnostic biomarkers of SE

Blood NSE, S100B and progranulin levels

Serum NSE levels were significantly higher in SE patients when compared with EPI patients and showed a non-significant increase as compared with CONT patients (Fig. 1B, Table 2). Both serum S100B and plasma progranulin levels were higher in SE patients when compared with EPI patients and CONT patients (Fig. 1B, Table 2). No significant difference of blood levels was found between CONT patients and EPI patients for any of the three biomarkers (Table 2).

CSF NSE, S100B and progranulin levels and CSF/blood ratios

Both CSF NSE and progranulin levels were significantly higher in SE patients when compared with CONT patients (Fig. 1C, Table 2). No significant difference was found for CSF S100B levels (Table 2). Similarly, we observed in SE patients an increase in the CSF/blood ratios for progranulin, while the CSF/blood ratios tended to increase for NSE and no difference was found for CSF/blood S100B ratios (Table 2).

SE diagnosis value

The ROC curves revealed good accuracy at detecting SE for: (1) serum S100B levels (AUC 0.748 [CI 95% 0.669–0.827]), with a sensitivity of 59.7%, specificity of 90.2%, positive predictive value (PPV) of 83.6% and negative predictive value (NPV) of 72.8% when using the cut-off of 0.09 ng/mL; and (2) plasma progranulin levels (AUC 0.756 [CI 95% 0.681–0.831]), with a sensitivity of 57.3%, specificity of 85.4%, PPV of 79.7% and NPV of

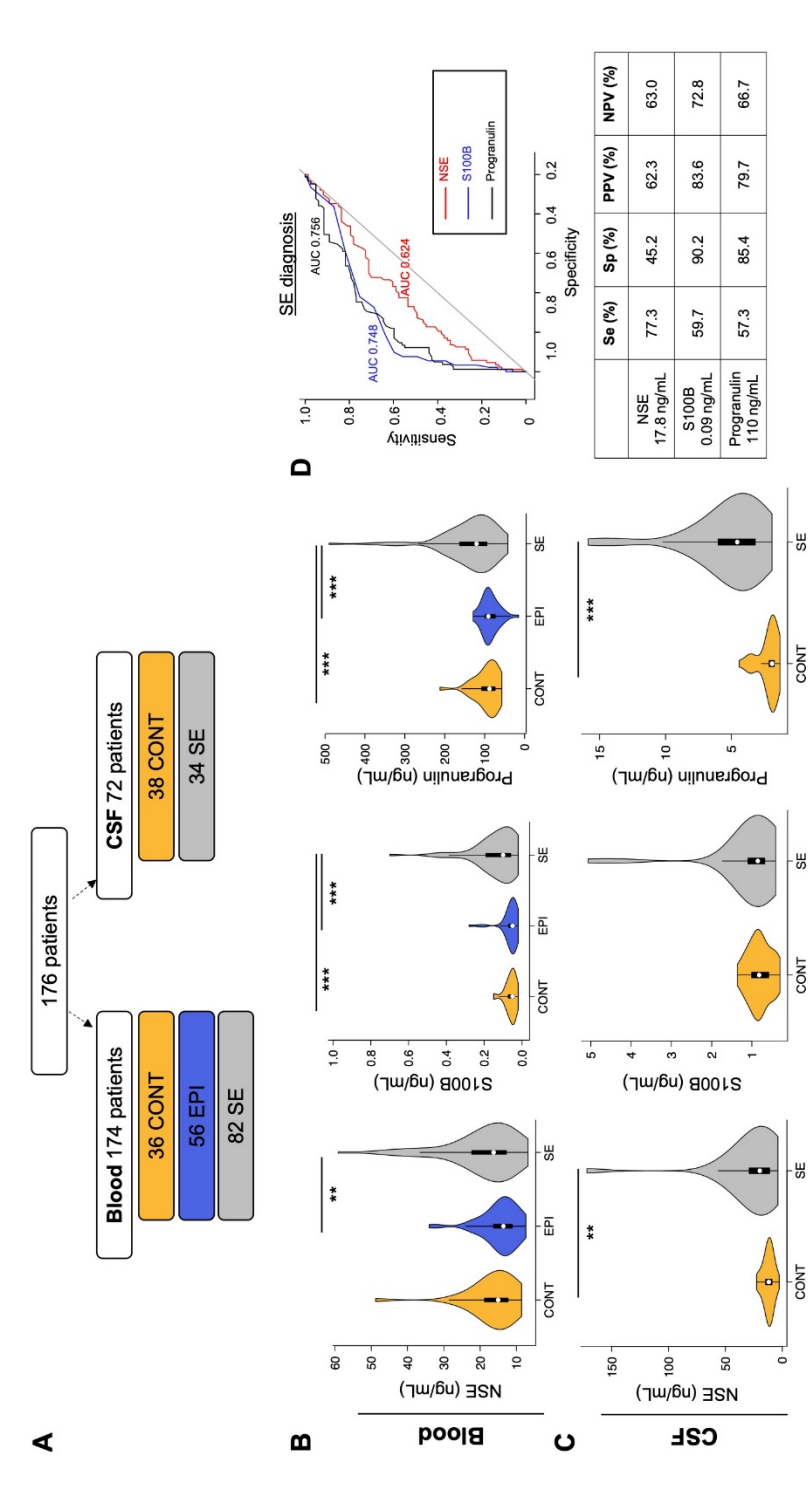

	Se (%)	Sp (%)	PPV (%)	NPV (%)
NSE 17.8 ng/mL	77.3	45.2	62.3	63.0
S100B 0.09 ng/mL	59.7	90.2	83.6	72.8
Progranulin 110 ng/mL	57.3	85.4	79.7	66.7

Fig. 1 Neuron Specific Enolase, S100-beta protein and progranulin as diagnosis biomarkers of status epilepticus; **A** represents the number of patients for each group (CONT, EPI, SE) and each biological compartment (blood, CSF); **B**, **C** represent, respectively, the distribution of NSE levels (left), S100B levels (center) and progranulin levels (right) in blood (**B**) and in CSF (**C**). The violin plots show the density of the data at different levels. The white point represents the median of the data, the dark box indicates the interquartile range, and the two end points represent, respectively, the maximum and the minimum values (expect for outliers); **D** shows the ROC curves for serum NSE (red), serum S100B (blue) and plasma progranulin (black) to identify patients with SE. The table below represents the values of sensitivity (Se), specificity (Sp), positive predictive value (PPV) and negative predictive value (NPV) for the best cut-off of each biological marker, defined according to the Youden's index

Table 1 Demographic characteristics of the study cohort

	Patients *N* (%)	Age (years ± SD)	Ratio M/F (%)
SE patients	82	49.8 ± 18.8	60
Acute	28 (34)	49.1 ± 19.7	57
Progressive	20 (24)	52.4 ± 19.8	70
Remote	24 (29)	48.8 ± 19.1	54
Unknown cryptogenic	10 (12)	49.4 ± 15.3	60
Patients who required immunomodulatory drugs	20 (24)	42.7 ± 21.0	60
NRSE	25 (30)	55.5 ± 16.7	64
RSE	32 (39)	51.3 ± 18.8	63
PSRSE	25 (30)	42.2 ± 18.8	52
EPI patients	56	35.9 ± 11.2	48
CONT patients	36	54.1 ± 20.7	50

Data are represented as percentages or mean ± standard deviation (SD)

CONT control patients, *EPI* pharmacoresistant epileptic patients, *F* female, *M* male, *NRSE* non-refractory status epilepticus, *PSRSE* prolonged super-refractory status epilepticus, *RSE* refractory status epilepticus, *SE* status epilepticus

66.7% when using the cut-off of 110 ng/mL (Fig. 1D). Serum NSE levels can detect SE with a lower discrimination (AUC 0.624 [CI 95% 0.536–0.713]).

Biomarkers levels according to SE refractoriness, SE semiology and SE etiology

SE refractoriness

We next wondered if blood biomarker levels differed according to SE refractoriness and to the delay between the ongoing SE onset and the blood collection. We found that only plasma progranulin levels differed according to the SE refractoriness ($p < 0.001$). Plasma progranulin levels were significantly higher for PSRSE patients when compared with RSE patients (177.1 ± 95.0 versus 107.7 ± 43.0, $p < 0.001$) and NRSE patients (177.1 ± 95.0 versus 137.5 ± 63.2, $p = 0.030$). Similarly, plasma progranulin levels were found correlated with the ongoing SE duration before the blood collection ($\rho = 0.360$, $p = 0.0032$) while no correlation was found for serum NSE and S100B levels (Fig. 2A). We did not look for the impact of SE refractoriness on CSF biomarkers levels as lumbar puncture was mostly done for refractory SE.

SE semiology

We then researched if these three biomarkers behave differentially according to SE semiology. Forty-two (51%) patients had a generalized convulsive SE, 33 (40%) had a focal convulsive SE and 7 (9%) had a focal non-convulsive SE. The blood or the CSF levels were not significantly

Table 2 Blood, CSF, CSF/blood ratio of NSE, S100B and progranulin in SE patients, control patients and EPI patients

	Blood			CSF			CSF/blood		
	NSE (ng/mL ± SD)	S100B (ng/mL ± SD)	Progranulin (ng/mL ± SD)	NSE (ng/mL ± SD)	S100B (ng/mL ± SD)	Progranulin (ng/mL ± SD)	NSE (AU)	S100B (AU)	Progranulin (AU)
SE	19.4 ± 10.2 ($n = 73$)	0.14 ± 0.12 ($n = 77$)	137.9 ± 73.5 ($n = 82$)	27.0 ± 31.4 ($n = 28$)	1.087 ± 0.953 ($n = 33$)	5.30 ± 3.08 ($n = 28$)	1.98 ± 2.93 ($n = 21$)	13.40 ± 12.51 ($n = 25$)	0.041 ± 0.027 ($n = 27$)
CONT	16.6 ± 7.37 ($n = 34$)	0.059 ± 0.030 ($n = 36$)	94.6 ± 31.3 ($n = 36$)	12.1 ± 4.63 ($n = 34$)	0.805 ± 0.283 ($n = 38$)	2.15 ± 0.766 ($n = 31$)	0.75 ± 0.36 ($n = 26$)	16.75 ± 9.84 ($n = 32$)	0.024 ± 0.0076 ($n = 31$)
EPI	14.5 ± 5.29 ($n = 54$)	0.061 ± 0.046 ($n = 56$)	86.6 ± 21.9 ($n = 46$)	–	–	–	–	–	–
p value SE-EPI Wilcoxon–test	0.0085	< 0.001	< 0.001	–	–	–	–	–	–
p value SE-CONT Wilcoxon–test	0.39	< 0.001	< 0.001	0.0067	0.46	< 0.001	0.087	0.20	0.019
p value CONT-EPI Wilcoxon–test	0.25	0.67	1	–	–	–	–	–	–

Data are represented as mean ± standard deviation (SD)

AU arbitrary units, *CONT* control patients, *EPI* pharmacoresistant epileptic patients, *SE* status epilepticus

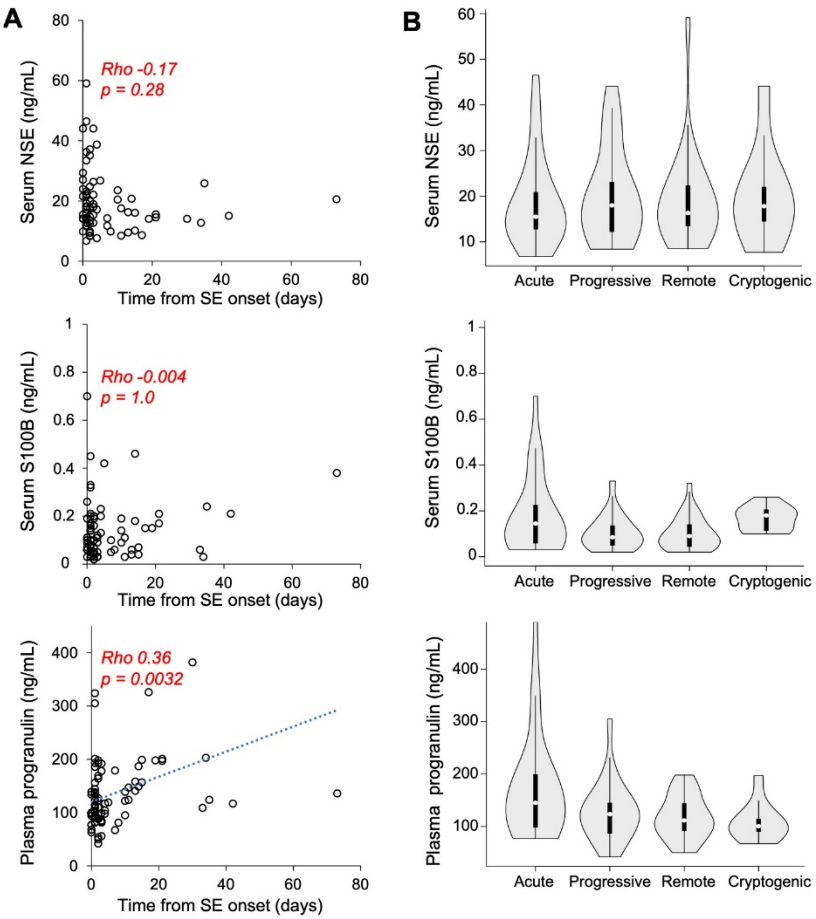

Fig. 2 Progranulin as a biomarker of inflammatory status epilepticus; **A** shows the relations between serum NSE levels (up), serum S100B levels (middle) and plasma progranulin levels (down) and the time between the SE onset and the blood sampling. The correlations were assessed with the Spearman test; **B** represents the distribution of serum NSE levels (up), serum S100B levels (middle) and plasma progranulin levels (down) according to the SE etiologies. The white points represent the median of the data, the dark boxes indicate the interquartile ranges, and the two end points represent, respectively, the maximum and the minimum values (expect for outliers)

different according to SE semiology for all the three markers (data not shown).

SE etiology

We then researched if these three biomarkers behave differentially according to SE etiology. The SE etiologies were classified as acute for 28 patients (34%), progressive for 20 patients (24%), remote for 24 patients (29%) and cryptogenic for 10 patients (12%). The CSF levels were not significantly different according to SE etiology for all the three markers (data not shown). Serum NSE levels were not significantly different according to SE etiology, whereas serum S100B and plasma progranulin levels tended to increase in acute SE (Fig. 2B). We observed a high heterogeneity of serum S100B levels (0.03–0.70 ng/mL) and plasma progranulin levels (77–490 ng/mL) for the patients with acute etiology (Fig. 2B). It might be explained by the heterogeneity of the underlying etiologies (encephalitis $n=19$, posterior reversible encephalopathy syndrome $n=3$, metabolic disturbances $n=2$, alcohol disorders $n=2$, subdural hematoma $n=2$).

Discussion

The identification of suitable biomarkers could help physicians to establish a more accurate diagnosis quickly, especially for difficult-to-diagnose form of SE.

The SE patients had higher CSF NSE levels when compared with control patients and higher serum levels when compared with pharmacoresistant epileptic patients. These results are in accordance with previous studies [7, 8], but were obtained in a larger cohort which support their accuracy. We showed, for the first time, that SE patients had higher S100B levels when compared with control (in serum and CSF samples) and pharmacoresistant epileptic patients

(in serum samples). Similarly, SE patients had higher progranulin levels when compared with control patients (in plasma and CSF samples) and pharmacoresistant epileptic patients (in plasma samples).

We may wonder if the increase of the biomarkers levels is related to SE onset, and therefore, biomarkers could be used for SE diagnosis; and/or if it reflects brain damage associated with SE. A mixed scenario can be considered with an unequal distribution according to the biomarkers. The NSE is a world-renowned biomarker to assess brain damage in acute neurological disorders or after cardiac arrest [16, 17, 21, 22]. Increased NSE levels following SE may be related to neuronal death and NSE could be preferentially used as a SE prognosis biomarker. Nevertheless, several arguments suggest that NSE could also be a SE diagnosis biomarker. First, while brain damage increased with the SE duration, we did not observe a correlation between the serum NSE levels and the ongoing SE duration before the blood collection. Second, serum NSE levels were not significantly different according to SE semiology, while generalized convulsive SE are known to be more severe than focal convulsive SE. Third, we previously reported that patients with seizures had higher blood NSE levels when compared with patients with periodic discharges at EEG despite periodic discharges were associated with higher brain damage [23, 24]. It suggested that increased NSE levels may be related to seizures onset and NSE could be used as a SE diagnosis biomarker. The S100B is a marker of astroglial injury and found increased in several acute neurological disorders [17, 21, 25]. While it was reported a quickly and progressive gliosis after SE, the absence of correlation between serum S100B levels and the ongoing SE duration before the blood collection suggests that the increase of S100B levels could be merely related to SE onset and, therefore, this biomarker could be used for SE diagnosis.

In contrast, plasma progranulin levels were higher in patients for whom the blood was collected several days after SE onset and therefore for PSRSE patients. The increase of the progranulin levels occurs primarily in activated microglia [13]. However, the microglial activation only occurs a few days after the SE onset which could explain the increased delay. The sustained SE may enhance the microglial activation and inflammation processes, and therefore, the increase of plasma progranulin levels could reflect the SE duration and subsequent consequences. Plasma progranulin levels might further testify the brain damage than the occurrence of SE. Nonetheless, as a microglial activation frequently occurs in SE of autoimmune origin [26], we may wonder if this biomarker might be also used to identify patients with SE of autoimmune origin and therefore guide the early treatment strategy.

Despite these three biomarkers were all increased in the blood of SE patients, and NSE and S100B increased could be related to SE onset, we believe that S100B is the most promising marker for SE diagnosis. Indeed, S100B had a higher AUC value than NSE, and it could be quickly assessed contrary to progranulin. We identified a cut-off at 0.09 ng/mL, which was accurately associated with a SE diagnosis for 84% of the patients. As control and pharmacoresistant epileptic patients rarely had serum S100B levels above 0.09 ng/mL (less than 10% in our cohort), it might be interesting to use serum S100B levels as an emergency triage marker. If a patient without any acute brain injury (trauma, hemorrhage) is admitted to the emergency department with convulsive movements, confusion or decreased alertness and has serum S100B levels above 0.09 ng/mL, clinicians may be prompted to keep the patient in the hospital for medical and neurological observation and to request an emergency EEG. Nonetheless, we believe that clinicians will not rely solely on this biomarker to decide on a return home. Our study highlights the potential of these biomarkers for SE diagnosis and allows to propose a cut-off for the clinical use of S100B.

We found no association between the SE etiology and the levels of serum NSE, as previously reported [8]. However, we observed a high heterogeneity in S100B and progranulin levels for patients with an acute SE. It could be explained by a heterogeneity of SE etiologies classified as an acute SE according to the International League Against Epilepsy Classification [18]. If this first classification is useful to categorize SE, it could be relevant to add biochemical biomarkers to this classification to distinguish acute SE with or without inflammatory underlying causes.

We investigated the potential of NSE, S100B and progranulin as SE biomarkers in a large cohort of patients for the first time. Although our population was heterogenous for SE etiology and for the delay of enrollment after the SE onset, we found promising results for the three biomarkers. We confirmed the increase of NSE levels in SE patients whatever the SE etiology. Serum S100B appears to be the most promising biomarker for SE diagnosis using the cut-off at 0.09 ng/mL. Plasma progranulin could be an interesting biomarker to reflect inflammatory processes.

There are some limitations for this study: it was conducted in a single center, most SE patients were enrolled in the Neuro-Intensive care unit specialized for the management of prolonged super-refractory SE, and therefore, the collection of blood and CSF samples was delayed for patients who were previously managed in another hospital. Due to the small number of patients, we were not able to specifically analyze the interest of blood and CSF biomarkers for non-convulsive SE patients. Nonetheless, the strengths of our study were to collect samples from a large cohort of patients and to provide cut-off for clinical use. Further studies are needed to investigate the diagnosis potential of the three biomarkers for non-convulsive SE and to investigate

the ability of progranulin to specifically distinguish inflammation processes related to a sustained SE (i.e., consequences of SE) from inflammation processes involved in the SE development (i.e., causes of SE) [27].

Author contributions Drafting the manuscript for content: AH and VN. Major role in the acquisition of data: AH, JAD, VF, FI-B, BR, CM, and VL. Study concept and design: AH, DB-R, SD, and VN. Analysis or interpretation of data: AH, JAD, VF, SD, and VN. Statistical analysis: AH. Obtaining funding: AH and VN. Revising the manuscript for content: JAD, VF, FI-B, BR, DB-R, CM, VL, and SD.

Funding This work received support from the "Investissements d'avenir" program ANR-10-IAIHU-06, from the "Fondation pour la Recherche Médicale" (FDM20170839111) and from the Fondation Assistance Publique-Hôpitaux de Paris (EPIRES- Marie Laure PLV Merchandising).

Availability of data and materials All data are available on request upon the corresponding author.

Code availability Not applicable.

Declarations

Conflicts of interest Vincent Navarro reports personal fees from UCB Pharma, EISAI, GW Pharma and LivaNova, outside the submitted work. Sophie Demeret reports individual payment from UCB Pharma, Regeneron and ARGENX. The other authors report no disclosures.

Ethical approval The protocol was approved by our local (2012, CPP Paris-VI) and by the INSERM ethic committees (C16-16, 20152482). The study was performed in accordance with the ethical standards as laid down in the 1964 Declaration of Helsinki and its later amendments or comparable ethical standards.

Consent to participate Patients or relatives were informed and give their consent.

Consent for publication Patients or relatives were informed and give their consent.

References

1. Trinka E, Kälviäinen R (2017) 25 years of advances in the definition, classification and treatment of status epilepticus. Seizure 44:65–73. https://doi.org/10.1016/j.seizure.2016.11.001
2. Alkhachroum A, Der-Nigoghossian CA, Rubinos C, Claassen J (2020) Markers in status epilepticus prognosis. J Clin Neurophysiol 37:422–428. https://doi.org/10.1097/WNP.0000000000000761
3. Claassen J, Goldstein JN (2017) Emergency neurological life support: status epilepticus. Neurocrit Care 27:152–158. https://doi.org/10.1007/s12028-017-0460-1
4. Leitinger M, Beniczky S, Rohracher A et al (2015) Salzburg consensus criteria for non-convulsive status epilepticus—approach to clinical application. Epilepsy Behav 49:158–163. https://doi.org/10.1016/j.yebeh.2015.05.007
5. Hanin A, Lambrecq V, Denis JA et al (2020) Cerebrospinal fluid and blood biomarkers of status epilepticus. Epilepsia 61:6–18. https://doi.org/10.1111/epi.16405
6. Correale J, Rabinowicz AL, Heck CN et al (1998) Status epilepticus increases CSF levels of neuron-specific enolase and alters the blood-brain barrier. Neurology 50:1388–1391
7. DeGiorgio CM, Correale JD, Gott PS et al (1995) Serum neuron-specific enolase in human status epilepticus. Neurology 45:1134–1137
8. DeGiorgio CM, Heck CN, Rabinowicz AL et al (1999) Serum neuron-specific enolase in the major subtypes of status epilepticus. Neurology 52:746–749
9. Gnanapavan S, Hegen H, Khalil M et al (2014) Guidelines for uniform reporting of body fluid biomarker studies in neurologic disorders. Neurology 83:1210–1216. https://doi.org/10.1212/WNL.0000000000000809
10. Vizuete AFK, Hennemann MM, Gonçalves CA, de Oliveira DL (2017) Phase-dependent astroglial alterations in li-pilocarpine-induced status epilepticus in young rats. Neurochem Res 42:2730–2742. https://doi.org/10.1007/s11064-017-2276-y
11. Freund Y, Bloom B, Bokobza J et al (2015) Predictive value of S100-B and copeptin for outcomes following seizure: the BISTRO International Cohort Study. PLoS ONE 10:e0122405. https://doi.org/10.1371/journal.pone.0122405
12. Asadollahi M, Simani L (2019) The diagnostic value of serum UCHL-1 and S100-B levels in differentiate epileptic seizures from psychogenic attacks. Brain Res 1704:11–15. https://doi.org/10.1016/j.brainres.2018.09.028
13. Zhu S, Tai C, Petkau TL et al (2013) Progranulin promotes activation of microglia/macrophage after pilocarpine-induced status epilepticus. Brain Res 1530:54–65. https://doi.org/10.1016/j.brainres.2013.07.023
14. Huchtemann T, Körtvélyessy P, Feistner H et al (2015) Progranulin levels in status epilepticus as a marker of neuronal recovery and neuroprotection. Epilepsy Behav 49:170–172. https://doi.org/10.1016/j.yebeh.2015.06.022
15. Cuschieri S (2019) The STROBE guidelines. Saudi J Anaesth 13:S31–S34. https://doi.org/10.4103/sja.SJA_543_18
16. Chou SH-Y, Macdonald RL, Keller E, Unruptured Intracranial Aneurysms, SAH CDE Project Investigators (2019) Biospecimens and molecular and cellular biomarkers in aneurysmal subarachnoid hemorrhage studies: common data elements and standard reporting recommendations. Neurocrit Care 30:46–59. https://doi.org/10.1007/s12028-019-00725-4
17. Helbok R, Beer R (2017) Cerebrospinal fluid and brain extracellular fluid in severe brain trauma. Handb Clin Neurol 146:237–258. https://doi.org/10.1016/B978-0-12-804279-3.00014-9
18. Trinka E, Cock H, Hesdorffer D et al (2015) A definition and classification of status epilepticus—report of the ILAE Task Force on classification of status epilepticus. Epilepsia 56:1515–1523. https://doi.org/10.1111/epi.13121
19. Hirsch LJ, Gaspard N, van Baalen A et al (2018) Proposed consensus definitions for new-onset refractory status epilepticus (NORSE), febrile infection-related epilepsy syndrome (FIRES), and related conditions. Epilepsia 59:739–744. https://doi.org/10.1111/epi.14016
20. Fluss R, Faraggi D, Reiser B (2005) Estimation of the Youden Index and its associated cutoff point. Biom J 47:458–472. https://doi.org/10.1002/bimj.200410135
21. Chou SH-Y, Robertson CS, Participants in the International Multi-disciplinary Consensus Conference on the Multimodality Monitoring (2014) Monitoring biomarkers of cellular injury and death in acute brain injury. Neurocrit Care 21(Suppl 2):S187-214. https://doi.org/10.1007/s12028-014-0039-z
22. Tawk RG, Grewal SS, Heckman MG et al (2016) The relationship between serum neuron-specific enolase levels and severity of bleeding and functional outcomes in patients with nontraumatic subarachnoid hemorrhage. Neurosurgery 78:487–491. https://doi.org/10.1227/NEU.0000000000001140

23. Hanin A, Demeret S, Denis JA et al (2021) Serum neuron-specific enolase: a new tool for seizure risk monitoring after status epilepticus. Eur J Neurol. https://doi.org/10.1111/ene.15154
24. Jaitly R, Sgro JA, Towne AR et al (1997) Prognostic value of EEG monitoring after status epilepticus: a prospective adult study. J Clin Neurophysiol 14:326–334
25. Sanchez-Peña P, Pereira A-R, Sourour N-A et al (2008) S100B as an additional prognostic marker in subarachnoid aneurysmal hemorrhage. Crit Care Med 36:2267–2273. https://doi.org/10.1097/CCM.0b013e3181809750
26. Tan TH-L, Perucca P, O'Brien TJ et al (2021) Inflammation, ictogenesis, and epileptogenesis: an exploration through human disease. Epilepsia 62:303–324. https://doi.org/10.1111/epi.16788
27. Abboud H, Probasco JC, Irani S et al (2021) Autoimmune encephalitis: proposed best practice recommendations for diagnosis and acute management. J Neurol Neurosurg Psychiatry. https://doi.org/10.1136/jnnp-2020-325300

Résumé

L'épilepsie se définit comme la répétition de crises, de symptomatologie variée, mais dont le caractère spontané et imprévisible rend compte du handicap chronique chez les patients. Près d'un tiers des patients est résistant aux médicaments antiépileptiques, c'est-à-dire que les crises d'épilepsie persistent malgré l'utilisation d'au moins deux molécules adaptées. L'étude des mécanismes sous-tendant la transition entre un état intercritique (littéralement « entre deux crises ») et la crise – l'ictogenèse – a longtemps suggéré l'existence de modifications précritiques. L'état précritique correspond à la période précédant la crise et constitue ainsi la pierre angulaire des méthodes de prédiction des crises. Individualiser des biomarqueurs précritiques sensibles et spécifiques pourrait permettre d'envisager des stratégies thérapeutiques afin de stopper la « route vers la crise ».

Mon travail de thèse a eu pour objectif de caractériser des états précritiques à l'aide : i) de symptômes cliniques subjectifs ; ii) de mesures standardisées de l'activité cardiaque et de connectivité fonctionnelle intracérébrale ; iii) d'enregistrements d'activités neuronales *in vivo* et d'activités épileptiques *in vitro* chez des patients atteints d'épilepsie.

Mon approche de l'état précritique s'est ainsi décomposée en plusieurs niveaux :

1) L'évaluation de symptômes prodromaux mesurés à l'aide d'auto-questionnaires quotidiens chez des patients hospitalisés : plusieurs algorithmes d'apprentissage automatique, basés sur des séparateurs à vastes marges, ont mis en évidence de bonnes performances de prédiction de l'état précritique. Une étude clinique à l'aide de l'application mobile Epiday – développée sur la base de mes travaux de thèse – permettra d'analyser cette approche de façon prospective et en condition de vie réelle.

2) L'analyse de la variabilité de la fréquence cardiaque – en tant que reflet de l'équilibre sympathique/parasympathique – au cours d'un protocole de repos standardisé quotidien, qui a permis une bonne distinction des états inter et précritiques à l'aide d'un classifieur. L'analyse pseudoprospective a montré des prévisions probabilistes du risque de crise(s) globalement correctes mais une sensibilité moyenne, nécessitant une amélioration dans l'optique d'une application clinique.

3) L'étude de la connectivité fonctionnelle à l'aide d'enregistrements EEG intracérébraux, également durant des protocoles de repos quotidiens : l'algorithme de classification basé sur la synchronie de phase a montré les meilleures performances de distinction entre les états inter et précritiques dans la bande thêta. Ces résultats étaient significativement supérieurs à ceux du classifieur basé sur les anomalies épileptiques intercritiques. Les prévisions probabilistes quotidiennes du risque de crise(s) étaient par ailleurs prometteuses. Transposer les données de connectivité dans un espace géométrique hyperbolique a montré des résultats similaires.

4) L'enregistrement *in vivo* de l'activité neuronale à l'aide de microélectrodes intracérébrales : j'ai pu, de façon préliminaire, identifier un grand nombre de neurones et suivre leur activité durant les heures précédant les crises. Je compte poursuivre mon travail de thèse en recherchant des modifications précritiques du comportement individuel et interindividuel de ces neurones.

5) L'enregistrement *in vitro* sur tranches de tissu cérébral épileptique post-opératoire m'a permis d'enregistrer, de façon préliminaire, des anomalies intercritiques et précritiques, que j'ai pu corréler avec des données acquises *in vivo*.

Mon travail de thèse a fourni de nouvelles données, suggérant l'existence de modifications dynamiques précritiques, en tirant bénéfice d'algorithmes d'apprentissage automatique et de la mise en place d'une évaluation quotidienne dans un état de repos standardisé. Mes travaux ouvrent la voie pour une analyse des modifications des activités neuronales enregistrées *in vivo* lors d'EEG intracérébraux.